

9C

NUREG/CR-3110  
PNL-4584  
Vol. 1

---

---

# Reliability of Nondestructive Examination

Chapters 1 - 6

---

---

Prepared by S. H. Bush

**Pacific Northwest Laboratory**  
Operated by  
Battelle Memorial Institute

Prepared for  
U.S. Nuclear Regulatory  
Commission

## NOTICE

This report was prepared as an account of work sponsored by an agency of the United States Government. Neither the United States Government nor any agency thereof, or any of their employees, makes any warranty, expressed or implied, or assumes any legal liability of responsibility for any third party's use, or the results of such use, of any information, apparatus, product or process disclosed in this report, or represents that its use by such third party would not infringe privately owned rights.

### Availability of Reference Materials Cited in NRC Publications

Most documents cited in NRC publications will be available from one of the following sources:

1. The NRC Public Document Room, 1717 H Street, N.W.  
Washington, DC 20555
2. The NRC/GPO Sales Program, U.S. Nuclear Regulatory Commission,  
Washington, DC 20555
3. The National Technical Information Service, Springfield, VA 22161

Although the listing that follows represents the majority of documents cited in NRC publications, it is not intended to be exhaustive.

Referenced documents available for inspection and copying for a fee from the NRC Public Document Room include NRC correspondence and internal NRC memoranda; NRC Office of Inspection and Enforcement bulletins, circulars, information notices, inspection and investigation notices; Licensee Event Reports; vendor reports and correspondence; Commission papers; and applicant and licensee documents and correspondence.

The following documents in the NUREG series are available for purchase from the NRC/GPO Sales Program: formal NRC staff and contractor reports, NRC-sponsored conference proceedings, and NRC booklets and brochures. Also available are Regulatory Guides, NRC regulations in the *Code of Federal Regulations*, and *Nuclear Regulatory Commission Issuances*.

Documents available from the National Technical Information Service include NUREG series reports and technical reports prepared by other federal agencies and reports prepared by the Atomic Energy Commission, forerunner agency to the Nuclear Regulatory Commission.

Documents available from public and special technical libraries include all open literature items, such as books, journal and periodical articles, and transactions. *Federal Register* notices, federal and state legislation, and congressional reports can usually be obtained from these libraries.

Documents such as theses, dissertations, foreign reports and translations, and non-NRC conference proceedings are available for purchase from the organization sponsoring the publication cited.

Single copies of NRC draft reports are available free upon written request to the Division of Technical Information and Document Control, U.S. Nuclear Regulatory Commission, Washington, DC 20555.

Copies of industry codes and standards used in a substantive manner in the NRC regulatory process are maintained at the NRC Library, 7920 Norfolk Avenue, Bethesda, Maryland, and are available there for reference use by the public. Codes and standards are usually copyrighted and may be purchased from the originating organization or, if they are American National Standards, from the American National Standards Institute, 1430 Broadway, New York, NY 10018.

---

---

# Reliability of Nondestructive Examination

Chapters 1 - 6

---

---

Manuscript Completed: August 1983  
Date Published: October 1983

Prepared by  
S. H. Bush

Pacific Northwest Laboratory  
Richland, WA 99352

Prepared for  
Division of Engineering Technology  
Office of Nuclear Regulatory Research  
U.S. Nuclear Regulatory Commission  
Washington, D.C. 20555  
NRC FIN B2289



## ABSTRACT

This eighteen-chapter, three-volume study evaluates the various nondestructive examination (NDE) techniques now used to detect flaws in components of nuclear systems so that the reliability of the techniques may be increased. The significance of flaws at various locations in pressure boundary components are assessed along with ways to optimize the NDE procedures needed to detect, locate and size them. Emphasis is placed on an integrated program which also considers design, fabrication procedures, and materials. The data available on the reliability of detecting, locating and sizing flaws by NDE are used to construct a probabilistic fracture mechanics model. The model highlights the significance of the failure to detect flaws, and to accurately locate or size them in the context of component failure probability.

This study was conducted under the U.S. Nuclear Regulatory Commission program on the "Integration of NDE Reliability and Fracture Mechanics." Its objectives include 1) improving examination procedures for incorporation into the American Society for Mechanical Engineers (ASME), Boiler and Pressure Vessel Codes, Section III, V, XI; and 2) gaining a better insight into the influence of improved reliability of NDE in detecting, locating and sizing flaws on component failure probabilities.



CONTENTS BY VOLUMES

VOLUME I

ABSTRACT . . . . .	iii
ACRONYMS . . . . .	vii
ACKNOWLEDGMENTS . . . . .	xi
CHAPTERS	
1.0 JUSTIFICATION, PURPOSE AND SCOPE . . . . .	1.0
2.0 NATIONAL AND INTERNATIONAL REGULATORY AND CODE REQUIREMENTS RELEVANT TO INSPECTION AND ACCEPTANCE/REJECTION OF FLAWS IN NUCLEAR PRESSURE BOUNDARY COMPONENTS . . . . .	2.0
3.0 DETECTION, LOCATION AND SIZING (The Pressure Vessel Research Committee Program) . . . . .	3.0
4.0 FLAW DETECTION . . . . .	4.0
5.0 FLAW SIZING AND LOCATION . . . . .	5.0
6.0 FLAW SIZING AND LOCATION--ADVANCED TECHNIQUES . . . . .	6.0

VOLUME II

ABSTRACT . . . . .	iii
ACRONYMS . . . . .	vii
ACKNOWLEDGMENTS . . . . .	xi
CHAPTERS	
7.0 ULTRASONIC EQUIPMENT--CHARACTERISTICS AND LIMITATIONS . . . . .	7.0
8.0 FLAW DETECTION AND SIZING--THEORETICAL BACKGROUND . . . . .	8.0
9.0 NOE--FOR MEASUREMENT OF PHYSICAL AND MECHANICAL PROPERTIES . . . . .	9.0
9A.0 MATHEMATICAL DERIVATIONS OF EQUATIONS FOR SECOND- AND THIRD-ORDER ELASTIC CONSTANTS . . . . .	9A.0

10.0	FAILURE STATISTICS AND FLAW SIGNIFICANCE . . . . .	10.0
11.0	RELEVANT STATISTICAL AND PROBABILISTIC MODELS . . . . .	11.0

VOLUME III

ABSTRACT . . . . .	fii
ACRONYMS . . . . .	vii
ACKNOWLEDGMENTS . . . . .	xi

CHAPTERS

12.0	PROBABILISTIC FRACTURE MECHANICS . . . . .	12.0
13.0	FACTORS INFLUENCING RELIABILITY OF FLAW DETECTION . . . . .	13.0
13A.0	PROBABILITY MODELS FOR RELIABILITY OF FLAW DETECTION . . . . .	13A.0
13B.0	ELASTIC WAVE PROPAGATION AND VELOCITY, SLOWNESS AND WAVE SURFACES . . . . .	13B.0
14.0	THE ASME COOES: TESTING TECHNIQUES, ANALYTIC PROCEDURES AND SUGGESTED MODIFICATIONS . . . . .	14.0
15.0	CONCLUSIONS AND RECOMMENDATIONS . . . . .	15.0



## ACRONYMS

ACRS	Advisory Committee on Reactor Safeguards
AD	Arbeitsgemeinschaft Druckbehälter
AD-RHP	Arbeitsgemeinschaft Druckbehälter-Reactor HP
AE	Acoustic Emission
AEC	Atomic Energy Commission
AEC/NRC	Atomic Energy Commission/Nuclear Regulatory Commission
AFML	Air Force Materials Lab
AH	Acoustic Holography
ALN	Adaptive Learning Network
ANL	Argonne National Laboratory
ARPA	Advanced Research Projects Agency
ASME	American Society for Mechanical Engineers
AVG	Abstand-Verstärker-Grosse
AVS	Distance Amplification Size
BNA	Barkhausen Noise Analysis
BWR	Boiling Water Reactor
CAP	Correct Acceptance Probability
CEGB	Central Electricity Generating Board
CRP	Correct Rejection Probability
DAC	Distance Amplitude Correction
DDP	Defect Detection Probability
DGS	Distance-Gain-Size
DG(z)	German Association for NDE Methods
DWR	Druckwasser Reaktor (German PWR)

EBS	Electronic Block Simulator
EDM	Electric Discharge Machining
EMA	Electromagnetic-Acoustic
EMAT	Electromagnetic Acoustic Transducers
EL	Error in Location
EPFM	Elastic-Plastic Fracture Mechanics
EPRI	Electric Power Research Institute
ES	Error in Sizing
ET	Engineering Testing
FRG	Federal Republic of Germany
GYFM	General Yield Fracture Mechanics
HAZ	Heat Affected Zone
HP	German Pressure Code Series
HSST	Heavy-Section Steel Technology
IAEA	International Atomic Energy Agency
ICP	Industry Cooperative Program
IGSCC	Intergranular Stress Corrosion Cracking
ISI	Inservice Inspection
ITV	Intermediate Test Vessel
IWG-RRPC	International Working Group on Reliability of Reactor Pressure Components
JAEC	Japan Atomic Energy Commission
LEFM	Linear Elastic Fracture Mechanics
LMFBR	Liquid Metal Fast Breeder Reactor
MPT	Magnetic Particle Testing
MMA	Manual Metal Arc (welding)

MIG	Metal Inert Gas (welding)
MITI	Ministry of Technology and Industry (Japan)
NASA	National Aeronautics and Space Administration
NBS	National Bureau of Standards
NDE	Nondestructive Examination
NRC-Res	Nuclear Regulatory Commission--Office of Research
PISC	Plate Inspection Steering Committee
PSI	Preservice Inspection
PT	Penetrant Testing
PVRC	Pressure Vessel Research Committee
PWHT	Post Weld Heat Treatments
PWR	Pressurized Water Reactor
PZT	Lead Zirconate Titanate (transducer)
QA	Quality of Acceptance
RF	Radio Frequency
RPV	Reactor Pressure Vessel
RSK	Reaktor-Sicherheit (German Reactor Safety Commission)
RT	Radiographic Testing
RTD-BAM	Röntgen-Technische-Dienst (RT)-Bundesanstalt für Materialprüfung (German Federal Institute for Material Testing)
SAFT-UT	Synthetic Aperture Focusing Technique for Ultrasonic Testing
SAR	Safety Analysis Report
SCC	Stress Corrosion Cracking
SET	Stress Exposure Technique
SMIRT	Structural Materials in Reactor Technology
SWP	Special Work Permit

USNRC     United States Nuclear Regulatory Commission  
UT         Ultrasonic Testing  
UT/ADP    Ultrasonic Automatic Data Processing System  
WRC        Welding Research Council

## ACKNOWLEDGMENTS

The support and assistance of the following members of the staff of Pacific Northwest Laboratory in preparing this document is greatly appreciated: Kay Drake, who assisted in all phases of its preparation; Pat Randklev, who coordinated and assisted in administering its production; Mary Sheeley, Kelly Feuerbacher, and Kay Chase, who prepared the camera-ready copy; and John Nageley, who edited it. The work of the PNL Graphics group, under Gene Wattenburger, is apparent on many pages of this report. Dr. Joseph Muscara was the USNRC Project Manager.

I wish to thank the following organizations and companies for granting permission to quote and cite, and include illustrative material, from the books, journals, reports and conference, seminar and symposium proceedings that they have published:

- Academic Press, Inc., New York, New York.
- Academic Press, Inc. Ltd., London, England.
- American Institute of Physics, New York, New York: Journal of Acoustical Society of America, Journal of Applied Physics, and Applied Physics Letters.
- American Nuclear Society, La Grange Park, Illinois: Nuclear Technology.
- American Physical Society, New York, New York: A Physical Review.
- American Society for Metals, Metals Park, Ohio.
- American Society for Nondestructive Testing, Inc., Columbus, Ohio: Materials Evaluation, Paper Summaries, and Conference Proceedings.
- American Society for Quality Control, Technometric Management Committee, Milwaukee, Wisconsin: Journal of Quality Technology and Technometrics.
- American Society for Testing and Materials, Philadelphia, Pennsylvania.
- American Society of Mechanical Engineers, New York, New York: Journal of Applied Mechanics, Journal of Engineering for Industry, and The Boiler Pressure Vessel Codes.

- American Statistical Association, Washington, D.C: Technometrics.
- American Welding Society, Miami, Florida: Welding Journal.
- Applied Science Publishers, Ltd., Essex, England: International Journal of Pressure Vessels and Piping, and Reliability Engineering.
- Architectural Institute of Japan, Tokyo, Japan.
- Argonne National Laboratory, Chicago, Illinois.
- Babcock and Wilcox, New Orleans, Louisiana.
- Battelle, Pacific Northwest Laboratories, Richland, Washington.
- Battelle's Columbus Laboratories, Columbus, Ohio.
- British Engine Insurance, Ltd., Manchester, England: Technical Report.
- British Institute of Nondestructive Testing, Northampton, England: British Journal of NDT.
- Bundesanstalt für Materialprüfung, Berlin, Germany.
- Butterworth Scientific, Ltd., (formerly IPC Science and Technology Press, Ltd.) London, England: Ultrasonics Journal, Ultrasonics International, Non-Destructive Testing, and NDT International.
- Central Electricity Generating Board, London, England.
- Combustion Engineering, Inc., Windsor, Connecticut.
- Comite Francaise d'Etude des Essais Non Destructifs, Laboratoire Nacional D'Essai, Paris, France.
- Commissariat a L'Énergie Atomique, Saclay, France.
- Commission of the European Communities, Brussels, Belgium.
- Committee on the Safety of Nuclear Installations of OECD Nuclear Energy Agency, Paris, France.
- Council of the Institution of Mechanical Engineers, London, England.
- Danish Welding Institute, Copenhagen, Denmark.
- Det Norske Veritas, Oslo, Norway.
- Deutsche Gesellschaft für Zerstörungsfreie Prüfung e.V., Berlin, Germany.

- Deutscher Verband für Materialprüfung, Duesseeldorf, Germany: Materialprüfung.
- Electric Power Research Institute, Palo Alto, California.
- Elsevier North-Holland, Inc., New York, New York.
- Fachinformationszentrum Energie, Physik, Mathematik, Lindau, Germany: 4th International Conference on NDE.
- General Electric Corporation, Fairfield, Connecticut.
- Hanford Engineering Development Laboratory, Richland, Washington.
- Holosonics, Inc., Richland, Washington.
- Institute of Electrical and Electronic Engineers, Inc., New York, New York: IEEE Transactions on Sonics and Ultrasonics, IEEE Proceedings.
- Institution of Civil Engineers, London, England: Journal of British Nuclear Energy Society.
- Institution of Nuclear Engineers, London, England.
- International Atomic Energy Agency, Vienna, Austria.
- International Institute of Welding, London, England: Welding in the World.
- Ishikawajima-Harima Heavy Industries Co., Ltd., Tokyo, Japan: IHI Engineering Review.
- Kobe Technical Institute, Kobe, Japan.
- Los Alamos National Laboratory, Los Alamos, New Mexico.
- Lund Institute of Technology, Lund, Sweden.
- M.A.N. Maschinenfabrik, Nurnberg, Germany.
- McGraw-Hill Book Company, New York, New York.
- National Aeronautics and Space Administration, Washington, D.C.
- National Bureau of Standards, Gaithersberg, Maryland.
- National Research Institute for Metals, Tokyo, Japan: Transactions of the National Research Institute for Metals.

- New England Institute, Ridgefield, Connecticut.
- North-Holland Publishing Company, Amsterdam, Holland: Nuclear Engineering and Design.
- Nuclear Engineering International, Surrey, England: Nuclear Engineering International.
- Oak Ridge National Laboratory, Oak Ridge, Tennessee: Nuclear Safety.
- Plenum Publishing Corporation, New York, New York: Soviet Journal of Nondestructive Testing.
- Pressure Vessel Research Committee, Welding Research Council, New York, New York: Welding Research Abroad.
- Rockwell International Corporation, Pittsburgh, Pennsylvania.
- Röntgen Technische Dienst. bv, Rotterdam, The Netherlands.
- The Royal Society, London, England: Proceedings.
- Scientific Applications, Inc., Palo Alto, California.
- Society for Experimental Stress Analysis, Brookfield Center, Connecticut: Experimental Mechanics.
- Southwest Research Institute, San Antonio, Texas.
- Studsvik Energiteknik AB (formerly Atomenergi AB), Nyköping, Sweden.
- Technischen Überwachungs Verein e.V., Rheinland Westphalia, Essen, Germany.
- United Kingdom Atomic Energy Authority, Harwell, England.
- U.S. Air Force, Wright Patterson Air Force Base, Ohio: USAF Technical Report.
- University of Tokyo Press, Tokyo, Japan.
- Welding Institute, Abington Hall, Cambridge, England: Welding Institute, Automatic Welding.
- Westinghouse Electric Corporation, Pittsburgh, Pennsylvania.
- John Wiley and Sons, New York, New York.



CHAPTER 1

JUSTIFICATION, PURPOSE AND SCOPE



## CONTENTS

1.1	INTRODUCTION . . . . .	1.1.1
1.2	JUSTIFICATION OF WHITE PAPER . . . . .	1.2.1
1.2.1	Background . . . . .	1.2.1
1.2.2	IAEA Meeting Conclusions . . . . .	1.2.1
1.3	PURPOSE OF WHITE PAPER . . . . .	1.3.1
1.4	SCOPE OF WHITE PAPER . . . . .	1.4.1
1.5	FORMAT OF WHITE PAPER . . . . .	1.5.1
1.6	REFERENCE . . . . .	1.6.1

FIGURES

1.3.1	Event Tree--Status NDE Techniques Relevant to Event Tree Factors . . . . .	1.3.2
1.3.2	Topics Relevant to Event Tree . . . . .	1.3.5

## CHAPTER 1

### JUSTIFICATION, PURPOSE AND SCOPE

#### 1.1

#### INTRODUCTION

The following white paper, "Reliability of Nondestructive Examination," consists of three volumes that include eighteen chapters related to the reliability of various nondestructive examination (NDE) techniques, the significance of lack of reliability in probabilistic terms, and factors and procedures that could enhance reliability. The reliability of detecting, locating and sizing flaws will be an input into a probabilistic fracture mechanics model whose purpose is to highlight the significance of failure to detect flaws or to inaccurately locate and size them in the context of component failure probability.

The emphasis of the white paper is on nuclear systems; however, relevant NDE data on a spectrum of materials and applications are examined to determine the applicability of the information to nuclear reactor systems.

The purpose of this exercise is not to generate a series of white papers on NDE practices. Rather, it is to pinpoint their strengths and weaknesses as input into experimental programs aimed at increasing the reliability of flaw detection. The hoped-for output of the combined detection reliability-probabilistic fracture mechanics program will be improved examination procedures for incorporation into the American Society for Mechanical Engineers (ASME) Boiler and Pressure Vessel Codes, Sections III, V, XI; and a better insight into component failure probabilities as they are influenced by improved reliability of detecting, locating and sizing flaws.



1.2.1 Background

Nondestructive examination, particularly ultrasonic, has been quite controversial. Its proponents claim high levels of flaw detection sensitivity and flaw sizing accuracy while its opponents denigrate ultrasonics as a viable examination procedure. As is usually the case with exaggerated claims, the truth lies somewhere in between. Just where in between is of intense interest to the utility operating a reactor and to the regulatory agencies concerned with the safe operation of the reactor. For example, the incorrect location and sizing of a detected flaw could lead to extensive downtime if the decision is made to repair. The preceding case is true for a relatively innocuous flaw incorrectly located nearer the surface than is physically true, or which is oversized by NDE. The alternate case of a potentially serious flaw in the context of being near the critical size for failure, which is assessed as of minor safety significance due to incorrectly locating or underestimating its size, has potentially serious safety implications.

1.2.2 IAEA Meeting Conclusions

The conclusions of an International Atomic Energy Agency (IAEA) sponsored technical meeting in 1977<sup>(1.2.1)</sup> highlight areas of concern and the differences of opinion that exist in the NDE field. The relevant conclusions follow:

- A need exists to understand better the similarities and differences between the various national in-service inspection (ISI) codes; it is suggested that existing codes be assembled in one location and, using ASME XI as a base, comparisons be made to detect and understand significant differences in philosophy and approach. To this end, all participating countries are invited to send to the Technical Secretariat International Working Group-Resonance for reactor pressure circuit (IWG-RRPC) copies of the most recent issues of their relevant requirements, regulations, specifications and guidelines relating to pre-service and in-service inspection of reactor primary circuit and

other coolant circuit components as soon as possible, and in the future to keep that Technical Secretariat informed of any changes, additions or deletions.

Such information is requested for all types of reactor systems. The Technical Secretariat is invited to maintain a library of such information, and also to take account of it in revision of the relevant IAEA International Safety guidelines documents.

- The question of the reliability of ultrasonic techniques in detecting rejectable defects was mentioned several times, and the important programmes of "round-robin" ultrasonic testing (UT) work being done currently in U.S. and Europe were mentioned. It is hoped that the results be made available to the IWG-RRPC at an early stage for them to discuss the implications and need for further work.
- The present information indicates that conventional UT techniques, especially as practiced with manual operation, have limitations in the sizing and detection of flaws.
- Ultrasonic examinations of welds in austenitic stainless-steel components, using conventional ultrasonic equipment and techniques is generally less effective, as compared to those used for welds in carbon-steel components, owing to the increased acoustic attenuation exhibited by these materials. Furthermore, large amplitude ultrasonic indications may occur in weld regions that are free of rejectable defects. The acoustic energy attenuation problems combined with the false indications encountered during the examination of austenitic stainless-steel welds, have emphasized the need for development of more effective ultrasonic methods to supplement the examination processes presently used during the fabrication of stainless-steel components. Improvements should be sought with emphasis on those aspects which will improve the probability of detecting any important flaws and taking appropriate action.
- Less information existed on the reliability of sizing and location of any defects reported. It was noted that work on B-scan, focused



probe, acoustic holography, phased-array and signal analysis devices all showed considerable evidence of some improvement, and it is desirable that a coordinated international programme to assess the accuracy, reliability and reproducibility of the various possible sizing methods be established and the IWG-RRPC be invited to consider this, possibly in collaboration with other international and national organizations. In particular, additional NDE including standard and advanced UT, acoustic holography, radiographic testing (RT) and penetrant testing (PT) would be a desirable extension of the Pressure Vessel Research Committee (PVRC) work on 201, 202 and 251J plates and of the PVRC-European Plate Inspection Steering Committee (PISC) programme to better understand the limitations of geometry, weldment design and material differences on the detectability and precise sizing of flaws. A compilation of past and ongoing work in the various countries would be a valuable first step. Possibly the Electric Power Research Institute (EPRI) could provide the service.

- A definite problem mentioned by several participants is in the inspection of dissimilar metal welds (e.g., bi-metallic or tri-metallic joints such as stainless to ferritic steels). These examinations can be complicated due to weld geometry, secondary reflecting artifacts, mode conversion, attenuation, soundwave diffraction and changes in propagation velocity. Improved methods for examination and for signal processing (e.g., of the original R.F. signal) such as those involving "Adaptive-Learning" techniques show promising results and should be vigorously encouraged and further information exchanged whenever possible.
- The ability of acoustic emission (AE) to detect flaws consistently, either in hydro-test or in on-line usage, is doubtful; even so it can be of sufficient value to justify its use provided that the limitations are recognized. The continuing growth of differing experience indicates the need for a further authoritative review to be made in 1-1/2 to 2-1/2 years time, and that the information then be critically appraised to provide a statement on the value of AE in various

applications to be included in Safety Guidelines on ISI. It is recommended that IAEA take appropriate action on these points.

It was noted that AE techniques can be of great value for leak detection and location, for "loose parts" and component movement detection and for detection of certain types of crack extension including some stress corrosion cracking. Emphasis on the development for these purposes of AE equipment and its application was recommended.

- The meeting noted that there was a real problem arising from ensuring that NDE personnel can maintain their effective ability for sustained periods under ISI conditions and also that there was a need to minimize radiation exposure of highly qualified personnel. Any improvements in these aspects that could be obtained by mechanization of equipment, by automation of the collection, recording and interpretation of data would be a major gain and should be actively encouraged.

Furthermore, all participating countries are invited to provide the Technical Secretariat with the data available concerning personnel radiation exposure, both total per plant and also subdivided according to details of specific examinations and locations, incurred as a result of in-service inspection. The Technical Secretariat is encouraged to file and periodically publish such data.

- Problems still exist with some of the currently used systems of the examination of steam generator tubes by eddy current testing. Masking of flaw signals due to tube supports, corrosion product buildup, denting, etc., as well as the lower reliability of detection of inner surface flaws indicate the need for improved techniques. Hopefully, the expanded effort now planned as well as the results already gained at least in one country, and reported during that meeting will yield the desired answers.
- Existing linear elastic fracture mechanics techniques such as embodied in Appendix A of ASME XI provide a conservative method of determining the acceptability of a detected flaw. Considering the major penalty in downtime facing a utility when such an analysis indicates

that repairs may be required, there is an incentive for developing an elastic-plastic fracture mechanics procedure acceptable to code and regulatory authorities. A necessary adjunct to such an approach is a better understanding of crack growth under complex loading with emphasis on bending.

- There should be more interaction between the system designer and the NDE expert. Optimization of design features and layout can in many cases greatly simplify the examination or its interpretation and can often minimize radiation exposure of examination personnel without affecting system reliability. Exchange of information on these aspects should be encouraged in future RRPC activities.
- This meeting had been particularly valuable in making clear that there was a large amount of research and development work currently being done in all these areas in several countries. This suggests that another specialist meeting on this topic be held in 2 to 4 years time, depending on availability of results and coordination with other international meetings. The IWG-RRPC is recommended to include such a proposal in drafts of future programs.



The purpose of the white paper is to assess the significance of flaws at various locations in pressure boundary components and to optimize the NDE procedures accordingly. If the presence of a flaw in a given location would result in a very high stress intensity factor due to location and loads, rigorous NDE procedures with a high detection reliability should be applied. On the other hand, much less rigorous criteria could be applied to innocuous defects such as slag, laminations or deeply embedded (small) flaws. Since the concern is with flaws in operating reactors, exposure of NDE operators to radiation is a critical factor and every effort should be made to reduce the time spent on geometric indications or in regions of minor safety significance so that the time can be spent in the areas of major safety significance.

Emphasis is on an integrated program. If component design and/or fabrication procedures adversely affect NDE detection of flaws, changes should be made. Where possible, materials should be selected that are amenable to NDE. Fracture mechanics and component failure statistics should be used to pinpoint critical locations where enhanced NDE may be required. Potential failure mechanisms should be examined to optimize the NDE for the types of cracks anticipated.

The preceding words are summarized in the event tree in Figure 1.3.1. As noted on the figure, a series of subjective judgments has been made concerning the current state of the art. While the event tree is believed to cover many of the critical factors, no claim is made that all factors were considered. Also, see Figure 1.3.2.

A -- Relevant to Flaws

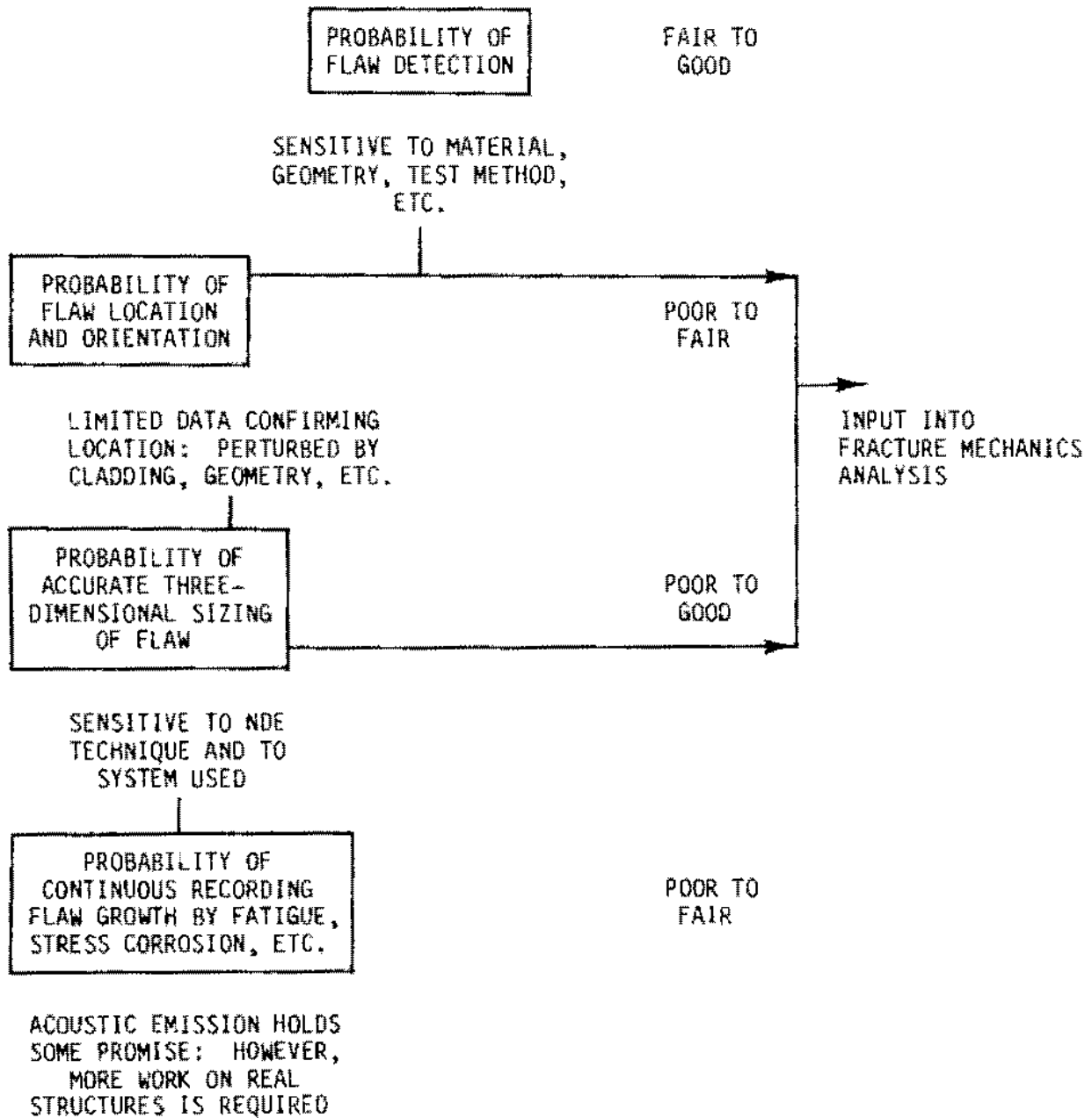


FIGURE 1.3.1. Event Tree--Status NDE Techniques Relevant to Event Tree Factors

B -- Relevant to Fracture Mechanics (LEFM, EPFM, GYFM)

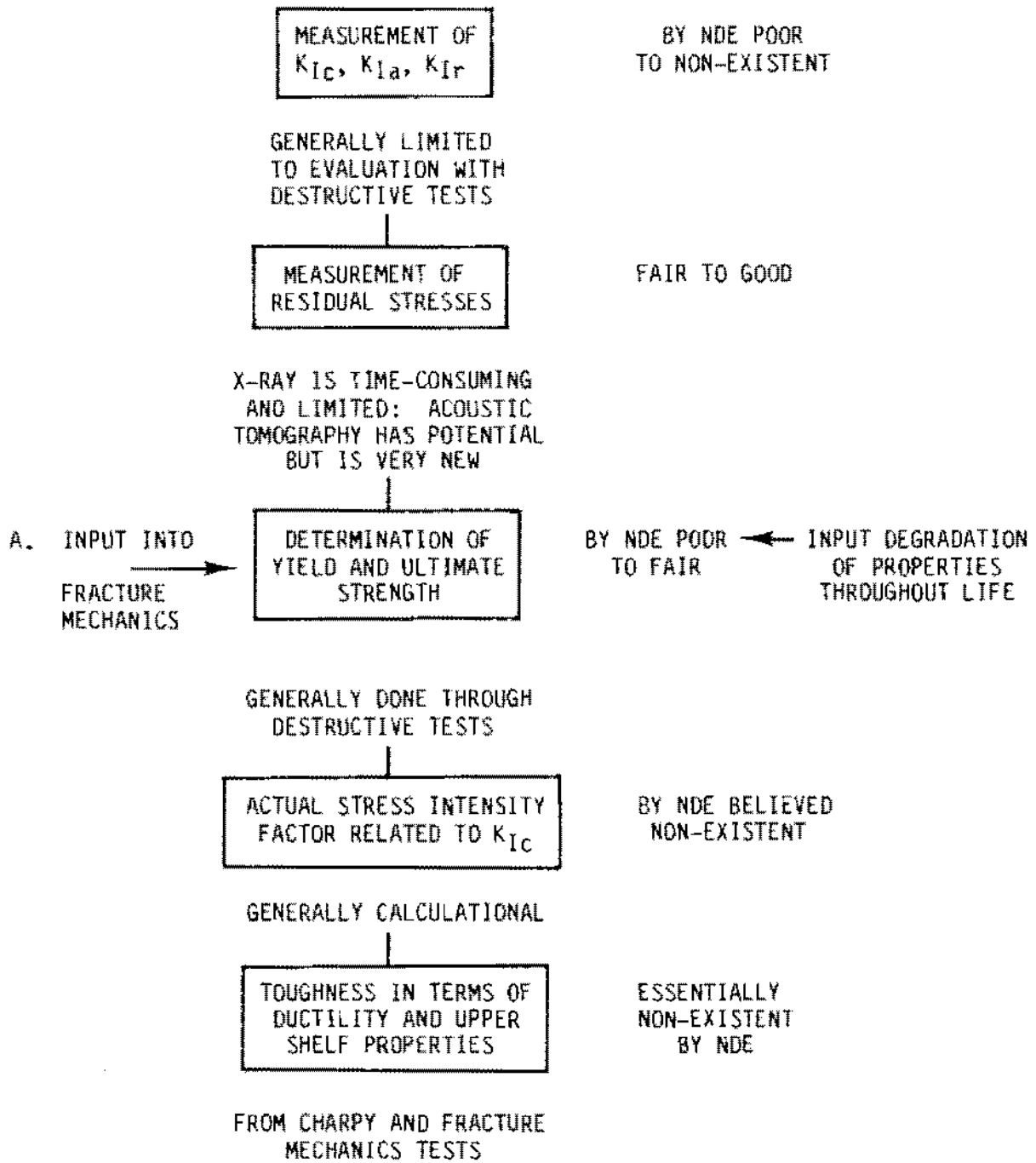


FIGURE 1.3.1. (contd)

C -- Relevant to Property Degradation Throughout Life, Exclusive of Flaw Growth (fatigue, creep, creep-rupture, etc.)

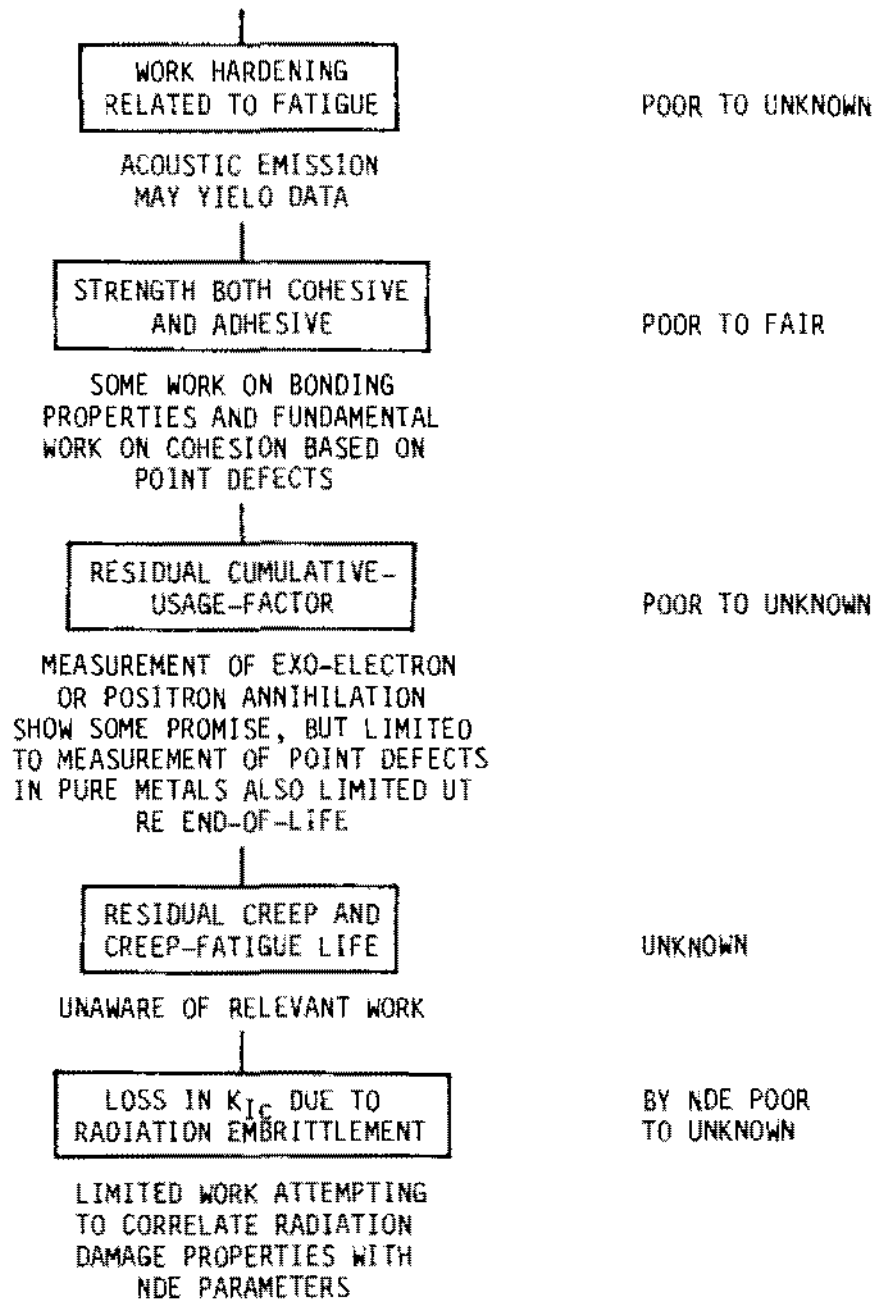


FIGURE 1.3.1. (contd)



SOURCES - NSA, DOD, OPEN LITERATURE

Library - Assuming NRC funding

NDE - Flaw detection

NDE - Pressure vessels, piping, etc.

NDE - UT, RT, PT, ET, MT

NDE - Flaw location, flaw orientation

NDE - Flaw sizing

NDE - Mechanical properties

NDE - Cohesive strength

NDE - Bond (adhesive strength)

NDE - Residual stress

NDE - Fracture mechanics

NDE - Fatigue

NDE - Exo-electron

NDE - Positron annihilation

NDE - Remaining fatigue life

NDE - Measurement creep, creep-fatigue,  
creep-rupture properties

NDE - End-of-life

NDE - Fatigue cracks

Probability-Flaw Detection

Probabilistic Fracture Mechanics

Elastic-Plastic Fracture Mechanics

Probability Density Functions-Flaws

FIGURE 1.3.2. Topics Relevant to Event Tree (Figure 1.3.1)



Consideration is given to all pressure boundary components where failures have safety or substantial economic significance. Emphasis is given to piping and to the reactor pressure vessel since much of the data relevant to these components can be applied to pumps, valves, steam generators, etc. Steam generator tubing is not covered extensively since there are extensive NDE efforts relevant to tubing and the information has been well reported to the relevant organizations.

The following paragraphs are an attempt to orient the reader on the coverage and scope of each chapter.

1. Justification, Purpose and Scope

Previously described in this chapter.

2. National and International Regulatory and Code Requirements Relevant to Inspection and Acceptance/Rejection of Flaws in Nuclear Pressure Boundary Components

The ASME III, V and XI Codes are compared to the Federal Republic of Germany (FRG) German Pressure Code Series (HP) 5/3 Construction/Inspection Code to assess the significance of differences in procedures and philosophies. The positive and negative impact of government regulations is examined.

3. Detection, Location and Sizing (The Pressure Vessel Research Committee Program)

The PVRC Industrial Cooperative Program complemented the Atomic Energy Commission/Nuclear Regulatory Commission (AEC/NRC) Heavy Section Steel Technology Program and concentrated on NDE flaw detection and sizing reliability. The results represent a major body of data pertinent to thick-steel sections such as plates, forgings and nozzles in plates or forgings. The use of a round-robin testing program highlights team variability as well as indicating the sensitivity of detection reliability to the NDE procedure followed.

4. Flaw Detection

The emphasis is on the factors influencing flaw detection such as material and surface characteristics, including coupling efficiency, geometry, etc. Results with commercial state-of-the-art equipment are emphasized.

5. Flaw Sizing and Location

The literature is reviewed relevant to errors in sizing of natural and artificial flaws, and the assessment of factors such as external loads, flaw roughness, beam spread, size of focal spot, etc., as they influence sizing.

6. Flaw Sizing and Location--Advanced Techniques

The emphasis is on UT, with a review of literature pertaining to focused probes, acoustic holography, and adaptive learning networks.

7. Ultrasonic Equipment--Characteristics and Limitations

Both theoretical upper-bound limits and variability typical of the electronic circuitry and transducers are considered. This chapter covers existing limitations and the possibilities for improvement.

8. Flaw Detection and Sizing--Theoretical Background

Several excellent papers are reviewed that have been written pertaining to wave behavior in solids. Some of the work should lead to new approaches in flaw location and sizing.

9. NDE--for Measurement of Physical and Mechanical Properties

The intent is to concentrate on those physical and mechanical properties directly pertinent to failure potential. Obvious choices include residual stress levels and distribution, approach to end-of-life by fatigue, and properties such as internal friction that may correlate with toughness and stress intensity. Ideally, one would like to measure parameters directly relevant to fracture mechanics.

9A. Mathematical Derivations of Equations for Second- and Third-Order Elastic Constants

Applying various NDE techniques to determine the physical and mechanical properties of solids is introduced through measuring engineering properties, developing general elasticity theory, simplifying the case of major interest, cubic metals such as steel, handling the preceding in terms of dynamic effects, and expanding to the nonlinear case. While the preceding uses solid mechanics rather than wave mechanics, both approaches converge to yield precisely the same equations.

10. Failure Statistics and Flaw Significance

An assessment is made of types and probability of failure by component size, specific location, etc., to benchmark the probabilistic fracture mechanics task.

11. Relevant Statistical and Probabilistic Models

An assessment is made of the preferred models for handling the available data. A review of elementary probability concepts and terminology is included. This chapter serves as an introduction to Chapter 12, Probabilistic Fracture Mechanics, and Chapter 13, Factors Influencing Reliability of Flaw Detection.

12. Probabilistic Fracture Mechanics

This chapter reviews work in probabilistic fracture mechanics. Inputs are used to characterize flaws as to their significance as functions of size, orientation and location. The aim is to define significance rather than to develop failure probability values in an absolute sense; deterministic fracture mechanics will be used as a base line.

13. Factors Influencing Reliability of Flaw Detection

The appropriate probability model will be selected as a vehicle for reviewing available data regarding flaw detection and for assisting

in developing the experimental program for amassing a statistically significant body of data on detection reliability and the factors affecting reliability.

13A. Probability Models for Reliability of Flaw Detection

General and specific probability models are examined, then pursued through correlation functions and field or production data. Examined also are statistical probability models for flaw detection. A section on nomenclature is included because of the spectrum of terminology.

13B. Elastic Wave Propagation and Velocity, Slowness and Wave Surfaces

Wave behavior in solid media is examined. The interaction of various waves in isotropic and anisotropic media is examined relative to such factors as wave direction; type of wave (shear, longitudinal); wave velocity; stresses and strains developed in various media because of wave propagation; the development of velocity, slowness and wave surfaces; and the effect of media on wave characteristics such as beam convergence or divergence.

14. The ASME Codes: Testing Techniques, Analytic Procedures and Suggested Modifications

Sections III, V and XI of the ASME Codes are examined to see whether there are changes in design, materials, or fabrication that could improve detection reliability in NDE procedures, and that could pinpoint significant flaws with greater reliability. Operational histories of existing nuclear plants are reviewed to optimize inservice inspection with personnel burnup, examination of significant areas, and assessment of the role of advanced NDE techniques.

15. Conclusions and Recommendations

Specific items were culled from all chapters to serve as guidance in future experimental and analytic programs.

The following criteria with regard to distribution and format are adopted for the preparation of this document. Inputs from sponsors and contributors have been incorporated into the criteria.

- Since the ultimate goal was to provide input to the experimental programs, the report was in draft form for two to three years. Thereafter, all approvals required for a formal report were obtained. We met our goal and converted to a final report.
- Updating has been on the basis of information becoming available. To minimize mailing costs, a nominal quantity was allowed to collect before sending it out for review, but for no longer than six months.
- Where possible, requests from members of the technical community outside the participants were honored when copies were available and with sponsor approval; when an obvious mutual advantage existed, an attempt was made to add such persons to the distribution list.





1.6

REFERENCE

- 1.2.1 Use of Non-Destructive Testing Techniques for Inservice Inspection of Reactor Pressure Components. IWG-RRPC-78/3, International Atomic Energy Agency, International Working Group on Reliability of Reactor Pressure Components, Kobe, Japan, April 25-27, 1977.



CHAPTER 2

NATIONAL AND INTERNATIONAL REGULATORY AND CODE REQUIREMENTS  
RELEVANT TO INSPECTION AND ACCEPTANCE/REJECTION OF FLAWS IN  
NUCLEAR PRESSURE BOUNDARY COMPONENTS



## CONTENTS

2.1	INTRODUCTION . . . . .	2.1.1
2.2	NATIONAL CODES--SIMILARITIES AND DIFFERENCES . . . . .	2.2.1
2.2.1	Equipment . . . . .	2.2.1
2.2.1.1	Ultrasonic Equipment . . . . .	2.2.1
2.2.1.2	Equipment Frequency . . . . .	2.2.1
2.2.1.3	Beam Angles . . . . .	2.2.1
2.2.1.4	Transducers . . . . .	2.2.3
2.2.2	Calibration . . . . .	2.2.3
2.2.3	Test Conditions . . . . .	2.2.3
2.2.3.1	Surface Finish . . . . .	2.2.3
2.2.3.2	Rate of Travel . . . . .	2.2.5
2.2.4	Examination . . . . .	2.2.5
2.2.4.1	UT Weld Examinations . . . . .	2.2.5
2.2.4.2	Cladding Examination . . . . .	2.2.5
2.2.5	Flaw Sizing and Location . . . . .	2.2.6
2.2.5.1	Recording Levels . . . . .	2.2.6
2.2.5.2	Acceptance/Rejection Limits . . . . .	2.2.6
2.2.5.3	Multiple Flaws or Indications . . . . .	2.2.9
2.3	PRESUMED LIMITATIONS: ASME XI VERSUS FRG CODES . . . . .	2.3.1
2.3.1	Difference in Philosophy: ASME Versus FRG . . . . .	2.3.1
2.3.2	Acceptance/Rejection Criteria . . . . .	2.3.10
2.3.3	Reporting Levels . . . . .	2.3.11
2.4	GOVERNMENTAL REGULATIONS . . . . .	2.4.1
2.4.1	Examples of NRC Concerns About ASME XI . . . . .	2.4.1

2.4.2	Positive Regulatory Actions	.	.	.	.	.	.	.	.	2.4.6
2.5	FOREIGN REGULATIONS	.	.	.	.	.	.	.	.	2.5.1
2.6	SUMMARY	.	.	.	.	.	.	.	.	2.6.1
2.7	REFERENCES	.	.	.	.	.	.	.	.	2.7.1

## FIGURES

2.2.1	General Distance Amplification Size Display Picture . . . . .	2.2.4
2.3.1	Comparison of Calibration Sensitivities According to ASME and HP 5/3 for Wall Thicknesses Between 4 and 6 in. . . . .	2.3.4
2.3.2	Flaw Detectability with 70° Angle Probe . . . . .	2.3.5
2.3.3	Weld Evaluation According to ASME and HP 5/3 . . . . .	2.3.7
2.3.4	Distribution of Introduced Defects in Pressure Vessel Circumferential Weld Seam-Wall Interface and Ultrasonic Probe Locations . . . . .	2.3.8
2.3.5	Measured and Theoretical Reduction in Ultrasonic Piping Inspection Sensitivity of the 1977 Edition of the ASME Code, Section XI as compared to the 1974 Edition . . . . .	2.3.14
2.5.1	Japanese Codes and Regulations for ISI . . . . .	2.5.3
2.5.2	Scope of Inservice Inspection (a) in Germany and (b) to ASME XI . . . . .	2.5.7

## TABLES

2.2.1	Examples of Use of Codes and Regulations by Various Countries . . . . .	2.2.2
2.2.2	Response Threshold as a Function of Nominal Wall Thickness . . . . .	2.2.7
2.2.3	Evaluation of Ultrasonic Findings . . . . .	2.2.8
2.2.4a	Allowable Planar Indications in Reactor Pressure Vessel . . . . .	2.2.10
2.2.4b	Allowable Laminar Indications . . . . .	2.2.10
2.2.5	Allowable Planar Indications--Piping . . . . .	2.2.11
2.3.1	Acceptable Defect Sizes and Numbers per Meter of Weld . . . . .	2.3.2
2.3.2	Comparison of Weld Examination According to HP 5/3 and ASME Code Section V for Wall Thickness Over 4 Through 6 in. . . . .	2.3.3
2.3.3	70° Probe ASME V 20% DAC FRG HP 5/3 . . . . .	2.3.6
2.3.4	Detection and Rejection on Bases of ASME V and HP 5/3 for Clad Pressure Vessel Wall . . . . .	2.3.9
2.3.5	Permissible Indications for Ultrasonic Examination . . . . .	2.3.12
2.3.6	Summary of Flaw Response Using 1974 and 1977 (1978 Summer Addendum) ASME XI Evaluation Criteria . . . . .	2.3.13
2.4.1	Augmented Inspections and Significant Requirements Added Since Summer 1975 Addenda . . . . .	2.4.7
2.5.1	Comparison of Selected ISI Requirements . . . . .	2.5.2



## CHAPTER 2

### NATIONAL AND INTERNATIONAL REGULATORY AND CODE REQUIREMENTS RELEVANT TO INSPECTION AND ACCEPTANCE/REJECTION OF FLAWS IN NUCLEAR PRESSURE BOUNDARY COMPONENTS

#### 2.1

#### INTRODUCTION

The detection, sizing and acceptance/rejection of flaws are sensitive to the particular National Codes, Standards and Regulations. With regard to examination requirements typical of thick-walled components used in light water reactors, two codes are pre-eminent and differ sufficiently to permit excellent comparisons. These codes are 1) the FRG Arbeitsgemeinschaft Druckbehälter (AD)-Markblätter [the specific one cited is manufacturing/inspection HP series<sup>(2.1.1,2.1.2)</sup>]; and 2) the US ASME Boiler and Pressure Vessel Codes. Those of relevance are ASME-III Construction,<sup>(2.1.3)</sup> ASME V NDE<sup>(2.1.4)</sup> and ASME XI ISI.<sup>(2.1.5)</sup> Since both the FRG and USA codes are compulsory, the differences have greater impact than do non-mandatory standards or codes in draft status.

The thinner-section austenitic stainless steel systems typical of Liquid Metal Fast Breeder Reactors (LMFBR) represent special problems in NDE. Basically, the existing LMFBRs are still prototypes and the relevant construction and inspection codes are under development.

The significant dividing line with regard to inspection codes occurs immediately prior to operation. The construction codes are in effect through code stamping so construction criteria apply with regard to acceptable indication sizes.

The period after stamping and before operation is somewhat unclear. Current practice is to conduct the preservice or baseline inspection during this period. Defect acceptance/rejection criteria then may differ from those applicable during construction. The operational phase differs in inspection

requirements and differs substantially in defect acceptance/rejection criteria. These factors will be discussed in this chapter.

The Boiler and Pressure Vessel Committee of ASME has considered shifting the preservice inspection now in ASME XI to ASME III. The reason for such a shift is essentially economic. Once a system or component is stamped, the responsibility shifts from the fabricator to the owner in most instances. Costs for baseline or preservice inspections after code stamping have been as high as \$1.25M, with a substantial percentage of the cost being an insurance policy to cover repairs of defects found by UT but not found by RT. Shifting the preservice inspection to ASME III and requiring both RT and UT will decrease the current preservice inspection costs. I suspect there will be an incremental increase in the fabrication costs to compensate for the anticipated increase in number of flaws detected that require evaluation and repair. The Boiler and Pressure Vessel Committee actively pursued this matter; however, no definitive action was taken and the action essentially is dead.

Since industrial codes serve as the basis for Regulatory modifications, the codes will be discussed prior to discussing Regulatory requirements.

In essence, exclusive of Russia and its satellites, two major national codes are used for the periodic inspection of nuclear reactor pressure boundaries. They are ASME Section XI and the FRG HP series of the AD-Markblätter. Other countries use one or the other or both of these codes suitably modified by governmental regulations, or depend on regulations. Recently, Sweden approved a code similar to ASME XI. The FRG HP codes cover both manufacture and inspection.<sup>(2.1.2,2.1.3)</sup> A similar situation occurs in the United States by adding ASME Sections III and V to Section XI<sup>(2.1.3,2.1.4,2.1.5)</sup> for coverage through manufacture and operation.

Some idea of the use made of the various codes can be obtained from Table 2.2.1. The emphasis on ASME XI may be due in part because it has been around longer.

### 2.2.1 Equipment

2.2.1.1 Ultrasonic Equipment represents a significant difference in philosophy between the FRG Codes and ASME. Both require the use of single probe pulse height equipment; however, in the FRG, the tandem technique is required in addition to single probe for wall thicknesses greater than 100 mm.

2.2.1.2 Equipment Frequency range is similar under both codes; however, the FRG Codes are more specific. For example,

<u>Angle Beam</u>	
Thickness < 24 mm	2 to 5 MHz
Thickness > 25 mm	1 to 2.5 MHz
<u>Longitudinal Beam</u> 2 to 5 MHz	

2.2.1.3 Beam Angles are similar with longitudinal beam, 40 to 55° (usually 45°) and 55 to 70° shear (usually 60°) cited with the proviso that at least 15° must separate the two shear angles used. The German requirements are more explicit with regard to testing cladding, depending upon whether it is

TABLE 2.2.1. Examples of Use of Codes and Regulations by Various Countries  
(not complete) (periodic inspection of light water reactors)

Country	Code		Regulations			Comment	Reference
	ASME XI	FRG-AD-M	Other	Yes	No		
Austria	X	X	X	X		Austrian Code	2.2.1(b)
Belgium	X					Relies on ASME and AD-M--Partial	2.2.2
France	X			X		Ministry Order Feb. 26, 1974 No. 33-19	2.2.1(e)
FRG		X	X			RSK	2.1.1 2.1.2
India	X			X			2.2.3
Italy	X						2.2.1(f)
Japan	X			X		MITI Technical Standards, Electric Utility Act	2.2.1(a)
Netherlands	X						2.2.2
Spain	X			X			2.2.2
Sweden	X		X			RPV follows ASME XI; Piping--special requirements	2.2.4
Switzerland	X		X	X		Writing code based on ASME XI	2.2.1(c)
U.S.	X			X			2.1.3 2.1.4 2.1.5 2.2.1(d)
IAEA			X			Modelled on ASME XI	2.2.5

done from the clad-side or the side opposite the clad. They require a longitudinal wave, at a defined angle. The same procedure is in use in the U.S., but there is no mandatory requirement.

2.2.1.4 Transducer requirements are similar in requiring definition of shape and size. In Germany, the near fields are fixed as functions of wall thickness; for  $t < 25$  mm, the near field is  $< 50$  mm; for  $t > 25$  mm, the near field is  $> 50$  mm.

## 2.2.2 Calibration

Calibration requirements represent the major difference in philosophy. Since calibration establishes sensitivity and may set acceptance/rejection criteria, many of the claims and counterclaims registered as to the superiority of one UT technique can be traced to the calibration criteria. The marked effect has been discussed by Meyer<sup>(2.2.6,2.2.7)</sup> and his data will be described in detail in a later section of this chapter. The ASME procedure uses a series of side-drilled holes varying in size as a function of calibration block thickness. The block(s) should compare in thickness to the component being tested and the acoustic properties of block and component should be essentially the same. The side-drilled hole sizes are 3/16 and 1/4 in. to thicknesses of 6 in. and holes, increasing in diameter by 1/16 in., are added for every additional 2 in. of block thickness.

German blocks use flat-bottom holes for calibration with either 3-mm or 10-mm dia used for accept/reject. Major emphasis is placed on use of the Krautkrämer Abstand-Verstärker-Grosse (AVG) distance-gain-size (DGS) diagram, which can be used in lieu of calibration blocks. Figure 2.2.1 is a typical AVG (DGS) diagram. Both ASME and DG(z) fP (German Association for NDE Methods) or Arbeitsgemeinschaft Druckbehälter-Reaktor HP (AD-RHP) 5/3 define linearity, control, screen height and calibration intervals; while there are differences, they are not considered major. Side-drilled holes often are used rather than flat-bottom holes.

## 2.2.3 Test Conditions

2.2.3.1 Surface Finish requirements are more severe in Germany. A surface finish of  $< 10$   $\mu\text{m}$  mean value is designated. ASME is more vague, simply

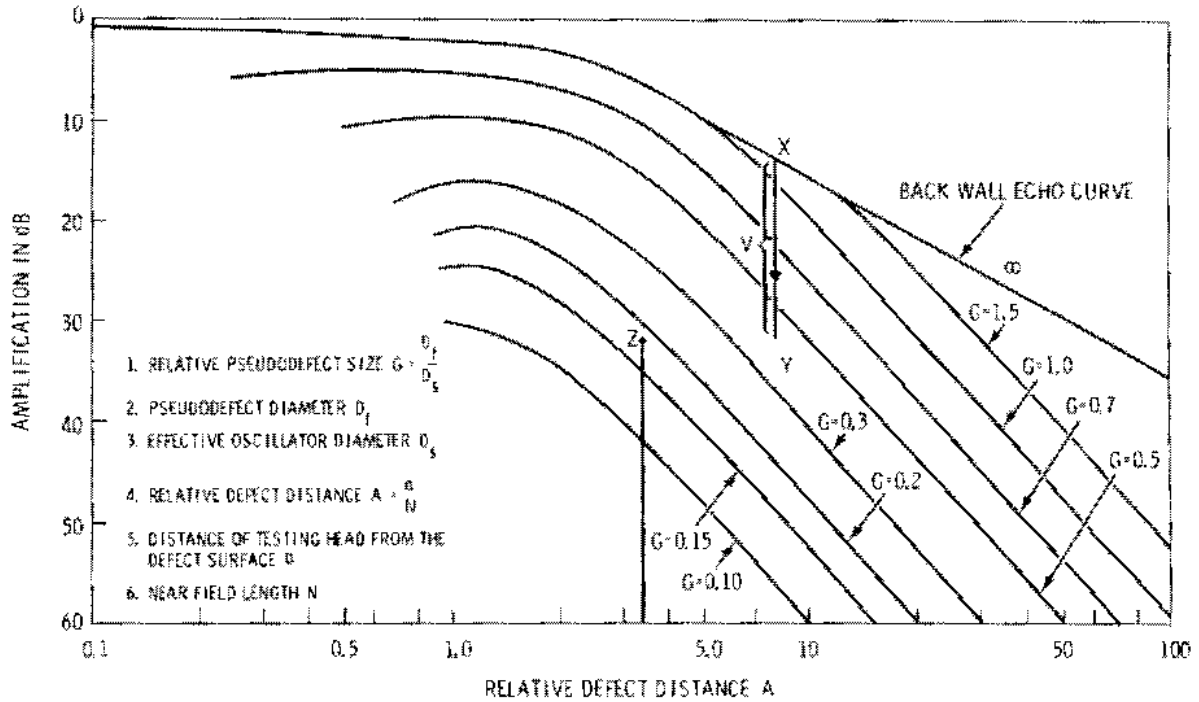


FIGURE 2.2.1. General Distance Amplification Size (AVG) Display Picture (Ref. 2.1.2)

The amplification value  $V$  for the defect echo, measured at the defect (e.g., 18 dB) is not plotted from the zero point but from the backwall echo curve and, in fact in each case, from that point  $X$  which on the backwall echo curve corresponds to the relative thickness of the sheet metal being examined (e.g., the value 8). By means of plotting of the amplification one comes to the point  $Y$ . Through the latter one draws a parallel to the abscissa which intersects in the point  $Z$  the parallels to the ordinate through the point of the relative spacing (e.g., the value 3.5). That curve in the family of curves which lies closest to the thus-obtained point  $Z$  in the display picture is associated with a specific pseudodeflect diameter from which one derives the pseudodeflect diameter; it corresponds to the diameter of the defect under consideration. For further information one should refer to the literature.

requiring that the surface be smooth, free of weld spatter, scale, etc. Both require that the weld region have no excessive elevations or depressions leading to probe tilt.

2.2.3.2 Rate of Travel of probe is limited to 6 in./sec in ASME. The German codes appear to be moot; however, this could be due to an inadequate search of the literature.

#### 2.2.4 Examination

2.2.4.1 UT Weld Examinations vary in degree. The differences are best seen by selecting a reactor pressure vessel such as a pressurized water reactor (PWR) where the wall will be about 250- to 300-mm thick. For preservice examinations, the German requirements include examination from both inside and outside, if possible, versus one or the other or a combination thereby in ASME XI. Examinations should be from both sides of the weld on the same surface, where possible, in both countries. German requirements include moving the probe in both directions along the weld plus rotating the probes to detect transverse cracks. For electroslag welds, an added beam traverse must be made at 45° to the weld. ASME XI requires examination of base metal to a distance  $t/2$  from the weld.

In the FRG, inservice examination must include at least 50-mm strips parallel to the weld for submerged-arc and manual welds, and >100 mm for electroslag welds. In the case of inservice examination, which is usually limited to either the inner or the outer surface, but not both, there is a German requirement to coordinate single probe and tandem examinations from the inner surface to permit the coverage of the most probable flaw orientations. At the preservice stage, the German requirement is to do 100% of the reactor pressure vessel (RPV) surface. In essence, this is done on U.S. PWRs due to the nature of the UT examination; however, it is not an ASME Code requirement. It is a requirement at the plate or forging state. Overlap coverage of the probe is the same; namely, >10%.

2.2.4.2 Cladding Examination differs to a major degree. For example, the ASME Code finds surface indications acceptable while the German Codes do not. The German Codes--[DG(z) FP] (AD-RHP 5/3) [Reaktor-Sicherheit (German Reactor

Safety Commission) (RSK) Directive for Druck Wasser Reaktor- (German PWR) (DWR) design April 24, 1974]--permit no cracks at the clad-base metal interface (ditto ASME III), and require angled longitudinal wave >2 MHz from the side opposite the clad or shear beam >2 MHz on the clad side. It is an RSK requirement that the required sensitivity be maintained through cladding. Sensitivity is set by using either a 2-mm-dia drilled hole parallel to the test surface at the interface with adjustment to full screen height, or a 2-mm flat-bottomed hole with bottom at the interface with the signal adjusted to 3/5 screen height. Added requirements include random examination with 70° angle probes Roentgen-Technische-Dienst (Radiological Testing)-Bundesanstalt für Materialprüfung (German Federal Institute for Material Testing) (RTD-BAM 70) for detecting crack-like defects at the interface.

#### 2.2.5 Flaw Sizing and Location

Flaw sizing and locating procedures are generally similar. The ASME Code requires sizing by measuring the maximum distance amplitude correction (DAC) value, then measuring the two ends on the basis of 50% of the maximum DAC value; the location must be recorded. In Germany the technique varies with thickness. For example,

if  $t < 10$  mm use vanishing echo  
10 <  $t < 40$  mm use 6-dB drop  
40 <  $t$  use 12-dB drop.

Again, the depth of the flaw must be recorded.

2.2.5.1 Recording Levels tend to be more specific in the FRG compared to ASME XI. The ASME XI requirement depends upon the edition and addenda. The requirement was 20% DAC initially, which was changed to 50% DAC because of the large number of geometric indications. Table 2.2.2 abstracted from Reference 2.1.2 contains the German recording thresholds.

2.2.5.2 Acceptance/Rejection Limits depend in both codes on whether the vessel is under the construction code, or in the preoperational or operational stage. Neither construction code (FRG or ASME III) will accept cracks or



TABLE 2.2.2. Response Threshold as a Function of Nominal Wall Thickness (all non-geometric signals exceeding limits in table must be recorded)

<u>Wall Thickness, t, mm<sup>(a)</sup></u>	<u>Diameter of Circular Disk Reflector, mm</u>
$\leq 10$	0.7
$10 < t \leq 15$	1.0
$15 < t \leq 20$	1.5
$20 < t \leq 40^{(b)}$	2.0
$t > 40^{(b)}$	3.0

(a) For differing wall thicknesses, the smaller controls regardless of the weld height.

(b) At angles of incidence above  $60^\circ$ , for close-to-surface defects an increase in sensitivity may be necessary. In tandem testing, all indications are to be recorded whose echo height attains or exceeds (that of) a corresponding circular disk reflector of 6-mm dia. The threshold value of the response can also be derived using other arbitrary test defects if at the same time it is made certain that no values arise which are larger than those in Table 2.2.2 above. The threshold value is to be lowered by 6 dB whenever those values are exceeded which are given in the AD Memorandum RHP 5/3 for the defect frequencies and extents which are admissible without control testing.

crack-like defects. Both will accept UT indications below certain sizes. For example, ASME III in NB-5330 permits the following:

$$\begin{aligned}
 &t < 19 \text{ mm } 6 \text{ mm indication}^{(a)} \\
 &19 < t < 57 \text{ mm } t/3 \\
 &t > 57 \text{ mm } 19 \text{ mm.}
 \end{aligned}$$

The German criteria are given in Table 2.2.3 for both longitudinal and transverse indications. Obviously, in the construction stage, ASME III is more restrictive than the FRG Code.

(a) If interpreted as a crack, unacceptable regardless of size.

**TABLE 2.2.3. Evaluation of Ultrasonic Findings**

Type of Defect	Wall Thickness $t$ in mm <sup>(a)</sup>	No. <sup>(b)</sup> per m of Joint Length	Admissible Defects, <sup>(c)</sup> Maximum Defect Length <sup>(b)</sup>	Echo Magnitude in dB
Longitudinal Defect	$\leq 10$	--	--	--
	$10 < t \leq 20$	10 and 3 and 1	10 20 10	6 6 12(d)
	$20 < t \leq 40$	10 and 3 and 1	10 25 10	6 6 12(d)
	$40 < t \leq 60$	10 and 3 and 1	10 30 10	6 6 12(d)
	$60 < t \leq 120$	10 and 3 and 1	10 40 10	6 6 12(d)
	$t > 120$	10 and 3 and 1	10 50 10	6 6 12(d)

Transverse and Oblique Defects All defects which are indicated in the transverse and oblique defect examination and for which it cannot be clearly demonstrated that they arise from a previously detected longitudinal defect shall be interpreted as transverse or oblique defects.

Wall Thickness $t$ in mm <sup>(a)</sup>	No. per m of Joint Length in Test Zone	Admissible Defects, <sup>(c,e)</sup> Maximum Defect Length	Echo Magnitude in dB
$t < 10$	--	--	--
$t > 10$	3	10	6

- (a) In the case of different wall thicknesses, the smaller is the decisive one, without regard to weld height. In the case of support weld joints, the wall thickness of the support is decisive for superimposed supports; for penetrating supports the wall thickness of the structural part is decisive. Nominal wall thicknesses above 60 mm may be subdivided into testing zones. The subdivision is carried out from both surfaces, with overlappings being allowed to occur. Each zone is evaluated like a weld in the thickness range between 40 and 60 mm; however, the maximum admissible recorded length (40 or 50 mm for wall thicknesses up to 120 mm or over 120 mm, respectively) must lie more than 20 mm below the final surface.
- (b) Flaws with the same depth position must be separated by at least twice the length of the largest flaw. The distance in the thickness direction must at least correspond to the length of the largest flaw.
- (c) If a condition (frequency, defect length or echo magnitude) is not met then a repair or a control test (e.g., a radiographic test or control opening) is required. A repair is always necessary whenever a control test is either impossible or shows no defect or does not clearly demonstrate a nonessential cause of the echo indication. Whenever the defect frequencies and defect lengths exceed those values which are admissible without control testing then reflection locations must also be interpreted as defects when their echo magnitudes are up to 6 dB below the recording response threshold given in the chapter, "Evaluation of Test Findings."
- (d) Random control tests are required.
- (e) If transverse flaws occur in groups, then improvements must be made if only a few of the readings lie above the recording threshold and the others exceed an echo magnitude which is 6 dB below this threshold value. Any deviation from this evaluation is only permissible, if by a random opening of the weld, it is found that the readings do not come from the cracks.

ASME XI defines a spectrum of acceptable flaws (not indications) at both the preservice and inservice stages. There are several tables covering acceptable flaw sizes. Tables 2.2.4a and b and 2.2.5 are representative. The reader is directed to ASME XI for the complete picture. The values in Table 2.2.4a and b represent rejection levels; however, for an operating vessel where the flaw exceeds the acceptable value, it is permissible to do a fracture mechanics analysis according to Appendix A of ASME XI and, if the analysis indicates the flaw does not exceed the criteria of IWB-3600, the vessel need not be repaired. However, the flaw must be monitored at several subsequent examinations.

2.2.5.3 Multiple Flaws or Indications are considered to be additive if they occur at the same depth and are closer than some specific value. ASME XI defines elaborate criteria; the German Code states indications are added unless separated by more than the length of the largest indication.

TABLE 2.2.4a. Allowable Planar Indications in Reactor Pressure Vessel. Material: Ferritic steels that meet the requirements of NB-2331 and have specified minimum yield strength of 50 ksi or less at 100°F. Thickness Range: 4 in. and greater.

<u>Aspect Ratio, <math>a/l</math> (a)</u>	<u>Surface Indications, <math>a/t</math> % (b)</u>	<u>Subsurface Indications, <math>a/t</math> % (b,c)</u>
0	1.8	2.3
0.05	2.0	2.4
0.10	2.2	2.6
0.15	2.4	2.9
0.20	2.7	3.2
0.25	3.1	3.7
0.30	3.5	4.1
0.35	3.5	4.6
0.40	3.5	5.2
0.45	3.5	5.8
0.50	3.5	6.5

- (a) For intermediate flaw-aspect ratios,  $a/l$ , linear interpolation is permissible.
- (b) Component thickness,  $t$ , is measured normal to pressure retaining surface of component. Where the section of thickness varies, the average thickness over the length of the indication is the component thickness.
- (c) The total allowable depth of subsurface indication is  $2a$ .

TABLE 2.2.4b. Allowable Laminar Indications

<u>Component Thickness <math>t</math>, inches (a)</u>	<u>Laminar Area <math>A</math>, square inches (b)</u>
4	18
6	18
8	24
10	30
12 and greater	36

- (a) For intermediate thicknesses, linear interpolation of area is permissible.
- (b) The area of a laminar flaw is defined in IWA-3360.

TABLE 2.2.5. Allowable Planar Indications--Piping. Material: Austenitic steels that meet the requirements of minimum yield strength of 35 ksi or less at 100°F.

Examination	Aspect Ratio, a/l <sup>(a)</sup>	Volumetric Examination Method								Surface Examination Method	
		Nominal Wall Thickness t, in. 0.312 or less <sup>(d)</sup>		1.0		2.0		3.0		Nominal Wall Thickness a/t, % <sup>(c)</sup>	Indication Length L, in.
		Surface Indication a/t, %	Subsurface Indication a/t, % <sup>(b)</sup>	Surface Indication a/t, %	Subsurface Indication a/t, % <sup>(b)</sup>	Surface Indication a/t, %	Subsurface Indication a/t, % <sup>(b)</sup>	Surface Indication a/t, %	Subsurface Indication a/t, % <sup>(b)</sup>		
Preservice	0	9.4	9.4	8.5	8.5	8.0	8.0	7.6	7.6	0.312 or less	1/8
	0.05	9.5	9.6	8.6	8.6	8.2	8.2	7.7	7.7		
	0.10	9.6	9.8	8.8	8.8	8.3	8.3	7.8	7.8	1.0	3/16
	0.15	9.9	9.9	8.9	8.9	8.4	8.4	7.9	7.9		
	0.20	10.0	10.0	9.1	9.1	8.6	8.6	8.1	8.1	2.0	1/4
	0.25	10.0	10.0	9.2	9.2	8.7	8.7	8.2	8.2		
	0.30	10.0	10.0	9.4	9.4	8.9	8.9	8.3	8.3	3.0 and over	1/4
	0.35	10.0	10.0	9.5	9.5	9.0	9.0	8.5	8.5		
	0.40	10.0	10.0	9.7	9.7	9.1	9.1	8.6	8.6		
	0.45	10.0	10.0	9.8	9.8	9.3	9.3	8.7	8.7		
0.50	10.0	10.0	10.0	10.0	9.4	9.4	8.9	8.9			
Inservice	0	11.7	11.7	10.6	10.6	10.0	10.0	9.5	9.5	0.312 or less	0.2
	0.05	12.0	12.0	10.7	10.7	10.2	10.2	9.6	9.6		
	0.10	12.2	12.2	11.0	11.0	10.4	10.4	9.7	9.7	1.0	0.25
	0.15	12.4	12.4	11.1	11.1	10.5	10.5	9.9	9.9		
	0.20	12.5	12.5	11.4	11.4	10.7	10.7	10.1	10.1	2.0	0.45
	0.25	12.5	12.5	11.5	11.5	10.9	10.9	10.2	10.2		
	0.30	12.5	12.5	11.7	11.7	11.1	11.1	10.4	10.4	3.0 and over	0.65
	0.35	12.5	12.5	11.9	11.9	11.2	11.2	10.6	10.6		
	0.40	12.5	12.5	12.1	12.1	11.4	11.4	10.7	10.7		
	0.45	12.5	12.5	12.2	12.2	11.6	11.6	10.9	10.9		
0.50	12.5	12.5	12.5	12.5	11.7	11.7	11.1	11.1			

(a) t is nominal wall thickness or actual wall thickness as determined by UT examination.  
 (b) The total depth of subsurface indication is 2a.  
 (c) For intermediate flaw aspect ratios a/L, and thickness t, linear interpolation is permissible.



Trumpfheller<sup>(2.3.1,2.3.2)</sup> argues that the ASME XI approach to flaw sizing is less thorough than the German Code rules, primarily because the ASME Code contains no criteria establishing when an indication should be interpreted as emanating from a crack-like defect. The preceding was based on the 1971 edition of ASME XI which did not contain the mandatory Appendix I covering UT procedures. Presumably, Appendix I in part supplies the missing criteria. A more pertinent claim is with regard to the recording and action levels of ASME XI. These levels have varied from 20% to 100% DAC, depending on the Code edition and addendum. The author<sup>(2.3.2)</sup> cites the Summer 1973 Addendum of ASME XI in a comparison with the FRG Code. A wall thickness of 250 mm will yield a recording level 6 dB below the amplitude of a cylindrical reflector with a diameter of 11 mm. A sound path of 500 mm results in the ASME XI recording level being 10 dB higher than the FRG Code, using 2-MHz crystals about 20-mm dia. If the sound path is increased to 1000 mm, the dB difference may rise to 12. Trumpfheller<sup>(2.3.2)</sup> argues that the decreased sensitivity such as cited in the above example, which is due to calibration against larger diameter flat-bottomed holes (ASME) versus the FRG 3-mm value, will decrease the probability of detecting relatively large flaws.

### 2.3.1 Difference in Philosophy: ASME Versus FRG

One further difference in code philosophy is cited by Trumpfheller.<sup>(2.3.1)</sup> A statistical or probabilistic approach is used in establishing the size and number of acceptable defects per specified volume of weld. The ASME codes emphasize size rather than numbers, see Table 2.3.1.

Meyer<sup>(2.2.6,2.2.7)</sup> conducted a series of experiments which highlight the similarities and differences of the FRG HP 5/3 and ASME V and XI Codes. Table 2.3.2 from Reference 2.2.7 provides an excellent comparison of these differences when applied to the examination of a weldment. The author's<sup>(2.2.6,2.2.7)</sup> approach was to conduct a testing program on different types of reference blocks of various thickness, containing natural and artificial reflectors of known size, location and orientation. He rigorously applied ASME and HP 5/3 with regard to calibration, testing, recording and reject/repair.

TABLE 2.3.1. Acceptable Defect Sizes and Numbers per Meter of Weld (Reference 2.3.1)

Wall Thick- ness, mm	Frequency of Defects		
	In Layers of Thickness, mm	Number of Defects per Meter of Weld	Size of Defect, mm
40 to 60	40 to 60	10	10
		3	30
60 to 120	60	10	10
		3	40
>120	60	10	10
		3	50

NOTE: Standard volume for frequencies cited is 1-m long by weld width by 60-mm thick.

While calibration procedures differ as noted in Table 2.3.2, the sensitivities in terms of dB have some interesting interrelationships as noted in Figure 2.3.1. Of greater interest are the detection sensitivity and the decision leading to recording or reject/repair. Figure 2.3.2 is a presentation of data using ASME and HP 5/3 procedures. The reference block, also illustrated in Figure 2.3.2, contains a series of 5-, 7-, 10-, 14-, and 20-mm flat-bottomed holes of various depths inclined  $6^\circ$  to the normal. Another variable was reference block thickness. Both  $45^\circ$  and  $70^\circ$  probes, as well as the tandem technique, were used. However, only  $70^\circ$  probe data are given in Figure 2.3.2. The symbols in Figure 2.3.2 denote whether the indicators are recordable or exceed the reject/repair levels using criteria in HP 5/3 and ASME 20% DAC and 50% DAC levels. The data in Figure 2.3.2 are repeated in tabular form in Table 2.3.3.

An analysis of the data in Table 2.3.3 is rather interesting. Without prejudging whether the accept/reject criteria of HP 5/3 are too restrictive or whether those of ASME V (X1) are too lenient, it is apparent that recording is synonymous with rejection in HP 5/3 whereas ASME Code rejection over the spectrum of flat-bottomed hole sizes used is limited to the largest diameter holes and not always there. It is interesting to note that the one case of rejection



TABLE 2.3.2. Comparison of Weld Examination According to HP 5/3 (Level C) and ASME Code Section V for Wall Thickness Over 4 Through 6 in.

<u>Sensitivity Setting</u>	<u>HP 5/3</u>	<u>ASME</u>
Calibration Method	+	0
Transfer Correction	+	0
Recording Level	+	0
Unacceptable Level	+	0
Higher Sensitivity According to Test Results	+	-
<u>Examination Technique</u>		
Longitudinal Flaws		
Two Different Beam Angles	+	+
Straight Beam Technique	+	+
Examination from Both Sides of the Weld	+	+
Tandem Technique	+	+
Transverse Flaws		
Two Different Beam Angles	+	+
Examination from One Surface	+	+
Tandem Technique	+	-
Evaluation of Flaws		
Evaluation of Flaw Amplitude	+	0
Length of Flaw	+	0
Depth of Flaw	+	+
Height of Flaw	+	0
Number of Flaws	+	-
Distance Between Flaws in Same Depth	+	-
Distance Between Flaws in Direction of Thickness	+	-

SYMBOLS: + + Same examination methods  
 + 0 Different examination methods  
 + - HP 5/3 examination method

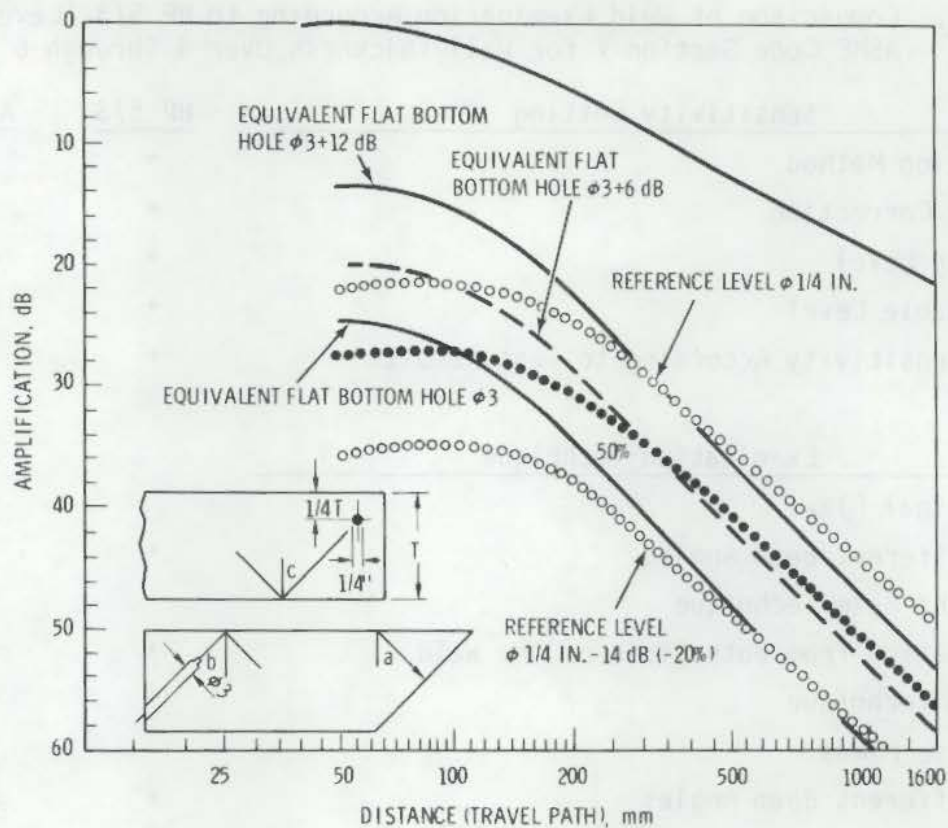


FIGURE 2.3.1. Comparison of Calibration Sensitivities According to ASME and HP 5/3 for Wall Thicknesses Between 4 and 6 in. (Reference 2.2.6)

occurred, at both 20% DAC and 50% DAC recording levels. Slight differences in detection sensitivity occurred at  $64^\circ$  versus  $76^\circ$ ; however, there were no definitive trends. The detection sensitivities of HP 5/3 and ASME at 20% DAC were virtually the same, indicating the principal difference is one of philosophy concerning indication acceptance for a given signal amplitude.

Figure 2.3.3 permits a comparison of recording and rejection as functions of ultrasonic beam travel path using both ASME and HP 5/3 sensitivity values. Figure 2.3.3 permits one to see how close to the boundaries the respective signal amplitudes were.

Meyer's conclusions in Reference 2.2.6 are more understandable having read his Reference 2.2.7 since some of the conclusions are not obvious from the report contents:

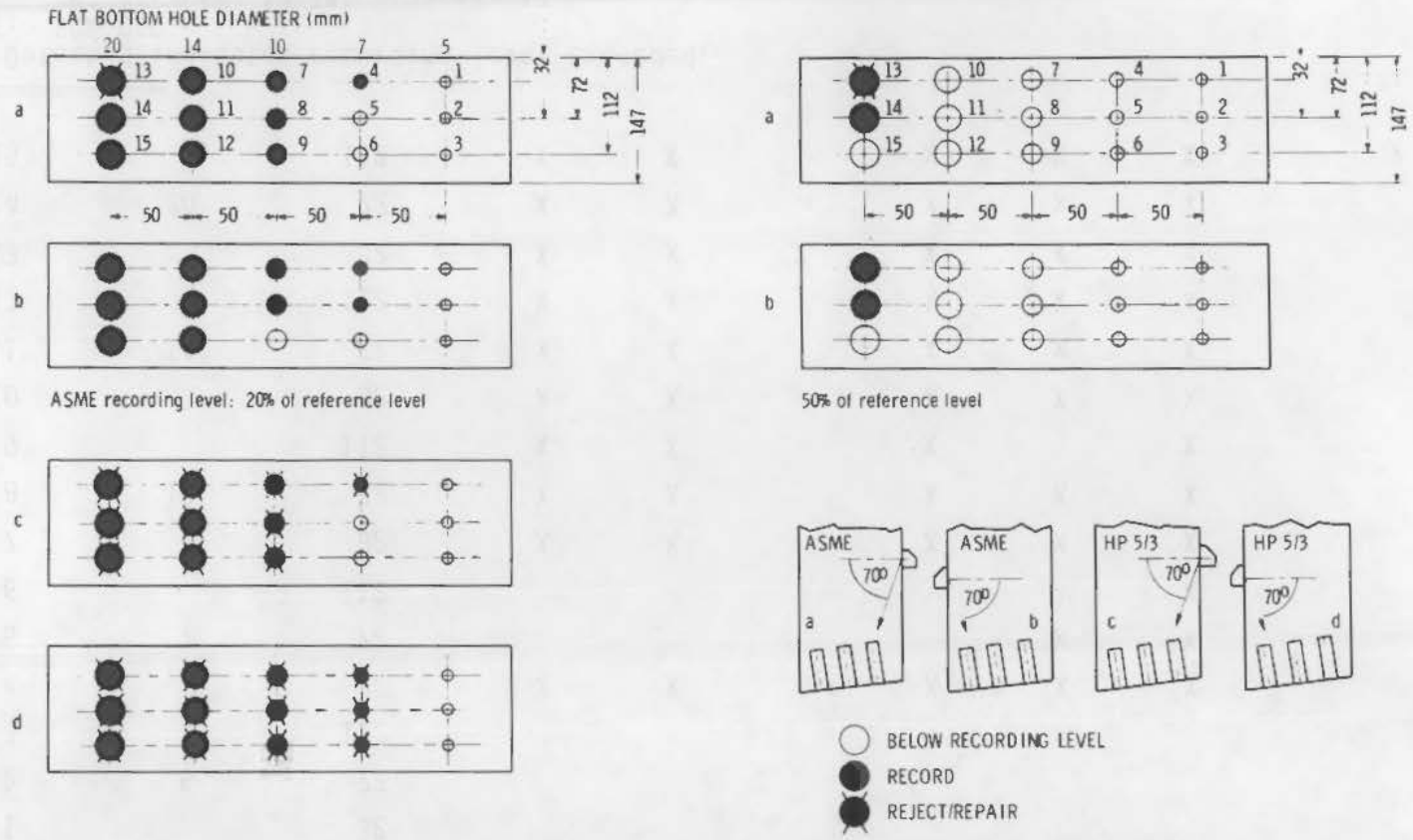


FIGURE 2.3.2. Flaw Detectability with 70° Angle Probe (Reference 2.2.6)

TABLE 2.3.3. 70° Probe ASME V 20% DAC FRG HP 5/3 (from Figure 2.3.2)

Hole No.	Hole Size (mm)	Centerline of Hole (mm)	64° Angle		ASME-A HP 5/3-C		76° Angle		ASME-B HP 5/3-D	
			Detected(a)		Rejected		Detected(a)		Rejected	
			ASME	HP 5/3	ASME	HP 5/3	ASME	HP 5/3	ASME	HP 5/3
1		32								
2	5	72								
3		112								
4		32	X	X		X	X	X		X
5	7	72					X	X		X
6		112						X		X
7		32	X	X		X	X	X		X
8	10	72	X	X		X	X	X		X
9		112	X	X		X		X		X
10		32	X	X		X	X	X		X
11	14	72	X	X		X	X	X		X
12		112	X	X		X	X	X		X
13		32	X	X	X	X	X	X		X
14	20	72	X	X		X	X	X		X
15		112	X	X		X	X	X		X

(a) Detected indicates recording level exceeded.

NOTE: 50% DAC

65° detected 13,14; rejected 13

76° detected 13,14

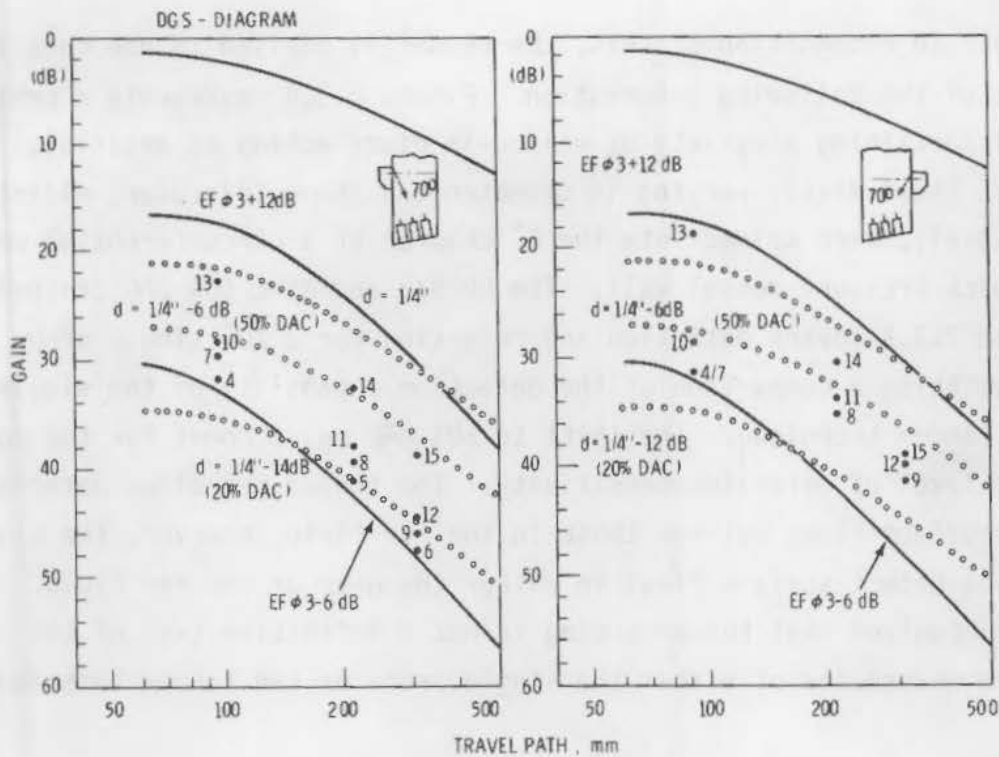
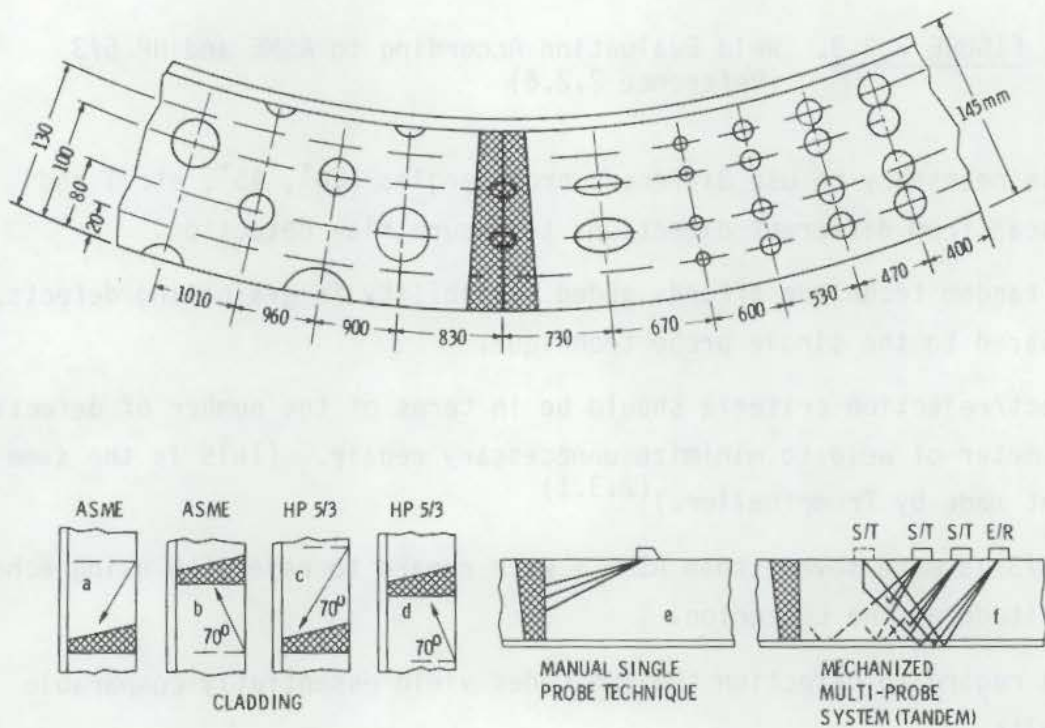


FIGURE 2.3.3. Weld Evaluation According to ASME and HP 5/3 (Reference 2.2.6)

- It is necessary to use different probe angles ( $70^\circ$ ,  $45^\circ$ , etc.) and to scan from different directions to ensure flaw detection.
- The tandem technique affords added reliability in evaluating defects, compared to the single probe technique.
- Defect/rejection criteria should be in terms of the number of defects per meter of weld to minimize unnecessary repair. (This is the same point made by Trumpfeller.) (2.3.1)
- HP 5/3 is more severe than ASME V with regard to rejection using echo amplitude as the criterion.
- With regard to detection the two codes yield essentially comparable results.

Meyer's second report, (2.2.7) while covering much of the information in the first report, (2.2.6) is limited in distribution and not for general

publication. In recognition of this, the reader is advised to use care in the further use of the following information. Figure 2.3.4 represents a pressure vessel wall containing a variety of welded-in discs acting as artificial reflectors. These discs, varying in diameter and shape (circular, elliptical, semi-elliptical), were welded into the 6° chamfer of a circumferential weld in a 145-mm thick pressure vessel wall. The HP 5/3 and ASME 50% DAC criteria were used. Table 2.3.4 covers detection and rejection for a 70° single probe as well as permitting a comparison of the detection capability of the single probe versus the tandem technique. The shift to 50% DAC may account for the apparently lower level of detection sensitivity. The tandem technique detected the near-field surface flaws but not those in the far field; however, the single probe did not detect surface flaws in either the near or the far field. It should be recognized that the preceding is not a definitive test of the strength and weaknesses of either the single probe or the tandem technique.



**FIGURE 2.3.4.** Distribution of Introduced Defects in Pressure Vessel Circumferential Weld Seam-Wall Interface and Ultrasonic Probe Locations (Reference 2.2.7)

**TABLE 2.3.4.** Detection and Rejection on Bases of ASME V and HP 5/3 for Clad Pressure Vessel Wall

Defect Code	ASME		HP 5/3		Single Probe	Detection Only Tandem
	a	b	c	d	e	f
80(a)		X	X	X	0	0
81		0	0	X	0	0
82			X	0	0	0
83						0
62	X	X	X	X	0	0
63			0	X	0	0
64			X		0	0
65					?	0
46	0	X	X	X	0	0
47	0	0	0	0	0	0
48	0	0	0	0	0	0
49	0	0	0	0	0	0
28	X	X	X	X	0	0
29	0	0	0	0	0	0
30	0	0	0	0	0	0
31	0	0	0	0	0	0
16		X	0	X	0	0
14		0	0	X	0	0
4	X	X	X	X	0	0
6	X	X	X	X	0	0
8(b)						
102			X	X	0	0
94			0	0	0	0
10						0
12						0
26			0		0	0
103		X	X	X	0	0
7						

(a) 80 is lower right in Figure 2.3.4. Numbers proceed up and to left to 9.

(b) 8 is lower left in Figure 2.3.4. Number proceeds up and to right to 9.

NOTE: 0 Detected  
X Rejected

Meyer<sup>(2.2.7)</sup> argues that the ASME procedure, where UT equipment is calibrated with notches or edges, is essentially unsatisfactory based on experience, whereas excellent correlations have been obtained with cylindrical boreholes (flat-bottomed holes). He makes the point that most national codes use flatbottomed holes for calibration.

Meyer<sup>(2.2.7)</sup> cited several factors adversely influencing the detection of flaws by UT such as the following:

- An adverse angle resulting from probe angle and flaw orientation may cause a majority of the UT beam not to be reflected back to the probe. (UT from both sides of the weld helps).
- Small planar defects normal to the surface are difficult to recognize from either side because most of the UT beam is reflected in different directions (the tandem technique may help).
- Laminations may shadow planar defects.
- Lack of fusion between weld beads will lead to curved surfaces which cause UT beam scatter.
- Shrinkage stresses may result in compressive loads on the crack rendering it transparent to the UT beam (with smooth surfaces and low frequencies complete transparency is probable at  $\geq 20 \text{ N/mm}^2$  compressive stress).
- There is an interaction between defect size and its orientation; small reflectors can be detected at steeper angles than large reflectors because such small reflectors behave as if they are spheres; as reflector size increases the UT beam is deflected in the opposite direction so that even at small angles of defect orientation no part of the beam is reflected back to the probe; this pertains to the tandem technique also.

### 2.3.2 Acceptance/Rejection Criteria

The ASME UT rejection criteria is quite straightforward. If the reduction in beam amplitude exceeds 100% DAC, the defect is rejectable. The situation is somewhat more complicated for HP 5/3. A definite dB value (6 or 12 dB) above



the recording level is the general criterion for repair. Between the recording level and the repair level there may exist a definite number of reflectors, depending on both length and number of indications, using 1-m weld length as the basis. If combined indications occur, the rejection level is usually reduced from 12 dB to 6 dB. A comparison is made with ASME V; however, it would be more relevant to use ASME XI where clustered defects are considered. Table 2.3.5 contains permissible longitudinal and transverse flaws as functions of wall thickness, flaw length, and number of flaws per meter of weld and maximum echo amplitude.

### 2.3.3 Reporting Levels

Work of Taylor and Selby<sup>(2.3.3)</sup> confirms some of the conclusions of Meyer.<sup>(2.2.6,2.2.7)</sup> The authors examined the 1974 edition of ASME XI (through Summer 1975 addendum) and the 1977 edition (through Summer 1978 addendum). These editions vary primarily in the reporting level of indications (20% DAC in 1974 versus 50% recording and 100% reporting in 1977) and in calibration standards (side-drilled holes 1974 versus notches 1977). The authors preferred notches on the basis that they more closely duplicated the physics of cracks. They felt that the decision to discard 20% DAC was unjustified on the basis that flaw detection reliability was markedly reduced. Table 2.3.6 contains data for detection of notches in a variety of sizes of piping. There is little doubt that 20% DAC yields more reliable results. Their point concerning notches versus side-drilled holes is confirmed in Figure 2.3.5. The notch is substantially less sensitive than the side-drilled holes.

TABLE 2.3.5. Permissible Indications for Ultrasonic Examination (HP 5/3) (CS CK)

Evaluation Group	Wall Thickness (mm)	Longitudinal Flaw			Transverse Flaw		
		Number per Weld	Flaw Length (mm)	Maximum Echo Amplitude per Weld	Number per Weld	Flaw Length (mm)	Maximum Echo Amplitude per Weld
CS - CK	$t < 10$	5	10	15	3	10	15
		10+	15	2	3	10	2
		3+	30	2			
	$10 \leq t \leq 20$	1	10	3			
		10+	15	3	3	10	3
		3+	40	3			
	$20 \leq t \leq 40$	1	10	5			
		10+	15	4	3	10	4
		3+	50	4			
$t > 40$	1	10	8				

TABLE 2.3.6. Summary of Flaw Response Using 1974 and 1977 (1978 Summer Addendum) ASME XI Evaluation Criteria

Pipe Diameter	Inspection Angle / Beam Path	ASME XI 1974 Ed Through 1975 Addendum		ASME XI 1977 Ed Through Summer 1978 Addendum		Total Measurements Made
		20% DAC		50% DAC	100% DAC	
		Number of Flaws Producing Recordable Response	Number of Flaws Producing Evaluation Response	Number of Flaws Producing Recordable Response	Number of Flaws Producing Evaluation Response	
4 in. Sch. 80 Carbon Steel	45° / 1/2 V	72	72	72	37	72
	45° / 3/2 V	72	72	65	19	72
	60° / 1/2 V	72	72	59	40	72
12 in. Sch. 80 304 Stainless Steel	45° / 1/2 V	108	108	86	25	108
	45° / 3/2 V	108	108	86	39	108
	60° / 1/2 V	108	108	105	51	108
20 in. Sch. 80 Carbon Steel	45° / 1/2 V	102	102	67	24	108
	45° / 3/2 V	98	98	48	9	108
	60° / 1/2 V	108	108	74	40	108
20 in. Sch. 80 304 Stainless Steel	45° / 1/2 V	101	101	17	0	108
	45° / 3/2 V	Sound attenuated; no flaw response.		Sound attenuated; no flaw response.		
	60° / 1/2 V	72	72	10	0	108
Total		1,021	1,021	689	284	1,080
Percent		94.5%	94.5%	63.8%	26.3%	

2.3.13

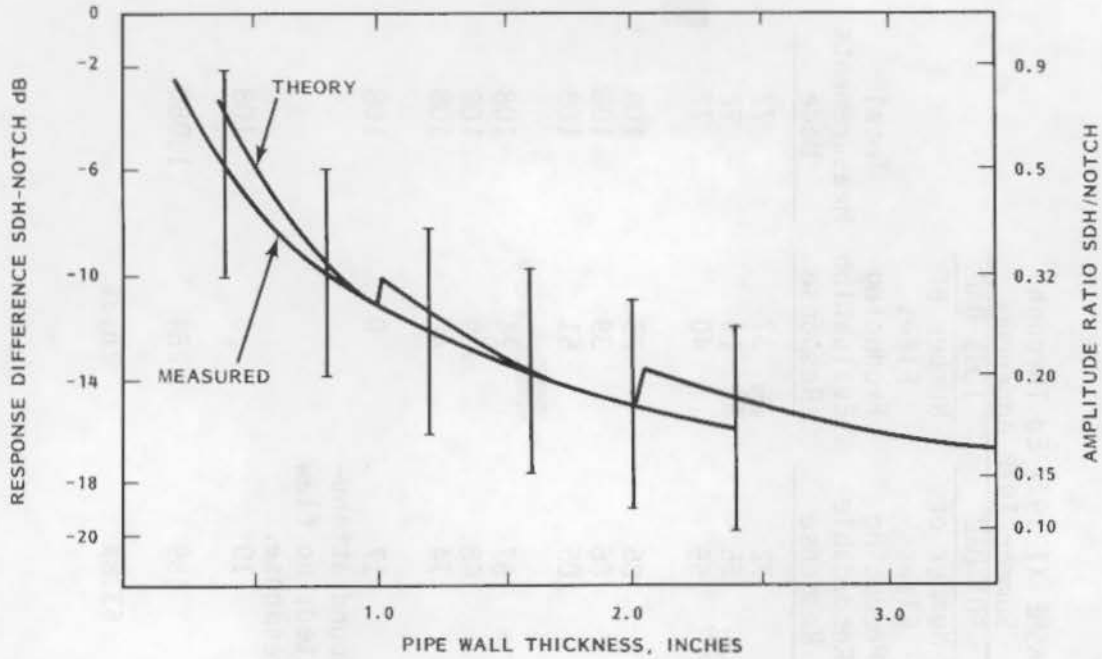


**FIGURE 2.3.5.** Measured and Theoretical Reduction in Ultrasonic Piping Inspection Sensitivity of the 1977 Edition of the ASME Code, Section XI (notch), as Compared to the 1974 Edition (side-drilled holes, SDH) for Piping, Illustrating Lower Sensitivity of the Notch

The government, whether in the United States or elsewhere, can have either a positive or a negative impact on the applicable codes covering NDE procedures and flaw acceptance levels. Emphasis will be given to the U.S. regulations because of greater familiarity. Examples of how positive changes may come about are contained in the Code of Federal Regulations Title 10 (10 CFR)<sup>(2.4.1)</sup> in Appendix A and Appendix B, and in 10 CFR Part 50.55(a), which deals specifically with ASME Codes. Positive actions also are promulgated through Regulatory Guides and Branch Technical Positions. Negative actions occur by failure to take action. For example, an August 1978 reading of 10 CFR Part 50.55(a) would reveal that ASME Section III, Division I, has been approved through the 1977 edition of this code including the Summer 1977 Addenda, while ASME Section XI was approved only through the 1974 edition including the Summer 1975 Addenda. This difference was due to reservations in the Regulatory staff about specific but limited items within the Section XI Code. One might consider such an approach as using the bludgeon rather than the rapier; however, it is quite effective in getting the attention of the Code groups. A further way to modify the requirements may be done by a utility on an individual basis. Requests may be made for exemptions to specific aspects of the ASME XI Code because of limited accessibility of older plants; preference for examination procedures embodied in Code Addenda not approved by USNRC, etc. These are reviewed case-by-case, and approved or denied, or further information may be requested. Some 18 plants currently are under review with the number of requests varying from a low of 4 to a high of 729. Obviously, such an approach may absorb a great deal of Regulatory Staff time.

#### 2.4.1 Examples of NRC Concerns About ASME XI

The negative action taken by NRC with regard to ASME XI was cited previously in failure to approve to 10 CFR 50:50(a)<sup>(2.4.1)</sup> beyond the 1974 Edition and Summer 1975 Addendum. The NRC concerns were reviewed in an RC-ASME XI meeting.<sup>(2.4.2)</sup> Beverly<sup>(2.4.3a)</sup> provided an excellent summary of the concerns as well as actions to be taken to resolve the concerns. These follow:

- NRC Concern

The Class 1 exemption criteria IWB-1220(d) based on postulated pipe failures and the Class 1 single stream concept for selection of welds for ISI, especially since it exempts many dissimilar metal welds from ISI, is an area of NRC concern.

Resolution

Section XI will be revised (Summer 1978 Addenda) to require examination of all high-stress welds, terminal ends, and all dissimilar metal welds each inspection interval. Additional welds will be selected (single loop selection is permissible) to make a 25% sample. NRC regulation will address "old" and "new" plants for application of the above sampling procedures.

- NRC Concern

Class 1 single stream concept will exempt many RPV nozzle-to-vessel welds (cat. B-D) from ISI.

Resolution

Section XI will be revised (Summer 1978 Addenda) to require 100% examination of all nozzle-to-vessel welds each inspection interval.

- NRC Concern

Surface examination only on branch pipe connections in Class 1 piping is not adequate; volumetric examination should be reinstated.

Resolution

Section XI will be revised (Summer 1978 Addenda) to require both a surface and a volumetric examination on branch pipe connections for piping greater than 2 in. and surface examination only on branch pipe connections for piping 2 in. and smaller, nominal pipe size. There is a 4-in. exemption in Summer 1975 and earlier editions.

- NRC Concern

ISI of steam generator tubes cannot be completely specified by Section XI since continuing problems require that each plant's steam generator ISI program be handled on a case basis.

Resolution

No revision of Section XI is needed at this time; NRC regulations will make reference to technical specification requirements for steam generator tube ISI.

- NRC Concern

Class 2 exemption criteria IWC-1220(b), (c), (d), and (f); Class 2 Figure IWC-1220-1; Class 2 examination category C-F as it relates to selection of welds for examination based on postulated pipe break criteria. Class 2 exemption criteria are subject to misinterpretation that would exempt piping that should not be exempted from ISI. Instead of allowing exemptions, Class 2 requirements should be stated in a positive sense by specifying which types of welds or systems should be examined.

Resolution

A joint ASME-NRC task group was established to rewrite portions of Subsection IWC to state the ISI examination requirements in a positive view. These revisions of IWC, which will be published in the Summer 1978 Addenda, include significant revisions of the Class 2 exemption criteria and a program for selecting welds for examination to assure ISI of the welds most susceptible to flaw initiation and growth.

The Class 2 exemption criteria based on postulated pipe break criteria, separation from essential systems and components, and exemption of supports and attachments that do not provide component support during normal conditions have been deleted. The other three Class 2 exemption criteria of IWC-1220 have been modified and are expected to read as follows:

- Components of systems or portions of systems that during normal plant operating conditions<sup>(a)</sup> are not required to operate or perform a system function but remain flooded under static conditions or at a pressure of at least 80% of the pressure that the component or system will be subject to when required to operate.
- Components of systems or portions of systems, other than Residual Heat Removal Systems and Emergency Core Cooling Systems, that are not required to operate above a pressure of 275 psig or above a temperature of 200°F.
- Component connections (including nozzles in vessels and pumps), piping and associated valves, and vessels (and their supports) that are 4-in. nominal pipe size and smaller.

The requirements for selection of circumferential piping welds for ISI examination have been changed to require that all highly stressed welds, all terminal ends of piping runs and branch runs, and all dissimilar metal welds be examined each inspection interval. Additionally, sufficient additional welds that are structural discontinuities shall be selected to complete a percentage sample (as specified in the revised IWC articles) of the piping welds for examination each inspection interval. These same welds would be reexamined during successive inspection intervals.

- NRC Concern

Revision of the preservice inspection (PSI) requirements for Class 2 components [IWC-2100(a)] which limits preservice inspection to those components initially selected for ISI is not justified.

---

(a) Normal conditions include operating conditions, reactor startup, operation at power, hot standby, and reactor cooldown to cold shutdown conditions. Test conditions are excluded.



### Resolution

Because of rapid advances in NDE technology, comparison of PSI and ISI flaw indication data is not as meaningful as was originally thought. Also, Class 2 systems are designed with a high degree of redundancy.

These factors indicate that a preservice examination of all nonexempt Class 2 components would serve no useful purpose. Therefore, no revision of Section XI is needed.

- NRC Concern

Using 100% of the UT reference level (DAC) as the criteria for investigation of flaw indications is not sufficiently sensitive to be permitted on a generic basis.

### Resolution

Section XI will be revised (Summer 1978 Addenda) to require that: 1) all ultrasonic reflectors which produce a response greater than 50% of the reference level shall be recorded and 2) the size of reflectors shall be measured between points which give amplitudes equal to 100% of the reference level. The NRC will continue to develop a regulatory guide to provide criteria for UT examination of austenitic piping.

- NRC Concern

Section XI requires a surface examination on Class 1 bolts and studs only if they are removed from the flange. NRC believes the surface examination of Class 1 bolts and studs is required; therefore, Section XI should require their removal from the flange.

### Resolution

Since tests are presently underway relating to these examinations of RPV studs, no revision of the Section XI Code or the NRC Regulatory Guide 1.65 will be made until further information develops.

The NRC is presently preparing an amendment of the 10 CFR 50.55(a) regulation that will upgrade the NRC's approval of Section XI Codes up through the Winter 1977 Addenda. However, the regulation will modify the ISI examination requirements of Section XI for the NRC "areas of concern" as discussed above. The NRC is also considering a "grandfathering" provision in the regulation for those operating plants which upgrade to the Winter 1977 Addenda, but the grandfathering would apply only to those examinations addressed by the NRC concerns. In such cases, the upgraded ISI program in the concern areas would be based on the Section XI requirements contained in the 1974 Edition with Addenda through the Summer 1975 Addenda. Additionally, the NRC is considering a relaxation of the upgrade frequency from the present 40 months for ISI and 20 months for pump and valve testing to as much as an inspection interval (e.g., up to 120 months). It is expected that this amendment of the 10 CFR 50.55(a) regulation will be published for public comment in the Federal Register in the next 3 to 6 months. (N.B.: This action has occurred.)

Presumably, there will be an update in 10 CFR 50.55(a) in the near future as noted in Beverly's report. (2.4.3b)(a)

It is reasonable to examine what may have been lost in enhanced examination through code actions taken since the Summer of 1975 which have not been approved by NRC. Table 2.4.1 contains specific changes made since then.

#### 2.4.2 Positive Regulatory Actions

An action not yet taken, but being considered by NRC, is to grandfather plants through 10 CFR 50.55(a). The requirement now is to update the new code every 40 months. Consideration is being given to 120 months, which would tend to coincide with the 10 year inspection interval. This would provide relief to both utilities and NRC staff who have been on a treadmill of updating of requests for exemption.

---

(a) A revision was released for comment in January 1979.

TABLE 2.4.1. Augmented Inspections and Significant Requirements  
Added Since Summer 1975 Addenda(2.4.3b)

Added Requirements Since Summer 1975 Addenda up to Winter 1976 Addenda	Current Code Requirements Up to Summer 1975 Addenda
W-1975--IWA-2233, IWB-2413, IWB-1210 Eddy-current examination of steam generator tubing added for pre-service and inservice examination.	Requirement for steam generator tubing examination not specified.
W-1975--IWA-2300 NDE personnel required to be qualified to SNT-TC-IA procedures.	Requirement for qualification of NDE personnel not specified.
W-1975--IWA-2410, IWB-2411 Adds accelerated inspection Program A to reduce overall exposure to NDE personnel. [Consistent with ALARA requirements of Regulatory Guide 8.8 and 10 CFR Part 20.1(c)].	Uniformly spaced inspection intervals may result in excessive radiation exposure to NDE personnel in later years of plant service.
W-1975--IWB-2100(c) Adds preservice examination requirements for component replacements, additions or alterations.	No preservice examination requirements specified for component replacements.
W-1975--Exam. Cat. B-A (Table IWB-2500) Increases examination of reactor vessel welds to 100% during first inspection interval, with 60% weld sampling examinations for subsequent inspection intervals.	Requires examination of only 5% circumferential welds and 10% longitudinal welds in reactor vessel during each inspection interval.
W-1975--Exam. Cat. B-B (Table IWB-2500) Increases examination of all steam generator (primary side) welds to 100% for first inspection interval, with 75% weld sampling examination of one generator for subsequent inspection intervals.	Requires examination of only 5% circumferential welds, and 10% longitudinal welds in each steam generator during each inspection interval.
W-1975--Exam. Cat. B-J (Table IWB-2500) Focuses examination on all pipe break locations in one reactor coolant loop, and selected branches during successive inspection intervals. Each selected weld receives four examinations in 40 years.	Requires examination of only 25% of randomly selected piping and branch connection welds in each loop, during each inspection interval. Each selected weld receives one examination in 40 years.
W-1975--Mandatory Appendix III Procedure for UT examination of ferritic steel piping added.	No procedures specified.
--Mandatory Appendix IV Eddy-current examination of steam generator tubing.	No examination specified.

TABLE 2.4.1. (contd)

Added Requirements Since Summer 1975 Addenda up to Winter 1976 Addenda	Current Code Requirement Up to Summer 1975 Addenda
S-1976--IWA-7000, IWB-7000 Adds rules for installation and preservice examination of component replacements, such as renewal parts, subassemblies, addition of valves and rerouting of piping.	No rules specified.
S-1976--Table IWC-2520 Increases the frequency of required component examinations from once in 40 years to once during each inspection interval of 10 years. Focuses examination upon all components in one stream of redundant systems rather than a reduced percentage distributed among all streams of the redundant system.	Distributes the required component examinations in one stream of each redundant system among its respective streams, and requires only one examination be completed in 40 years.
W-1976--IWA-1400(1) Owner held responsible to retain all calibration blocks used for ultrasonic examination of components in service.	No responsibility specified.
W-1976--IWB-3500 Flaw evaluation standards extended to cover each Examination Category and replace Section III acceptance standards.	Where flaw evaluation standards are not specified, Section III standards must be applied, which are not always practical.
W-1976-- Added steam generator tube plugging technique for defective tubes.	No rules specified.
1977 Edition--Appendix I now Article 4 of Section V	No effect.
S-1977--IWA-2300 Contains clarification with regard to qualifications of NDE personnel.	
W-1977-- Four types of visual examination defined; V-1, V-2, V-3, V-4; these are specific to particular types of defects. Examination categories B-H and B-K-1 changed to volumetric. Examination categories B-L-1 and B-M-1 changed to volumetric.	Surface or volumetric permitted. Volumetric (surface) as required acceptable.

Examples of positive actions taken through Regulatory Guides or positions in NUREG documents have been cited by Lagleder.<sup>(2.4.3c)</sup> Supplemental surface examinations are required in reactor vessel closure studs per Regulatory Guide 1.65. In Regulatory Guide 1.14, Revision 1, added UT examinations are required on pump flywheels. Regulatory Guide 1.83, Revision 1 in essence replaces the code criteria for steam generator tubing examination and acceptance. NUREG-0312 addresses the concerns of boiling water reactor (BWR) feedwater and control rod drive return line nozzle cracking and recommends enhanced UT. In NUREG-0313, the stress corrosion of BWR austenitic stainless steel primary pressure boundary piping is considered and prescribed an augmented ISI program for plants not conforming to a cited specification.

Example of positive action taken through regulatory bodies or positions in such documents have been cited by Eggleston (2004, 2005). Supplemental to these examinations are required in reaction to the 2003-2004 period performance year 1.02. In regulatory bodies 1.14, version 1, added to examination are required on data (financial regulatory bodies 1.05, version 1 in 2003-2004). The code criteria for the general purpose examination and audit-able, which 2003 address the concept of holding water (BWA) 1.05. In addition, the other, completion of the sufficient standard level per very practice because given its condition and prescribed as suggested 1.01. Issues for plants not complying to a 50% effectiveness.

Switzerland recently introduced an inservice inspection code borrowing from features of ASME XI and the FRG KTA. Baschek<sup>(2.5.1)</sup> reported on this code, discussing similarities and differences to these codes. Table 2.5.1 permits a comparison of these similarities and differences. Some aspects parallel the NRC regulations; for example, consideration of access for ISI at the design stage. There is no specific UT technique explicitly required; however, tandem and single probe are favored. The detail relevant to NDE of ASME Class 2 and 3 systems tends to be more explicit than ASME XI. For example, Class 2 is divided into two categories on the basis of risk. The higher risk is handled like Class 1.

In Japan the status of construction examinations and inservice inspection of nuclear systems appears to have stabilized.<sup>(2.5.2)</sup> The Ministry of Technology and Industry (MITI) has jurisdiction over nuclear power plants under the Electric Utility Industry Law of 1965. Two regulations were developed on the basis of this law; namely,

1. Ordinance No. 81 (MITI) "Technical Requirements for Welding of Electrical Facilities (Nuclear and Non-Nuclear)"
2. Notification No. 501 (MITI) "Technical Requirements for Construction of Pressure Vessels and Other Facilities (Nuclear Only)."

The preceding were strongly influenced by the ASME Codes, differing in stricter RT requirements than in ASME III, V.

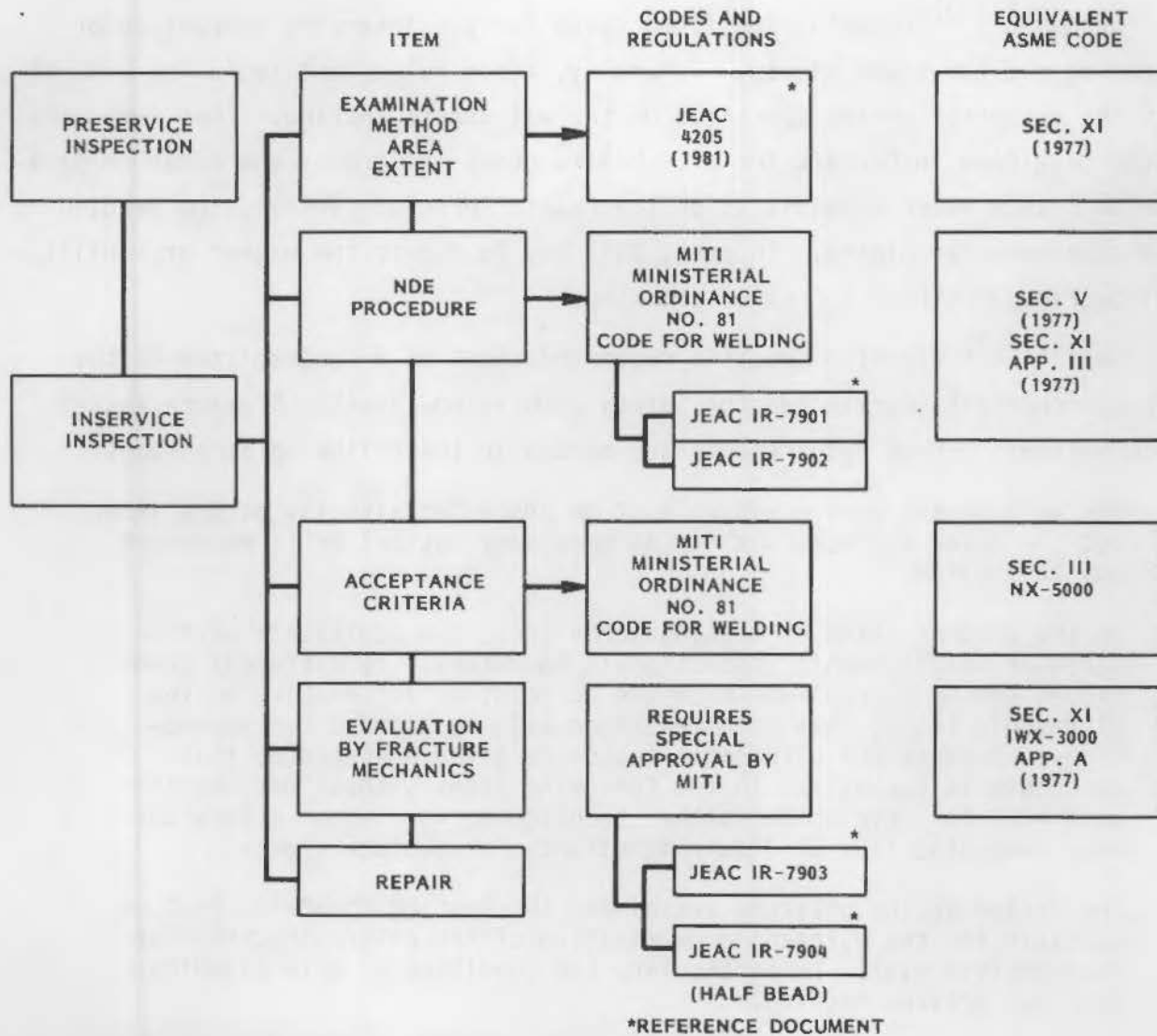
In Japan the MITI codes which govern the design and fabrication of components are still valid in the stage after plant operation as the maintenance criteria.

JEAC-4205, "Inservice Inspection of component for light water nuclear power plant," which specifies the detail of Inservice Inspection program was revised in 1981; and the requirements of ASME Boiler and Pressure Vessel Code, Section XI 1974 Edition (partially 1977), have been incorporated except that the MITI code acceptance criteria of nondestructive examination is applied. The relation between MITI codes and JEAC-4205 is shown in Figure 2.5.1.

TABLE 2.5.1. Comparison of Selected ISI Requirements--Inspection Methods and Areas

Switzerland NE 14, Draft 1	USA ASME XI, 1977 Edition	Germany (FRG) RSK (Draft)/KTA (Draft)
<p>Volumetric Examinations:</p> <ul style="list-style-type: none"> <li>● <u>UT preferred</u> but application of alternative NDT methods possible.</li> <li>● Particular technique not specified.</li> </ul>	<p>Volumetric Examinations:</p> <ul style="list-style-type: none"> <li>● <u>UT, RT and EC listed in the code</u>, but alternative methods possible.</li> <li>● Performance of UT examinations for Class 1 and 2 vessel and piping welds specified.</li> </ul>	<p>Volumetric Examinations:</p> <ul style="list-style-type: none"> <li>● <u>UT for RPV and RCP strongly recommended</u>, but alternative methods possible in certain cases.</li> <li>● <u>Combination of Tandem and single probe technique favored for RPV and RCP.</u></li> </ul>
<p>Surface Examinations:</p> <ul style="list-style-type: none"> <li>● Suitable and approved methods should be used. <u>UT acceptable in special cases.</u></li> </ul>	<p>Surface Examinations:</p> <ul style="list-style-type: none"> <li>● MP and LP examinations, but alternative methods possible.</li> </ul>	<p>Surface Examinations:</p> <ul style="list-style-type: none"> <li>● MP, LP, EC allowed.</li> </ul>
Examination of Welds in Piping Includes Weld Joint		
<p>Plus Y2 T (but min. Y2 in.) on each side of the weld for all examination.</p>	<p>Plus Y2 in. on each side for surface and Y4 in. for volumetric examinations.</p>	<p>Plus 1 T but not more than 2 in. on each side for all examination.</p>





JEAC 4205 "INSERVICE INSPECTIONS OF LWR POWER PLANT COMPONENTS"

FIGURE 2.5.1. Japanese Codes and Regulations for ISI

Evaluation of an indication which exceeds the acceptance criteria of construction codes by fracture mechanics is not allowed without approval of MITI and its advisory committee.

In addition, MITI requires additional examination for special problems. One example is the case of IGSCC of stainless steel piping. A weld joint for which the IGSCC countermeasure is not applied has been ultrasonically examined more frequently than specified in JEAC 4205 with both 45° and 60° transducers to get higher crack detectability and to ensure the integrity.

Sweden<sup>(2.5.3)</sup> recently published rules for the inservice inspection of operating nuclear power plants. Generally, these rules tend to follow ASME XI with the exception of the specifics of the ultrasonic testing. They favor the P-scan developed in Denmark for UT. Unlike codes in Germany and under preparation in France where emphasis is on the reactor pressure vessel, the Swedish code does consider piping. In part, this may be due to the higher probability of intergranular stress corrosion cracking.

Haas<sup>(2.5.4)</sup> reported specific recommendations of a subcommittee of the Reaktorsicherheit (German Reactor Safety Commission--Reactor Pressure Vessel Subcommittee). These requirements are quoted in the following paragraphs:

The wall of the entire vessel must be inspected visually at the inner and the outer surface. As far as necessary optical or TV equipment may be applied.

In the present state of testing techniques, the additional performance of an ultrasonic inspection is mandatory. If different techniques can be introduced which are at least as informative as the ultrasonic tests, this recommendation will be amended correspondingly. Because the ultrasonic tests are given preference, this technique is emphasized in the following items without denying the potential for developing further techniques, for instance eddy current, magnetic flux or liquid penetrants for surface cracks.

The design of the pressure vessel and the testing apparatus must be suitable for the ultrasonic examination of the entire thickness of the complete wall. In particular, the condition of weld cladding must not prevent testing.

As the dose rate of radiation in the vicinity of the pressure vessel at the time of in-service inspections cannot be predicted with sufficient accuracy, the ultrasonic inspection should be carried out by a fairly mechanized system. For regions where the theoretical dose rate of radiation will be low, and where, therefore, tests are usually performed by hand, it must be demonstrated how mechanized remote control testing systems can be made feasible in the case of an unexpected high dose rate prohibiting the presence of testing personnel.

The maximum of testing feasibilities is required, because, with regard to the youth of the technology of the nuclear power industry, operational experience is still not sufficient to provide the essential information for suitable selection of the vessel parts to be tested. Nevertheless, it is intended to apply ultrasonic testing procedures to those vessel parts which appear to be important and

representative according to the present state of knowledge. The areas to be tested could be extended, if future experience should make it desirable.

The process of selecting the parts to be tested in a preliminary state has been based upon the possibilities of hidden defects created by manufacturing or of operational stress. Thus, the following parts are to be tested as a minimum; all butt and nozzle welds, ligaments between the holes for the control rod penetrating the head (PWR) or the bottom (BWR), inner edges of the coolant nozzle holes, bolts and nuts of the flange connection between the head and the vessel.

Ultrasonic tests can be conducted by directing the sonic beam from the inner as well as from the outer vessel surface. Because the testing equipment which is provided for any of these cases can fail, and because it may become necessary to carry out the ultrasonic test from a complementary surface in order to check or interpret indications which might be found within the applied system, it must be demonstrated in what manner such supplementary tests can be made possible at all times after the vessel has been put into service.

The testing procedure has to be suitable, in order to be able to detect free crack surfaces in the interior of the vessel wall which are oriented vertically to the essential stress directions. This means, for a large part of the region to be tested, that the ultrasonic beam has to be directed perpendicularly to these crack faces or that a tandem or pitch and catch technique has to be applied. In order to find cracks which are located close to the vessel surface, the use of effective angular reflections may be applied. Testing with a single probe technique which cannot fulfill one of these conditions for the beam directions is only acceptable if a more suitable technique is not feasible.

The transfer losses in the entire testing area and for each sonic beam path are to be determined and accounted for as much as is feasible. If the coupling is not secured by immersion technique, it must be monitored continuously.

The sensitivity calibration depends upon the methods which are applied in the individual case and the conditions in the testing area. Therefore, requirements for the testing sensitivity have to be defined on a case-by-case basis. However, the following conditions and rules should be met.

If the ultrasonic beam can be directed vertically to the expected crack surfaces or if the tandem or pitch and catch technique is applied with regard to the expected crack orientation, the level for flaw registration has to be set 6 dB lower than the echo level of an

equally oriented circular reflector of 10 mm dia. These conditions have to be met at each point of the beam cross-section which is being applied.

If only a single probe technique is applied, the effect of angular reflection cannot be used, and the direction of the beam is not perpendicular to the surface of the expected defect; therefore a higher sensitivity must be calibrated. Circular reflectors with a diameter of 3 mm which may be oriented vertically to the main beam determine the registration limit to potential flaw echoes. This condition must be met at each point of the beam cross-section which is used in the tests.

For different techniques, the required sensitivity calibration has to be determined by experiments. If in this manner only tests with a relatively low sensitivity can be conducted, then the intervals between these tests have to be correspondingly small.

Engl and Elsner<sup>(2.5.5)</sup> compared the FRG requirements for ISI with those of ASME XI. This paper tends to update the comments of Haas<sup>(2.5.4)</sup> by incorporating items covered in the draft version of KTA-3201.4. Emphasis is on the examination of the reactor pressure vessel with little attention given to piping. There is a preference for the tandem UT technique for welds with sufficient accessibility because of enhanced reliability of detection of planar defects. Figure 2.5.2 compares ISI by the FRG requirements to ASME XI. An examination of this paper highlights the basic differences in ISI philosophy between FRG and U.S. An obvious example being the FRG requirement for access to an NDE from both inner and outer surfaces of the pressure vessel.

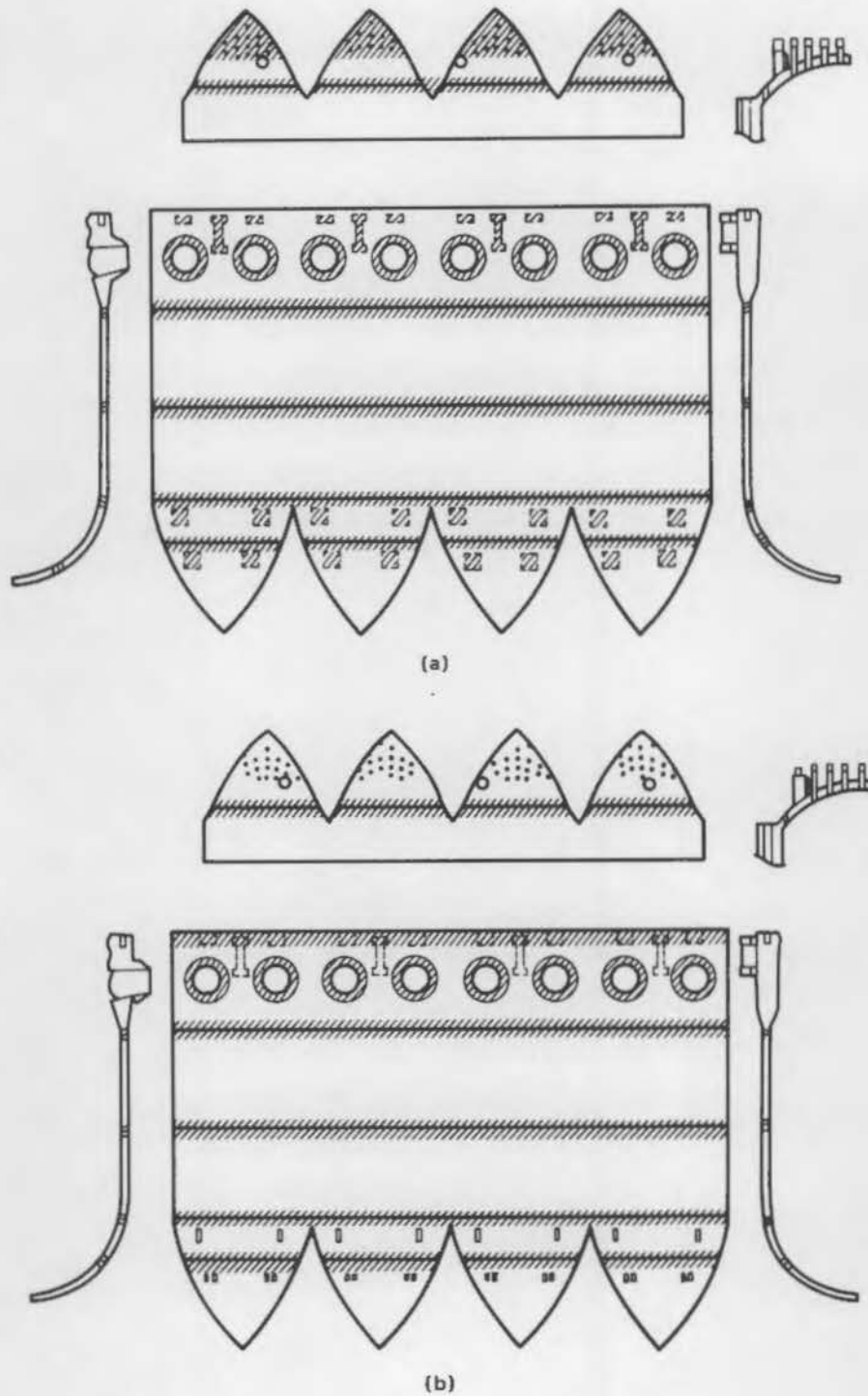


FIGURE 2.5.2. Scope of Inservice Inspection (a) in Germany and (b) to ASME XI

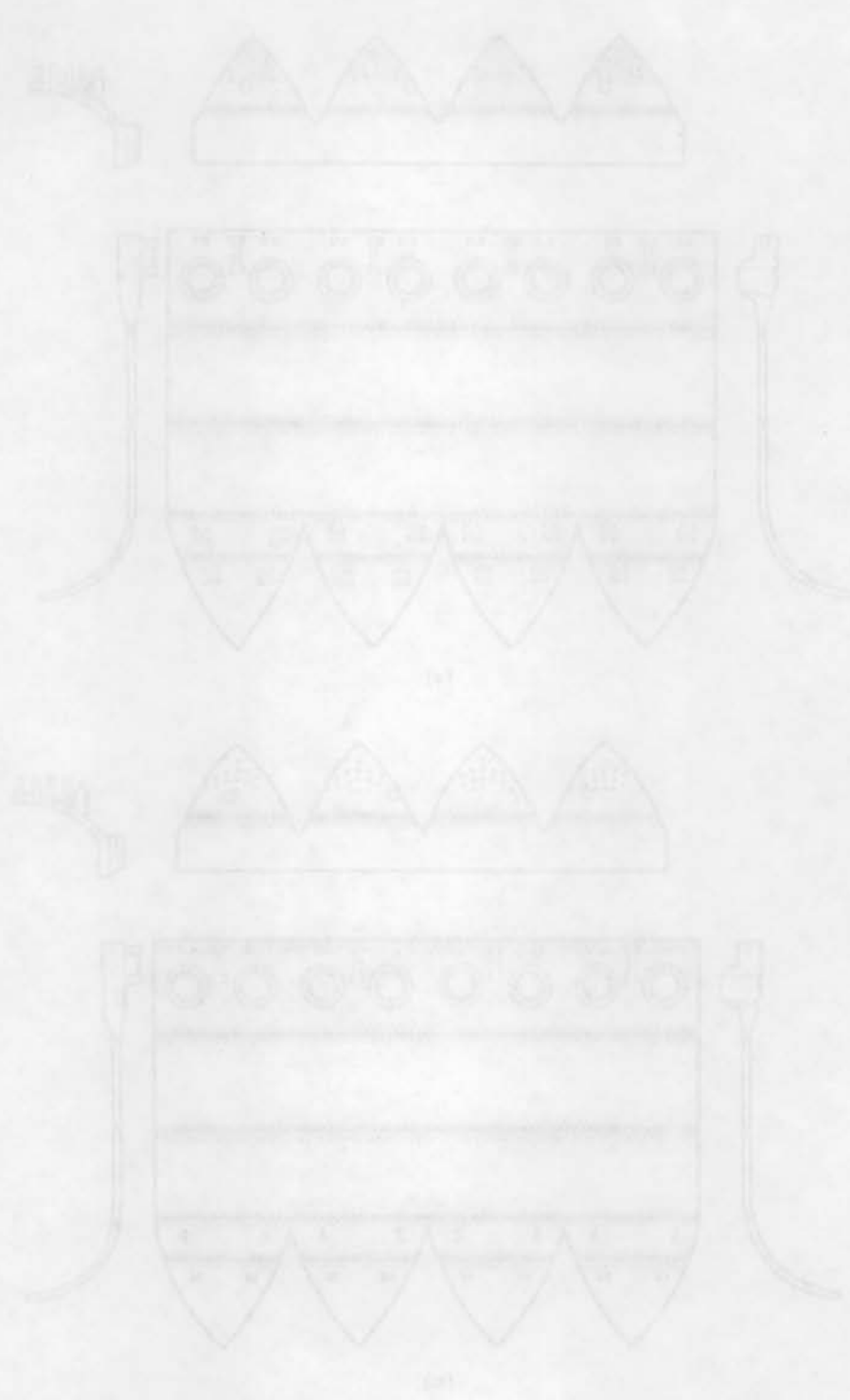


Figure 5.212. Scales of insecticide injection (a) in Germany and (b) in USA.

Major differences in NDE philosophy exist between the ASME XI Code and the FRG HP 5/3 Code. These differences have been discussed in this chapter. It appears that the principal difference is in the acceptance/rejection thresholds for indications rather than in the detection of flaws.

Major differences between the two topography exist between the two 1700 and the 1800. These differences have been observed in this chapter. It appears that the prime difference is in the amount of vegetation for the two periods rather than in the location of the



- 2.1.1 "Compilation and Comparative Examination of Existing Guidelines and Specifications for the Design, Fabrication, Testing, and Inspection of Steel Pressure Vessels for Reactors—Final Report." GERRSR-21 (Vol. 2), General Electric Corporation, originally EUR-5402d (Vol. 2), December 1974.
- 2.1.2 "Compilation and Comparative Examination of Existing Guidelines and Specifications for the Design, Fabrication, Testing, and Inspection of Steel Pressure Vessels for Reactors—Final Report." GERRSR-21 (Vol. 3), General Electric Corporation, originally EUR-5402d (Vol. 3), December 1974.
- 2.1.3 "Nuclear Power Plant Components," ASME Section III, Division 1, 1977 Edition.
- 2.1.4 "Non-Destructive Examination," ASME Section V, 1977 Edition.
- 2.1.5 "Rules for In-Service Inspection of Nuclear Power Plant Components," ASME Section XI, Division 1, 1977 Edition.
- 2.2.1a Takahashi, H., "Regulations on ISI in Japan." Use of Non-Destructive Testing Techniques for In-Service Inspection of Reactor Pressure Components, IWG-RRPC-78/3, International Atomic Energy Agency, International Working Group on Reliability of Reactor Pressure Components, Kobe, Japan, pp. 4-7, April 25-27, 1977,
- 2.2.1b Theiretzbacher, H., "Regulations for ISI of Reactor Pressure Vessels in Austria." Use of Non-Destructive Testing Techniques for In-Service Inspection of Reactor Pressure Components, IWG-RRPC-78/3, International Atomic Energy Agency, International Working Group on Reliability of Reactor Pressure Components, Kobe, Japan, pp. 7-11, April 25-27, 1977.
- 2.2.1c Bashek, H., "ISI of Reactor Pressure Components in Switzerland." Use of Non-Destructive Testing Techniques for In-Service Inspection of Reactor Pressure Components, IWG-RRPC-78/3, International Atomic Energy Agency, International Working Group on Reliability of Reactor Pressure Components, Kobe, Japan, pp. 11-22, April 25-27, 1977.
- 2.2.1d Chockie, L. J., "ASME Section XI." Use of Non-Destructive Testing Techniques for In-Service Inspection of Reactor Pressure Components, IWG-RRPC-78/3, International Atomic Energy Agency, International Working Group on Reliability of Reactor Pressure Components, Kobe, Japan, pp. 23-33, April 25-27, 1977.

- 2.2.1e Prot, A. C. and Saglio, R., "Survey of the French Developments in the Field of ISI." Use of Nondestructive Testing Techniques for Inservice Inspection of Reactor Pressure Components, IWG-RRPC-78/3, International Atomic Energy Agency, International Working Group on Reliability of Reactor Pressure Components, Kobe, Japan, pp. 38-62, April 25-27, 1977.
- 2.2.1f Cioli, F. and Messore, G., "Italian Experience on NDT Techniques for ISI of Reactor Pressure Components." Use of Non-Destructive Testing Techniques for In-Service Inspection of Reactor Pressure Components, IWG-RRPC-78/3, International Atomic Energy Agency, International Working Group on Reliability of Reactor Pressure Components, Kobe, Japan, pp. 62-63, April 25-27, 1977.
- 2.2.2 Watkins, B., Swithenbank, T. and Jackson, H., "Experiences in the Pre-service and Inservice Inspection of Light Water Reactors." Periodic Inspection of Pressurized Components, Institute of Mechanical Engineers, London, England, pp. 118-128, 1974.
- 2.2.3 Kothare, V. V. and Nanjundeswaran, K., "In-Service Inspection of Tarapur Units No. 1 and No. 2 Reactor Pressure Vessels and Primary Coolant Pressure Boundary." Periodic Inspection of Pressurized Components, Institute of Mechanical Engineers, London, England, pp. 157-164, 1976.
- 2.2.4 Lautzenheiser, C. E., "In-Service Inspection of Nuclear Power-Plant Pressure Components." Nucl. Saf. 17(6):133-143, November-December 1976.
- 2.2.5 "IAEA Safety Guide on In-Service Inspection." International Atomic Energy Agency, Draft Copy, September 9, 1976.
- 2.2.6 Meyer, H. J., "Relation Between Ultrasonic Indications and Flaw Size in Pressure Vessel Welds." NDE Conference, Babcock and Wilcox/Technischen Überwachungs Verein e.V., Rheinland Westphalia, Washington, D.C., November 18, 1976.
- 2.2.7 Meyer, H. J., "Probability of Detecting Planar Defects in Heavy Wall Welds by Ultrasonic Techniques According to Existing Codes." Report to Subcommittee V (Ultrasonics) of Commission V, International Institute of Welding on Quantitative Evaluation of UT Indication, 1977.
- 2.3.1 Trumpfheller, R., "The Sizes of the Largest Defects Which may be Overlooked by Non-Destructive Testing Methods in Germany." Technischen Überwachungs Verein e.V., Rheinland Westphalia, Essen, Germany, Translated ABH, April 11, 1972.
- 2.3.2 Trumpfheller, R., "Requirements for In-Service Inspection of Water-Cooled Reactor Vessels by Non-Destructive Testing Methods in Germany." Periodic Inspection of Pressurized Components, Institute of Mechanical Engineers, London, England, pp. 114-117, 1974.

- 2.3.3 Taylor, T. T. and Selby, G. P., "Evaluation of ASME Section XI Reference Level Sensitivity for Initiation of Ultrasonic Inspection Examination." NUREG/CR-1957, U.S. Nuclear Regulatory Commission, Washington, D.C., 1981. Also PNL-3692, Pacific Northwest Laboratory, Richland, Washington, 1981.
- 2.4.1 Code of Federal Regulations (U.S.), Title 10 (Energy), Part 50.55(a), Codes and Standards of Part 50—Licensing of Production and Utilization Facilities, Effective May 24, 1978.
- 2.4.2 Minutes Special Meeting of ASME Subcommittee on "Nuclear In-Service Inspection and U.S. Nuclear Regulatory Commission," October 11, 1977.
- 2.4.3a Beverly, R. L., "Review of ASME Section XI Codes: 1974 Edition Through the Winter 1977 Addenda." Nuclear Power Education Seminar, Southwest Research Institute, San Antonio, Texas, April 17-21, 1978.
- 2.4.3b Beverly, R. L., "The Impact of the Upgrade Criterion on Access Design Review Programs." Nuclear Power Education Seminar, Southwest Research Institute, San Antonio, Texas, pp. C-1 to C-4, April 17-21, 1978.
- 2.4.3c Lagleder, G. L., "The Effect of Codes and Regulatory Changes on Pre-service and Inservice Examinations." Nuclear Power Education Seminar, Southwest Research Institute, San Antonio, Texas, April 17-21, 1978.
- 2.5.1 Baschek, H., "Requirements for Inservice Inspection in Switzerland and Their Comparisons with the Requirements in Other Countries Under Particular Consideration of ASME Code Section XI." NDE in the Nuclear Industry, American Society for Metals, pp. 271-280, 1980.
- 2.5.2 Ando, Y., "Non-Destructive Examination Relating to Structural Integrity of Light Water Nuclear Power Plants; Recent Trend in Japan." Post Structural Materials in Reactor Technology Conference, Paris, France, August 1981.
- 2.5.3 "Regler För Återkommande Besiktning Och Provning I Kärnkraft-Anläggningar." 1981-04-01, (Rules for Inservice Inspection of Nuclear Power Plants), Sweden, April 1, 1981.
- 2.5.4 Haas, B., "Discussion re. Requirements of German Reactor Safety Commission (RKS) by Reactor Pressure Vessels Subcommittee." Periodic Inspection of Pressure Vessels, Institute of Mechanical Engineers, London, England, pp. 241-242, 1972.
- 2.5.5 Engl, G. O. and Elsner, H. J., "Comparison of Requirements for Inservice Inspection in Germany with Section XI, ASME, BAPV Code." NDE in the Nuclear Industry, American Society for Metals, 1980.

- 2.4.1 Taylor, T. J. and Selby, G. P., "Evaluation of RBE for the induction of dicentric chromosomes in lymphocytes by ultraviolet radiation", *Journal of Cellular Biochemistry*, 1991, 41: 1-10.
- 2.4.2 Taylor, T. J. and Selby, G. P., "Evaluation of RBE for the induction of dicentric chromosomes in lymphocytes by ultraviolet radiation", *Journal of Cellular Biochemistry*, 1991, 41: 1-10.
- 2.4.3 Taylor, T. J. and Selby, G. P., "Evaluation of RBE for the induction of dicentric chromosomes in lymphocytes by ultraviolet radiation", *Journal of Cellular Biochemistry*, 1991, 41: 1-10.
- 2.4.4 Taylor, T. J. and Selby, G. P., "Evaluation of RBE for the induction of dicentric chromosomes in lymphocytes by ultraviolet radiation", *Journal of Cellular Biochemistry*, 1991, 41: 1-10.
- 2.4.5 Taylor, T. J. and Selby, G. P., "Evaluation of RBE for the induction of dicentric chromosomes in lymphocytes by ultraviolet radiation", *Journal of Cellular Biochemistry*, 1991, 41: 1-10.
- 2.4.6 Taylor, T. J. and Selby, G. P., "Evaluation of RBE for the induction of dicentric chromosomes in lymphocytes by ultraviolet radiation", *Journal of Cellular Biochemistry*, 1991, 41: 1-10.
- 2.4.7 Taylor, T. J. and Selby, G. P., "Evaluation of RBE for the induction of dicentric chromosomes in lymphocytes by ultraviolet radiation", *Journal of Cellular Biochemistry*, 1991, 41: 1-10.
- 2.4.8 Taylor, T. J. and Selby, G. P., "Evaluation of RBE for the induction of dicentric chromosomes in lymphocytes by ultraviolet radiation", *Journal of Cellular Biochemistry*, 1991, 41: 1-10.
- 2.4.9 Taylor, T. J. and Selby, G. P., "Evaluation of RBE for the induction of dicentric chromosomes in lymphocytes by ultraviolet radiation", *Journal of Cellular Biochemistry*, 1991, 41: 1-10.
- 2.4.10 Taylor, T. J. and Selby, G. P., "Evaluation of RBE for the induction of dicentric chromosomes in lymphocytes by ultraviolet radiation", *Journal of Cellular Biochemistry*, 1991, 41: 1-10.

CHAPTER 3

DETECTION, LOCATION AND SIZING

(The Pressure Vessel Research Committee Program)

CHAPTER 3

THE STATE OF TEXAS

(The State of Texas is a state of the United States of America.)

## CONTENTS

3.1	INTRODUCTION . . . . .	3.1.1
3.1.1	ACRS Letter . . . . .	3.1.1
3.1.2	AEC Concerns . . . . .	3.1.2
3.1.3	Heavy-Section Steel Technology and Industry Cooperative Program Projects Relevant to NDE . . . . .	3.1.3
3.1.3.1	Project 3: Effects of Process Variables on Mechanical Properties . . . . .	3.1.3
3.1.3.2	Project 8: Development of Improved Ultrasonic Testing of Weldments . . . . .	3.1.3
3.1.3.3	Project 9: Development of Ultrasonic Techniques for Inspecting Vessels in Service . . . . .	3.1.4
3.1.3.4	Project 10: Evaluation and Development of Advanced Concepts in Nondestructive Testing of Pressure Vessels in Service . . . . .	3.1.4
3.1.3.5	ICP-PVRC NDE Programs . . . . .	3.1.4
3.2	STATUS OF EARLY PVRC TESTS . . . . .	3.2.1
3.2.1	Early Period . . . . .	3.2.1
3.2.2	New UT Procedures . . . . .	3.2.1
3.2.3	PVRC Specimen 201 . . . . .	3.2.4
3.2.4	PVRC Specimen 251J . . . . .	3.2.6
3.2.4.1	Acoustic Holography . . . . .	3.2.19
3.2.4.2	Statistical Evaluation . . . . .	3.2.19
3.2.4.3	Conclusions--251J . . . . .	3.2.22
3.3	RECENT PVRC PROGRAMS . . . . .	3.3.1
3.3.1	PVRC Specimen 155 . . . . .	3.3.2
3.3.2	PVRC Specimen 202 . . . . .	3.3.6
3.3.3	PVRC Specimen 203 . . . . .	3.3.13

3.4	COMPARISONS . . . . .	3.4.1
3.5	THE EUROPEAN PLATE INSPECTION STEERING COMMITTEE PROGRAM . . . . .	3.5.1
3.5.1	PVRC (PISC) Specimen 50-52 . . . . .	3.5.5
3.5.2	PVRC (PISC) Specimen 51-53 . . . . .	3.5.8
3.5.3	PVRC (PISC) Plate 204 . . . . .	3.5.10
3.5.4	Information Relevant to All Three Plates . . . . .	3.5.11
3.5.5	Conclusions and Recommendations . . . . .	3.5.25
3.6	GENERAL CONCLUSIONS . . . . .	3.6.1
3.7	REFERENCES . . . . .	3.7.1



FIGURES

3.2.1	PVRC Plate-Weld Specimen 201 . . . . .	3.2.5
3.2.2	Nondestructive Examination of PVRC Plate-Weld Specimen 201 . . . . .	3.2.9
3.2.3	PVRC Specimen 251J . . . . .	3.2.14
3.2.4	Nondestructive Examinations of PVRC Plate-Weld Specimen 251J . . . . .	3.2.18
3.3.1	PVRC Weld Specimen 155 . . . . .	3.3.2
3.3.2	Summary Drawing of Radiographic Results on PVRC Specimen 155 . . . . .	3.3.5
3.3.3	Discontinuity Locations in PVRC Specimen 202 . . . . .	3.3.6
3.3.4	Summary Drawing of Radiographic Results on PVRC Specimen 202 . . . . .	3.3.11
3.3.5	Graphical Representation of PVRC 202 Block Data After Coincidence Analysis . . . . .	3.3.12
3.3.6	PVRC Weld Specimen 203 . . . . .	3.3.13
3.3.7	Discontinuity Locations in PVRC Specimen 203 . . . . .	3.3.17
3.3.8	Summary Drawing of Radiographic Results on PVRC Specimen 203 . . . . .	3.3.18
3.5.1	PVRC Weld Specimen 50-52 . . . . .	3.5.2
3.5.2	PVRC Weld Specimen 51-53 . . . . .	3.5.2
3.5.3	PVRC Weld Specimen 204 . . . . .	3.5.3
3.5.4	Plate 50-52 Defect Number 1, Application of Full ASME XI IWB-3000 Proximity Rules and PISC Procedures . . . . .	3.5.6
3.5.5	Plate 50-52 Defect Number 1, Full ASME XI Proximity Rules Applied . . . . .	3.5.7
3.5.6	Defect Detection Probability for Defect Number 2 in Plate 50-52 as a Function of the Tolerance in Detection-Location of the Defect . . . . .	3.5.8
3.5.7	Full ASME XI Proximity Rules Applied to Plate 51-53 for Defect Number 1 . . . . .	3.5.9

3.5.8	Percentage DAC as a Function of the Sizing Quality . . . . .	3.5.13
3.5.9	Estimated Defect Size as a Function of Actual Defect Size . . . . .	3.5.14
3.5.10	DDP as a Function of Actual Defect Size; PISC UT Procedure Used . . . . .	3.5.15
3.5.11	DDP as a Function of Actual Defect Size; Alternative UT Procedures Used . . . . .	3.5.16
3.5.12	CRP as a Function of the Actual Defect Size; PISC UT Procedure Used . . . . .	3.5.17
3.5.13	CRP as a Function of the Actual Defect Size; Alternative UT Procedures Used . . . . .	3.5.17
3.5.14	Acceptable and Unacceptable Defects Based on ASME XI IWB-3500 Criteria . . . . .	3.5.18
3.5.15	Correlation Between Quality of Sizing and DDP . . . . .	3.5.19
3.5.16	Average $\overline{DDP}$ as a Function of the Defect Position in Plate Thickness . . . . .	3.5.20
3.5.17	Average Cumulative Diagrams of Defect Detection and Correct Rejection or Acceptance as a Function of the Defect Categories a, b, c, d . . . . .	3.5.25

TABLES

3.2.1	PVRC-ICP Test Block Descriptions . . . . .	3.2.2
3.2.2	Estimates of Present Status of Various PVRC Plate-Weld Samples . . . . .	3.2.3
3.2.3	Ultrasonic Testing Procedure . . . . .	3.2.4
3.2.4	Nondestructive Examination of PVRC Plate-Weld Specimen 201 . . . . .	3.2.7
3.2.5	Comparison of Detection of Defects in Clad PVRC Block 201 . . . . .	3.2.9
3.2.6	Variability of Results on Specimen 201 . . . . .	3.2.11
3.2.7a	Nondestructive Examination of PVRC Plate-Weld Specimen 251J . . . . .	3.2.15
3.2.7b	Nondestructive Examination (RT) of PVRC Plate-Weld Specimen 251J . . . . .	3.2.17
3.2.8	Acoustic Holography Examination from Unclad Side on Clad Plate . . . . .	3.2.20
3.2.9	Comparisons of Examination Results for Plates 201 and 251J, Means $\bar{X}$ and Standard Deviations . . . . .	3.2.21
3.2.10	Analysis of Plate 251J Using Criterion of Relative Flaw Significance; Comparison Limited to Ultrasonic Testing . . . . .	3.2.23
3.2.11	PVRC Plate 251J Ratios of Effectiveness of Detection . . . . .	3.2.25
3.3.1	Team Rating Factors, Specimen 155 . . . . .	3.3.4
3.3.2	Summary of Ultrasonic Examination Results, PVRC Specimen 202 . . . . .	3.3.7
3.3.3	Team Rating Factors, Specimen 202 . . . . .	3.3.8
3.3.4	Presumed Locations of Flaws in PVRC Plate-Weld Specimen 202 . . . . .	3.3.9
3.3.5	Radiographic Indications in Block No. 202 . . . . .	3.3.10
3.3.6	Summary of Ultrasonic Examination Results, PVRC Specimen 203 . . . . .	3.3.14
3.3.7	Team Rating Factors, Specimen 203 . . . . .	3.3.15

3.3.8	Comparison of Intended Flaw Locations in PVRC Specimen 203 with Radiographs . . . . .	3.3.16
3.4.1	Comparison of Rating Factors Achieved by Different UT Examination Procedures on PVRC Specimens . . . . .	3.4.2
3.4.2	Comparisons of the Two Methods of Analyses on PVRC Specimens 155, 202 and 203 . . . . .	3.4.3
3.5.1	Main Parameters Considered in the Evaluation of PVRC Plates 50-52, 51-53 and 204 . . . . .	3.5.4
3.5.2	Effect of Subdividing Defect 1 in Plate 51-53 into a Set of Eight Defects . . . . .	3.5.10
3.5.3	Acceptable Defects--PISC Procedure . . . . .	3.5.21
3.5.4	Rejectable Defects--PISC Procedure . . . . .	3.5.22
3.5.5	Acceptable Defects--Alternative Procedures . . . . .	3.5.23
3.5.6	Rejectable Defects--Alternative Procedures . . . . .	3.5.24

## CHAPTER 3

### DETECTION, LOCATION AND SIZING

#### (The Pressure Vessel Research Committee Program)

### 3.1

#### INTRODUCTION

The Advisory Committee on Reactor Safeguards (ACRS) wrote a letter dated November 24, 1965<sup>(3.1.1)</sup> recommending that work be done to reduce still further the probability of reactor pressure vessel failure. The text follows:

#### 3.1.1 ACRS Letter

##### Text of ACRS Letter to Atomic Energy Commission

Dear Dr. Seaborg:

The design of pressurized and boiling water nuclear power plants has undergone many improvements with regard to safety, improvements which markedly reduce the risk of significant radiation exposure to the public in the unlikely event of certain accidents or system failures in such reactors.

There is a facet of current pressurized and boiling water reactor design practice which should be recognized, however. Containment design is generally predicted on the basis that a sudden, large scale rupture of the reactor pressure vessel or its closure is incredible. Reactor designers have supported this view by detailing the extreme care to be taken in design, fabrication, and inspection of a vessel, and by specifying pressurization only at temperatures above the nil ductility transition temperature. They further cite the excellent record for large pressure vessels which comply with the ASME Boiler and Pressure Vessel Code.

The Committee believes, with the industry, that the probability of a sudden major pressure vessel failure leading to breaching the containment is very low. Nevertheless, it seems desirable and possible to make some provisions in future designs against this very unlikely accident.

1. To reduce further the already small probability of pressure vessel failure, the Committee suggests that the industry and the AEC give still further attention to methods and details of stress analysis, to the development and implementation of improved methods of inspection during fabrication and vessel service life, and to the

improvement of means for evaluating the factors that may affect the nil ductility transition temperature and the propagation of flaws during vessel life.

2. The ACRS also recommends that means be developed to ameliorate the consequences of a major pressure vessel rupture. Some possible approaches include:

- a) Design to cope with pressure buildup in the containment and to assure that no internally generated missile can breach the containment.
- b) Provide adequate core cooling or flooding which will function reliably in spite of vessel movement and rupture.
- c) If breaching the containment cannot be precluded, provide other means of preventing uncontrolled releases of large quantities of radioactivity to the atmosphere.

In view of the very small probability of pressure vessel rupture the Committee reconfirms its belief that no undue hazard to the health and safety of the public exists, but suggests that the orderly growth of the industry with concomitant increase in number, size, power level, and proximity of nuclear power reactors to large population centers will in the future make desirable, even prudent, incorporating in many reactors the design approaches whose development is recommended above.

Sincerely yours,

/s/W. D. Manly

### 3.1.2 AEC Concerns

The concerns in the above letter together with others cited by the AEC can be written as the six questions:

1. What are the properties of and how effective are inspection techniques for heavy-section steels?
2. What effect does the variation of properties and flaws have on the behavior of vessels fabricated of heavy-section steels?
3. How effective are currently used inspection techniques and what new inspection techniques may be applied to weldments and fabrication of vessels fabricated of heavy-section steels?

4. What inspection and surveillance techniques may be effectively applied to vessels in service?
5. How effective is the enforcement of ASME Boiler and Pressure Vessel Section III requirements?
6. What control does the owner or his representative (Nuclear Engineer) exercise over the materials, fabrication, and installation of the reactor vessels?

### 3.1.3 Heavy-Section Steel Technology (HSST) and Industry Cooperative Program (ICP) Projects Relevant to NDE

The response to generating answers to these questions was twofold. The AEC funded the HSST Program managed by Oak Ridge National Laboratory (ORNL). Industry funded an ICP which was directed and managed by PVRC.

The HSST program concentrated on material testing and analytic studies in 12 tasks, whereas the ICP work was divided into 10 projects. Project 3, in part, and projects 8 through 10 dealt specifically with nondestructive examination. The original scopes are given below. Obviously, neither the time nor cost schedules should be considered as representative since the programs are still underway.

#### 3.1.3.1 Project 3: Effects of Process Variables on Mechanical Properties

The effects of process variables on the mechanical properties of heavy-section steels 10 to 12 in. thick will be studied. Included in this project are studies of the "scatter" of test data, variation of properties at different locations in the plate, effect of rolling reduction ratio, property dependence on heat treatment, and identification of discontinuities detected by nondestructive inspection. Estimated cost: \$833,000. Estimated schedule: 30 months.

#### 3.1.3.2 Project 8: Development of Improved Ultrasonic Testing of Weldments

Ultrasonic testing is currently employed to inspect welds in many applications; however, the equipment and techniques have not been generally accepted because of the inability to detect, define, and interpret indications. A

sophisticated method will be developed for the ultrasonic inspection of weldments. It is proposed that the weld be automatically scanned and the resultant ultrasonic data be fed into a computer which will analyze it and provide a readout of exact flaw size and location. The equipment will also mark the location of the flaw on the piece being tested. Many practical problems must be resolved before such a system can be developed. Estimated cost: \$267,000. Estimated schedule: 42 months.

#### 3.1.3.3 Project 9: Development of Ultrasonic Techniques for Inspecting Vessels in Service

Two methods are proposed for inspecting reactor vessels in service utilizing conventional ultrasonic testing techniques. Although both methods now seem feasible, many problems must be resolved before a satisfactory technique can be developed and demonstrated. One technique involves designing and building a complex positioner and recording device for immersion testing from inside the vessel; the other presupposes that inspection of 100% of the vessel will not be required and that all critical areas can be identified and monitored by ultrasonic transducers permanently affixed to the outside of the vessel. Estimated cost: \$478,000. Estimated schedule: 36 months.

#### 3.1.3.4 Project 10: Evaluation and Development of Advanced Concepts in Nondestructive Testing of Pressure Vessels in Service

Ultrasonic testing, utilizing conventional techniques, is being proposed as a promising method for inspecting vessels in service; however, other more sophisticated advanced concepts are in various stages of development. Their applicability will be investigated and appropriate development work will be performed to culminate in a satisfactory system for evaluating reactor vessels in service. Estimated cost: \$819,000. Estimated schedule: 48 months.

#### 3.1.3.5 ICP-PVRC NDE Programs

The ICP-PVRC NDE programs can be divided into a series of progressive plateaus, each of which will be discussed more fully later. The plateaus can be summarized as follows:



- round-robin ultrasonic or radiographic examination of weldments containing natural flaws using the operators own equipment and procedures
- UT or RT examinations to one specific set of procedures which forbade certain techniques and limited type of equipment
- UT examination through weld overlay clad to existing procedures, but with no provisions for internal calibration of weldment
- improved UT examination through weld overlay clad to existing procedures plus provisions for internal calibration
- use of advanced techniques (acoustic holography, etc.) for evaluation of flaws in weldments
- statistical evaluation of round-robin data using assumed flaw sizes and locations
- sectioning of weldments and correlation of actual flaw sizes and locations with values determined by NDE.



Several plates of various thickness were butt-welded, with measures taken to introduce a spectrum of weld defects (porosity, slag, lack-of-fusion, cracking). Additionally, nozzles were welded into plates with defects introduced into the weldment. These weldments are summarized in Table 3.2.1. The current status of programs on each weldment studied or under study is given in Table 3.2.2.

### 3.2.1 Early Period

During the period 1967 to 1968, four butt-welds and four nozzle-welds containing defects were examined, usually by five teams from different organizations. These teams had the option of using their own examination procedures or using ASME Section III, Appendix 9. It soon became apparent that some degree of standardization was required to permit a comparison of the data; therefore, the reporting level was set at 25% Distance Amplitude Correction (DAC), the specific angle-beam transfer method was recognized, and one couplant, glycerine, was selected. Even with these variables set, virtually no agreement was found among the teams. As a result of this lack of agreement, steps were taken to control the following parameters:

- transfer method
- half- or full-node technique
- depth measurement technique
- instrument and transducer variables
- gain multiple for scanning sensitivity
- dual transducer techniques
- personnel.

### 3.2.2 New UT Procedures

The control of these parameters was obtained through a series of revisions to the so-called "old PVRC Testing Procedure."<sup>(3.2.1)</sup> The differences are compared in Table 3.2.3.

Changes continued culminating in two articles published in Welding Research Bulletin 235<sup>(3.2.2)</sup> in 1978:

TABLE 3.2.1. PVRC-ICP Test Block Descriptions

<u>Identity</u>	<u>Fabricator</u>	<u>Approximate Thickness</u>	<u>Type of Weld</u>	<u>Intended Flaws</u>
50 - 52	Babcock & Wilcox	11 in. (27 cm)	Butt-weld, ES	Gross cracks
51 - 53	Babcock & Wilcox	8 in. (20 cm)	Butt-weld, sub arc	Gross cracks
155	Babcock & Wilcox	8-3/4 in. (22 cm)	18 in. (45 cm) forged nozzle sub arc with cladding	4, all cracks
156	Babcock & Wilcox	5 in. (13 cm)	18 in. (45 cm) cast nozzle sub arc	3, areas of flaws of varied sizes
201	Chicago Bridge & Iron	8 in. (20 cm)	Butt-weld	10, varied types
202	Chicago Bridge & Iron	8 in. (20 cm)	Butt-weld manual metal with cladding	9, varied types
203	Chicago Bridge & Iron	8 in. (20 cm)	21 in. (54 cm) forged nozzle manual metal arc	9, varied types
204	Chicago Bridge & Iron	8 in. (20 cm)	18 in. (45 cm) forged nozzle manual metal arc	9, varied types
251-J	Combustion Engineering	11 in. (27 cm)	Butt-weld sub arc	15, varied types
252-J	Combustion Engineering	8 in. (20 cm)	Butt-weld elec- troslag	3, areas of flaws of varied types
253-J	Combustion Engineering	11 in. (27 cm)	24 in. (60 cm) forged nozzle sub arc	20, varied types
254-J	Combustion Engineering	10 in. (25 cm)	17 in. (43 cm) forged nozzle sub arc	25, varied types

TABLE 3.2.2. Estimates of Present Status of Various PVRC Plate-Weld Samples (1981)

Weld Specimen Number	Size and Type (in.)	Ultrasonic and Radiographic Examination	Analysis of UT, RT	Sectioning
201	8.5-in.-thick butt-welded flat plate	Completed by 5 UT participants + 6 radiographic + 2 special techniques	Unclad section Reference 3.2.1 clad section Reference 3.2.7	Completed Reference 3.2.7
251J	11-in.-thick x 36 x 50 1/2 butt-welded flat plate	Completed by 6 UT participants + 7 radiographic + special techniques	Completed and published Reference 3.2.6	Completed; reports to sub-committee
202	8-5/16 x 24 x 34.6 butt-welded flat plate	Completed UT, RT special techniques	Reference 3.3.1 - 3.3.2	To JPVRC
155	8-5/8 x 39-7/8 x 10-1/4 curved plate with 18-7/8 OD and 9-13/16 ID nozzle welded in	Completed UT, RT	Reference 3.3.1 - 3.3.2	To EPRI
203	8-5/16 x 48 x 48 20.8 OD and 11.4 ID nozzle welded in	Completed UT, RT	Reference 3.3.1 - 3.3.2	To JPVRC
204	8-5/16 x 40 x 40 18 OD and 6 ID nozzle welded in	Completed	See PISC	Reference 3.5.1 - 3.5.6
50 - 52	11 x 36.5 x 55.25 butt-weld flat plate	Completed	See PISC	Reference 3.5.1 - 3.5.6
51 - 53	8 x 36 x 40.75 butt-welded flat plate	Completed	See PISC	Reference 3.5.1 - 3.5.6

TABLE 3.2.3. Ultrasonic Testing Procedure (PVRC)

Parameter	Old	New
Specifies Couplant	No	Yes
Transducer Limited to One Type and Heat	No	Yes
Instruments Standardized	No	Yes
75% Response of Test Block for Both Angled and Straight Beam	No	Yes
Transfer Methods Used	Yes	Only 1:1
Scanning Gain Setting	2 x Sensitivity	> 10 x Sensitivity
Records	All > 25% DAC	All > 10% DAC

"Improved Repeatability in Ultrasonic Examination" and "Ultrasonic Testing System Standardization Requirements." Additionally, ASME Section XI<sup>(3.2.3)</sup> developed Mandatory Appendices I and III for UT examination of pressure vessels and piping. Subsequently, Appendix I was transferred to ASME Section V.<sup>(3.2.4)</sup>

The period 1967 to 1968 resulted in what has been defined as the first plateau where virtually no consistency of results was observed from team to team due to a lack of control over procedures. Achievement of better results denoted as higher plateaus will be discussed under the specific PVRC specimens.

### 3.2.3 PVRC Specimen 201

Specimen 201 consisted of two plates nominally 8-in. thick joined by a manual metal arc butt-weld (Figure 3.2.1) in which ten flaws were introduced. In addition, two laminations adjacent to the weld were detected in later studies. Both RT and UT were conducted. The data reported are based on the use of the improved NDE test procedures. The data were analyzed in several fashions. Formal releases of information were in an article in the Welding Research Journal in 1971;<sup>(3.2.1)</sup> and in reports to the PVRC NDE Subcommittee.<sup>(3.2.5,3.2.7)</sup> In essence, the following chronology has been in effect:

1. Radiography and ultrasonics (revised procedures on unclad plate);  
Plateau-2.

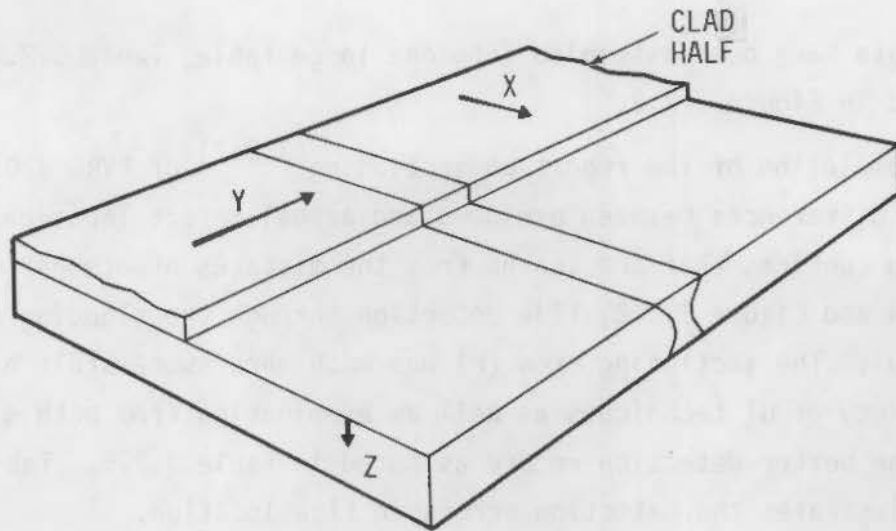


FIGURE 3.2.1. PVRC Plate-Weld Specimen 201

2. Division of weldment into two sections with one destructively sectioned and the other weld-overlay clad; this clad weld was re-examined using Plateau-2 procedures; Plateau-3.
3. The clad plate was examined with conventional UT using additional angles; drilled holes were incorporated for internal calibration of the clad plate; Plateau-4.
4. Improved techniques such as acoustic holography<sup>(3.2.5)</sup> and focused transducers were used to dimension the flaws; Plateau-5.

A variety of analytic tools were used to compare the performance of the various teams as well as to examine the detectability of each flaw.

Four ratios were utilized; namely,

$$R_I = \frac{F}{F+U} \times 100 \quad R_{III} = \frac{F}{F-U}$$

$$R_{II} = \frac{F-f}{F+U} \times 100 \quad R = \frac{F}{F+U+f} \times 100$$

where F = number of introduced flaws found  
 U = number of introduced flaws unfound  
 f = number of false indications.

The data have been assembled into one large table, Table 3.2.4, and represented in Figure 3.2.2.

The completion of the report on sectioning<sup>(3.2.7)</sup> of PVRC #201 plate highlights the differences between presumed and actual defect locations. The report also confirms that one learns from the mistakes of others; As noted in Table 3.2.4 and Figure 3.2.2, flaw detection through the cladding was quite unsuccessful. The sectioning crew (F) was much more successful; however, they used a variety of UT techniques as well as examination from both sides in amassing the better detection record as noted in Table 3.2.5. Table 3.2.6 further illustrates the detection errors in flaw location.

It is apparent that a definite need exists for definitive and restrictive UT procedures. Also, cladding seriously perturbs the validity of UT unless actions are taken for internal calibration to correct for the effects of cladding. The UT data yield nominal locations, but do not give flaw dimensions.

#### 3.2.4 PVRC Specimen 251J

PVRC specimen 251J consisted of two 11-in. plates welded together using a submerged-arc single electrode multiple pass technique. Fifteen welding defects (slag, transverse cracks, longitudinal cracks) were deliberately introduced.

Sufficient work had been completed on PVRC-201 to highlight potential problem areas. Therefore, the 251J examination was directed toward a re-examination of the problem areas. Specifically, the following programs were carried out:

1. Radiography by one team; later by six teams
2. UT 45° angle beam, 2.25 MHz using old PVRC procedures, plate unclad
3. UT 45° angle beam, 2.25 MHz using new PVRC procedures, plate unclad
4. (3) after cladding
5. UT straight beam, 2.25 MHz using old PVRC procedures, plate unclad
6. UT straight beam, 2.25 MHz using new PVRC procedures, plate unclad







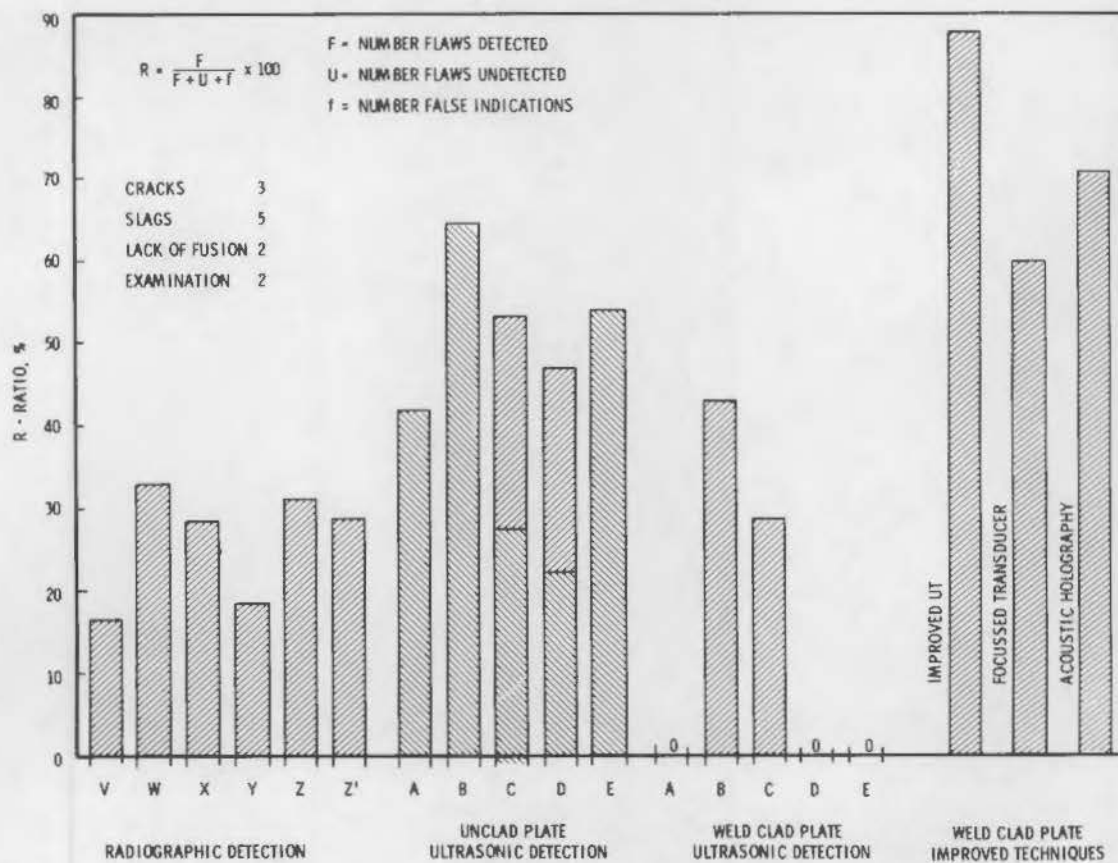


FIGURE 3.2.2. Nondestructive Examination of PVRC Plate-Weld Specimen 201 (8.5 in. thick)

TABLE 3.2.5. Comparison of Detection of Defects in Clad PVRC Block 201 by Teams A, B, C, D, E, and by Sectioning Crew (F)

Flaw	Detection					Sectioning Crew (F)					
	Clad Surface <sup>(a)</sup>					Clad Surface			Unclad Surface		
	A	B	C	D	E	0°	45°	60°	0°	45°	60°
B	U	F	F	U	U	U	F	F	U	U	U
C	U	U	U	U	U	U	F	F	U	U	U
G	U	U	U	U	U	U	U	U	U	F	F
H	U	F	F	U	U	F	F	F	U	U	F
I	U	F	U	U	U	U	U	U	F	F	F
1	U	U	U	U	U	F	U	U	F	U	U
2	U	U	U	U	U	F	U	U	F	U	U

(a) Probably 45° 2.25 MHz.



FIGURE 3.5.5. Comparison of defect detection in PCB layout by using the proposed method.

TABLE 3.5.5. Comparison of defect detection in PCB layout by using the proposed method.

Defect Type	Proposed Method		Reference Method	
	Count	Percentage (%)	Count	Percentage (%)
Missing Pad	10	100	2	20
Wrong Pad	8	100	1	12.5
Wrong Drill	6	100	1	16.67
Wrong Layer	5	100	1	20
Wrong Via	4	100	1	25
Wrong Trace	3	100	1	33.33
Wrong Component	2	100	1	50
Wrong Orientation	1	100	1	100
Wrong Value	1	100	1	100
Wrong Pin	1	100	1	100
Wrong Label	1	100	1	100
Wrong Reference	1	100	1	100
Wrong Net	1	100	1	100
Wrong Bus	1	100	1	100
Wrong Signal	1	100	1	100
Wrong Power	1	100	1	100
Wrong Ground	1	100	1	100
Wrong Connect	1	100	1	100
Wrong Disconnect	1	100	1	100
Wrong Component Value	1	100	1	100
Wrong Component Pin	1	100	1	100
Wrong Component Label	1	100	1	100
Wrong Component Reference	1	100	1	100
Wrong Component Net	1	100	1	100
Wrong Component Bus	1	100	1	100
Wrong Component Signal	1	100	1	100
Wrong Component Power	1	100	1	100
Wrong Component Ground	1	100	1	100
Wrong Component Connect	1	100	1	100
Wrong Component Disconnect	1	100	1	100
Wrong Component Value Pin	1	100	1	100
Wrong Component Value Label	1	100	1	100
Wrong Component Value Reference	1	100	1	100
Wrong Component Value Net	1	100	1	100
Wrong Component Value Bus	1	100	1	100
Wrong Component Value Signal	1	100	1	100
Wrong Component Value Power	1	100	1	100
Wrong Component Value Ground	1	100	1	100
Wrong Component Value Connect	1	100	1	100
Wrong Component Value Disconnect	1	100	1	100

(a) Proposed Method.

TABLE 3.2.6. Variability of Results on Specimen 201

		A <sub>Δ</sub>	B <sub>Δ</sub>	C <sub>Δ</sub>	D <sub>Δ</sub>	E <sub>Δ</sub>	F <sub>Δ</sub>	G <sub>Δ</sub>	H <sub>Δ</sub>	I <sub>Δ</sub>	12 <sub>Δ</sub>	1 <sub>Δ</sub>	2 <sub>Δ</sub>
Assumed	X	14.75	15.0	14.0	16.0	14.0	15.0	14.0	16.0	15.74			
	Y	19.75	3.0	5.75	17.0	21.0	16.0	0.83	5.0	1.0			
	Z	4.125	2.0	1.0	0.5	5.5	5.5	7.0	7.5	7.0			
Measured	X	15.0	15.4	14.3	16.0	13.9	15.2	14.7	15.7	15.8	14.8	14.3	14.3
	Y	19.3 to 21.1	2.3 to 3.6	5.4 to 7.2	16.8 to 17.8	21.1 to 22.1	15.9 to 16.9	-0.8 to 1.2	4.3 to 6.0	0.3 to 1.6	21.1	0.1 to 2.1	9.1 to 9.9
	Z	4.2	2.0	1.0	0.5	1.25	5.4	7.6	7.4	7.9	2.5	4.6	4.5
A	X	15.0	15.7		15.9		14.9				14.9		
	Y	19.8	2.2		17.5		15.3				21.3		
	Z	4.1	2.0		0.7		5.0				34.0		
B	X	15.1	15.8	14.1	15.9	13.9	15.4	14.3	15.6	16.5			
	Y	19.4		6.4	17.0	22.0	16.4	0.3	4.9	--			
	Z	4.0	2.5	0.8	1.0	1.0	5.3	7.5	7.5	7.3			
C	X	15.1	15.5				15.5		15.8	-16.0			
	Y	19.6	3.0				16.0		4.5	1.3			
	Z	4.0 to 4.6	2.0				5.3		7.0 to 8.0	7.8			
D	X	15.0	15.4	14.2	16.3		15.5		15.8	15.8			
	Y	18.5		4.8	14.3		14.3		3.8	2.4			
	Z	4.3	2.1	1.1	0.9		5.5		7.8	7.1			
E	X	15.1	15.5	14.4	16.0		15.8		16.1	15.0			
	Y	20.5	2.5	6.3	17.0		16.0		4.8	1.0			
	Z	4.0	2.0	1.0	0.8		5.3		6.8	7.5			
F	X		15.8	14.6				14.0	15.5	16.3		14.5	14.5
	Y		1.8 to 3.5	5.0 to 6.3				-0.8 to 0.5	3.3 to 5.9	3.1		0.8 to 2.4	8.5 to 9.6
	Z		1.8	1.0				7.3	7.4	7.3		4.3	4.5
FOC.	X		15.2						15.3			14.3 to 15.3	
	Y		2.6 to 3.6						4.4 to 6.1			-0.6 to 6.6	
	Z		2.0						7.3			4.4	
A.H.	X		15.0	14.6				14.8	16.0	16.5			
	Y		3.0	6.0				0.0	4.4	1.0			
	Z		2.0	1.0				7.5	7.5	7.5			
B-CLAD	X		15.6						16.3	16.5			
	Y		3.0						5.0	1.0			
	Z		2.4						7.7	8.1			
C-CLAD	X		15.5						15.0				
	Y		3.0						4.3				
	Z		2.25						8.0				
Δ Spread	X	-0.2 to 10.1	-0.4 + 0.4	-2.0 + 3.0	-0.1 + 0.3	+0.0	-0.2 + 0.6	-7.0 + 0.1	-0.4 + 0.6	-0.8 + 0.7	+0.1	+1.0	+0.2
	Y	-0.8	-0.5 + 0.0	-1.1 + 0.0	-2.5 + 0.0	+0.0	-2.6 + 0.0	+0.0	-1.0 + 1.0	-0.0 + 1.5	0.0 + 0.3	-0.5 + 4.5	-0.6 + 0
	Z	-0.2 + 10.4	-0.2 + 1.0	-0.2 + 0.1	-0.0 + 0.5	-3.0 + 0.0	-0.4 + 0.1	-0.6 + 0.0	-0.6 + 0.6	-0.9 + 0.2	+0.9	-0.3 + 0.0	0.0

NOTE: Δ - Deviation from measured value.



7. (6) after cladding
8. UT 60° angle beam, 2.25 MHz using old PVRC procedures, plate unclad
9. UT 45° angle beam, 1.0 MHz using new PVRC procedures, plate unclad
10. UT straight beam, 1.0 MHz using new PVRC procedures, plate unclad
11. UT 45° angle beam, 1.0 MHz using new PVRC procedures, examination from clad side
12. UT 45° angle beam, 2.25 MHz using new PVRC procedures, examination from unclad side.

In addition, an acoustic holography examination was conducted from the unclad side of the clad plate.

The raw data were statistically analyzed by Buchanan<sup>(3.2.6)</sup> using a defect identification criterion to permit an intercomparison of the teams. This criterion consisted of adding certain tolerances to the intended defect dimensions. If the dimensions fell within the bounds, the indication was accepted as a correct defect identification. Two criteria were used, one with a 1.0-in. tolerance and the other with a 1.5-in. tolerance. This approach tends to assume that the flaw size and location are about as stated in the fabrication document and that errors are due to examination procedures; however, the currently available sectioning data indicate that neither the flaw sizes nor the flaw locations was precisely as indicated.<sup>(3.2.7,3.2.8)</sup> In some instances, the flaws were much larger than presumed. It should be recognized that the data presented in the tables assumed that the predicted sizes and locations were correct. Figure 3.2.3 from Reference 3.2.6 illustrates the presumed size and location of flaws. Table 3.2.7a describes the presumed flaws and presumed locations and contains the results of the NDE studies cited previously. The data are included as are values for  $R_I$ ,  $R_{II}$ ,  $R_{III}$ , and  $R$ . The data for  $R$  are given in Figure 3.2.4.

Table 3.2.7b summarizes the RT data using a format similar to Table 3.2.7a.

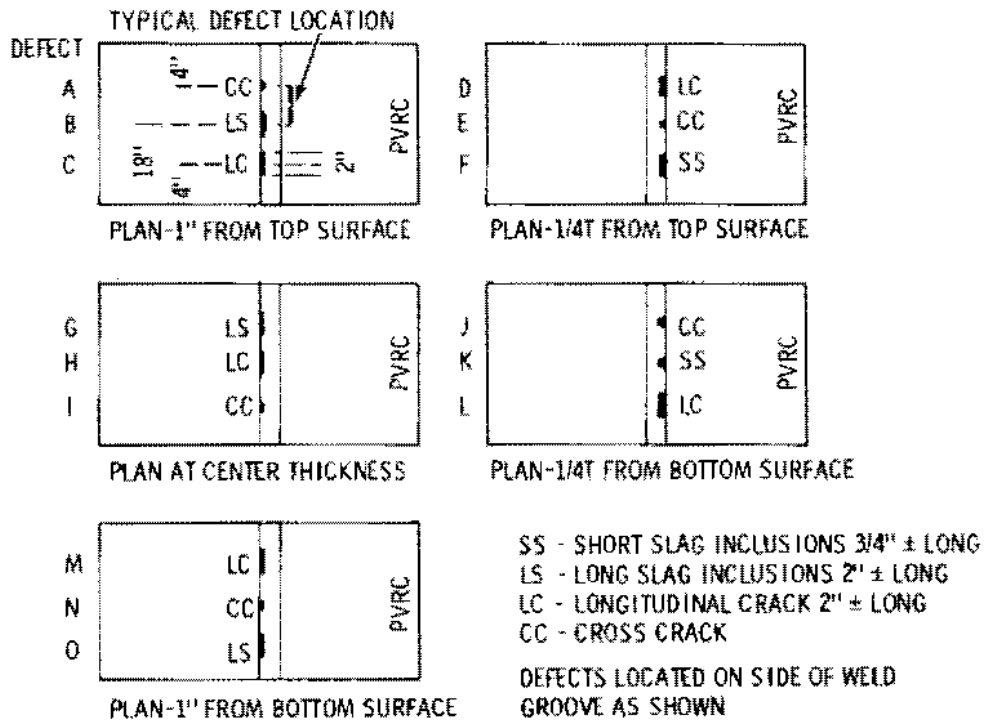
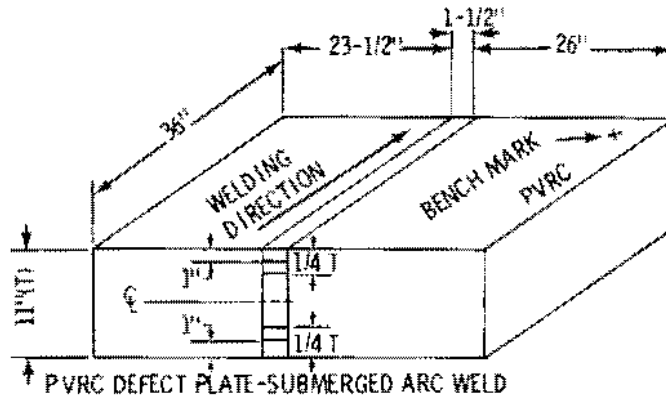


FIGURE 3.2.3. PVRC Specimen 251J







TABLE 3.2.7b. Nondestructive Examination (RT) of PVRC Plate-Weld Specimen 251J

Flaw Characteristics	Radiographic Examination Team (1.5-in. Tolerance where given)							Detected
	C <sup>(a)</sup>	1 <sup>(b)</sup>	2	3	4	5	6	
A. Cross-Crack	U	U	U	U	U	U	U	0/7
B. Long Slag Inclusion	F	F	F	U	F	U	F	5/7
C. Longitudinal Crack	U	U	U	U	U	U	U	0/7
D. Longitudinal Crack	U	F	U	F	F	F	F	5/7
E. Cross-Crack	U	U	U	U	U	U	U	0/7
F. Short Slag Inclusion	U	F	U	F	F	F	F	5/7
G. Long Slag Inclusion	F	F	F	F	F	F	F	7/7
H. Longitudinal Crack	U	F	F	F	F	F	F	6/7
I. Cross-Crack	U	U	U	U	U	U	U	0/7
J. Cross-Crack	U	U	U	U	U	U	U	0/7
K. Short Slag Inclusion	F	F	F	F	F	F	F	7/7
L. Longitudinal Crack	U	U	U	U	U	U	U	0/7
M. Longitudinal Crack	F	U	F	F	F	F	F	6/7
N. Cross-Crack	U	U	U	U	U	U	U	0/7
O. Long Slag Inclusion	F	F	U	F	F	F	F	6/7
F	5	7	5	7	8	7	8	
U	10	1	4	0	0	0	1	
f	4	8	10	8	7	8	7	
R <sub>I</sub>	33	47	33	47	53	47	53	
R <sub>II</sub>	7	40	7	47	53	47	47	
R <sub>III</sub>	6.36	0.79	0.36	0.88	1.29	0.88	1.00	

(a) Used three angles 0, +15°, -15°.

(b) Defects not identified in WRC-259. Values assumed lack of ±15° prevented Z dimensioning.

3.2.18

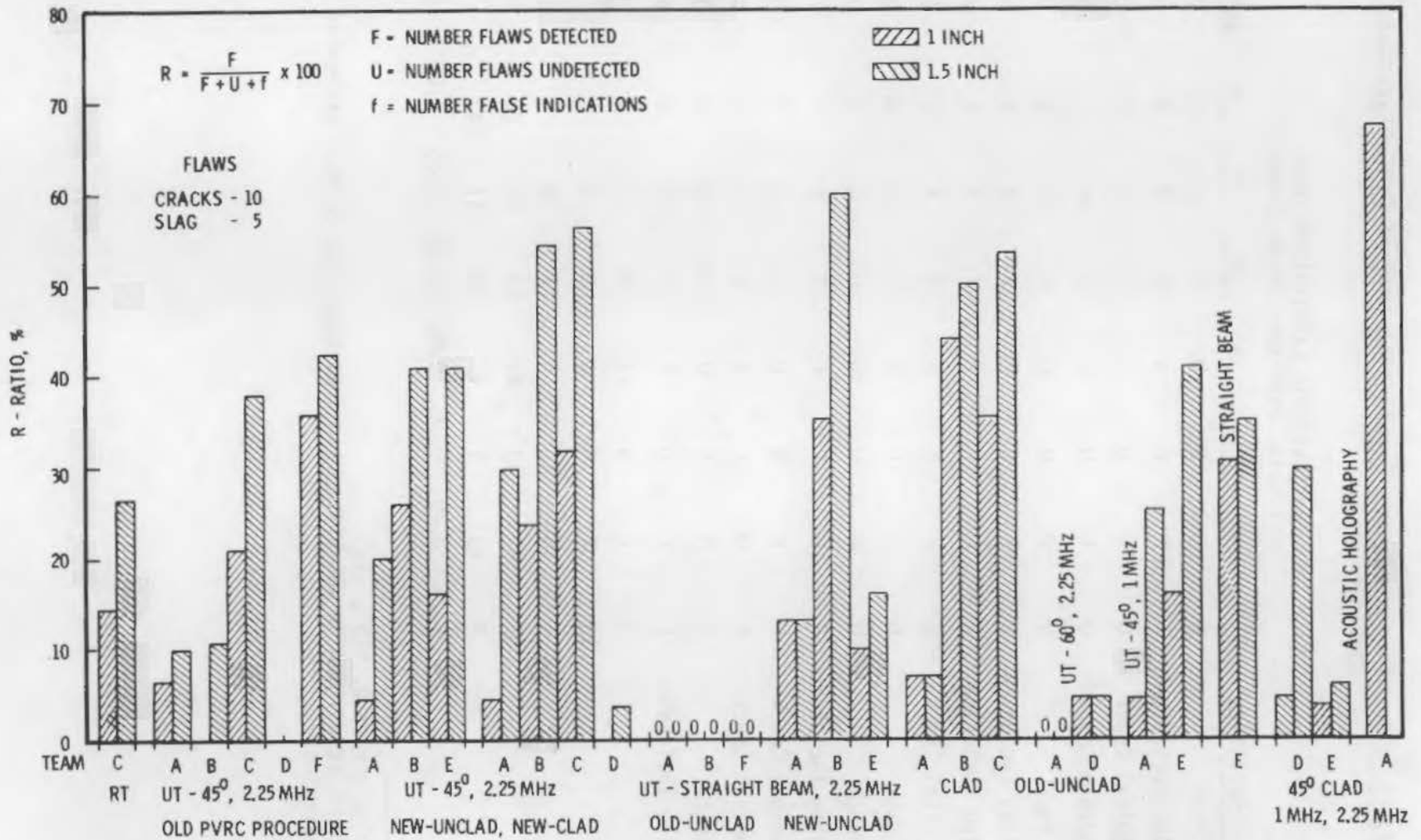


FIGURE 3.2.4. Nondestructive Examinations of PVRC Plate-Weld Specimen 251J (11 in. thick)

#### 3.2.4.1 Acoustic Holography

General Electric<sup>(3.2.9)</sup> examined the clad plate using acoustic holography. Initial examination indicated poor image quality through the cladding so further studies were limited to the unclad side. Examinations were with 2 and 3 MHz longitudinal and 45° shear wave. The data are presented in Table 3.2.8. A significant item is the lack of imaging from flaws too close to the surface when examination is limited or non-existent from the other surface.

The significance of actual flaw location versus presumed flaw location is highlighted from a limited and rather cursory study of RT and UT C-scan after initial sectioning of Specimen 251J. Thirteen data points change from false (f) to found (F) which increases the values for the 45°, 2.25 MHz new procedure--from a cumulative  $R_{II}$  of 0 to  $R_{II}$  of 58%.

#### 3.2.4.2 Statistical Evaluation

The preceding helps clarify some of the apparent discrepancies in statistical evaluation contained in Table 3.2.9 where the averages and standard deviations from  $R_I$ ,  $R_{II}$  and  $R_{III}$  are compared within and between Specimens 201 and 251J. A similar plot will need to be made for corrected 251J data to establish the actual degree of improvement resulting from the new procedures.

Another way to examine the data is to consider the significance of the various flaws in terms of fracture mechanics parameters. The following are two major assumptions for such an approach:

- Cracks are more critical than slag inclusions.
- Flaws near surfaces are more critical because residual, thermal and bending stresses are higher there;
  - Most critical are A, C, M, N;
  - Less critical are D, E, J, L.
- Least critical of cracks are H, I;
  - Minor significance are slag inclusions B, F, G, K, O.

TABLE 3.2.8. Acoustic Holography Examination from Unclad Side on Clad Plate(3.2.9)

	Code in NE DO-2735	Fall Within Tolerance				Dimensions and Orientation			Detected by
		1.0			1.0	Height	Length	Degrees	
		X	Y	Z	1.0				
A	13	-	-	-	U	-	-	-	Not detected
B	14	N	Y	Y	F	1.7A	2.0A		Longitudinal; 45° shear perpendicular (⊥) to weld
C	15	-	-	-	U	-	-	-	Not imaged
D	10	Y	Y	Y	F	1.7	2.9	98	45° shear; ⊥ weld
E	11	Y	N	Y	F	1.9A	1.0A	-	45° shear; ⊥ weld
F	12	N	Y	Y	F	1.4A	2.4A	-	45° shear; ⊥ weld
G	7	Y	Y	Y	F	2.2	1.9	114	45° shear; ⊥ weld
H	8	Y	Y	Y	F	1.3	5.6	85	Longitudinal; 45° shear parallel (//) and ⊥ weld
I	9	Y	Y	Y	F	0.7A	1.7A	-	45° shear // weld
J	4	Y	Y	Y	F	0.7 to 0.9A	2.7 to 2.9	-	45° shear ⊥ and // weld
K	5	Y	Y	Y	F	0.7	0.6	69	Longitudinal; 45° shear ⊥ weld
L	6	Y	Y	Y	F	1.0	3.9	80	Longitudinal; 45° shear ⊥ weld
M	1	-	-	-	U	-	-	-	Not imaged; too close to surface
N	2	-	-	-	U	-	-	-	Not imaged; too close to surface
O	3	-	-	-	U	-	-	-	Not imaged; too close to surface
F								10	
U								5	
f								0	
R <sub>I</sub>								67	
R <sub>II</sub>								67	
R <sub>III</sub>								2.0	

TABLE 3.2.9. Comparisons of Examination Results for Plates 201 and 251J, Means  $\bar{X}$  and Standard Deviations ( $\sigma$ )

Test Conditions		Parameter					
		$R_I$		$R_{II}$		$R_{III}$	
		1.0	1.5	1.00	1.5	1.0	1.5
Plate 251J 45°; 2.25 MHz							
Old PVRC	$\bar{X}$	23	32	-41	-23	0.18	0.32
	$\sigma$	28	30	30	38	0.24	0.33
New PVRC	$\bar{X}$	31	53	-51	0	0.20	0.54
	$\sigma$	27	24	19	10	0.15	0.25
New PVRC (clad)	$\bar{X}$	25	47	-47	7	0.21	0.73
	$\sigma$	26	35	44	55	0.22	0.60
Straight Beam 2.25 MHz							
Old PVRC	$\bar{X}$	0	0	-2	-2	0.0	0.0
	$\sigma$	0	0	4	4	0.0	0.0
New PVRC	$\bar{X}$	22	31	7	22	0.27	0.61
	$\sigma$	16	25	24	34	0.24	0.77
New PVRC (clad)	$\bar{X}$	31	38	25	36	0.47	0.74
	$\sigma$	21	27	17	25	0.36	0.58
Radiography	$\bar{X}$	20	33	-20	7	0.17	0.36
Holography	$\bar{X}$	67		67		2.0	
Plate 201							
Old PVRC	$\bar{X}$	54		27		0.92	
	$\sigma$	15		27		0.52	
Old PVRC (clad)	$\bar{X}$	14		14		0.23	
	$\sigma$	20		20		0.25	
New PVRC (clad)	$\bar{X}$	100		86		7.0	
Radiography	$\bar{X}$	29		2		0.35	
	$\sigma$	10		7		0.12	
Holography	$\bar{X}$	71		71		2.5	

Table 3.2.10 gives some idea of the relative effectiveness of both techniques and operators in detecting the various flaws. It is interesting to observe that the 45° angle beam 2.25 MHz was quite effective in detecting flaws through the clad.

An attempt to quantify the results of NDE is given in Table 3.2.11 where the ratio of found-to-found plus unfound flaws is used to evaluate both flaw detectability and effectiveness of a given technique.

Recognizing that the final results will depend on the size and location of flaws, the following interim conclusions are believed to be of interest and, probably, not subject to substantial change.

#### 3.2.4.3 Conclusions--251J

- Team F results should be discarded since their participation was limited to one survey; (N.B., it is interesting to note the F record of finding all slag and no cracks).
- Operators B and C did better than the others; their results were essentially comparable; there was no significant difference in performance with angled and straight beam (new) techniques.
- The D operator was consistently the least effective, particularly since he did no straight beam testing.
- Operator E appeared slightly better than A but the difference was not significant (generally both did better on angled beam than straight beam); both were more effective than D, but generally less effective than B and C.
- The new PVRC procedure was substantially better than the old procedure for the same conditions of angle and frequency.
- With the new procedure there seemed to be little or no difference in detection reliability for either clad or unclad condition.



TABLE 3.2.10. Analysis of Plate 251J Using Criterion of Relative Flaw Significance; Comparison Limited to Ultrasonic Testing

UT TEST CONDITIONS	DETECTION OF FLAWS																			
	MOST CRITICAL (INEAREST SURFACE)					LESS CRITICAL (DEEPLY BURIED)					LEAST CRITICAL (CENTER OF PLATE)				SLAG					
	A	C	M	N	Σ	D	E	J	L	Σ	H	I	Σ	B	F	G	K	O	Σ	
1. 45°, 2.25 MHz (A, B, C, D, F) OLD PVRC; UNCLAD	C A, B, D, F	C A, B, D, F	A, C B, D, F	B, C A, D, F	A, B, 4C 3A, 3B, 4D, 4F	C A, B, D, F	C A, B, D, F		A B, C, D, F	A, 2C 3A, 4B, 2C, 4D, 4F	A, B, C, D, F	A, B, C, D, F	2A, 2B, 2C, 2D, 2F	C, F A, B, D	F A, B, C, D	C, F A, B, D	A, B, F C, D	F A, B, C, D	A, B, 2C, 5F 4A, 4B, 3C, 5D	
2. 45°, 2.25 MHz (A, B, E) NEW PVRC; UNCLAD	A, E B	B, E A	B A, E	B A, E	A, 3B, 2E 3A, B, 2E	A, B, F	B, E A		B A, E	A, 3B, 2E 3A, B, 2E	A, B E	B A, E	A, 2B A, 2E	E A, B	A, B, E A	B, E A	B, E A	E A, B	A, 3B, 5E 4A, 2B	
3. 45°, 2.25 MHz (A, B, C, D) NEW PVRC; CLAD	B A, C, D	A, B, C D	A, B, C D	B A, C, D	2A, 4B, 2C 2A, 2C, 4D	A, B, C D	C A, B, D		B A, C, D	2A, 3B, 3C, D 2A, B, C, 3D	B, C A, D	B A, C, D	2B, C 2A, C, 2D	A, B, C, D	B, C A, D	A, B, C D	B, C A, D	B A, C, D	A, 4B, 3C 4A, B, 2C, 5D	
4. STRAIGHT BEAM, 2.25 MHz (A, B, F) OLD PVRC; UNCLAD	A, B, E	A, B, E	A, B, E	A, B, E	4A, 4B, 4E	A, B, E	A, B, E		A, B, E	4A, 4B, 4E	A, B, E	A, B, E	2A, 2B, 2E	A, B, E	A, B, E	A, B, E	A, B, E	A, B, E	A, B, E	5A, 5B, 5E
5. STRAIGHT BEAM, 2.25 MHz (A, B, E) NEW PVRC; UNCLAD	A, B, E	B A, E	B A, E	B A, E	3B 4A, B, 4E	A, B, E		B A, E	A, B 2A, 3B, E 2A, B, 3E	2A, 3B, E 2A, B, 3E	B A, E	B, E A	2B, E 2A, E	A, B, E	A, B, F	A, B, E	B A, E	E A, B	B, E 5A, 4B, 4E	
6. STRAIGHT BEAM, 2.25 MHz (A, B, C) NEW PVRC; CLAD	A, B, C	B, C A	B, C A	B A, C	3B, 2C 4A, B, 2C	A, B, C		C A, B, C	A, B, 3C 3A, 3B, C	A, B, 3C 3A, 3B, C	B, C A	A, B, C	B, C 2A, B, C	A, B, C	B A, C	B, C A	B, C A	A, B, C	3B, 2C 5A, 2B, 3C	
7. STRAIGHT BEAM, 1.0 MHz (E) NEW PVRC; UNCLAD	E	E	E	E	E 3E	E		E	3E E	3E E	E	E	E E	E	E	E	E	E	E	3E 2E
8. 60°, 2.25 MHz (A, D) OLD PVRC; UNCLAD	A, D	D A	A, D	A, D	4A, 3D	A, D		A, D	4A, 4D	4A, 4D	A, D	A, D	2A, 2D	A, D	A, D	A, D	A, D	A, D	A, D	5A, 5D
9. 45°, 1.0 MHz (A, E) NEW PVRC; UNCLAD	A, E	E A	A, E	A, E	A, 2E 3A, 2E	A, E		E A	A, 2E 3A, 2E	A, 2E 3A, 2E	A E	A, E	A A, 2E	E A	A, E	A, E	E A	E A	A	2A, 5E 3A
10. 45°, 1.0 MHz (D) NEW PVRC; CLAD SIDE	D	D	D	D	2D 2D	D		D	2D 2D	2D 2D	D	D	2D	D	D	D	D	D	D	D 4D
11. 45°, 2.25 MHz (E) NEW PVRC; CLAD-UNCLAD SIDE	E	E	E	E	4E	E		E	E 3E	E 3E	E	E	2E	E	E	E	E	E	E	2E 3E
$\frac{2A, B, C, 2E}{6A, 5B, 2C, 4D, 4E, F}$ $\frac{2A, 4B, 3C, D, E}{6A, 2B, 3D, 5E, F}$					$\frac{5A, 4B, 3C, D, 4F}{3A, 2B, 3D, E, F}$ $\frac{2B, C, D, E}{8A, 3B, 2C, 3D, 4E, F}$					$\frac{2A, 4B, 2C}{6A, 2B, C, 4D, 6E, F}$				$\frac{C, 2E, F}{8A, 6B, 2C, 4D, 4E}$ $\frac{2A, 3B, 3C, D, 3E, F}{6A, 3B, 3D, 3E}$ $\frac{B, 4E, F}{8A, 5B, 3C, 4D, 2E}$						
HARDEST → EASIEST N, A, M, C R RATIOS: A 0.16, B 0.59, C 0.67, D 0.19, E 0.21, F 0.0					E, J, L, D					I, H				HARDEST → EASIEST B, O, F, G, K R RATIOS: A 0.125, B 0.59, C 0.47, D 0.05, E 0.17, F 1.0						
OVERALL BEST → WORST					C, B					E				A, D						

NOTE: YES (FOUND) / NO (NOT FOUND) EXAMPLE C / A, B, D, F



TABLE 3.2.11. PVRC Plate 251J Ratios of Effectiveness of Detection

Test Condition	Most Critical					Less Critical					Least Critical					Slag						
	A	B	C	D	E	A	B	C	D	E	A	B	C	D	E	Σ	A	B	C	D	E	Σ
1	0.25	0.25	1.0	0.0	--	0.25	0.0	0.5	0.0	--	0.0	0.0	0.0	0	--	0.2	0.2	0.2	0.4	0.0	--	0.20
2	0.25	0.75	--	--	0.5	0.25	0.75	--	--	0.5	0.5	1.0	--	-	0.0	0.5	0.2	0.6	--	--	1.0	0.60
3	0.5	1.0	0.5	0.0	--	0.5	0.75	0.75	0.25	--	0.0	1.0	0.5	0	--	0.5	0.2	0.8	0.6	0.0	--	0.40
4	0.0	0.0	--	--	0.0	0.0	0.0	--	--	0.0	0.0	0.0	--	-	0.0	0.0	0.0	--	--	0.0	0.0	
5	0.0	0.75	--	--	0.0	0.5	0.75	--	--	0.25	0.0	1.0	--	-	0.5	0.4	0.0	0.2	--	--	0.2	0.13
6	0.0	1.0	0.5	--	--	0.25	0.25	0.75	--	--	0.0	0.5	0.5	-	--	0.4	0.0	0.6	0.4	--	--	0.33
7	--	--	--	--	0.25	--	--	--	--	0.75	--	--	--	-	0.5	0.5	--	--	--	--	0.6	0.6
8	0.0	--	--	0.25	--	0.0	--	--	0.0	--	0.0	--	--	0	--	0.4	0.0	--	--	0.0	--	0.0
9	0.25	--	--	--	0.5	0.25	--	--	--	0.5	0.5	--	--	-	0.0	0.33	0.4	--	--	--	1.0	0.7
10	--	--	--	0.5	--	--	--	--	0.5	--	--	--	--	0	--	0.33	--	--	--	0.2	--	0.2
11	--	--	--	--	0.00	--	--	--	--	0.25	--	--	--	0	0.0	0.08	--	--	--	--	0.4	0.4
All	0.16	0.62	0.55	0.19	0.21	0.25	0.41	0.67	0.19	0.37	0.12	0.60	0.33	0	0.17	0.33	0.12	0.4	0.47	0.05	0.53	0.32
Without Straight Beam	0.25	0.67	0.56	0.19	0.33	0.25	0.50	0.63	0.19	0.50	0.20	0.67	0.27	0	0.0	0.35	0.20	0.53	0.50	0.07	0.80	0.44
Only Straight Beam	0.0	0.58	0.50	--	0.08	0.25	0.33	0.75	--	0.33	0.0	0.50	0.50	-	0.33	0.35	0.0	0.27	0.40	0.0	0.27	0.19

NOTE: Ratios  $\frac{\text{Found}}{\text{Found} + \text{Unfound}}$

Table 1  
Summary of Results

Run	Time (min)	Temp (°C)	Pressure (mm Hg)	Flow (ml/min)	Concn. (%)	Yield (%)	Refractive Index	Boiling Point (°C)	Density (g/ml)
1	10	120	1.0	1.0	0.1	0.1	1.000	100	0.80
2	15	130	1.0	1.0	0.2	0.2	1.000	100	0.80
3	20	140	1.0	1.0	0.3	0.3	1.000	100	0.80
4	25	150	1.0	1.0	0.4	0.4	1.000	100	0.80
5	30	160	1.0	1.0	0.5	0.5	1.000	100	0.80
6	35	170	1.0	1.0	0.6	0.6	1.000	100	0.80
7	40	180	1.0	1.0	0.7	0.7	1.000	100	0.80
8	45	190	1.0	1.0	0.8	0.8	1.000	100	0.80
9	50	200	1.0	1.0	0.9	0.9	1.000	100	0.80
10	55	210	1.0	1.0	1.0	1.0	1.000	100	0.80

TABLE 1. Summary of Results of Distillation of Methylacetylene.

During 1974, a new program was initiated for NDE of PVRC Specimens 155, 202 and 203. The examination criteria were based on an evaluation of the results of Specimens 201 and 251J and of the effect of modified procedures on these results. The procedure selected on for the new program (155, 202, 203), in essence, consisted of an expansion of Appendix I of ASME Section XI.<sup>(3.2.2)</sup> The specific procedures denoted as the PVRC Section XI UT Procedure are included as Appendix I to the Buchanan Interim Report to PVRC.<sup>(3.2.6)</sup> This approach was believed to permit a verification of the code procedure and to determine whether a more restrictive procedure would produce more accurate results.

Steps taken to further control the examination included the following:

- All examinations were in one location.
- Each team used a matched set of transducers and one of three matched Krautkramer US1P-11 instruments.
- Operators were instructed to perform in strict compliance with the procedures.
- The same scan paths were used.
- Data were recorded on the same format data sheets.
- A modification midway through the testing required increased scanning gain from 2x to 5x calibration level and permitted intermediate scan paths to better locate the indication peak (most, but not all, teams repeated their examination using the new procedure).

Other aspects of the recent PVRC programs bearing on future work included studies of electronic systems variability and variability in the overall test system. These studies culminated in a single document<sup>(3.2.2)</sup> covering two topics:

1. "Improved Repeatability in Ultrasonic Examination"<sup>(3.2.2a)</sup> which was aimed at limiting the significant variations existing in "off the shelf" search units,

2. "Ultrasonic Testing System Standardization Requirements"(3.2.2b) which defines minimum performance for the system defined as the instrument (pulser-receiver, CRT, gate), coaxial cable and search unit.

### 3.3.1 PVRC Specimen 155

PVRC Specimen 155 consisted of a nozzle welded into a plate (Figure 3.3.1). This specimen was intended to contain four flaws. These flaws were located at approximately 90° intervals around the nozzle in weld built-up regions immediately adjacent to the nozzle-plate weldment on the nozzle side of the weldment. The flaws were about in the mid-section insofar as plate thickness was concerned. An attempt was made to orient the flaws with respect to the nozzle wall at (approximately) 30°, 45°(2), and 60°.

Thirteen teams round robin examined Specimen 155 and reported (collectively) 56 indications including data for 0°, 45°, and 60° beam angles at 2.25 MHz. Buchanan<sup>(3.3.1)</sup> initially used the procedure developed for the analysis of 251J, namely, tolerances of 0.5, 1.0 and 1.5 in. on the x, y, z, (R,  $\theta$ , z) values of the flaws. Results were surprising and discouraging. Two indications fell within the 0.5-in.-tolerance level for Flaw 2. At 1.0 in. only one flaw (No. 2) was correctly identified by 11 of the 56 indications.

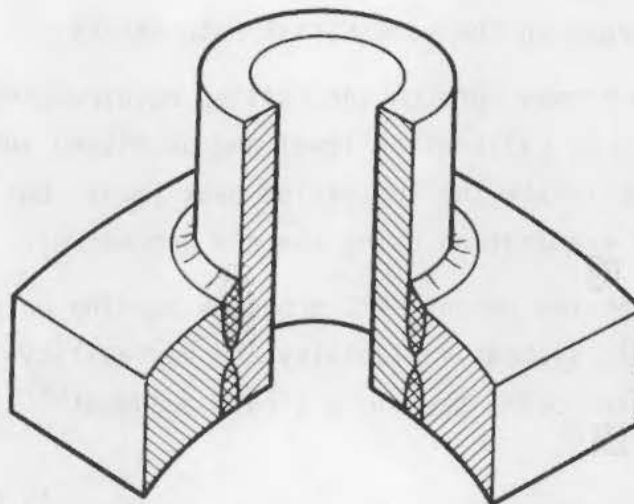


FIGURE 3.3.1. PVRC Weld Specimen 155, 40 (102 cm) x 48 (210 cm) x 8-1/2 (22 cm)

At 1.5 in. only Flaw 2 was correctly identified by 32 of the 56 indications. None of the correct indications was by straight beam. Of the 45° and 60°, it appeared that the 45° angle beam was somewhat more effective; e.g., 38 indications for 45° and 7 for 60°.

Flaw (or discontinuity) 2 was oriented at about 45° to the vertical; however, factors other than orientation of this flaw may have resulted in overall poor performance. For example, the plate into which the nozzle was welded was not flat. It had a radius of curvature of 120 in. along one axis where Flaws 2 and 4 were located. On the other axis at 90° the plate had zero curvature (Flaws 1 and 3). An added factor was the internal cladding of the nozzle so that through-wall UT from the nozzle bore would be through cladding.

The required tangential and radial scan pattern was inscribed on the surface. No indications were noted in the tangential scans; all resulted from radial scans.

Eleven of the 13 teams detected Flaw 2. None detected Flaws 1, 3, or 4 at tolerance levels as great as 1.5 in. Table 3.3.1 (Table 6 of Reference 3.3.1) contains  $R_{III}$  values at 1.0 in.-tolerance level to permit comparison to Specimens 201 and 251J.

A potential source of the very low team ratings could be related to the validity of the basic assumption that the intentional flaws are located exactly where intended. Obviously, if an indication is judged to be correct only if it matched, within tolerances, the intended location, and if the actual locations differed considerably from the intended locations, large errors could result.

A review of available radiographic data indicated that the size, shape and location of the actual flaws differed significantly from the intended values. Figure 3.3.2 contains the radiographic data as well as the presumed locations of the four flaws. The narrow dimension (width) of the four flaws was supposed to have been about 0.5 in., which would have been the distance around the circumference.

As an alternate to the tolerance system a two-point coincidence method was developed which was to determine whether a given UT indication was correct without assuming actual flaw locations. The two-point coincidence method

TABLE 3.3.1. Team Rating Factors, Specimen 155, 1.0-in. Tolerance Level, Standard Method of Analysis

a) UT Data					b) RT Data				
Team	F	u	f	$R_{III}$	Team	F	u	f	$R_{III}$
1	1	3	1	0.25	A	10	9	0	1.1
2	0	4	4	0.0	B	15	5	1	2.5
3	0	4	5	0.0	C	14	6	2	1.8
4	0	4	6	0.0	D	12	8	1	1.3
5	1	3	2	0.20	E	14	6	1	2.0
6	0	4	6	0.0	F	13	7	1	$\frac{1.6}{1.7^{(a)}}$
7	1	3	0	0.33					
8	1	3	3	0.17					
9	1	3	1	0.25					
10	0	4	4	0.0					
11	0	4	0	0.0					
12	0	4	12	0.0					
13	1	3	1	$\frac{0.25}{0.11^{(a)}}$					

(a)  $R_{III}$  average.

consists of an analytic division of the specimen into a large number of small essentially cubic elements. If any portion of two or more indications fall within a given element, a discontinuity is said to exist and all indications in that element are treated as correct indications.

Three different volume element sizes were used to be somewhat consistent with the previous method of analysis; e.g., the normal edge dimensions were 0.45, 0.90 and 1.35 in. respectively, compared to tolerances of  $\pm 0.5$ ,  $\pm 1.0$  and  $\pm 1.5$  in.

The percentage of reported indications found to be correct with the two-point coincidence method ranged from 74% for the smallest volume element to 80% for the largest volume element.



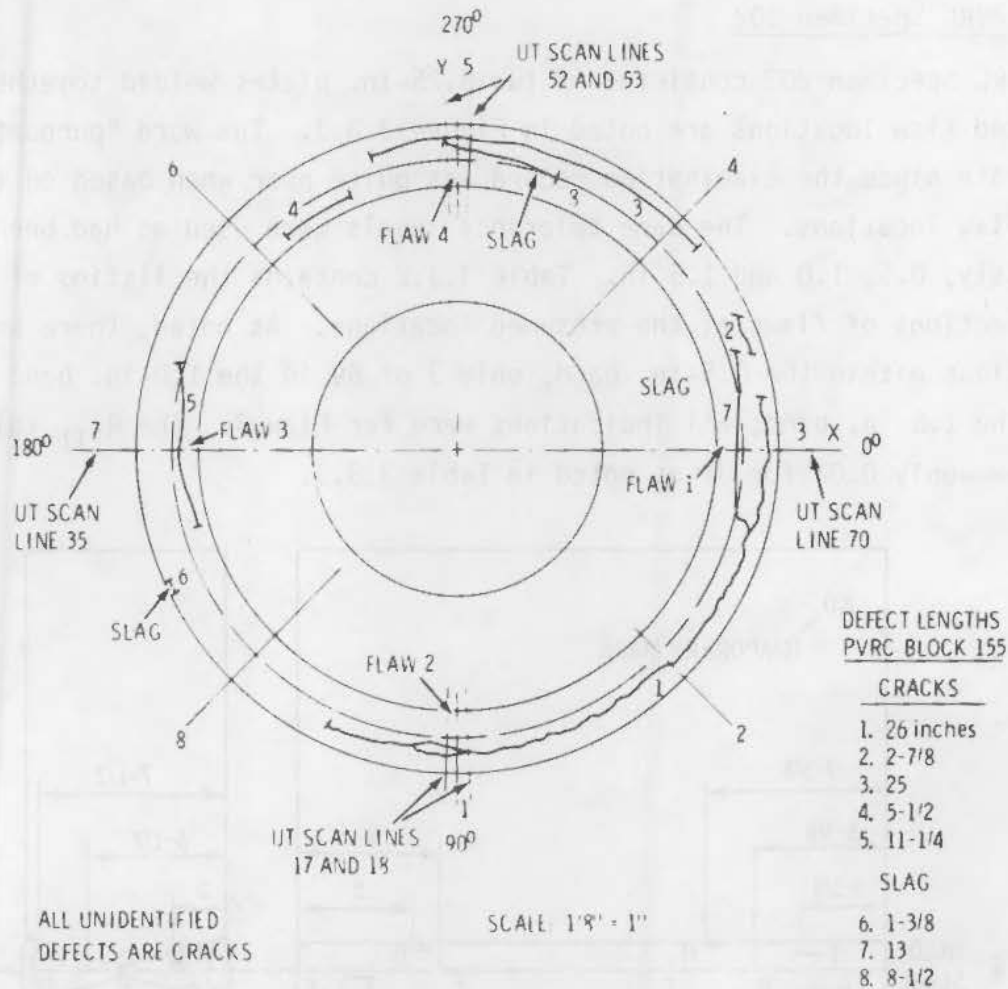


**FIGURE 3.3.2.** Summary Drawing of Radiographic Results on PVRC Specimen 155

The analysis was expanded to determine the effect on the percentage rating if the number of points required for coincidence were increased. For the 0.9-in.-element size (76.8% with 2-point), the data were analyzed using 3-, 4-, 5-, 6- and 7-point coincidence requirements; yielding percentages of 67.9, 62.5, 62.5, 62.5 and 62.5, respectively; a decrease from 2-point to 4-point, then remaining constant to 7-point.

An intercomparison will be made later with Specimens 201 and 251J as well as 202 and 203.

### 3.3.2 PVRC Specimen 202

PVRC Specimen 202 consisted of two 8.25-in. plates welded together. The purported flaw locations are noted in Figure 3.3.3. The word "purported" is deliberate since the examination record was quite poor when based on the presumed flaw locations. The same tolerance levels were used as had been used previously, 0.5, 1.0 and 1.5 in. Table 3.3.2 contains the listing of successful detections of flaws at the presumed locations. As noted, there were no indications within the 0.5-in. band; only 3 of 69 in the 1.0-in. band and 5 of 69 in the 1.5-in. band; all indications were for Flaw 3. The  $R_{III}$  values are very low--only 0.02 for UT as noted in Table 3.3.3.

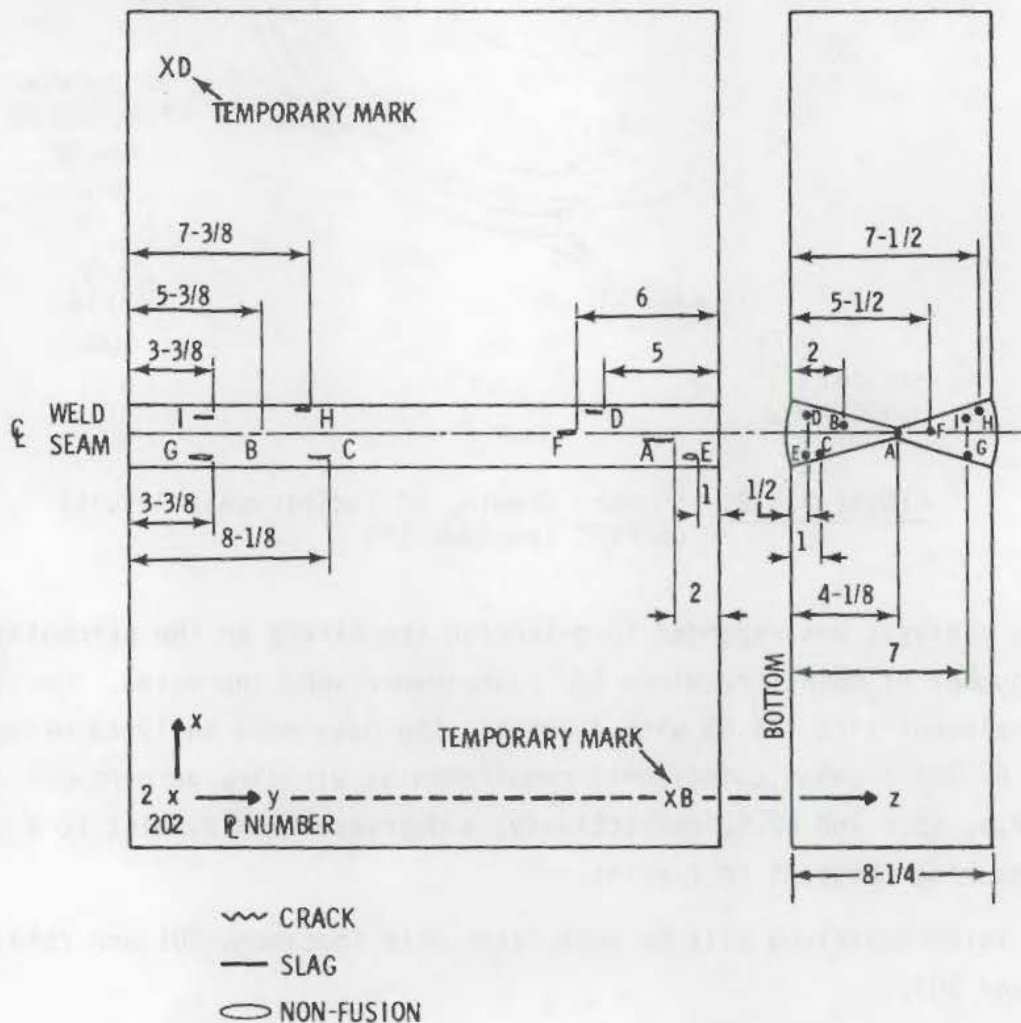


FIGURE 3.3.3. Discontinuity Locations in PVRC Specimen 202

TABLE 3.3.2. Summary of Ultrasonic Examination Results, PVRC Specimen 202, Standard Method of Analysis

<u>Discontinuity Number</u>	<u>Tolerance Level (in.)</u>	<u>Discontinuity Type</u>	<u>Indication Number</u>	<u>Correctly Identified by Team Number</u>	<u>Ultrasonic Inspection Mode (shear wave)</u>
(a)	0.5				
3	1.0	Crack	24	6	45°
			29	7	45°
			65	13	60°
3	1.5	Crack	4	2	45°
			24	6	45°
			29	7	45°
			61	13	45°
			65	13	60°

(a) No correct identifications.

3.3.7

TABLE 3.3.3. Team Rating Factors, Specimen 202, 1.0-in. Tolerance Level, Standard Method of Analysis

a) UT Data					b) RT Data												
Team	F	u	f	R <sub>III</sub>	Team	F			u			f			R <sub>III</sub>		
						1-2	2-3	3-4	1-2	2-3	3-4	1-2	2-3	3-4	1-2	2-3	3-4
1	0	9	2	0.0	A M	17	0	12	8	1	15	0	0	0	0.9	0	0.8
2	0	9	5	0.0	B	3	0	9	12	1	18	0	1	0	0.3	0	0.5
3	0	9	4	0.0	C	8	0	12	7	1	15	0	0	0	1.1	0	0.8
4	0	9	3	0.0	D	13	0	16	2	1	11	1	0	1	4.3	0	1.3
5	0	9	3	0.0	E	9	0	15	6	1	12	0	1	0	1.5	0	1.3
6	1	8	10	0.06	F	8	0	12	7	1	15	0	0	0	1.1	0	0.8
7	1	8	3	0.09	G	11	0	14	4	1	13	0	0	1	2.8	0	1.0
8	0	9	10	0.0	H	11	0	15	4	1	12	0	0	2	2.8	0	1.1
9	0	9	5	0.0	I	12	1	19	3	0	8	2	12	6	2.4	0.8	1.4
10	0	9	3	0.0	AAA	8	0	15	7	1	12	0	0	1	1.1	0	1.2
11	0	9	3	0.0	B	--	0	--	--	1	--	-	0	-	--	0	--
12	0	9	6	0.0	C	11	0	13	4	1	14	1	0	0	2.2	1	0.9
13	1	8	9	0.06	D	--	0	--	--	1	--	-	0	0	--	0	--
				0.02 <sup>(a)</sup>	E	9	1	13	6	0	14	0	0	0	1.5	∞	0.9
					F	8	0	12	7	1	15	0	0	0	1.1	0	0.8
					G	8	1	12	7	0	15	0	0	0	1.1	∞	0.7
					H	8	0	13	7	1	14	0	0	0	1.1	0	0.9
						134		202							1.7 <sup>(a)</sup>		0.96

(a) R<sub>III</sub> average.

NOTE: M and AA film sets considered independent.

3.3.8

The next step was to use a 2-point coincidence method of analysis as had been done with PVRC Specimen 155. The percentage of reported indications found to be correct with the 2-point coincidence method for 0.45-, 0.90- and 1.35-in. volume-element sizes were 76.8, 84.1 and 81.2%. The 0.9-in. element was analyzed using 3-, 4-, 5-, 6- and 7-point coincidence in addition to the 2-point. The resultant percentages of reported indications found to be correct were 84.1, 81.2, 71.0, 49.3, 46.4 and 37.7%, respectively.

Radiography data have been reported in three references (3.3.1, 3.3.2, 3.3.3). Unfortunately, the references do not contain flaw dimensions in the context of plate dimensions so it is not possible to quantify the actual (based on RT) versus presumed flaw locations. Presumably, the final reports will permit a more definitive analysis of flaw types, sizes and locations. An interesting aspect is the analyses of all flaws as slag in one set of RT data.<sup>(3.3.1)</sup> Another set<sup>(3.3.3)</sup> disagrees with other RT data as well as presumed flaw locations. See Tables 3.3.3b, 3.3.4, and 3.3.5, and Figures 3.3.3 and 3.3.4.

TABLE 3.3.4. Presumed Locations of Flaws in PVRC Plate-Weld Specimen 202<sup>(3.3.1)</sup>

Discontinuity		X	Y <sub>1</sub>	Y <sub>2</sub>	ΔY	Z
Number	Letter					
1	A	16.20	18.75	20.00	1.25	4.12
2	B	16.67	2.62	3.38	0.76	2.00
3	C	15.62	5.12	6.12	1.00	1.00
4	D	17.27	16.25	17.00	0.75	0.50
5	E	15.59	20.25	21.00	0.75	0.50
6	F	16.44	15.25	16.00	0.0	5.50
7	G	15.62	0.38	1.38	1.00	7.00
8	H	17.37	4.62	5.38	0.76	7.50
9	I	17.07	0.02	1.38	0.76	7.00

NOTE: Dimensions in inches.  
Add 2 in. to Y to shift to plate edge.

3.3.10

TABLE 3.3.5. Radiographic Indications in Block No. 202

Indication No. (arbitrary)	Dimension A <sup>(a)</sup>		Dimension B		Dimension C		Depth		Length		Characterized As
	(mm)	(in.)	(mm)	(in.)	(mm)	(in.)	(mm)	(in.)	(mm)	(in.)	
A 9	605	23.8	10	0.4	48	1.99	?		22	0.87	Crack
B 6	465	18.29	150	5.91	56	2.20	71	2.79	36	1.42	Non-fusion
C Not in Sequence	201	7.91	414	16.29	81	3.19	?		20	0.79	Slag or void
D	188	7.40	427	16.9	104	4.09	26	1.02	16	0.63	Slag or void
E 3	169	5.65	446	18.55	52	2.04	?		30	1.18	Crack
F 4	133	5.23	482	18.97	80	3.15	161	6.33	31	1.22	Void or slag
G 2	72	2.83	543	21.37	48	1.99	38	1.49	41	1.61	Void or non-fusion
H 1	72	2.83	543	21.37	102	4.01	38	1.49	45	1.77	Void or slag

(a) Not same locations or terminology as flaws identified in PVRC Documents.

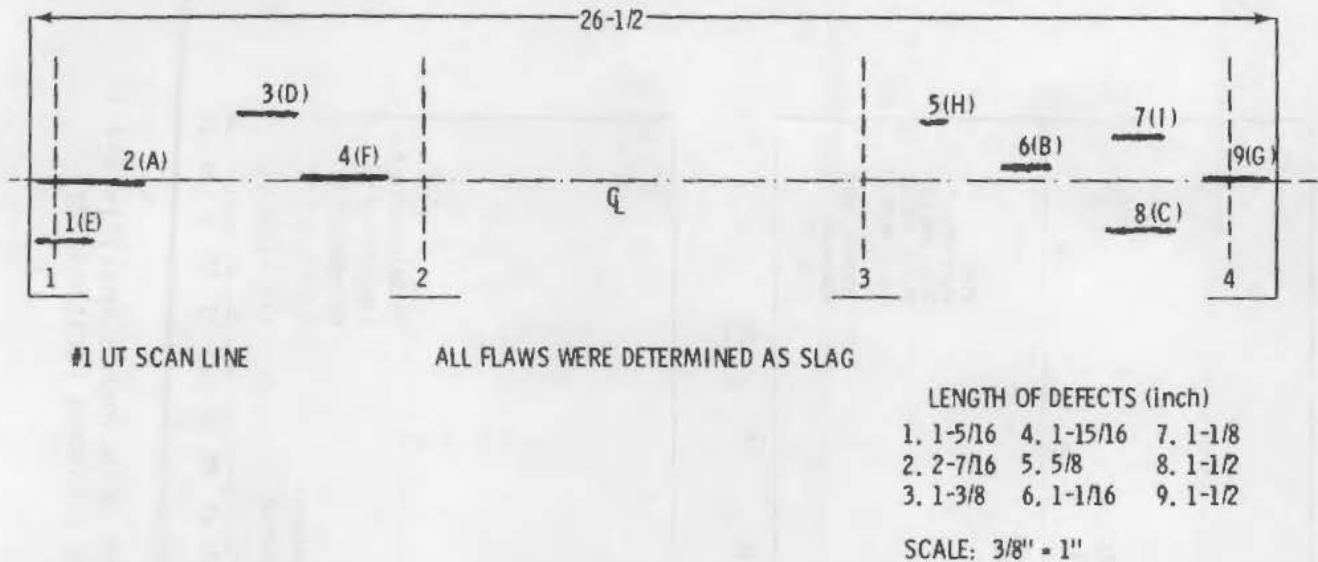


FIGURE 3.3.4. Summary Drawing of Radiographic Results on PVRC Specimen 202

Special UT studies were conducted by one team using three procedures: 1) the ASME Section XI procedures, 2) the UT procedures used in Germany for reactor pressure vessels, and 3) a tandem UT procedure, also used in Germany. The tandem procedure could not be completely calibrated for the cladding on one-half of the 202 plate, rendering much of the data questionable. This technique did not prove too successful in locating flaws--identifying only two. (3.3.3)

The ASME XI and German procedures were more successful. ASME XI procedures located 13 flaws and German procedures located 23.

Two flaws were located by RT, tandem UT, ASME UT and German UT; three flaws were located by RT, ASME XI UT and German UT; two flaws were located by RT and German UT; one flaw was located by RT and ASME XI UT; and one flaw was located by RT. Other indications were located by UT but not by RT. Four were located by both ASME XI UT and German UT. Apparent dimensions and locations were given for all indications.

Figure 3.3.5 graphically presents the collective ultrasonic data on PVRC block No. 202 as reported in various studies. (3.3.1, 3.3.3, 3.3.4) Some idea of the degree of overlap of team data as well as the difference between presumed

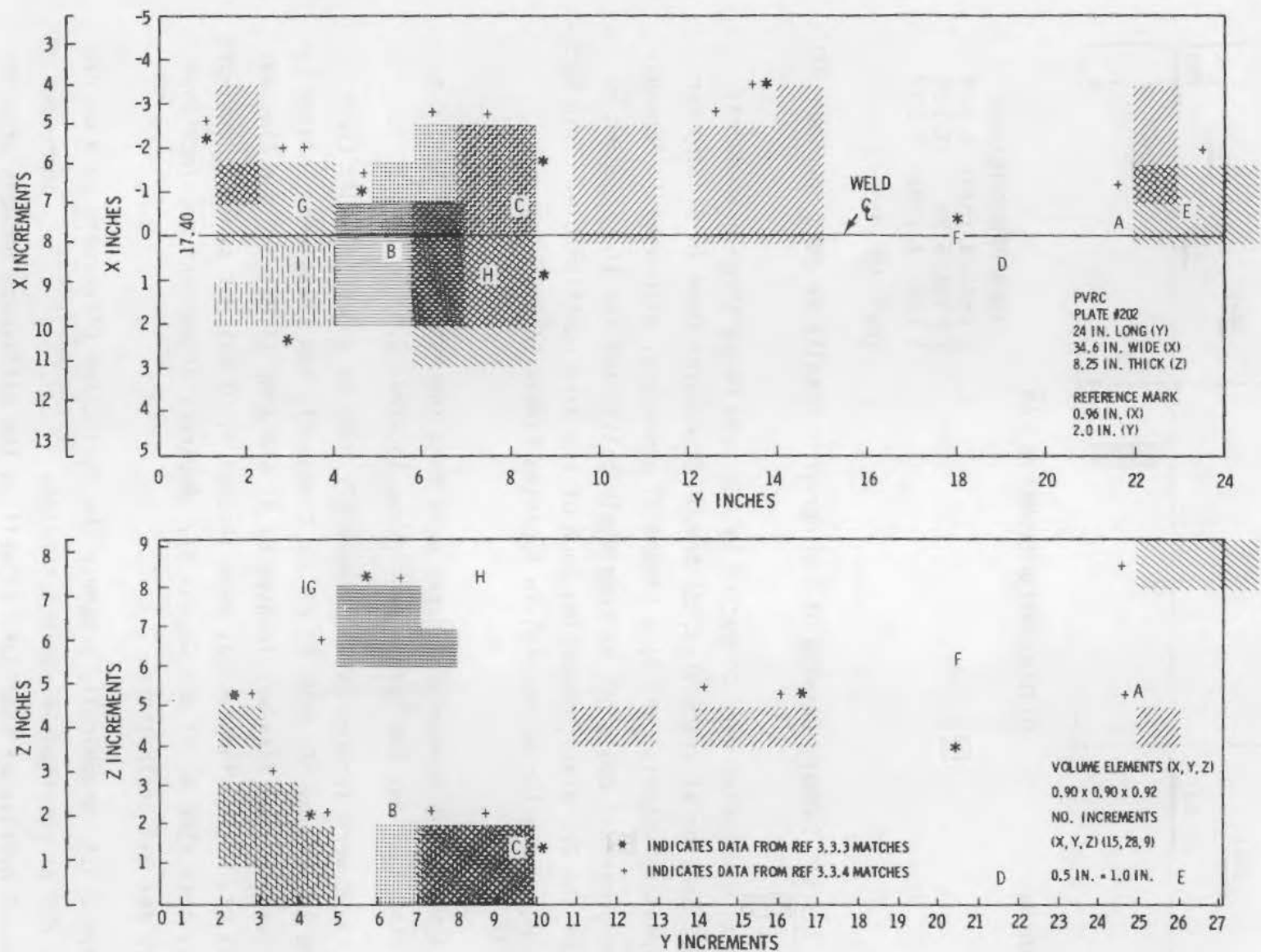


FIGURE 3.3.5. Graphical Representation of PVRC 202 Block Data After Coincidence Analysis(3.3.1) References 3.3.3 and 3.3.4 Included. Letters denote presumed locations of discontinuities.



locations of discontinuities versus reported locations can be obtained from this figure. Reference 3.3.4 covers an Immersion C-Scan Technique.

### 3.3.3 PVRC Specimen 203

PVRC Specimen 203 consisted of a nozzle welded into an 8.3-in. plate (see Figure 3.3.6). Table 3.3.6 contains a summary of UT results at the three tolerances. All flaws were detected by angle beam, either 45° or 60°. One flaw (7) was detected in the 0.5-in. tolerance, five (1, 3, 4, 7, 9) in 1.0-in. tolerance and the same five in the 1.5-in. tolerance band. Six teams were successful in locating one or more flaws. The  $R_{III}$  values are low, only 0.07, as noted in Table 3.3.7.

The presumed locations of the flaws are given in Figure 3.3.7. Radiography indicated substantial disagreement in detected flaw locations versus presumed locations (see Figure 3.3.8 and Table 3.3.8).

The 2-point coincidence method was used with 0.45-, 0.9- and 1.35-in. volume elements. Percentages of correct indications were 54.5, 61.4, and 72.7%, respectively. The analysis for 2- to 7-point coincidence and 0.9-in. volume elements were 61.4, 45.5, 38.6, 36.4, and 36.4%.

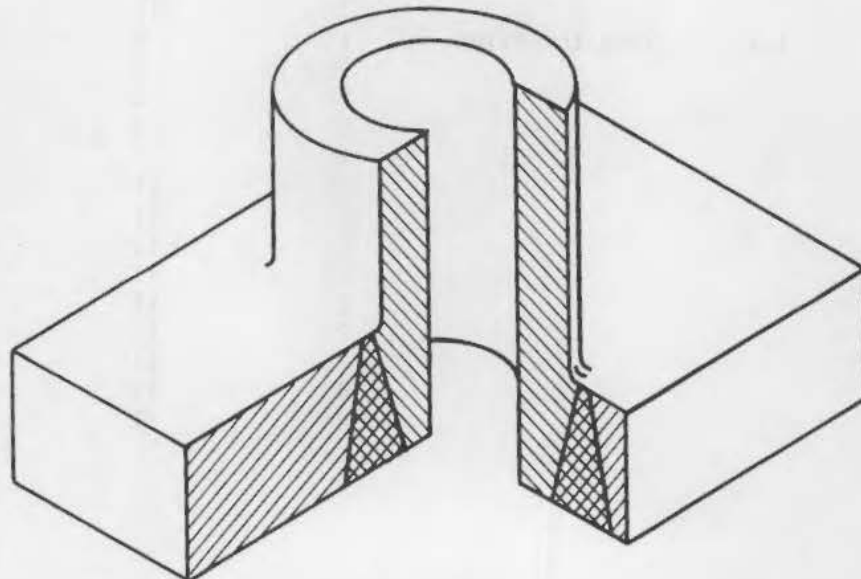


FIGURE 3.3.6. PVRC Weld Specimen 203 48-1/2 (123 cm) x 48-1/2 (123 cm) x 8-1/4 (21 cm)

**TABLE 3.3.6. Summary of Ultrasonic Examination Results, PVRC Specimen 203, Method**

Discontinuity Number	Tolerance Level (in.)	Discontinuity Type	Indication Number	Correctly Identified by Team Number	Ultrasonic Inspection Mode (shear wave)
7	0.5	Slag inclusion	30	11	45°
1	1.0	Slag inclusion	38	12	60°
3	1.0	Non-fusion zone	13	6	60°
4	1.0	Slag inclusion	12	6	60°
7	1.0	Slag inclusion	28	11	45°
			30	11	45°
			31	11	45°
			32	11	45°
9	1.0	Slag inclusion	11	6	60°
			16	8	60°
			17	8	60°
			18	8	60°
			44	13	45°
1	1.5	Slag inclusion	8	4	60°
			38	12	60°
3	1.5	Non-fusion zone	13	6	60°
4	1.5	Slag inclusion	12	6	60°
			42	13	60°
7	1.5	Slag inclusion	27	11	45°
			28	11	45°
			29	11	45°
			30	11	45°
			31	11	45°
			32	11	45°
9	1.5	Slag inclusion	11	6	60°
			15	8	45°
			16	8	60°
			17	8	60°
			18	8	60°
			21	11	45°
			22	11	45°
			23	11	45°
			24	11	45°
			25	11	45°
			26	11	45°
			36	11	45°
			43	11	45°
			44	11	45°

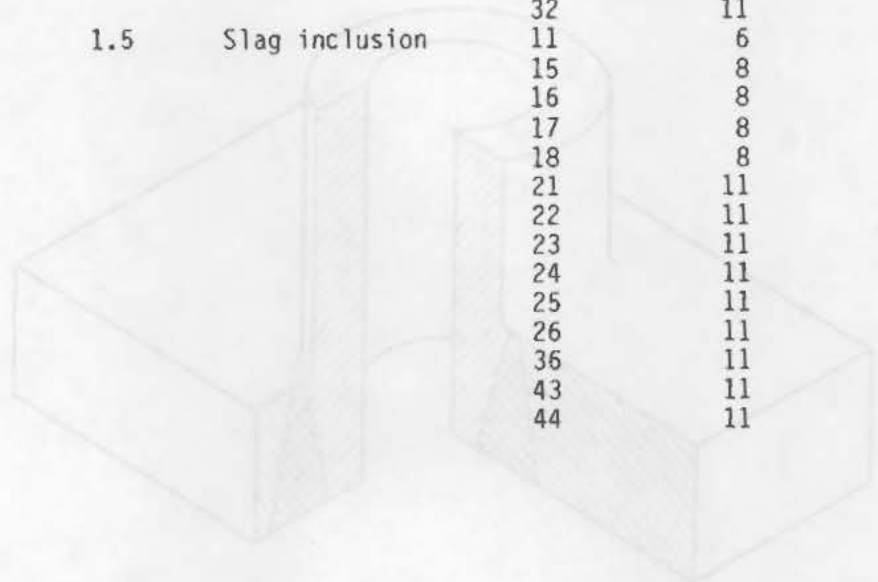


TABLE 3.3.7. Team Rating Factors, Specimen 203,  
1.0-in. Tolerance Level, Standard  
Method of Analysis

<u>Team</u>	<u>F</u>	<u>u</u>	<u>f</u>	<u>R<sub>III</sub></u>
1	0	9	3	0.0
2	0	9	1	0.0
3	0	9	2	0.0
4	0	9	3	0.0
5	0	9	1	0.0
6	3	6	0	0.50
7	0	9	1	0.0
8	1	8	1	0.11
9	0	9	2	0.0
10	0	9	0	0.0
11	1	8	8	0.06
12	1	8	6	0.07
13	1	8	4	$\frac{0.12}{0.07^{(a)}}$

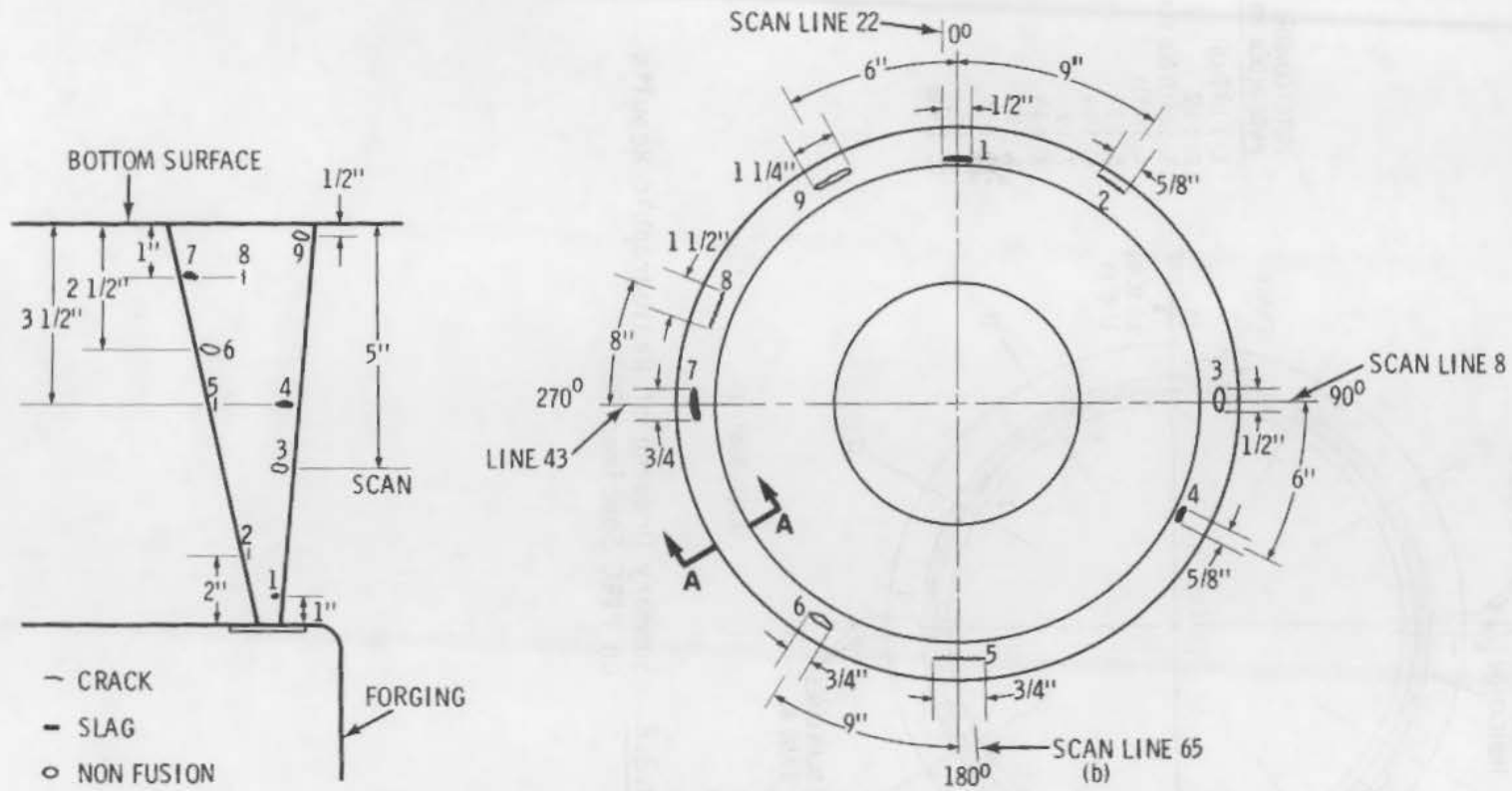
(a) R<sub>III</sub> average.

TABLE 3.3.8. Comparison of Intended Flaw Locations in PVRC Specimen 203 with Radiographs(3.3.2)

Flaw Identification		Intent		RT		Intent		Intent Z, in.
Intent	RT	$R_1R_2$ , in.	$R_1R_2$ , in.	$e_1$ Length	$e_2$ Length	$e_1$ Length(a)	$e_2$ Length(a)	
1(A)	11	11.6	12.6	88.8° 0.5 in.	91.2°	84° 1.5 in.	90°	1
2(B)	12	13.3	12.8	46.7° 0.6 in.	49.6°	51° 1.6 in.	58°	2
3(C)	1	11.4	11.4	358.8° 0.5 in.	1.2°	350° 1.3 in.	356°	3.75
4(D)	2	11.3	11.3	330.6° 0.6 in.	333.5°	321° 1.5 in.	328°	4.75
5(E)	4	13.8	13.8	268.3° 0.8 in.	271.4°	262° 1.9 in.	270°	4.75
6(F)	5	14.0	14.0	226.4° 0.8 in.	229.9°	233° 1.8 in.	240°	5.75
7(G)	6	14.2	14.2	178.3° 0.8 in.	181.4°	176° 1.3 in.	180°	7.25
8(H)	8	12.3	12.8	129.3° 1.5 in.	146.3°	136° 2.4 in.	146°	7.25
9(J)	10	11.0	12.2	115.0° 1.3 in.	120.8°	111° 1.4 in.	117°	7.75
	3						295 300 scattered slag	
	7		12.8			171° 0.5 in.		
	9		13.0			133° spot		

(a) Lengths as reported by radiographer; angles are approximate.

3.3.17



NOTE: DEFECTS NOT TO SCALE

FIGURE 3.3.7. Discontinuity Locations in PVRC Specimen 203

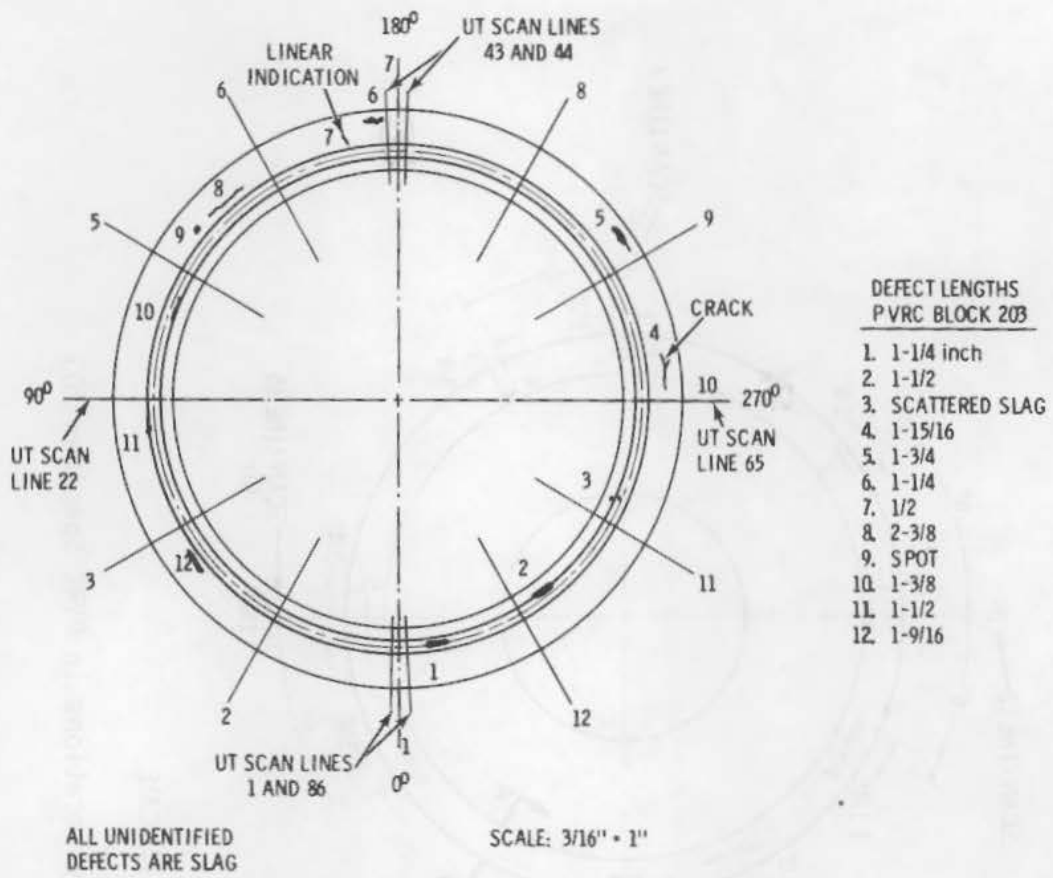


**FIGURE 3.3.8.** Summary Drawing of Radiographic Results on PVRC Specimen 203

Tables 3.4.1 and 3.4.2 permit intercomparisons. The  $R_{III}$  values range from 0.02 to 1.52. The primary reason for the low values is the difference in actual versus presumed flaw locations.

Table 3.4.2 compares the standard method, based on tolerance levels and assumed flaw locations versus 2-point coincidence.

It will be necessary to await results of sectioning before we can assess these UT results.

TABLE 3.4.1. Comparison of Rating Factors Achieved by Different UT Examination Procedures on PVRC Specimens

<u>Specimen</u>	<u>Specimen Type</u>	<u>Stage of Analysis</u>	<u>UT Examination Procedure Employed</u>	<u>R<sub>III</sub> (average)</u>
201	Plate-weld	Metallurgically sectioned	PVRC procedure for ultrasonic examination of welds in Plates 201 and 202 for Pressure Vessel Research Committee Program--As published in <u>Welding Journal</u> , December 1971, p. 529s.	1.52
251J	Plate-weld	Metallurgically sectioned	Ultrasonic examination of welds for Pressure Vessel Research Committee Program--February 16, 1968.	0.11
			Ultrasonic examination of welds in plates 201 and 202 for Pressure Vessel Research Committee Program--March 19, 1970.	0.24
155	Nozzle-weld	Not as yet metallurgically sectioned	Procedure for manual ultrasonic examination of PVRC welded test blocks--June 27, 1974; Supplement--August 9, 1974; Modification--September 18, 1974.	0.11
202	Plate-weld	Not as yet metallurgically sectioned	Procedure for manual ultrasonic examination of PVRC welded test blocks--June 27, 1974; Supplement--August 9, 1974; Modification--September 18, 1974.	0.02
203	Nozzle-weld	Not as yet metallurgically sectioned	Procedure for manual ultrasonic examination of PVRC welded test blocks--June 27, 1974; Supplement--August 9, 1974; Modification--September 18, 1974.	0.07



TABLE 3.4.2. Comparisons of the Two Methods of Analyses on PVRC Specimens 155, 202 and 203

Specimen	Percentage of Reported <sup>(a)</sup>					
	Standard Method <sup>(b)</sup>			Two-Point		
	Tolerance Level (in.)			Coincidence Method <sup>(c)</sup>		
	0.5	1.0	1.5	0.45	0.9	1.35
155	3.6	19.6	57.1	71.4	76.8	80.4
202	0.0	4.3	7.2	76.8	84.1	81.2
203	2.3	27.3	56.8	54.5	61.4	72.7

- (a) Based on Intended discontinuity locations.  
 (b) Indications considered correct.  
 (c) Nominal volume-element size (in.).

TABLE 2. Accuracy of the Two Methods of Analysis on RWC  
 Specimens 152, 505 and 509

Specimen	Reference Level (%)		Standard Method (a)		Two-Point Concubine Method (b)	
	1.0	1.5	1.0	1.5	1.0	1.5
152	19.8	27.1	17.4	25.8	18.5	26.4
505	4.5	5.2	4.8	5.1	4.1	4.5
509	23.9	28.0	24.5	28.4	21.8	25.3

(a) Data on internal distortion factor  
 (b) Distortion factor correct  
 (c) Initial value of water stress (%)

### 3.5 THE EUROPEAN PLATE INSPECTION STEERING COMMITTEE (PISC) PROGRAM

The European Community expressed an interest in the early 1970s in participating in the ICP-PVRC NDE programs. Arrangements were formalized through PISC during 1975 and NDE began in 1976. Ten countries participated, represented by 34 organizations, of which 28 carried out NDE on the test plates. All of the 28 used the basic PISC technique, essentially the same procedure as that in the 1974 Appendix I of ASME XI, which was used in recent PVRC programs. In addition, seven teams used the "improved" PISC techniques which differed only in setting 20% DAC as the recording level rather than 50% DAC. Nineteen of the teams used one or more alternative procedures in addition to the basic PISC/PVRC/ASME XI--Appendix I procedure. These alternative procedures included inspection from the inside surface, focused probes using the immersion technique, focused probes using the contact technique, tandem techniques, automated NDE, acoustic holography, high frequency back scattering techniques, amplitude-time locus curves, delta technique, phased arrays, full skip, longitudinal wave angle probes and other standard probes.

Three PVRC test plates were made available to PISC. They were Plates 50-52, 51-53 and 204 described in Tables 3.2.1 and 3.2.2. Plate 50-52 consisted of two 11-in. (27-cm) plates joined with a butt-weld (Figure 3.5.1); Plate 51-53 consisted of two 8-3/4-in. (22-cm) plates joined with a submerged arc butt-weld (Figure 3.5.2); and 204 consisted of an 18-in. (45-cm) forged nozzle welded into an 8-in. (20-cm) -thick plate with manual metal arc weld (Figure 3.5.3). A variety of defects was included in the welds.

The NDE phase was completed during 1978 and the destructive examination to establish flaw size and location was essentially completed in the first half of 1979. The available information covering both NDE and destructive testing has been stored in a computer and evaluated.

The status as of late 1980 is as follows:

- Six reports were prepared to be presented at post-SMIRT (Structural Materials in Reactor Technology) Conference in Berlin in August 1979. The reports dealt with 1) materials, <sup>(3.5.1)</sup> 2) UT, <sup>(3.5.2)</sup>

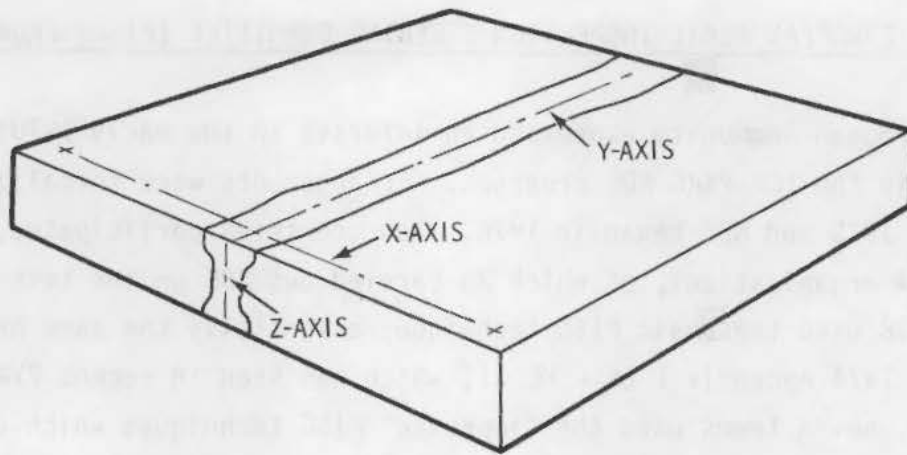


FIGURE 3.5.1. PVRC Weld Specimen 50-52

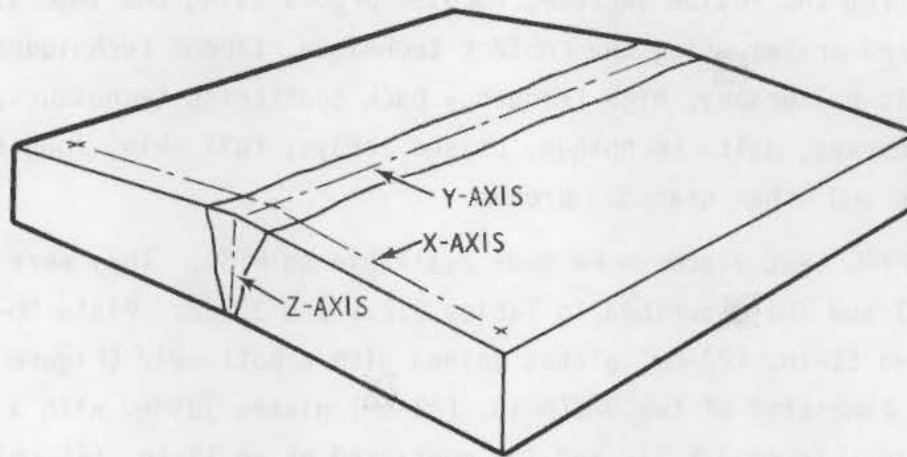


FIGURE 3.5.2. PVRC Weld Specimen 51-53

3) Sectioning, <sup>(3.5.3)</sup> 4) Analysis, <sup>(3.5.4)</sup> 5) Evaluation <sup>(3.5.5)</sup>  
 and 6) Summary, Conclusions and Recommendations. <sup>(3.5.6)</sup>

- Further reports are planned addressing specific alternative NDE procedures. A significant aspect of the PISC program is the data evaluation which will be discussed in Section 3.5.4. The nomenclature differs somewhat from that used in other PVRC reports. It is introduced here in the following paragraph and in Table 3.5.1, rather than later.

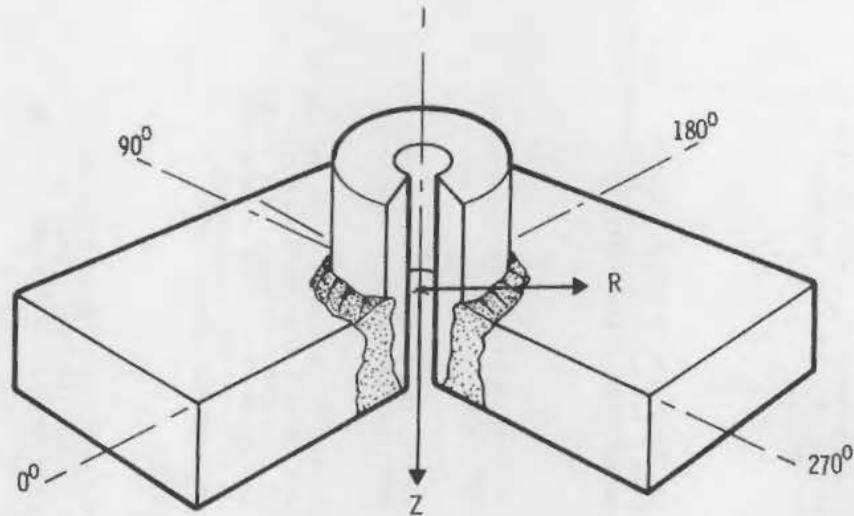


FIGURE 3.5.3. PVRC Weld Specimen 204

Several terms defining parameters used in the evaluation of the PISC-NDE data were used in the study. They are presented here, together with their ranges of values. The latter is given because such ranges are highly sensitive to the bounding conditions utilized. For example, the rejection criterion is relevant to sub-surface defects only due to the decision of PISC to consider all defects in the three plates as sub-surface defects. This simplification permits a direct comparison of all defects from an NDE point of view. If more specific criteria were to be used, such as 1) sub-surface defects criteria, 2) surface defects criteria, and/or 3) nozzle weld defects criteria, the values of parameters [or quality of acceptance (QA)] and the correct rejection probability (CRP) or the correct acceptance probability (CAP) defined below would change. Therefore, the values cited elsewhere in this section apply only for the specific boundary conditions and should not be extrapolated without first considering the implications of the bounding conditions.

For all factors other than error in location (EL) and error in sizing (ES), a value of one (1) indicates a perfect result for a single team. Since values are averages of several teams, care must be exercised in assessing the significance. Perfect value for EL or ES is zero (0).

TABLE 3.5.1. Main Parameters Considered in the Evaluation of PVRC Plates 50-52, 51-53 and 204 by the Plate Inspection Steering Committee (PISC)

Parameter	Perfect Result <sup>(a)</sup>	Deviations from Perfect Result	Significance of Deviations and Remarks
Correct Acceptance Probability (CAP) This is a conditional probability. If a defect is detected, CAP indicates how well it is accepted.	<u>1</u>	0 > <u>1</u>	Zero indicates failure to correctly classify CAP (and CRP) and is related to QA or QR. These values are evaluated using a modified form of ASME XI permissible flaw-size standards for sub-surface defects.
Correct Rejection Probability (CRP) Definition similar to CAP except for rejection.	<u>1</u>	0 > <u>1</u>	
Defect Detection Probability (DDP) This probability is determined in terms of the maximum tolerance considered for the purpose of deciding whether detection has or has not occurred. This tolerance is generally 50 mm.	<u>1</u>	0 > <u>1</u>	Zero indicates a failure to detect. Numbers between 0 and <u>1</u> are averages of all teams for one flaw or for flaws collectively.
Error in Location (EL) Values are given for EL in the X, Y, Z directions.	0	Positive; >0	Deviations in terms of "known" location, values plus 2 $\sigma$ error band.
Error in Sizing (ES) As with EL, in X, Y, Z directions, plus a summation value.	0	><0	If ES is negative, the defect is undersized. If ES is positive, the defect is oversized.
Quality of Acceptance (QA) QA (and QR) of the defect is based on the INB-3500 criteria of ASME XI, modified for through-thickness separation and disregarding surface proximity. They apply only for planar sub-surface indications.	1	><0	QA may exceed one (1) indicating on the average no acceptable defects were wrongly rejected even though they were oversized. QA < 0 indicates on average teams rejected an acceptable defect. QA > 0 indicates teams correctly accepted an acceptable defect.
Quality of Rejection (QR) Defined above under QA.	<u>1</u>	><0	As for QA above.
Quality of Location (QL) A measure of the ability to correctly locate flaw in the Y direction.	<u>1</u>	>< <u>1</u>	QL > 1 indicates average flaw location was higher in through-thickness (rare); QL < <u>1</u> indicates average flaw location was lower in through-thickness.
Quality of Sizing (QS) A measure of the ability to correctly size the flaw in the Z direction.	<u>1</u>	>< <u>1</u>	QS < <u>1</u> indicates on average teams underestimated size. QS > <u>1</u> indicates on average teams over-estimated size of defect.

NOTE: All errors are given for a 95% confidence level ( $\pm 2 \sigma$ ).

(a) Values in the following tables are averages of several examinations, not a single value.

### 3.5.1 PVRC (PISC) Specimen 50-52

Because of the large number of defects in the three test pieces, it became necessary to use the ASME XI proximity rules given in IWB-3000. Both the proximity of a defect to the surface and the proximity of multiple defects to one another are considered in combining defects. In addition to the direct application of IWB-3000, a modified procedure was developed to permit an intercomparison of flaw sizes from test piece to test piece. In the modified procedure, the surface proximity rules were ignored (defects near the surface retain their actual size) and for combinations of defects in the YZ plane, Z is not compared to 2a, but to 0.5 in. (13 mm) as prescribed in ASME XI for defects in the X-direction. YZ was considered the plane of maximum principal stress for the analysis.

Obviously, the preceding rules apply equally to all three test pieces. In the case of 50-52, the application of either IWB-3000 or the modified form, yields the same result; namely, two separate unacceptable defects.

The larger defect (No. 1) was missed by one team (No. 1); generally the defect was located and sized reasonably well as noted in Figure 3.5.4. Figure 3.5.5 illustrates the variation in sizing from procedure to procedure. PISC DS5 refers to the comparison with Data Sheet 6, constructed by the computer from Data Sheet 5, given by teams following the PISC procedure. Specifically, DS-5 represents responses along each scanning line. In the case of PISC DS6, the comparison is with Data Sheet 6 given by teams following the PISC procedure. Data Sheet 6 contains team sizings of individual defects. ALT refers to the comparison with Data Sheets 6 given by teams following alternative procedures.

The defect detection probability (DDP) as noted in Table 3.5.1 is that DDP at some tolerance value considered for the purpose of deciding whether detection has or has not occurred. Three values were investigated: 100 mm, 50 mm, 25 mm, where the values denote a cube size within which the center of a defect is considered to fall. As noted in Figure 3.5.6 a cube size (length) of 50 mm is adequate to yield a high and reproducible value of DDP.

Most of the comparisons relevant to Plate 50-52 will be given in Section 3.5.4.

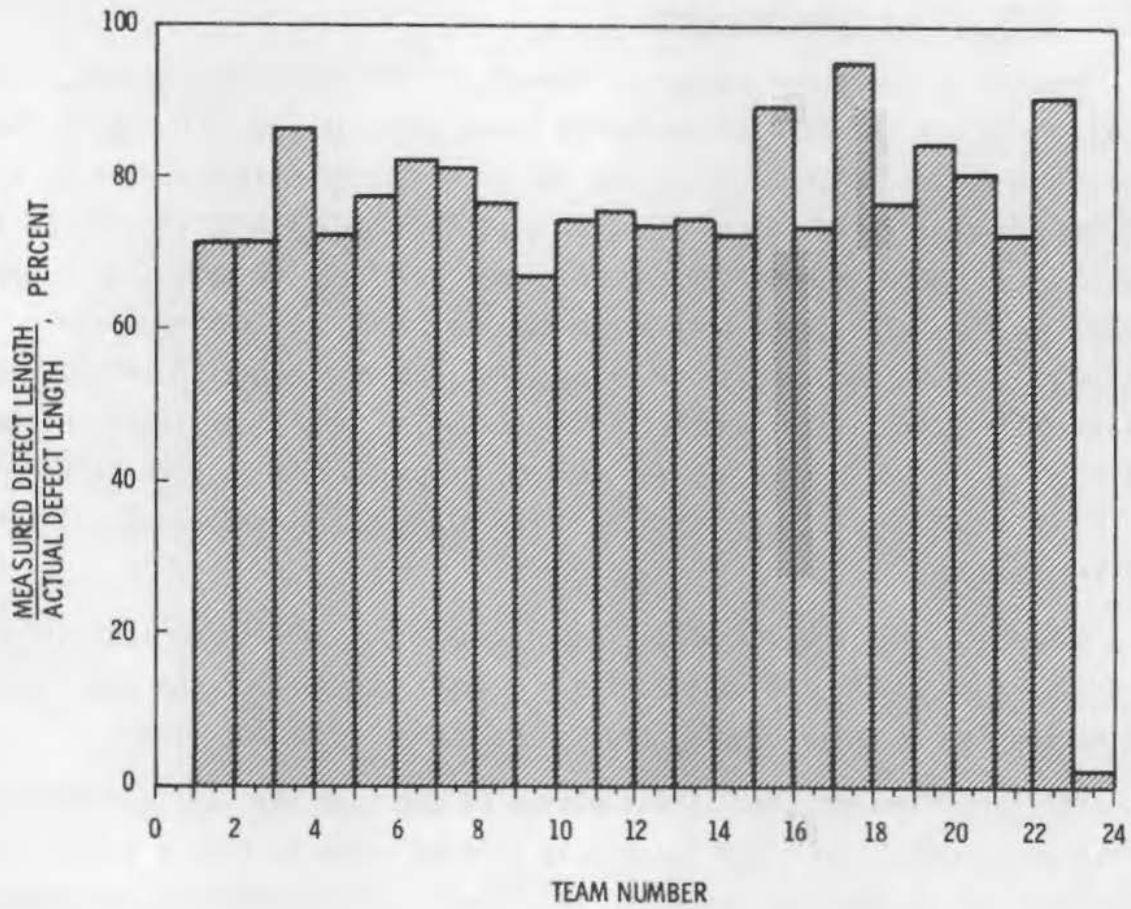
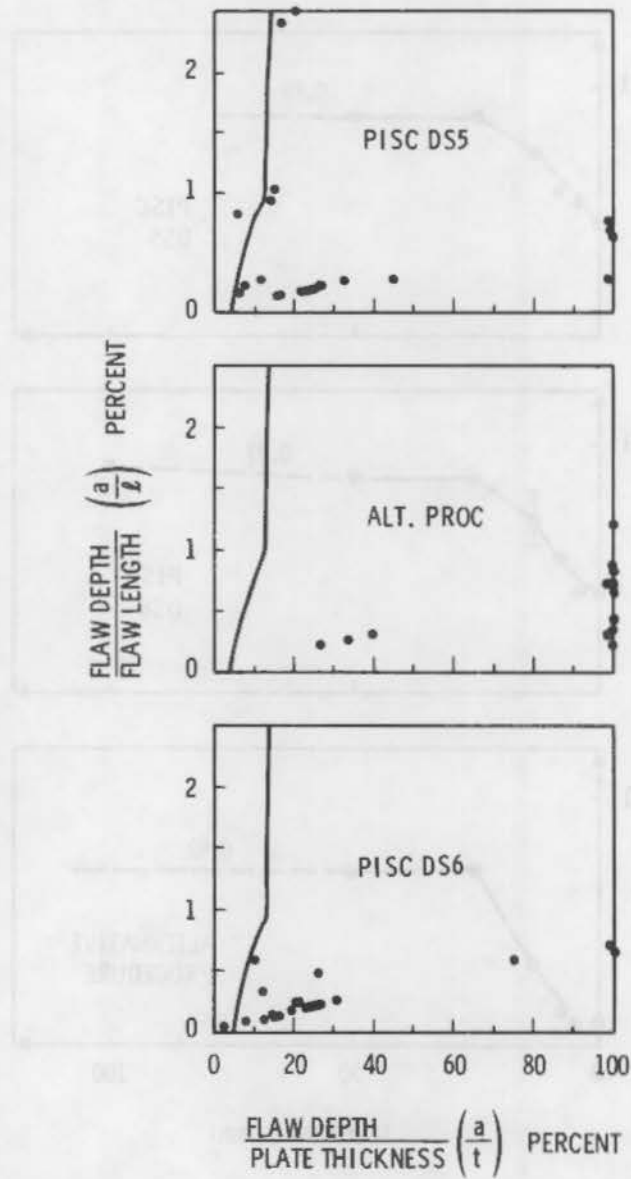


FIGURE 3.5.4. Plate 50-52 Defect Number 1, Application of Full ASME XI IWB-3000 Proximity Rules and PISC Procedures; Presented Team by Team





**FIGURE 3.5.5.** Plate 50-52 Defect Number 1, Full ASME XI Proximity Rules Applied; Boundary Line Defined Using ASME XI Upper Bound Flaw Standards Values Condition for Plane YZ, the Plane of Maximum Principal Stress

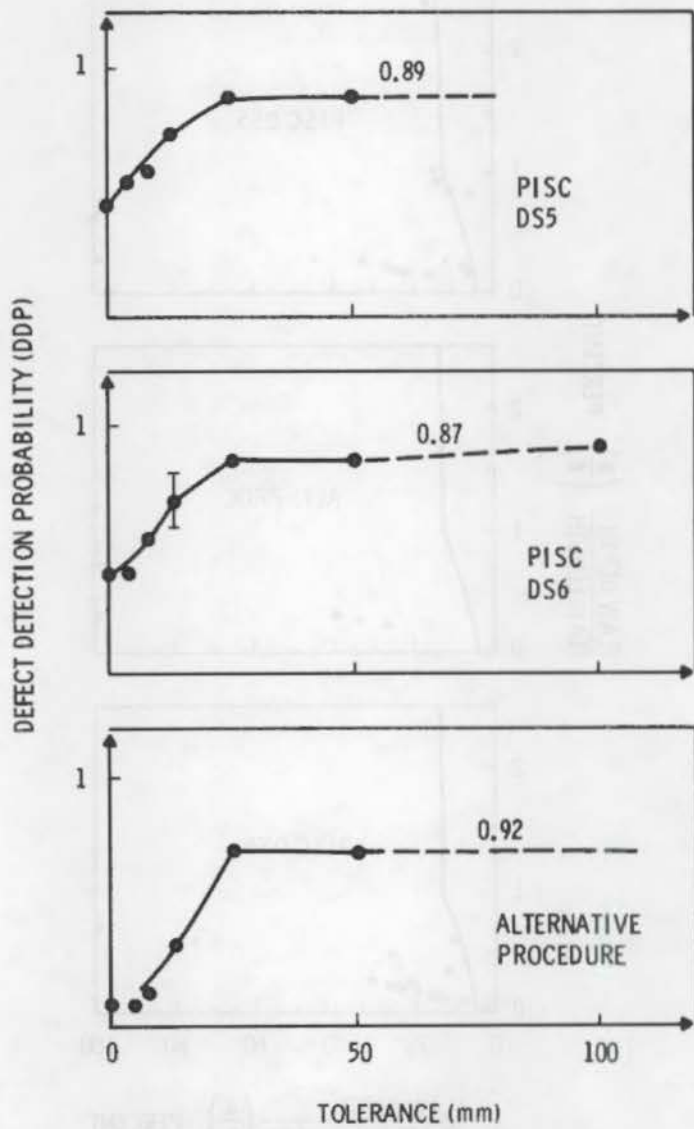


FIGURE 3.5.6. Defect Detection Probability for Defect Number 2 in Plate 50-52 as a Function of the Tolerance in Detection-Location of the Defect

### 3.5.2 PVRC (PISC) Specimen 51-53

An application of the flaw proximity rules to Plate 51-53 indicates there is one large rejectable flaw. The data also reveal the sensitivity of the proximity rules to missing small defects that are between large ones. Figure 3.5.7 illustrates this effect. The population is divided into teams that

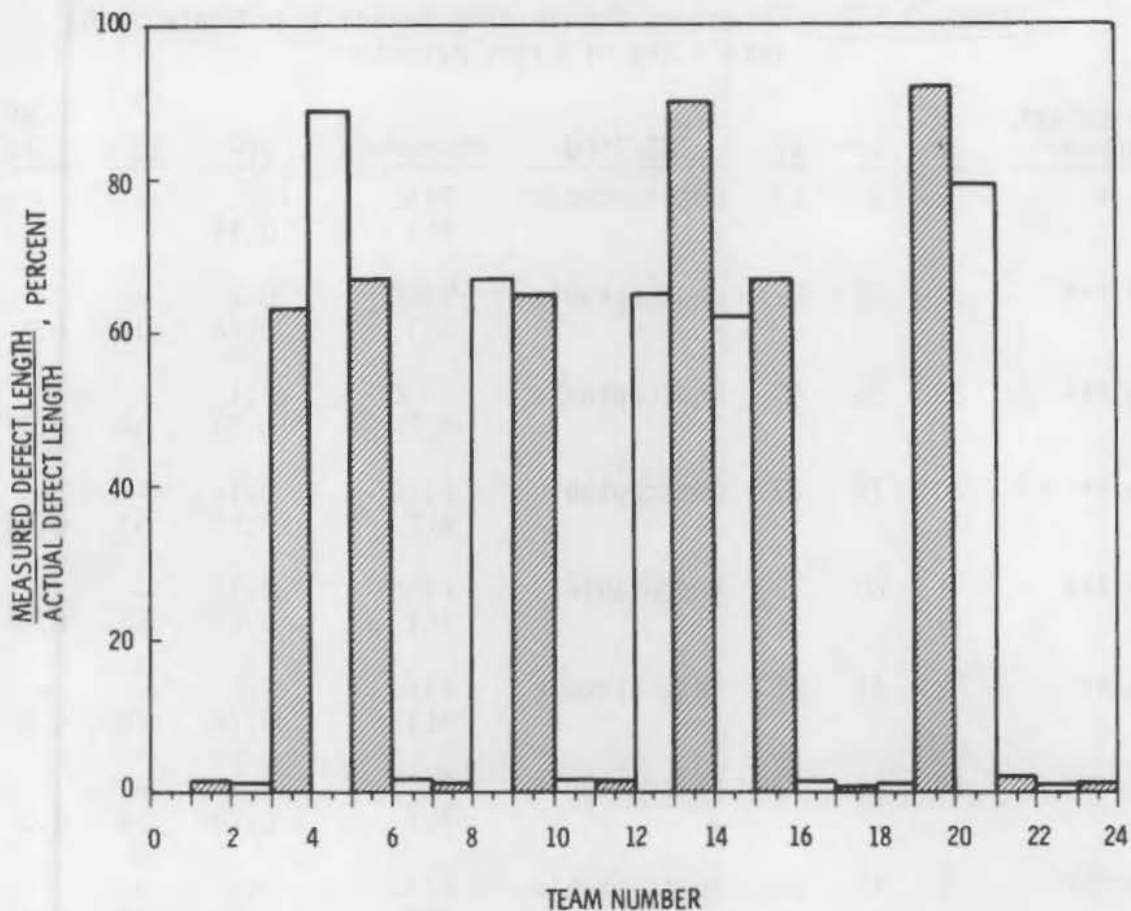


FIGURE 3.5.7. Full ASME XI Proximity Rules Applied to Plate 51-53 for Defect Number 1; Team by Team

missed just enough not to have the full combination of defects, and the fortunate teams that detected the necessary defects.

The effects of NDE procedure on correct detection and classification of the large defect in 51-53, when subdivided into eight smaller defects, can be seen in Table 3.5.2. The alternative procedures clearly yield superior results compared to the PISC procedure. However, even with the alternative procedures, CRPs are quite low and errors in sizing are high. As with 50-52 most of the 51-53 data will be given in Section 3.5.4.

TABLE 3.5.2. Effect of Subdividing Defect 1 in Plate 51-53 into a Set of Eight Defects

<u>Sub-Defect Number</u>	<u><math>\Delta X</math></u>	<u><math>\Delta Y</math></u>	<u><math>\Delta Z</math></u>	<u>IWB-3500</u>	<u>Procedure</u>	<u>DDP</u>	<u>ES</u>	<u>CRP (CAP)</u>
1.1 *	2	15	13	Unacceptable	PISC ALT	<0.1 0.44	-	-
1.2 ***	22	30	22	Unacceptable	PISC ALT	<0.1 0.78	- >10	- 0.3
1.3 ***	29	58	40	Unacceptable	PISC ALT	<0.1 0.78	- >4	- 0.3
1.4 **	20	75	13	Unacceptable	PISC ALT	0.17 0.87	- >1	- 0.54
1.5 ***	1	60	5	Acceptable	PISC ALT	<0.1 0.78	- >5	- 0.48
1.6 **	2	45	11	Unacceptable	PISC ALT	<0.1 0.78	- >20	- 0.8
1.7 ***	10	45	11	Unacceptable	PISC ALT	<0.1 0.78	- >4	- 0.3
1.8 ***	2	45	20	Unacceptable	PISC ALT	<0.1 0.78	- >4	- 0.3

### 3.5.3 PVRC (PISC) Plate 204

Plate 204 basically is similar to Plate 203 illustrated in Figure 3.3.6. Unlike Plates 50-52 and 50-53, defects in it were scattered so that the proximity rules did not apply. Only one of the several defects was considered rejectable.

Plate 204 examination suffered from some limitations such as size; the plate was too small to permit a full 60° probe examination. In addition, the rough-weld surface prevented examination of the weld top by either 45° or 60° probes. Alternative procedures detected a cloud of small defects when applied by a few of the teams. Even with these few teams, detection was quite local and sizing quality was low. One team indicated the defect (cloud) continued for about 90°. Only one defect was designated as unacceptable, and that was not a large one.

Several defects in the base metal led to confusion; these defects were eliminated from the data. Generally, alternative procedures yielded better results; these relatively small defects consistently were oversized; also, the relationship between size of defect and its detection was not always clear because of the nature of some of the defects.

#### 3.5.4 Information Relevant to All Three Plates

The NDE of Plates 50-52, 51-53 and 204 was subject to both adverse and beneficial factors. Human error entered into the incorrect location of defects. When found, the defects were correctly relocated by changing coordinate systems, inversion of coordinates, rotation of coordinates, or redimensioning of defects.

Operator error entered in the failure to record all of the data, probably because of fatigue, since there was a very large number of defects to record.

On the positive side, conditions were much closer to ideal than would occur in a nuclear power plant so that the results could be more optimistic than would be true under "real" conditions.

The data are presented in the following figures and tables. In general the trends are similar to those reported under Section 3.3, "Recent PVRC Programs."

In the following figures, the numbers 1, 2, and 3, or a, b, c, and d appear. These designate the following:

- 1 Acceptable defects
- 2 Large single defects
- 3 Sets of defects.
- a  $0 \leq \Delta Z \leq 10 \text{ mm}$  (all type of defects)
- b  $10 \text{ mm} \leq \Delta Z \leq 15\%T$  (vertical cracks)
- c  $15\%T \leq \Delta Z \leq T$  (vertical defects)
- d  $10 \text{ mm} \leq \Delta Z \leq T$  (composite rejectable defects)

T is the plate thickness and  $\Delta Z$  the height of the defect.

Figure 3.5.8 relates amplitude of detection signal in terms of percentage DAC to the sizing quality  $QS$  in the YZ plane. There are no consistent trends; however, one might argue that the large flaws in Plate 50-52 do tend to develop a trend relationship.

Figure 3.5.9 relates the measured flaw dimension  $2a$  (designated by  $\Delta Z$ ) to the actual flaw size. It is apparent that the collective alternative procedures yield much better results than with the PISC procedure.

DDP is determined in terms of defect size for the flaw families 1, 2, and 3 using both PISC and alternative procedures. The trends are random for the acceptable defects, 1. For the PISC procedure (Figure 3.5.10) sets of defects, 3, have lower probabilities of detection than do single large defects, 2. This difference essentially disappears for alternative procedures (Figure 3.5.11) where differences between 2 and 3 are minimal.

The effects reported for DDP are generally repeated for the CRP. Figures 3.5.12 and 3.5.13 contain relevant information. Since 1 represents acceptable defects, these data are omitted. The PISC procedure is relatively unsuccessful for sets of defects, having very low values of CRP, (Figure 3.5.12).

The alternative procedures are more successful. While sets of defects have lower values of CRP than do single defects, definite trends develop in CRP with increasing defect size. Figure 3.5.14 presents the data in a different fashion. The data are in the same form as in Figure 3.5.5 except that Figure 3.5.14 presents defect data for the three plates.

Trends similar to the preceding for PISC procedures versus alternative procedures occur for quality of sizing  $\overline{QS}$  versus DDP. Values of  $\overline{QS}$  with the PISC procedure are underpredicted with low values of DDP for unacceptable defects as noted in Figure 3.5.15a. With alternative procedures, Figure 3.5.15b, values of both DDP and  $\overline{QS}$  trend toward the optimum of 1.

A significant trend that could have definite implications with regard to the average detection probability  $\overline{DDP}$  is given in Figure 3.5.16. The probability of detection DDP approaches zero near the examining surface. This is

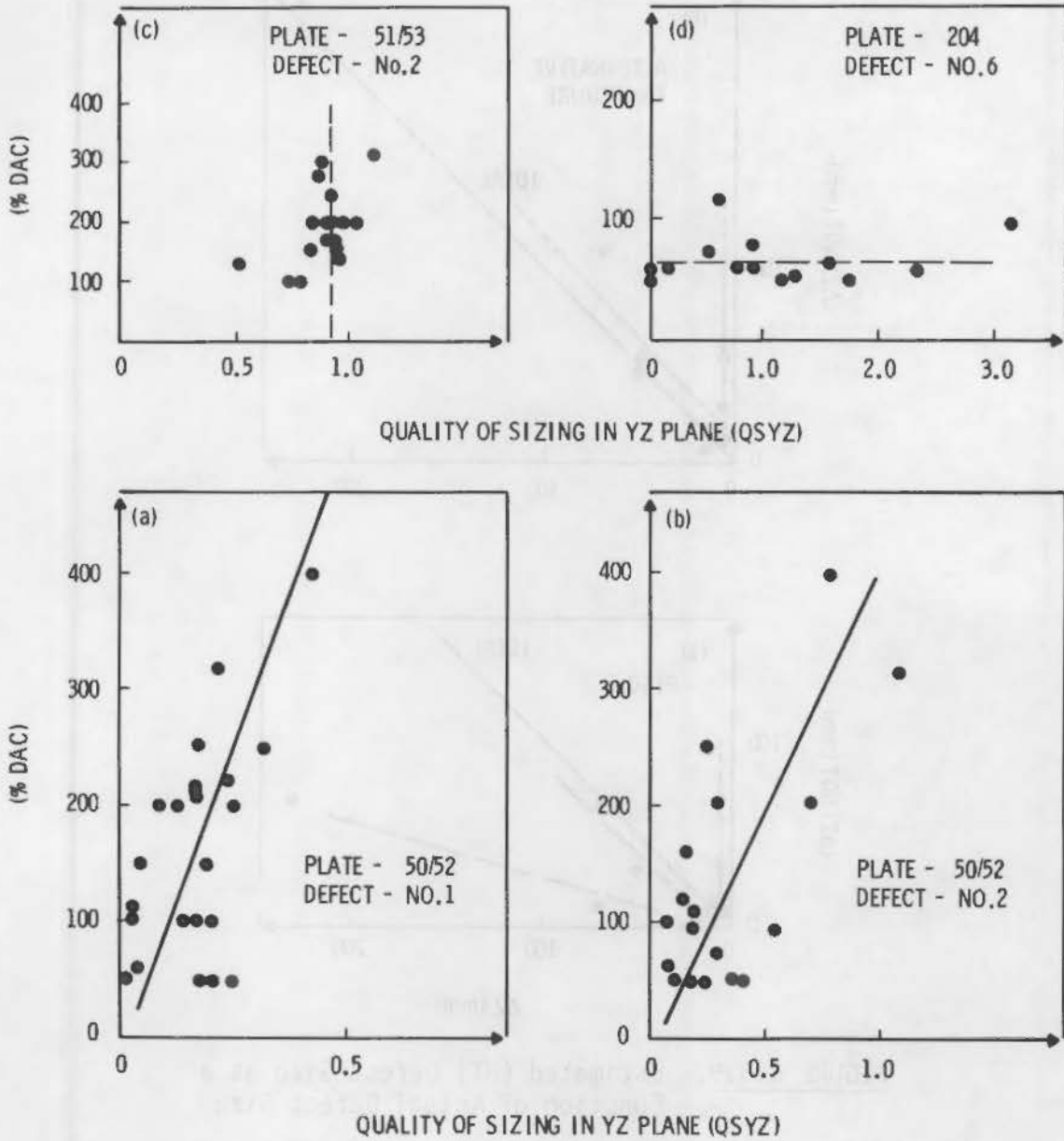
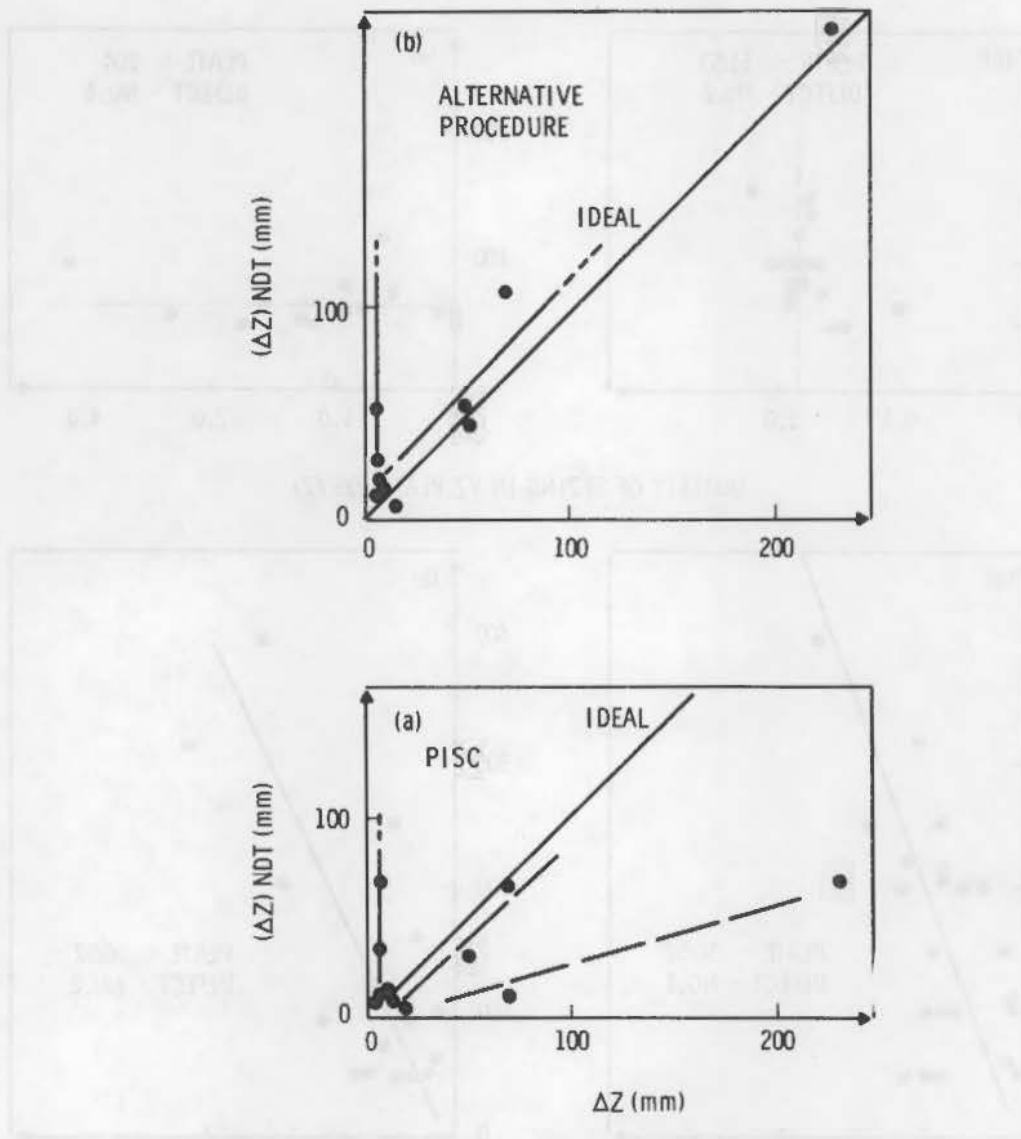


FIGURE 3.5.8. Percentage DAC as a Function of the Sizing Quality

not too surprising considering the near-field dead zone. What is surprising is the minimum occurring near the mid-thickness region. This is true for both PISC and alternative procedures. The far-field back-face region behaves as anticipated with a high probability of detecting flaws.



**FIGURE 3.5.9.** Estimated (UT) Defect Size as a Function of Actual Defect Size

The collective data for both PISC and alternative procedures, using a breakdown of acceptable and unacceptable defects, are presented in Tables 3.5.3 through 3.5.6 for the three plates. Values given include DDP, QL, QS, QA (QR), CAP (CRP).

Figure 3.5.17 provides an overview of the reliability of detection and sizing as functions of the three categories of NDE technique used. In essence, this figure provides an overall summary of the PISC results.



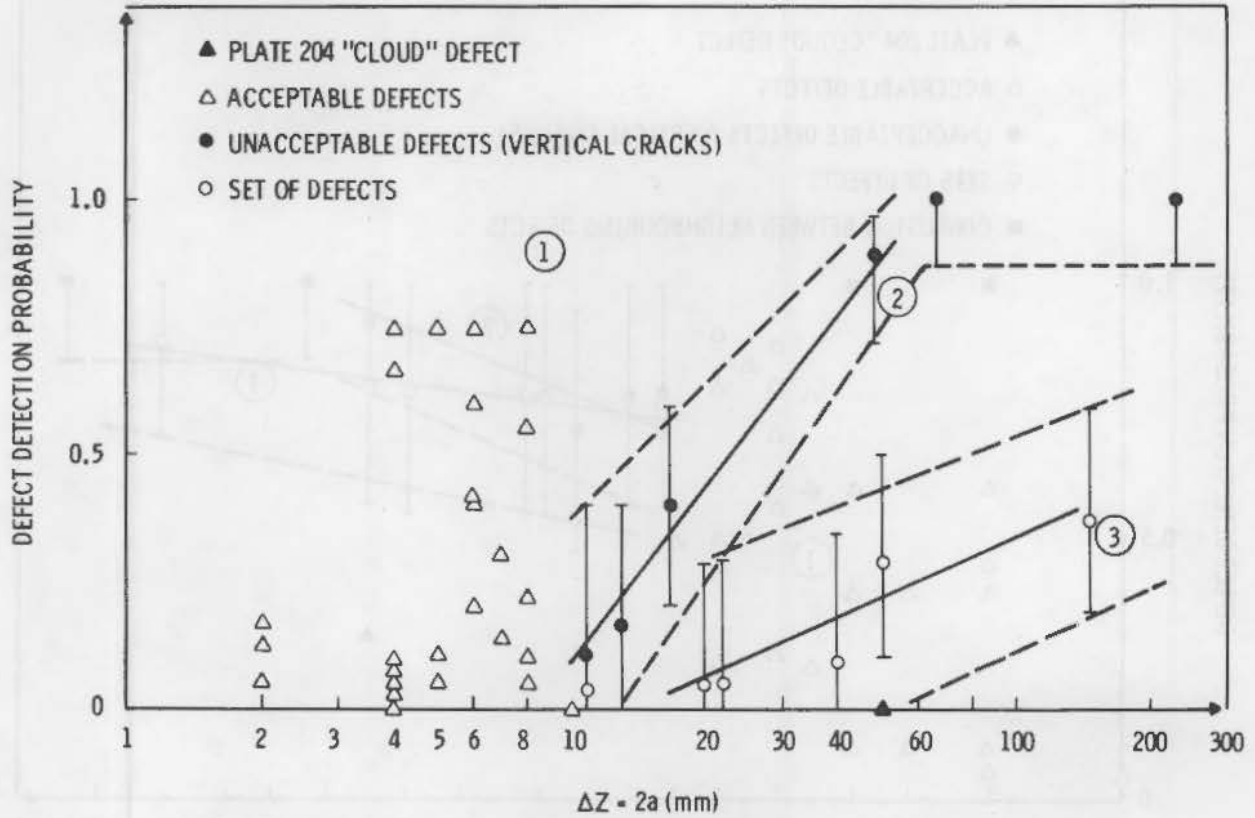


FIGURE 3.5.10. DOP as a Function of Actual Defect Size; PISC UT Procedure Used

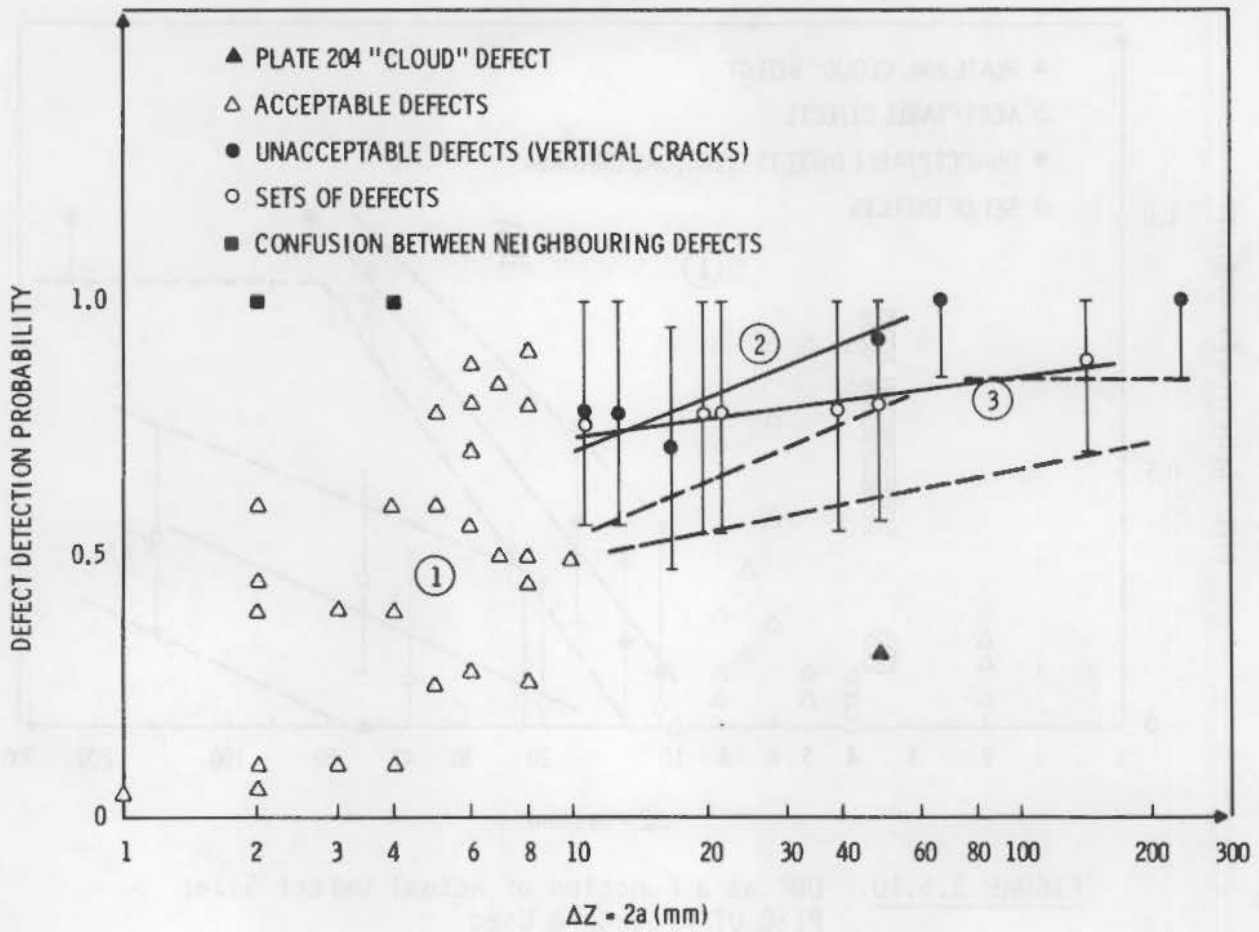


FIGURE 3.5.11. DDP as a Function of Actual Defect Size; Alternative UT Procedures Used

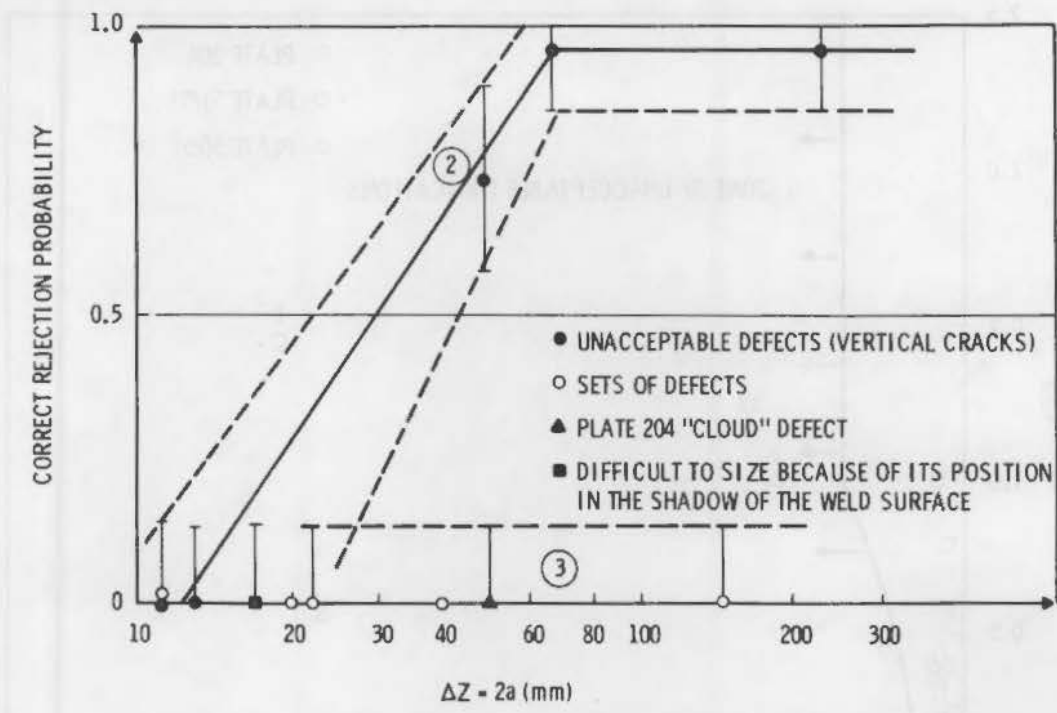


FIGURE 3.5.12. CRP as a Function of the Actual Defect Size; PISC UT Procedure Used

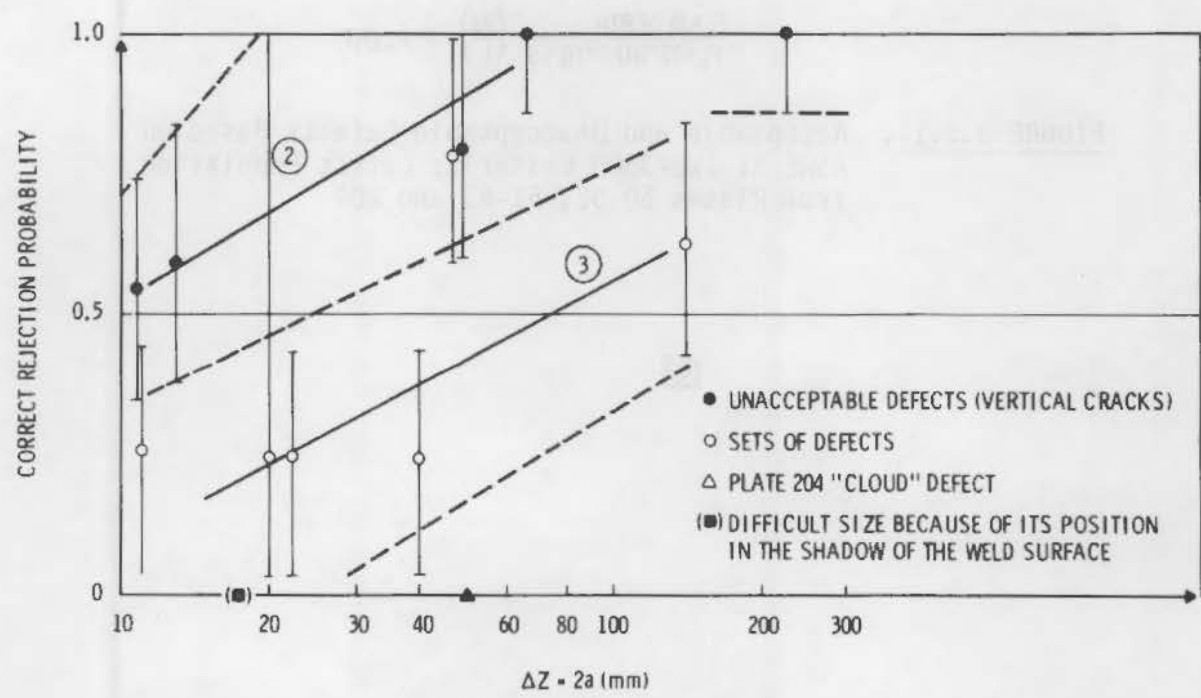


FIGURE 3.5.13. CRP as a Function of the Actual Defect Size; Alternative UT Procedures Used

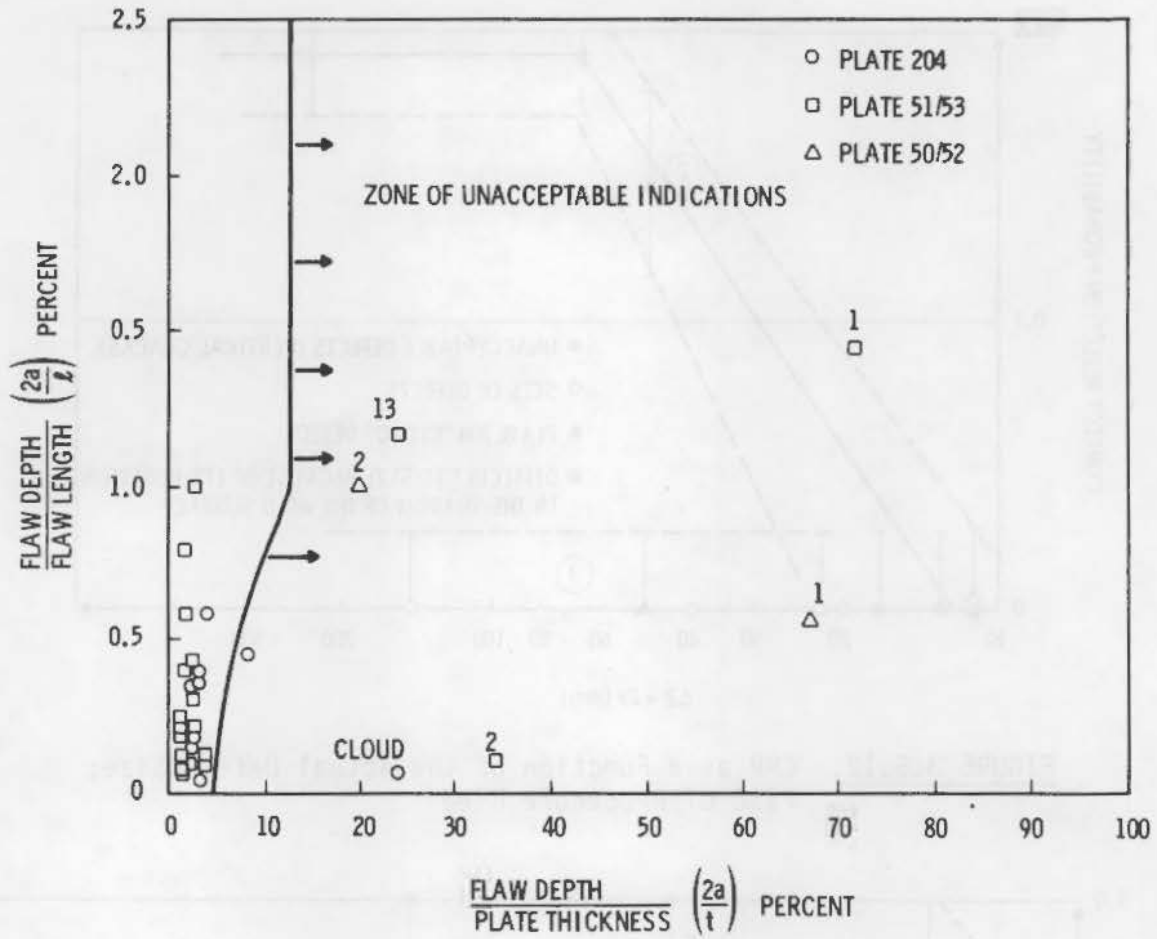
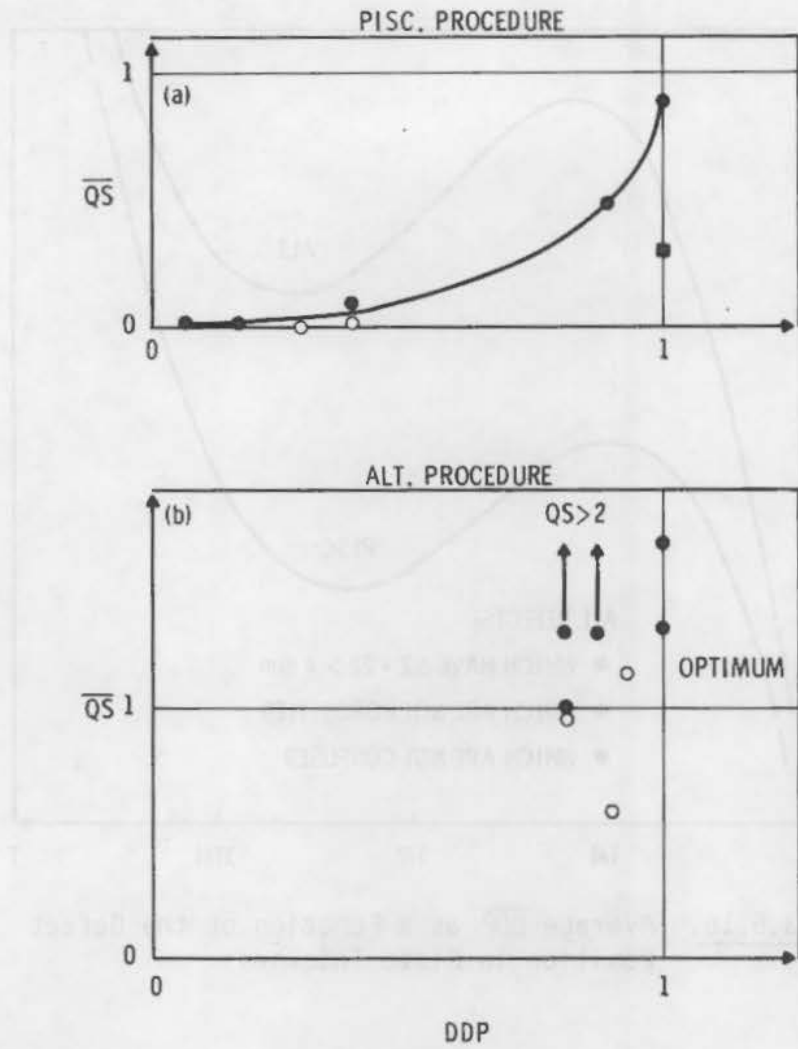


FIGURE 3.5.14. Acceptable and Unacceptable Defects Based on ASME XI IWB-3500 Criteria; Defect Population from Plates 50-52, 51-53 and 204



**FIGURE 3.5.15.** Correlation Between Quality of Sizing and DDP. Only unacceptable defects were considered: a) PISC UT procedure; b) alternative procedure

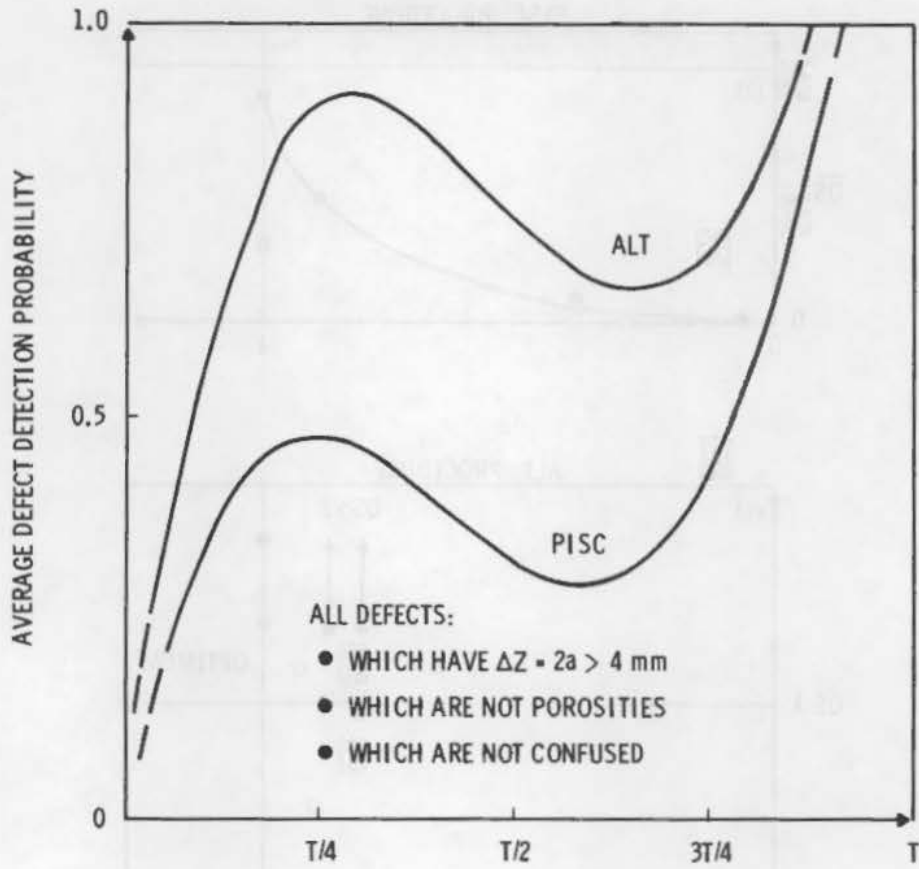


FIGURE 3.5.16. Average  $\overline{DDP}$  as a Function of the Defect Position in Plate Thickness

TABLE 3.5.3. Acceptable Defects--PISC Procedure

Defect No. Plate No.	Size (mm)			DDP	QLY		QLY		QA	CAP	Remarks
	$\Delta X$	$\Delta Y$	$\Delta Z$		Mean	$\bar{S}$	Mean	$\bar{S}$			
50-52											
3	2	10	2	0.0	--	--	--	--	--	--	
4	2	4	1	0.54	--	--	--	--	--	--	
51-53											
1.5	1	60	5	<0.1	--	--	--	--	--	--	(a)
3	3	216	4	0.67	0.83	0.4	2.6	3.5	2.0	0.57	
4	1	6	5	0.1	--	--	--	--	--	--	
5	11	14	6	0.6	--	--	--	--	--	--	(b)
6	8	31	7	0.13	--	--	1.17	1.65	--	--	
7	10	86	8	0.21	--	--	1.29	1.54	1.0	0.0	
8	2	18	2	0.13	--	--	--	--	--	--	(b)
9	1	16	2	0.92	--	--	--	--	--	--	(b)
10	6	10	4	0.75	0.90	0.3	2.0	1.0	2.3	0.7	
11	1	12	2	<0.1	--	--	--	--	--	--	
12	3	8	2	0.17	--	--	--	--	--	--	(b)
14	2	1	10	0.0	--	--	--	--	--	--	
15	3	7	4	<0.1	--	--	--	--	--	--	
16	9	20	6	0.75	--	--	1.40	1.23	3.0	0.7	
17	3	24	4	<0.1	--	--	--	--	--	--	(b)
18	3	5	4	0.0	--	--	--	--	--	--	
19	4	16	2	0.0	--	--	--	--	--	--	(b)
204											
2	17	42.4	6	0.41	0.93	0.25	0.5	0.5	0.57	0.36	
3	2	17	6	0.18	--	--	0.92	0.87	--	--	
4	7	140	7	0.4	--	--	0.97	1.06	--	--	
5	9	32	4	0.14	--	--	2.17	0.63	--	--	
6	8	22	8	0.73	0.97	0.4	0.8	0.8	1.4	0.5	
7	17	37	6	0.3	--	--	1.51	1.02	--	--	
8	6	20.3	8	0.59	0.94	0.1	0.73	0.75	2.7	0.5	
9	4	23.7	5	0.73	0.95	0.12	1.5	1.5	1.98	--	
10	27	70	8	<0.1	--	--	--	--	--	--	
11	2	13.6	8	0.1	--	--	--	--	--	--	
12	13	42.4	4	<0.1	--	--	--	--	--	--	
13	10	11	1	<0.1	--	--	--	--	--	--	
14	1	12.7	2	<0.1	--	--	--	--	--	--	
Mean	--	--	--	0.29	0.92	--	1.38	--	1.87	0.48	

(a) Set of small defects.  
 (b) Confusion with other defects.

TABLE 3.5.4. Rejectable Defects—PISC Procedure

Defect No. Plate No.	Size (mm)			DDP	QLY		QSZ		QR	CRP	Remarks
	$\Delta X$	$\Delta Y$	$\Delta Z$		Mean	$\bar{S}$	Mean	$\bar{S}$			
50-52											
1	57	400	236	1.0	0.98	1.0	0.30	0.2	0.15	0.95	
2	2	50	50	0.89	0.96	0.1	0.61	0.35	0.35	0.73	
51-53											
1.0	43	105	148	0.38	--	--	0.17	0.28	-0.02	0.0	(a)
1.1	2	15	43	<0.1	--	--	--	--	--	--	(b)
1.2	22	30	22	<0.1	--	--	--	--	--	--	(a)
1.3	29	58	40	<0.1	--	--	--	--	--	--	(a)
1.4	20	75	13	0.17	--	--	--	--	--	--	
1.6	2	45	11	<0.1	--	--	--	--	--	--	
1.7	10	45	11	<0.1	--	--	--	--	--	--	(a)
1.8	2	45	20	<0.1	--	--	--	--	--	--	(a)
2.0	44	700	69	1.0	0.87	1.5	1.26	0.35	0.93	0.96	
13.0	37	42	50	0.3	--	--	--	--	--	--	(a)
204											
1.0	<u>2</u>	<u>38.2</u>	<u>17</u>	<u>0.4</u>	<u>0.99</u>	<u>0.11</u>	<u>0.1</u>	<u>0.02</u>	<u>-4.0</u>	<u>0.0</u>	
Mean	--	--	--	0.36	0.95	--	0.49	--	-0.52	0.53	

(a) Set of defects.

(b) Defect near to the edge of the plate.



TABLE 3.5.5. Acceptable Defects--Alternative Procedures

Defect No. Plate No.	Size (mm)			DDP	QLY		QSZ		QA	CAP	Remarks
	$\Delta X$	$\Delta Y$	$\Delta Z$		Mean	$\bar{s}$	Mean	$\bar{s}$			
50-52											
3	2	10	2	<0.1	--	--	--	--	--	--	
4	2	4	1	0.44	--	--	--	--	--	--	(a)
51-53											
1.5	1	60	5	0.78	--	--	>6.0	--	--	0.48	(a)
3	3	216	4	1.0	0.80	0.6	1.14	11.0	-0.25	0.5	
4	1	6	5	0.25	--	--	--	--	--	--	
5	11	14	6	0.7	--	--	--	--	--	--	(a)
6	8	31	7	0.5	--	--	3.9	3.2	--	--	
7	10	86	8	0.5	--	--	3.1	3.9	--	--	
8	2	18	2	1.0	--	--	--	--	--	--	(a)
9	1	16	2	0.9	--	--	--	--	--	--	(a)
10	6	10	4	1.0	--	--	0.57	0.65	--	--	(a)
11	1	12	2	0.6	--	--	--	--	--	--	(a)
12	3	8	2	0.4	--	--	--	--	--	--	(a)
14	2	1	10	0.5	--	--	--	--	--	--	(a)
15	3	7	4	0.5	--	--	--	--	--	--	(a)
16	9	20	6	0.88	--	--	--	--	--	--	(a)
17	3	24	4	0.40	--	--	--	--	--	--	(a)
18	3	5	4	0.1	--	--	--	--	--	--	
19	4	16	2	0.45	--	--	--	--	--	--	(a)
204											
2	17	42.4	6	0.8	1.0	0.17	2.3	2.0	-2	0.4	
3	2	17	6	0.20	--	--	1.0	1.4	--	--	
4	7	140	7	0.8	--	--	1.71	1.6	1.5	0.53	
5	9	32	4	0.7	--	--	3.8	6.0	2.1	0.3	
6	8	22	8	0.9	0.93	0.13	2.67	2.4	-2.0	0.41	
7	17	37	6	0.8	--	--	1.48	1.4	0.9	0.4	
8	8	20.3	8	0.82	0.97	0.9	2.4	1.7	-1.7	0.7	
9	4	23.7	5	0.6	1.0	0.02	0.95	1.0	-1.7	0.6	
10	27	70	8	0.3	--	--	0.25	0.22	--	--	
11	2	13.6	8	0.5	--	--	2.35	2.0	--	--	
12	3	42.4	4	0.4	--	--	2.81	2.4	--	--	
13	10	11	1	<0.1	--	--	--	--	--	--	
14	1	12.7	2	<0.1	--	--	--	--	--	--	
Mean	--	--	--	0.56	0.94	--	2.28	--	-0.39	0.48	

(a) Defect often included in other defects.

TABLE 3.5.6. Rejectable Defects—Alternative Procedures

Defect No. Plate No.	Size (mm)			DDP	QLY		QSZ		QR	CAP	Remarks
	$\Delta X$	$\Delta Y$	$\Delta Z$		Mean	$\bar{s}$	Mean	$\bar{s}$			
50-52											
1	57	400	236	1.0	0.96	0.65	1.42	1.0	0.76	1.0	
2	2	50	50	0.92	0.99	0.16	1.17	0.9	1.44	0.8	(a)
51-53											
1.0	43	105	148	0.89	--	--	1.51	1.1	0.23	0.63	
1.1	2	15	13	0.44	--	--	--	--	--	--	(b)
1.2	22	30	22	0.78	--	--	>10.0	--	--	0.3	(a)
1.3	29	58	40	0.78	--	--	>4.0	--	--	0.3	(a)
1.4	20	75	13	0.87	--	--	>1.0	--	--	0.54	(c)
1.6	2	45	11	0.78	--	--	>20.0	--	--	0.6	(c)
1.7	10	45	11	0.78	--	--	>4.0	--	--	0.3	(a)
1.8	2	45	20	0.78	--	--	>4.0	--	--	0.3	(a)
2.0	44	700	69	1.0	0.4	0.3	1.83	0.8	1.04	1.0	
13.0	37	42	50	0.8	--	--	1.07	0.67	0.95	0.8	(a)
204											
1	<u>2</u>	<u>38.2</u>	<u>17</u>	<u>0.8</u>	<u>0.94</u>	<u>0.12</u>	<u>0.5</u>	<u>0.6</u>	<u>-4.0</u>	<u>0.0</u>	
Mean	--	--	--	0.82	0.82	--	4.21	--	0.07	0.55	

(a) Set of defects.

(b) Defect too near to the edges.

(c) Defect often confused with another defect.

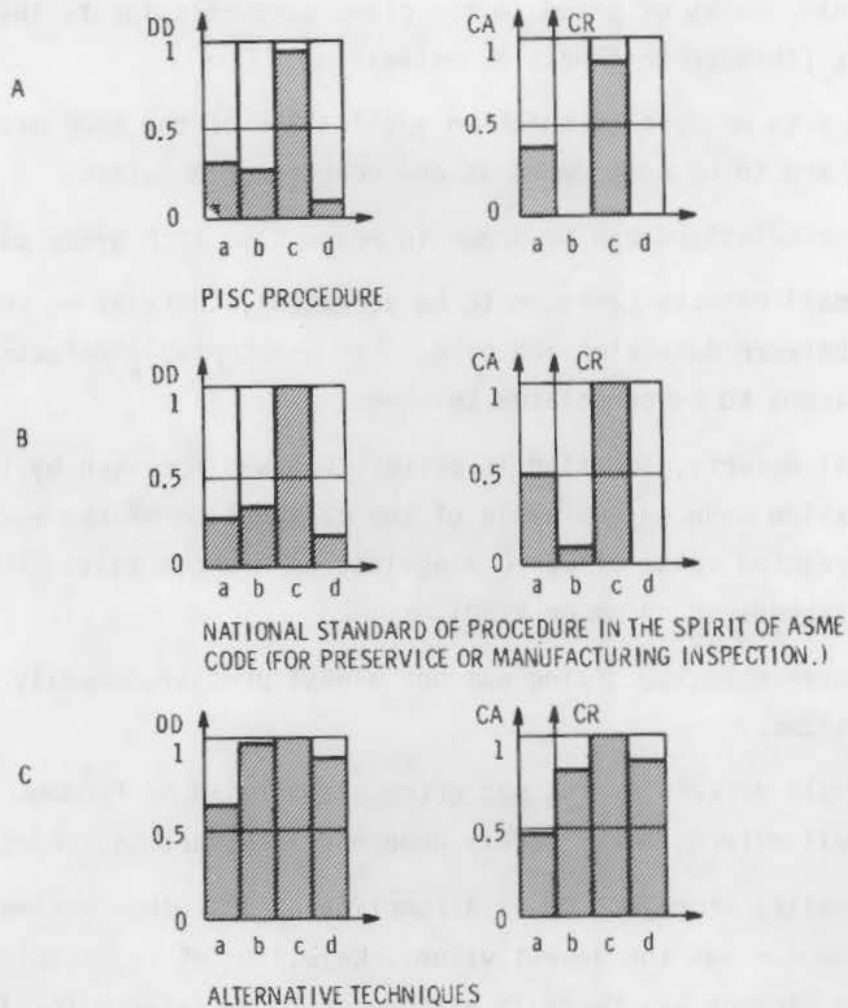


**FIGURE 3.5.17.** Average Cumulative Diagrams of Defect Detection (DD) and Correct Rejection or Acceptance [CR(CA)] as a Function of the Defect Categories a,b,c,d

### 3.5.5 Conclusions and Recommendations

Conclusions and recommendations relevant to the three plates are presented in the following paragraphs. In some instances, as noted, there are rather definite trends.

- Analysis of the results shows that the defects fall naturally into three main groups:
  - Small defects having a general volumetric character (sometimes consisting of many small cracks)

- Discrete cracks oriented in the plane perpendicular to the maximum stress (through-thickness oriented)
- Large sets of defects which on application of the ASME proximity rules are to be considered as one unacceptable defect.
- Separate conclusions can be drawn in respect to each group as follows:
  - For small defects (defects to be accepted), there is no correlation between detection and size. For unacceptable defects, detection seems to be correlated to size.
  - For all defects, location is better than was foreseen by the error evaluation made on the basis of the calibration of the equipment (a predicted value of EL  $\approx$  0.9 against an average value of 0.1) (corresponds to  $\sim$ 9 mm or  $t/20$ ).
  - For large defects, sizing was not always precise, usually undersized.

For small defects sizing was often exaggerated or random. Sets of small defects were largely underestimated and not rejected.

- The quality of rejection is a function of all other parameters and thus appears as the lowest value. Rejection of rejectable defects is not certain and there is a tendency to acceptance for large defects.

For small acceptable defects there is a tendency for rejection.

- Defect detection on an average for all "PISC Defects" is more a function of the position of defects in the plate than of other defect characteristics. Due to the principle of the echo technique, DDP is lower for defects in the middle part of the plate when the defect surface is smooth.

The large defect (No. 1) of plate 50-52, when considered as a set of three adjacent defects, demonstrated a very important weakness of the PISC procedure, which is confirmed for other plates.

Detection probability and sizing are better for defects near the inner surface of the plate, and are worse for defects near the upper surface of the plate and for defects in the central part of the plate.

Through-thickness oriented cracks could have a low detection probability and the most optimistic statement that can be made is that cracks which have a height greater than about  $\Delta Z = 2a = 50$  mm have a good probability ( $>0.95$ ) of being detected.

- The limitations existing on Plate 204 for defects located in the upper and lower zones of the weld (viz., the length of the plate for the  $60^\circ$  angle probes, and the unground surface of the weld) did not impede detection of those defects. Conclusions about the CRP of those defects should, nevertheless, not be drawn (Defect No. 1 or Plate 204, between brackets in Figure 3.5.14).
- Correlation between real defect size and estimated defect size is lower than one might have reasonably expected for the PVRC plates provided.

Application of the full ASME XI proximity rules does not change the general conclusions obtained with the restricted rules.

If means and standard deviations given by the DS 5 (sheet of results presented by teams as a straight record of instrumentation results) and DS 6 (after team interpretation) are statistically equivalent, it appears that:

- the interpretation made by the teams (DS 6) is in the wrong sense for five defects among the six rejectable defects, both for DDP and ES
- when looking at the results given by the full ASME reduction procedure, this "human factor" never appears positively
- for the acceptable defects, teams generally appear to give, as an average, safer results after interpretation of the instrumentation data.

- Defects perpendicular to the surface were not consistently detected except when close to the bottom wall. From the results of the PISC exercise, probably the most optimistic statement that can be made is that cracks which have a depth greater than about  $Z = 2a = 50$  mm have a probability of 0.95 of being detected. This conclusion is based on a linear fit to the logarithmic plot of DDP versus  $\Delta Z$  (Figure 3.5.10). It is important to note that data are missing in the region between  $\Delta Z = 20$  and  $\Delta Z = 50$  mm. Nevertheless, this result does suggest that vertical cracks of less than 50 mm in depth have a probability of detection which at best is of the order of 0.95. [The results for CRP are similar although the fall-off of the optimistic limit with decreasing  $\Delta Z$  is faster (Figure 3.5.12).]
- The difference which exists between the values of DDP, EL, and ES for the two PISC procedure declarations (DS 5 and DS 6) is only indicative of a trend. When the large errors are taken into account, statistical tests cannot for most cases disprove the hypotheses:

$$(DDP) \text{ DS } 5 = (DDP) \text{ DS } 6$$

$$(ES) \text{ DS } 5 = (ES) \text{ DS } 6.$$

- Concerning the whole set of the alternative procedures, the following can be stated:
  - Alternative procedures seem on the average to give better values for all parameters. For large defects (rejectable defects) the detection appears high and often equal to 1 but further studies are necessary.
  - The very long defective zone of Plate 204 (HAZ) has been detected by some teams. Its configuration is such that only tandem techniques focused probe techniques from the inside or high frequency

techniques are able to detect it, bearing in mind that tandem techniques can be fully applied only on plates of bigger dimensions.

This large quantity of small cracks and inclusions could perhaps be a zone for the propagation of fatigue cracks and further investigation are needed for evaluating the significance of this defective zone.

- Base material defects, which are numerous and extended, have produced confusion for the evaluation of results. Some calculated values of DDP are not precise and in some cases (Defect No. 6 of Plate 204) this value can be increased by including those defective zones. Such an increase is, nevertheless, within the error bands.
- Instrumentation seems to be always correct in that all indications correspond to some physical reality, either effective defects or localized structure variation which appear clearly on micrographs.

No false indication has, therefore, been reported.

The results of all the alternative procedures were considered together. Some of the procedures were very close to the PISC method, differing only as to the calibration technique, or scanning surface used; others are in fact the PISC procedure with a 20% DAC cut-off instead of 50% DAC.

It should be noted that all these procedures satisfy the requirements of the ASME Code, Section XI and that some are used for quality control and inservice inspection.

From the analysis carried out so far, there are strong indications that certain alternative procedures, when considered on their own merits, could give a very reliable detection, sizing and rejection of all "rejectable" defects regardless of their size, location and nature.

This observation is subject to confirmation by further detailed analysis which will be carried out in due course.

With regard to recommendations, the following should be considered tentative and subject to future revision:

- It is necessary to perform a detailed analysis of all the alternative procedures used and this study has to consider each procedure or groups of similar procedures separately to determine the correct performance of each one.

Recommendations concerning the improvement of ultrasonic performance will depend on this detailed analysis.

- A critical study of all the major defects should be conducted for:
  - the defect surface state and its relationship to defects found in service
  - the defect importance considering fracture mechanics evaluation procedures.

This study should lead to more accurate conclusions from the PISC exercise.

- New round-robin tests are recommended and should be carefully prepared with regard to the following:
  - type of defects
    - surface defects
    - defects near to the acceptance limit
    - discrete defects to simplify the destructive examination and evaluation and thus the costs
    - same defects located in different positions of depth in the plate
    - both austenitic clad plates as well as unclad
  - type of material and welding process
  - geometry of test block
  - procedures for UT and influence of equipment characterization
  - marking of plates and collection of data.



- Some of the variables mentioned above could be examined in a parametric study, not necessarily involving an exercise of the round-robin type.
- Round-robin tests on austenitic stainless steels should be arranged in view of their extensive use in power reactor primary circuits.

... of the ... ..  
... ..

... ..  
... ..

Certain trends were observed in both the PVRC and/or PISC NDE programs. These are cited in the following paragraphs:

- Reliability of detection and sizing of defects using a single combination of transducer beam angle and frequency was substantially lower than had been anticipated.
- Combinations of angles and frequencies used for detecting and sizing a given defect enhanced the reliability.
- Examination through cladding grossly reduced reliability of detection compared to examining the same flaws with the same techniques in the absence of cladding.
- Some of the alternative UT techniques used in the PISC program appeared to yield better detection and sizing reliabilities, however, test results were relatively limited and no examinations were made through cladding. Further examinations (PISC-II) are required to determine whether alternate techniques substantially enhance reliability.
- The gross level of impurities in 50-52 and 51-53 plates tended to obscure the relative detection reliability.
- Flaws oriented at angles substantially away from the normal to the surface were difficult to detect with conventional UT (see PVRC-155).
- Radiography was less reliable than anticipated for cracks. Reliability was high for slag and porosity.
- Further tests are required to quantify reliability of detection of near-field cracks, particularly through cladding.
- The human variable is quite marked. Some teams achieved acceptable overall reliabilities of detection for a given series of examinations whereas other teams using similar equipment or the same procedures

have poor reliabilities. This means the composite results do not portray the correct picture since the distribution tends to be bimodal.

- Location of defects was consistently poor. The teams consistently did not relate measurements to the benchmarks or did not read dimensions correctly.

- 3.1.1 Manly, W. D. (ACRS) to Seaborg, G. (AEC), Subject: "Pressure Vessel Failure," November 24, 1965.
- 3.2.1 PVRC Subcommittee Report, "Nondestructive Examination of PVRC Plate-Weld Specimen 201." Welding Research Supp., pp. 529S-538S, December 1971.
- 3.2.2a Birks, A. S. and Lawrie, W. E., "Improved Repeatability in Ultrasonic Examination." Weld. Res. Council Bull. 235, February 1978.
- 3.2.2b "Ultrasonic Testing System Standardization Requirements." Weld. Res. Council Bull. 235, February 1978.
- 3.2.3 "Rules for In-Service Inspection of Nuclear Power Plant Components," ASME Section XI, Division 1, 1977 Edition.
- 3.2.4 "Non-Destructive Examination," ASME Section V, 1977 Edition.
- 3.2.5 Collins, H. D. and Gribble, R. P., "PVRC Plate-Weld Specimen 201, Inspection by Acoustical Holography." Holosonics, Inc., Internal Report, September 1972.
- 3.2.6 Buchanan, R. A., "Analysis of the Nondestructive Examination of PVRC Plate-Weld Specimen 251J--Part A." Weld. Res. Council Bull. 221, November 1976.
- 3.2.7 Adamonis, D. C. and Hughes, E. T., "Ultrasonic Evaluation and Sectioning of PVRC Plate-Weld Specimen 201." WCAP-9378, Westinghouse Electric Corporation, Pittsburgh, Pennsylvania, September 1978. Also Weld. Res. Council Bull. 252.
- 3.2.8 Graber, H. C. and Hedden, O. F., "PVRC Round Robin Ultrasonic Inspection Results of Thick Section Weldments." Pressure Vessel Research Committee Internal Report, 1978.
- 3.2.9 Sharon, G. M. and Witek, R. R., "Acoustic Holography Examination of PVRC Plate-Weld Specimen 251J." NEDO-20735, General Electric, Nuclear Energy Division, December 1974.
- 3.3.1 Buchanan, R. A., "Analyses of the Ultrasonic Examinations of PVRC Weld Specimens 155, 202, and 203 by Standard and Two-Point Coincidence Methods." Interim Report to Pressure Vessel Research Committee NDE Subcommittee, June 1978. Also Weld. Res. Council Bull. 257.
- 3.3.2 Ruescher, E. H., "Analysis of the Radiographic Evaluation of PVRC Weld Specimens 155, 202, 203, and 251J." Final Report to Pressure Vessel Research Committee by Southwest Research Institute, San Antonio, Texas, October 1978. Also Weld. Res. Council Bull. 259.

- 3.3.3 Ferree, D. V., "Tandem and Conventional Ultrasonic Examination and Radiography of PVRC Test Block 202." Report to Pressure Vessel Research Committee NDE Subcommittee by Babcock and Wilcox, Mt. Vernon, Indiana, March 17, 1978.
- 3.3.4 Birks, A. to Berry, F., Subject: "Immersion Ultrasonic Examination of PVRC Block 202," February 12, 1979.
- 3.5.1 Plate Inspection Steering Committee Report No. 1, "A Description of the PISC Project." May 1979, issued as an European Commission of the European Communities Report, September 1979.
- 3.5.2 Plate Inspection Steering Committee Report No. 2, "Ultrasonic Examination of the PVRC Plates No. 50-52, 51-53 and 204." May 1979, issued as an European Commission of the European Communities Report, September 1979.
- 3.5.3 Plate Inspection Steering Committee Report No. 3, "Destructive Examination of the PVRC Plates No. 50-52, 51-53 and 204." May 1979, issued as an European Commission of the European Communities Report, September 1979.
- 3.5.4 Plate Inspection Steering Committee Report No. 4, "Analysis Scheme of the PISC Trials Results." May 1979, issued as an European Commission of the European Communities Report, September 1979.
- 3.5.5 Plate Inspection Steering Committee Report No. 5, "Evaluation of PISC Trials Results." May 1979, issued as an European Commission of the European Communities Report, September 1979.
- 3.5.6 Plate Inspection Steering Committee Report No. 6, "Analysis of the PISC Trials Results for Alternative Procedures." EUR 6371 EN, June 1980.

CHAPTER 4

FLAW DETECTION

SECRET

CONFIDENTIAL



## CONTENTS

4.1	INTRODUCTION . . . . .	4.1.1
4.2	SURFACE FLAWS . . . . .	4.2.1
4.2.1	Detection Probability--Fatigue Cracks . . . . .	4.2.1
4.2.1.1	Flaw Dimensions . . . . .	4.2.2
4.2.1.2	Fatigue Cracks . . . . .	4.2.11
4.2.2	Flaw Detection Probability--Fabrication Defects . . . . .	4.2.12
4.2.2.1	Flaw Sizes . . . . .	4.2.14
4.2.2.2	Influence of Stress . . . . .	4.2.16
4.2.3	Factors Affecting Detection Reliability . . . . .	4.2.16
4.2.4	Statistical Analyses--NDE Data . . . . .	4.2.17
4.2.4.1	Machined Versus Fatigue Flaws . . . . .	4.2.18
4.3	EMBEDDED FLAWS . . . . .	4.3.1
4.4	COMPARISON--SURFACE VERSUS SUBSURFACE FLAWS . . . . .	4.4.1
4.5	LIMITING CONSIDERATIONS . . . . .	4.5.1
4.5.1	External Factors . . . . .	4.5.1
4.5.1.1	Equipment Variability . . . . .	4.5.1
4.5.1.2	Human Factor . . . . .	4.5.3
4.5.1.3	Calibration . . . . .	4.5.3
4.5.1.4	Calibration Blocks . . . . .	4.5.5
4.5.1.5	Acoustic Properties . . . . .	4.5.6
4.5.1.6	Acceptance Criteria . . . . .	4.5.6
4.5.2	Internal Factors . . . . .	4.5.7
4.5.2.1	Component Surface . . . . .	4.5.7
4.5.2.2	Component Geometry . . . . .	4.5.10

4.5.2.3	Material Variables	. . . . .	4.5.12
4.5.2.4	Flaw Characteristics	. . . . .	4.5.32
4.5.3	Detection—RT	. . . . .	4.5.34
4.6	FLAW SIZING FACTORS	. . . . .	4.6.1
4.6.1	Limitations in Detection and Sizing	. . . . .	4.6.1
4.6.2	AVG-DGS	. . . . .	4.6.2
4.6.3	Stress on Flaw	. . . . .	4.6.2
4.6.4	Flaw Orientation	. . . . .	4.6.9
4.7	CORRECTIVE ACTIONS	. . . . .	4.7.1
4.8	REFERENCES	. . . . .	4.8.1

## FIGURES

4.2.1	Crack Detection Probability of the X-Radiographic Inspection Method Plotted by Actual Crack Length at 95% Probability and 95% Confidence Level . . . . .	4.2.3
4.2.2	Crack Detection Probability of the X-Radiographic Inspection Method Plotted by Actual Crack Depth at 95% Probability and 95% Confidence Level . . . . .	4.2.3
4.2.3	Crack Detection Probability of the Penetrant Inspection Method Plotted by Actual Crack Length at 95% Probability and 95% Confidence Level . . . . .	4.2.4
4.2.4	Crack Detection Probability of the Penetrant Inspection Method Plotted by Actual Crack Depth at 95% Probability and 95% Confidence Level . . . . .	4.2.4
4.2.5	Crack Detection Probability of the Ultrasonic Inspection Method Plotted by Actual Crack Length at 95% Probability and 95% Confidence Level . . . . .	4.2.5
4.2.6	Crack Detection Probability of the Ultrasonic Inspection Method Plotted by Actual Crack Depth at 95% Probability and 95% Confidence Level . . . . .	4.2.5
4.2.7	Crack Detection Probability of the Eddy Current Inspection Method Plotted by Actual Crack Length at 95% Probability and 95% Confidence Level . . . . .	4.2.6
4.2.8	Crack Detection Probability of the Eddy Current Inspection Method Plotted by Actual Crack Depth at 95% Probability and 95% Confidence Level . . . . .	4.2.6
4.2.9	Sensitivity of NDE Methods in Detecting Surface Fatigue Cracks in 7075-T6511 Aluminum . . . . .	4.2.11
4.2.10	Sensitivity of Crack Length $2c$ , Indication by NDE in 4330V Modified Steel Heat-Treated to 220 to 240 ksi Ultimate Strength . . . . .	4.2.12
4.2.11	Inspection Results by NDE Method . . . . .	4.2.13
4.2.12	Results of Liquid Penetrant Testing as Function of Flaw Depth . . . . .	4.2.14
4.2.13	MT Production Detection Capability--95% Confidence Level . . . . .	4.2.18
4.2.14	Probability of Detection for 2219-T87 Al Using Ultrasonic Surface Waves . . . . .	4.2.19

4.2.15	Optimum Probability Method of Data Cumulation . . . .	4.2.20
4.2.16	Overlapping Sixty-Point Method of Data Cumulation . . . .	4.2.21
4.3.1	Agreement with the Number of Flaw Locations Given . . . .	4.3.3
4.5.1	Examples of Various Weldment Geometry Problems That Can Adversely Influence Flaw Detection by Ultrasonics . . . .	4.5.12
4.5.2	Number of Indications of Inservice Inspections . . . .	4.5.13
4.5.3	Influence of Cladding on Angle-Beam Penetration . . . .	4.5.14
4.5.4	The Amplitude Variation by Frequency, Marked for the Test Steel and Steel of Poorer Quality . . . .	4.5.17
4.5.5	Example of Influence of Differences of Attenuation on UT Beam Path on DAC Values . . . .	4.5.19
4.5.6	Laboratory and Test Team Characterization of Welds . . . .	4.5.23
4.5.7	Original and Modified Weld Profiles for Optimization of Ultrasonic Examination . . . .	4.5.28
4.5.8	Purpose--Optimization of UT; 90° to Tube Axis . . . .	4.5.28
4.5.9	Purpose--Optimization of UT; 55° to Tube Axis . . . .	4.5.29
4.5.10	Mode Conversion . . . .	4.5.33
4.5.11	Minimum Detectable Crack Cross-Sectional Areas . . . .	4.5.35
4.5.12	Minimum Detectable Crack Dimensions . . . .	4.5.36
4.5.13	Ultrasonic Attenuation as a Function of Direction of Propagation Relative to the Welding Direction . . . .	4.5.39
4.6.1	Limitations to Flaw Detection, Sizing, Location . . . .	4.6.1
4.6.2	Changes Due to Applied Tensile Loads, in Ultrasonic Reflection Amplitude as Determined by Three Analysis Methods . . . .	4.6.4
4.6.3	Optimum Ultrasonic Techniques for Detecting Fatigue Cracks Under Both Zero Load and Compressive Stresses When Using 45°, 60°, and 70° Probes . . . .	4.6.5
4.6.4	Ultrasonic Response to Fatigue Cracks Under Compression Using 45° Probes at Different Frequencies and Scanning Positions . . . .	4.6.6

4.6.5	Signal Amplitude Responses from Fatigue Cracks Under Compression in the As-welded, Stress-relieved and Normalized Welds Using a 45° Probe . . . . .	4.6.7
4.6.6	Ultrasonic Examination of Test Block F Using Various Techniques . . . . .	4.6.10
4.6.7	The Effects of Liquid in Cracks When Unloaded and Under Compression . . . . .	4.6.11
4.6.8	Static and Dynamic Angular Dependency with Various UT Techniques . . . . .	4.6.15

## TABLES

4.2.1	Materials and NDE Techniques Used in Detection of Surface Flaws . . . . .	4.2.1
4.2.2	Detection Probability as Function of Flaw Size . . . . .	4.2.2
4.2.3	Sensitivity of Detection of Surface Flaws in Aluminum and Steel Cylinders . . . . .	4.2.7
4.2.4	Comparison of Detection Sensitivities of Production and Laboratory NDE . . . . .	4.2.8
4.2.5	Summary of Selected Detection Sensitivities of Some Commercial NDE Processes . . . . .	4.2.9
4.2.6	Flaw Sizes Detectable at Known Confidence Limits . . . . .	4.2.10
4.2.7	Flaw Depths Yielding 90% Detection Probability at 95% Confidences . . . . .	4.2.15
4.2.8	Reliability of Detection with MT as Function of Flaw Depth . . . . .	4.2.17
4.2.9	Parametric Effects for Calculating $D_0$ , the Difference Between the Ultrasonic Signals from Machined Flaws and Fatigue Cracks in Reference Blocks . . . . .	4.2.22
4.2.10	The Gain $G$ (dB) Which Must Be Added to Ultrasonic Equipment Calibrated on Machined Flaws to Have 95% Confidence of Detecting Fatigue Cracks in Reference Blocks . . . . .	4.2.23
4.2.11	Analysis of Variance for Ultrasonic Signals from Twelve Different Flawed Blocks and Nine Different Transducers . . . . .	4.2.24
4.2.12	The Flaw Echo Strength Relative to the Background Signals . . . . .	4.2.25
4.3.1	Detection of Flaws in Five Reactor Pressure Vessels . . . . .	4.3.2
4.5.1	Theoretical Considerations . . . . .	4.5.2
4.5.2	Summary of Flaw Response Using 20% and 50% to 100% Reference Level Evaluation Criteria . . . . .	4.5.8
4.5.3	Effect of Surface Condition on Ultrasonic Coupling . . . . .	4.5.9
4.5.4	Shear-Wave Attenuation . . . . .	4.5.15
4.5.5	Shear-Wave Misdirection Angle . . . . .	4.5.16

4.5.6a	Assessment of Radiographs of B.E.R.T.A. Specimen (Radiation Source: X-Ray and Cobalt-60)	. . . . .	4.5.37
4.5.6b	Assessment of Radiographs of B.E.R.T.A. Specimen (Radiation Source: X-Ray and Cobalt-60)	. . . . .	4.5.37
4.5.6c	Assessment of Radiographs of B.E.R.T.A. Specimen (Radiation Source: 300 kV C.P. Unit)	. . . . .	4.5.37
4.5.6d	Assessment of Radiographs of B.E.R.T.A. Specimen (Radiation Source: 18 MeV Betatron)	. . . . .	4.5.37
4.5.6e	Assessment of Radiographs of B.E.R.T.A. Specimen (Radiation Source: 4.3 MeV Linear Accelerator)	. . . . .	4.5.37
4.6.1	Factors for Optimizing System Selection Based on Specific Application(s)	. . . . .	4.6.16

4.2.2	Assessment of radiography of B.E. 2.11A Section (Radiation source: A-44 and C-14-50)	4.2.2
4.2.3	Assessment of radiography of B.E. 2.1A Section (Radiation source: A-44 and C-14-50)	4.2.3
4.2.4	Assessment of radiography of B.E. 2.7A Section (Radiation source: C-14-50)	4.2.4
4.2.5	Assessment of radiography of B.E. 2.7A Section (Radiation source: B-14-50)	4.2.5
4.2.6	Assessment of radiography of B.E. 2.7A Section (Radiation source: C-14-50)	4.2.6
4.3	Factors for determining cyclic life based on both the radiations	4.3



## CHAPTER 4

### FLAW DETECTION

#### 4.1

#### INTRODUCTION

A critical aspect related to the reliability of strength-bearing components is the ability to detect flaws in the component. Such detection is only the initial step in sizing and locating flaws as input into a fracture mechanics analysis. Obviously, undetected flaws represent unsized and unlocated flaws so reliability of detection and the parameters influencing such reliability, either favorably or adversely, are of major significance.

This chapter will review the available information pertinent to flaw detection with the spectrum of NDE techniques. An arbitrary division is made between surface flaws and subsurface flaws. In the case of subsurface flaws, the effect of section thickness and material will be examined. The final section deals with those parameters affecting flaw detection.

FLAW DETECTION

INTRODUCTION

A critical aspect related to the reliability of structural analysis is the ability to detect flaws in the component. Such detection is only possible if the flaw is large enough to be detected by a fracture mechanics analysis. Obviously, undetected flaws represent a hazard and a potential cause of failure. The probability of detection and the probability of failure are related by either favorably or unfavorably, the of major significance.

This chapter will review the available information pertinent to flaw detection with the spectrum of our techniques. An obvious distinction is made between surface flaws and subsurface flaws. In the case of subsurface flaws, the effect of section thickness and material will be examined. The final chapter deals with those parameters affecting flaw detection.

Extensive programs on surface flaw detection reliability have been sponsored by the Air Force and by the National Aeronautics and Space Administration (NASA). These programs related to military planes and to space vehicles. A relatively limited number of materials were investigated. These are cited in Table 4.2.1, together with the NDE used. In most instances, the cracks were surface fatigue cracks varying in depth and length.

#### 4.2.1 Detection Probability--Fatigue Cracks

A substantial program sponsored by NASA<sup>(4.2.1)</sup> quantitatively evaluated the probability of detecting fatigue cracks in 2219-T87 aluminum as functions

TABLE 4.2.1. Materials and NDE Techniques Used in Detection of Surface Flaws

<u>Material</u>	<u>Thickness</u>	<u>NDE</u>	<u>Reference</u>
2219 A1	0.060, 0.210 in.	RT, PT, UT, ET	4.2.1
4330 Steel	Cylinders 0.25 in.	RT, PT, MT, UT	4.2.2
7075 A1	Wall	RT, PT, UT	
7075 A1		UT, PT, RT, VT, ET	4.2.3
4330-V Steel		Plus MT	
2219 A1		UT, PT, RT, VT, ET	
2014		UT, PT, RT, VT, ET	
D6AC Steel		Plus MT	
HP-9 Steel		MT	4.2.4
Ti 6Al-4V		PT	
Aluminum		PT, UT	
Ti		PT, UT, ET	4.2.5
A1		PT, UT, ET	
Steel		PT, MT, UT, ET	
2218 A1	0.060, 0.0225, 0.25 in.	PT, ET	4.2.6
D6AC Steel	Irregular shape	MT, Delta UT	4.2.7
Ti-6Al-4V	Ingot, billet, plate, bar	RT, UT, ET, PT	4.2.8
7075 A1	0.25 in., sheet	UT	4.2.9
7075	0.5 in., sheet	ET	4.2.10

of flaw size, surface finish, loading, and the NDE technique used. Two section thicknesses (0.060, 0.210 in.) were used. Surface finishes in the as-machined state ranged from 28 to 64 rms smooth to 125-420 rms rough. After chemical milling the surface finishes were 35 to 100 rms smooth and 120 to 300 rms rough. Some chemically milled specimens were loaded to proof stress (85% of yield strength) before NDE. Four NDE techniques were used: 1) RT, 2) penetrant testing (PT), 3) UT, and 4) engineering testing (ET). There were 118 specimens containing a total of 328 cracks. These cracks varied in length from 1.27 to 0.018 cm and in depth from 0.451 to 0.003 cm. Statistical techniques were used to examine the reliability of each NDE technique. Limits of 95% detection probability and 95% confidence were used for this quantification. Each NDE technique was examined as a function of flaw length and flaw depth.

#### 4.2.1.1 Flaw Dimensions

Some idea of the detection probability with respect to flaw dimensions can be seen from Table 4.2.2.

The detection probability distributions as functions of flaw length and depth at 95% probability and 95% confidence levels are given for RT, PT, UT, and ET in Figures 4.2.1 through 4.2.8. It is apparent that RT is of marginal

TABLE 4.2.2. Detection Probability as Function of Flaw Size<sup>(a)</sup>

NDE Technique	Dimension	As-Machined (in.)	Chemically Milled (in.)	Chemically Milled Plus Proof Stress (in.)
RT	Length	<0.20 at 0.4	~0.60 at 0.1	0.6 at 0.1
	Depth	~0.50 at 0.14	~0.80 at 0.04	~0.6 at 0.04
PT	Length	~0.60 at 0.1	~0.90 at 0.1	0.90 at 0.1
	Depth	0.60 at 0.02	~0.90 at 0.02	~0.90 at 0.02
UT	Length	~0.90 at 0.1	~0.90 at 0.1	>0.90 at 0.1
	Depth	~0.90 at 0.02	~0.90 at 0.02	>0.90 at 0.02
ET	Length	~0.80 at 0.1	~0.90 at 0.1	>0.90 at 0.1
	Depth	~0.80 at 0.04	>0.80 at 0.04	>0.90 at 0.04

(a) Probability as fraction of 1.0.

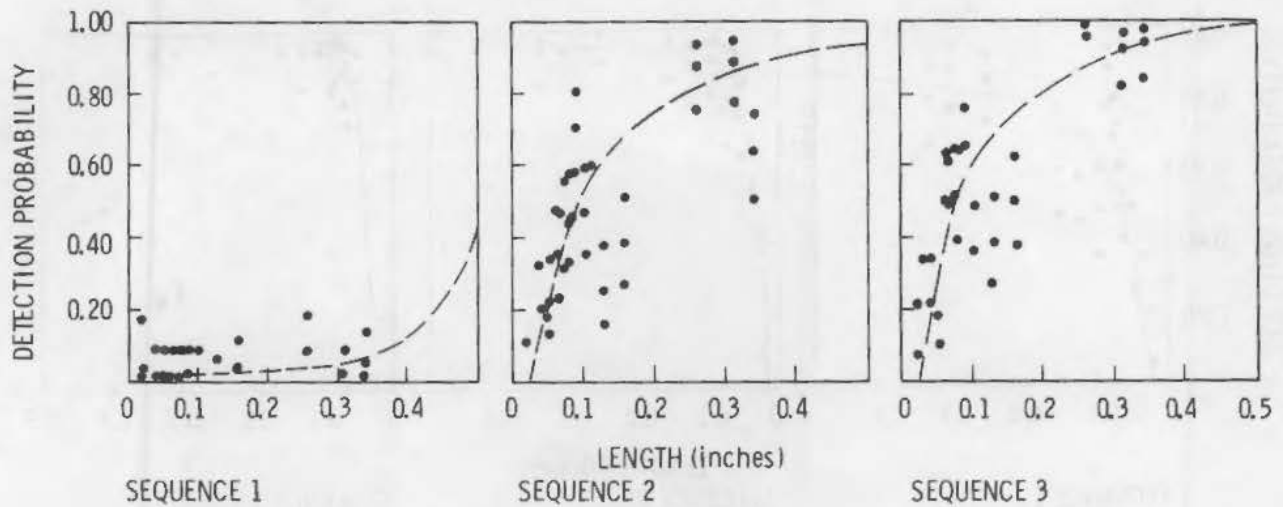


**FIGURE 4.2.1.** Crack Detection Probability of the X-Radiographic Inspection Method Plotted by Actual Crack Length at 95% Probability and 95% Confidence Level

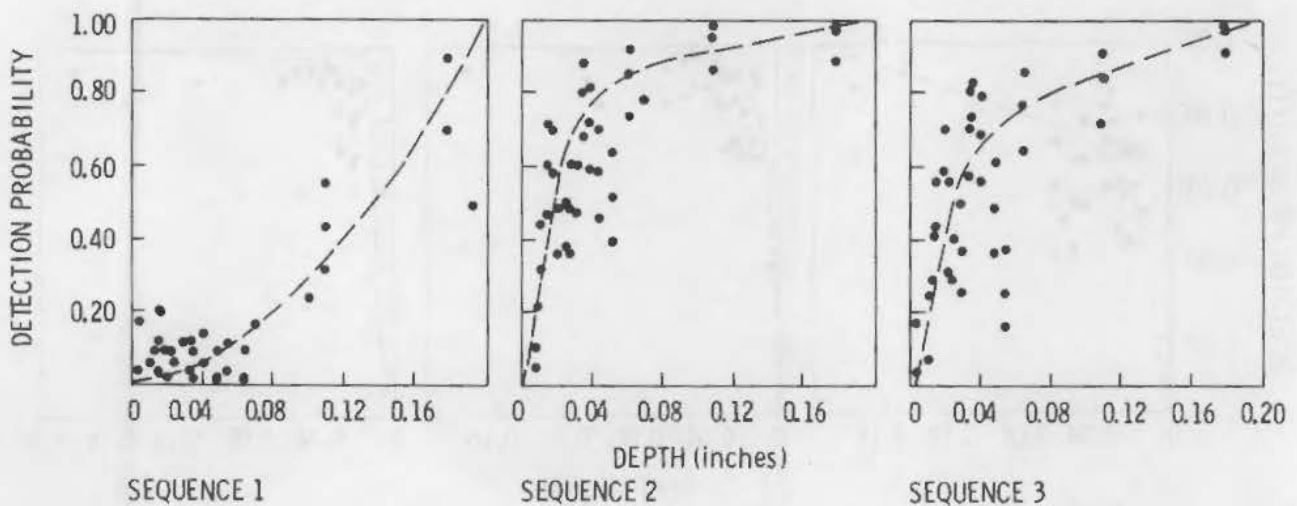


**FIGURE 4.2.2.** Crack Detection Probability of the X-Radiographic Inspection Method Plotted by Actual Crack Depth at 95% Probability and 95% Confidence Level

value. Surface finish appears to be a factor, albeit not of major significance for UT, PT, and ET. Several UT techniques were evaluated; namely, shear wave, surface wave, Lamb wave and Delta modes at 2.25, and 10 MHz with C-scan as reference.

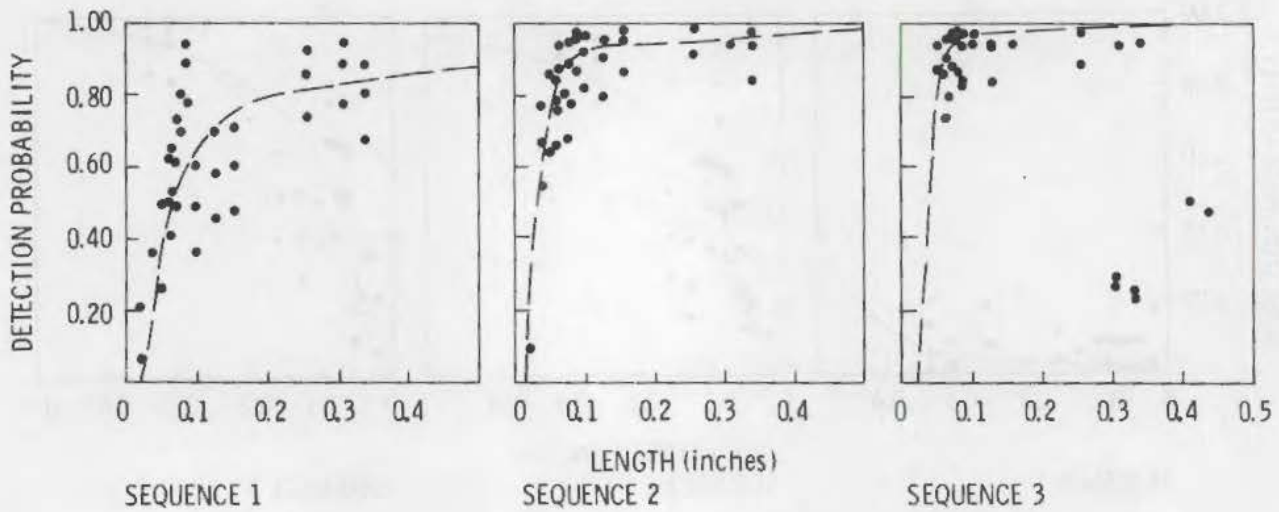


FIGURE 4.2.3. Crack Detection Probability of the Penetrant Inspection Method Plotted by Actual Crack Length at 95% Probability and 95% Confidence Level

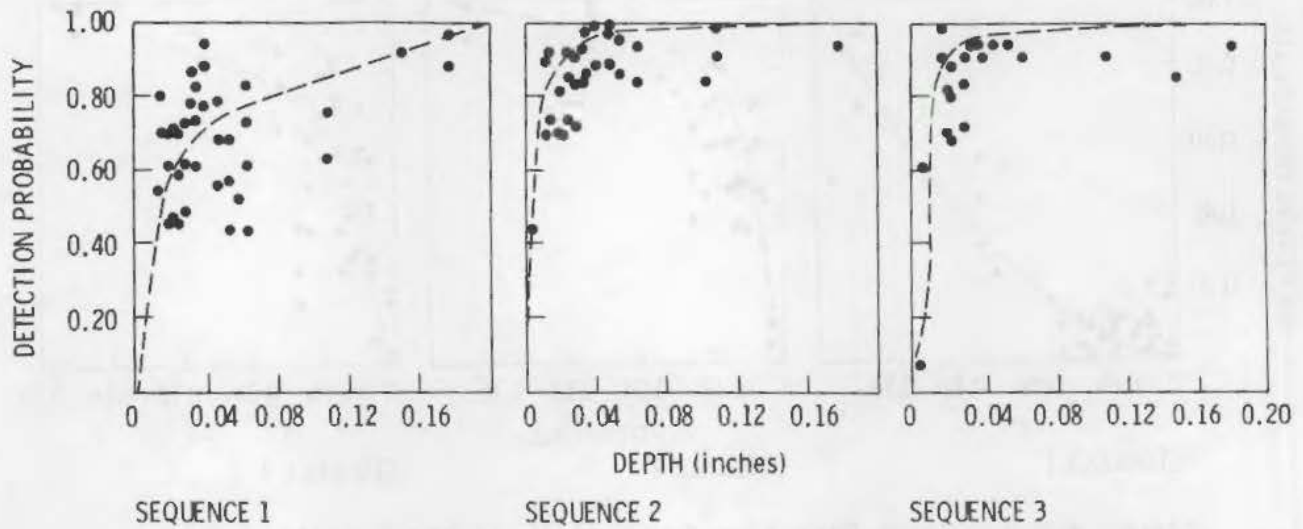


FIGURE 4.2.4. Crack Detection Probability of the Penetrant Inspection Method Plotted by Actual Crack Depth at 95% Probability and 95% Confidence Level

Packman et al. (4.2.2,4.2.3,4.2.4) reported data on fatigue cracks in 4330 steel and in 7075 aluminum. The samples were 3-in.-dia cylinders with a 0.25-in. wall. The emphasis was on correlating NDE results with Linear Elastic Fracture Mechanics (LEFM). This aspect is discussed in another chapter. The following NDE techniques were evaluated: RT, PT, magnetic particle testing

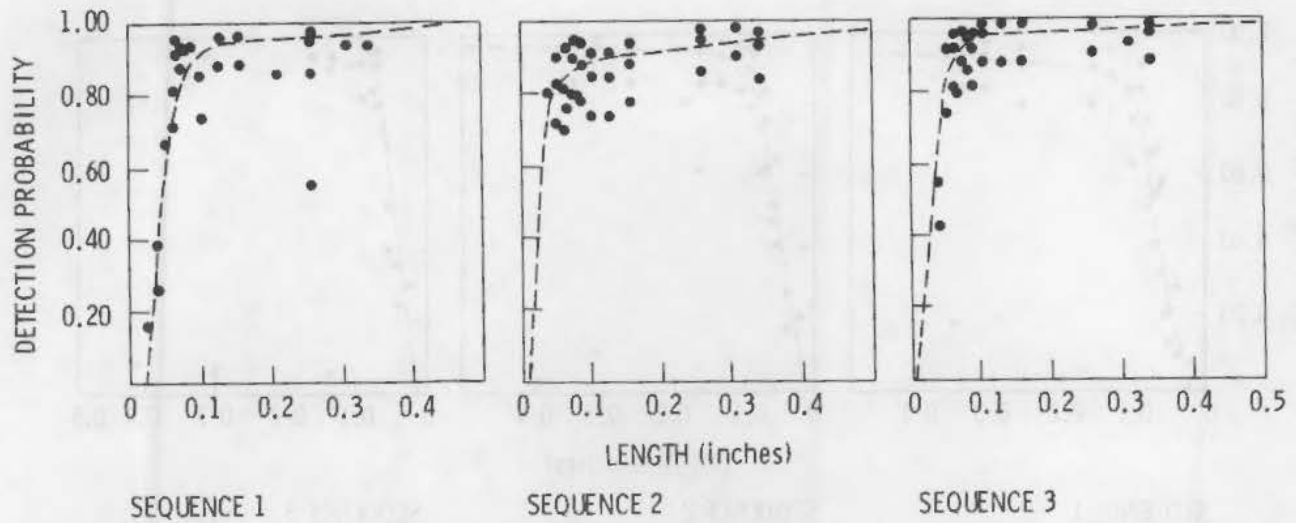


FIGURE 4.2.5. Crack Detection Probability of the Ultrasonic Inspection Method Plotted by Actual Crack Length at 95% Probability and 95% Confidence Level

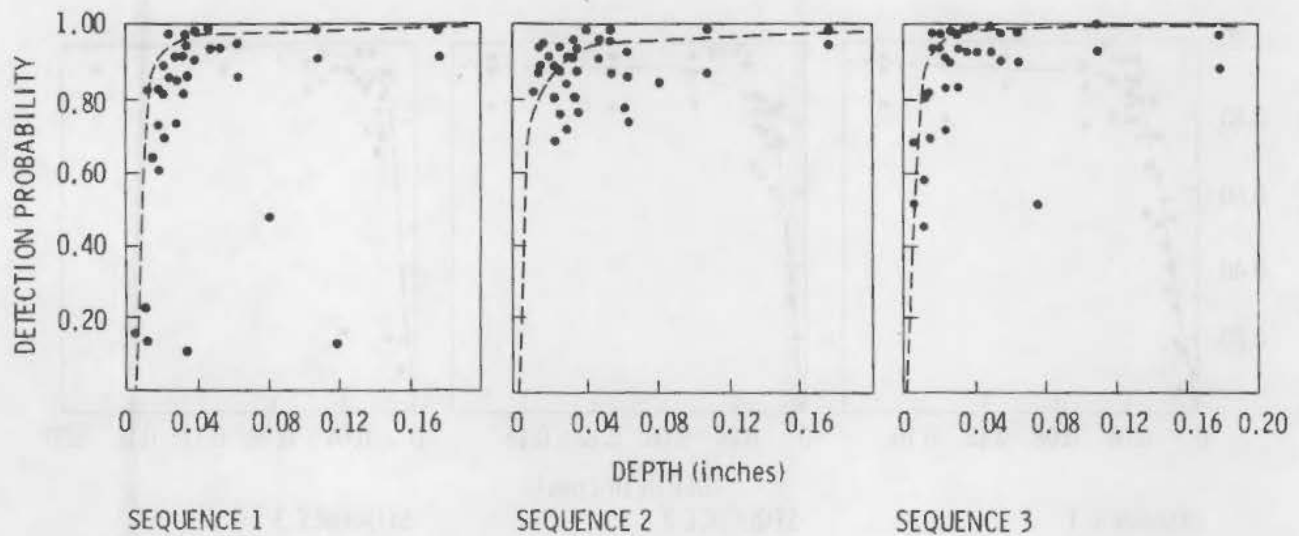


FIGURE 4.2.6. Crack Detection Probability of the Ultrasonic Inspection Method Plotted by Actual Crack Depth at 95% Probability and 95% Confidence Level

(MT), and UT. The sensitivity, which is a measurement of the probability of detection, is denoted by

$$S(NDE) = \frac{N_f(NDE)}{N} \quad (4.2.1)$$

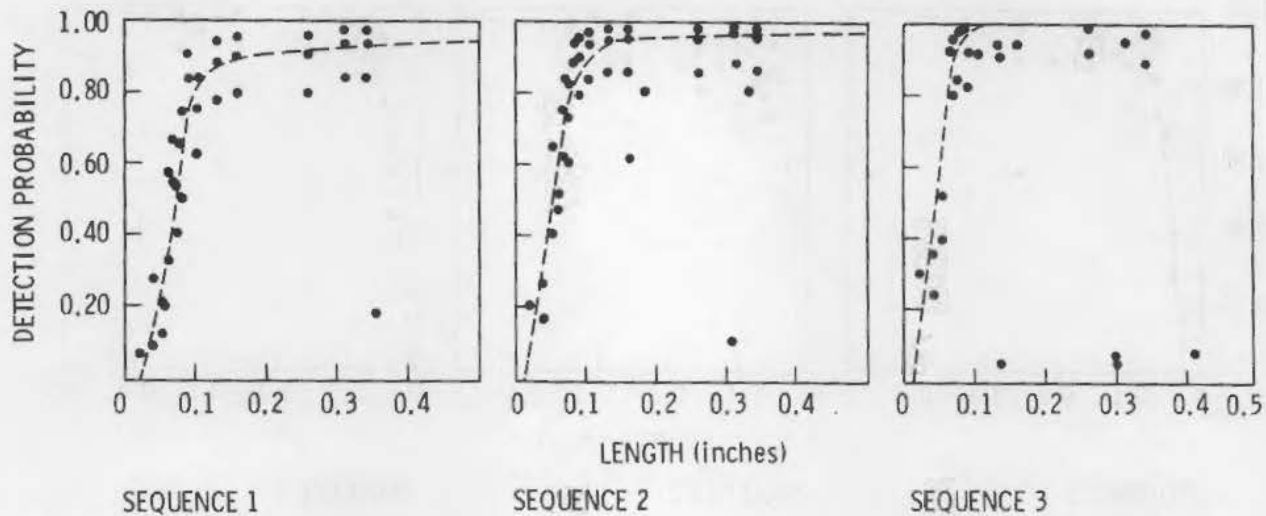


FIGURE 4.2.7. Crack Detection Probability of the Eddy Current Inspection Method Plotted by Actual Crack Length at 95% Probability and 95% Confidence Level

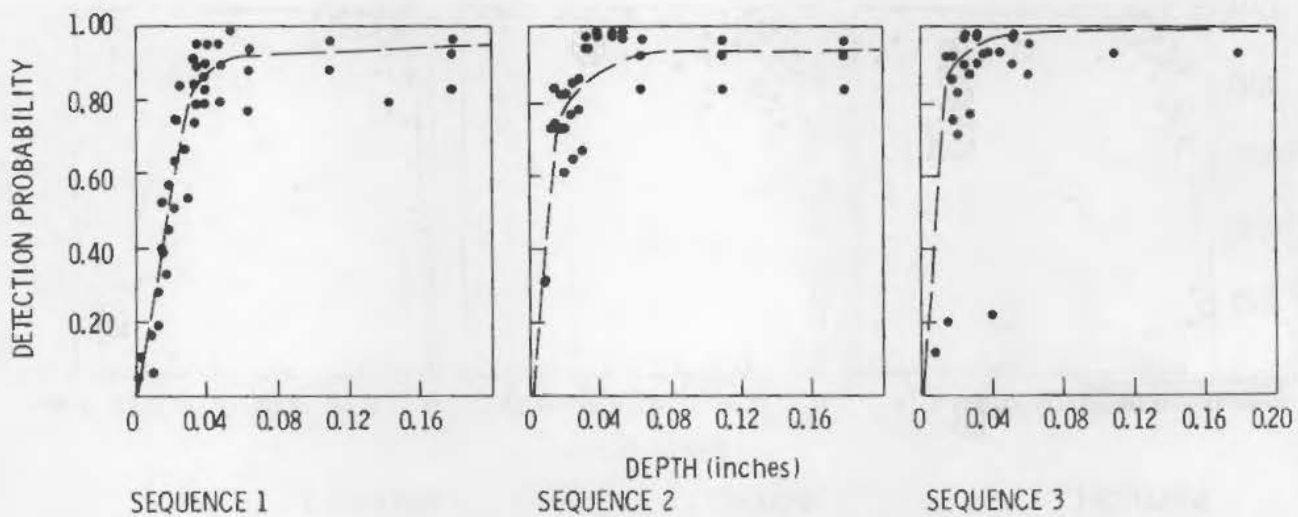


FIGURE 4.2.8. Crack Detection Probability of the Eddy Current Inspection Method Plotted by Actual Crack Depth at 95% Probability and 95% Confidence Level

The relevant data are given in Table 4.2.3. Production and laboratory NDE procedures were compared for flaw detection for aluminum (PT) and steel (PT, MT, ET, and UT). These results are given in Table 4.2.4.

In Reference 4.2.3, the author summarizes detection sensitivities for several materials and NDE procedures. These are given in Table 4.2.5.



TABLE 4.2.3. Sensitivity of Detection of Surface Flaws in Aluminum and Steel Cylinders (4.2.2)

Actual Crack Range (2C) in.	Aluminum			Steel			
	PT	UT	RT	PT	UT	MT	RT
No Crack	0.9333	0.8667	0.9333	0.8889	0.7778	0.7778	
0.000 to 0.050	0.0667	0.1333	0.0667	0.1111	0.2222	0.2222	0.3900
0.051 to 0.100	0.1538	0.4615	0.0000	0.4000	0.4000	0.6000	0.0000
0.101 to 0.150	0.2917	0.6250	0.0417	0.3333	0.8000	0.9333	0.0000
0.151 to 0.200	0.3636	0.5000	0.0000	0.3000	0.9000	0.9333	0.0000
0.201 to 0.250	0.8571	0.8571	0.0000	0.6000	1.0000	0.9000	0.0000
0.251 to 0.300	1.0000	1.0000	1.0000	0.7978	1.0000	0.8889	0.2222
0.301 to 0.350	1.0000	1.0000	0.1111	0.6250	0.8750	1.0000	0.1250
0.351 to 0.400	1.0000	1.0000	0.0000	1.0000	1.0000	1.0000	0.0000
0.401 to 0.450	1.0000	1.0000	0.2500	1.0000	1.0000	1.0000	0.0000
0.451 to 0.500	1.0000	1.0000	0.8333	1.0000	1.0000	1.0000	0.5000

One further data collection of significance is given in Reference 4.2.4. The probability of detection at 95% confidence level for a spectrum of flaw sizes in steel titanium and aluminum for MT, PT and UT is given in Table 4.2.6.

Some of the conclusions from Reference 4.2.2 are relevant to the work reported in References 4.2.2 to 4.2.4 with regard to detection sensitivity:

- The reliability of NDE needs to be improved.
- For 7075 aluminum cylinders containing surface fatigue cracks, the order of preference for NDE would be, for crack length less than 0.20 in., a) UT, b) PT, c) RT; for crack length 0.20 to 0.50 in., a) PT, b) UT, and c) RT.
- For 4330V steel cylinders containing surface fatigue cracks, the order of preference for NDE would be, for crack length less than 0.015 in., a) UT, b) MT, c) PT, d) RT; for crack length 0.15 to 0.50 in., a) MT, b) UT, c) PT, and d) RT.
- All NDE methods were quite accurate in detecting the location of the crack (RT was not included because of the low sensitivity of this technique).

TABLE 4.2.4. Comparison of Detection Sensitivities of Production and Laboratory NDE(4.2.2)

Actual Crack Length (2C) Range (in.)	Aluminum				Steel			
	PT		RT		MT		ET	UT
	Prod.	Lab	Prod.	Lab	Prod.	Lab	Lab	Lab
0.0 to 0.05	NA	0.0667	NA <sup>(a)</sup>	0.1111	0.2105	0.2222	0.0000	0.2222
0.05 to 0.10	0.0000	0.1538	(0.5000)	0.4000	(0.5000)	0.6000	0.2000	0.4000
0.10 to 0.15	0.0909	0.2917	(0.1000)	0.3333	0.6667	0.9333	0.1250	0.8000
0.15 to 0.20	0.0833	0.3636	(0.6667)	0.3000	0.7500	0.9000	0.2857	0.9000
0.20 to 0.25	1.0000	0.8571	(0.3000)	0.6000	0.6000	0.8889	(1.0000)	1.0000
0.25 to 0.30	(0.3333) <sup>(b)</sup>	1.0000	(1.0000)	0.7778	1.0000	1.0000	(1.0000)	1.0000
0.30 to 0.35	(0.5000)	1.0000	(1.0000)	0.6250	1.0000	1.0000	(1.0000)	1.0000
0.35 to 0.40	NA <sup>(a)</sup>	1.0000	(1.0000)	1.0000	1.0000	1.0000	(1.0000)	1.0000
0.40 to 0.45	NA <sup>(a)</sup>	1.0000	NA <sup>(a)</sup>	1.0000	NA <sup>(a)</sup>	1.0000	NA <sup>(a)</sup>	1.0000
0.45 to 0.50	(1.0000)	1.0000	(1.0000)	1.0000	(1.0000)	1.0000	(1.0000)	1.0000

(a) Number specimens containing cracks of this size range were inspected by the particular technique.

(b) Number in parentheses based on three specimens or less.

**TABLE 4.2.5. Summary of Selected Detection Sensitivities of Some Commercial NDE Processes**

Technique	Material	Size (mm)	Comments
Visual	7075-T6511	0.7	Fatigue crack magnification
Ultrasonics	7075-T6511	6.3	Fatigue 5.0 MHz 6 mm shear transducer
Penetrant	7075-T6511	6.3	Fatigue. No pre-etch ZL-2 penetrant ZE-3 emulsifier ZP-4 developer
X-ray	7075-T6511	13.0	Fatigue 110 kVp 5 mA 0.9 m distance 2 min exp, D-4 film
Visual	4330 V	0.7	Fatigue crack magnification
Ultrasonics	4330 V	5.0	Fatigue crack 5.0 MHz 0.6 m shear transducer
Penetrant	4330 V	9.0	See 3
Magnetic Particle	4330 V	7.8	Fatigue crack mag 20 A 20,000 A turns
Ultrasonics: Surface Wave	2219-T87	5.0	Fatigue crack preproof
Penetrant	2219-T87	5.0	Fatigue crack URE SC OP-133 Dry Developer 2L2A penetrant 2E44 emulsifier 2P4A developer
Eddy Current	2219-T87	5.0	Fatigue crack
Ultrasonics: Shear Wave	2219-T87	6.3	Fatigue crack 2.25 to 15 MHz various configurations
X-ray	2219-T87 + welded	7.6	Fatigue crack
Delta Scan	D6AC	3.8	Induced flaws
Magnetic Rubber	D6AC	0.9	Induced flaws
Delta Wheel	2014A1	>0.3	Porosity
Ultrasonics: 60° Angle	2014	>0.3	Porosity
X-ray	2014, 2219	>0.3	Porosity
Penetrant	7075-T6	1.9	Fatigue P51 = 2.5 penetrant
Magnetic Particle	D6AC	2.5	Fatigue Fluor, magnetic particle

TABLE 4.2.6. Flaw Sizes Detectable at Known Confidence Limits (in.)

<u>Flaw Size Range</u>	<u>Probability of Detection (%)</u>	<u>Confidence Levels (%)</u>
0.030 to 0.75 (2c)	75	95
0.076 to 0.100 (2c)	90	95
0.101 to 0.150 (2c)	95 Mag particle-HP-9 steel, MTL-I-6868 with 0.1 to 0.15 ml per 100 ml SO <sub>2</sub>	95
0.030 to 0.075 (2c)	90	95
0.076 to 0.100 (2c)	90 P5F2.5 penetrant system Ti6Al-4V 0.5 mil etch	95
0.030 to 0.075 (2c)	90 Instaviz P5F 1.0 penetrant-alum. 0.5 mil etch	95
0.076 to 0.100 (2c)	90 P5F-1 Penetrant-alum. RHR 65 or better 0.5 mil etch	95
0.030 to 0.075 (2c)	90	95
0.076 to 0.100 (2c)	90 4 MHz 45° and 70° duplex inspection	95
0.030 to 0.050 (2c)	90 Mag rubber double inspection	95

- RT was unable to detect small tight surface fatigue cracks in aluminum and steel cylinders.
- The sensitivity of UT to detect small cracks appears to be superior to all other methods examined.
- MT is the most rewarding for 4330V steel cylinders.
- Production inspection methods are as sensitive to cracks of length 0.20 to 0.50 in. as are laboratory methods. Laboratory methods appear to be more sensitive for small crack lengths.
- ET is less sensitive than UT for cracks from 0.20 to 0.50 in.

These conclusions are borne out in the following figures--for 7075 aluminum, Figure 4.2.9; and for 4330 steel, Figure 4.2.10.

Padilla and Park<sup>(4.2.10)</sup> utilized eddy currents to detect and size small fatigue cracks in thin aluminum sheets. The report dealt primarily with sizing; however, the method was quite sensitive to detection with cracks as small as 0.005 in. in depth.

#### 4.2.1.2 Fatigue Cracks

A study reported by Pettit and Hoepfner<sup>(4.2.11)</sup> on the 2219-T87 aluminum alloy containing fatigue cracks unloaded or with applied tensile loads utilized RT, PT, UT and ET. A round robin among three laboratories revealed significantly poorer results in the case of Laboratory II compared to I and III, primarily due to less time to optimize and to poorer working conditions. The most significant results pertained to NDE in the as-fatigued condition and after

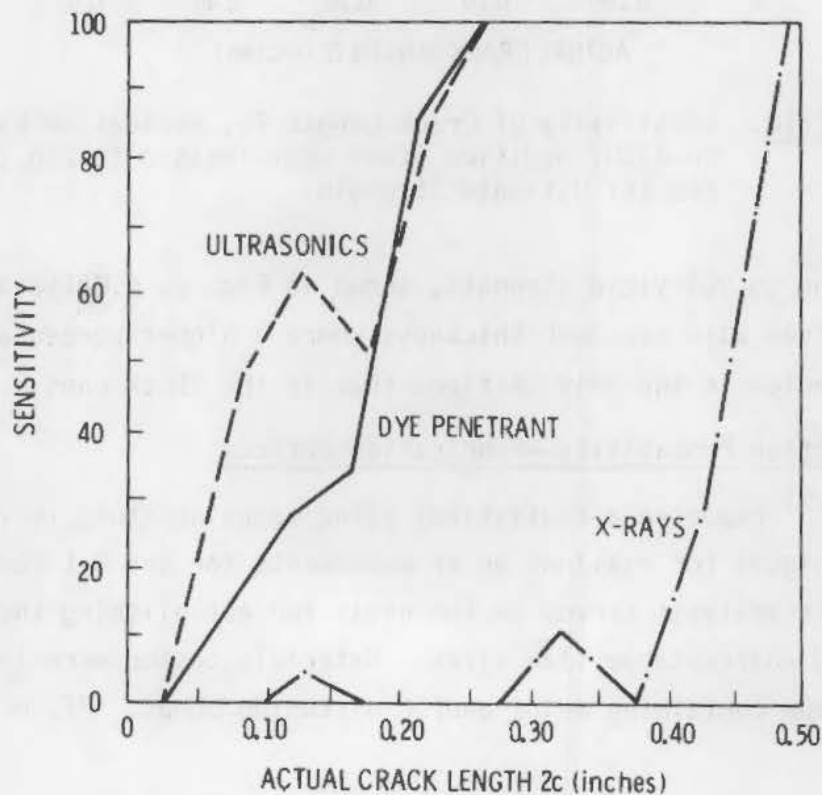


FIGURE 4.2.9. Sensitivity of NDE Methods in Detecting Surface Fatigue Cracks in 7075-T6511 Aluminum

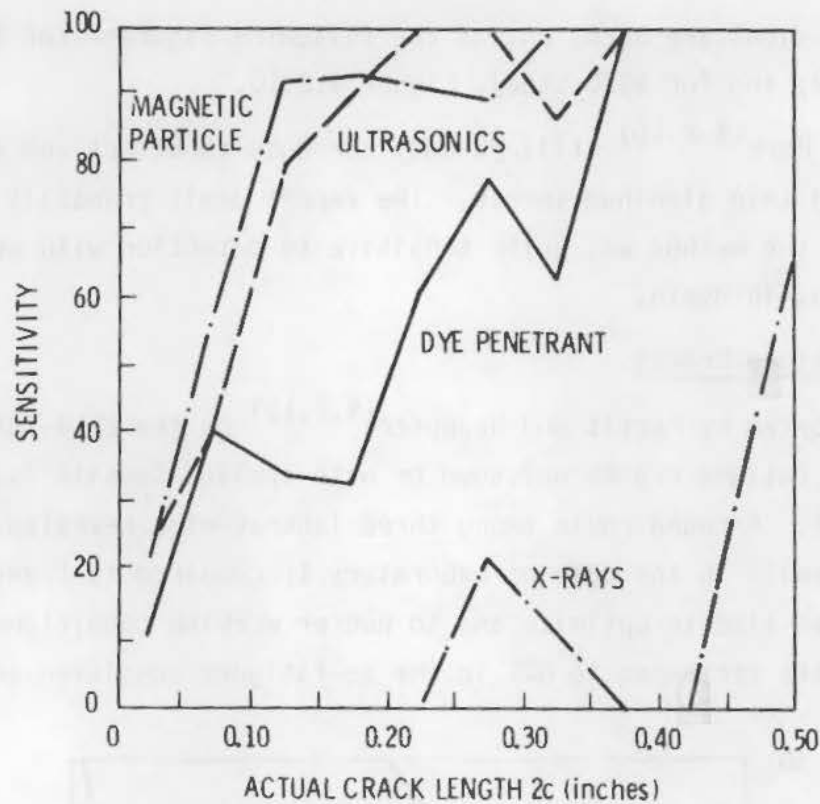
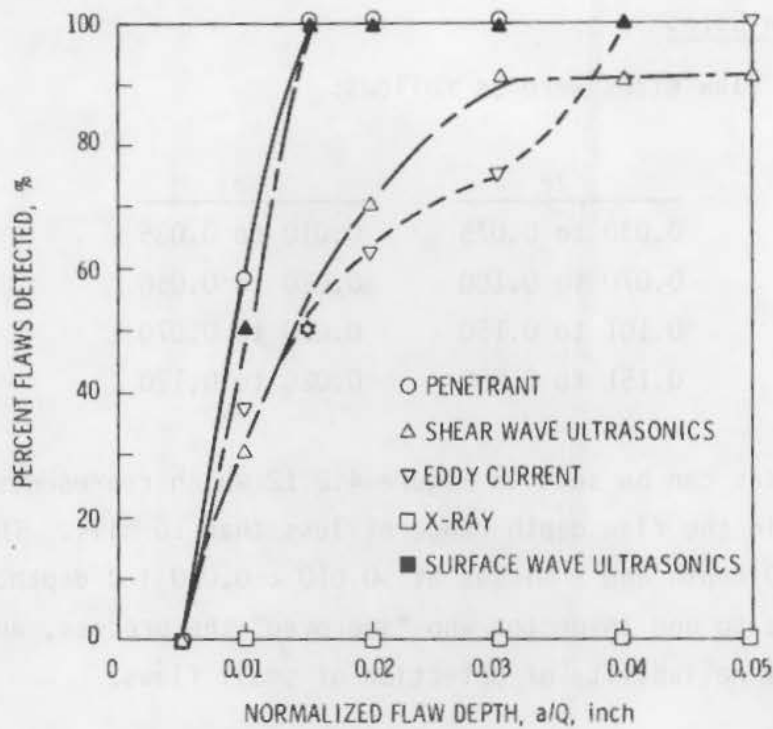


FIGURE 4.2.10. Sensitivity of Crack Length  $2c$ , Indication by NDE in 4330V Modified Steel Heat-Treated to 220 to 240 ksi Ultimate Strength

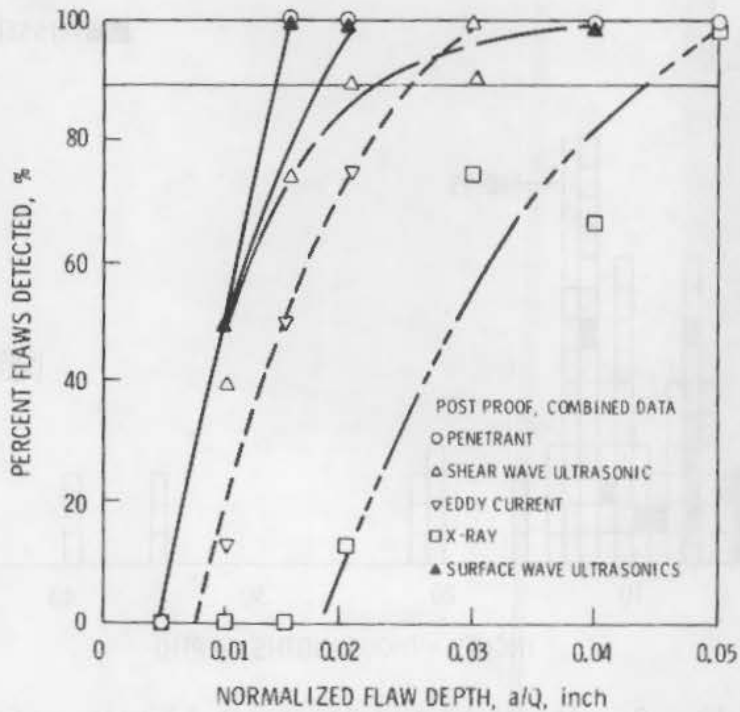
post-proof loading to 90% yield strength, shown in Figures 4.2.11a and 4.2.11b. A trend was observed with specimen thickness where a higher percentage of defects were detected in the thin sections than in the thick ones.

#### 4.2.2 Flaw Detection Probability--Fabrication Defects

Caustin<sup>(4.2.5)</sup> reported a statistical blind sampling study to validate various NDE techniques for examination of components for the B-1 bomber. A fracture mechanics analysis served as the basis for establishing the spectrum of acceptable and unacceptable flaw sizes. Materials tested were titanium, steel, and aluminum containing welds and/or diffusion bonds. PT, MT, UT or ET were used.



(a) ALL PREPROOF DATA



(b) ALL POSTPROOF (90% Y.S.) DATA

FIGURE 4.2.11. Inspection Results by NDE Method

#### 4.2.2.1 Flaw Sizes

The range of flaw sizes were as follows:

<u>2c</u>	<u>a</u>
0.030 to 0.075	0.010 to 0.035
0.070 to 0.100	0.020 to 0.050
0.101 to 0.150	0.020 to 0.070
0.151 to 0.250	0.020 to 0.120

An example of misses can be seen in Figure 4.2.12 which represents results with PT. Misses were in the flaw depth range of less than 10 mils. There were 11 misses below 0.010 depth and 2 misses at  $>0.010 < 0.020$  in. depth. Four of the 11 misses were due to one inspector who "improved" the process, and, in so doing, reduced the reliability of detection of small flaws.

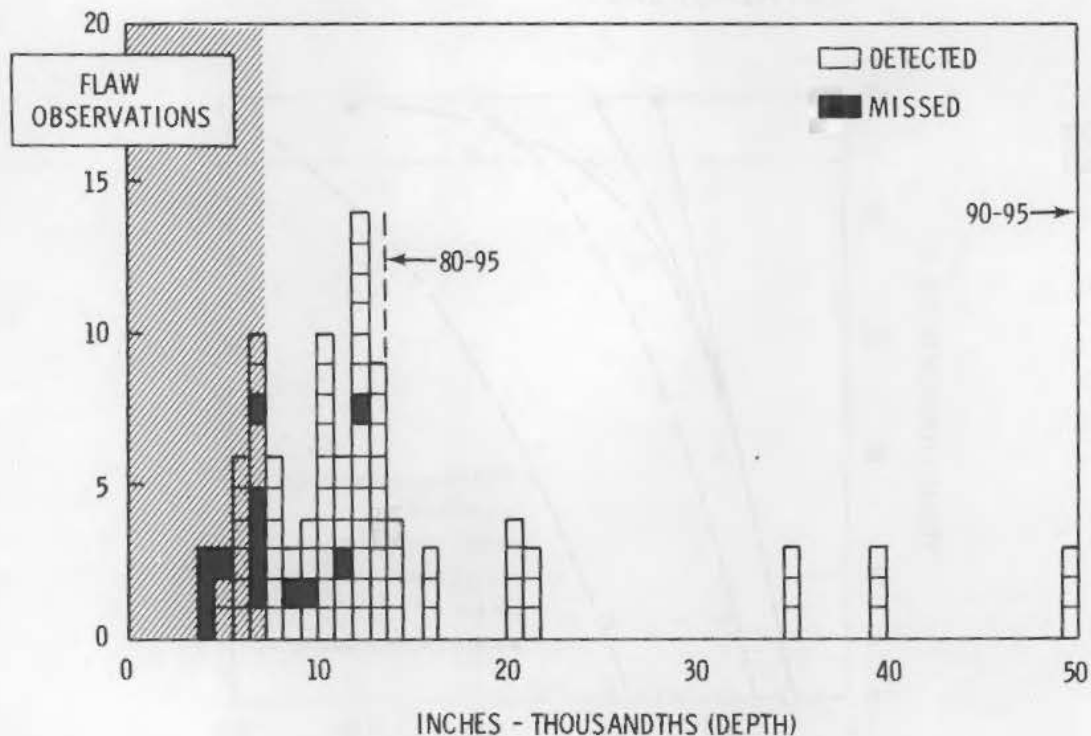


FIGURE 4.2.12. Results of Liquid Penetrant Testing as Function of Flaw Depth



The 90% probability--95% confidence limits were met for the depths shown in Table 4.2.7 with the NDE techniques cited.

The results are quite interesting when one considers the following ground rules:

- Defects were to be fabrication type, not fatigue nor environmentally induced.
- The procedures were to be those approved for the B-1.
- Inspection personnel used were limited to those certified to work on the B-1.
- Flaw sizes were to be confirmed by destructive testing.
- To ensure blind sampling, the specimens were intermixed with similar B-1 test pieces passing through inspection.

Hagamaier<sup>(4.2.6)</sup> has plotted the data of others as functions of flaw length and depth dimensions. Typical plots using surface flaw data are similar to Figures 4.2.9 and 4.2.10.

TABLE 4.2.7. Flaw Depths Yielding 90% Detection Probability at 95% Confidences

<u>NDE Technique</u>	<u>Material</u>	<u>Depth (in.)</u>
PT	Steel	0.040
PT	Aluminum	0.035
PT	Titanium	0.035
MT	Steel	0.050
UT <sup>(a)</sup>	---	0.046
UT <sup>(b)</sup>	Steel	0.050
UT <sup>(b)</sup>	Titanium	0.035
ET	---	0.030

(a) Longitudinal.  
(b) Shear.

#### 4.2.2.2 Influence of Stress

Corbly et al.<sup>(4.2.9)</sup> have examined the influence of stress on a flaw on the accuracy and precision of UT shear-wave measurements. While the data are more related to flaw sizing, the conclusions are applicable to detection, particularly with high DAC cutoffs.

- Natural cracks can be used for calibration and correlate well with the actual flaw depth. The accuracy of the technique is high and decreases with increasing stress on a flaw.
- The precision of the UT technique measured by the standard deviation increases with increasing stress on a flaw.
- UT shear-wave measurements do not measure the true depth of the flaws, but only the depth for which the crack opening displacement is greater than some critical amount; hence, upon stressing the flaw, the apparent indicated crack depth increases. This increase in apparent crack depth indication appears to be a linear function of the stress.

#### 4.2.3 Factors Affecting Detection Reliability

The NDE personnel factor may be quite significant with regard to reliability of detection of flaws. Herr<sup>(4.2.7)</sup> discusses the following factors affecting reliability:

- selection and training of personnel
- retention of trained personnel through higher wages
- definitive accept-reject criteria
- operating environment (noise, lighting, etc.)
- uniform reference standards
- standardization of equipment
- automation
- role of prior manufacturing operations in masking defects.

A specific magnetic particle testing (MT) program on D6AC steel test specimens of irregular shape illustrates the influence of flaw size on sensitivity to detection.

Table 4.2.8 compares failure to detect to number of tests. These data are plotted in Figure 4.2.13 for 95% confidence levels.

Extensive work on titanium alloys has been reported by Lord<sup>(4.2.8)</sup> for tight cracks, gross cracks and porosity. A majority of the work was with PT; however, RT, UT and ET were investigated for selected specimens.

#### 4.2.4 Statistical Analyses--NDE Data

The most extensive statistical analysis of NDE data relevant to detection was reported by Yee et al.<sup>(4.2.12)</sup> The authors reviewed 23 potentially useful data sets, then limited the study to seven on the basis of availability and completeness of data. All seven data sets were derived from NASA or Air Force programs. Several statistical models for evaluating the data were reviewed to determine their relevance to accurately modeling the probability of flaw detection. Included were binomial, normal, Poisson, Chi-square, and binomial exact. The following three statistical procedures were used to manipulate the data:

1. range interval (RI)
2. overlapping 60 points
3. optimized probability method (OPM).

Some 112 subsets of data were analyzed statistically. Although the data pool included some 34,000 measurements, there were many gaps in the information.

TABLE 4.2.8. Reliability of Detection with MT as Function of Flaw Depth

<u>Flaw Surface Length (in.)</u>	<u>Number of Trials</u>	<u>Number of Misses</u>
Less than 0.010	16	16
0.010 to 0.019	105	37
0.020 to 0.029	510	71
0.030 to 0.039	451	17
0.040 to 0.049	207	8
0.050 to 0.059	329	9
0.060 or Larger	<u>518</u>	<u>4</u>
	2,136	162

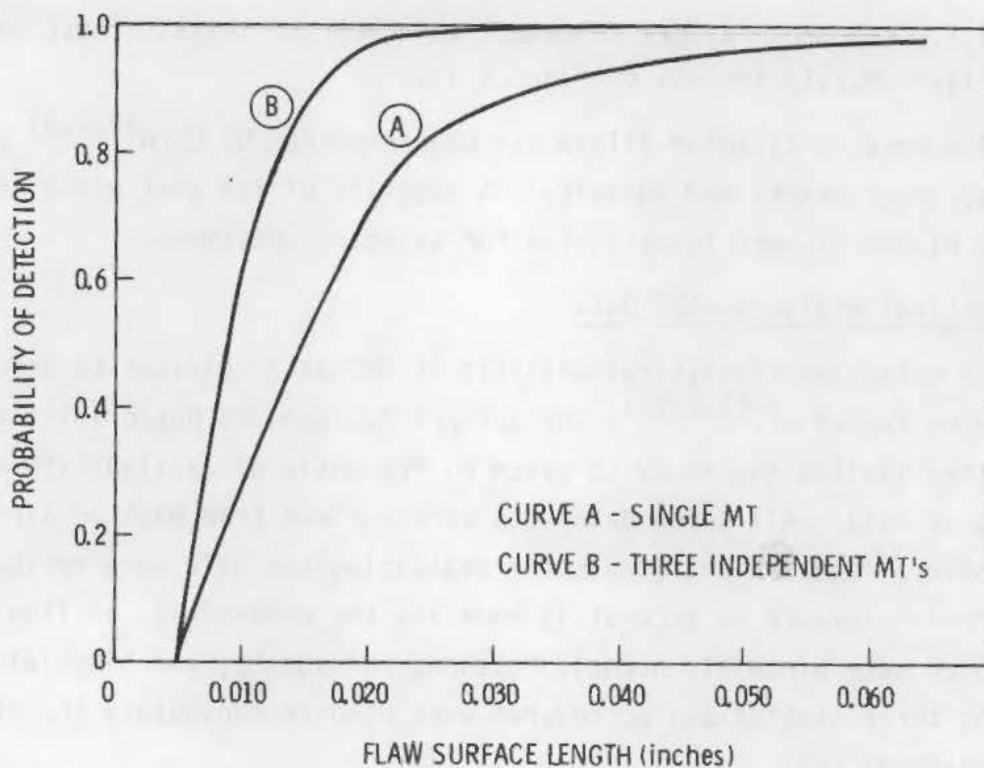


FIGURE 4.2.13. MT Production Detection Capability--  
95% Confidence Level

Examples of the statistical formats are given for the same data set covering probability of detection of fatigue cracks in 2219-T87 aluminum using UT surface waves. Figure 4.2.14 is a plot with the RI method. Figure 4.2.15 uses the OPM and Figure 4.2.16 uses the overlapping sixty-point method. It is obvious why the authors preferred OPM.

The major conclusion, which wasn't too surprising, was that human factors dominate NDE reliability. Another conclusion, confirmed by many workers, was the lack of sensitivity of RT in detecting fatigue cracks.

#### 4.2.4.1 Machined Versus Fatigue Flaws

An excellent paper by Birchak and Gardner<sup>(4.2.13)</sup> compared the response of machined flaws as standards for fatigue by quantitatively evaluating machined versus fatigue flaws under the same conditions. Flaw shapes simulated those commonly encountered in fatigue; namely, triangular, rectangular and half

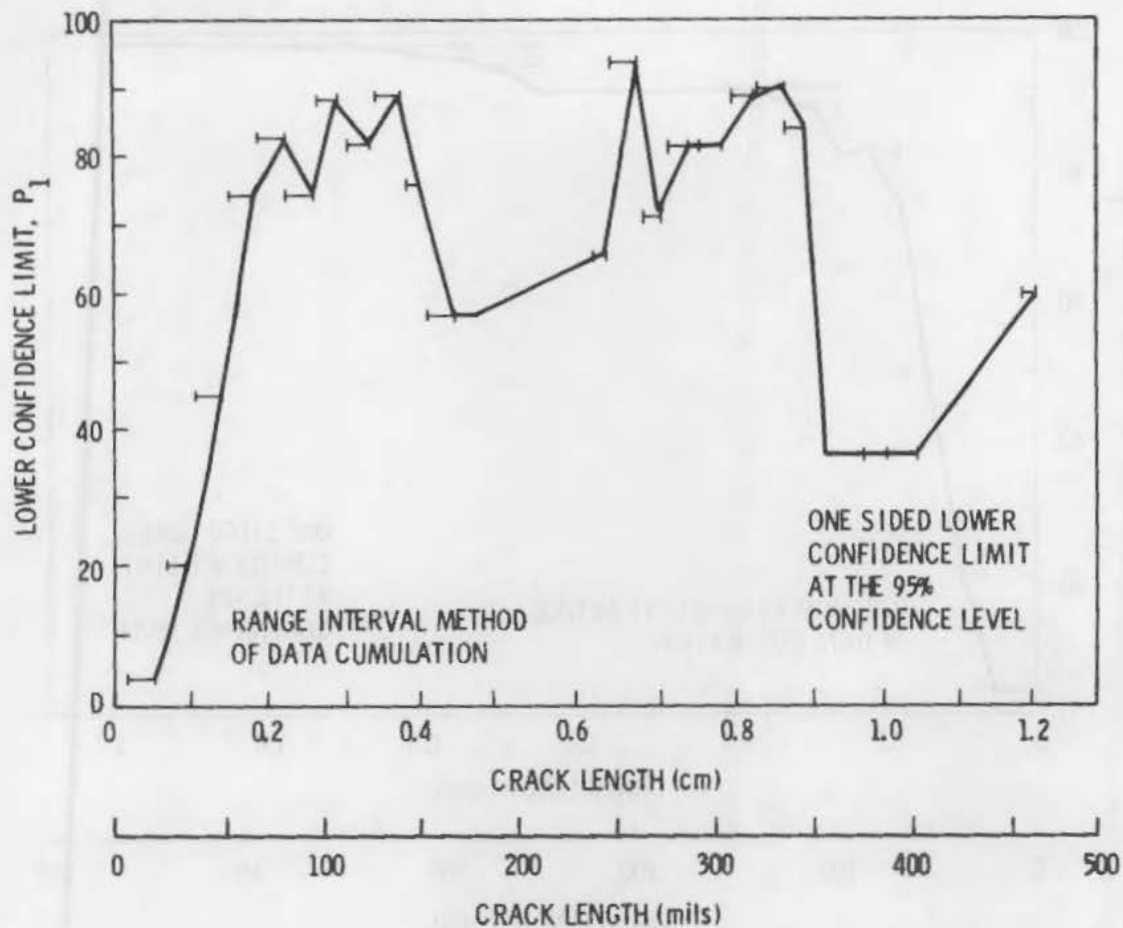


**FIGURE 4.2.14.** Probability of Detection for 2219-T87 Al Using Ultrasonic Surface Waves; Fatigue Cracks in Flat Plates; Laboratory Environment

penny. Artificial flaws were saw slits or electric discharge machining (EDM) notches. Fatigue cracks were either low or high cycle.

Significant UT parameters investigated included frequency (2.25 to 10 MHz) bandwidth and wave mode.

Substantial differences in signal were observed between artificial and fatigue cracks. For example, 10 to 34 dB added gain was required for reliable fatigue crack detection, which was attributed to partial transparency of the fatigue cracks and diffuse scattering due to surface roughness.

The data were statistically analyzed to quantify the differences between machined and fatigue cracks assuming the differences ( $D$ ) arose from random

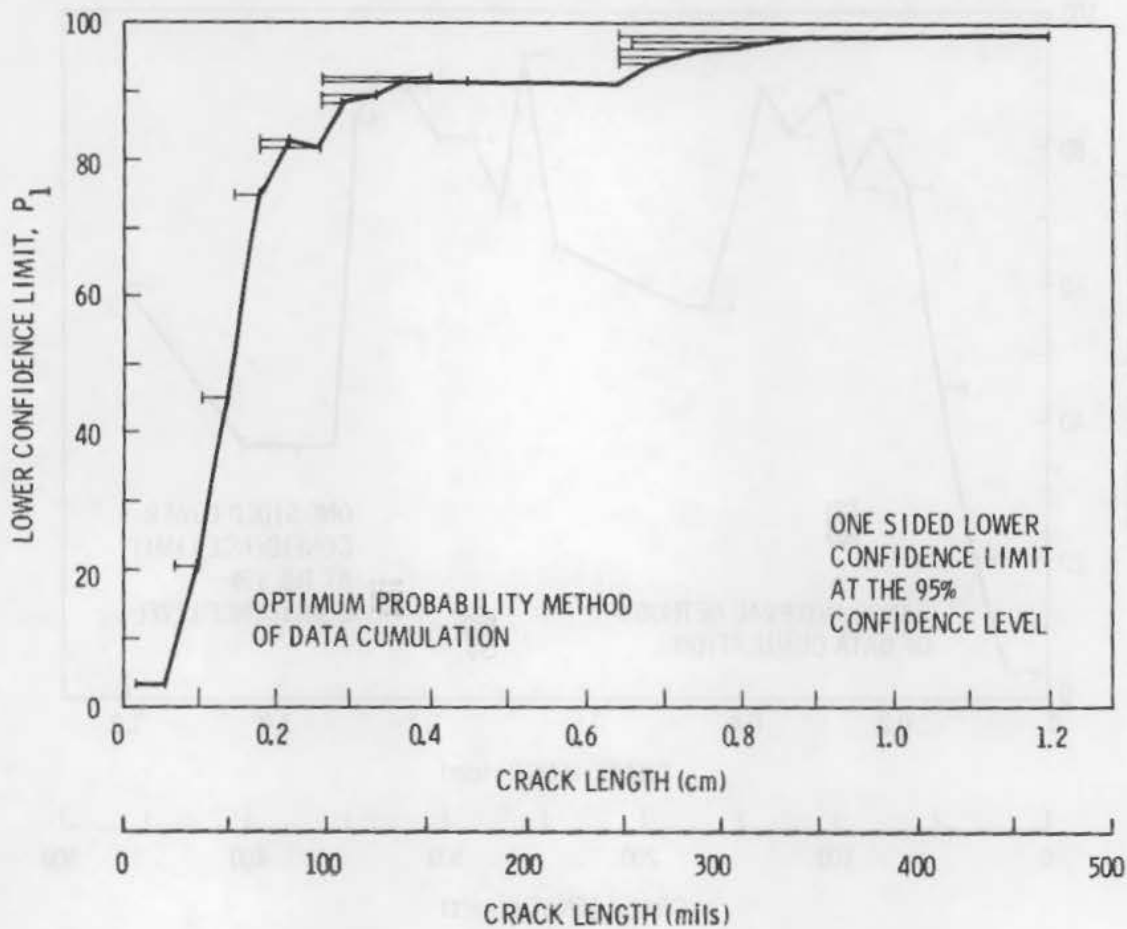


FIGURE 4.2.15. Optimum Probability Method of Data Cumulation

effects. The assumption proved invalid since they were not normally distributed. The overall average difference  $\bar{D}$  based on 54 measurements was 11.3 dB. The four parameters (viz.,  $\Delta_{Ti}$ ,  $\Delta_{Si}$ ,  $\Delta_{Fi}$ , and  $\Delta_{Mi}$ ), fatigue crack type, fatigue crack shape, UT frequency and UT wave mode can be calculated from the relationship

$$D = \bar{D} + \Delta_{Ti} + \Delta_{Si} + \Delta_{Fi} + \Delta_{Mi} \quad (4.2.2)$$

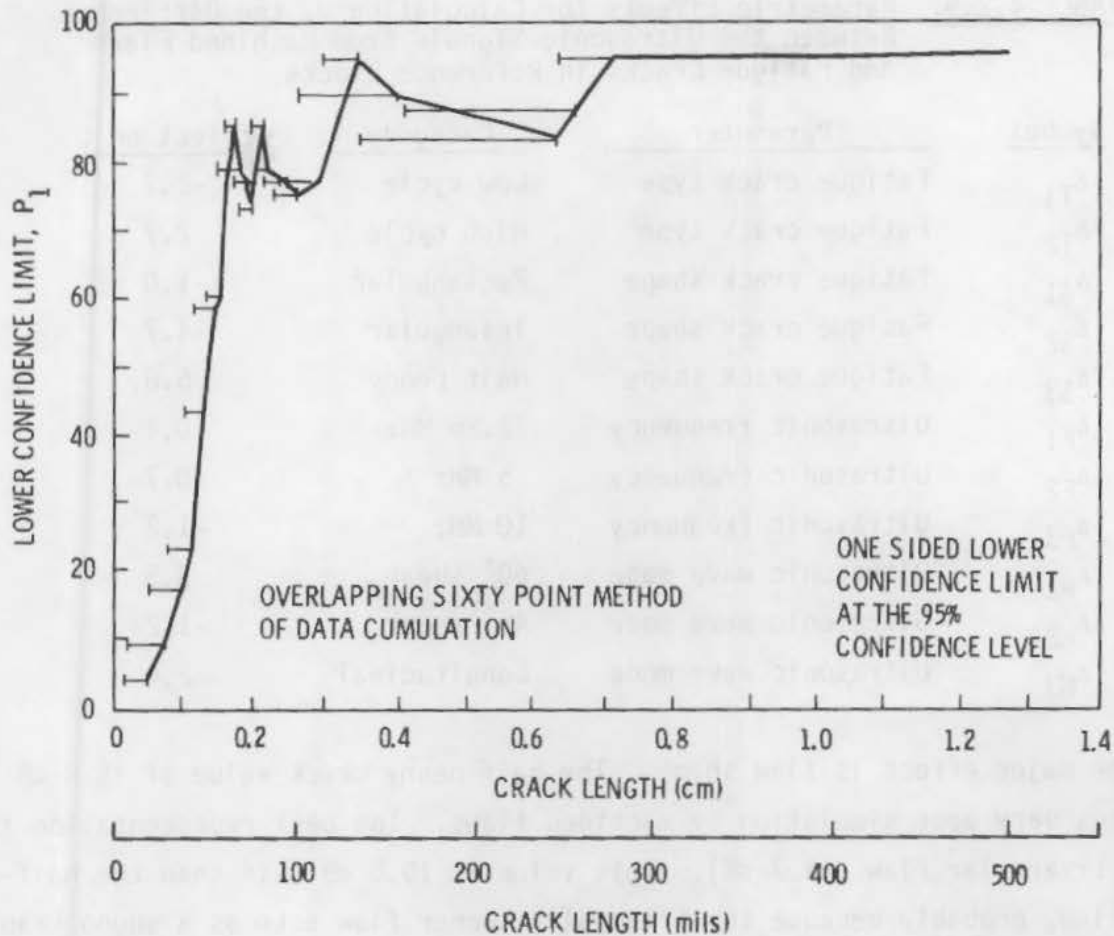


FIGURE 4.2.16. Overlapping Sixty-Point Method of Data Cumulation

Table 4.2.9 gives the values for each parametric state, permitting one to estimate the change in  $D$  with a change in any parameter. For example, in shifting from low-cycle fatigue to high-cycle fatigue,

$$\Delta_{T2} - \Delta_{T1} = 2.7 - (-2.7) = 5.4 \text{ dB} \quad (4.2.3)$$

or  $\bar{D}_{T2}$  for high-cycle flaws is 5.4 dB greater than  $\bar{D}_{T1}$  for low-cycle flaws. Qualitatively, this is what is anticipated because the higher stress of low-cycle fatigue will result in lower residual stress and larger crack opening displacement which will result in stronger reflections and smaller  $D$ .

TABLE 4.2.9. Parametric Effects for Calculating D, the Difference Between the Ultrasonic Signals from Machined Flaws and Fatigue Cracks in Reference Blocks

<u>Symbol</u>	<u>Parameter</u>	<u>Category</u>	<u>Effect on D</u>
$\Delta_{T1}$	Fatigue crack type	Low cycle	-2.7
$\Delta_{T2}$	Fatigue crack type	High cycle	2.7
$\Delta_{S1}$	Fatigue crack shape	Rectangular	-1.0
$\Delta_{S2}$	Fatigue crack shape	Triangular	-4.7
$\Delta_{S3}$	Fatigue crack shape	Half penny	5.8
$\Delta_{F1}$	Ultrasonic frequency	2.25 MHz	0.4
$\Delta_{F2}$	Ultrasonic frequency	5 MHz	0.7
$\Delta_{F3}$	Ultrasonic frequency	10 MHz	-1.2
$\Delta_{M1}$	Ultrasonic wave mode	60° shear	3.5
$\Delta_{M2}$	Ultrasonic wave mode	45° shear	-1.2
$\Delta_{M3}$	Ultrasonic wave mode	Longitudinal	-2.4

The major effect is flaw shape. The half-penny crack value of +5.8 dB indicates very poor simulation by machined flaws. The best representation is with a triangular flaw (-4.7 dB). This value is 10.5 dB less than the half-penny flaw, probably because the triangular corner flaw acts as a sound trap directing the scattered energy to the transducer.

The authors<sup>(4.2.13)</sup> discuss the direct application of the data in Table 4.2.9 to a specific examination by selecting an appropriate confidence level for detecting similar cracks in a structure. The added gain required can be calculated from Student-t values found in statistical tables. Table 4.2.10 presents such data. The range 10 to 34 dB cited previously is obtained from this analysis.

The importance of signal sensitivity is emphasized. While a small D is recommended, it is possible to have signals so small that they are essentially undetectable. The effect of the various parameters on signal strength is shown in Table 4.2.11. Analysis of variance was used to establish the influence of the various parameters on signal strength.



TABLE 4.2.10. The Gain G (dB) Which Must Be Added to Ultrasonic Equipment Calibrated on Machined Flaws to Have 95% Confidence of Detecting Fatigue Cracks in Reference Blocks

Flaw Type	Flaw Shape	60° Shear Transducers			45° Shear Transducers			Longitudinal Transducers		
		2.25 MHz	5 MHz	10 MHz	2.25 MHz	5 MHz	10 MHz	2.25 MHz	5 MHz	10 MHz
LC	R	21	22	20	17	17	15	15	16	14
LC	T	18	18	16	13	13	11	12	12	10
LC	HP	28	29	27	23	24	22	22	23	21
HC	R	27	27	25	22	22	21	21	21	19
HC	T	23	23	22	18	19	17	17	17	16
HC	HP	34	34	32	29	29	27	28	28	26

NOTE: The flaw types are low-cycle (LC) and high-cycle (HC) fatigue cracks; the flaw shapes are rectangular (R), triangular (T), and half penny (HP).

The influence of broad band versus narrow band is shown in Table 4.2.12. As anticipated the broad band is less sensitive. The effect of back scattering can be seen in Table 4.2.12 where the last two columns subtract the scattering background. Here the broad band yields better discontinuities, probably due to differences in frequency-dependent attenuation. These effects are more pronounced in the far field.

TABLE 4.2.11. Analysis of Variance for Ultrasonic Signals from Twelve Different Flawed Blocks and Nine Different Transducers

<u>Flaw Type</u>	<u>Mean Signal (dB)</u>	<u>Flaw Shape</u>	<u>Mean Signal (dB)</u>
Low	24.7	Rectangular	29.6
High	19.2	Half penny	29.7
Saw	33.5	Triangular	23.7
EDM	33.2		
Confidence	99.5%	Confidence	80%
Std. error	2.2	Std. error	2

<u>Transducer Frequency (MHz)</u>	<u>Mean Signal (dB)</u>	<u>Transducer Mode</u>	<u>Mean Signal (dB)</u>
2.25	31.0	60°	20.8
5	37.4	45°	28.3
10	14.7	Longitudinal	34.0
Confidence	95%	Confidence	80%
Std. error	4.3	Std. error	4.3

NOTE: The signal strengths are the receiver attenuation (dB) to produce a 2-in. (5.08-cm) deflection on the cathode ray tube (CRT) of the Reflectoscope.

TABLE 4.2.12. The Flaw Echo Strength Relative to the Background Signals

Frequency (MHz)	Mode	Signal		Signal Minus Background	
		Broad Band (dB)	Narrow Band (dB)	Broad Band (dB)	Narrow Band (dB)
2.25	60° shear	36	53	22	17
2.25	45° shear	39	56	24	22
2.25	Longitudinal	45	63	17	15
5	60° shear	34	49	28	27
5	45° shear	44	56	26	21
5	Longitudinal	47	62	23	17
10	60° shear	2	13	28	13
10	45° shear	6	28	31	16
10	Longitudinal	32	52	26	23

NOTE: For nine transducers the flaw signals (averaged for 12 specimens) are listed for broad- and narrow-band pulser/receivers. Additionally, the difference between these signals and the background level of an unflawed specimen is presented. Measurements were made with maximum pulse length at the far transducer location.

For 2.25 MHz, the longitudinal data refer only to the signals from the rectangular flaws because the triangular and half-penny flaw echoes could not be distinguished from the background.

TABLE 3.1. Signal-to-noise ratios for the different signals.

Signal-to-noise ratio	Signal		Noise	
	Low	High	Low	High
10	20	40	10	20
15	30	60	15	30
20	40	80	20	40
25	50	100	25	50
30	60	120	30	60
35	70	140	35	70
40	80	160	40	80
45	90	180	45	90
50	100	200	50	100

The signal-to-noise ratios for the different signals are given in Table 3.1. The signal-to-noise ratios are defined as the ratio of the signal power to the noise power. The signal power is defined as the average power of the signal over the observation interval. The noise power is defined as the average power of the noise over the observation interval. The signal-to-noise ratios are given in Table 3.1 for different values of the signal-to-noise ratio and the observation interval. The signal-to-noise ratios are given in Table 3.1 for different values of the signal-to-noise ratio and the observation interval. The signal-to-noise ratios are given in Table 3.1 for different values of the signal-to-noise ratio and the observation interval.

The relatively high sensitivity of detection of relatively insignificant flaws such as centerline porosity was reported by Katz and Caplan.<sup>(4.3.1)</sup> These results in thick section plate parallel the data reported on the PVRC test specimens. Such voids are detectable with both RT and UT. An interesting dichotomy exists in that the ASME III using RT may find them acceptable whereas ASME XI using UT may not. Hopefully, the long-range plans to resolve such code differences may prevent unnecessary repairs.

Caplan<sup>(4.3.2)</sup> reported NDE results on 36 reactor pressure vessels examined by UT and RT. Five of the 36 contained rejectable defects which were repaired. The results are summarized in Table 4.3.1. While one cannot be sure how many flaws were not detected by UT, it is obvious that RT missed many that UT detected. It is interesting to note that flaws in three of the five reactor pressure vessels would not have been detected if UT had been limited to the outer surface.

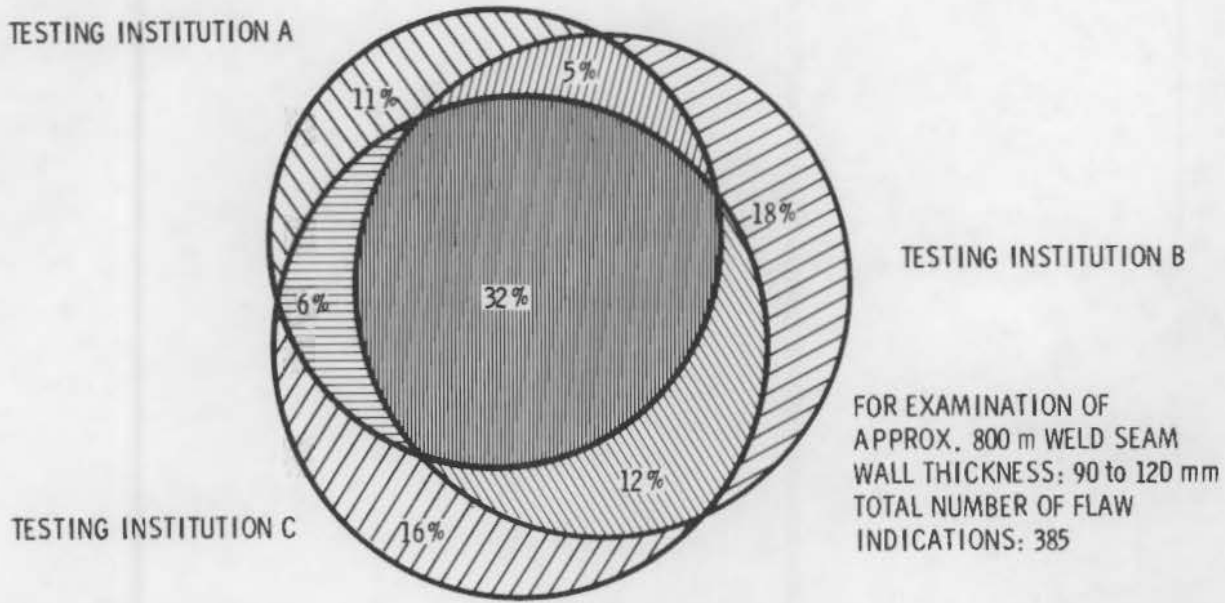
The results reported by Caplan<sup>(4.3.2)</sup> were confirmed in the Doel<sup>(4.3.3)</sup> reactor pressure vessel. NDE during construction consisted of both UT and RT from the outer surface. Later, during the baseline examination, UT from the inner surface detected a planar defect near a nozzle that was about 2.5 in. long by about 0.1 in. deep. If construction UT had included examination from the inner surface, the flaw probably would have been detected.

Trumpfheller<sup>(4.3.4)</sup> reported the degree of agreement among three different UT testing institutions in examining the same 800 m of weldment in relatively thick sections (90 to 120 mm). Figure 4.3.1 permits a comparison of the ability to detect flaws. It is interesting to note that only 32% were found by all three organizations. While the report does not define the makeup of the flaw population, the detection distribution is typical of teams with greater abilities to detect one class, e.g., slag to another.

TABLE 4.3.1. Detection of Flaws in Five Reactor Pressure Vessels

Vessel	UT Data	RT Data
RPV-1	Twenty-three indications found, 8 to 400% DAC with 40° angle beam; also 60%. Lack of fusion -12, slag inclusions -11.	None of 23 detected with initial RT. Only 4 with subsequent RT.
RPV-2	Fourteen indications in 6 of 8 nozzles-to-shell welds. Five greater than 100% DAC. Detected by straight beam from bore side. UT from outer surface by straight and 45° beam did not detect. Porous structure produced by solidification after liquation.	None detected by initial RT; however, this had incorrect beam alignment. With correct alignment 12 of 14 were found by RT with 9 code rejectable.
RPV-3	Sixteen indications in nozzle welds detected by straight beam (>100% DAC) from bore side.	No indications with initial RT; more sensitive RT detected 9 of 16.
RPV-4	Low amplitude signals detected in 2 longitudinal welds with 45° beam; from inside 60° gave negligible response. There was a complete lack of detection from the outside. Straight beam detected nothing from inside nor did angle beam directed along the weld characterized as slag porosity; lack of fusion and freeze-line shrinkage or liquation cracking.	No detection in either initial or subsequent RT.
RPV-5	45° angle beam detected rejectable indications in circumferential weld between head dome and flange. Lack of fusion.	Nothing in RTs.

TESTING INSTITUTION A



TESTING INSTITUTION B

TESTING INSTITUTION C

FOR EXAMINATION OF  
APPROX. 800 m WELD SEAM  
WALL THICKNESS: 90 to 120 mm  
TOTAL NUMBER OF FLAW  
INDICATIONS: 385

FIGURE 4.3.1. Agreement with the Number of Flaw Locations Given

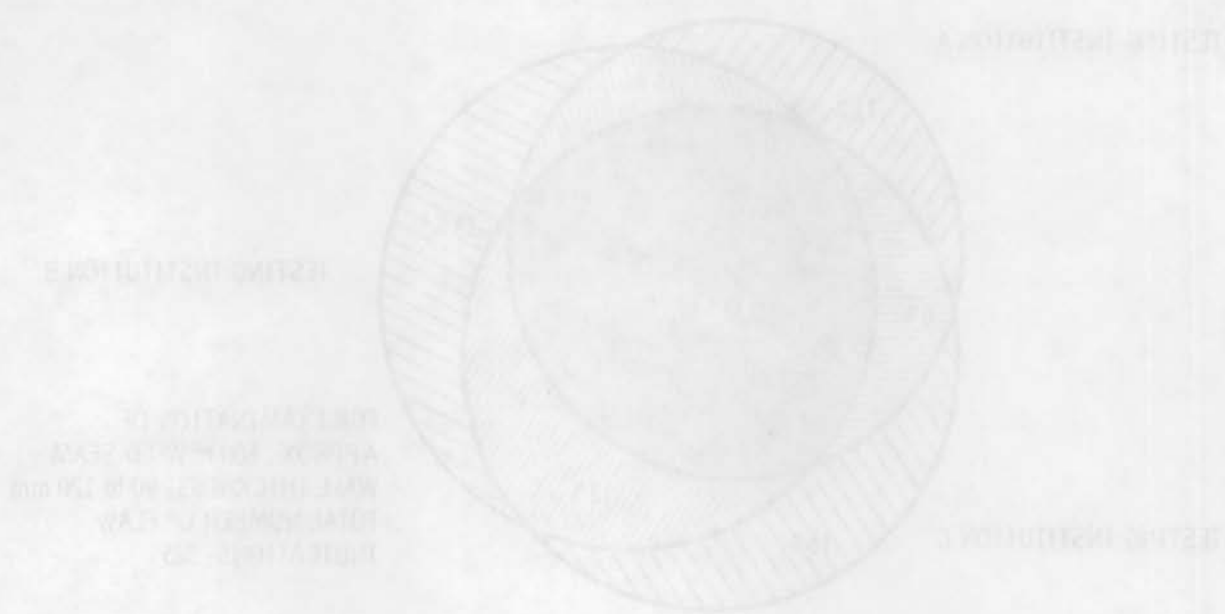


FIGURE 4.3.1. Agreement with the number of raw locations given



An examination of the extensive (but still inadequate) surface flaw data confirms the high probability of detection of relatively small flaws by one or more NDE techniques. Unfortunately, these results cannot be extrapolated to embedded flaws in thicker sections. While the data on such flaws is relatively limited in this chapter, a review extended to Chapter 3 on PVRC blocks leads to the conclusion that RT is not reliable for tight cracks and that UT may miss cracks due to location, flaw orientation and flaw size. The parameters causing such UT variability are reviewed in the next section.

As a result of the extensive (but still inadequate) surface finish  
investigation, the high probability of detection of relatively small flaws by one of  
the techniques mentioned above, these results cannot be extrapolated to  
include flaws in these sections. While the data on each flaw is relatively  
limited in this context, a review of the data on flaws in these sections  
leads to the conclusion that it is not reliable for small cracks and that the  
flaws due to location, the orientation and the size. The generalizing  
each of the data are reserved to the next section.

Table 4.5.1 touches on a few of the limitations derived from theoretical evaluations. Of particular interest is Haines<sup>(4.5.3)</sup> work which relates directly to ASME XI and German code threshold reporting values. The significance of flaw surface condition and flaw tilt for a given beam angle helps explain the missed flaws when examinations were limited to one surface and one or two beam angles.

#### 4.5.1 External Factors

The obvious external factors influencing reliability of UT are equipment and operator. Others to be considered also are calibration and acoustic properties.

##### 4.5.1.1 Equipment Variability

Equipment variability has been examined and reported in conjunction with the PVRC program.<sup>(4.5.5)</sup> The equipment testing, round robin, indicates that the two most important parameters are 1) the system operating frequency spectrum observed at the instrument video detector, and 2) the beam profile or radiation pattern of the search unit in the material under consideration.

It is significant to note that gain adjustment using calibration blocks does not eliminate response variation caused by variations in frequency or search unit size. This is because, with most calibration blocks, the energy impinges on the reference hole at normal incidence so that the effect of variations in beam profiles does not become apparent. However, when poorly oriented defects are detected, the interaction of beam profiles may significantly reduce the amplitude. This latter result is due to the dependency of interaction of search unit and defect radiation patterns. Generally, this program confirms the earlier conclusion of Hislop.<sup>(4.5.6)</sup>

Transducers represent another source of variation. The radiation pattern, intensity, and the frequency response generally cannot be reproduced to within 20% even when two transducers are obtained from the same manufacturer.<sup>(4.5.1)</sup> In addition, transducer characteristics decay with usage, with the mean useful

## TABLE 4.5.1. Theoretical Considerations

Beam attenuation and dispersion not taken into account—ultrasound discontinuity interactions treat as case of infinite plane waves incident on a single discrete discontinuity such as cylinder, sphere, etc.

Need solutions for spatially bounded—wave packets incident on discontinuities embedded in an attenuating medium.<sup>(4.5.1)</sup>

Thompson<sup>(4.5.2)</sup> cites a first principle approach to defect sizing where the known systematic error in the approximation theory led to most of the absolute error of 15% on height and 37% on diameter.

The Central Electricity Generating Board (CEGB)<sup>(4.5.3)</sup> has a theoretical model of pulse reflection from surfaces that takes account of crack size, shape, orientation and surface roughness as well as UT pulse shape. Specific geometries investigated include elliptic planar (rough and smooth), cylindrical, and spherical. The model does not consider attenuation caused by surface condition, presence of cladding, etc. Therefore, the model is assumed to yield the maximum signal amplitude with a pulse echo UT system.

If the reporting threshold criteria of ASME XI and the German code are used, the significance of the theoretical model becomes obvious. The thresholds are:

- ASME XI—reporting threshold for a defect at depth of 100 mm is 50% of the amplitude from a 0.25-in.-dia (6.35-mm) hole. This corresponds to -7.2 dB for compression and -9.9 dB for shear waves relative to the 6-mm-dia reference flat bottom hole (FBH) assumed;
- The German code recommends a 3-mm FBH at normal incidence as the reporting threshold. The area is 25% of the reference 6-mm disc and corresponds to a level of -12 dB.

Significant aspects of the theoretical model were:

- Theory predicts a saturation value due to a finite beam width of a transducer. Experimental results confirm such saturation; e.g., for 5-MHz 12-mm transducer saturation at -12 dB occurs relative to a 6-mm FBH for a reflector area of  $100 \text{ mm}^2$ , corresponding to a 12-mm dia disc;
- An increase in roughness of an assumed crack will reduce the signal amplitude; e.g., at  $0^\circ$  tilt a smooth ( $<5 \text{ } \mu\text{m rms}$ ) surface will register -12 dB higher than a rough ( $41 \text{ } \mu\text{m rms}$ ) surface. Experiment closely conforms to theory. Above for 5-MHz 12-mm transducer;
- Reducing the frequency reduces impact of flaw surface roughness;
- The flaw surface roughness approach will not hold for extremely angular surface which will not obey a Gaussian distribution. A possible approach, not evaluated yet, would be to establish probability density function for facet occurrence as functions of facet size and orientation;
- The necessity of using more than one beam angle is borne out; relatively large assumed flaws as discs would be missed using ASME XI threshold if the angle of incidence is greater than  $11^\circ$  for a compression wave (at 100 mm) and greater than  $6.5^\circ$  for a shear wave (at 200 mm);
  - In essence a crack normal to the surface using a  $60^\circ$  shear-wave probe would require that the threshold be at least 20 dB below that set by ASME XI;
  - Suggested means of detecting under these circumstances include lowering the level 20 dB and using the German tandem system.

Thompson and Evans<sup>(4.5.4)</sup> cite work on characterizing defects based on measurements of scattered fields. Ultrasonic spectroscopy is an outgrowth utilizing the inferred frequency dependence of scattered signals.

Both aperture and wave vectors are finite so resolution is limited; however, theoretical considerations can lead to an optimization aimed at high resolution. For example a resolution of 0.25 in. would require an ideal imaging system with a numerical aperture of 0.5 which would have to operate at greater than 10 MHz. Such systems are under development, but are not commercially available.

life being about six months. The programs funded by Advanced Research Projects Agency (ARPA) and Air Force Materials Lab (AFML) may lead to transducers with more controlled parameters.<sup>(4.5.1)</sup>

The variability within a given class of transducers is significant as noted by Yee and Couchman.<sup>(4.5.1)</sup> The situation is much worse between classes of transducers. For example, Bastien<sup>(4.5.7)</sup> found quartz transducers conditionally acceptable, but considered the use of barium titanate transducers inadvisable for quantitative work due to their poor agreement with theoretical curves in the far field and their lack of discrimination in the near field.

The problems cited by Bastien<sup>(4.5.7)</sup> are repeated elsewhere. Lautzenheiser et al.<sup>(4.5.8)</sup> reported on the old and new PVRC test procedures. The old procedure recommended the use of 1-in. x 1-in. quartz transducers, but allowed the use of other transducers such as 0.5-in. x 1-in. barium titanate, lithium sulfate or lead metaniobate. The new PVRC procedure specifies that a 1-in. x 0.5-in. lead metaniobate transducer shall be used.

#### 4.5.1.2 Human Factor

The human factor has been discussed previously. Both Caustin<sup>(4.2.5)</sup> and Herr<sup>(4.2.7)</sup> emphasize the need to minimize this variable. An examination of the results of the PVRC program illustrate the significant differences possible from one team to another. The current trend is toward automation to minimize or eliminate the human factor; however, we still lack the equipment capable of scanning and inspecting complex geometries.<sup>(4.5.1)</sup>

#### 4.5.1.3 Calibration

Some of the problems arising from calibration are a direct result of using amplitude as a means of detecting and sizing defects. The use of flat bottomed or side-drilled holes (SDHs) is misleading in that there is no high correlation with real defects.<sup>(4.5.9)</sup> Mundry<sup>(4.5.10)</sup> in discussing the DGS technique, stresses that no real defect size determination takes place because the echo of a real flaw often differs greatly from that of an ideal circular disc on which the DGS system is based. The same point is made by Hislop.<sup>(4.5.6)</sup>

The problems of calibration block comparability, as well as those of examination accuracy and reproducibility, were examined as three Combustion Engineering internal reports. (4.5.11,4.5.12,4.5.13) Acoustic similarity was established by reading and comparing results from the same reference holes in several calibration blocks. This approach was used in recognition of the difficulty in measuring attenuation. One block was arbitrarily selected as the reference, comparing its DAC curve to the DAC curves of other blocks. Variables included surface roughness, changes in calibration reflectors and acoustic differences.

Reproducibility of attenuation measurements was poor and operator reproducibility was fair to good. While in a strict sense the blocks are not interchangeable, the reasons are less acoustic than factors such as surface roughness. Clad surfaces do not correlate either from one area to another on the same block or from block to block.

Further work (4.5.12) concentrated on repeatability and accuracy using statistical analyses to quantify. The following are some interesting conclusions of the study:

- The largest single factor is due to differences in length measurement.
- Differences are due to reflectors being sized either smaller or larger in both length and height rather than random differences.
- There is little self-cancellation in measurements governing length although there may be significant ones in height.

The third study (4.5.13) utilized both broad-band and narrow-band equipment to detect reflectors. Significant differences were noted with both 45° and 60° probes with the narrow band detecting less than half the number of reflectors found with broad-band equipment. The equipment variability was 2 to 3 times that of the inspector.

A similar study by Taylor and Selby (4.5.14) compared the SDHs of the calibration block specified by Appendix III of ASME XI to end-milled notches. A large number of measurements (540) were made using 34 different standards to

yield statistically significant values. Notches produced higher reflected values than SDHs. The notches provide less sensitive inspection values which varies with specimen thickness. For example, the difference is -6 dB for 0.4-in. wall (a factor of 2) and -16 dB for 2.4-in. wall (a factor of 6.3). The preceding values related to 45° 2.25 MHz. With 60°, results were not statistically significant.

The SDH reflection is normal incidence without mode conversion. With notches, two reflections occur. One is at the incident angle; the other is at the complementary angle because the wave is reflected from both the back and the notch surfaces. At 45°, both reflections are above the critical angle for longitudinal wave mode conversion; therefore, the wave is completely reflected. At 60°, the complementary angle is 30° below the angle of total reflection so only 15% of the 30° angle is reflected as a shear wave with the remainder mode converted to longitudinal wave which does not return to the search unit.

The authors<sup>(4.5.14)</sup> conclude that the notch is a more appropriate reflector than SDH because a notch more closely approximates the physics of reflection of a crack. In their estimation, the calibration blocks of Appendix III of ASME XI are inadequate for detection of minimum size unacceptable flaws.

#### 4.5.1.4 Calibration Blocks

An EPRI funded study,<sup>(4.5.15)</sup> whose primary purpose was the UT examination of BWR piping welds, highlighted the differences that can exist between apparently equivalent calibration blocks. One block was identified as being 316 stainless steel (SS), 10-in. dia, Schedule 160 piping. The other probably was 304 SS. The following differences were unexpected:

- There was a significant difference in UT test response (~8 dB) between two dimensionally equivalent stainless steel calibration blocks.
- The apparent shear-wave beam angle of the search unit can change from calibration block (33°) to calibration block (42°), and from calibration block to test specimen (44°). The difference in wave velocities between the two calibration blocks was only 2% which was insufficient to explain the angular differences.

- The ultrasonic response from an intergranular stress corrosion cracking (IGSCC) flaw can be much lower than the response from an artificial calibration reflector, such as a notch machined flaw to a depth of 10% of the pipe wall thickness.

These results were obtained with a 45° shear wave.

#### 4.5.1.5 Acoustic Properties

Another source of error is in the differences in acoustic properties from one reference block to another. Lautzenheiser et al.<sup>(4.5.8)</sup> cite the case of two A-533, Grade B reference standard blocks which differed by nearly a factor of 10 in attenuation due to the amount, distribution and size of nonmetallic inclusions in one block compared to the other. The situation may be even more pronounced in reference blocks fabricated of austenitic stainless steel weld metal. The welding procedure can result in major variations in attenuation due to the size and orientation of the dendritic grains.

#### 4.5.1.6 Acceptance Criteria

Administrative or political decisions may play a significant role in the number of defects reported as detected. The ASME XI code uses a percentage of distance-amplitude-correction (DAC) based on calibration curves. Earlier versions of ASME XI (1974) required reporting at 20% DAC. Based on industry complaints concerning the large number of geometric defects necessitating evaluation, the Code was changed in 1977 to require recording at 50% DAC and reporting at 100% DAC. Concern as to the adequacy of these more relaxed values by USNRC personnel led to a program aimed at comparing the two criteria.<sup>(4.5.14)</sup> Blocks containing artificial defects of various depths, aspect ratios and orientations were examined with nominal 2.25 MHz and 45° and 60° shear waves. Two instruments, one wide band and the other narrow band, were used coupled to a range of transducer sizes. Both 1/2-V and 3/2-V were used.

The aim of the program was to provide engineering data, hopefully statistically significant, concerning the adequacies or inadequacies of the 20% DAC versus 50% to 100% DAC criteria. Both ferritic and austenitic piping were used as test materials. The authors<sup>(4.5.14)</sup> concluded that 100% DAC is not adequate



to detect flaws of the minimum size defined as rejectable by ASME XI. They felt that 20% DAC was needed to assure detection of 90% of the "flaws" used in the study.

The data in Table 4.5.2 illustrate the implications of higher DAC levels vis-a-vis the reporting of rejectable flaws.

#### 4.5.2 Internal Factors

Even when external variables are controlled and calibration is done with real defects, the internal factors may grossly bias the results. This section will consider the following factors--component surface, component geometry, material variables, and flaw characteristics (orientation, geometry, etc.).

##### 4.5.2.1 Component Surface

The component surface is a major variable as indicated in Haines<sup>(4.5.3)</sup> theoretical analysis, where an ideal surface was assumed, any surface degradation further reduces the signal amplitude. Silk and Lidington<sup>(4.5.9)</sup> cite the relation of surface to relative efficiency of coupling (see Table 4.5.3).

The preceding applies to contact probes. Under immersion conditions coupling should be a relatively minor problem. A condition controlled by the surface is attenuation due to temperature. If temperatures are too high or too low conventional liquid couplants cannot be used.<sup>(4.5.16)</sup> Even where the couplants are usable, temperature is a factor since there is a 2-dB attenuation loss for every 25°F (14°C) increase in temperature.<sup>(4.5.17)</sup>

An extensive study by Coffey<sup>(4.5.18)</sup> clearly defined the significance of surface finish on variability of ultrasonic examination. Weld caps were deposited onto an IIW test block then ground away in successive stages. At each stage, the echo strengths and beam shapes of nine commercial probes were determined by reflection of the SDHs in the block. Results were analyzed in terms of loss of sensitivity, errors in defect position and errors in sizing introduced by the nonideal surface. Three classes of surface texture were considered: errors in form such as crown, undercut, etc.; waviness; and roughness.

TABLE 4.5.2. Summary of Flaw Response Using 20% and 50% to 100% Reference Level Evaluation Criteria

Pipe Diameter	Inspection Angle / Beam Path	20% DAC		50% DAC	100% DAC	Total Measurements Made
		Number of Flaws Producing Recordable Response	Number of Flaws Producing Evaluation Response	Number of Flaws Producing Recordable Response	Number of Flaws Producing Evaluation Response	
4 in. Sch. 80 Carbon Steel	45° / 1/2 V	72	72	72	37	144
	45° / 3/2 V	72	72	65	19	144
	60° / 1/2 V	72	72	59	40	144
12 in. Sch. 80 304 Stainless Steel	45° / 1/2 V	108	108	86	25	216
	45° / 3/2 V	108	108	86	39	216
	60° / 1/2 V	108	108	105	51	216
20 in. Sch. 80 Carbon Steel	45° / 1/2 V	102	102	67	24	216
	45° / 3/2 V	98	98	48	9	216
	60° / 1/2 V	108	108	74	40	216
20 in. Sch. 80 304 Stainless Steel	45° / 1/2 V	101	101	17	0	216
	45° / 3/2 V	Sound attenuated; no flaw response.		Sound attenuated; no flaw response.		
	60° / 1/2 V	72	72	10	0	216
TOTAL		1,021	1,021	689	284	2,160
PERCENTAGE		94.5%	94.5%	63.8%	26.3%	

4.5.8

TABLE 4.5.3. Effect of Surface Condition on Ultrasonic Coupling

<u>Type of Surface</u>	<u>Relative Efficiency of Coupling (%)</u>
Smooth Machined Finish	100
Ground by Hand Grinder	76
Smooth but Rusty	70
Adhering Scale	72
Rusty and Pitted	48

The following conclusions and recommendations are reproduced because they are felt to be decidedly pertinent:

Conclusions

1. On an irregular surface, ultrasonic test sensitivity varies erratically from place to place. On the average, the sensitivity loss depends mainly on the surface texture and little on the probe design. On the best hand-ground surfaces, typical losses vary between 2 and 6 decibels.
2. The deleterious effects of poor surface finish are most pronounced with high angle (e.g., 70°) probes. Single defects can appear as two or more, and errors in through-wall size can be large.
3. On an uneven surface, the 20-dB Drop sizing technique will systematically underestimate a defect's through-wall extent. The Maximum Amplitude technique does not suffer this shortcoming, though it is still impaired by component roughness.
4. The errors in defect measurement arising from nonideal surface finish can be estimated using equations cited in the report.
5. For reliable ultrasonic inspection, the probe contact surface must be smooth and even. Fine scale roughness should be less than 3.2  $\mu\text{m}$   $R_a$  over an 0.8-mm sampling length (BS 1134). The

error of form should not allow an 0.5-mm gap to develop under a 50-mm long straight edge (or curved template for pipe welds) placed against the surface.

#### Recommendations

1. The surface finish requirements cited in this report should be seriously considered for incorporation into ESI ultrasonic testing specifications.
2. Further experiments should examine directly the effects of surface texture on circumferential.

#### 4.5.2.2 Component Geometry

Component geometry is a critical factor. There is ample evidence that a combination of flaw location and orientation in a nozzle region may result in 1) no detection when examined from one surface while 2) the flaw is detected when examined from the other surface. A third possibility is failure to detect from either surface. The PVRC work cited in Chapter 3, Caplan's work<sup>(4.3.2)</sup> and UT of the Doel reactor<sup>(4.3.3)</sup> all confirm the unreliability of examination from only one surface. Wüstenberg and Mundry<sup>(4.5.19)</sup> cite the measures necessary to detect cracks on the inner radius of a nozzle. When examined from the outer surface, changes in geometry along the circumference of the vessel require a series of beam angles for each crack position. While such a need may be recognized, there is no compliance.

Another problem with geometry is the opposite of lack of detection. A rule of thumb for systems such as piping is that geometric reflectors outnumber flaw reflectors 1000 to 1 at a threshold value such as 20% DAC.<sup>(4.5.17)</sup> Examples include mode conversions due to beam reflection from the weld preparation counterbore. The severity of the geometric reflector problem is apparent from an example cited<sup>(4.5.17)</sup> where one 22-in. pipe weld required nearly 60 crew hours to plot and analyze due to 422 separate indications with essentially all being geometric.

A special form of geometric problem is related to welds having a substantial crown. If the crown is not removed, the transducer will ride up on the weld making examination of the upper portion of the weld difficult or impossible. (4.5.17)

Another example of geometry causing problems relates to typical pipe weld joint designs. The weld root geometry may register 200% DAC while a through-wall stress corrosion crack (SCC) may register 80% DAC.

The effects of component geometry, specifically weld joint design, has been examined by Flack and Watson. (4.5.20) The axial position of the counterbore and the angle of taper of the counterbore can cause mode conversion. The shorter counterbore is more prone to do so. Mismatch of the weld joint can result in a high-low condition with extraneous UT signals. Size and profile of the weld root pass is important. Excess concavity or convexity, or internal undercut may cause return reflections. The weld crown, if irregular, is another source of UT reflections. Excessive crown height or width will limit UT accessibility, precluding adequate examination of the root pass. If the crown is asymmetric, the weld  $\zeta$  will be mislocated, resulting in incorrect recording of surface distances and errors in the data plots. Lack of control of the welding operation is another source of error. Uncontrolled welding or excessive repair can lead to excessive joint distortion, undue shrinkage, etc. Examples of the defects cited appear in Figure 4.5.1.

Another aspect of specimen geometry including counterbore configuration is the added ultrasonic signals arising from these geometric configurations. A major reason for the change in DAC reporting level from 20% in the 1974 ASME XI Code to 50% to 100% in the 1977 ASME XI Code was the extensive time spent in differentiating geometric signals from flaw signals. Wüstenberg and Engl (4.5.21) reported on work at Kraftwerk Union (KWU) related to the number of indications at inservice inspections. Figure 4.5.2 presents these data. As noted, the great preponderance of signals are due to geometry. Only a small number are due to the indications above the evaluation threshold.

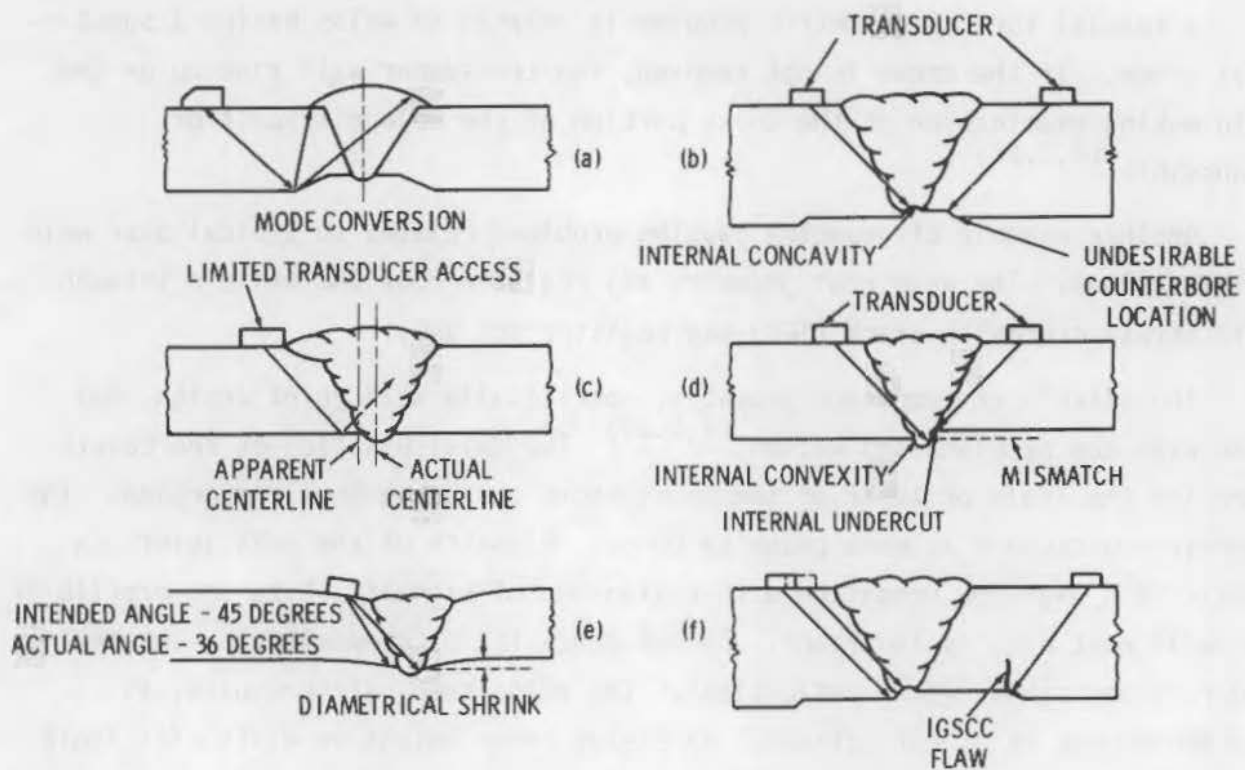


**FIGURE 4.5.1.** Examples of Various Weldment Geometry Problems That Can Adversely Influence Flaw Detection by Ultrasonics

#### 4.5.2.3 Material Variables

Material variables represent another major source of error in UT. While an earlier and slightly pessimistic conclusion by I. I. Win in 1969 stated that it is very difficult or impossible to UT test the majority of austenitic materials in sections greater than 100 mm, <sup>(4.5.16)</sup> it is still true that, though possible now, such examinations are not easy. The same statement applies to coarse grained cast materials (iron, copper, bronze, aluminum, etc.).

4.5.2.3.1 Austenitic Stainless Steel Overlay Clad. A special example of cast structure is the austenitic stainless steel overlay clad used in nuclear pressure vessels. The PVRC work with UT on clad and unclad test blocks clearly indicates the difficulty of detection in clad components when no compensation is made for such cladding. This point is also made by Wüstenberg and Mundry. <sup>(4.5.19)</sup>

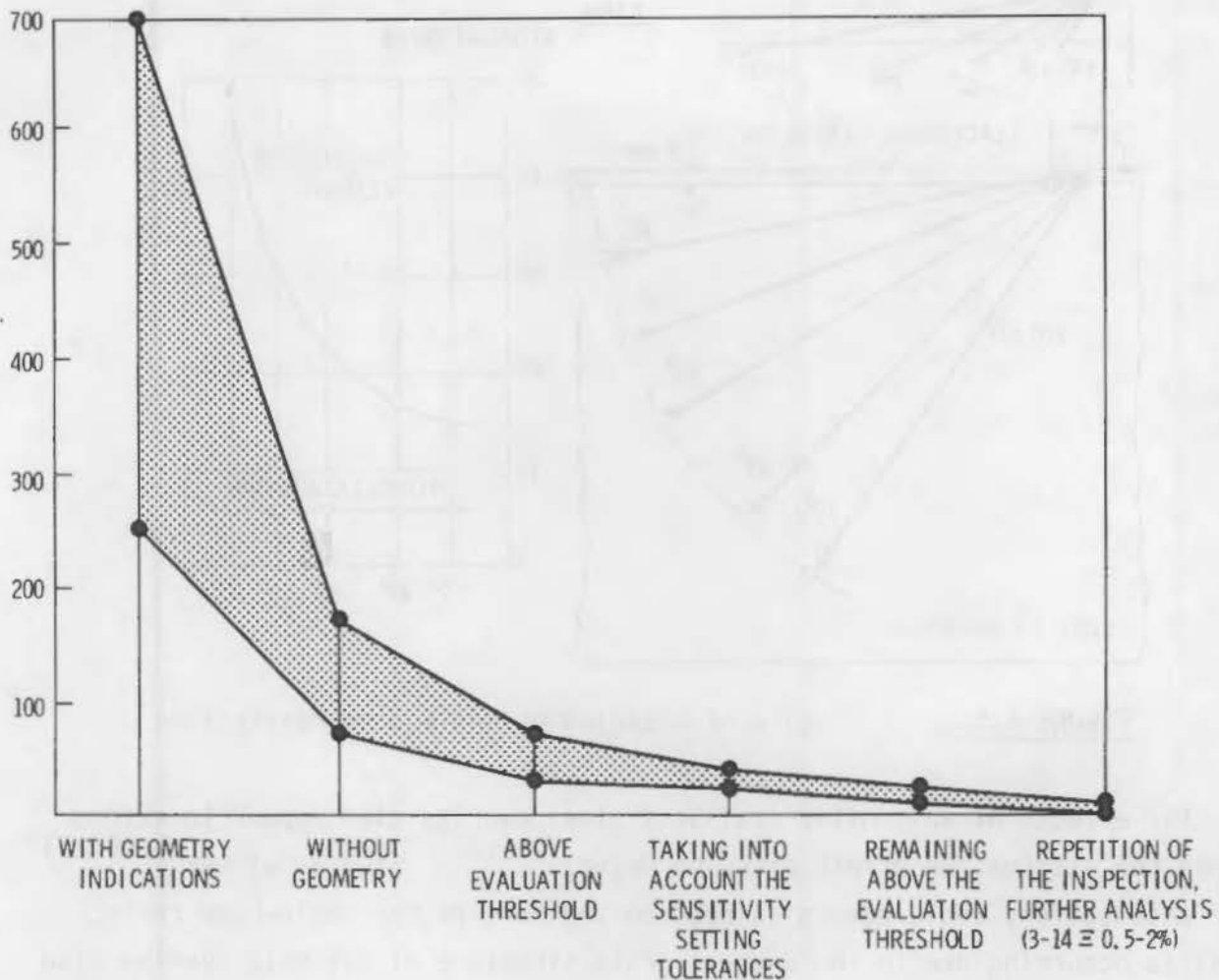


FIGURE 4.5.2. Number of Indications of Inservice Inspections (KWU data)

Meyer<sup>(4.5.22)</sup> discusses the austenitic cladding problem in terms of attenuation. Figure 4.5.3 graphically illustrates the attenuation as a function of beam angle. As noted there is approximately a 50-fold increase in attenuation through cladding compared to the ferritic base metal. Meyer<sup>(4.5.22)</sup> cites a further problem of concern in inservice inspection. There is a definite shift in beam angle for either immersion or contact UT as the system temperature changes. For example, a 45° immersion probe measuring 45° at 20°C will drop to 42.2° at 50°C. A contact probe shifts from 45° at 20°C to 46.3° at 50°C. The change is even more marked with a 70° probe. In immersion, it drops from 70° to 63.8° with a temperature change of 20°C to 50°C. With contact, the change is 70° to 66.3° over the same range.

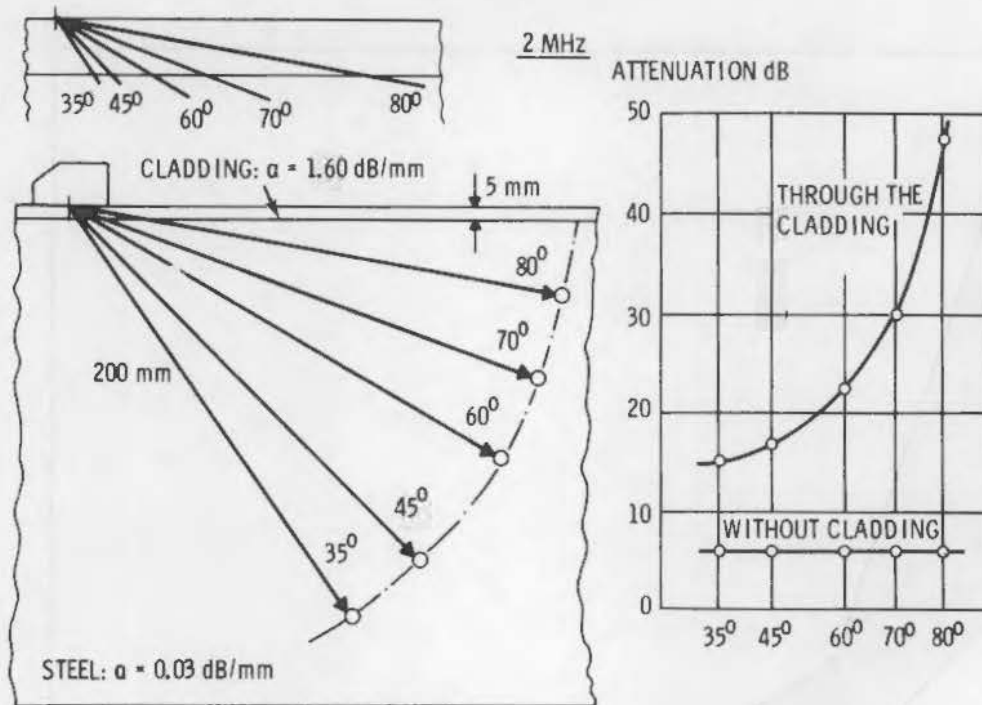


FIGURE 4.5.3. Influence of Cladding on Angle-Beam Penetration

The effects of austenitic stainless steel overlay clad appear to extend beyond the attenuation effect cited by Meyer.<sup>(4.5.22)</sup> Studies at KAPL<sup>(4.5.23)</sup> cite attenuation, angle-beam misdirection and zero-degree angle-beam reflections as occurring due to the unusual grain structure of the weld overlay cladding. These effects are sensitive to the direction of clad welding, being significantly greater if the beam (45° shear wave) is perpendicular to the welding direction.

The zero-degree angle-beam reflection appears as a false 3/8 node shear-wave signal which is postulated to have been caused by scattering on the concave surfaces of the weld beads. The authors define this as a zero-degree shear wave because the beam reflects back along the initial path. The following characteristics typified the beam:

- The signal always appeared at the 3/8 node regardless of forging thickness.



- The signal could be moved in space by placing a reflector directly below the transducer, but outside the sonic path of the incident 45° shear wave.
- The signal could not be dampened.
- The time required to appear at the 3/8 node was very close to the time for a shear wave to undergo a simple reflection.
- A large diameter transducer at a low test frequency eliminated the signal.
- A small diameter transducer at a high frequency enhanced the signal.
- A real flaw at the 3/8-node position should have a longer travel time.

Measurements of attenuation due to the cladding were obtained by removing the ferritic steel, indicating about 20 dB/in. difference between clad and base metal. In the case of a longitudinal wave, the extra attenuation due to presence of cladding is about 30% of the typical incident signal. In the case of shear waves, attenuation was determined by a relative technique using notches in clad and unclad steel blocks. The effects of frequency and transducer dimensions can be seen in Table 4.5.4.

Redirection of the shear wave may occur due to the clad/base metal interface. The degree of refraction depends on coarseness of grains and degree of unevenness of the interface more than on the impedance differences between the two metals. Both frequency and, to a lesser degree, beam size affects the misdirection (refraction) as noted in Table 4.5.5.

TABLE 4.5.4. Shear-Wave Attenuation

<u>Transducer Dimensions</u>	<u>Test Frequency, MHz</u>	<u>Relative Response Clad/Unclad, dB</u>
0.5-in. dia.	2.25	10 ± 20
0.5 x 1.0 in.	2.25	8 ± 2
0.5 x 1.0 in.	1.00	2 ± 1

TABLE 4.5.5. Shear-Wave Misdirection Angle

Transducer Dimension (in.)	Test Frequency MHz	Maximum Reflection Angle (degrees)	Material
0.5 x 1.0	2.25	45	Alloy steel
0.5 x 1.0	2.25	26	Cladded steel
0.5 x 1.0	1.00	45	Cladded steel
0.5 dia.	2.25	38	Cladded steel

4.5.2.3.2 Scattering at Grain Boundaries. Silk and Lindington<sup>(4.5.9)</sup> conducted a series of experiments to rebut Böttcher's<sup>(4.5.24)</sup> claim that the basic cause of the UT signal detected is due to scattering at the grain boundaries of the material. The authors<sup>(4.5.9)</sup> argued that a major cause of amplitude variation was due to inclusions in the steel rather than grain size alone. Qualitative experiments were conducted on two steels where the second had a much higher inclusion count than the first. The effect of inclusions was quite marked (Figure 4.5.4); such a variation in amplitude could seriously affect the validity of the UT technique.

The results of Silk and Lidington<sup>(4.5.9)</sup> parallel those cited by Lautzenheiser et al.<sup>(4.5.8)</sup> where one block had 2-dB ultrasound attenuation per inch of beam travel while another block had nearly 20-dB attenuation per inch of beam travel. The variation was attributed principally to the amount, distribution and size of nonmetallic inclusions.

The significance of attenuation difference, unless accounted for, can be substantial. For example, if the attenuation is greater than 20 dB between standard and weld, the weld will not be adequately examined.<sup>(4.5.17)</sup>

In relatively coarse-grained materials, such as austenitic weldments, grain echoes contribute to the background noise due to scattering. Bilgutay et al.<sup>(4.5.25)</sup> cite techniques to reduce background noise by frequency wobbling and signal averaging. This scattering depends on the ratio of ultrasonic wavelength to the grain size. If the transmitted frequency is varied, grain echoes can be markedly reduced without affecting the flaw echoes which leads to an enhancement of signal-to-noise ratio.

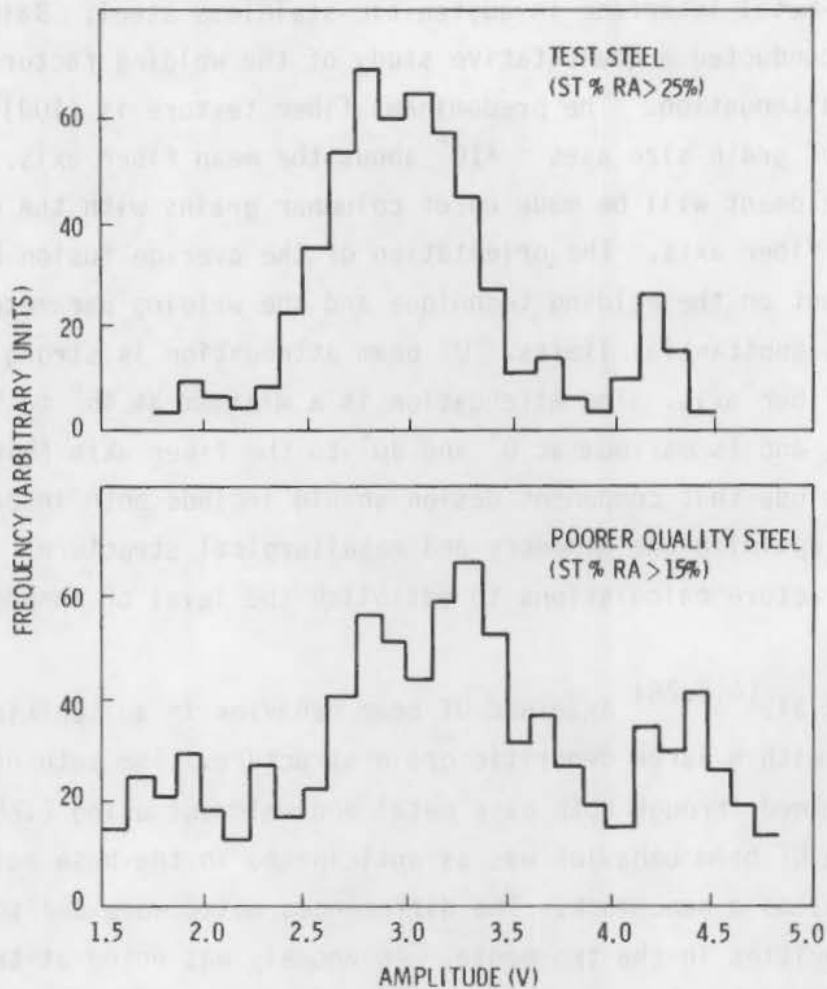


FIGURE 4.5.4. The Amplitude Variation by Frequency, Marked for the Test Steel and Steel of Poorer Quality

4.5.2.3.3 Crack Tip. Another potential source of error, related partially to the flaw and partially to the material, has to do with regions of high stress such as may occur in the crack-tip volume. Silk and Lidington<sup>(4.5.22)</sup> argue that such regions represent centers for acoustic scattering. Since local regions of high residual stress may be associated with structural discontinuities, it is not necessary to associate them with flaws. There is a need for further work to establish the significance of this factor.

4.5.2.3.4 Weld-Metal/Base-Metal Interface. Perhaps the most significant material variable influencing UT is the discontinuity existing at the

weld-metal/base-metal interface in austenitic stainless steel. Baikie et al. (4.5.27) conducted a quantitative study of the welding factors influencing UT beam attenuation. The predominant fiber texture is (100) with the angular spread of grain size axes  $\sim \pm 10^\circ$  about the mean fiber axis. Generally, an austenitic weldment will be made up of columnar grains with the grain axes parallel to the fiber axis. The orientation of the average fusion boundary is strongly dependent on the welding technique and the welding parameters, and may be varied within substantial limits. UT beam attenuation is strongly correlated with the fiber axis. The attenuation is a minimum at  $45^\circ$  to the fiber axis (6000 m/s), and is maximum at  $0^\circ$  and  $90^\circ$  to the fiber axis (5400 m/s). The authors conclude that component design should include both inspection requirements to optimize the geometry and metallurgical structure. This should be coupled to fracture calculations to establish the level of inspection sensitivity required.

Yoneyama et al. (4.5.28) examined UT beam behavior in austenitic shielded metal arc welds with a large dendritic grain structure. The path of the wave train was determined through both base metal and weldment using 2.25 MHz and  $45^\circ$  C-scan. The UT beam behavior was as anticipated in the base metal using ferritic material as a benchmark. The differences noted were due to the differences in velocities in the two media. An anomaly was noted at the base metal-weld interface where a greatly enhanced transmission occurred. To date there is no satisfactory explanation for this behavior.

Another anomaly occurred in the weldment. On entering the weldment, the UT beam bent until it was essentially perpendicular to the surface. This behavior was attributed to the pronounced dendritic pattern where, it was believed, the UT beam was channeled along the columnar grains with the grains acting as acoustic channels. As the columnar grain structure changes to one that is randomly oriented, the sound path reverts to a random walk pattern through the weld zone.

An extensive analytic study using computer modeling and supported by some experimental work assessed the reliability of the angle-beam DAC curve for the interrogation of weldments. (4.5.29) The author concludes that the current procedure cannot produce the quantitative information required for realistic

flaw detection because of the unusually high weldment attenuation. He cites procedures which can reduce or even eliminate the errors.

Weldment studied was Inconel 600-Inconel weld--carbon steel.

The point was made that differences in attenuation in base metal and weld still influence predicted flaw size based on amplitude. Modifying the DAC curve to apply to welds still results in errors because of different ratios of path length in base metal and in weld (see Figure 4.5.5).

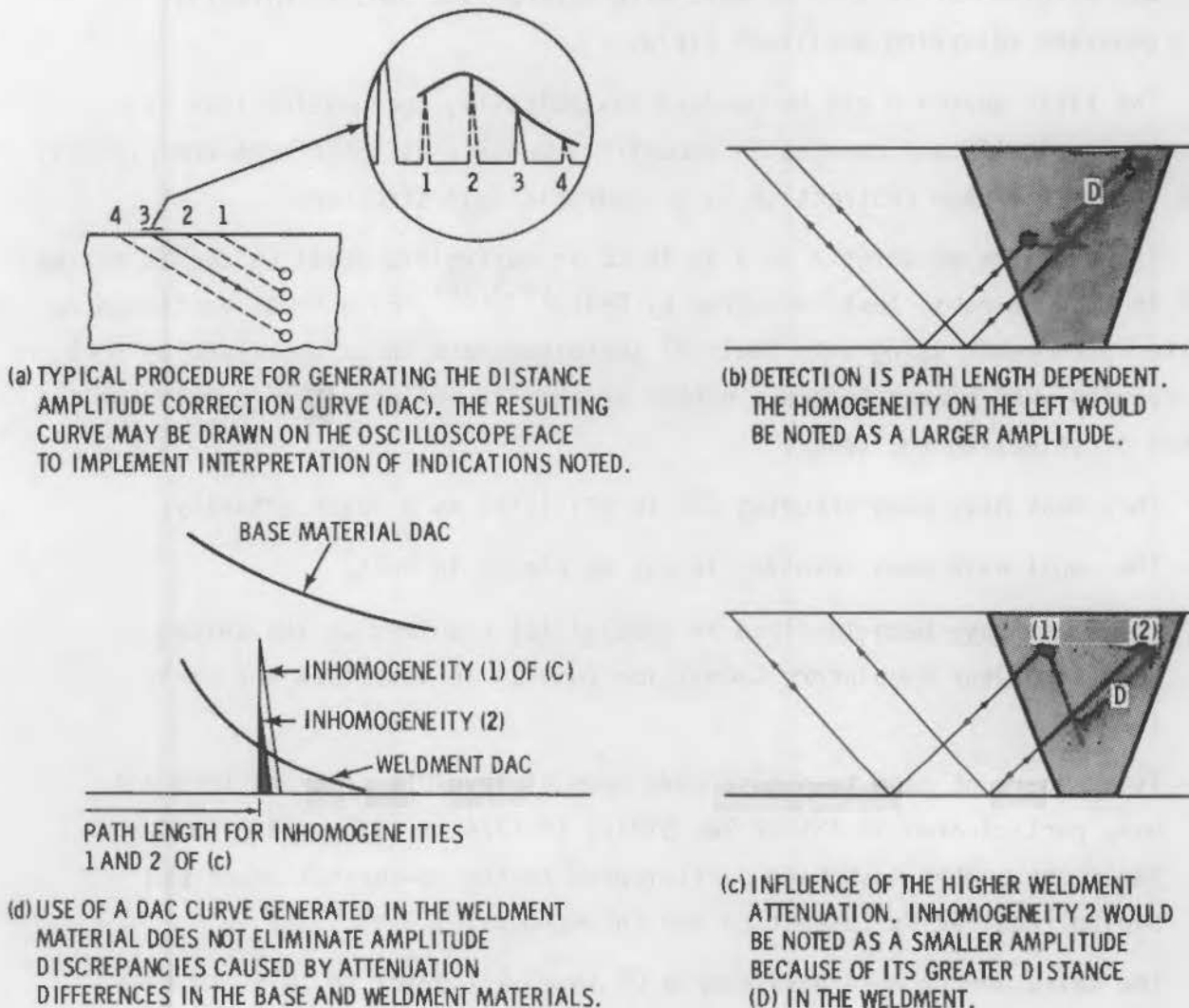


FIGURE 4.5.5. Example of Influence of Differences of Attenuation on UT Beam Path on DAC Values

The Inconel-steel system tends to be isotropic; however, there are large differences in attenuation. The weldment has even higher attenuation. UT interrogation is preferred from the side with attenuation characteristics closest to those of weld.

The following are possible approaches to better DAC corrections:

- make appropriate corrections to the conventional DAC curve obtained from a block of base material.
- use specimen or section of weld with appropriate SDHs to directly generate returning amplitude field.

The first approach can be handled analytically, recognizing that it assumes no significant changes in acoustic impedance at interfaces and probably does not assume beam redirection in a dendritic weld structure.

The problems of defects such as IGSCC in austenitic steel weldments can be seen in a round-robin test conducted by EPRI.<sup>(4.5.30)</sup> Five teams participated in the round robin using both their UT techniques and those specified by EPRI. The results were biased toward a higher probability of detection due to the method of selecting the teams:

- They must have been offering ISI to utilities as a major activity.
- They must have been involved in ISI of piping in BWRs.
- They must have been involved in special ISI required by the United States Nuclear Regulatory Commission (USNRC) in late 1974 and early 1975.
- Two members of each team must have been UT level II prior to 1975 and have participated in ISI of BWR piping in 1974 to 1975 period; and at least one member must have participated in the re-inspection of BWR piping required by Inspection and Enforcement.
- The third member must have been a UT level III prior to 1975 and have participated in the ISIs cited above. (Personnel training specifically for IGSCC was considered the single most important factor.)

- Five teams (CONAM, GE-NED, NSC, Peabody, SWRI) of eight meeting the above criteria were selected on the basis of overall experience.

Procedures consisted of the following:

- Each team used their own inspection procedure, equipment and standards in the first phase.
- A reference procedure and standards defined by EPRI were used in the second phase. (The EPRI standard used contained 3% notches on the inside and outside both axial and radial plus SDHs.)
- Specimens consisted of BWR piping containing IGSCC, fabrication defects, and no defects.
- Sufficient residual radioactivity remained so that examinations were done in special work permit (SWP) clothing.
- A time limit was placed on each examination.

The piping specimens were examined independently prior to the round robin. These results, together with the two round robins, are given in Figure 4.5.6. While the detection of IGSCC was quite good (43/50), the correct interpretation was less satisfactory (28/43). The same can be said for fabrication defects. All participants detected the defects (18/18); however, only 10/18 analyzed them correctly. False calls also were a problem. There were (23/90) called cracked with one reflector accounting for 7 miscalls. (This could have been identified more correctly as a defect based on destructive examination.)

The following factors adversely influenced flaw detection:

- crack orientation--skewed cracks (which are relatively rare) were very difficult to detect with normal UT procedures; rotating the transducer as suggested in the German HP 5/3 code improved detection.
- larger transducers--they were less effective, primarily because of physical interference between the front edge of the transducer and the raised weld crown.
- plotting the weld cross-section on cross-section paper, together with the data, definitely improved detection.

The first part of the report deals with the general situation of the country and the results of the survey. The second part is devoted to the analysis of the data and the third part to the conclusions and recommendations.

The survey was carried out in the period from 1981 to 1983. The results are presented in the following tables:

Table	Description
Table 1	General situation of the country
Table 2	Results of the survey
Table 3	Analysis of the data
Table 4	Conclusions and recommendations

The survey was carried out in the period from 1981 to 1983. The results are presented in the following tables:

The survey was carried out in the period from 1981 to 1983. The results are presented in the following tables:

The survey was carried out in the period from 1981 to 1983. The results are presented in the following tables:



SAMPLE IDENTIFICATION AND NOMINAL PIPE DIAMETER, IN.	DESCRIPTION	DYE PENETRANT (PT)	SHEAR WAVE ULTRASONIC ANALYSIS (UT)	RADIOGRAPHIC CONFIRMATION (RT)	FLAW DESCRIPTION (UT <sup>a</sup> CONFIRMED BY DPT <sup>b</sup> )	BASIS FOR EVALUATION	TEST TEAM RESULTS <sup>g</sup>					EVALUATION CRITERIA
							A	B	C	D	E	
19AL, 10	DUTCHMAN TO SAFE END, WELDS GROUND FLUSH ID AND OD (180° SECTION)	THROUGH WALL AXIAL CRACK 1.25 in. ON ID BY 0.60 in. ON OD, SCC	SIGNALS FROM TWO SOURCES, ONE CONFIRMED, ONE UNCONFIRMED, HIGH AMPLITUDE SIGNALS	THROUGH-WALL FLAW AGREES WITH UT AND PT, EASY TO READ, POSSIBLE SECOND CRACK	SCC <sup>c</sup> , AXIAL, THROUGH WALL 1 WELD $\zeta$	■	■	■	■	■	PIPE MUST BE CALLED "CRACKED" ON EPRI FORM	
1028A, 10	DUTCHMAN TO PIPE WELD, CONSIDERABLE DROP THROUGH, IS PARTIALLY GROUND (36° SECTION)	RADIAL CRACK COMPLETELY ACROSS SAMPLE, CONFIRMED AS SCC, DEPTH OF 0.120 in. BY ELECTRIC RESISTANCE GAUGE (ERG) MEASUREMENT	HIGH AMPLITUDE SIGNALS FROM FLAW, SEVERAL SPURIOUS SIGNALS	GOOD AGREEMENT WITH PT, EASY TO READ	SCC, RADIAL, ACROSS SAMPLE <sup>d</sup> , II WELD $\zeta$	■	■	■	■	■		
1028B, 10	AS ABOVE (36° SECTION)	THREE SHORT RADIAL CRACKS 1 in. LONG CONTINUATION OF THE CRACKS IN 1028A; CONFIRMED AS SCCs, DEPTH OF 0.10 in. BY ERG	HIGH AMPLITUDE SIGNAL FROM FLAW, SPURIOUS SIGNALS FROM WELD ROOT	GOOD AGREEMENT WITH PT, EASY TO READ	SCC, SKEWED ANGLE, EDGE CRACK <sup>d</sup>	■	■	■	■	■		
1024A, 10	DUTCHMAN TO PIPE WELD, PARTIALLY GROUND CROWN (180° SECTION)	EIGHT CRACKS DETECTED, ONE AXIAL, ONE RADIAL, THE REST SKEWED AT 45°. VERY TIGHT CRACKS, ALL ARE CONSIDERED SCCs DEPTHS BY ERG ARE 0.10 TO 0.12 in.	EXTREMELY DIFFICULT TO FIND AND CHARACTERIZE ALL CRACKS. TRANSDUCER MUST BE OSCILLATED ±45° INTO WELD TO DETECT SKEWED CRACKS	MAJORITY OF FLAWS CONFIRMED BUT VERY DIFFICULT TO READ	SCC, RADIAL, AXIAL, AND SKEWED, SPOTTY <sup>d</sup>	■	■	■	■	■	PIPE MUST BE CALLED "CRACKED" OR "LACK OF FUSION."	
B2A, 4	PIPE TO ELBOW, WELDS GROUND SMOOTH, SHARP COUNTERBORE ON ID (360° SECTION)	TWO SMALL INDICATIONS ANALYZED AS POSSIBLE SCCs	LOW AMPLITUDE SIGNALS FROM FLAW, MANY SIGNALS FROM GEOMETRY	NOT PERFORMED	SCC, SMALL SPOTS, SINGLE POROSITY PER DESTRUCTIVE TEST	■	□	□	■	□		
10K18, 10	PIPE TO 90° ELBOW, PARTIALLY GROUND CROWN (360° SECTION)	INTERMITTENT RADIAL INDICATIONS, ONE CRACK CONFIRMED UT INDICATIONS, 0.03 TO 0.06 in. DEPTH BY ERG	MANY GEOMETRIC INDICATIONS, TWO EVALUATED AS POSSIBLE RADIAL CRACKS, DIFFICULT TO UT	SHARP REENTRY, LACK OF FUSION	LACK OF FUSION <sup>e</sup>	■	■	■	■	■		
1021, 10	ELBOW TO PIPE WELD, CROWN IS PARTIALLY GROUND (360° SECTION)	STRAIGHT RADIAL INDICATION, ~7.87 in. LONG POSSIBLE LACK OF FUSION	SERIES OF HIGH UT SIGNALS CORRESPOND TO PT INDICATIONS, SEVERAL UNCONFIRMED SIGNALS	LONG CRACKLIKE INDICATION CONFIRMS PT	LAP <sup>e</sup> RADIAL, 1 in. LONG	■	■	■	NO TEST	■	INDICATIONS MUST NOT BE CALLED CRACKS	
10K17L, 10	PIPE TO 90° ELBOW, PARTIALLY GROUND CROWN (360° SECTION)	TWO SMALL SPOTS WITH POSSIBLE RADIAL INTERCONNECTING CRACK 1.50 in. LONG; INTERNALLY GROUND AREA	MANY GEOMETRIC SIGNALS, UT SIGNALS AGREE WITH PT INDICATIONS, VERY DIFFICULT TO UT	SHARP UNDERCUT	POROSITY	■	■	■	■	■		
10K17, 10	PIPE TO PIPE (360° SECTION)	NO INDICATIONS	GEOMETRIC SIGNALS COMPLETELY AROUND WELD	UNDERCUT AND SHARP REENTRY	NONE BY PENETRANT	■	■	■	■	■		
1020A, 10	PIPE TO ELBOW (360° SECTION)	NO INDICATIONS	LIMITED NUMBER OF GEOMETRIC SIGNALS	NOT PERFORMED	WELD ROOT OVERLAP <sup>e</sup>	■	■	■	■	■		
1024B, 10	DUTCHMAN TO PIPE (180° SECTION)	NO INDICATIONS	AS ABOVE	NOT PERFORMED	NONE BY PENETRANT	■	■	■	■	■		
1028C, 10	DUTCHMAN TO PIPE WELD, CONSIDERABLE DROP THROUGH, IS PARTIALLY GROUND (36° SECTION)	NO INDICATIONS	SPURIOUS SIGNALS FROM WELD ROOT	SHARP REENTRY OR ROOT CRACK	NONE BY PENETRANT	■	■	■	■	■		
1028D, 10	AS ABOVE (36° SECTION)	NO INDICATIONS	AS ABOVE	AS ABOVE	NONE BY PENETRANT	■	■	■	■	■		
1019A, 10	PIPE TO ELBOW, UNGROUND CROWN, EXTREME SUCK-UP ON ID (360° SECTION)	NO INDICATIONS	FEW INDICATIONS	POROSITY, LINEAR INDICATIONS, SUCK-UP	NONE BY PENETRANT	■	■	■	■	■		
198BL, 10	DUTCHMAN TO SAFE END, WELDS GROUND FLUSH, ID AND OD (180° SECTION)	NO INDICATIONS	MANY GEOMETRIC INDICATIONS, TIME CONSUMING TO RECORD, PLOT AND EVALUATE	APPEARS CLEAN	INTERNAL REFLECTOR FROM WELD <sup>e</sup> (FABRICATION DEFECT)	■	■	■	■	■		
A9A, 4	PIPE TO ELBOW, WELDS GROUND SMOOTH, SHARP COUNTERBORE ON ID (360° SECTION)	NO INDICATIONS	-----	-----	NONE BY PENETRANT	■	■	■	■	■		

- a - ULTRASONIC TEST
- b - DYE PENETRANT TEST
- c - FLAW INTERPRETED AS STRESS CORROSION CRACK
- d - SCC CONFIRMED BY METALLURGY
- e - CONFIRMED BY METALLURGY

- f -  UNFLAWED  FLAWED
- g - TEST PROCEDURE, PHASE A (INSPECTION GROUP) →  ← PHASE B (EPRI) RESULTS AS SHOWN:
  - CRACK CALLED
  - NO CRACK DETECTED
  - ◻ CRACK SIGNAL DETECTED, CRACK NOT CALLED

FIGURE 4.5.6. Laboratory and Test Team Characterization of Welds

Table 1. Summary of the results of the 1998 survey of the 100 most important factors for the success of a business.

Rank	Factor	Percentage of respondents who ranked it as important	Percentage of respondents who ranked it as very important
1	Quality of products and services	85%	15%
2	Customer service	82%	18%
3	Price	78%	22%
4	Location	75%	25%
5	Staff	72%	28%
6	Facilities	68%	32%
7	Reputation	65%	35%
8	Marketing	62%	38%
9	Management	60%	40%
10	Financial strength	58%	42%
11	Product range	55%	45%
12	Customer loyalty	52%	48%
13	Brand name	50%	50%
14	Customer feedback	48%	52%
15	Employee training	45%	55%
16	Customer satisfaction	42%	58%
17	Product quality	40%	60%
18	Customer retention	38%	62%
19	Product innovation	35%	65%
20	Customer loyalty programs	32%	68%
21	Product variety	30%	70%
22	Customer service training	28%	72%
23	Product reliability	25%	75%
24	Customer service excellence	22%	78%
25	Product consistency	20%	80%
26	Customer service responsiveness	18%	82%
27	Product quality control	15%	85%
28	Customer service recovery	12%	88%
29	Product quality assurance	10%	90%
30	Customer service excellence programs	8%	92%
31	Product quality management	5%	95%
32	Customer service excellence awards	3%	97%
33	Product quality improvement	2%	98%
34	Customer service excellence recognition	1%	99%
35	Product quality excellence	0%	100%

Source: Author's survey of 100 most important factors for the success of a business.

The results shown in Figure 4.5.6 underline the major problems in detection cited in the previous paragraph. Even with very experienced teams, there is a fundamental problem in correctly recognizing the signal as emanating from a flaw rather than from innocuous sources such as fabrication anomalies. On the basis of the preceding results, several suggestions were made that were expected to improve the detection reliability. These follow (EPRI is or has followed up on several cited):

- Evaluate transducers to determine what parameters enhance detection and analysis of IGSCC (partially done).
- Develop specialized equipment using flawed specimens to improve detection, particularly with regard to enhancing signal-to-noise ratio (underway).
- Train UT personnel on defective piping.
- Improve the methods for detecting off-axis flaws either with improvements in technique or scanning procedure (underway).
- A long-term project is the modification of field welding procedures and weld configurations to improve ISI. Obvious possibilities include moving the counterbore away from the weld fusion zone reducing the taper in the counterbore, modifying rules regarding drop-through or suckup and controlling weld crown.
- Develop methods of processing the UT data or use supplemental NDE techniques.

The preceding study represents a milestone in defining UT limitations as well as suggesting corrective actions. The ultimate impact of the suggested actions awaits completion of ongoing work and reporting of the data.

Substantial work was reported in 1978 pertinent to the behavior of an ultrasonic beam in an austenitic weldment. The information presented in Reference 4.5.28 complements these reports. (4.5.31,4.5.32,4.5.33)

Kupperman and Reimann reported essentially the same information in two papers. (4.5.31) Their results closely paralleled those of Baikie

et al.<sup>(4.5.27)</sup> with regard to directions of minimum and maximum beam attenuation in dendritic weldments. They conclude that convergence of UT beams along the direction of maximum velocity may be a major factor in attenuation. This conclusion, together with the following factors, said to affect attenuation in welds, may explain the results of Yoneyama et al.<sup>(4.5.28)</sup>

- Grain boundary scattering which is a function of wavelength and polarization.
- Mode conversion which will differ not only for longitudinal and shear waves, but also for shear waves of various polarizations.
- The guiding of beams from their wave normal, which is characteristic of single crystal and preferred texture material.

The third item should explain the data of Yoneyama et al.<sup>(4.5.28)</sup>

This paper<sup>(4.5.31)</sup> contains an extensive development of velocity/elastic constant relationships.

A paper by Tomlinson, Wagg and Whittle<sup>(4.5.32)</sup> expands extensively on the previous results of Baikie et al.<sup>(4.5.27)</sup> In fact, several figures and conclusions are identical. Their theoretical calculations further confirm the experimental results of Yoneyama et al.<sup>(4.5.28)</sup> in predicting that shear waves may deviate as much as 50° from the expected direction of propagation in an anisotropic medium such as a dendritic weld.

The theoretical concepts developed were used to redesign weld geometries to optimize UT examination. This aspect is developed further in subsequent paragraphs.

The authors do an excellent job of presenting the interrelationship of weld design, metallurgical properties and UT procedures, and the way changes can be made to improve the reliability.

#### Equipment Factors

- Compression (longitudinal) waves are less sensitive to weld anisotropy than are shear waves and are favored where it is possible to use them. Their lack of sensitivity is due to the following:

- Most of the energy scattered by grains is in the shear mode which contributes to noise level.
- Beam skewing effects are less for compression waves.
- Short-pulse probes are preferred because they result in less energy scatter along the beam; e.g., lower noise.
- The other approach to reducing noise due to energy scatter is to reduce the beam spread because scatter is a volume effect; this can be done through use of focused probes; however, their use may introduce other problems.

#### Metallurgical Factors

Attenuation can be minimized if the angle between the ultrasonic beam and the columnar grains in the weld is  $45^\circ$ ; this infers not only a controlled orientation but also a uniform orientation. The problems in achieving such are discussed under welding.

#### Weld Joint Design

If the weld joint can be designed for enhanced accessibility in several directions, advantage can be taken of the positive aspects of longitudinal waves; an example of joint redesign to achieve this objective is given in Figure 4.5.7. The modified design permits examination at right angles to the fusion faces.

#### Welding Technique and Process

As cited previously, it is necessary to control both fiber texture insofar as orientation is concerned and be sure that this orientation remains consistent throughout. Examples of success and failure follow:

- Typically, welds either butt or fillet are made with the pieces (such as piping) in the horizontal position; at the top (12 o'clock) the welding is horizontal-vertical; at 3 o'clock it is vertical-up, etc. With this procedure (Figure 4.5.8a), grain orientation relative to the tube axis varies in zone repetitive patterns around the weld (Figure 4.5.8b) which makes weld examination by UT very difficult.

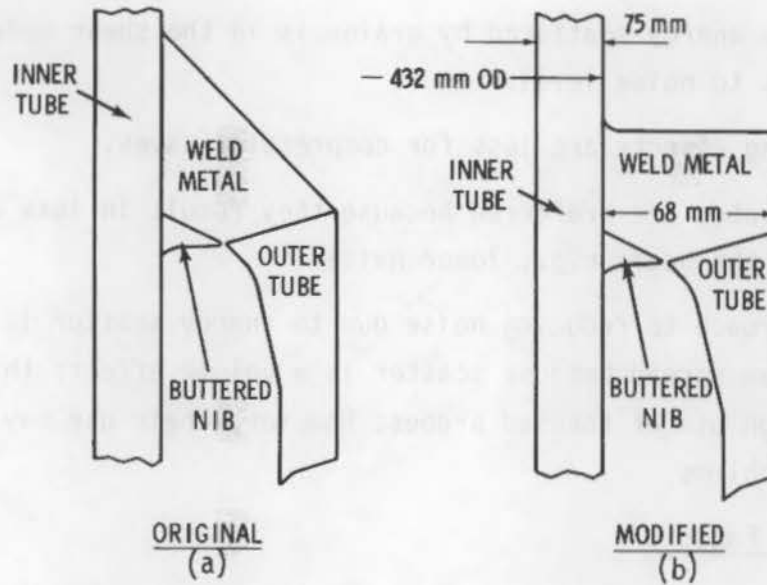


FIGURE 4.5.7. Original (a) and Modified (b) Weld Profiles for Optimization of Ultrasonic Examination

DEPOSITION OF WELD LAYERS AT 90° TO TUBE AXIS

RESULTANT ANGLES BETWEEN BEAM AXES AND GRAIN AXES AROUND WELD

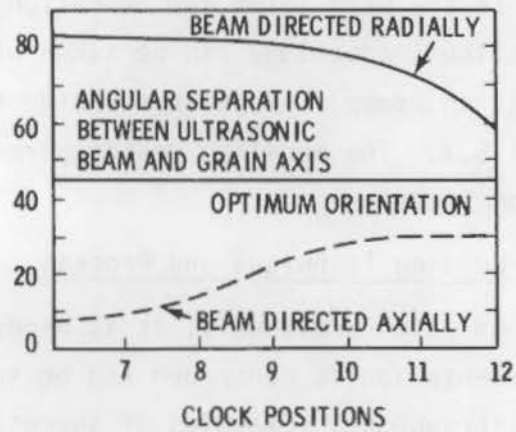
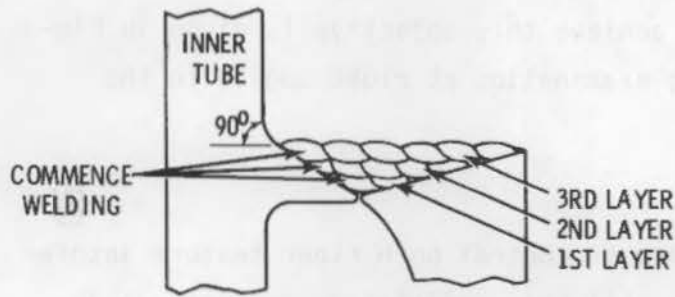


FIGURE 4.5.8. Purpose--Optimization of UT; 90° to Tube Axis

- If the welding process is modified to deposit metal at  $55^\circ$  to the tube axis rather than  $90^\circ$  (Figure 4.5.9a), the orientation variation is minimized (Figure 4.5.9b). Even with such a procedure there is given distribution about the optimum.
- Welding process can markedly influence orientation. Examples of this effect can be seen in the following where butt welds were made by both the manual metal arc (MMA) and the metal inert gas (MIG) processes. A butt weld varies from a fillet weld such as shown in Figure 4.5.7 in ratio of volume of weld metal to area of weld at the fusion faces. This ratio is much larger in the fillet weld than in the butt weld. The higher ratio of contact area in a butt weld results in significant cooling, producing smaller grains and changing the orientation:
  - The MMA weld produces long grains growing epitaxially across many weld beads with a well-defined orientation. While this weldment has a very low attenuation when examined down the center of the weld, there is severe beam skewing and a bimodal energy distribution. These effects were attributed to the inhomogeneous nature

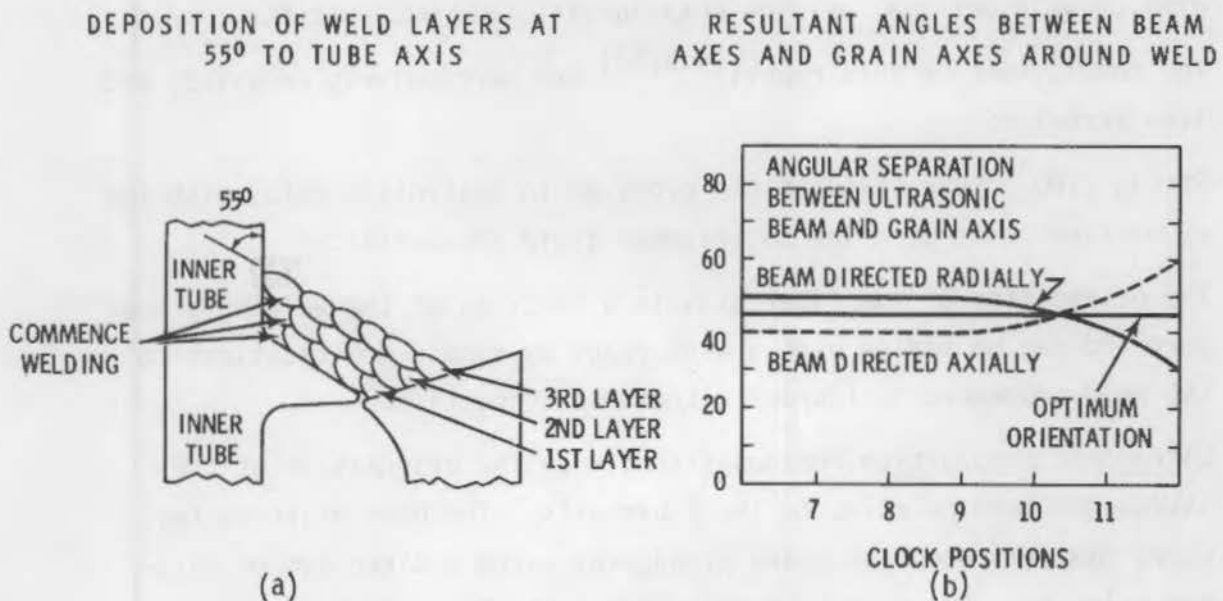


FIGURE 4.5.9. Purpose--Optimization of UT;  $55^\circ$  to Tube Axis

of the weld metal, permitting the sound beam to find more than one path, resulting in double images in some instances.

- The MIG process produced a weld with fans of grains within each weld bead with little or no extension into adjacent layers of beads. The MIG process generates a higher and more localized heat input with deeper remelting leading to curved liquid-solid boundaries. This less ordered grain structure leads to higher beam attenuation; however, there was no beam skewing. The MIG weld is intermediate between the pronounced orientation of the MMA weld and the isotropic structure of a forging.

Variability in orientation can be particularly troublesome in sizing a defect since substantial fluctuations in orientation negate the techniques depending on dB drop or vanishing echo.

The authors emphasize the need to optimize equipment, metallurgical structure and joint design. Even with the optimization, the detection and sizing of defects in austenitic weldments will be inferior to ferritic weldments.

With these sizing problems, there will be a greater need for fracture mechanics to assess safety margins. This approach illustrates the need for synergism of weld designs, welding metallurgist, and NDE operator.

The conclusions of this report<sup>(4.5.32)</sup> are particularly relevant, and are given verbatim:

- Strong  $\langle 100 \rangle$  fiber textures are produced in austenitic welds with the  $\langle 100 \rangle$  fiber axis parallel to columnar grain boundaries.
- The orientation of the fiber axis is a function of the welding procedure and can be varied over a wide range by simple modifications to the weld procedure to improve ultrasonic inspection.
- Ultrasonic propagation depends strongly on the orientation of the ultrasonic beam relative to the fiber axis. The beam width varies, being smallest when the sound propagates along a direction of maximum velocity. The signal-to-noise ratio is also a maximum when the



beam is along such a direction (approximately  $45^\circ$  to the fiber axis). The beam axis, in general deviates from the direction that it would have in equiaxed austenitic steel.

- Consideration and control of the weld structure must precede attempts to improve inspection sensitivity by the use of special transducers or signal processing methods.
- Sensitivity to small defects is, in general, unlikely to be as high for austenitic welds as for ferritic even when the weld structure has been optimized. Austenitic welds should, therefore, be examined to acceptance standards based on fracture considerations.
- Plant designers should take account of the limitations of ultrasonic inspection when applied to austenitic structures at the earliest possible stage.

A paper by Newmann et al. (4.5.33) is devoted primarily to a discussion of special UT equipment to be used in the examination of austenitic welds in the German LMFBR, SNR-300; however, they also cite several factors affecting such UT examinations either beneficially or adversely. Their goal was to develop a technique (UT) effective in materials with high attenuation levels ( $>0.3$  dB/mm) with low signals and high noise due to grain scattering. To accomplish this goal required an optimization of transducer dimensions. Kirchoff diffraction theory was used for this optimization which proved to be quite complicated requiring significant approximations. The use of a specially developed computer program capable of calculating transducer dimensions for a given region and given coupling surface geometry made the calculations feasible.

Factors that must be controlled if optimum results are to be obtained include the following:

- The incident angle must be optimized for each examination zone in the structure; for example, near the surface the angle is  $70^\circ$ .
- The coupling surface of the probe must be mated to that of the component with the gap less than 0.2 mm.
- The surface finish should be smooth without significant ripples.

- Short, broad-band pulses should be used to suppress reflections from coarse grains and to yield higher resolution.
- This effective bandwidth can be increased further by appropriate signal processing (deconvolution).

The authors used the above criteria in a UT examination of an austenitic weldment. These results were compared with RT results with the comparison being quite good; however, a final assessment should be deferred until the specimen is destructively tested.

#### 4.5.2.4 Flaw Characteristics

Flaw characteristics such as orientation and dimensions are quite sensitive to the UT conditions. The flaw characteristics per se can minimize detection when conventional UT procedures and equipment are used. Similarly, variations in equipment and technique will influence the probabilities of flaw detection, flaw sizing and flaw location.

Typical UT uses only the amplitude to indicate the presence of a discontinuity. If the size of discontinuity exceeds the transducer diameter, we are limited to estimating the discontinuity cross section because present instrumentation is not amenable to correction of beam spread and beam attenuation. (4.5.1)

Signals from flaws can be adversely affected by mode conversion due to relations between shear angles and geometries. (4.5.34) Shear-waves incident on a steel-water interface at angles between  $34^\circ$  and  $89^\circ$  from the normal to the interface will reflect at the same angle on the other side of the normal. Figure 4.5.10 illustrates how shear waves at angles between  $1^\circ$  and  $33^\circ$  will partially mode convert into longitudinal waves and longitudinal waves at angles between  $1^\circ$  and  $89^\circ$  will partially mode convert into shear waves. On Figure 4.5.10, the percentage of energy converted is read vertically above the longitudinal wave beam angle regardless of whether the longitudinal angle is incident or mode converted.

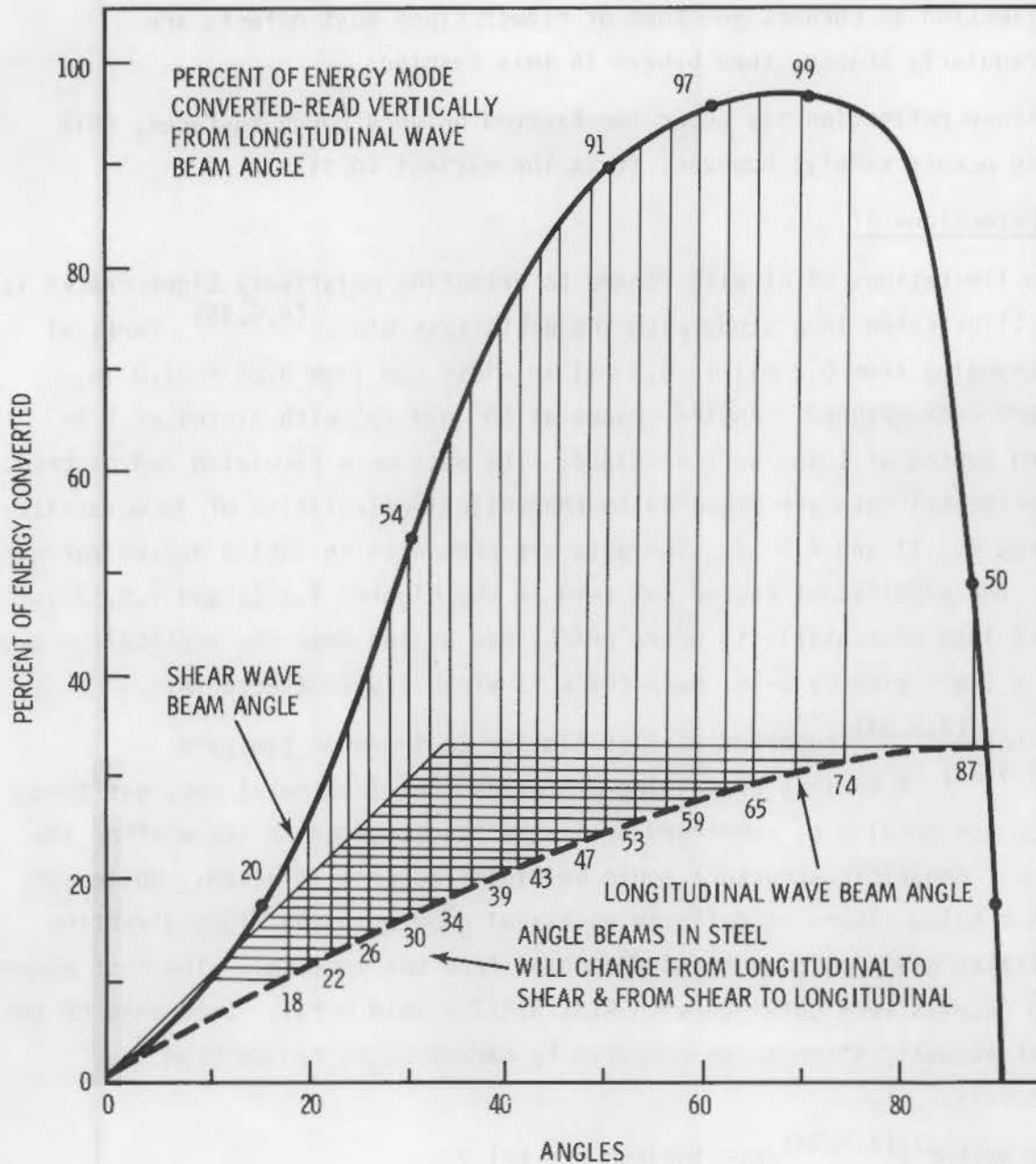


FIGURE 4.5.10. Mode Conversion

Three mechanisms of reflection of UT waves at defect surfaces are discussed by Erhard et al.: (4.5.35)

- Geometric reflection usually occurring for defects much larger than the wave length.

- Reflection at corners and tops of flaws; since most defects are irregularly shaped, they behave in this fashion.
- Diffuse reflection may occur for faceted or very rough surfaces; this case occurs rarely; however, it is the easiest to size.

#### 4.5.3 Detection--RT

The limitations of RT with regard to detecting relatively tight cracks is clearly illustrated in a study with the BERTA test block.<sup>(4.5.36)</sup> Vertical cracks--ranging from 0.2 mil to 0.5 mil in width and from 0.25 to 1.0 in. deep--were radiographed. Angled cracks at 10° and 30° with widths of 1 or 5 mil and depths of 1 in. were examined. The data were tabulated and plotted. The experimental data are compared to theoretical calculation of detectability in Figures 4.5.11 and 4.5.12. The data are presented in Tables 4.5.6a through 4.5.6e. The significant factor not seen in the Figures 4.5.11 and 4.5.12 is the gross loss of sensitivity where cracks are angled from the vertical; e.g., at 30°, a 1-mil wide by 1-in. deep crack is virtually undetectable.

Macecek<sup>(4.5.37)</sup> reported results similar to those of Yoneyama et al.<sup>(4.5.28)</sup> A variety of welding processes (shielded metal arc, gas tungsten arc, gas metal arc, submerged arc) were investigated to see whether the anisotropic dendritic structure could be minimized or eliminated. While submerged arc helps, there is definite epitaxial growth in the <100> direction with definite grain alignment and deviation from the vertical. The most unpredictable results were obtained with AISI 304/308 weld metal. Some idea of the degree of acoustic attenuation compared to carbon steel can be seen in Figure 4.5.13.

The author's<sup>(4.5.37)</sup> conclusions are relevant:

- The coarse grained fibrous structure of stainless steel weld with dominant preferred orientation of fibers results in anisotropy of the ultrasonic velocity and attenuation.
- There is a direction of minimal ultrasonic attenuation in weld structures. This offers the way of achieving a good penetration of weld metal, especially for fully austenitic weld metals, if the structure of the weld metal is known.

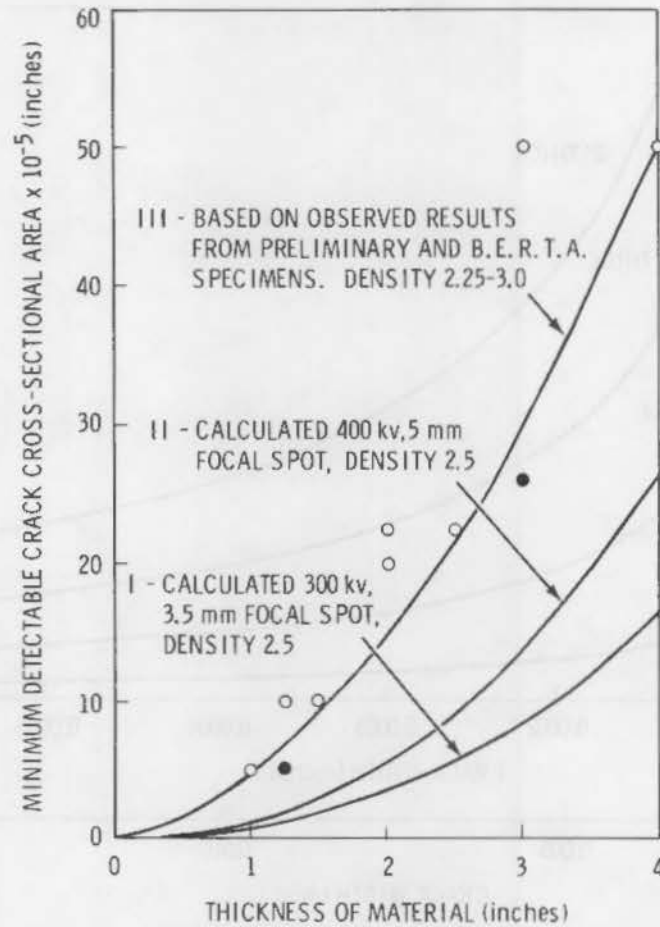


**FIGURE 4.5.11.** Minimum Detectable Crack Cross-Sectional Areas (calculated and observed results)

- The structure of weld metal depends on the material and more on the welding technique used. The features which determine the ultrasonic characteristic of the weld metal are not fully understood yet due to the complexity and interplay of individual factors.
- Due to the weld structure and properties, the total coverage cannot be secured with one probe. However, simple multiprobe arrangement can succeed in inspection of butt-welds up to 3-in. thick.

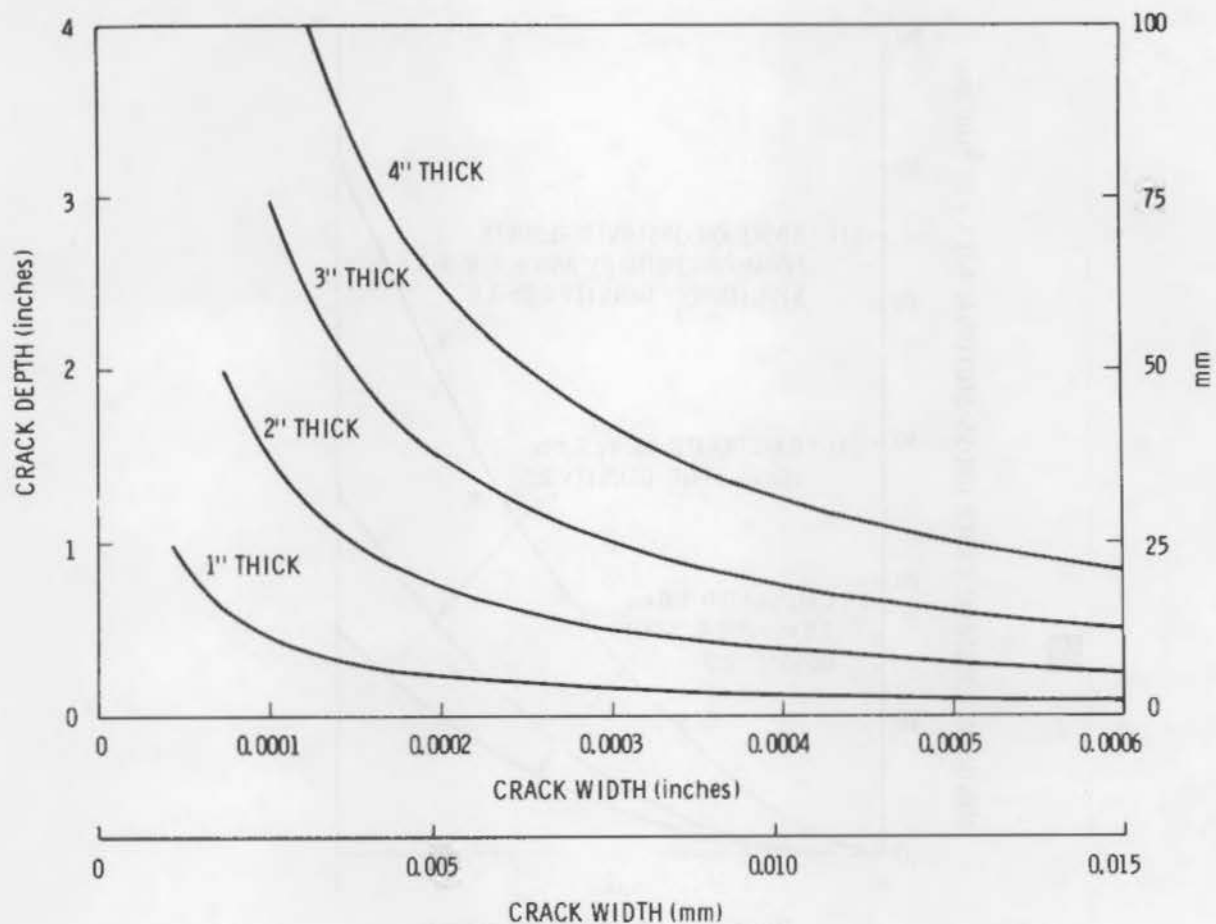


FIGURE 4.5.12. Minimum Detectable Crack Dimensions (based on observed results)

He recommends some items relevant to the philosophy of ultrasonic testing of austenitics:

- The inspection of austenitic weldments should not be divorced from welding procedures and the link between these directions should be established in future NDE inspections.
- Welding procedures and methods should be recorded and made available for ultrasonic inspection. The direction of ultrasonic attenuation can then be established.
- Codes should be modified to make use of the fitness for purpose approach; i.e., to take into account special properties (toughness) of austenitic steels.







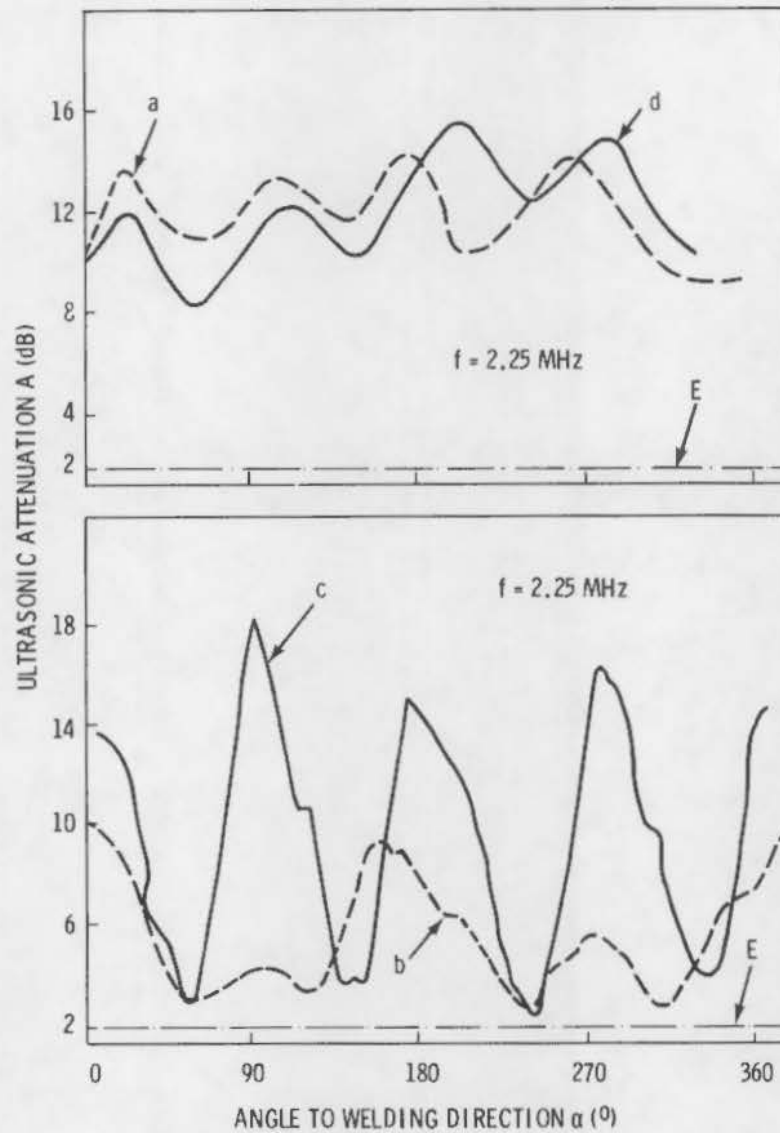


**FIGURE 4.5.13.** Ultrasonic Attenuation as a Function of Direction of Propagation Relative to the Welding Direction  
 (a) AISI 308 welded in horizontal position (GTA Method)  
 (b) AISI 316 steel, horizontally welded (SMA Method)  
 (c) AISI 310 steel, horizontally welded (GMA Method)  
 (d) AISI 308 steel, horizontally welded (GTA Method) (with oscillating electrode)  
 (e) Carbon steel



Figure 1.1.2.100 and 1.1.2.101 show the current amplitude versus well location distance for the two different well locations. The current amplitude is shown in Amperes (A) and the well location distance is shown in meters (m). The current amplitude is generally higher for the well location shown in Figure 1.1.2.101 compared to Figure 1.1.2.100.

4.6.1 Limitations in Detection and Sizing

Since factors related to flaw detection are entwined with factors related to flaw location and sizing, this section will combine them to lead into information relevant to sizing and location. We need to remind ourselves that two reliable and two unreliable conditions exist. The reliable conditions are 1) flaw is detected that exists, and 2) flaw is detected that does not exist. The unreliable conditions are 1) flaw is not detected that exists--of safety significance, and 2) flaw is detected that does not exist--of economic significance.

An attempt will be made to establish materials, geometric and equipment factors playing a significant role in detection unreliability. Comments will be limited to ultrasonic techniques since that is where the major questions exist. Figure 4.6.1 schematically outlines the areas considered significant.

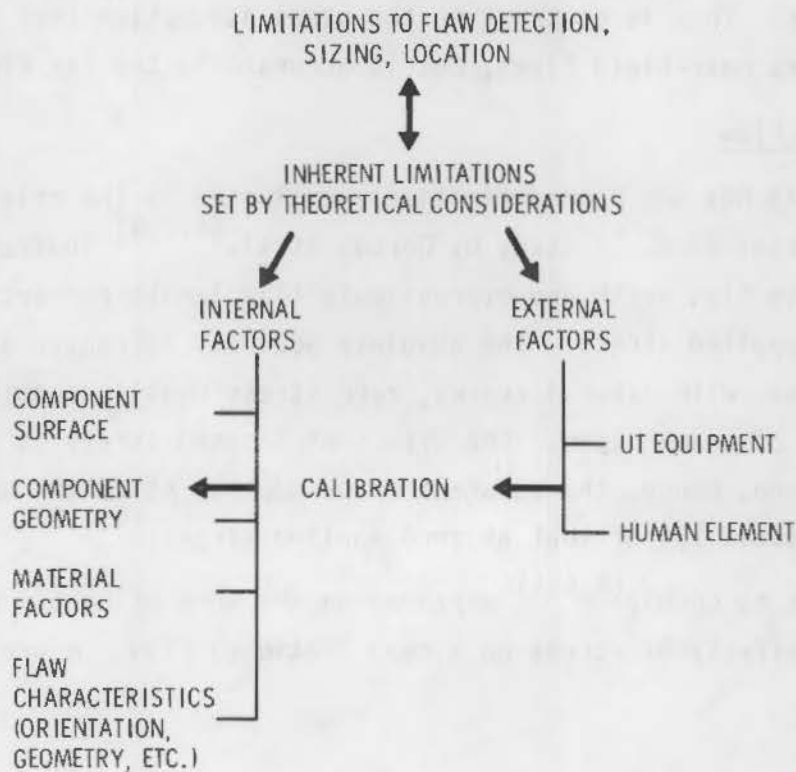


FIGURE 4.6.1. Limitations to Flaw Detection, Sizing, Location

Factors leading to an underestimation of crack depth and, possibly, crack length include 1) tight cracks where transmission losses differ from open cracks, 2) specular reflection from smooth surfaces which is often the case for the lowest or latest generated section of a fatigue crack, 3) crack branching, 4) diffraction effects,<sup>(4.6.1)</sup> and 5) premature mode conversion of Rayleigh waves, possibly from irregularities down a fatigue crack face.<sup>(4.6.2)</sup>

#### 4.6.2 AVG-DGS

The AVG or DGS technique has been used to determine flaw sizes; however, several factors can adversely influence accurate dimensions such as beam attenuation, geometric features, and search unit access. For surface flaws a further source of error is the pronounced magnification effect.<sup>(4.6.3)</sup> Further errors that may occur with the DGS system include overestimation of defect size as distance from transducer to flaw increases. Since the S-scale is logarithmic, the error is substantially greater than indicated on cursory examination.<sup>(4.6.4)</sup> Another source of error is variability of pulse strength. For distant reflectors, an increase in energy input will cause the apparent defect to be much larger. This is contrary to the usual assumption that the DGS system underestimates near-field flaws, but is accurate in the far field.<sup>(4.6.4)</sup>

#### 4.6.3 Stress on Flaw

A factor that has not been definitively evaluated is the role of stress on a real or artificial flaw. A study by Corbly et al.<sup>(4.2.9)</sup> indicates that UT will underestimate flaw depth and overestimate flaw length for artificial flaws subjected to an applied stress. The absolute accuracy increases slightly with increasing stress. With natural cracks, zero stress usually permits an accurate measurement of crack depth. The effect of imposed stress is to increase the peak height and, hence, the apparent crack depth. At 20 ksi applied stress the accuracy is about 10% of that at zero applied stress.<sup>(4.2.9)</sup>

Further work by Corbly<sup>(4.6.5)</sup> expanded on the work of Corbly et al.<sup>(4.2.9)</sup> relevant to the effects of stress on a real (fatigue) flaw. A broad-band 6-MHz

transducer was used to scan the crack-tip region as well as the near-surface edges of the crack. A 7075-T651 aluminum fatigue specimen was used. Three measurement techniques were used:

1. first reflection—the interaction of the leading edge of the sonic field with the crack tip.
2. tip amplitude—the value corresponding to the centerline of the transducer at the crack tip.
3. integral—the integrated signal response from a 0.25-in. scan over the crack tip.

A major conclusion was that crack closure can significantly affect the UT response from fatigue cracks in the near-tip region. Tensile loading will increase the magnitude of UT reflection at the crack tip. Figure 4.6.2 illustrates the effects of loading on UT signal amplitude both at the crack centerline and at the crack edge. In the latter case, the signal change is quite marked.

The following are other conclusions having implications with regard to reliability of crack detection by UT:

- The stress state at the crack tip influences the crack closure and the UT signal.
- The combined effects of crack closure and crack surface topography make it impossible to develop a usable correlation between the ultrasonic response from reference notches and fatigue cracks.

The final conclusion is quite significant and merits additional work to verify or to refute it.

Ibrahim and Whittaker<sup>(4.6.6)</sup> examined the effects of compressive stress on fatigue cracks in mild steel weldments. They used the following combinations:

Frequency - 2, 5 MHz

Shear Angles - 45°, 60°, 70°

Scanning - 1/2 skip, full-skip

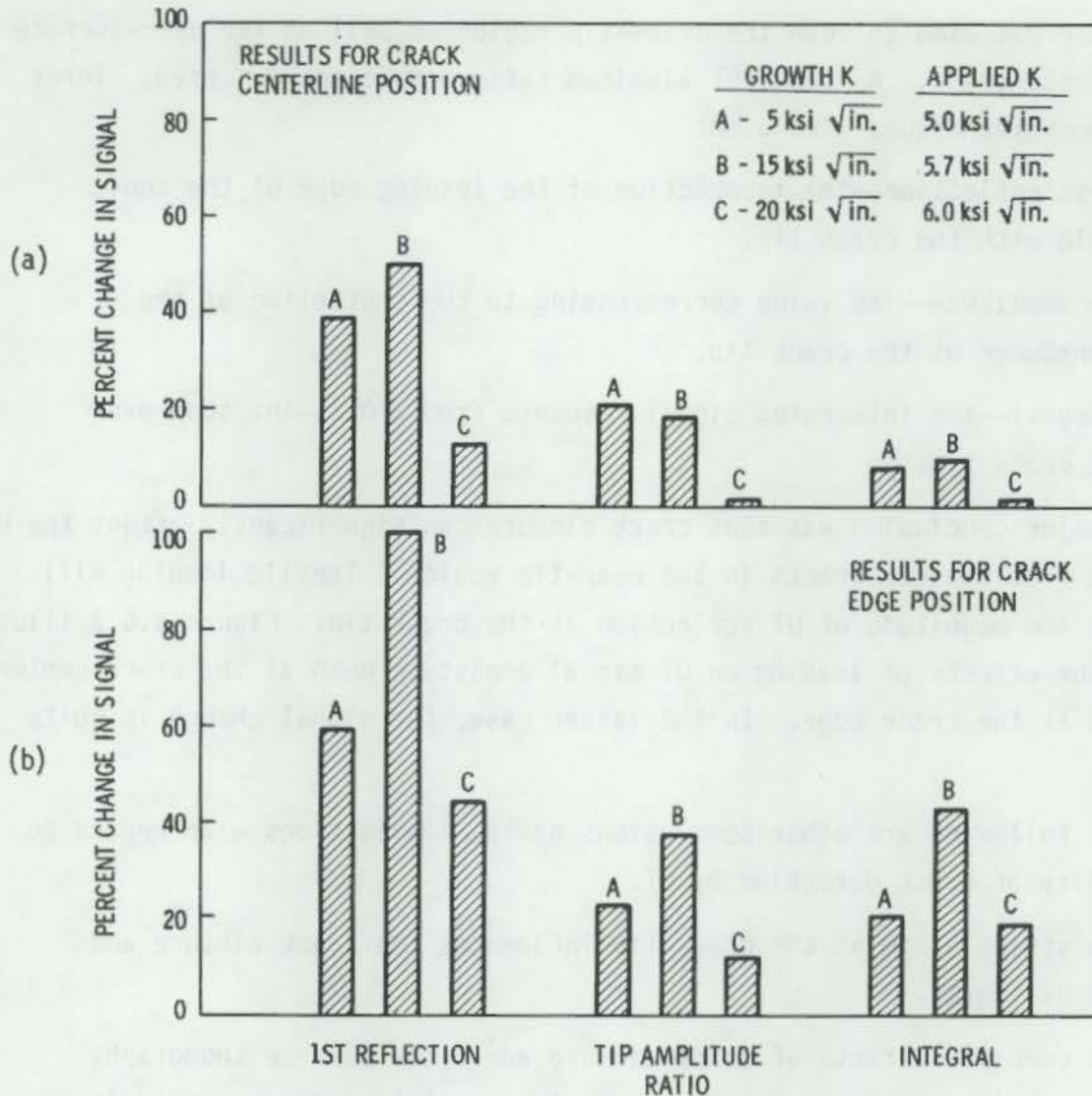


FIGURE 4.6.2. Changes Due to Applied Tensile Loads, in Ultrasonic Reflection Amplitude as Determined by Three Analysis Methods  
 (a) Results for crack centerline position  
 (b) Results for crack edge position

Optimum conditions were 5 MHz, 45°, 1/2 skip. The 2 MHz had poor signal-to-noise ratios. Use of 60° led to substantial mode conversion with loss of signal.

The 45° probe was preferred because the acoustic wave was essentially perpendicular to the facets of the fatigue cracks. This became more apparent in

stress relieved and normalized specimens compared to as-welded because crack facets were larger in the stress-relieved and normalized conditions.

Figure 4.6.3 compares results of 45°, 60°, and 70° at 5 MHz, 1/2 skip confirming the problems with 60° probes. Figure 4.6.4 covers the spectrum of tests with 45° probes, and Figure 4.6.5 illustrates the influence of prior heat treatment or signals from fatigue cracks.

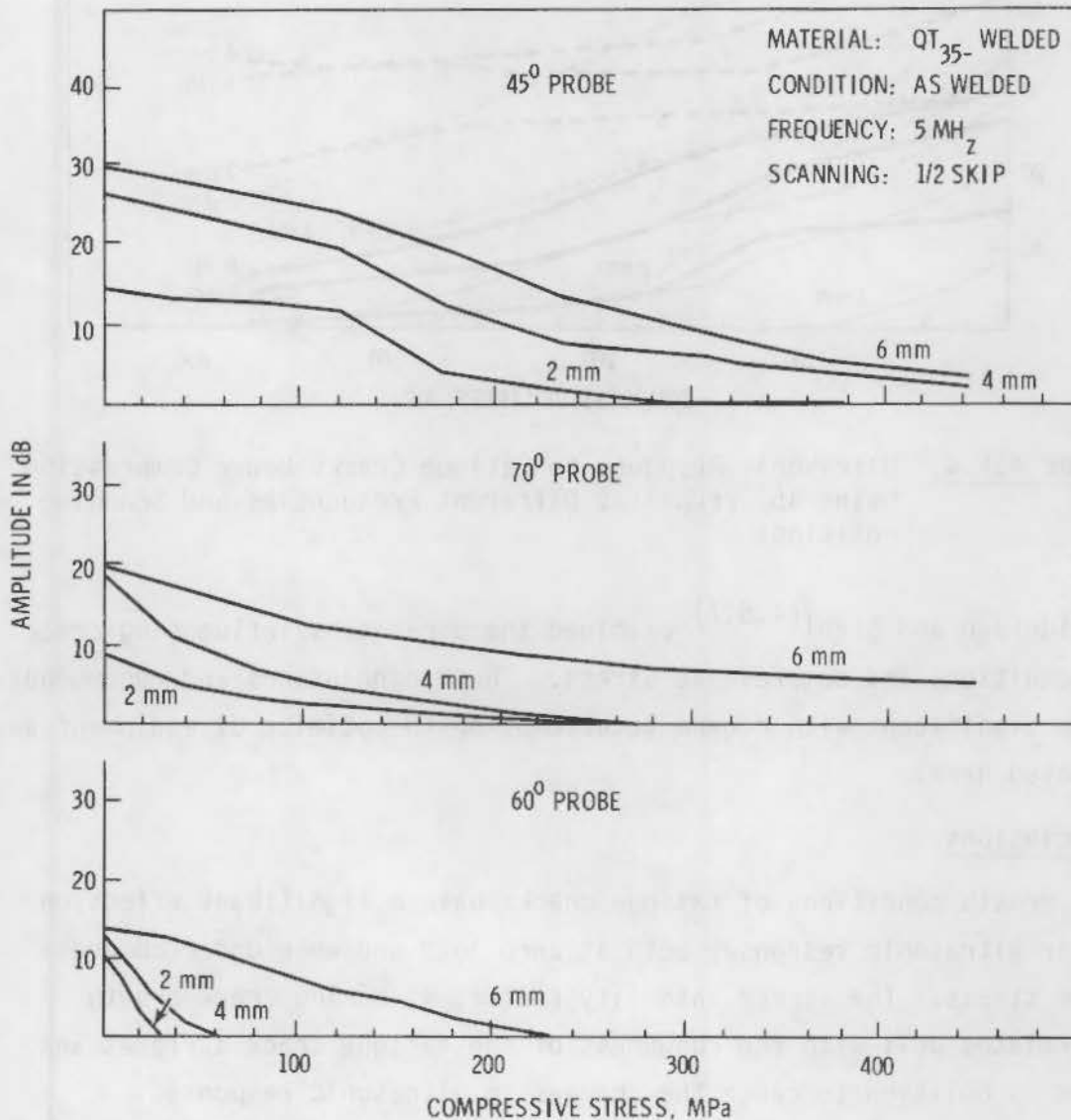


**FIGURE 4.6.3.** Optimum Ultrasonic Techniques for Detecting Fatigue Cracks Under Both Zero Load and Compressive Stresses When Using 45°, 60°, and 70° probes (5 MHz at 1/2-skip scanning)

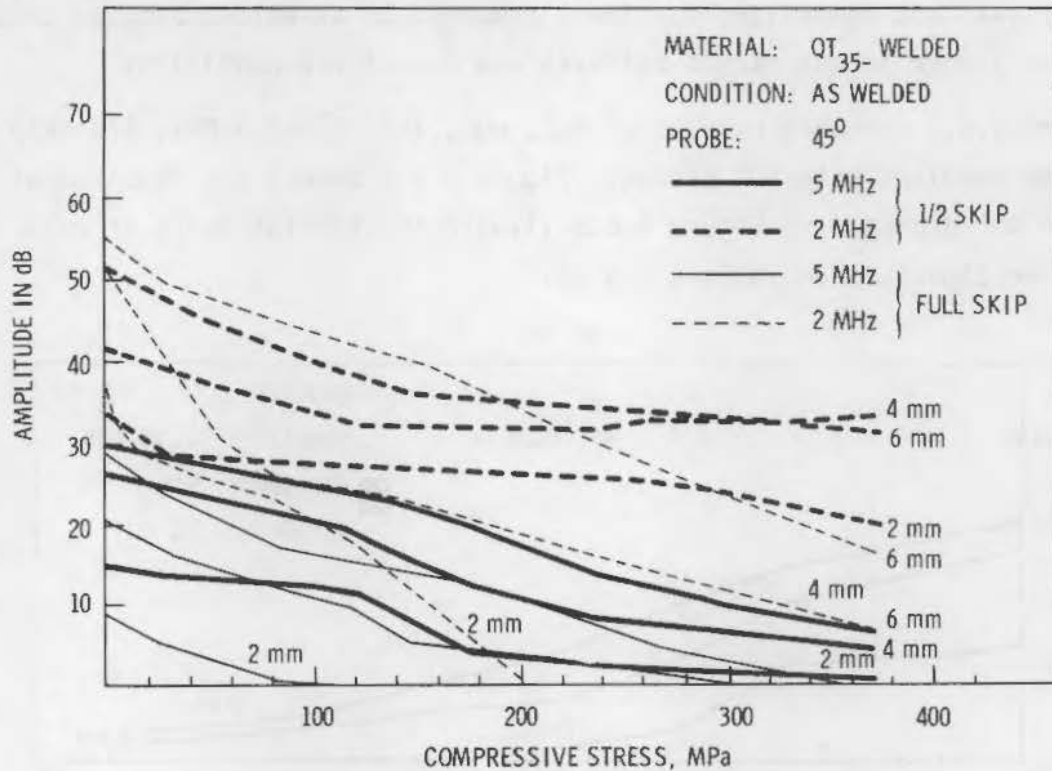


FIGURE 4.6.4. Ultrasonic Response to Fatigue Cracks Under Compression Using 45° Probes at Different Frequencies and Scanning Positions

Wooldridge and Steel<sup>(4.6.7)</sup> examined the parameters influencing crack growth conditions and compressive stress. Their conclusions and recommendations are significant with regard to attempting to optimize UT equipment and are repeated here:

#### Conclusions

1. The growth conditions of fatigue cracks have a significant effect on their ultrasonic response, both at zero load and when under compressive stress. The stress intensity factor,  $K$ , during crack growth correlates well with the roughness of the fatigue crack surfaces and this is believed to cause the changes in ultrasonic response.
2. Both increasing crack roughness and increasing compressive stresses reduce the specular reflection from fatigue cracks. Decreases of up to 10 dB may be caused by crack roughness while large compressive



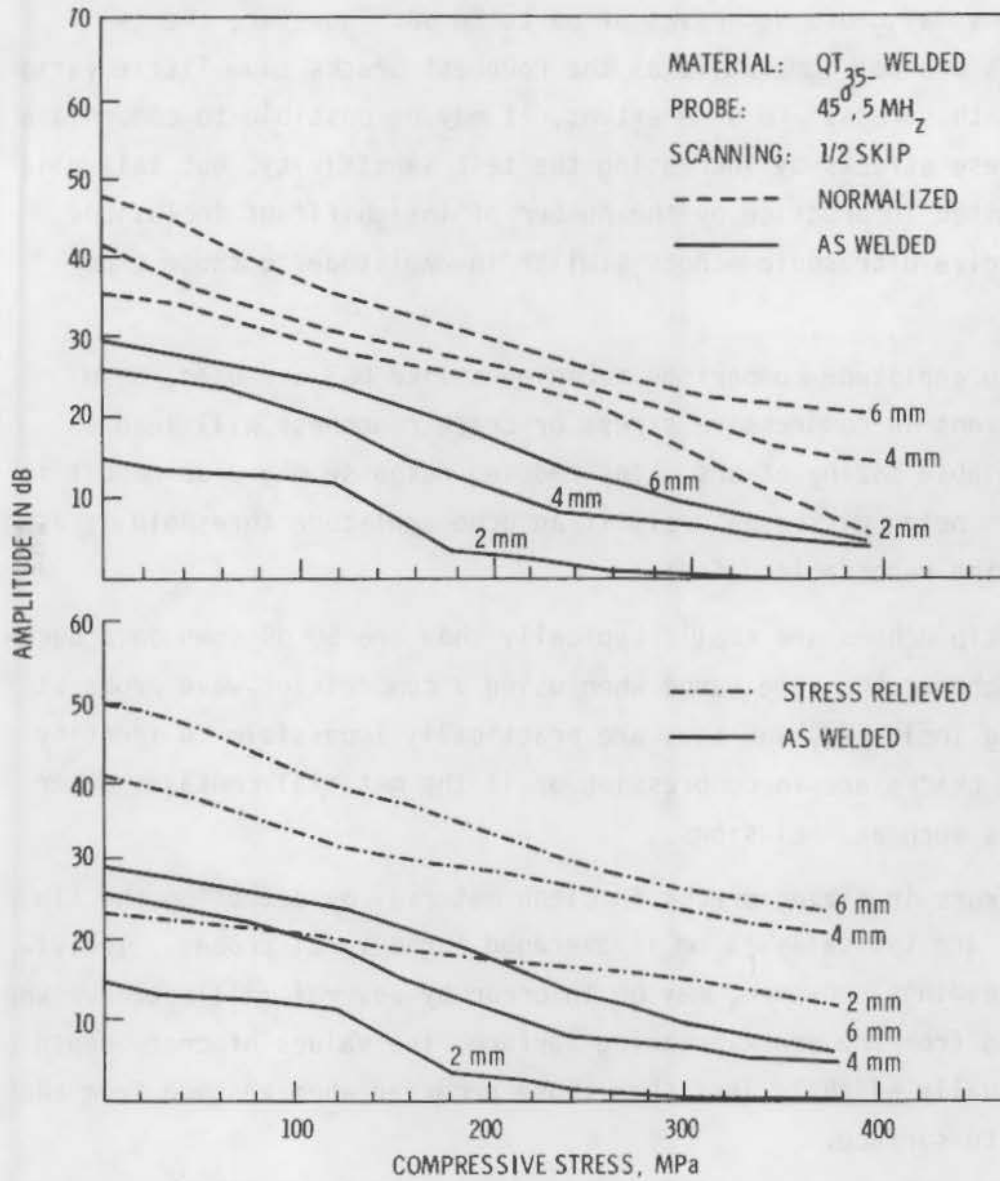


FIGURE 4.6.5. Signal Amplitude Responses from Fatigue Cracks Under Compression in the As-welded, Stress-relieved and Normalized Welds Using a 45° Probe (5 MHz at 1/2-skip Scanning)

stresses may cause decreases of up to 20 dB. However, the two effects are not cumulative as the roughest cracks show little variation with stress. To some extent, it may be possible to compensate for these effects by increasing the test sensitivity, but this will be limited in practice by the number of insignificant inclusions which give ultrasonic echoes similar in amplitude to those from cracks.

3. If echo amplitude comparison techniques like DGS are used, then variations in compressive stress or crack roughness will lead to appreciable sizing errors. The reduced response may also result in defects being missed entirely if an echo amplitude threshold is used to define recordable defects.
4. Crack-tip echoes are small; typically they are 50 dB down on a back-wall echo at the same range when using a compression-wave probe at grazing incidence, and they are practically impossible to identify if the cracks are in compression or if the material contains other defects such as inclusions.
5. The errors in sizing cracks in clean material by detecting the tip echoes are typically  $\pm 1$  mm if averaged for several probes. Individual readings, however, may be in error by several millimeters. When testing from the crack-breaking surface, the values of crack depth are usually slightly less than those recorded when testing from the opposite surface.
6. The presence of liquid in a crack causes a marginal increase in reflection for shear-wave beams incident at  $20^\circ$  to the crack normal. Modest decreases in reflection occur for beams incident at  $45^\circ$ , while considerable decreases are likely at  $30^\circ$  incidence.
7. Although compressive residual stresses may lead to cracks being undersized, fracture mechanics predictions of growth rates may nevertheless be conservative because these stresses reduce the resultant stress intensity at the crack tip.

### Recommendations

1. When designing inspections to detect high-cycle fatigue cracks the orientations of the ultrasonic beams relative to the likely directions of crack growth should be such that the specularly reflected waves are detected. Realistic estimates of crack growth directions and compressive stresses during testing are necessary if reliable and cost-effective inspections are to be achieved.
2. Sizing using crack-tip echoes should only be relied upon if the region of the crack tip is known to be unstressed or under tension.
3. The ultrasonic responses and surface profiles of fatigue cracks should be measured for a wide range of  $\Delta K$  and R values so that the dependence of the crack roughness on the growth conditions can be firmly established. This should be repeated for several materials with different values of yield stress using both parent plate and weld metal.

Test blocks typically were 350 x 50 x 40 mm in size with side grooves and a V-notch as a crack initiator. Fatigue cracks were generated by cycling under bending loads, and repeating in some instances to deepen the cracks. Figure 4.6.6 permits a comparison of compressive stress as detection of cracks with various probes. As noted, Delta-scan, 45° shear and surface waves are most effective. Figure 4.6.7 is a compression of the effects of water in the crack together with a compressive load. Wet cracks cause a definite decrease in signal amplitude.

#### 4.6.4 Flaw Orientation

Flaw orientation is a critical factor. As noted in the theoretical analyses of Haines,<sup>(4.5.3)</sup> a tilt of about 10° is sufficient to prevent detection with a given beam angle. Experimental work has confirmed that such flaws may not be detected, probably because certain flaw types and orientations do not interact sufficiently strongly with the UT wave.<sup>(4.5.4)</sup> An example is single-probe analysis of lack of fusion on a square butt-weld where the echo does not return to the probe.<sup>(4.5.16)</sup>

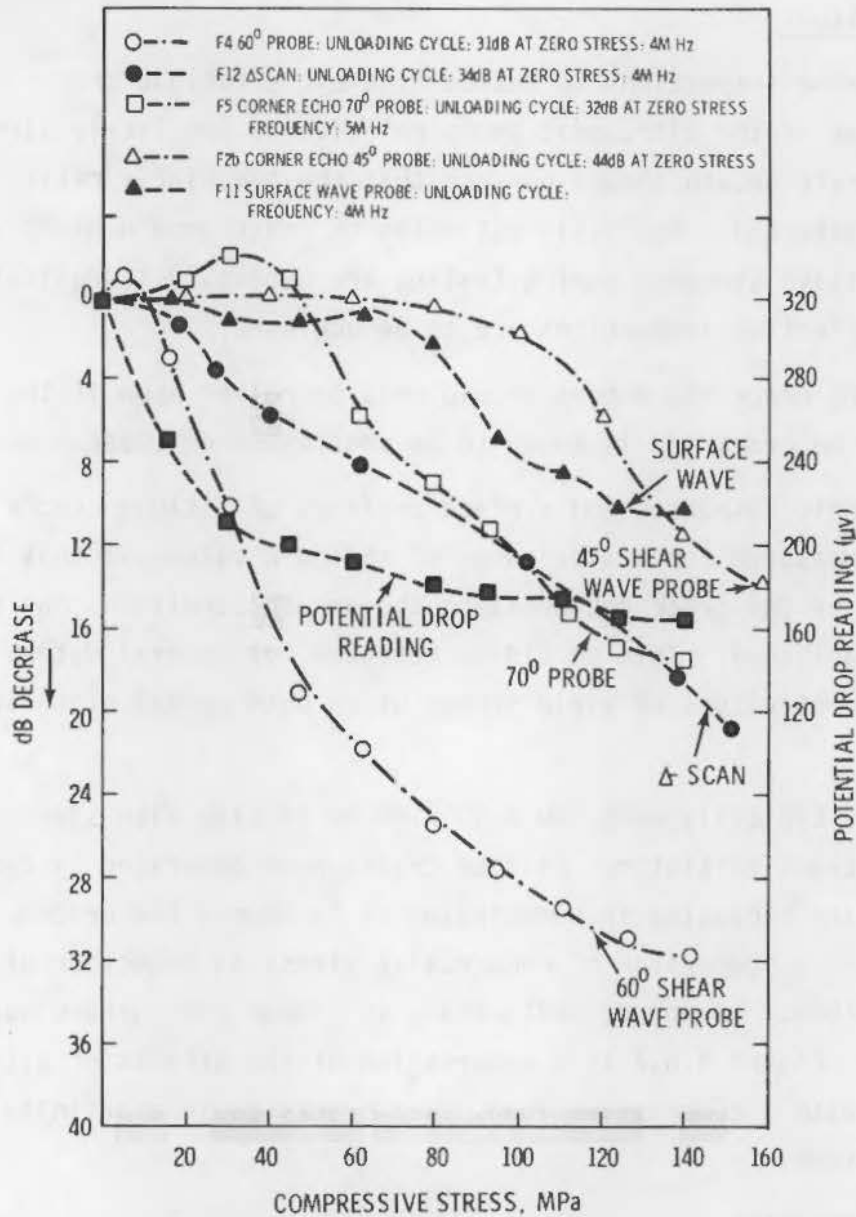


FIGURE 4.6.6. Ultrasonic Examination of Test Block F Using Various Techniques

Several factors leading to missing a defect or underestimating its size have been cited.<sup>(4.5.16)</sup> An orientation related item has to do with insufficient reflection if the sound beam travels at too flat an angle in relation to the defect. Laminations may result in beam deviations and possible failure to detect flaws. Another structure leading to the missing of flaws may occur in certain weldments where "cold shuts" between each individual bead and the pass

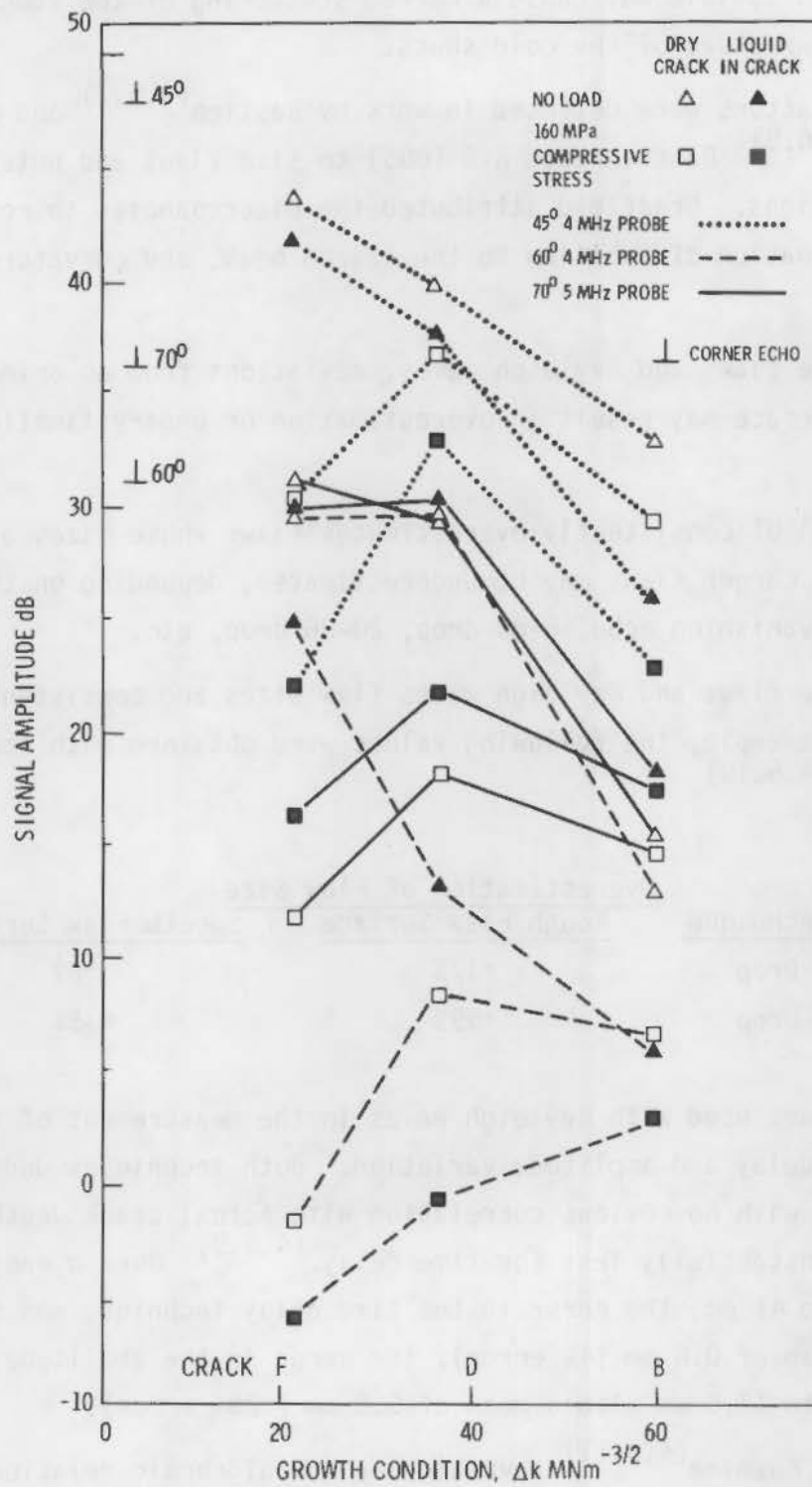


FIGURE 4.6.7. The Effects of Liquid in Cracks When Unloaded and Under Compression

on which the bead is laid may cause a marked scattering of the sound beam because of the curvature of the cold shuts.

The above factors were detected in work by Bastien<sup>(4.5.7)</sup> and discussed by Bradfield.<sup>(4.6.8)</sup> Bastien used AVG (DGS) to size flaws and noted discrepancies in dimensions. Bradfield attributed the discrepancies to roughness of the flaws, inclination of the flaw to the search beam, and curvature of the flaw surfaces.

With surface flaws and Rayleigh waves, deviations from an orientation normal to the surface may result in overestimation or underestimation of flaw depth.<sup>(4.6.9)</sup>

Conventional UT consistently overestimates flaws whose sizes are less than the focal spot. Larger flaws may be underestimated, depending on the sizing technique used--vanishing echo, 6-dB drop, 20-dB drop, etc.

With surface flaws and Rayleigh waves flaw sizes are consistently overestimated. For example, the following values were obtained with smooth and rough surfaces:<sup>(4.6.10)</sup>

Sizing Technique	Overestimation of Flaw Size	
	Rough Flaw Surface	Smooth Flaw Surface
6-dB Drop	+17%	~0%
20-dB Drop	+59%	+35%

Two techniques used with Rayleigh waves in the measurement of surface cracks are time delay and amplitude variation. Both techniques underestimated or overestimated with no obvious correlation with actual crack depth; however, the error was substantially less for time delay.<sup>(4.5.9)</sup> Over a range of crack depths from 10 to 41 mm, the error in the time delay technique was from 0.1 to 1.8 mm with a mean of 0.8 mm (4% error); the error in the amplitude technique ranged from 0.6 to 17.8 mm with a mean of 5.5 mm (~28% error).

Gurvich and Kuzmina<sup>(4.6.11)</sup> investigated the algebraic relationships used in measuring defect height (depth) with the dB-drop and vanishing-echo techniques. The derivations are given in Chapter 5.

An excellent paper by Wüstenberg et al.<sup>(4.6.12)</sup> complements the information in Haines article<sup>(4.5.3)</sup> concerning the implications of flaw orientation as it influences detection. Their study emphasized defect orientation; however, this was in the context of other factors influencing the overall echo amplitude. Their list included the following:

- orientation of the flaw surface referred to the UT beam axis
- flaw (reflector) size
- the sound field of the search unit or the inspection system
- scanning motion
- pulse shape
- roughness of reflector (flaw) surface.

Both a theoretical study and a series of experiments were conducted to evaluate the influence of the preceding factors.

The following are some general conclusions:

- Orientation, if poor with respect to the UT beam, may result in large defects giving smaller signals than favorably oriented small defects.
- Surface roughness will cause beam diffusion when peak-to-valley ratios are  $R_a > \lambda/2$ .
- Scanning motion may yield a higher echo amplitude than a stationary probe. The two values will converge with increased beam divergence.
- Pulse shape may be a factor, depending on whether a harmonic signal does or does not occur; a nonharmonic signal is more detectable.

The angular dependence of defect detection was modeled with a computer for the single transducer and tandem cases. These analytic results were compared to experimental data obtained from spark-eroded notches at various orientations. Agreement was excellent.

Both static and dynamic cases were examined for an extinction angle of  $20^\circ$  for single probes, tandem probes and focused probes. These studies indicated that the tandem technique has maximum orientation dependence for a backwall defect. Focused probes exhibited a definite superiority to the other two techniques for detecting poorly oriented flaws under static conditions; however,

this superiority is markedly reduced for the (moving probe) case. Generally, a moving probe reduced the orientation dependence for all probes. Since one type of probe responded more than another type in a given angular range, the possibility of optimizing by combining two systems such as single probe and tandem probe warrants consideration. A majority of the preceding information was collected on 45° probes; however, the limited work on a 60° single probe revealed no major differences.

Figure 4.6.8 compares the three probes under static and dynamic conditions for the 0° to 20° range of defect orientation. The effects of movement as well as the differences from probe type to probe type can be seen.

Table 4.6.1 provides criteria for optimizing for detection, sizing, etc.

One can conclude that, for high detection probability with an adequate signal-to-noise ratio, inspection systems with medium divergence probes are the best choice. The other systems are preferred for sizing.

An analytic study for Serabian and Lawrie<sup>(4.6.13)</sup> examined the limitations of pulse echo for flaw sizing in the context of such variables as orientation, surface contours, flaw surface roughness, transducer size and shape, and frequency. This particular study was limited to beams perpendicular to both flat and convex surfaces. Presumably, future work will cover angled beams.

The orientation of the flaw with respect to the beam results in signal amplitude distributed in a Gaussian distribution. Presumably, if the distribution is well defined (which is improbable), the size of the flaw could be defined for various orientations.

The pitfalls of distance-amplitude relationships are exemplified in their study. A 2.25-MHz 0.25-in.-dia transducer predicts an 0.125-in.-dia reflector at 5-in. depth to be 2 in. in size using a 6-dB drop technique. A 1-in.-dia reflector will be reported as 0.40 in. for the same depth--dB-drop conditions. Obviously, there is a proportionality relating flaw depth and transducer size. The tendency is to overestimate small flaws and to underestimate large ones.

If one could achieve the ideal combination of transducer size to defect size, it should be possible to accurately estimate flaw size, given that the



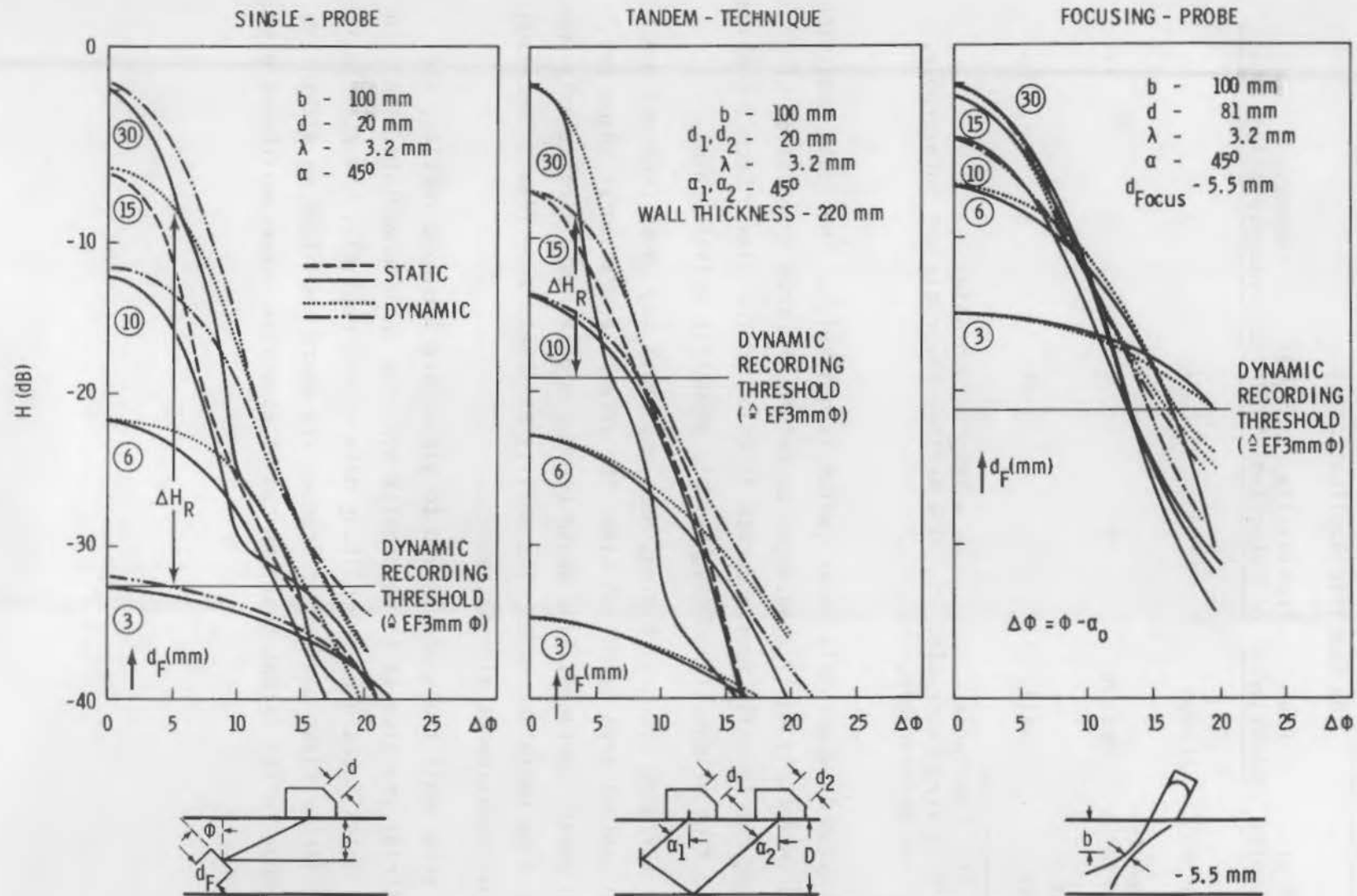


FIGURE 4.6.8. Static and Dynamic Angular Dependency with Various UT Techniques

TABLE 4.6.1. Factors for Optimizing System Selection Based on Specific Application(s)

<u>Type of Probe System</u>	<u>Beam Divergence</u>	<u>Probability of Detection</u>	<u>Signal to Noise</u>	<u>Readout Interpretation</u>	<u>Costs</u>
Acoustic Holography	Large	++	--	+	-
Most Commercial Probes	Medium	+	+	0	++
Focused Probes	Small	-	++	++	-

NOTE: + = Favorable, -- = Very Unfavorable  
 ++ = Very Favorable; 0 = Neither Favorable nor Unfavorable.  
 - = Unfavorable;

flaw orientation is accurately known (which is unlikely). The ideal condition would be an infinitely small transducer to obtain the true orientation of a flaw assuming the (usually two) accurate location of the flaw. Such a combination permits true orientation through simple geometric relationships.

Convex surfaces (such as piping, nozzles, etc.) may cause problems due to the limited contact area which can alter the effective transducer shape and size. With convex surfaces, flaw depth becomes significant, particularly when shallow; as flaw depth increases, the ability to obtain true flaw orientation with a single measurement also increases.

While very small transducers tend to yield more accurate results, the usual industrial practice is to compromise by using an intermediate size. In general, an intelligent use of amplitude data is not possible. An example is the case of larger flaws and larger transducers where amplitude is within the nonlinear range to the extent that one cannot associate large amplitudes with large flaws.

Several actions can be taken to minimize or eliminate the above limitations. A very basic one would be to reduce or eliminate the dependence on signal amplitude as an indicator of defects. Recognizing that such a change is so major that early action is unlikely, other possibilities are suggested:

- Minimize equipment variability by standardizing. Pick either tuned system or broad band, but not both.
- Minimize the human variable through automation, special training, etc.
- Use as many beam angles and traverses from as many surfaces as economically feasible to minimize inherent limitations in defect detection.
- Move toward reference blocks containing real defects not drilled holes.
- Minimize coupling problems by suitable surface preparation.
- Have NDE input into component design to optimize material properties, joint design, welding procedure.
- Modify the codes to eliminate or minimize UT in the noncritical central portion of components. Based on LEFM, flaws in the region surrounding the neutral axis have minimal safety significance. This approach should eliminate a large number of geometric indicators.
- Consider the feasibility of varying the recording and analysis thresholds as functions of stress intensity factors. This approach would drop DAC levels to 5 to 10% at the surface, rising rapidly as one moves away from the surface.
- Use LEFM, Elastic-Plastic Fracture Mechanics (EPFM), and/or General Yield Fracture Mechanics (GYFM) to establish necessary UT sensitivity flaw requirement.
- Minimize beam attenuation, etc., through appropriate control of material quality and fabrication process, particularly welding.

EXERCISE 1

- Level 1 solution can be taken to minimize or eliminate the above 1 mile-  
long. A very basic one would be to reduce or eliminate the dependence on sig-  
nal amplifiers as an indicator of defects. Research has shown that such a method is  
notionally that early sector is usually, other possibilities are suggested:
  - Minimize equipment variability by standardizing. Test with a fixed  
system of ground leads, but not data.
  - Minimize the human variable through automation, sector or wiring  
etc.
  - Use as many beam angles and traveled from as many sectors as  
economically feasible to minimize potential falsification in defect  
detection.
  - Use lower reference lines containing non-defects as detailed  
below.
  - Minimize complex problems by suitable sector presentation.
  - Have the final data computer design to detect the actual properties  
total design, wiring procedure.
  - Minimize the need to eliminate or minimize it in the non-defect can-  
diate portion of components. Used in LEM, also in the region sur-  
rounding the defect. Use a variable inductance circuit, etc. (see later).
  - Minimize the need to eliminate a large sector of geometric tolerances.  
Consider the feasibility of varying the recording mechanism  
to detect as a function of stress intensity factors. This approach  
would vary the level to keep the at the surface, rising rapidly as  
one moves away from the surface.
  - Use CRR, Electro-Phase Pattern Reference (EPR), and/or similar  
type fracture detection methods for the necessary of sensitivity  
the instrument.
  - Minimize the detection etc., through automatic control of wave-  
length, voltage and frequency power, particularly when

- 4.2.1 Rummel, W. D. and Rathke, R. A., "Detection and Measurement of Fatigue Cracks in Aluminum Alloy Sheet by Non-Destructive Evaluation Techniques." Prevention of Structural Failure: The Role of Quantitative Non-Destructive Evaluation, T. D. Cooper and P. F. Packman, eds., American Society for Metals, pp. 146-160, 1975.
- 4.2.2 Packman, P. F., et al., "Definition of Fatigue Cracks Through Nondestructive Testing." J. Mater. 4:666-700, 1969.
- 4.2.3 Packman, P. F., "Fracture Toughness and NDT Requirements for Aircraft Design." Nondestructive Testing, pp. 314-324, December 1973.
- 4.2.4 Packman, P. F., "Status of Non-Destructive Inspection Techniques with Special References to Welding Defects." Proceedings of Japan-U.S. Seminar, T. Kanazawa and A. S. Kobayaski, eds., Univ. of Tokyo Press, Tokyo, Japan, 1973.
- 4.2.5 Caustin, E. L., "State of Art NDE in Quantitative Inspection." Proceedings of the Interdisciplinary Workshop for Quantitative Flaw Definition. AFML-TR-74-238, USAF Technical Report, June 17-20, 1974.
- 4.2.6 Hagamaier, D., "State-of-the-Art Inspection of Aircraft Structures." Prevention of Structural Failure: The Role of Quantitative Nondestructive Evaluation, T. D. Cooper and P. F. Packman, eds., American Society for Metals, pp. 161-187, 1975.
- 4.2.7 Herr, J. C., "Human Factors in NDE." Prevention of Structural Failure: The Role of Quantitative Non-Destructive Evaluation, T. D. Cooper and P. F. Packman, eds., American Society for Metals, pp. 226-241, 1975.
- 4.2.8 Lord, R. J., "Evaluation of the Reliability and Sensitivity of NDT Methods for Titanium Alloys." AFML-TR-73-107, Vol. II, USAF Technical Report, June 1974.
- 4.2.9 Corbly, D. M., Packman, P. F. and Pearson, H. S., "The Accuracy and Precision of Ultrasonic Shear Wave Flaw Measurements as a Function of Stress in the Flaw." Mater. Eval. 28:103-110, May 1970.
- 4.2.10 Padilla, V. E. and Parks, J. W., "Definition of Fatigue Crack Geometry by Eddy Current Techniques." American Society of Nondestructive Testing 7th Symposium on NDT, San Antonio, Texas, 1969.
- 4.2.11 Pettit, D. E. and Hoepfner, D. W., "The Influence of Nondestructive Inspection Parameters on the Preproof and Postproof Fatigue Crack Detection Limits for Fracture Mechanics Applications." Proceedings of 9th Symposium on NDE, San Antonio, Texas, pp. 434-441, April 25-27, 1973.

- 4.2.12 Yee, B. G. W., "Assessment of NDE Reliability Data." NASA-CR-134994, National Aeronautics and Space Administration, October 1976.
- 4.2.13 Birchak, J. R. and Gardner, C. G., "Comparative Ultrasonic Response of Machined Slots and Fatigue Cracks in 7075 Aluminum." Mater. Eval., pp. 275-280, December 1976.
- 4.3.1 Katz, L. R. and Caplan, J. S., "Shrinkage Voids in Reactor Vessel Plate Materials." 1st International Conference on Periodic Inspection, Institute of Mechanical Engineers, London, England, pp. 101-106, 1970.
- 4.3.2 Caplan, J. S., "The Ultrasonic Shop Map and Its Use in Pre-Service Inspection." 2nd International Conference on Periodic Inspection, Institute of Mechanical Engineers, London, England, pp. 19-28, 1974.
- 4.3.3 "The Doel Defect." Nucl. Eng. Int., p. 543, July 1974.
- 4.3.4 Trumpfheller, R., "Reliability in Non-Destructive Examination." International Conference on NDE, Lindau, FRG, May 1981.
- 4.5.1 Yee, B. G. W. and Couchman, J. C., "Application of Ultrasound to NDE of Materials." IEEE Trans. Sonics Ultrason. SU-23(5):299-305, September 1976.
- 4.5.2 Thompson, D. O., "Interdisciplinary Program for Quantitative Flaw Definition, Semi-Annual Report." July 1, 1977 to July 1, 1978 for Advanced Research Projects Agency by Rockwell International, SCC 595 32SA, 1978.
- 4.5.3 Haines, N. F., "The Reliability of Ultrasonic Inspection." IAEA-SM-218/41, International Symposium on Application of Reliability Technology to Nuclear Power Plants, Vienna, Austria, October 10-13, 1977.
- 4.5.4 Thompson, R. B. and Evans, A. G., "Goals and Objectives of Quantitative Ultrasonics." IEEE Trans. Sonics Ultrason. SU-23(5):292-299, September 1976.
- 4.5.5 Birks, A. S. and Lawrie, W. E., "Improved Repeatability in Ultrasonic Examination." Also "Ultrasonic Testing System Standardization Requirements." Weld. Res. Council. Bull. 235, February 1978.
- 4.5.6 Hislop, J. D., "Flaw Size Evaluation in Immersed Ultrasonic Testing." Nondestructive Testing, pp. 182-192, August 1967.
- 4.5.7 Bastien, P., "Difficulties in the Ultrasonic Evaluation of Defect Size." Nondestructive Testing 1(5):147-151, February 1968.

- 4.5.8 Lautzenheiser, C. E., Whiting, A. R. and McElroy, J. T., "Ultrasonic Variables Affecting Inspection." 3rd International Conference on Periodic Inspection, pp. 107-111, 1976.
- 4.5.9 Silk, M. G. and Lidington, B. H., "The Potential of Scattered or Diffracted Ultrasound in the Determination of Crack Depth." Nondestructive Testing, pp. 146-151, June 1975.
- 4.5.10 Mundry, E., "Defect Evaluation of Ultrasonics." Nondestructive Testing, pp. 290-297, October 1972.
- 4.5.11 McDearman, W. R., Benton, L. S. and Pade, E. R., "Phase 1—Acoustic Comparison of Calibration Blocks." MML-75-111, Combustion Engineering, July 29, 1975.
- 4.5.12 Gothard, M. E., et al., "Accuracy and Repeatability in Section XI Ultrasonic Test Techniques." Phase I, Task A, MML-76-138, Combustion Engineering, April 29, 1977.
- 4.5.13 Gothard, M. E., et al., "Accuracy and Repeatability in Section XI Ultrasonic Test Techniques." Phase II, Task A, MML-76-138, Combustion Engineering, April 29, 1977.
- 4.5.14 Taylor, T. T. and Selby, G. P., "Evaluation of ASME Section XI Reference Level Sensitivity for Initiation of Ultrasonic Inspection Examination." NUREG/CR-1957, U.S. Nuclear Regulatory Commission, Washington, D.C., 1981. Also PNL-3692, Pacific Northwest Laboratory, Richland, Washington, 1981.
- 4.5.15 Cook, J. F., "ANC UT Examination of EPRI BWR Piping Welds." NP-797-SR, Electric Power Research Institute, Palo Alto, California, August 1978.
- 4.5.16 "Limitations Inherent in the Use of Ultrasonics for the Examination of Welds." Weld. World 6(4):31-33, 1968.
- 4.5.17 Dau, G. J., ed., Proceedings of NDE Experts Workshop on Austenitic Pipe Inspection, SR-30, Electric Power Research Institute, Palo Alto, California, February 1976.
- 4.5.18 Coffey, J. M., "An Experimental Study of the Effects of Surface Finish, as Produced by Hand Grinding, on Ultrasonic Inspection." NW/SSD/RR/85/79, Central Electricity Generating Board, July 1979.
- 4.5.19 Wüstenberg, H. and Mundry, E., "Limiting Influences on the Reliability of Ultrasonic In-Service Inspection Methods." Paper C 112/74, 2nd Conference on Periodic Inspection, Institute of Mechanical Engineers, London, England, 1974.

- 4.5.20 Flach, W. T. and Watson, P. D., "Effects of Construction Practices on the Ultrasonic Inspectability of Piping Welds." Paper Summaries, American Society of Nondestructive Testing, National Spring Conference, April 3-6, 1978.
- 4.5.21 Wüstenberg, H. and Engl, G., "Recent Developments in Ultrasonic Inspection of Reactor Pressure Vessel Weldments in the Federal Republic of Germany." Post-Conference Seminar, NDE in Relation to Structural Integrity, Structural Materials in Reactor Technology Conference, Paris, France, August 24, 1981.
- 4.5.22 Meyer, H. J., "Discussion Periodic Inspection of Pressure Vessels." 1st Conference on Periodic Inspection of Pressure Vessels, Institute of Mechanical Engineers, London, England, 197:246-249, 1972.
- 4.5.23 Anderson, P. and Gavin, P. A., "Ultrasonic Inspection of Austenitic Cladded Steel." KAPL-P4045, Conference 76D506, Eastern Testing Conference, Hartford, Connecticut, May 1976.
- 4.5.24 Böttcher, B., Schulz, E. and Wüstenberg, H., "A New Method of Crack Depth Determination in Ultrasonic Materials Testing." 7th International Conference on NDT, Warsaw, Poland, 1973.
- 4.5.25 Bilgutay, M. M., et al., "Flaw-to-Grain Echo Enhancement." Proceedings of Ultrasonics International Conference, Graz, Austria, May 15-18, 1979.
- 4.5.26 Silk, M. G. and Lidington, B. H., "An Evaluation of Single Probe Bulk-Wave Time-Delay Technique in Sizing Cracks in Steel." NDT Int., pp. 129-134, June 1977.
- 4.5.27 Baikie, B. L., et al., "Ultrasonic Inspection of Austenitic Welds." J. Br. Nucl. Energy Soc. 15(3):257-261, July 1976.
- 4.5.28 Yoneyama, H., Shibata, S. and Kishigami, M., "Ultrasonic Testing of Austenitic Stainless Steel Welds—False Indications and the Cause of Their Occurrence." Nondestructive Testing, pp. 3-8, February 1978.
- 4.5.29 Serabian, S., "Influence of Attenuation Upon the Weld Interrogation Distance-Amplitude Curve." Mater. Eval., pp. 265-274, December 1976.
- 4.5.30 Reinhart, E. R., "A Study of In-Service Ultrasonic Inspection Practice for BWR Piping Welds." NP-436-SR, Electric Power Research Institute, Palo Alto, California, August 1977.
- 4.5.31a Kupperman, D. S. and Reimann, K. J., "Effect of Shear-Wave Polarization on Defect Detection in Stainless Steel Weld Metal." Ultrasonics, pp. 21-27, January 1978.



- 4.5.31b Kupperman, D. S. and Reimann, K. J., "Acoustic Properties of Stainless Steel Weld Metal." NDE in the Nuclear Industry, American Society for Metals, pp. 370-380, 1978.
- 4.5.32 Tomlinson, J. R., Wagg, A. R. and Whittle, M. J., "Ultrasonic Inspection of Austenitic Welds." NDE in the Nuclear Industry, American Society for Metals, pp. 64-83, 1978.
- 4.5.33 Neumann, E., et al., "Development and Improvement of Ultrasonic Testing Techniques for Austenitic Nuclear Components." NDE in the Nuclear Industry, American Society for Metals, pp. 84-105, 1978.
- 4.5.34 McGaughey, W. C. and Lautzenheiser, C. E., "Detectability of Intergranular Stress Corrosion Cracking Using Field Proven Ultrasonic Techniques." CSNI Specialist Meeting "On the Applicability of Ultrasonic Testing Techniques for Coarse Grain Austenitic Welds," Brussels, Belgium, May 29-30, 1980.
- 4.5.35 Erhard, A., et al., "Reliability and Redundancy in Ultrasonic Flaw Sizing Methods." NDE in the Nuclear Industry, American Society for Metals, pp. 253-268, 1980.
- 4.5.36 "Limitations of Radiography in Detecting Crack-Like Defects in Thick Sections." British Engine Insurance, England, Technical Report, March 1962, Vol. IV, pp. 57-87, October 1970.
- 4.5.37 Macecek, M., "Metallurgical Causes of Difficulties with Ultrasonic Inspection of Austenitic Welds." 78-PVP-8, Transactions of the ASME, Journal of Applied Mechanics, 1978.
- 4.6.1 Digiacomo, G., Corisci, J. R. and Goldspiel, S., "An Ultrasonic Method for Measuring Crack Depth in Structural Weldments." Mater. Eval., pp. 189-204, September 1970.
- 4.6.2 Hudgell, R. J., Morgan, L. L. and Lumb, R. F., "Nondestructive Measurement of the Depth of Surface Breaking Cracks Using Ultrasonic Rayleigh Waves." Br. J. Nondestr. Test., pp. 144-149, September 1974.
- 4.6.3 Minton, W. C., "Flaw Sizing in Piping Welds with Ultrasonics." Nuclear Power Education Seminar, Southwest Research Institute, San Antonio, Texas, 1978.
- 4.6.4 Chapman, H., "Defect Size Estimation with Ultrasonic Angle Beam Probes and the DGS Diagram." Report 8-11, 6th International Conference on NDT, Hanover, Germany, pp. 122-133, 1970.
- 4.6.5 Corbly, D. M., "Ultrasonic Signal Response as a Function of Crack Closure." USAF Materials Laboratory, Wright-Patterson AFB, Fairborn, Ohio, Paper Summaries, American Society of Nondestructive Testing National Spring Conference, New Orleans, Louisiana, pp. 72-77, April 3-6, 1978.

- 4.6.6 Ibrahim, S. I. and Whittaker, V. N., "The Influence of Crack Topography and Compressive Stresses on the Ultrasonic Detection of Fatigue Cracks in Submerged Arc Welds." Br. J. Nondestr. Test., pp. 233-240, 1981.
- 4.6.7 Wooldridge, A. B. and Steel, G., "The Influence of Crack Growth Conditions and Compressive Stress on the Ultrasonic Detection and Sizing of Fatigue Cracks." NW/SSD/RR/45/80, Central Electricity Generating Board, 1980.
- 4.6.8 Bradfield, G., "Correlating Echo and Flaw Magnitudes." Nondestructive Testing 1(5):317-318, 1968.
- 4.6.9 Lidington, B. H. and Silk, M. G., "Crack Depth Measurements Using a Single Surface Wave Probe." Br. J. Nondestr. Test., pp. 165-167, November 1975.
- 4.6.10 Silk, M. G. and Lidington, B. H., "A Preliminary Study of the Effects of Defect Shape and Roughness on Ultrasonic Size Estimation." Nondestructive Testing, pp. 27-32, February 1975.
- 4.6.11 Gurvich, A. K. and Kuzmina, L. I., "Investigation of Methods of Measuring the Apparent Height of Defects in the Case of Scanning with an Inclined Probe." Sov. J. Nondestr. Test., pp. 678-684, 1971.
- 4.6.12 Wüstenberg, H., Kutzner, J. and Engl, G., "Dependence of Echo Amplitude on Defect Orientation in Ultrasonic Examinations." 8th World Conference on NDT, Cannes, France, Paper 3H-4, 1976.
- 4.6.13 Serabian, S. and Lawrie, W. E., "A Detection Model for Pulse Echo Ultrasonics." Paper Summaries, 37th National Fall Conference, American Society of Nondestructive Testing, pp. 133-145, Fall 1977.

CHAPTER 5

FLAW SIZING AND LOCATION

CHAPTER 2

PLASMA SPINNING AND FIBRILATION

## CONTENTS

5.1	INTROOUCTION . . . . .	5.1.1
5.2	UT FLAW SIZING TECHNIQUES . . . . .	5.2.1
5.2.1	dB Drop . . . . .	5.2.1
5.2.2	Vanishing Echo . . . . .	5.2.1
5.2.3	ASME Section V . . . . .	5.2.2
5.2.4	The AVG (DGS) Diagram . . . . .	5.2.2
5.2.4.1	Strengths and Weaknesses . . . . .	5.2.2
5.2.4.2	Relationships . . . . .	5.2.11
5.2.4.3	Calibration Blocks . . . . .	5.2.13
5.2.4.4	Beam Attenuation . . . . .	5.2.14
5.2.4.5	Frequency . . . . .	5.2.16
5.2.4.6	Pulse Strength . . . . .	5.2.18
5.2.5	Comparison of Sizing Techniques . . . . .	5.2.20
5.3	FACTORS INFLUENCING ACCURACY OF SIZING . . . . .	5.3.1
5.3.1	Statistical Treatment . . . . .	5.3.1
5.3.1.1	Individual Error . . . . .	5.3.2
5.3.2	External Variability . . . . .	5.3.7
5.3.3	Theoretical Limitations . . . . .	5.3.7
5.3.4	Factors Affecting Echo Strength . . . . .	5.3.10
5.3.4.1	Spheres . . . . .	5.3.10
5.3.4.2	Cylinders . . . . .	5.3.10
5.3.4.3	Flat Plate . . . . .	5.3.10
5.3.4.4	Rough Cracks . . . . .	5.3.10

5.3.5	Problems in Detection . . . . .	5.3.11
5.3.5.1	Defect . . . . .	5.3.11
5.3.5.2	Equipment and Procedure . . . . .	5.3.11
5.3.5.3	Signal-to-Noise Ratio . . . . .	5.3.11
5.3.6	Code Criteria Relevant to Sensitivity . . . . .	5.3.11
5.3.6.1	Minimum Detectable Flaw Size in Example . . . . .	5.3.12
5.3.7	Influence of Defect Surface Roughness . . . . .	5.3.13
5.3.7.1	Theoretical Bases for Figure 5.3.3 . . . . .	5.3.14
5.3.8	Detection Probability for Large Rough Flaws . . . . .	5.3.15
5.3.9	Limitations in Flaw Sizing . . . . .	5.3.16
5.4	DEFECT SIZING--PROBE MOVEMENT . . . . .	5.4.1
5.4.1	Russian Approach . . . . .	5.4.1
5.4.2	Sizing of Surface Flaws . . . . .	5.4.3
5.4.2.1	Artificial Flaws . . . . .	5.4.3
5.4.2.2	Real Surface Flaws . . . . .	5.4.9
5.4.2.3	Real and Artificial Flaws . . . . .	5.4.17
5.4.3	Sizing Cladding Cracks . . . . .	5.4.17
5.5	OTHER SURFACE SIZING TECHNIQUES . . . . .	5.5.1
5.5.1	Delta Scan and Shear Wave . . . . .	5.5.1
5.5.1.1	Theoretical Study . . . . .	5.5.1
5.5.1.2	Frequency Modulation . . . . .	5.5.2
5.5.2	Surface (Rayleigh) Waves . . . . .	5.5.2
5.5.2.1	Time Delay . . . . .	5.5.4
5.5.3	Eddy Current . . . . .	5.5.5
5.5.4	Image Reconstruction . . . . .	5.5.7

5.5.5	Possible Limitations	. . . . .	5.5.11
5.5.6	Opposite Surface	. . . . .	5.5.13
5.5.6.1	Diffraction	. . . . .	5.5.15
5.6	EMBEDDED FLAWS	. . . . .	5.6.1
5.6.1	Artificial Flaws	. . . . .	5.6.1
5.6.2	Real Flaws	. . . . .	5.6.1
5.6.2.1	Effect of Cladding	. . . . .	5.6.1
5.6.2.2	Probe-to-Specimen Contact	. . . . .	5.6.3
5.6.2.3	ASME XI NDE-UT	. . . . .	5.6.4
5.6.2.4	Undercladding Cracks	. . . . .	5.6.5
5.6.2.5	Other Detection Techniques	. . . . .	5.6.9
5.6.2.6	Defect Sizing	. . . . .	5.6.11
5.6.2.7	Geometric Effects	. . . . .	5.6.23
5.7	CONCLUSIONS	. . . . .	5.7.1
5.8	REFERENCES	. . . . .	5.8.1

## FIGURES

5.1.1	a) Typical Flaw Size Frequency Distribution $\phi(a)$ ; $a_u$ is the Maximum Flaw Size and $a_m$ is the Allowable Flaw Size; b) Ideal Flaw Detection Function $\phi'(a)$ Required for Quantitative Failure Prediction . . . . .	5.1.2
5.1.2	Probability of Flaw Detection for Specific Sensitivity Setting as Function of Flaw Size, Showing "False" Signals and Indicating 95% Confidence Level . . . . .	5.1.3
5.1.3	Flaw Detection Function Derived from Figures 5.1.1a and 5.1.2 . . . . .	5.1.3
5.1.4	Example of Flaw Size Measurement Required for Quantitative Ultrasonics Showing Typical Confidence Band and Detectability Limit, $a_0$ . . . . .	5.1.4
5.2.1	General Distance Amplification Size Display Picture . . . . .	5.2.3
5.2.2a	AVG Diagram Obtained in Water, Probe Type Q2SX . . . . .	5.2.4
5.2.2b	AVG Diagram Obtained in Water, Probe Type Q4SX . . . . .	5.2.5
5.2.3a	AVG Diagram Obtained in Steel, Probe Type Q2SX . . . . .	5.2.6
5.2.3b	AVG Diagram Obtained in Steel, Probe Type Q4SX . . . . .	5.2.6
5.2.4	Comparison of Various Artificial and Natural Defects as They Influence the Shape of a DGS Diagram . . . . .	5.2.10
5.2.5	Relation of dB Scales and the Commonly Used Percentage Scale . . . . .	5.2.11
5.2.6	Distance-Amplitude Curve; Plot of the Variation of Sound Intensity Along the Beam Axis in Water, Produced with a Spherical Target . . . . .	5.2.12
5.2.7	Distance-Amplitude Curves for Three Probes, Showing How the Shape of the Curve Varies with the N-Point . . . . .	5.2.13
5.2.8	Comparison of Actual Defects in Steel Forgings and Flat-Bottomed Holes Giving Identical Indications . . . . .	5.2.15
5.2.9	Flaws in Forged Steel . . . . .	5.2.16
5.2.10	Flaws in Forged Titanium Alloy . . . . .	5.2.17
5.2.11	Flaws in Forged INCO 901 . . . . .	5.2.17



5.2.12	A DGS Diagram Calculated by the Double-Probe Method for a Quartz Probe of 10-mm Dia at 2 MHz . . . . .	5.2.19
5.2.13	A DGS Diagram for a Normal Probe of 10-mm Dia at 2 MHz Calculated by the Single-Probe Method . . . . .	5.2.20
5.2.14	A DGS Diagram for an Angle Probe Calculated by the Single-Probe Technique . . . . .	5.2.21
5.3.1	Limit of Resolution of an Ultrasonic Test . . . . .	5.3.9
5.3.2	Echo Amplitude from Edge of Semi-Infinite Straight Cracks Relative to Echo from Infinite Mirror at Same Range, R . . . . .	5.3.12
5.3.3	Probable Values of Echo Amplitude, as a Function of Defect's Surface Roughness . . . . .	5.3.14
5.4.1	Determination of the Apparent Height of Defects . . . . .	5.4.2
5.4.2	Calculated Dependences of the Apparent Height of a Reflector with a Circular Scattering Indicatrix on its Depth . . . . .	5.4.4
5.4.3	Data from Sawn and Spark-Eroded Slits for 5-MHz Angle Probes . . . . .	5.4.9
5.4.4	Accuracy of Crack Indication versus Applied Stress, ksi . . . . .	5.4.18
5.4.5a	Schematic of Effect of Stress on Reflected Peak . . . . .	5.4.19
5.4.5b	Schematic Showing Decrease in Accuracy and Increase in Precision of Ultrasonic Indications . . . . .	5.4.20
5.4.6	CRT Pattern from Shear-Wave Angle Probe . . . . .	5.4.21
5.4.7	Mechanism and Dimensions of Longitudinal Wave Twin-Crystal Angle Probe . . . . .	5.4.22
5.4.8	Variation in Directional Characteristics from Difference in Refraction Angle of Angle-Beam Probe . . . . .	5.4.22
5.5.1	Estimates of Crack Depth in a T-Butt Weld Using a Surface-Wave Pulse Echo Technique . . . . .	5.5.3
5.5.2a	Actual Crack Profile Compared with Ultrasonic; Old Timing . . . . .	5.5.6
5.5.2b	Actual Crack Profile Compared with Ultrasonic; New Timing . . . . .	5.5.7

5.5.3	Relationship Between Actual and Predicted Crack Depth; Eddy Current, 7075-T73 Aluminum . . . . .	5.5.8
5.5.4	Correlations of Eddy Current Responses with Crack Depths in Titanium . . . . .	5.5.9
5.5.5	a) Comparison of Responses from Three Kinds of Defects; b) Responses from Crack Perpendicular to Hole Axis . . . . .	5.5.9
5.5.6	Reconstruction . . . . .	5.5.10
5.5.7	Reconstruction: Results . . . . .	5.5.11
5.5.8	Estimation of Depth of Fatigue Cracks by Rayleigh Wave Transmission . . . . .	5.5.13
5.5.9a	Estimation of Depth Profile of Fatigue Cracks by Rayleigh Mode Conversion . . . . .	5.5.14
5.5.9b	Estimation of Depth Profile of Fatigue Cracks by Rayleigh Mode Conversion . . . . .	5.5.15
5.5.10a	Estimates of Crack Depth in a T-Butt Weld Using Ultra- sonic Diffraction with the Probes Placed on the Face Opposite the Weld, Compared with the Actual Crack Profile . . . . .	5.5.16
5.5.10b	Estimates of Crack Depth in a T-Butt Weld Using Diffracted Ultrasound, Compared with the Actual Crack Profile . . . . .	5.5.16
5.5.11	a) Diffracted Ultrasound used for Crack Depth Measure- ment with Cracks on the Same Surface as the Probe; b) Ultrasonic Diffraction Techniques also used when Cracks are Present on the Surface Opposite to the Probe . . . . .	5.5.17
5.6.1	Relation Between Actual Defect Size and Indicated Length of Flaw . . . . .	5.6.2
5.6.2	Comparison Between the Sizes of Defects Measured by Ultrasonic and Radiographic Testing . . . . .	5.6.4
5.6.3	Depth-Amplitude-Drop Relation . . . . .	5.6.7
5.6.4	Comparison of Estimates of Size of Reflectors Inclined at 60° . . . . .	5.6.10
5.6.5	Comparison of Defect Lengths Estimated by Various Inspection Methods to Actual Defect Lengths . . . . .	5.6.16
5.6.6	Relation Between $\mu_L B$ and $\zeta L$ . . . . .	5.6.17

5.6.7	Relation Between $x_L$ and $s_L$	. . . . .	5.6.17
5.6.8	Relation Between $u_{HA}$ and $s_H$	. . . . .	5.6.18
5.6.9	Relation Between $u_{HB}$ and $s_H$	. . . . .	5.6.18

TABLES

5.2.1	Results of Tests on the Forged Piece . . . . .	5.2.7
5.2.2	Typical Results of Tests to Check the AVG Diagram . . . . .	5.2.14
5.2.3	Equations for Empirical Backwalls . . . . .	5.2.18
5.3.1	Combining Various Sources of Variability . . . . .	5.3.3
5.3.2	Error Estimates for Various Sources of Variation . . . . .	5.3.4
5.3.3	Error Values for Various Defects . . . . .	5.3.4
5.3.4	Error Spreads Implied by Various Values of the Standard Deviation . . . . .	5.3.5
5.3.5	Standard Deviation for Various UT Measuring Techniques . . . . .	5.3.6
5.3.6	Individual Sources of Variability . . . . .	5.3.6
5.3.7	Simplified Equations for Relative Echo Amplitude . . . . .	5.3.8
5.3.8	Examples of Probabilities of Detecting Rough, Through-Wall Cracks with a 70°, 2.5-MHz Probe . . . . .	5.3.16
5.3.9	Defect Diameter-Wavelength-Beam Diameter Relationships . . . . .	5.3.18
5.4.1	Ultrasonic Shear-Wave Crack Indications . . . . .	5.4.5
5.4.2	Artificial Crack Depth Estimates by Time Delay and from Amplitude . . . . .	5.4.6
5.4.3a	Observed Maxima and Minima . . . . .	5.4.8
5.4.3b	Predicted and Experimental Results . . . . .	5.4.8
5.4.4	Estimates of Depth of Artificial Slits . . . . .	5.4.10
5.4.5	NDE Inspection of Aluminum Cylinders . . . . .	5.4.12
5.4.6	NDE Inspection of Steel Cylinders . . . . .	5.4.13
5.4.7	Actual versus Measured Crack Size in Pressure Tubes . . . . .	5.4.14
5.4.8	Summary of Maximum Crack Lengths Possible for Zero Indicated Crack Lengths and Test Accuracies for the Various Nondestructive Testing Techniques on the Four Alloys and Four Section Thicknesses . . . . .	5.4.15

5.4.9	Summary of Maximum Crack Depths Possible for Zero Indicated Crack Depths and Test Accuracies for the Ultrasonic-Shear and Delta-Testing Techniques on Four Alloys and Three Section Thicknesses . . . . .	5.4.16
5.4.10	Correlation Between Actual Crack Depth and Depth by Ultrasonics (L-wave) . . . . .	5.4.23
5.5.1	Estimates of the Depth of Natural Cracks, Using the Improved Surface-Wave Transmission Techniques . . . . .	5.5.4
5.5.2	Estimates of the Depth of Natural Cracks, Using the Maximum Echo Position for the Mode-Converted Shear Wave . . . . .	5.5.5
5.5.3	Degree of Agreement Between Crack Size Measurements Using a Cathetometer and the Single-Probe Technique at Normal Incidence . . . . .	5.5.18
5.6.1	Comparison of Flaw Sizes Estimated from Ultrasonic Test and Radiography . . . . .	5.6.3
5.6.2	Sizing of Defects with UT Plane Transducers, Both Contact and Immersion . . . . .	5.6.6
5.6.3	Sizing of Defects Located at Cladding—Base-Metal Interface . . . . .	5.6.8
5.6.4	Comparison of Actual Flaw Sizes and UT Estimate in Large Forgings . . . . .	5.6.9
5.6.5	Test Series Data . . . . .	5.6.12
5.6.6	Test Program—Outline and Terminology . . . . .	5.6.13
5.6.7	Statistical Data for Population Tested by Specified Method . . . . .	5.6.14
5.6.8	Specimen Details and Testing Conducted - Welding Institute Non-Planar Defects Program . . . . .	5.6.19
5.6.9	Positional and Size Data: Various Ultrasonic Techniques . . . . .	5.6.20
5.6.10	Specimen Details and Testing for Planar Defects - Welding Institute . . . . .	5.6.25
5.6.11	Details and Testing of Laboratory Specimens Having Complex Geometries - Welding Institute Planar Defects Program . . . . .	5.6.27



## CHAPTER 5

### FLAW SIZING AND LOCATION--WITH NDE

#### 5.1

#### INTRODUCTION

Thompson and Evans<sup>(5.1.1)</sup> described the next frontier for ultrasonics to be the provision of quantitative information needed to distinguish between small flaws that are benign with respect to failure and larger flaws that are critical with respect to failure. Figures 5.1.1 through 5.1.4, taken from their paper, nicely illustrate the ideal quantitative condition and the real semi-quantitative condition. Figure 5.1.1a is a typical flaw size frequency function with a large distribution of small flaws and very few large ones. If  $a_m$  is the maximum tolerable flaw size (division between flaws benign throughout life and flaws that may grow to critical size), the ideal NDE technique would detect nothing below  $a_m$  and everything above it (see Figure 5.1.1b). This is readily apparent in Figure 5.1.2 where a typical detection probability is superposed on the ideal step function for flaw detection. Figure 5.1.3 is the combined Figure 5.1.1a and the flaw detection probability portion of Figure 5.1.2. The boundaries assume a statistically significant number of NDE measurements. Figure 5.1.4 is a semi-idealized curve with a sharp flaw size--NDE detection cutoff  $a_0$  and a line comparing actual to measured flaw size. If truly quantitative, the line would have a 45° slope and there would be a one-to-one correlation. The confidence limits represent a return to real life with regard to sizing.

The authors<sup>(5.1.1)</sup> assess the significance of flaw profile and location. This is quoted verbatim:

Flaw profile definition is less important than flaw size determination, because  $Y^{(a)}$  is relatively invariant; typically  $Y$  varies between  $\pi^{1/2}$  and  $2/\pi^{1/2}$ . Therefore, strenuous efforts at defining the flaw shape are not merited. Similarly, flaw location although important, does not usually demand high accuracy because the stress in most components is not a strong function of location.

---

(a)  $Y$  is the flaw profile parameter usually given in terms of  $\phi$  or  $Q$ .

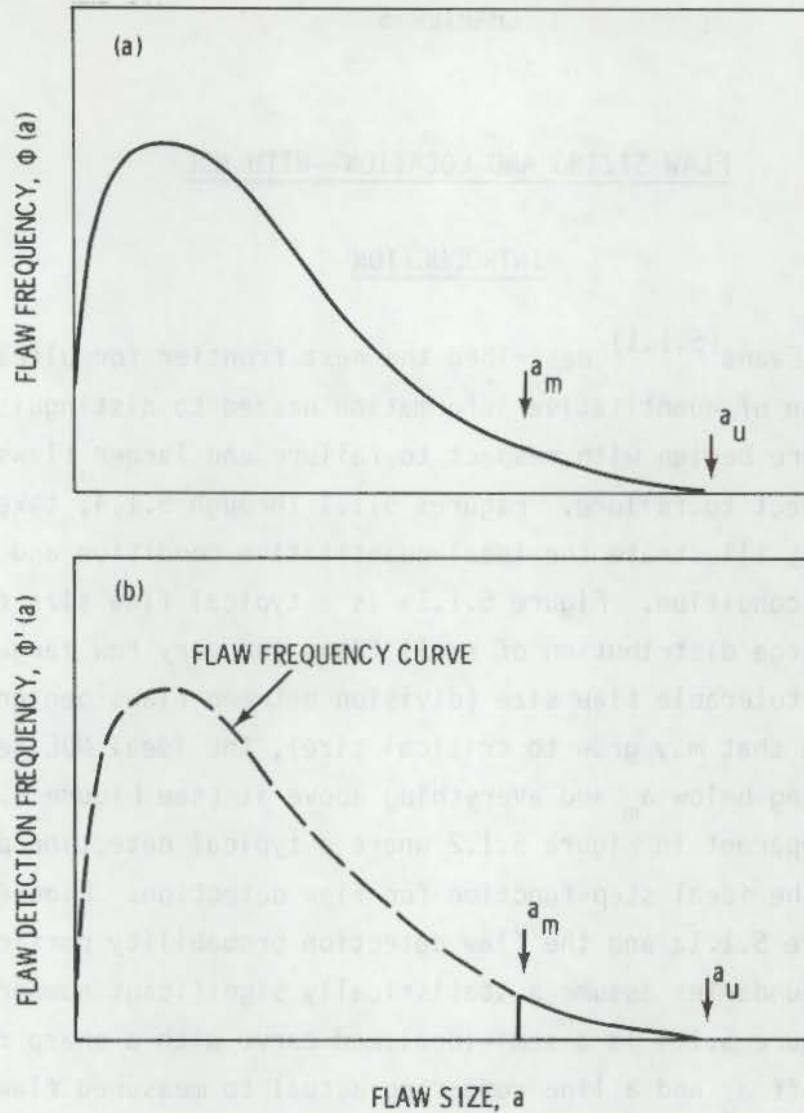


**FIGURE 5.1.1.** a) Typical Flaw Size Frequency Distribution  $\phi(a)$ ;  $a_u$  is the Maximum Flaw Size and  $a_m$  is the Allowable Flaw Size; b) Ideal Flaw Detection Function  $\phi'(a)$  Required for Quantitative Failure Prediction. Typical of bounded extremal Weibull distribution.

The authors are probably correct concerning the relative unimportance of flaw shape compared to flaw size; however, I would argue that flaw location can be quite significant, particularly where there is a high bending stress. Under these circumstances near-surface or surface flaws may become critical.



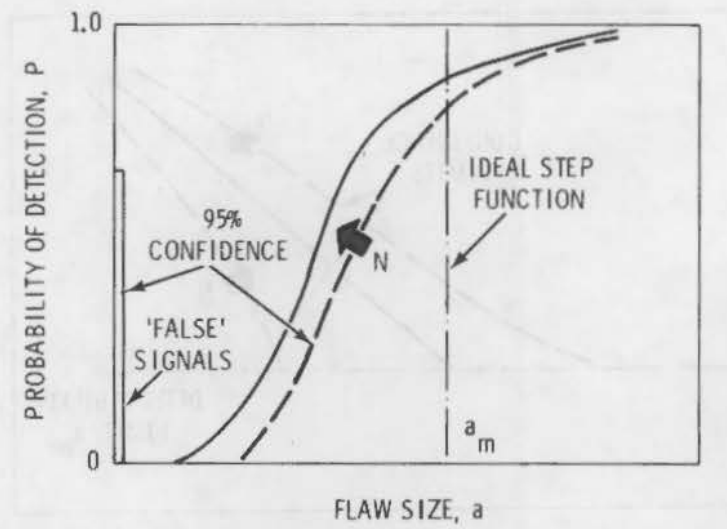


**FIGURE 5.1.2.** Probability of Flaw Detection for Specific Sensitivity Setting as Function of Flaw Size, Showing "False" Signals and Indicating 95% Confidence Level

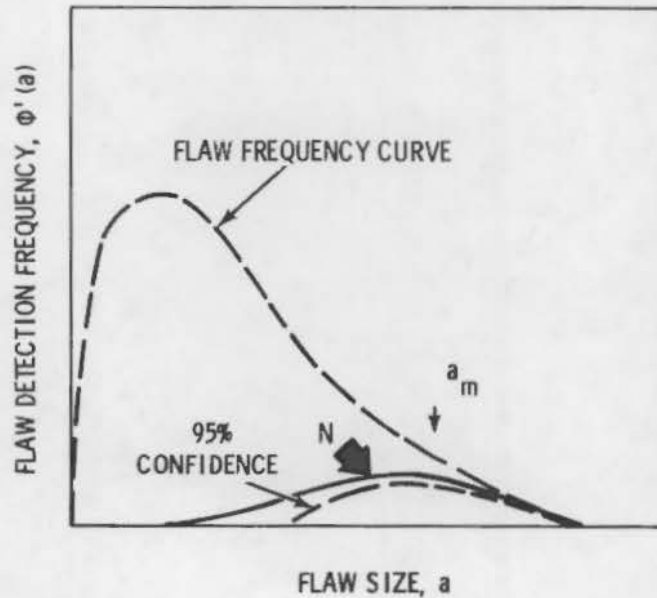


**FIGURE 5.1.3.** Flaw Detection Function Derived from Figures 5.1.1a and 5.1.2

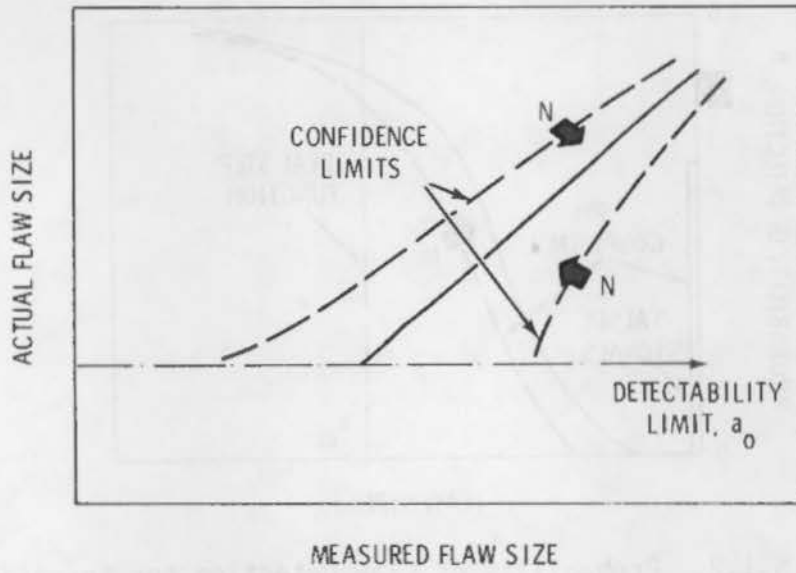


**FIGURE 5.1.4.** Example of Flaw Size Measurement Required for Quantitative Ultrasonics Showing Typical Confidence Band and Detectability Limit,  $a_0$



Several rather arbitrary dB values have been used to denote the points at which a flaw is considered to begin and end. A common one is to determine the maximum dB for a given flaw then move the search unit parallel to the flaw until the maximum dB drops by a specific amount. Critical dB drops that are routinely used are the following:

### 5.2.1 dB Drop

6 dB--AWS D1. 1-72 Structural Welding Code "Ultrasonic Testing of Groove Welds"

10 dB--BS 3923, Part I, Appendix B 1968 "Methods for Ultrasonic Examination of Welds"

20 dB--Same as for 10 dB plus IIW VC-265 1973 "Recommended Practice for the Ultrasonic Examination of Welds"

N.B.: for 20 dB a correction is made for effective beam width.

Values other than 6, 10 and 20 have been used; however, these are the most common.

In the case of surface flaws examined with Rayleigh waves, the same changes in signal amplitude used for conventional UT may be applied; e.g., 6 dB, 10 dB, and 20 dB. An alternate approach is to measure the time delay between the transmitted and received signals and correlate this with crack depth. The relative accuracy of the two approaches will be reviewed in a later section.

### 5.2.2 Vanishing Echo

Another approach is the vanishing echo. Here the maximum signal is determined and the probe is moved parallel (in both directions) until the echo vanishes. The total travel length is recorded.

The preceding techniques have been used extensively so that a large volume of data exist, permitting evaluation of their relative reliability.

### 5.2.3 ASME Section V

Another technique is contained in ASME Section V.<sup>(5.2.1)</sup> Unfortunately, no reports are available permitting an evaluation of its reliability. Basically, in this technique the UT equipment is calibrated against side-drilled holes in a reference block. Any flaw with DAC greater than 50% uses a 50% DAC cutoff to denote both ends of the flaw. If the maximum signal exceeds 100% DAC, the cutoff is 50% of the maximum signal. The procedure is extensively documented; however, nothing is given regarding its expected accuracy.

Once one has measured the flaw with the above techniques, it is possible to refine the measurements since it is recognized that amplitude values are dependent upon several parameters such as distance from surface, beam attenuation, and geometric features, all serving as sources of error.

### 5.2.4 The AVG (DGS) Diagram

One approach used extensively in Europe makes use of the Krautkrämer Abstand-Verstärkung-Grosse (AVG) Diagram.<sup>(5.2.2)</sup> The English translation is Distance-Gain-Size (DGS), and AVG or DGS are used interchangeably in describing the use of these diagrams. The parameters are defined as follows:

$$A(D) = \frac{\text{Distance between reflector and probe}}{\text{Near-field length}}$$

$$V(G) = \frac{\text{Echo amplitude at reflector (measured in dB)}}{\text{Reference echo amplitude}}$$

$$G(S) = \frac{\text{Diameter of reflector}}{\text{Diameter of probe}}$$

Figure 5.2.1 is the theoretical AVG (DGS) diagram. Limitations inherent in the AVG approach will be covered in a later section.

#### 5.2.4.1 Strengths and Weaknesses

The following paragraphs are one assessment of the strengths and weaknesses of the AVG (DGS) technique.

Bastien<sup>(5.2.3)</sup> in a report prepared by the French Nondestructive Testing Commission of the Committee for the Coordination of Welding Research (CCRS)

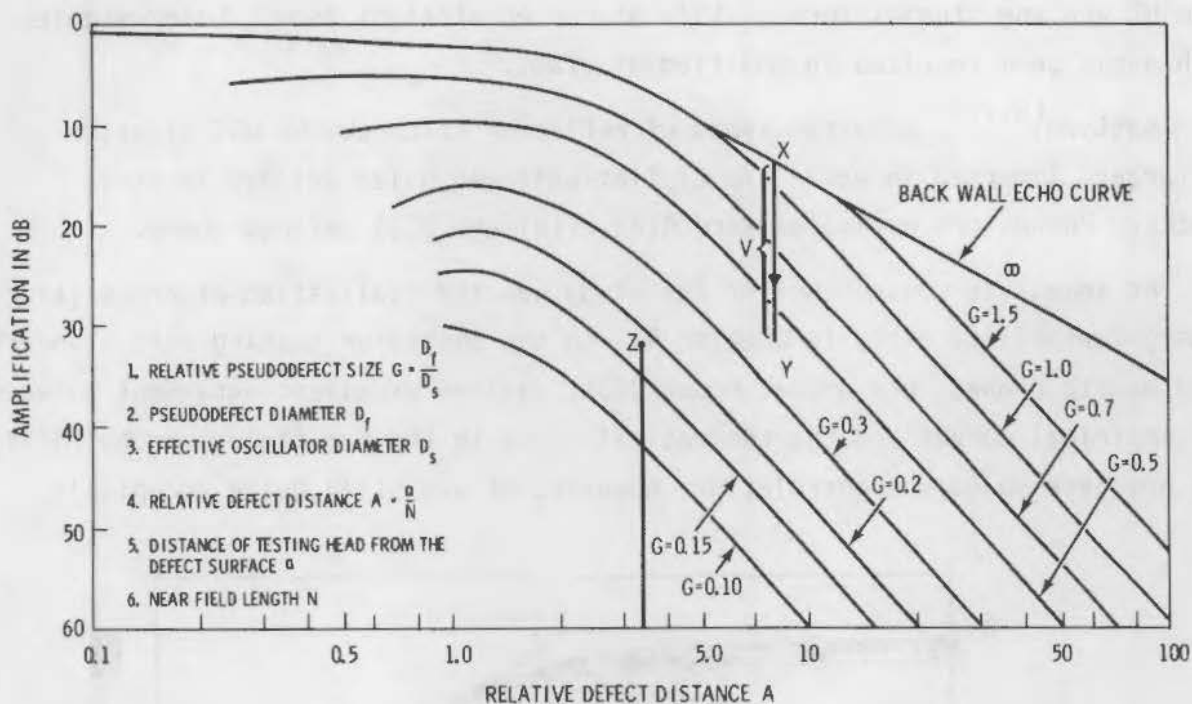


FIGURE 5.2.1. General Distance Amplification Size (AVG) Display Picture(5.2.2)

The amplification value  $V$  for the defect echo, measured at the defect (e.g., 18 dB), is not plotted from the zero point but from the back wall echo curve and in fact in each case from that point  $X$  which on the back wall echo curve corresponds to the relative thickness of the sheet metal being examined (for example, the value 8). By means of plotting of the amplification one comes to the point  $Y$ . Through the latter one draws a parallel to the abscissa which intersects in the point  $Z$  the parallels to the ordinate through the point of the relative spacing (for example, the value 3.5). That the thus-obtained point  $Z$  in the display picture is associated with a specific pseudodeflect diameter from which one derives the pseudodeflect diameter; it corresponds to the diameter of the defect under consideration. For further information one should refer to the literature.

discussed some of the simplifying assumptions that are inherent in the DGS diagram. Examples are the beam shape and the beam propagation. Both influence accuracy, but the errors are within acceptable bounds. The situation is less certain with regard to shape and orientation of defect. The original work leading to the development of the AVG diagram<sup>(5.2.2)</sup> was limited to straight

beam UT and the studies through 1970 also used straight beam. Later studies with angle beam resulted in modified diagrams.

Bastien<sup>(5.2.3)</sup> used two types of reflector to check the DGS diagram: 1) targets immersed in water and 2) flat-bottomed holes drilled in steel blocks. Parameters evaluated were  $A(D)$ ,  $V(G)$  and  $G(S)$  defined above.

An immediate consequence of the study was the realization of probe (transducer) variability cited in Chapter 4. In the immersion testing with standardized quartz probes, one probe, Probe Q2SX, yielded excellent agreement between the empirical curves and the theoretical lines in the far field. Probe (Q4SX) did not give so good a correlation; however, it was still quite acceptable.

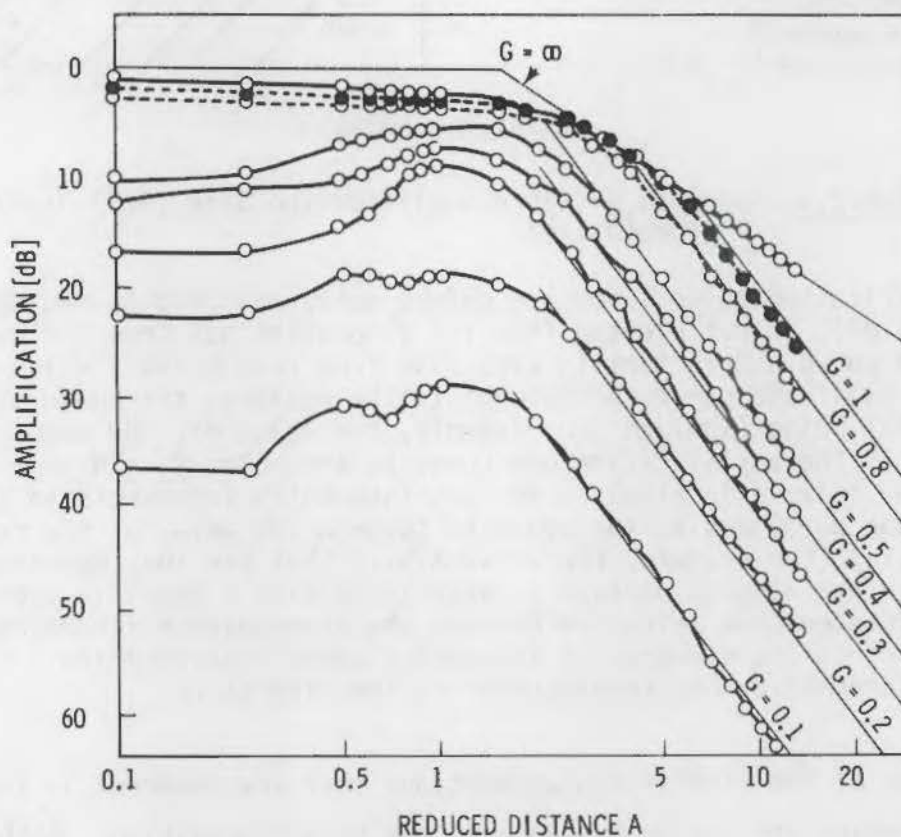


FIGURE 5.2.2a. AVG (DGS) Diagram Obtained in Water, Probe Type Q2SX.  $A$ ,  $V$  and  $G$  are reduced parameters which enable a direct comparison to be made between probes of different diameters and different frequencies.

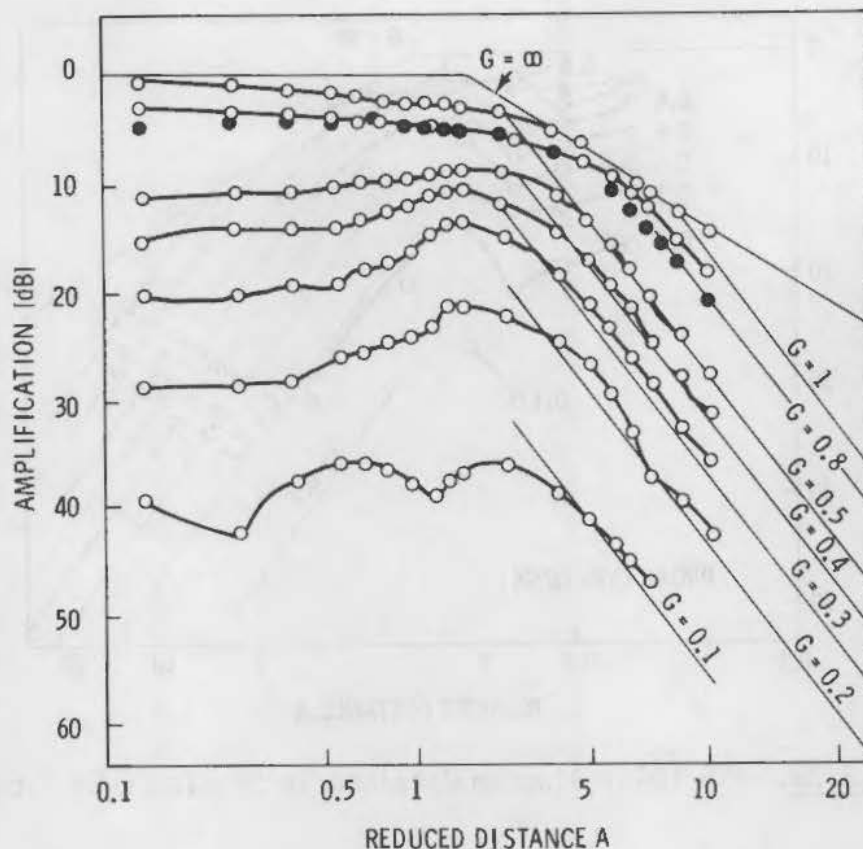


FIGURE 5.2.2b. AVG (DGS) Diagram Obtained in Water, Probe Type Q4SX. A, V and G are reduced parameters which enable a direct comparison to be made between probes of different diameters and different frequencies.

The degree of fit can be seen in Figures 5.2.2a and 5.2.2b. Other quartz probe tests differed more in the far field and all probes differed from one another in the near field.

Tests with barium titanate probes were quite unsatisfactory. The curves obtained were very closely packed in the near field and did not agree with the theoretical curves in the far field.

Figures 5.2.3a and 5.2.3b represent results made in steel, primarily in the near field. Agreement was good in the far field; but marked differences were observed in the near field and close-in far field. Some of the difference was attributed to poorer coupling plus the possibility that maximum signal in the near field does not correspond to coincidence of probe and hole axes.

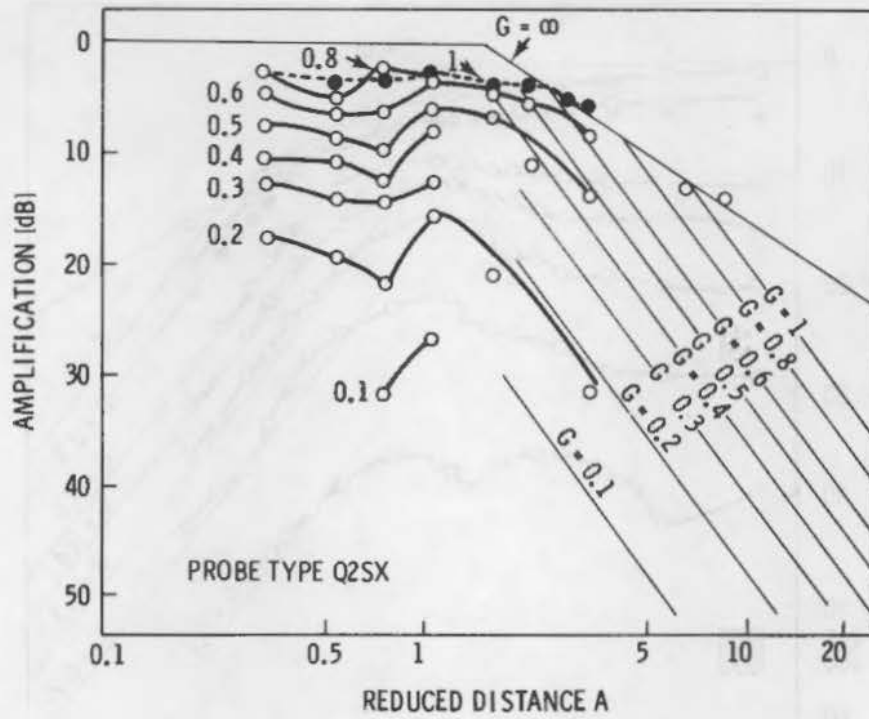


FIGURE 5.2.3a. AVG (DGS) Diagram Obtained in Steel, Probe Type Q2SX

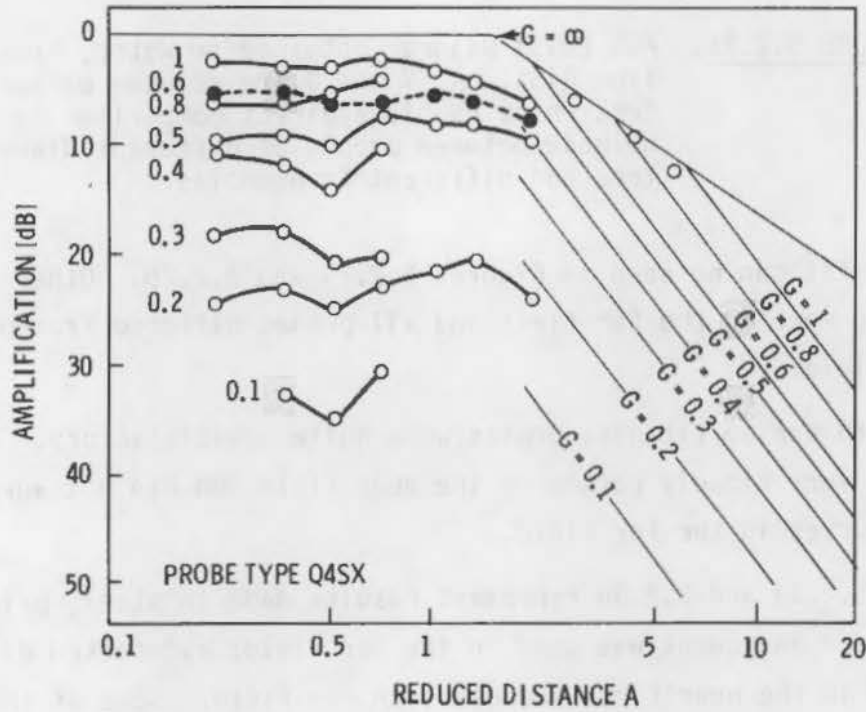


FIGURE 5.2.3b. AVG (DGS) Diagram Obtained in Steel, Probe Type Q4SX



It should be recognized that Krautkrämer warned that the diagram has no general validity in the near field, being completely empirical in the region near  $0.5S$ . The DGS curves were developed on the basis of flat discs with smooth surfaces perpendicular to the UT beam. Deviations with real flaws should not come as a surprise.

Bastien<sup>(5.2.3)</sup> cited the UT examination of flaws in forgings and rolled plate. After examination the pieces were sectioned and the actual flaw sizes were determined. Unfortunately, barium titanate probes were used which render the results suspect. In addition to examining the forging, which introduces geometrical complexities to the UT, similar UT was conducted on standardized samples cut from the test piece. These samples contained flaws, and machining was done so that the defects were known distances from the test surfaces. In Table 5.2.1, the actual flaw area is converted to an equivalent diameter and the ratio of calculated to real (equivalent) diameters compared. Results are given for both 2 and 4 MHz. At a given frequency, different results were obtained for examination of the inner versus outer surface. Bastien<sup>(5.2.3)</sup> concluded that the error depends on whether the defect is situated in the near field or the far field. The changes were more marked at the higher frequency.

TABLE 5.2.1. Results of Tests on the Forged Piece

Defect	Examination of Testpiece				Examination of Sample				Effective Surface Area of Defect and Corresponding Diameter
	Frequency 2 MHz		Frequency 4 MHz		Frequency 2 MHz		Frequency 4 MHz		
	Equivalent Diameter (mm)	Ratio Calculated Diameter Real Diameter	Equivalent Diameter (mm)	Ratio Calculated Diameter Real Diameter	Equivalent Diameter (mm)	Ratio Calculated Diameter Real Diameter	Equivalent Diameter (mm)	Ratio Calculated Diameter Real Diameter	
A--Tested from									
Internal Surface	13.2	0.94	5.0	0.35	14.4	1.02	7.2	0.5	157 mm <sup>2</sup>
External Surface	19.2	1.46	14.5	1.03	24.0	1.7	14.1	1.02	(14.1 mm)
B--Tested from									
Internal Surface	7.2	2.4	2.4	0.8	9.6	3.2	4.8	1.6	7 mm <sup>2</sup>
External Surface	7.2	2.4	2.4	0.8	9.6	3.2	9.6	3.2	(3.0 mm)
C--Tested from									
Internal Surface	4.8	0.96	1.9	0.38	4.8	0.96	2.1	0.48	20 mm <sup>2</sup>
External Surface	4.8	0.96	4.8	0.96	4.8	0.96	7.2	1.44	(5 mm)

The changes in ratios were even more pronounced in the sample, again with the larger change in the near field.

Bastien<sup>(5.2.3)</sup> argues that the correct evaluation of a defect will depend upon the prior solution of the following problem:

1. identification of the defect from the indications provided by the ultrasonic equipment
2. knowledge of the reflecting properties of the defects likely to be found, in terms of their shape, orientation and surface condition.

While a great deal of work has been done on the first problem, it is sufficiently complex to present a consistent limitation. The second problem requires a great deal more work, preferably with real defects.

One final difficulty cited was the use of angle probes, the usual type used in examining welds. More work is required concerning their limitations.

Bradfield<sup>(5.2.4)</sup> commented on Bastien's<sup>(5.2.3)</sup> paper with regard to limitations in the DGS diagram and the discrepancies noted with real flaws. Bradfield emphasized that the main reason for poor consistency in the range 0.4 to 0.65S is fundamental. For idealized conditions a theoretically zero response should exist at 0.5S. The idealized conditions include small flaw size, pure "piston" excitation (i.e., uniform particle velocity over the probe face), and baffle operation in a medium equivalent to a fluid; the excitation should be continuous, not pulsed. Since the pulsed beam represents a definite departure from idealized conditions, behavior from probe to probe will be distinctly variable in this region. Bradfield<sup>(5.2.4)</sup> mentioned that the results of Bastien<sup>(5.2.3)</sup> would have been more consistent if he had used a probe three-quarters the size used. The probe face excitation has a Gaussian, not a uniform distribution.

Another aspect of operating near 0.5S is that probe behavior is not dependent on the probe alone but involves the frequency spectrum. This is further perturbed by variability of coupling which can change the frequency spectrum.

Bradfield<sup>(5.2.4)</sup> attributes the variation in measured to real flaw size to flaw dependent factors, assuming adequate and accurate calibration. The three major factors for such errors are

1. roughness of the flaw
2. inclination of the flaw to the search beam direction (orientation)
3. curvature of the front and back of the flaw.

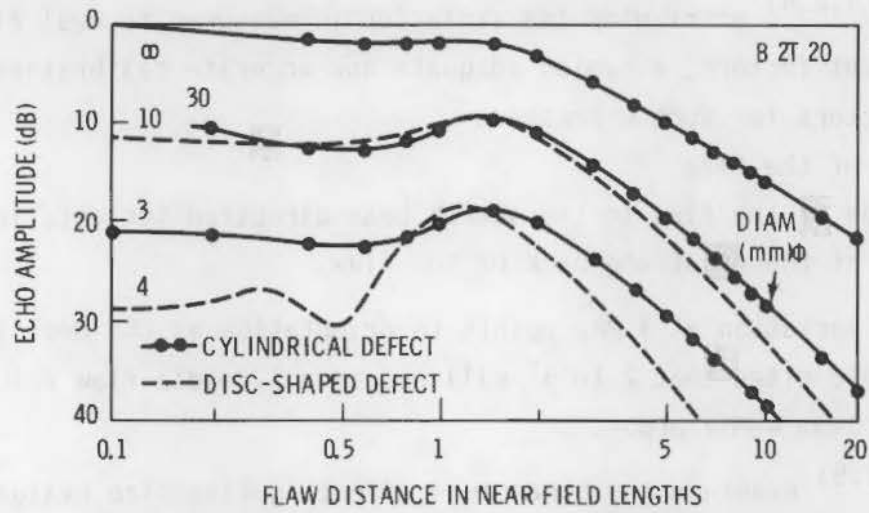
The major variation at 4 MHz points to orientation as the most likely cause. Bradfield cites that 2 to 3° will reduce a 1-cm-dia flaw return signal by half for a 20-mm 4-MHz probe.

Hislop<sup>(5.2.5)</sup> examined the parameters affecting flaw size evaluation and discussed the strengths and weaknesses of various systems as well as suggesting other approaches.

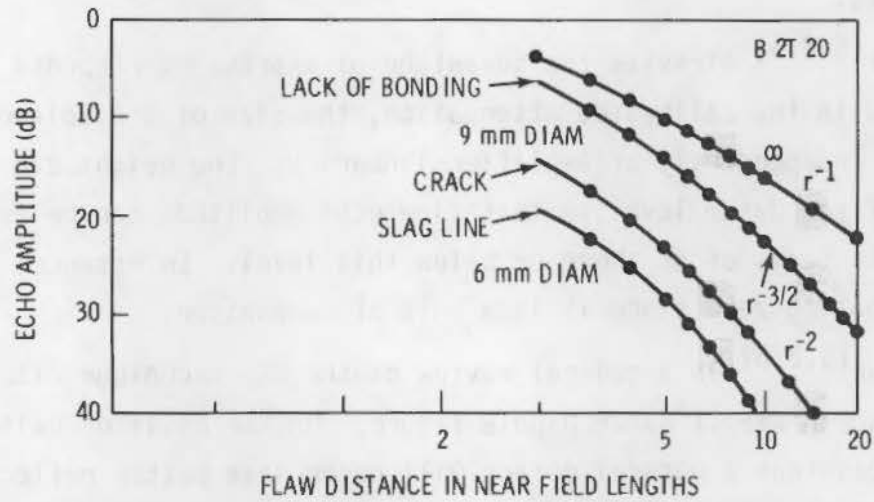
The author<sup>(5.2.5)</sup> stresses the advantage of expressing response in terms of decibels. With the calibrated attenuation, the size of a displayed signal can be reduced independently of amplifier linearity. The height can be adjusted to a fixed datum level so that flaw echo amplitude can be expressed unambiguously in terms of dB above or below this level. In essence, the dB scale has a floating zero since it is a unit of comparison.

Krautkrämer<sup>(5.2.6)</sup> in a general review of the DGS technique cited its origin from a World War II Radar Dipole figure. On the basis of existing theory, he concludes that a natural defect will never have better reflection conditions than the plane disc-shaped defect, vertical to the beam (concave reflectors are excepted). Therefore, the actual defect will always be larger than the equivalent defect. This is in contrast to a statement by Bastien et al.<sup>(5.2.3)</sup>

Krautkrämer<sup>(5.2.6)</sup> argues against setting up special DGS diagrams for different cases such as transverse borings simulating slag inclusions, etc. The apparent gain is lost in the added detail. In fact, Figures 5.2.4a and 5.2.4b confirm that a long slag inclusion behaves like a disc-shaped defect as soon as the complete defect is located within the sound beam diameter. In such a case,



(a) DGS-DIAGRAM FOR CYLINDRICAL AND DISC-SHAPED DEFECT



(b) BEHAVIOUR OF NATURAL WELD DEFECTS

FIGURE 5.2.4. Comparison of Various Artificial and Natural Defects as They Influence the Shape of a DGS Diagram

the area could be calculated from the equivalent defect size of a disc-shaped defect within the known uncertainty band. Therefore, a cylindrical equivalent defect offers no advantages.

#### 5.2.4.2 Relationships

Some specific relationships with dB are of interest. If the area of a source such as a flat-bottomed hole is doubled, the amplitude will increase by 6 dB. If the diameter is doubled, the amplitude will increase by 12 dB. This is applicable to all materials. Figure 5.2.5 compares the two commonly used scales of linear amplitude and linear dB.

Actual data may differ substantially from the theoretical beam shape usually due to non-uniform vibration of the transducer or to mechanical clamping of the transducer.

A typical distance-amplitude curve will have a shape such as shown in Figure 5.2.6. The N-point is the point of maximum sensitivity and roughly represents the end of the near zone and the beginning of the far zone. The N-point is not a fixed point being dependent on the transducer diameter (D) and the

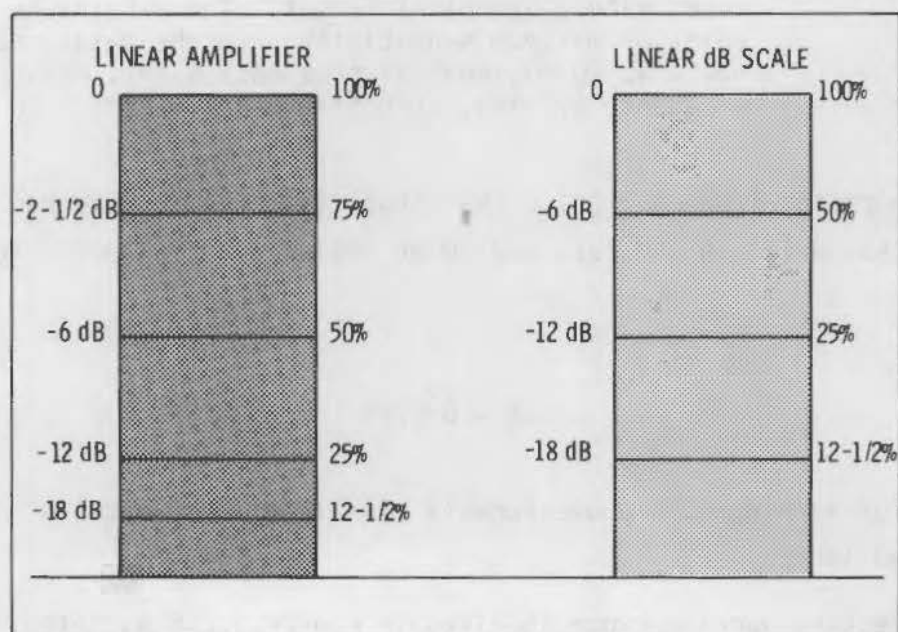


FIGURE 5.2.5. Relation of dB Scales and the Commonly Used Percentage Scale. The same 6 dB difference is found for all echoes with a relative amplitude of 2:1.

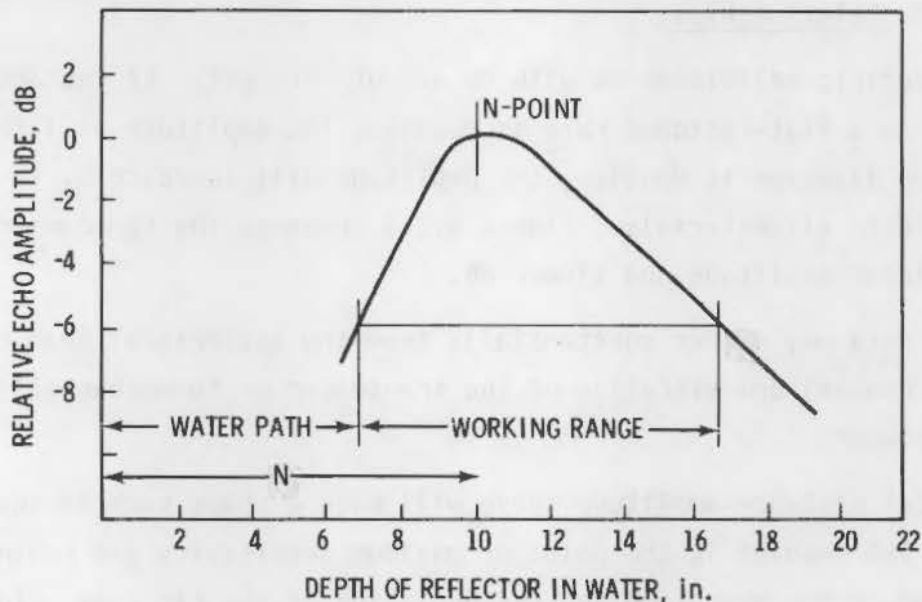


FIGURE 5.2.6. Distance-Amplitude Curve; Plot of the Variation of Sound Intensity Along the Beam Axis in Water, Produced with a Spherical Target. The N-Point is the point of maximum sensitivity. (probe data: nominal dia. 20 mm, nominal frequency 6 MHz, measured frequency 5.2 MHz, effective dia 17.1 mm)

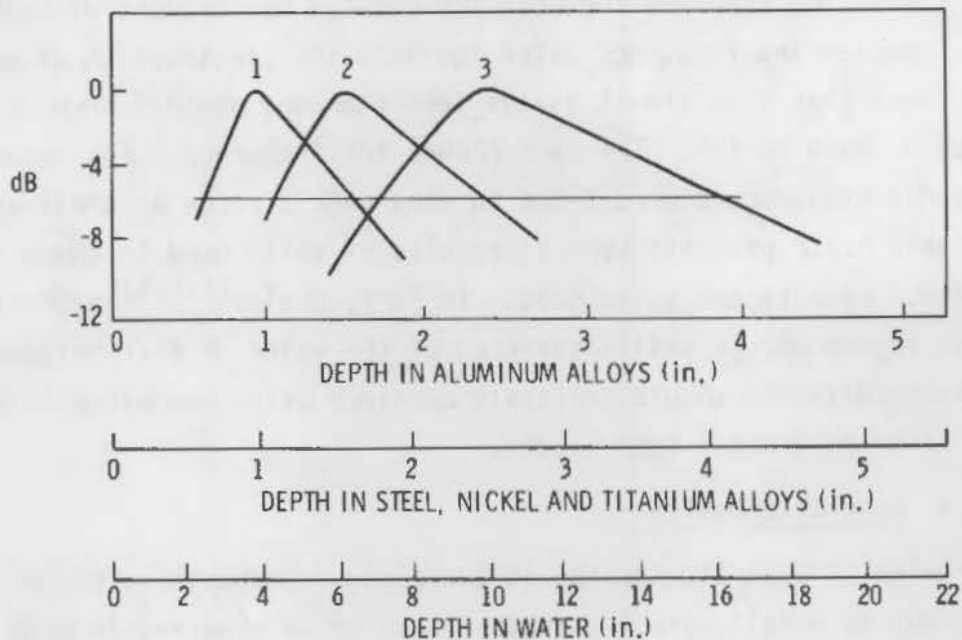
effective operating frequency ( $f$ ). The actual distance is governed by the velocity of sound ( $V$ ) in the test medium or media. The following formula has been used:

$$N = D^2 f / 4V \quad (5.2.1)$$

A word of warning--the above formula usually overestimates  $N$ . The reasons are discussed later.

The effective working range is given in Figure 5.2.6 as noted. This is the part of the beam which never falls more than 6 dB below the maximum. This corresponds to 50% DAC.

Careful selection of probe and frequency permits one to tailor the DAC curve to the specific needs. This is illustrated in Figure 5.2.7 where it can



CURVE 1. N = 4 in. PREFERRED WATER GAP = 2-3/4 in. WORKING RANGE = 3-3/4 in. WATER (1 in. STEEL APPROX)

CURVE 2. N = 6 in. PREFERRED WATER GAP = 4-1/4 in. WORKING RANGE = 5-3/4 in. WATER (1-1/2 in. STEEL APPROX)

CURVE 3. N = 10 in. PREFERRED WATER GAP = 7 in. WORKING RANGE = 9-1/2 in. WATER (2-1/2 in. STEEL APPROX)

**FIGURE 5.2.7.** Distance Amplitude Curves for Three Probes, Showing How the Shape of the Curve Varies with the N-Point

be seen it is possible to optimize for examination at different depths in a medium such as steel. As noted, the horizontal scale is expanded.

#### 5.2.4.3 Calibration Blocks

The preceding comments apply in some respects to the DGS diagram; the near-field problems cited by Krautkrämer,<sup>(5.2.2)</sup> Bastien,<sup>(5.2.3)</sup> and Bradfield<sup>(5.2.4)</sup> are confirmed by Hislop.<sup>(5.2.5)</sup> However, he comments that similar problems exist with the use of calibration blocks since blocks are inherently least useful in the near field owing to the rapid fluctuation of probe sensitivity for a small change in material thickness. Hislop<sup>(5.2.5)</sup> cites work that indicates excellent agreement of test data with the DGS diagram

in the far field. He stresses the need for careful measurement of both effective probe diameter and frequency which involves the construction of a DAC curve. He found that D is almost always less than the nominal probe diameter, sometimes by as much as 15%. The same occurs for frequency. For example, so-called 5-MHz transducers were found to vary over a range as great as 3.8 to 5.5 MHz. Table 5.2.2 presents typical results of tests used to check the DGS (AVG) diagram. Results are quite good. In fact, Hislop<sup>(5.2.5)</sup> expresses the opinion that anyone who is still convinced of the value of flat-bottomed targets for standardization should seriously consider using one piece of paper instead of 72 or more metal test blocks.

#### 5.2.4.4 Beam Attenuation

The problem of beam attenuation is addressed. Emphasis is placed on the attenuation due to metallurgical structure such as is observed in high nickel alloys and in cast stainless steels. No attention is given to attenuation due to inclusions. The frequency sensitivity of attenuation is noted with attenuation increasing with increase in frequency.

Hislop<sup>(5.2.5)</sup> is pessimistic concerning correlating actual flaw sizes in terms of flat-bottomed holes. He cites work of Claydon who found correction factors of one to five were needed to compare flaw sizes in aluminum forgings

TABLE 5.2.2. Typical Results of Tests to Check the AVG Diagram (see text)

True Size (in.)	1		2	
	Estimated Size (in.)	Error (%)	Estimated Size (in.)	Error (%)
0.047	0.036	20	0.045	4
0.078	0.065	16	0.080	3
0.125	0.100	20	0.122	3
0.188	0.146	22	0.180	4

NOTE: Probe data; nominal frequency 4.0 MHz, nominal dia 20 mm, calculated N 10.6 in., measured N 8.0 in. measured frequency 3.5 MHz, effective dia 18.5 mm.



to areas of equivalent flat-bottomed holes. Figure 5.2.8 illustrates the consistent underprediction of actual flaw size by as much as a factor of 4.4. Hislop<sup>(5.2.5)</sup> comments that work of several years invariably resulted in defects after fracture that were considerably larger than predicted from flat-bottomed hole evaluation. Unfortunately, early results were generated before the significance of frequency was recognized. (N.B.: I suspect these were by direct comparison to reference blocks, not probe travel).

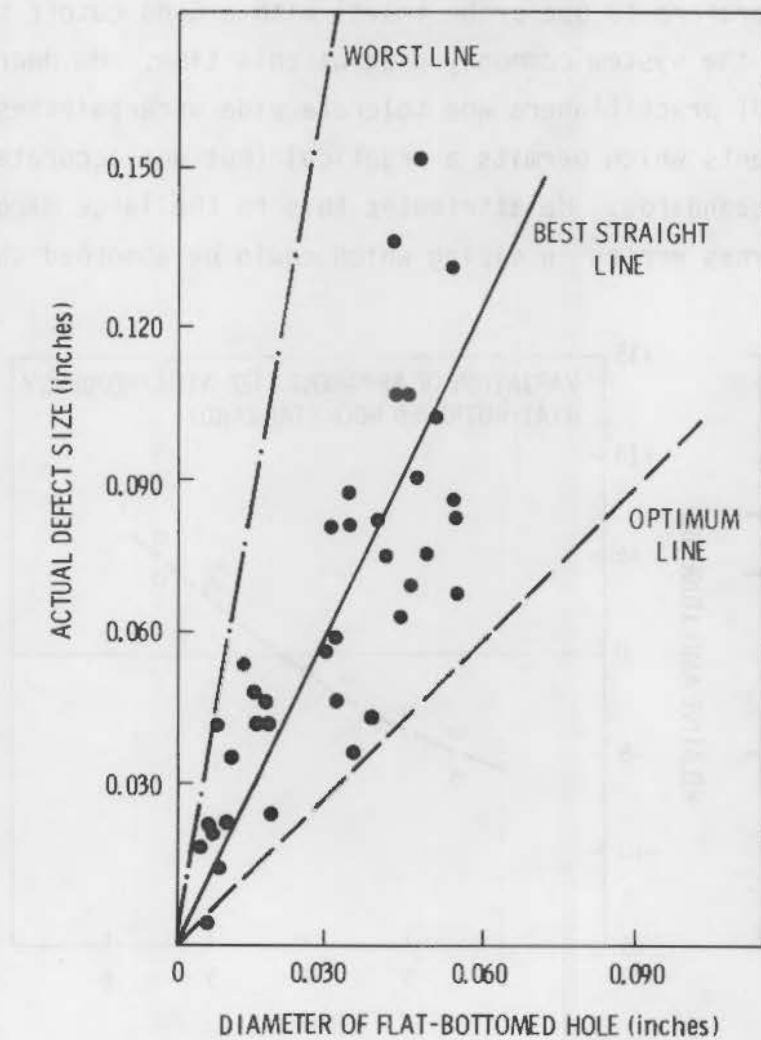


**FIGURE 5.2.8.** Comparison of Actual Defects in Steel Forgings and Flat-Bottomed Holes Giving Identical Indications. Correction factors: worst line x 6.0 on dia, best straight line x 2.1 on dia, optimum line x 1.0 on dia.

#### 5.2.4.5 Frequency

The implications of frequency, or more specifically cases where the actual frequency differed markedly from the assumed value, can be seen in Figures 5.2.9, 5.2.10, and 5.2.11. Not only is there a variation in apparent size with frequency, there is a difference in slope with material. In steel the slope is positive, while in titanium it is negative. The preceding figures compare apparent sizes of actual flaws to equivalent flat-bottomed hole sizes.

Hislop<sup>(5.2.5)</sup> prefers to use probe travel with a 6-dB cutoff to determine flaw size. This is the system commonly used at this time. He decries the casual attitude of UT practitioners who tolerate wide uncertainties in amplitude-based measurements which permits a practical (but not accurate) scheme of quality acceptance standards. He attributes this to the large margins of safety permitting gross errors in sizing which could be absorbed safely. As

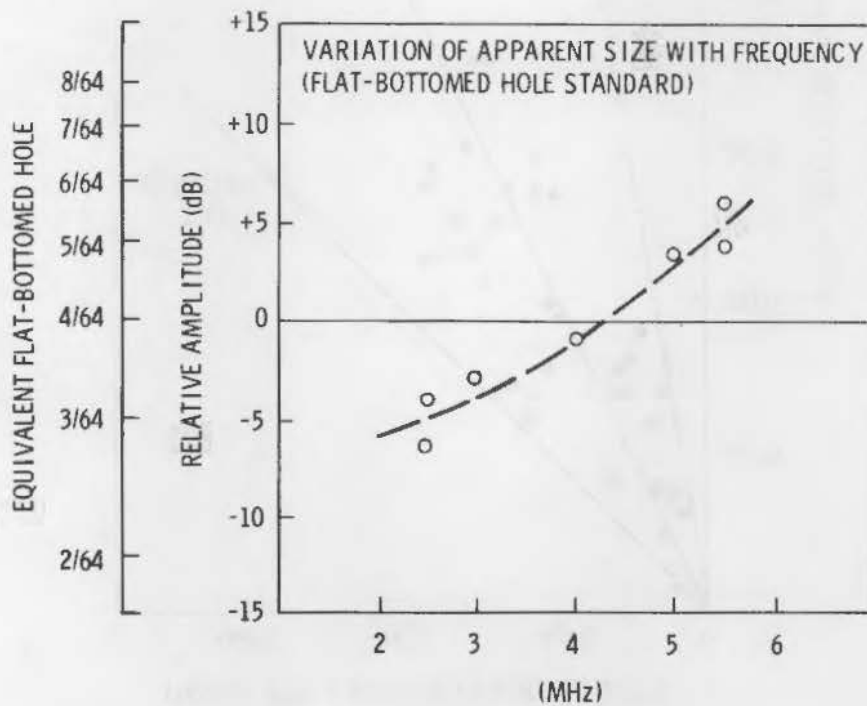


FIGURE 5.2.9. Flaws in Forged Steel

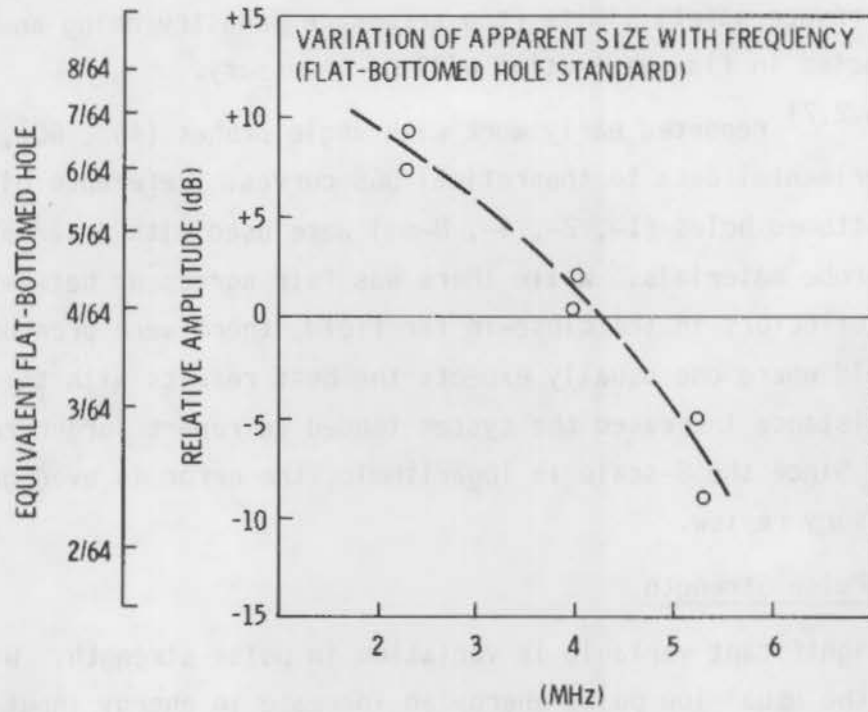


FIGURE 5.2.10. Flaws in Forged Titanium Alloy

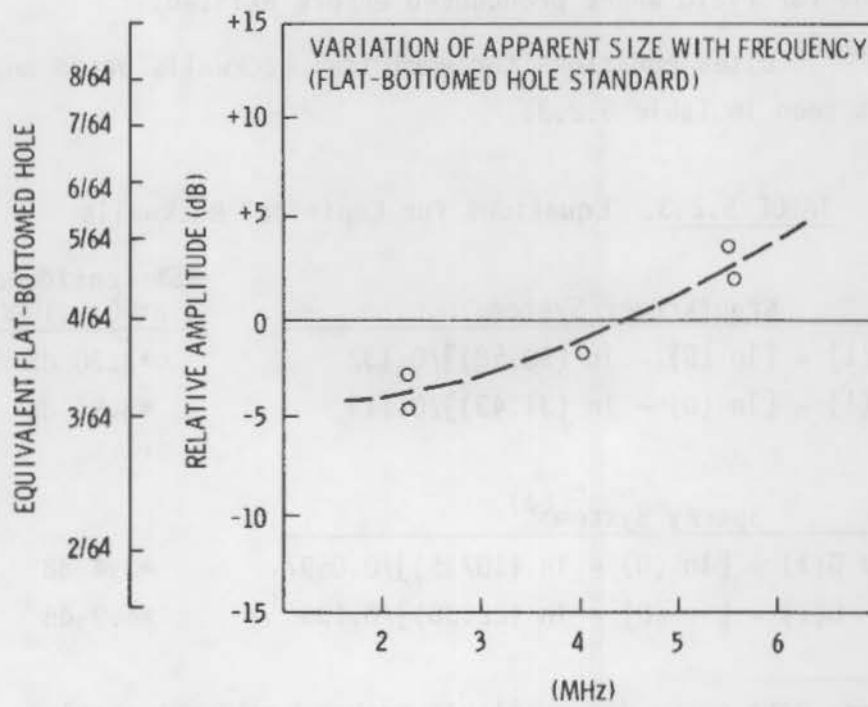


FIGURE 5.2.11. Flaws in Forged INCO 901

one wishes to reduce safety limits (the aerospace industry being an example), greater accuracies in flaw estimation will be necessary.

Chapman<sup>(5.2.7)</sup> reported early work with angle probes (45°, 60°, 70°) to correlate experimental data to theoretical DGS curves. Reference blocks with angled flat-bottomed holes (1-, 2-, 4-, 8-mm) were used with a variety of frequencies and probe materials. While there was fair agreement between DGS lines and measured reflectors in the close-in far field, there were pronounced errors in the far field where one usually expects the best results with the DGS diagram. As distance increased the system tended to report larger reflectors than existed. Since the S-scale is logarithmic, the error is even greater than assumed by cursory review.

#### 5.2.4.6 Pulse Strength

Another significant variable is variation in pulse strength. With distant reflectors at the usual low pulse energy an increase in energy input makes the reflector appear much larger. The author concluded that the results from the various instrument-probe combinations were not as precise as anticipated, particularly in the far field where pronounced errors existed.

Chapman<sup>(5.2.7)</sup> cites equations for empirical backwalls based on repetitive testing as seen in Table 5.2.3.

TABLE 5.2.3. Equations for Empirical Backwalls

Krautkramer System	95% Confidence at D = 1000
2 MHz $G(1) = [\ln(D) - \ln(90.58)]/0.132$	±2.30 dB
4 MHz $G(1) = [\ln(D) - \ln(31.43)]/0.119$	±3.9 dB
Sperry System <sup>(a)</sup>	
2.25 MHz $G(1) = [\ln(D) - \ln(107.5)]/0.0697$	±3.4 dB
5 MHz $G(1) = [\ln(D) - \ln(22.30)]/0.135$	±4.9 dB

(a) Sperry data censored—available probes would not resolve the distant backwall.

Mundry<sup>(5.2.8)</sup> discusses factors influencing DGS diagrams. Specific examples of DGS diagrams tailored to equipment are given in Figures 5.2.12, 5.2.13 and 5.2.14. Figure 5.2.13 is a modification of Figure 5.2.1 for straight beam. Figure 5.2.12 is a diagram calculated for double probes. Figure 5.2.14 is a generalized DGS diagram for the spectrum of angle probes typically used in shear-wave examination. This diagram is considered valid for distances greater than 0.7 near-field length.

Mundry<sup>(5.2.8)</sup> reiterates the warning that no real defect size determination takes place because the echo of a real flaw often differs greatly from that of an ideal circular disc on which the DGS system is based. He cites the

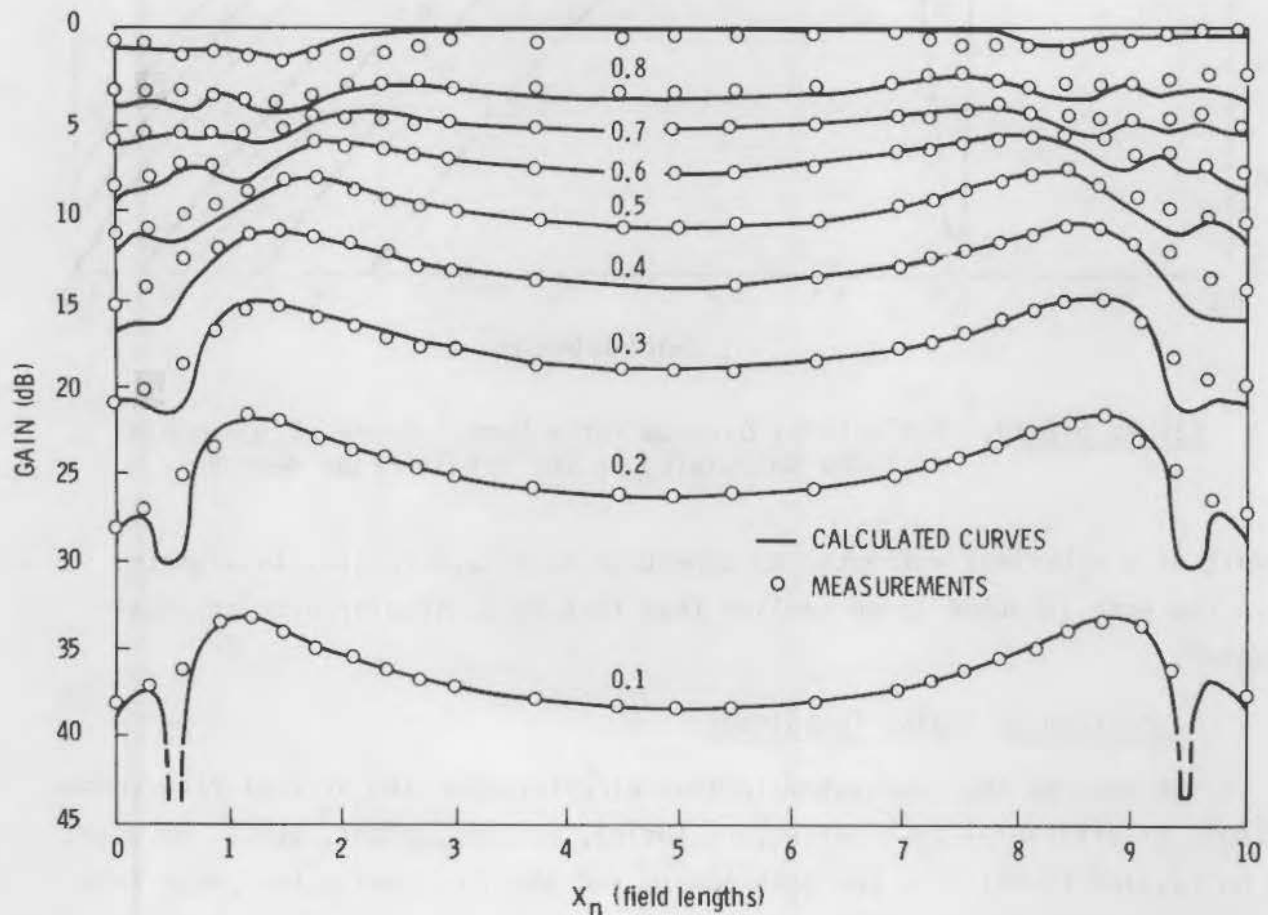


FIGURE 5.2.12. A DGS (AVG) Diagram Calculated by the Double-Probe Method for a Quartz Probe of 10-mm Dia at 2 MHz

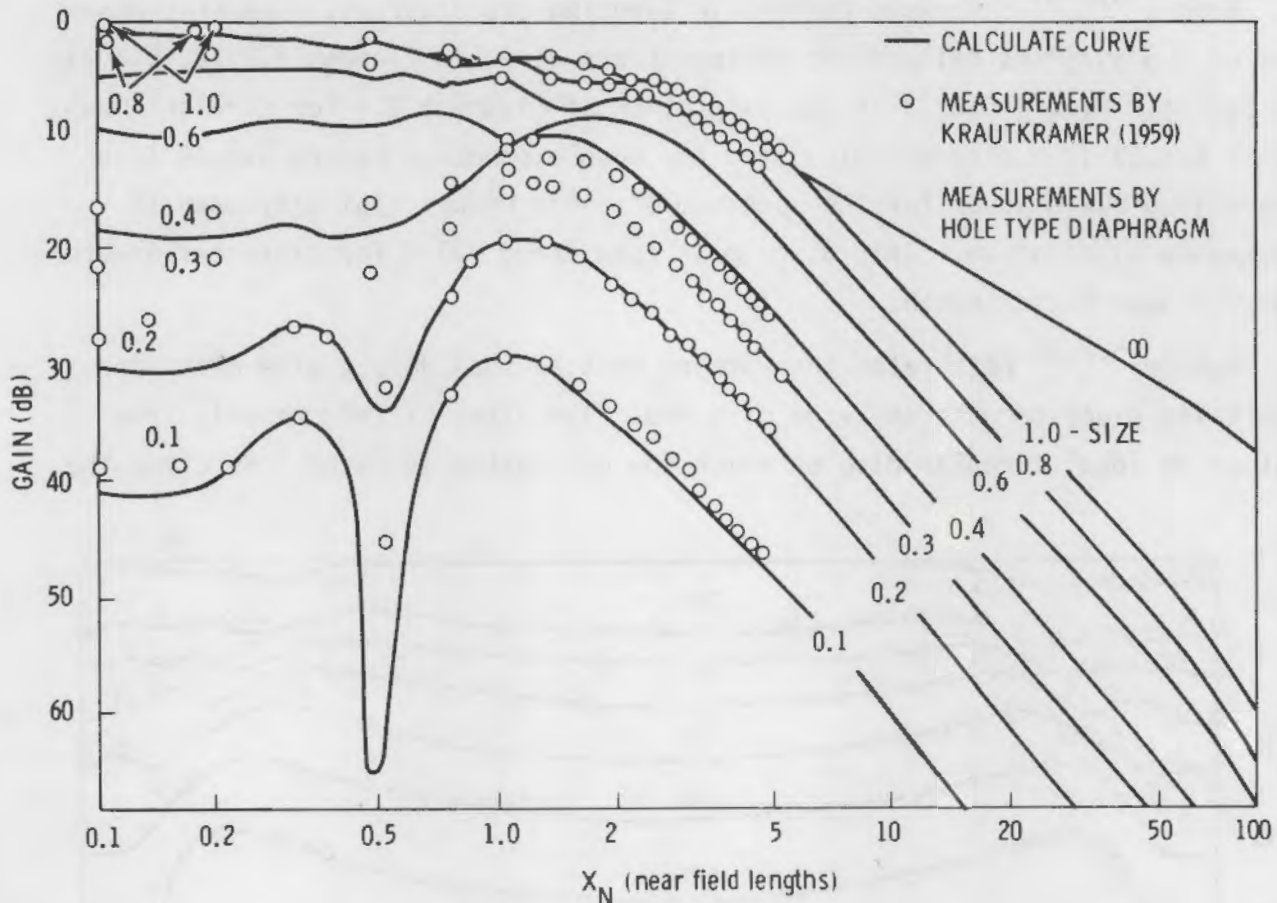


FIGURE 5.2.13. A DGS (AVG) Diagram for a Normal Probe of 10-mm Dia at 2 MHz Calculated by the Single-Probe Method

example of a spherical reflector no more than three wavelengths in diameter where the echo is about 35 dB smaller than that of a circular disc of equal diameter.

### 5.2.5 Comparison of Sizing Techniques

Alternates to the DGS system include direct comparison of real flaw echoes to those of artificial test reflectors (holes, notches, edges, etc.), or using the half-value (6-dB) drop for both length and depth by moving the probe from the maximum magnitude to points of 6-dB drop.

Mundry<sup>(5.2.8)</sup> mentions limited work on using pulse shape as an aid to defect evaluation. He believes a systematic pulse spectrum analysis could supply better information than that available from amplitude.

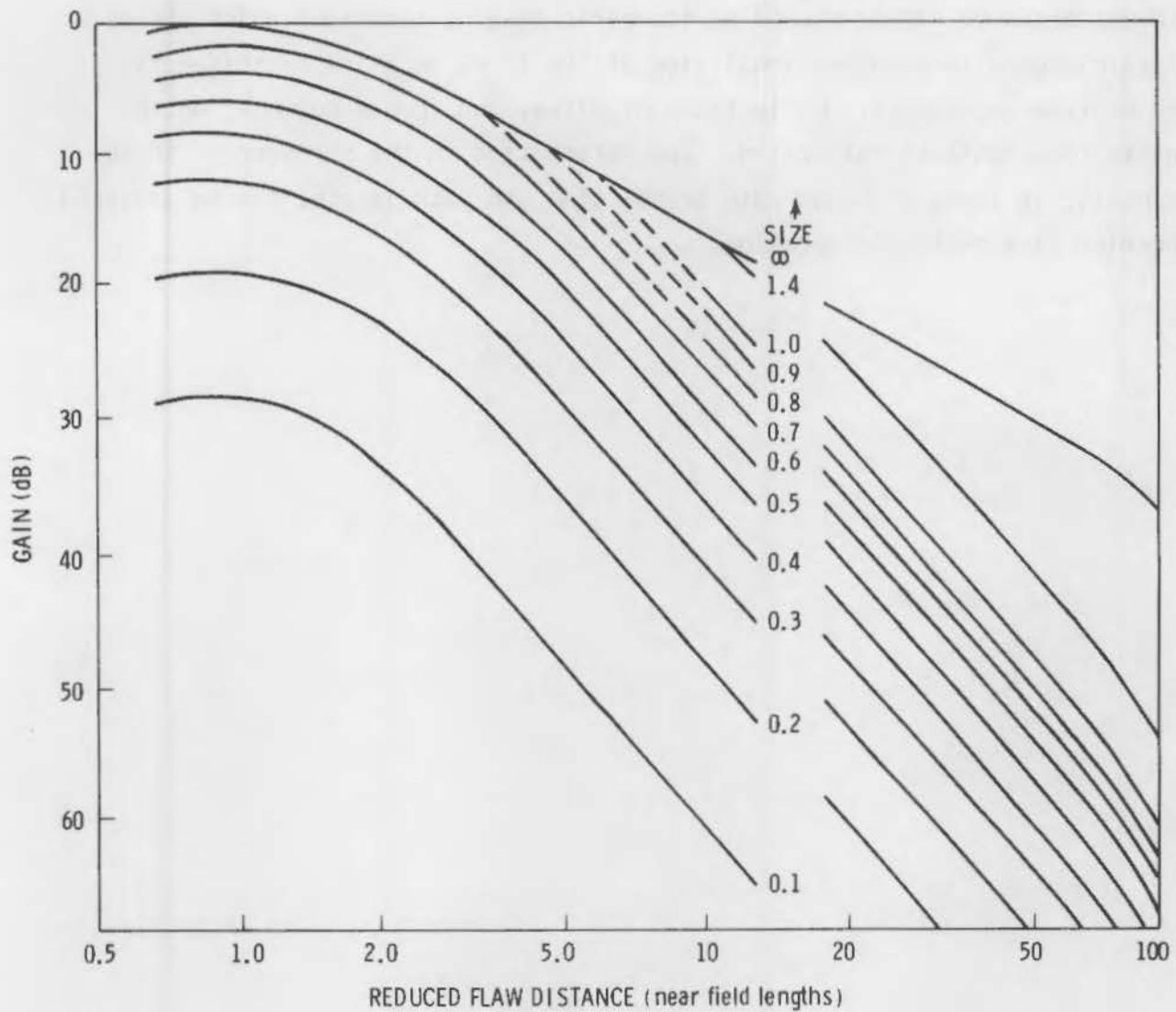


FIGURE 5.2.14. A DGS (AVG) Diagram for an Angle Probe Calculated by the Single-Probe Technique

Minton<sup>(5.2.9)</sup> discusses various methods of determining flaw size such as DGS, scan-movement dependent, isometric imaging, and time-dependent method. With regard to DGS, he argues that no method of sizing of flaws larger than the sound beam can depend on flaw amplitude alone. Since search units of practical size and the resulting sound beams are almost always equal to or smaller than flaws of interest in nuclear work, the DGS system is not usable under such circumstances. Techniques not depending on amplitude values alone include scan-movement-dependent methods where a typical value used is 6-dB drop.

Southwest Research has developed an isometric imaging technique which yields a realistic pseudo three-dimensional view of the flaw. A third technique is based on time-dependence. Reflections of ultrasound from a notch or defect leads to components of reflection. The information in the stronger of these components, in terms of sound path travel time and path length, can be analyzed to predict flaw depth and location.





5.3.1 Statistical Treatment

Silk<sup>(5.3.1)</sup> examined a segment of the published experimental and theoretical data to estimate the magnitude of some of the individual sources of error in ultrasonic defect sizing. He found the dominant sources of error in fatigue crack examination by UT to be those associated with the defect itself; namely, defect roughness, orientation and transparency with the latter being the most important. The data are relatively limited for other defects. The potential usefulness of the technique is examined by estimates of the error inherent in the study of various defect types. This study appears to be a major step toward quantifying the factors leading to variability in flaw sizing. It is an important step but only a step. An examination of the data reveals how limited the quantitative information is. Silk<sup>(5.3.1)</sup> emphasizes the need to quantify the magnitude of individual error sources rather than limiting estimates to the total error. A knowledge of the magnitude of individual error would enable more realistic estimates to be made in advance of errors occurring in a particular investigation. Unfortunately, a statistical basis for individual error is limited; a possible alternate approach is to provide enough complementary data to make realistic estimates of the importance of the various sources of error by the use of suitable weighting factors. An obvious outcome of this exercise was to prove how little the available data were applicable, which points out the need for the use of statistical design of experiments. Specific sources of error cited were as follows:

1. defect orientation
2. defect roughness
3. interference effects (diffracted-reflected interference)
4. transparency (tight crack)
5. attenuation (material attenuation and scatter)
6. coupling factors (film thickness variation, surface roughness, etc.)
7. operator and equipment variables.

In addition, another source of error relates to range factors due to spread of and interference within the UT beam. This factor and the attenuation factor are believed to be small. (N.B.: Attenuation will not be small in a dirty

steel or in materials such as high nickel alloys, cast stainless steel, etc.). Of the seven factors cited, one cannot be represented in terms of a random function; the interference factor (3) cannot since the variation in reflected intensity is a non-random function of defect size and orientation.

#### 5.3.1.1 Individual Error

Silk<sup>(5.3.1)</sup> considers the preferred approach to handling individual errors to assume they follow a log-normal distribution. While the data are insufficient to confirm such a distribution, it appears to be a reasonable assumption.

The logical way of expressing errors and standard deviations is in terms of decibels; e.g., error =  $\pm 6$  dB; this in turn can be correlated to equivalent defect size. If  $\sigma$  is the standard distribution and  $\sigma_n$  is the standard distribution from the error source n, then

$$\sigma_T^2 = \sigma_1^2 + \sigma_2^2 + \sigma_3^2 = \sigma_n^2 \quad (5.3.1)$$

The author<sup>(5.3.1)</sup> suggests that weighting factors be used with the factors in the above equation. In the absence of data, he suggests limiting the weighting factor to values of 0 and 1 where significant sources are rated 1 and lesser sources 0. Hopefully, in the future, more definitive values can be assigned to the weighting factors.

A substantial body of data was reviewed and standard deviations given to them. Some but not all of the references will be discussed further in this chapter. Table 5.3.1 contains the significant sources of error, the standard deviation resulting from the combined sources of error, an independent calculation of  $\sigma_T$  from the values cited in Table 5.3.2, the significance (weight) placed on each data set, and the source.

Table 5.3.2 gives best estimate values for each source of variation in terms of  $\sigma_n = \pm$ dB. As noted previously, the major source of variability is the crack and its transparency. The author<sup>(5.3.1)</sup> suggests it would be prudent to allow an additional error of  $\pm 0.5$  dB on all estimates to allow for variation among the experimental data.

TABLE 5.3.1. Combining Various Sources of Variability

Equation	Weight	Reference	SD Estimated from Experimental Data (to nearest 0.5 dB)	SD Calculated from Final Estimates of $\sigma_n$ (to nearest 0.5 dB)
$\sigma_T^2 = \sigma_1^2 = \sigma_2^2 = 20.5$	4	4	4-1/2	4-1/2
$\sigma_T^2 = \sigma_1^2 + \sigma_2^2 + \sigma_4^2 + \sigma_6^2 = 49$	4	5	7	6-1/2
$\sigma_T^2 = \sigma_4^2 = 20.25$	1	6a	4-1/2	4
$\sigma_T^2 = \sigma_1^2 + \sigma_2^2 + \sigma_4^2 = 36$	1	6b	6	6
$\sigma_T^2 + \sigma_1^2 + \sigma_2^2 + \sigma_4^2 = 42.25$	2	7	6-1/2	6
$\sigma_T^2 = \sigma_4^2 = 16$	1	8	4	4
$\sigma_T^2 = \sigma_1^2 + \sigma_2^2 + \sigma_4^2 = 36$	2	14a	6	6
$\sigma_T^2 = \sigma_4^2 = 12.25$	1	14b	3-1/2	4
$\sigma_T^2 = \sigma_1^2 + \sigma_2^2 + \sigma_4^2 = 25$	2	9	5	6
$\sigma_T^2 = \sigma_2^2 = 9$	2	10	3	3
$\sigma_T^2 = \sigma_1^2 + \sigma_2^2 + \sigma_4^2 = 25$	2	11	5	6
$\sigma_T^2 = \sigma_6^2 + \sigma_7^2 = 9$	4	2	3	3
$\sigma_T^2 = \sigma_1^2 + \sigma_2^2 + \sigma_4^2 = 30.25$	1	15	5-1/2	6
$\sigma_T^2 = \sigma_1^2 + \sigma_4^2 = 16$	1	16a	4	5-1/2
$\sigma_T^2 = \sigma_7^2 = 4$	2	16b	2	2
$\sigma_T^2 = \sigma_1^2 + \sigma_2^2 + \sigma_4^2 + \sigma_6^2 + \sigma_7^2 = 56.25$	2	17	7-1/2	7

Notes: SD = Standard Deviation.  
Reference numbers cited are in original source (5.3.1).

TABLE 5.3.2. Error Estimates for Various Sources of Variation

<u>Source of Variation</u>	<u>Estimate of Error (<math>\sigma_n</math>)</u>
Defect Orientation	±3.5 dB
Defect Roughness	±3.0 dB
Interference Effects	Not quantified
Transparency	±4.0 dB
Attenuation	Not quantified
Coupling Factors	±2.0 dB
Operator Variables	±2.0 dB

The preceding data are primarily from examination of fatigue cracks in aluminum and steel. Care should be exercised in extrapolating from them to stress corrosion cracks or, in general, to cracks in austenitic stainless steel.

Table 5.3.3 covers the limited data pertaining to other defect types; namely, lack of fusion, slag inclusions and gas pores. It is interesting to note that the variability is less than anticipated using fatigue data for comparison, probably because the transparency of these defects is less subject to extraneous influences. In fact, one would surmise that these defects would not be particularly transparent.

An examination of all the data<sup>(5.3.1)</sup> suggests that in a clean material with a good surface finish, the range corrected response to fatigue cracks should show a total variability of ±6.7 dB at one standard deviation.

TABLE 5.3.3. Error Values for Various Defects

<u>Defect Type</u>	<u>Spread in Data</u>	<u>Best Estimate of <math>\sigma_T</math></u>
Lack of Fusion/Incomplete Penetration	6 dB	2 dB
Slag Inclusions	10 dB	2-1/2 dB
Gas Pores	10 dB	3 dB

Placed in perspective, 95% of the data would fall within extreme limits differing from the mean by a factor of 5, or 5% will fall outside these limits (see Table 5.3.4). Since the relationship between defect size and amplitude is broadly linear, this implies a similar spread in the estimate of defect size. An obvious problem with such error magnitudes is that an assumed defect, which is assumed to be close to the upper limit of reflected amplitude ( $\sim 2\sigma$  above the mean), will result in a rejection of 25% of the flaws of the same size if the reporting level is set at a factor of five below this level. At a factor of ten the rejection rate is 15%. In fact, a factor of 40 would be necessary to ensure that >99% of all defects are detected. This represents obvious difficulties. If a more realistic defect standard is used, yielding a response closer to the mean, the factor governing reporting level can be reduced from 40 to about 8.

If one uses dB drop instead of changes in amplitude, the concern is in rate of change rather than absolute values. In one study, the variability of the dB-drop technique was  $\sigma_T = \pm 3.5$  dB compared to the absolute value of nearly  $\pm 7$  dB.

Another check on values of  $\sigma_n$  is obtained by varying the UT technique. Pitch and catch should be insensitive to flaw roughness and flaw orientation,

TABLE 5.3.4. Error Spreads Implied by Various Values of the Standard Deviation

Factor/ Assumed SD	Percentage of Size Estimates Differing from the Mean Value by a Factor Greater than that Indicated (left)			
	3 dB	4 dB	5 dB	7 dB
1.50	24	38	48	62
2.00	4.5	13.5	23	39
3.00	0.7	1.6	5.6	17
5.00	0.0004 <sup>(a)</sup>	0.04	0.5	4.5

(a) Deviation exceeds  $2\sigma$ ; figure presented as a guide only.  
NOTE: SD = Standard Deviation.

but sensitive to transparency, compared to a single probe technique. This is borne out by the estimate of  $\sigma_T = \pm 2.5$  dB for pitch and catch. These data are given in Table 5.3.5.

Some other factors that lead to error and an assessment of the variability are given in Table 5.3.6. Obviously, the major factor is transparency based on available data.

**TABLE 5.3.5.** Standard Deviation for Various UT Measuring Techniques

<u>Technique</u>	<u>Value of SD</u>
Amplitude as a Basis for Defect Size Estimate	$\pm 6.75$ dB
Decibel Drop	$\pm 4$ dB
Pitch and Catch	$\pm 3$ dB

NOTE: SD = Standard Deviation.

**TABLE 5.3.6.** Individual Sources of Variability

<u>Factor</u>	<u>SD, dB</u>	<u>Comment</u>
Defect Orientation	3.5	8% of population exceed factor of 2
Alignment Changes ( $\leq 3^\circ$ )		Change in amplitude of a factor of 4
Defect Roughness	3.0	4.5% of population would differ by factor $\geq 2$
Roughness $\sim \lambda/8^{\text{RMS}}$		Theory predicts factor of 4
Transparency		13.5% of defects should differ from mean by factor $\geq 2$

NOTE: SD = Standard Deviation.

### 5.3.2 External Variability

With regard to coupling and operator values, the author<sup>(5.3.1)</sup> considers the available values of  $\pm 2$  dB for each to be reasonable.

The preceding values contain no allowance for material attenuation and interference effects. Also, there may need to be another set of values for poor surfaces and working difficulties. An obvious advantage of the preceding approach is that such quantitative data on individual sources of variability can be extracted from sets of largely non-specific measurements; however, it should be recognized that the data suffer from several limitations:

- The amount of useful data so far discovered is limited.
- Very few workers publish their data in a form most useful to this type of analysis and these estimates of variability are second hand.
- Weighting as yet is only crudely applied.
- Data on the decibel-drop approach and on defects other than fatigue crack are limited.

### 5.3.3 Theoretical Limitations

Coffey<sup>(5.3.2)</sup> discussed the theoretical limitations of detection and sizing in terms of specific flaw geometries. He examined the sphere, cylinder, mirror-flat plane, and rough crack which was considered to represent the following:

- sphere--gas pores and small slag inclusions
- cylinder--slag lines and worm holes
- flat plane--laminations, lack of bond, lack of fusion, fusion cracks
- rough cracks--heat-affected-zone cracks, stress corrosion cracks, creep cracks.

Coffey<sup>(5.3.2)</sup> describes the inherent characteristics of these classes of defects in terms of theoretical behavior in the ultrasonic beam and cites simplified formulae for determining the relative echo amplitudes. These simplified formulae, which are presented in Table 5.3.7, relate the response to

TABLE 5.3.7. Simplified Equations for Relative Echo Amplitude

<u>Defect</u>	<u>Range</u>	<u>Diameter or Dimension</u>	<u>Echo Amplitude Equation</u>
Flat Mirror	R	---	1
Sphere	R	d	$\sim(d/2R)$
Cylinder	R	d	$\sim(d/2R)^{1/2}$
Ribbon-Like Crack	R	w-width	$\sim(w/\lambda R)^{1/2}$
Flat-Bottomed Hole	R	d	$\sim\pi d^2/2\lambda R$
Rough-Surface Crack (can drop signal 20 to 30 dB)			

defect size and to a normalized beam range. The unpublished work of Wickham is cited as the basis for the theoretical derivations pertaining to certain classes of cracks, particularly the ribbon-like crack. Apparently, the simplified formulae are related to those of Haines<sup>(5.3.3)</sup> and Haines and Langston<sup>(5.3.4)</sup> discussed in Chapter 4. An attempt will be made in Chapter 8 to correlate the simplified formulae with the rigorous equations to establish the limitations and errors in using the simplified equations.

In the preceding table, it is assumed that the echo from a large flat mirror at Range R is normalized to one; and the echo amplitudes for the cited classes of defects will have echo amplitudes derived from the formulae.

An overriding caveat with the preceding formulae is that any defect, irrespective of its detailed shape, if less than one wavelength in dimension, will have an amplitude of back-scattered echo essentially independent of the incident beam direction. Figure 5.3.1<sup>(5.3.2)</sup> does a good job of illustrating the inherent limits of detection and sizing in terms of flaw size and wavelength. Figure 5.3.1a represents a probe scanning ahead that is about to detect reflectors B and C. If they are separated by more than  $\lambda/4$ , they will be resolved by time-of-flight since the reflected pulses are  $\lambda/2$  apart, which is sufficient for their respective peaks not to overlap. An alternate case is where A and B are at the same range (R) so their echoes overlap for all positions of the probe. In this case, the reflectors A and B will be resolved only if they are sufficiently far enough apart so that, as the probe scans forward, the echo



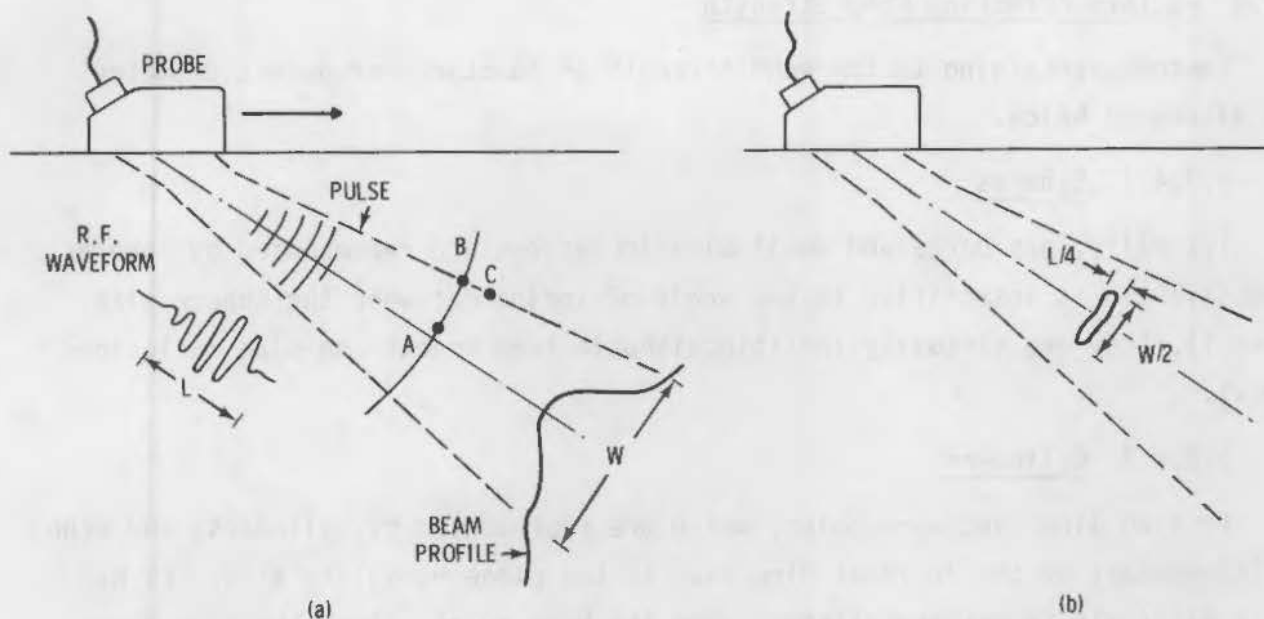


FIGURE 5.3.1. Limit of Resolution of an Ultrasonic Test

from A can rise and then fall significantly before further fall is masked by the rising echo from B. This condition is met if the lateral separation of A and B is at least  $W/2$ , where  $W$  is the beam profile.

The situation pertaining to resolution is given in Figure 5.3.1b where a defect is represented by the roughly elliptical area with major axis  $W/2$  and minor axis  $L/4$ . Assume the beam rotates about its axis, or the flaw rotates about the fixed beam axis: two point reflectors will not be resolved if both are within the ellipsoidal volume, which means the limit of resolution will depend on the relative orientation of the defects in the probe beam.

This concept is significant because it clearly denotes the importance of resolution in defect size estimation because sizing involves the measurement of distance between the opposite edges of a flaw. The accuracy can be no better than approximately the limit of resolution. Additionally, there may be problems in recognition of echoes from the flaw edges and of errors in measuring echo range and flaw position. The methods of improving resolution are discussed in the following paragraphs.

#### 5.3.4 Factors Affecting Echo Strength

Factors pertaining to the echo strength as functions of defect geometry are discussed below.

##### 5.3.4.1 Spheres

Typically, gas pores and small slag inclusions are represented by spheres. Echo strength is insensitive to the angle of incidence; when the sphere size is small, they are virtually indistinguishable from cracks and slag inclusions ( $<1 \lambda$ ).

##### 5.3.4.2 Cylinders

In slag lines and worm holes, which are represented by cylinders, the echo is independent of the incident direction in the plane normal to axis. (N.B.: it is difficult to detect cylinders when the beam points along the axis since only the ends "see" the signal or flat-bottomed hole.)

##### 5.3.4.3 Flat Plate

An RLM plate can be used to represent laminations, lack of bond, lack of fusion, and fatigue cracks; in essence, that plate is a mirror so the beam needs to be at nearly normal incidence; e.g., angle of incidence  $<10^\circ$  from normal, preferably  $<5^\circ$  to obtain significant back scattering. An exact solution of this case, purportedly done by Wickham, is mentioned but not given.

##### 5.3.4.4 Rough Cracks

Rough cracks such as those in a heat-affected-zone, due to stress corrosion, or to creep, result in diffuse scatter so that the echo amplitude is less, but the reflection is greater. Quantitative work is underway within Central Electricity Generating Board (CEGB).

The flat plate, and to a degree the rough crack case, highlight one of the problems of using echo amplitude. Amplitude is sensitive but not discriminating. It may miss large cracks when not appropriately oriented and get a large signal from properly oriented small defects.

### 5.3.5 Problems in Detection

Coffey<sup>(5.3.2)</sup> presented a test example which exemplifies some of the problems inherent in the detection of flaws.

#### 5.3.5.1 Defect

The defect selected consisted of lack-of-fusion at the weld/base-metal interface in a butt-weld consisting of a 30° double-V weld preparation in the thick plate of a pressure vessel.

#### 5.3.5.2 Equipment and Procedure

A 70° shear-wave probe was selected, which is only 5° from the ideal value of 75°, since the beam needs to be as close to normal incidence at the fusion boundary as is possible. The top half of the weld should be examined from the external surface and the bottom half of the weld should be examined from the internal surface. The equipment selected was a 2.5-MHz, 15-mm-dia 70 crystal. The beam path at the weld root (1/2 t) location will be ~60-mm long and 25-mm wide at the weld root location.

#### 5.3.5.3 Signal-to-Noise Ratio

The signal-to-noise ratio will establish the sensitivity. A "clean" material will have very low noise; however, in practice there is noise from sources such as slag inclusions, rough surfaces, etc. For the purposes of this example, it was assumed that there are a large number of spherical slag particles and gas pores up to 4 mm in dia in the weld. Using the formulae in Table 5.3.7, 4-mm-dia spheres will reflect to the same degree as a 1.3-mm-dia flat-bottomed hole. (The work of Jessop at the Welding Institute indicates that at 4 to 5 MHz such slag inclusions reflect less than 1.5 mm and often less than 1.0-mm-dia flat-bottomed holes.)

### 5.3.6 Code Criteria Relevant to Sensitivity

The ASME and German codes set somewhat relaxed thresholds. This is particularly true for ASME XI where the test sensitivity "primary reference level" for thickness of 110 mm is based on a series of 0.25-in. (6.35-mm) holes. On the basis of the formulae in Table 5.3.7, the 50% DAC level (sensitivity twice the primary level) is equivalent to a 3.0-mm flat-bottomed hole sensitivity

which is 15 dB lower than the limiting sensitivity set by slag inclusions. This 3.0-mm flat-bottomed hole is recommended by the German codes. The ASME XI 20% DAC level, which is five times more sensitive than the primary reference level (0.25-in. holes), is equivalent (in sensitivity) to a 1.0-mm flat-bottomed hole; in this example the level is only less than that of the limiting value set by slag. The probable system standard deviations will mean the noise level may include such holes.

#### 5.3.6.1 Minimum Detectable Flaw Size in Example

The minimum defect size will be a function of its shape; however, for a given size, the strongest echo for a given size is likely to arise from a long, parallel-sided reflector parallel to the surface. Figure 5.3.2 uses the Wickham data to illustrate echo amplitude behavior. For defects in the weld/base-metal interface, the limit of resolution with a 70° probe is about W/2 or 12 mm. If the defect is narrower than 12 mm, the edge waves will interfere so the results shown in Figure 5.3.2 will not apply; however, additional work by

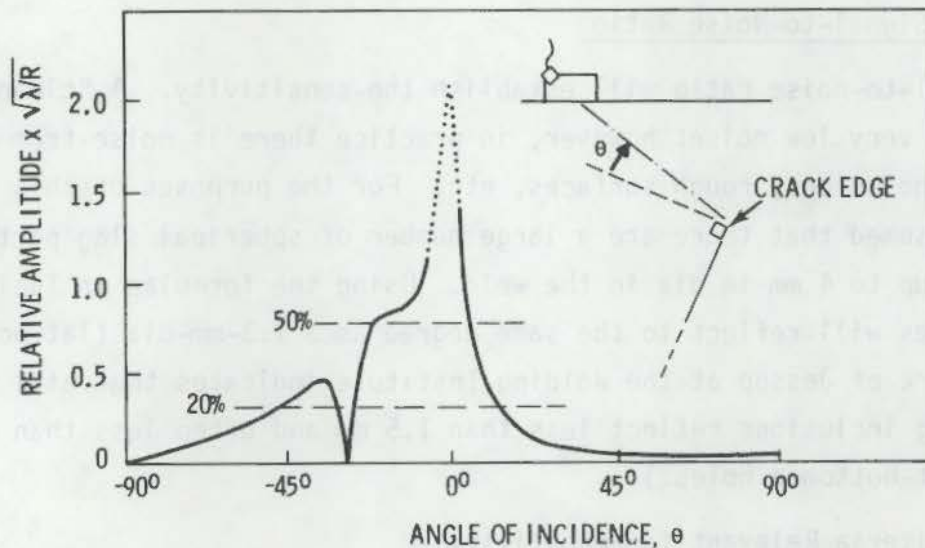


**FIGURE 5.3.2.** Echo Amplitude from Edge of Semi-Infinite Straight Cracks Relative to Echo from Infinite Mirror at Same Range, R. The lines at 50% and 20% are ASME Primary Reference Levels.

Wickham on narrow ribbon-like cracks shows that if such defects extend more than 1.3 mm through the weld, they would be detected even at the ASME 50% DAC sensitivity.

While these results indicate that a smaller flaw than originally assumed can be detected at the optimum angle of incidence, the situation degrades substantially if the angle becomes greater than  $\pm 10^\circ$  to the normal. For example, if a  $60^\circ$  probe had been chosen rather than the  $70^\circ$  probe, giving an angle of incidence of  $15^\circ$ , no smooth ribbon-like crack, even up to 5 mm through the wall will exceed the 50% DAC level. If the flaw width exceeds 5 mm, which now exceeds the limit of resolution for a  $60^\circ$  2.5-MHz probe, then Figure 5.3.2 will apply, and the lower crack edge would be detected at the 20% DAC level, but the upper crack edge would not. This illustrates the sensitivity of echo-amplitude from smooth, flat cracks to the angle of incidence, which covers the entire family of smooth cracks (fatigue, lack of fusion, etc.).

#### 5.3.7 Influence of Defect Surface Roughness

In the smooth mirror-like flaw, only the directly back-scattered edge waves are significant so the use of a  $60^\circ$  probe would lead to nearly zero probability of detection of the example defect. However, if the defect has rough surfaces, which is typical of most weld flaws, the probability of detection is enhanced. If a vertical (through-wall orientation) crack is assumed to exist in addition to the lack of fusion defect, the  $70^\circ$  probe may detect both. Figure 5.3.3 covers the case of the expected echo response from a rough vertically-oriented crack. The dashed line represents the anticipated response of a crack of varying roughness and facet angle. If the peak value is considered to be the most probable amplitude, it is 25 dB weaker than obtained from a smooth mirror at normal incidence. The assumed defect sizes applicable to Figure 5.3.3 are about equal to the limit of resolution, or about 5 mm for a  $70^\circ$  probe incident on a vertical crack. The probability distribution of the echo amplitude,  $y$ , can be approximated with a Rayleigh function of the form  $y \exp(-a^2 y^2)$ ; integration indicates there is a 30 to 40% probability of detection at 50% DAC, rising to 80 to 90% at 20% DAC. If any signal above the noise level set by the inclusions is considered, then the probability of detection will rise to greater than 95%.

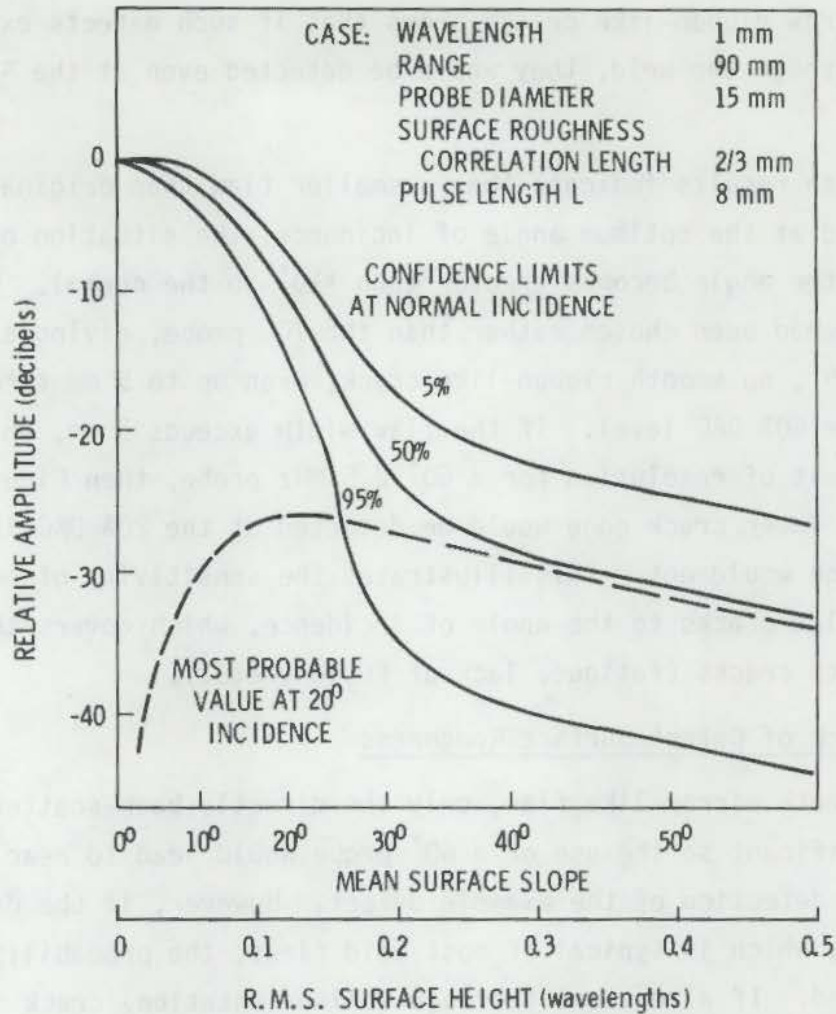


**FIGURE 5.3.3.** Probable Values of Echo Amplitude, as a Function of Defect's Surface Roughness. Case of macroscopically flat reflector, equal to or greater in size than limit of resolution. Echo measured relative to signal from mirror of normal incidence.

The preceding probabilities are very sensitive to threshold level. For example, if the most likely echo amplitude were -30 dB, not -26 dB below the mirror echo value, the probability of detecting the 5-mm rough through-wall value at 50% DAC decreases from 30 to 40% to less than 10%.

#### 5.3.7.1 Theoretical Bases for Figure 5.3.3

The CEGB has quantitative studies underway to examine reflections from rough cracks. The only meaningful way of discussing reflection from rough

surfaces is by using statistics relating the statistical properties of the crack surface to the statistical properties of the detected signal. Coffey<sup>(5.3.2)</sup> reported that the diffraction process can be modeled crudely with scalar Kirchoff theory (radar) and was used in developing Figure 5.3.3. The echo-amplitude relative to a mirror-like defect will depend on the root-mean-square surface height in terms of the beam wavelength,  $\lambda$ , on the mean slope of the crack's profile and on the area occulted by the beam. For normal incidence, as the roughness increases, the echo amplitude falls which assumes the reflections are random because of interference within the beam over the beam area occulting the flaw. In Figure 5.3.3, the solid diverging lines are the 95%, 50% and 5% confidence limits that the signal will exceed the level shown. The knee in the curves occurs when the root-mean-square surface height is approximately  $\lambda/5$ . Below  $\lambda/5$ , the sound is considered to be scattered incoherently. Above  $\lambda/5$ , the coherent component of the sound beam will travel in the specular direction, which means it will not be detected for oblique incidence (e.g.,  $\theta \neq 10$ ); the incoherent portion of the back-scattered echo will be weak, whatever the crack's roughness. The specific case shown in Figure 5.3.3 pertains to the variation of back-scattered signal for a pulse incident at  $20^\circ$  onto a large rough surface. The values predicted by theory are that crack roughness will decrease the signal 20 to 30 dB compared to an optimum smooth crack. Initial experiments support the 20 to 30 dB-drop values.

#### 5.3.8 Detection Probability for Large Rough Flaws

Rough flaws that are factors of  $n$  greater than the limit of resolution in size will result in cyclic shifts in echo amplitude as the probe beam traverses the flaw; this is due to changes in the local interference effects. For this case, the probability of detection of the defect is given by the probability that one of the echo peaks will exceed the recording threshold level. The function used is  $1 - (1 - p)^{n-1}$  where  $p$  is the probability that any one peak chosen at random will exceed the threshold. Values of  $p$  are given in an article by Rice cited as Reference 7 in Coffey.<sup>(5.3.2)</sup> Rice's article is an extensive dissertation on random noise with only one portion (III) dealing with the statistical properties of random noise circuits. Coffey<sup>(5.3.2)</sup> uses the

values of Rice to determine the probabilities of detecting flaws. Table 5.3.8 presents two specific cases of such probability values.

Coffey<sup>(5.3.2)</sup> emphasizes that the probabilities quoted are not generally applicable. A factor not included in the analysis, and often leading to an underestimation of flaw size, is operator error. (N.B.: The probabilities cited will not be improved by repeating the inspection procedure.)

The author<sup>(5.3.2)</sup> gets in a dig at ASME XI with the following statement-question: "It is clear that very high confidence in finding all but the largest cracks can be attained only by careful design of the test and by using quite a high sensitivity. Is the sensitivity required by ASME XI for the inservice inspection of PWR vessels high enough to justify the confidence placed in the test results?"

**TABLE 5.3.8.** Examples of Probabilities of Detecting Rough, Through-Wall Cracks with a 70°, 2.5-MHz Probe Using Relationship  $1 - (1 - p)^{n-1}$

Case 1:	n = 2	Crack 10 mm	Through-wall
50% ASME	DAC	Sensitivity <sup>(a)</sup>	60%
20% ASME	DAC	Sensitivity <sup>(a)</sup>	95%
Case 2:	n = 5	Crack 25 mm	Through-wall
50% ASME	DAC	Sensitivity	98%
20% ASME	DAC	Sensitivity	99.5%

(a) Limiting sensitivity set by slag, 99.5%.

### 5.3.9 Limitations in Flaw Sizing

The following represent some specific problems in sizing.

Flaws smaller than the limit of resolution cannot be measured by probe displacement because the ends cannot be distinguished. An alternate to sizing by probe displacement is by measurement of echo amplitude; however, it should be recognized that echo amplitude is dependent on several parameters, particularly the defect shape. For specific types of defects experience often permits fairly accurate prediction of size. With larger flaws, a lack of resolution



results in errors in sizing. The obvious solution is to improve the resolution which can be accomplished by changing the angle of incidence to assure that the defect is struck obliquely by the beam. With most probes resolution of about 2 mm can be achieved. The accuracy should be enhanced by examining the defect from several directions with high frequency probes.

The use of oblique incidence may introduce another set of problems such as the following:

- Smooth cracks will back scatter only the weak edge waves which may be mistaken for slag lines.
- Rough cracks may have such an undulating echo that they appear to be the same as slag clusters.

Normal beam incidence with respect to the defect may be required for the sizing of several classes of defects. Improved resolution will increase the accuracy; such improvement can be achieved by decreasing the effective beam width which is what is done with both focused probes and acoustic holography.

With focused probes performance away from the focus can be poor. Additionally, there are stringent requirements on the surface profile of the component which results from the large probes used to get fine detail.

The situation is similar to focused probes for acoustic holography; however, the depth resolution is relatively poor—poorer than A-scan.

Coffey<sup>(5.3.2)</sup> emphasizes the need to get input early. It should be required at the design stage touching on such items as degree of surface finish, joint design, welding procedure, etc.

Höller<sup>(5.3.5)</sup> touched on the following significant UT parameters influencing flaw size:

- design of the defect
- wavelength of the UT beam
- diameter of the UT beam.

These parameters may yield different responses depending on characteristics of the defect. Four categories were cited (see Table 5.3.9).

TABLE 5.3.9. Defect Diameter-Wavelength-Beam Diameter Relationships

1. The diameter of the defect is small compared to the wavelength and the beam diameter. In this case there will be oscillation of the wave field with incoherent scattering.
2. The diameter of the defect is comparable to the wavelength but smaller than the beam diameter. This leads to a very complicated behavior where the wave is diffracted at the defect, resonance occurs and small changes in the ratio of defect diameter to wavelength result in significant changes. There will be limited diffraction over a small angle rather than diffracted and scattering echo emitted over a wide angle.
3. The defect diameter is greater than the wavelength but smaller than the beam diameter. There will be a diffracted wave from the sides or corners of the defect, as well as geometrical reflection from the flat area of the defect. The reflected beam spread will decrease with increased defect size.
4. The diameter of the defect is greater than the beam diameter. The defect will behave as if it were an infinitely large mirror, at least in the central portion of the beam. The defect results in complete geometric reflection.

In reactor pressure vessels, the concern is with flaws having areas on an order of square centimeters. Most of the testing will be in the far field so Category 3 above applies. Both pulse-echo and tandem are applicable as is through-transmission.

As Category 4 is approached the system must rely more and more on geometrical reflection. A special subset falling into Category 4 is the case of a Category 3 flaw in the far field examined by conventional transducers. If focused probes are used the flaw may shift to Category 4.

A limitation in UT is the zone of low sensitivity near the incident beam surface. This zone is smaller with direct coupling than it is for immersion. Since the severity of the flaw as well as its potential for growth is greater near the surface, consideration may need to be given to complementary methods for near-surface examination or to the upgrading of UT systems to permit acceptable examination of this region.

Defect sizing by probe movement is the technique used for flaws larger than the beam size. While something has been said concerning the use of cutoff values, such as 6 dB or vanishing echo, the algebraic relationships have not been developed previously. Since several of the papers discussed later depend upon these relationships, they will be developed now.

#### 5.4.1 Russian Approach

Gurvich and Kuzimina<sup>(5.4.1)</sup> reported on the measurement of the defect configuration, orientation and its depth in terms of a scattering indicatrix. Figure 5.4.1 illustrates their technique which depends on the accurate measurement of probe travel. The values of  $H$ ,  $\Delta H$ , and  $X$ ,  $\Delta X$  are obvious. Flaw length is defined as  $2h$ ; angle  $\gamma$ , the orientation of the defect with respect to the normal to the surface, also is apparent. The angle,  $\gamma$ , is the angle of inclination of the acoustic axis of the probe which is usually equal to the entry angles of the UT beam. The angles  $\alpha_I$  and  $\alpha_{II}$  represent certain angles of refraction at which the defect is irradiated with ultrasonic waves.

Various equations can be developed in terms of the geometric relationships of surface, defect, and UT beam. The general equations are

$$\Delta X = (H - h \cos \gamma) (\tan \alpha_{II} - \tan \alpha_I) + 2 h \sin \rho \quad (5.4.1)$$

$$\Delta H = H (\sec \alpha_{II} - \sec \alpha_I) \cos \alpha_0 + h (\sec \alpha_{II} + \alpha_I) \cos \alpha_0 \cos \gamma \quad (5.4.2)$$

Specific cases of the above general cases follow. For the vertical defect typical of surface fatigue and nonfusion ( $\gamma = 0$ ),

$$\Delta X = (H - h) (\tan \alpha_{II} - \tan \alpha_I) \quad (5.4.3)$$

$$\Delta H = H (\sec \alpha_{II} - \sec \alpha_I) \cos \alpha_0 + h (\sec \alpha_{II} + \alpha_I) \cos \alpha_0 \quad (5.4.4)$$

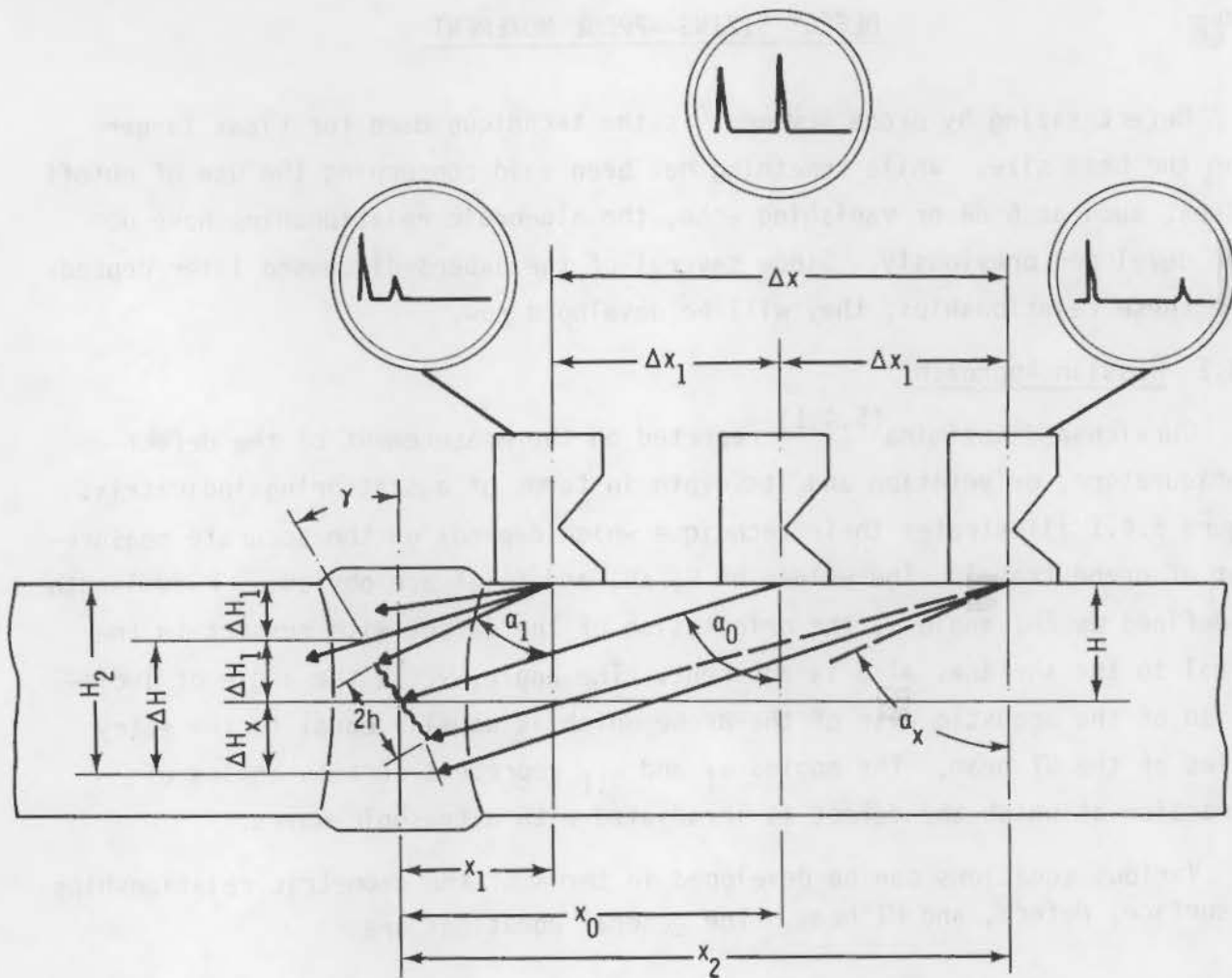


FIGURE 5.4.1. Determination of the Apparent Height of Defects

For horizontal nonfusion and lamination defects ( $\gamma = 90^\circ$ ),

$$\Delta X = H (\tan \alpha_{II} - \tan \alpha_I) + 2h \quad (5.4.5)$$

$$\Delta H = H (\sec \alpha_{II} - \sec \alpha_I) \cos \alpha_0 \quad (5.4.6)$$

For very small defects such as pores or point slag ( $H \cong 0$ ),

$$\Delta X = H (\tan \alpha_{II} - \tan \alpha_I) \quad (5.4.7)$$

$$\Delta H = H (\sec \alpha_{II} - \sec \alpha_I) \cos \alpha_0 \quad (5.4.8)$$

The authors examined the dB drop and a technique analogous to vanishing echo (fixed value above background). They cite the relationships pertaining to apparent defect height and pulse amplitude which are not discussed here, <sup>(5.4.1)</sup> the scattering indicatrix, which is the configuration and orientation of the reflecting surface and depth. The damping factor ( $\delta$ ) of ultrasound in the specific medium and the relative cutoff level A, which is the quantity  $\Delta U/U_{b \text{ max}}$ , are the two parameters used in evaluation. A or  $\Delta U/u_{b \text{ max}}$  defined the cutoff level of pulses in the receiving circuit of the flaw detector with respect to the maximum echo pulse from the given defect ( $U_{b \text{ max}}$ ). With a fixed dB drop, the clipping threshold,  $\Delta U$ , defines the cutoff level. If the vanishing echo is used, the cutoff level depends on the peak amplitude in addition to the clipping threshold. How significant the difference in approach is can be seen from Figure 5.4.2.

#### 5.4.2 Sizing of Surface Flaws

Since sizing techniques applicable to surface flaws may not be applicable to embedded flaws, the two will be discussed separately. Both surface and embedded flaws are made up of two subsets; namely, real and artificial flaws. One can go still further in that there is a variety of both real and artificial flaws with different acoustic response characteristics. An attempt to evaluate these different characteristics is made in the following sections.

##### 5.4.2.1 Artificial Flaws

Artificial flaws have been examined extensively with both surface-wave and shear-wave techniques. Corbly et al. <sup>(5.4.2)</sup> used shear wave to size the lengths and depths of both artificial and real flaws. The authors <sup>(5.4.2)</sup> introduced stress on the flaw as a variable. A 7075-T6511 aluminum was used; semi-circular notches were cut into flat plates with the cuts ranging from 0.010- to 0.050-in. deep. Table 5.4.1 illustrates the relative accuracy of length and depth measurements at various levels of stress in bending. With artificial flaws, the depth was severely underestimated and the length over-estimated. Applied stress led to a decrease in error with regard to depth and an increase in error with regard to length. As noted later, real flaws yielded more accurate results than artificial.

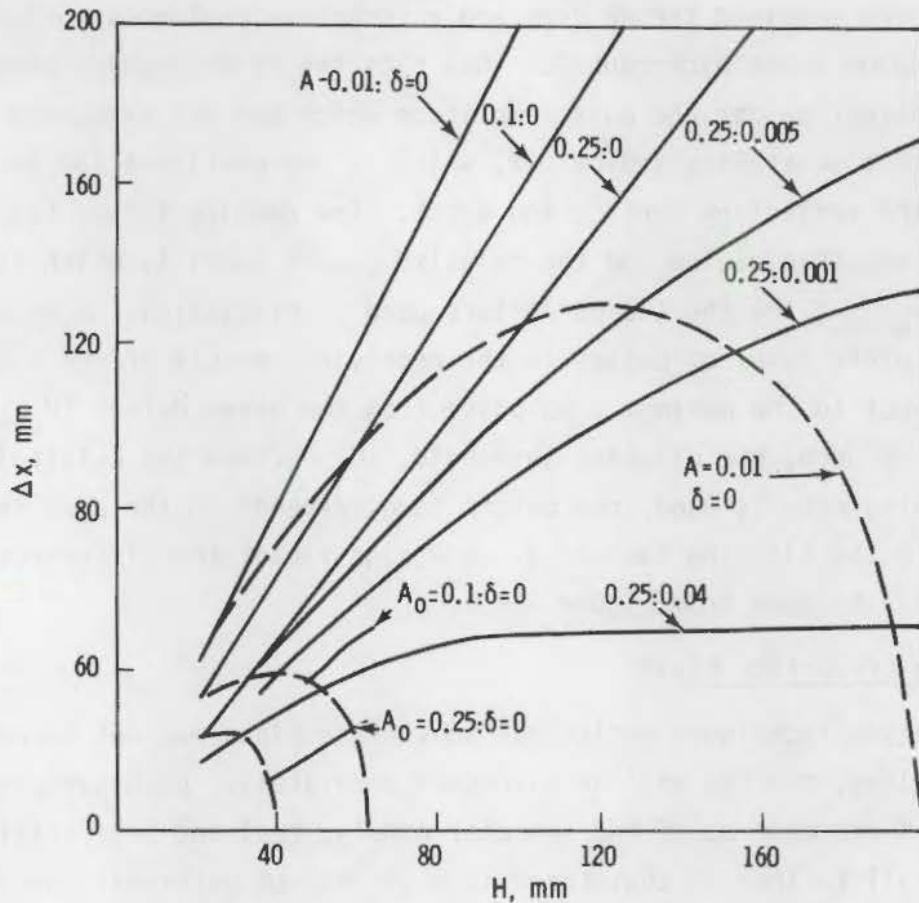


FIGURE 5.4.2. Calculated Dependences of the Apparent Height of a Reflector with a Circular Scattering Indicatrix on its Depth: (——) for the First Measurement Method; (-----) for the Second

Silk and Lidington<sup>(5.4.3)</sup> examined two commonly used techniques for sizing flaws, the 6-dB drop used in Europe and the 20-dB drop used in the United Kingdom. A 5-MHz straight beam probe was used. Rough, medium and fine files were used with the teeth simulating planar or half-round defects. Both the 6-dB and 20-dB techniques overestimated the "defect" size with the error greater in 20 dB. As the roughness increased the error increased. The 6-dB technique was 17% high with the rough file and essentially correct with the smooth file. The 20-dB was 59% high with the rough and 35% high with the smooth.

TABLE 5.4.1. Ultrasonic Shear-Wave Crack Indications (using artificial flaws as calibrations) (results from two tests)

<u>a Actual</u>	<u>2c Actual</u>	<u><math>\sigma</math> Applied</u>	<u>a NDT</u>	<u>2c NDT</u>	<u>Accuracy A (a)</u>
0.052	0.114	0	0.002	0.32	0.039
		3,240	0.002	0.34	0.039
		6,900	0.003	0.38	0.058
		10,200	0.004	0.40	0.077
		16,500	0.006	0.41	0.116
		20,300	0.008	0.42	0.154
		24,000	0.009	0.44	0.174
		0.041	0.082	0	0.001
1,800	0.001	0.273		0.024	
4,440	0.002	0.273		0.049	
8,220	0.002	0.277		0.049	
11,430	0.003	0.277		0.074	
14,700	0.003	0.293		0.074	
17,850	0.003	0.310		0.074	
11,750	0.004	0.332		0.098	

The same authors<sup>(5.4.4)</sup> used a pitch-catch system where the diffracted longitudinal wave was used to measure the flaw depth. Time delay rather than peak amplitude was used to size the defect. Due to the shallow angle of beam entry, very accurate timing on the order of nanoseconds is required; however, such accuracy is possible electronically.

Stepped slits were measured with accuracies of  $\pm 0.2$  to 0.3 mm demonstrated. The authors anticipated similar accuracies with real defects.

Silk and Lidington<sup>(5.4.5)</sup> investigated both time delay and amplitude change in the estimation of the depth of artificial flaws. Several sources of error were discussed in Chapter 4 and will not be repeated here.

A spectrum of probe angles and probe separations were examined. For smaller slits, results were relatively poor, apparently because signals from slits less than 20-mm deep are very close to the noise level.

Shallower angle probes with greater separations yielded poorer resolution but gave good results for slits >5-mm deep. Table 5.4.2 permits a comparison of the accuracy of time delay on amplitude. Crack depths of 10 to 41 mm were examined at 2-mm and 40-mm probe separations. The time delay results were very good, particularly when compared to the poor results using amplitude.

TABLE 5.4.2. Artificial Crack Depth Estimates by Time Delay and from Amplitude

Probe Separation	Actual Crack Depth (mm)	Depth Estimated from Time Delay (mm)	Error (mm)	Depth Estimated from Amplitude (mm)	Error (mm)
2 mm <sup>(a)</sup>	10.0	10.5	0.5 (5%)	27.5	17.5
	13.9	12.5	1.4 (10%)	10.0	3.9
	17.8	16.0	1.8 (10%)	0.0	17.8
	21.7	22.0	0.3 (1.5%)	20.0	1.7
	25.5	26.0	0.5 (2%)	27.5	2.0
	29.4	29.5	0.1 (0%)	30.0	0.6
	33.2	33.5	0.3 (1%)	35.0	1.8
	37.1	38.5	1.4 (4%)	36.0	1.1
	41.0	--	--	42.0	1.0
40 mm <sup>(b)</sup>	10.0	10.0	0.0 (0%)	29.0	19.0
	13.9	14.5	0.6 (5%)	32.5	18.0
	17.8	18.0	0.2 (1%)	17.0	1.0
	21.7	21.5	0.2 (1%)	0.0	21.5
	25.5	26.5	0.1 (4%)	-0.5	26.0
	29.4	29.5	0.1 (0%)	0.0	29.5
	33.2	34.5	1.3 (4%)	35.5	2.3
	41.0	--	--	40.5	0.5

(a) Mean Error = 0.8 mm (4%); Mean Error = 5.5 mm.

(b) Mean Error = 0.5 mm (2%); Mean Error = 13.2 mm.



The error with time delay ranges from 0.0 to 1.8 mm with maximum mean error 4%; whereas amplitude errors ranged from 0.5 to 29.5 mm with mean error 66%. The error was much greater for 40-mm probe separation (55%) versus 2-mm probe separation (28%).

Lidington et al.<sup>(5.4.6)</sup> used small sawn and spark eroded slits to examine the postulate that flaw measurements are only reliable when the depth is less than  $1/4 \lambda_{UT}$ . The data in this report would suggest the optimum ranges are  $1/4$  to  $1/2 \lambda_{UT}$  and  $>4 \lambda_{UT}$ , at least when sawn slits were examined. Results were substantially different with spark eroded slits. The authors considered that spark eroded slits should more closely simulate crack surfaces which led them to the conclusion that real cracks should be subject to large and unpredictable errors. A simplified model was used to predict maxima and minima arising from wavelength-linked interference. Table 5.4.3a contains predictions of maxima and minima for a given frequency. Table 5.4.3b permits a comparison of experimental data versus prediction. As noted the results were similar. The situation is less obvious when comparing the results of sawn slits and spark eroded slits. Figure 5.4.3 illustrates the substantial scatter from spark eroded slits, presumably due to the roughness of surface.

Lidington and Silk<sup>(5.4.7)</sup> used UT surface waves to determine crack depths. Both artificial and real cracks were measured. In essence, the procedure consisted of measuring the time interval between two pulse echoes—that at the surface of the crack and that of the crack tip. Obviously, the latter is a measurement to the crack tip rather than to the depth. An angled crack to a given depth will yield different results than a vertical crack. Errors were quite small, on the order of  $\pm 0.2$  mm or 1%.

Silk<sup>(5.4.8)</sup> extended the previous work to examine cracks at angles other than normal incidence so that there was both a vertical and a horizontal component. He compared surface-wave measurements to direct shear-wave measurements using several artificial slits of various depths. In addition, the calculations are available for handling a crack normal to the surface, changes in direction of a crack, changing direction of a crack tip, and a triangulation method using a time-delay path. Table 5.4.4 presents data on the estimation

TABLE 5.4.3a. Observed Maxima and Minima

	<u>2 1/2 MHz (mm)</u>	<u>5 MHz (mm)</u>	<u>2 1/2 MHz (λ)</u>	<u>5 MHz (λ)</u>	<u>Calculated (mm)</u>
Probe (60°)					
First Max	0.8	0.4	0.65	0.65	
First Min	1.6	0.8	1.25	1.25	1.4 0.7
Second Max	2.4	1.3	1.95	2.05	
Second Min	3.2	1.6	2.60	2.60	
Third Max	~4.0	~1.9	~3.25	~3.15	
Probe (45°)					
First Max	0.63	0.3	0.3	0.50	
First Min	1.1	0.6	0.9	0.95	1.0 0.5
Second Max	1.6	1.0	1.30	1.60	
Second Min	2.0	1.3	1.60	2.05	
Third Max	~2.7	1.8	~2.10	~2.85	
Third Min	~3.1	2.1	~2.50	~3.5	

TABLE 5.4.3b. Predicted and Experimental Results

<u>Frequency (MHz)</u>	<u>Expected Δt/2 1/2 Cycle (mm)</u>	<u>Observed Value Δt/2 (mm)</u>	<u>Mean Δt/2 (mm)</u>
60° 2 1/2	0.7	0.8, 0.8, 0.8, 0.8	0.8
5	0.3	0.4, 0.5, 0.3, 0.3	0.4
45° 2 1/2	0.5	0.45, 0.5, 0.4, 0.7, 0.4	0.5
5	0.25	0.3, 0.4, 0.3, 0.5, 0.3	0.33

NOTE: Above results indicate serious predictive error in flaw sizing.

of the depth using both surface-wave transmission and shear-wave transmission in conjunction with time-delay. Obviously, the two techniques yield similar results.

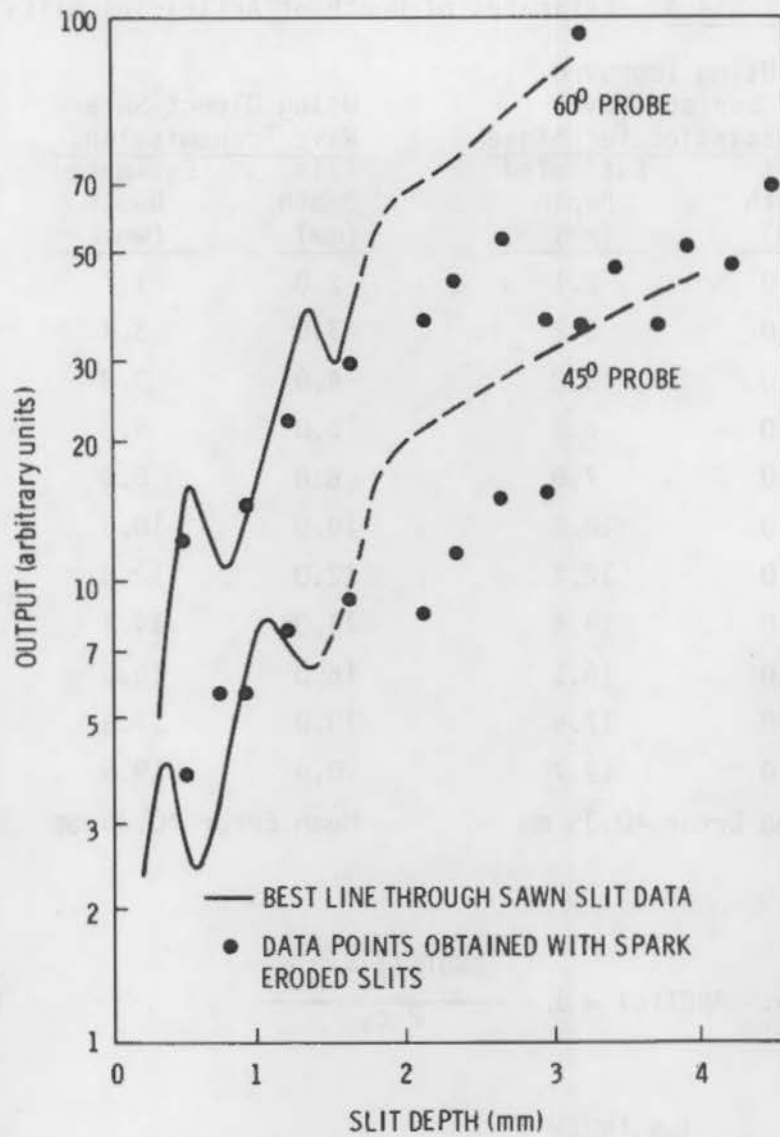


FIGURE 5.4.3. Data from Sawn and Spark-Eroded Slits for 5-MHz Angle Probes

#### 5.4.2.2 Real Surface Flaws

Real surface flaws have been considered in several studies. Early work by Packman et al.<sup>(5.4.9)</sup> considered sensitivity of flaw detection, accuracy in sizing, accuracy in locating, precision (or repeatability) of measurement, validity of measurement, and an assurance index, which considers all of the foregoing parameters. Sensitivity was considered in Chapter 4.

TABLE 5.4.4. Estimates of Depth of Artificial Slits

Using Improved Surface-Wave Transmission Technique		Using Direct Shear-Wave Transmission,	
Slit Depth (mm)	Estimated Depth (mm)	Slit Depth (mm)	Estimated Depth (mm)
2.0	2.1	2.0	1.7
3.0	3.2	3.0	3.4
4.0	3.8	4.0	3.8
6.0	6.3	6.0	6.3
8.0	7.8	8.0	8.4
10.0	10.6	10.0	10.6
12.0	12.4	12.0	12.0
14.0	14.4	14.0	14.4
16.0	16.1	16.0	16.0
18.0	17.5	18.0	17.8
20.0	19.7	20.0	19.6
Mean Error $\pm 0.35$ mm		Mean Error $\pm 0.36$ mm	

Accuracy: (of size) 
$$ANDT(c) = 1 - \frac{2c_{NDT(i)} - 2c_i}{2c_i} \quad (5.4.9)$$

or 
$$\frac{1}{N_f(NDT)} \sum_{i=1}^{i=N_f(NDT)} \left( 1 - \frac{2c_{NDT(i)} - 2c_i}{2c_i} \right) \quad (5.4.10)$$

Accuracy: (of location) 
$$ANDT(l) = \frac{1}{N_f(NDT)} \sum_{i=1}^{i=N_f(NDT)} \left( 1 - \frac{l_{NDT(i)} - l_i}{l_i} \right) \quad (5.4.11)$$

or 
$$ANDT(e) = \frac{1}{N_f(NDT)} \sum_{i=1}^{i=N_f(NDT)} \left( 1 - \frac{e_{NDT(i)} - e_i}{e_i} \right) \quad (5.4.12)$$

Precision: standard deviation of measurements

Validity: measurements valid or spurious Assurance

$$\text{Assurance Index: } AS_{(NDT)} = S_{NDT} A_{NDT(c)} A_{NDT(l)} A_{NDT(\theta)} \text{---} P_{NDT(i)} P_{NDT(l)}$$

Specimens consisted of steel and aluminum cylinders containing surface fatigue cracks. NDE techniques evaluated included PT, UT, RT for aluminum and PT, MT, UT, RT for steel. Table 5.4.5 contains accuracy (PT, UT), sensitivity (PT, UT, RT), and Assurance Index (PT, UT, RT) values for aluminum. Obvious trends include the high accuracy of flaw location by PT and UT compared to lower accuracies for sizing. In terms of the Assurance Index the results are highly variable.

Table 5.4.6 contains accuracy (PT, UT, MT), sensitivity (PT, UT, MT, RT), and Assurance Index (PT, UT, MT, RT) data for steel. The same trends were observed for steel that were observed for aluminum; namely, high accuracy in locating flaws, lesser accuracy in sizing and variable Assurance Index values.

The work of Rummel and Rathke<sup>(5.4.10)</sup> was discussed in Chapter 4 in terms of detection probability. The authors evaluated crack size in aluminum alloy sheet in terms of length and depth of flaws by RT, PT, UT and ET. No attempt was made to evaluate the data statistically. The same sequences discussed in Chapter 4 applied here; namely, 1) as machined, 2) etched, and 3) post-proof stress. The only reasonable conclusion is that there is a general trend of estimated values to actual values; however, the scatter of the data is very large.

Kupcis<sup>(5.4.11)</sup> reported on the detection and sizing of cracks in rolled joints on the pressure tubes used at the Pickering Nuclear Generating Station (a CANDU). The approach used was somewhat simplistic; arbitrary defect length-to-depth ratios were assumed; namely, semi-elliptical flaws with an aspect ratio of 3.5:1. This permitted a depth to be determined from the measured length. In a few instances, metallography was used to establish flaw dimensions which were compared to the UT results based on 4-dB drop. Table 5.4.7 contains the limited data.

TABLE 5.4.5. NDE Inspection of Aluminum Cylinders

Actual Crack Range (2c)(in.)	Accuracy by Dye Penetrant			Accuracy by Ultrasonics			Sensitivity			Assurance Index		
	Crack Length	Crack Location, $\lambda$	Crack Location, $\theta$	Crack Length	Crack Location, $\lambda$	Crack Location, $\theta$	Dye Penetrant	Ultra- sonics	X-ray	Dye Penetrant	Ultra- sonics	X-ray
No Crack	--	--	--	--	--	--	0.9333	0.8667	0.9333	0.9333	0.8667	0.9333
0.000 0.050	0.0000	0.0000	0.0000	0.0000	0.0000	0.0000	0.0667	0.1333	0.0667	--	--	--
0.051 0.100	0.265	0.9986	0.9527	0.7272	0.9961	0.9737	0.1538	0.4615	0.0000	0.0387	0.3255	0.0000
0.101 0.150	0.8528	0.9968	0.9817	0.6918	0.9961	0.9860	0.2917	0.6250	0.0417	0.2434	0.4247	0.0417
0.151 0.200	0.7033	0.9968	0.9674	0.7598	0.9978	0.9639	0.3636	0.5000	0.0000	0.2466	0.3654	0.0000
0.201 0.250	0.0157	0.9981	0.9350	0.7131	0.9970	0.9669	0.8571	0.8571	0.0000	0.6525	0.5893	0.0000
0.251 0.300	0.8954	0.9985	0.9742	0.6390	0.9533	0.9879	1.0000	1.0000	1.0000	0.8710	0.6018	0.0000
0.301 0.350	0.8406	0.9829	0.9418	0.7475	0.9835	0.9527	1.0000	1.0000	0.1111	0.7781	0.7004	0.1111
0.351 0.400	0.7871	0.9969	0.9682	0.7292	0.9959	0.9882	1.0000	1.0000	0.0000	0.7597	0.7176	0.0000
0.401 0.450	0.9038	0.9979	0.9700	0.7702	0.9965	0.9719	1.0000	1.0000	0.2500	0.8748	0.7459	0.2500
0.451 0.500	0.9395	0.9863	0.9233	0.6383	0.9845	0.9340	1.0000	1.0000	0.8333	0.8555	0.5806	0.8333

5.4.12

5.4.13

TABLE 5.4.6. NDE Inspection of Steel Cylinders

Actual Crack Range (2c)(in.)	Accuracy									Sensitivity				Assurance Index				
	Penetrant			Ultrasonics			Magnetic Particle			Pene- trant	Ultra- sonics	Magnetic Particle	X-ray	Pene- trant	Ultra- sonics	Magnetic Particle	X-ray	
	Crack Length	Crack Location, $\pm$	Crack Location, $\theta$	Crack Length	Crack Location, $\pm$	Crack Location, $\theta$	Crack Length	Crack Location, $\pm$	Crack Location, $\theta$									
No Crack	--	--	--	--	--	--	--	--	--	0.8889	0.7778	0.7778	--	--	--	--	--	
0.001	0.050	0.0000	0.0000	0.0000	0.0000	0.0000	0.0000	0.0000	0.0000	0.1111	0.2222	0.2222	0.390	--	--	--	--	
0.051	0.100	0.3587	0.9972	0.9822	0.6662	0.9929	0.9082	0.4130	0.9979	0.9809	0.4000	0.4000	0.6000	0.0000	0.1405	0.2615	0.2426	0.0000
0.101	0.150	0.6381	0.9976	0.9894	0.6987	0.9972	0.9038	0.4527	0.9972	0.9459	0.3333	0.8000	0.9333	0.0000	0.2099	0.5038	0.3985	0.0000
0.151	0.200	0.2220	0.9960	0.9757	0.6493	0.9969	0.9841	0.8564	0.9966	0.9878	0.3000	0.9000	0.9333	0.0000	0.0647	0.5733	0.7868	0.0000
0.201	0.250	0.7731	0.9987	0.9563	0.6687	0.9962	0.9811	0.8097	0.9976	0.9837	0.6000	1.0000	0.9000	0.0000	0.4430	0.6836	0.7151	0.0000
0.251	0.300	0.7652	0.9986	0.9984	0.7478	0.9966	0.9885	0.7503	0.9984	0.9898	0.7978	1.0000	0.8889	0.2222	0.5874	0.7367	0.6591	0.2222
0.301	0.350	0.7571	0.9981	0.9621	0.6639	0.9984	0.9871	0.7838	0.9968	0.9704	0.6250	0.8740	1.0000	0.1250	0.4544	0.5725	0.7582	0.1250
0.351	0.400	0.6880	0.9850	0.9422	0.5793	0.9968	0.9448	0.7483	0.9979	0.9545	1.0000	1.0000	1.0000	0.0000	0.8241	0.5456	0.7128	0.0000
0.401	0.450	0.5491	0.9988	0.8970	0.6484	0.9784	0.9105	0.7917	0.9989	0.9513	1.0000	1.0000	1.0000	0.0000	0.4920	0.5776	0.7523	0.0000
0.451	0.500	0.8007	0.9970	0.8424	0.5458	0.9977	0.9307	0.8408	0.9984	0.9872	1.0000	1.0000	1.0000	0.5000	0.6725	0.5068	0.8287	0.5000

TABLE 5.4.7. Actual versus Measured Crack Size in Pressure Tubes

Crack Number	Actual Size (mm) by Metallography		Estimated Length (mm) 4-dB Drop	Ratio Length/Depth	Percent Error
	Length	Depth			
1	1.58	0.54	1.8	~3.0	+14
2	--	--	1.8	--	--
3	1.29	0.50	1.5	~2.5	+16
4	1.42	0.50	1.7	~2.8	+20
5	--	0.54	1.7	--	--

Sattler<sup>(5.4.12)</sup> examined RT, PT, and UT (both shear and Delta) with aluminum and titanium alloys of various thickness to establish the accuracy of sizing surface and embedded flaws as an input into fracture mechanics calculations. Results ranged from fair to good for the determination of length, and from fair to poor for the determination of flaw depth. The latter results are given in Tables 5.4.8 and 5.4.9.

Corbly et al.<sup>(5.4.2)</sup> investigated the influence of applied stress on the sizing of real as well as of the artificial flaw cited previously. The most significant conclusions related to natural cracks were as follows:

- Natural flaws can be used for calibration and correlate well with the actual crack depth. The accuracy of the technique is high and decreases with increasing stress on the flaw.
- The precision of the ultrasonic technique measured by the standard deviation increases with increasing stress on the flaw.
- Ultrasonic shear-wave measurements do not measure the true depth of the flaw, but only the depth for which the crack opening displacement is greater than some critical amount; hence, upon stressing the flaw, the apparent indicated crack depth increases. This increase in apparent crack depth indication appears to be a linear function of the stress.

As noted in the discussion by the same authors<sup>(5.4.2)</sup> of artificial flaws, such flaws cannot be used to calibrate the height of the reflected peak



TABLE 5.4.8. Summary of Maximum Crack Lengths Possible for Zero Indicated Crack Lengths and Test Accuracies for the Various Nondestructive Testing Techniques on the Four Alloys and Four Section Thicknesses<sup>(a)</sup>

Thickness	Alloy	Maximum Crack Length for Zero Indicated Length and $\pm 3 \sigma$ Limit							
		Radiographic		Penetrant		Ultrasonic Shear		Ultrasonic Delta	
		MCL <sup>(b)</sup>	$\pm 3 \sigma$	MCL <sup>(b)</sup>	$\pm 3 \sigma$	MCL <sup>(b)</sup>	$\pm 3 \sigma$	MCL <sup>(b)</sup>	$\pm 3 \sigma$
0.020	2014 & 2219A1	(c)	(c)	0.040	0.036	0.048	0.062	---	---
0.020	6-4 & 5-2.5Ti	0.069	0.051	0.032	0.027	0.097	0.084	---	---
0.200	6Al-4V-Ti	---	---	---	---	0.051	0.039	---	---
0.125	2014 & 2219A1	(c)	(c)	0.029	0.032	(c)	(c)	(c)	(c)
0.125	6-4 & 5-2.5Ti	0.130	0.086	0.050	0.067	---	---	0.061	0.105
0.125	6Al-4V-Ti	---	---	---	---	(c)	(c)	(c)	(c)
0.125	5Al-2.5Sn-Ti	---	---	---	---	0.092	0.070	0.057	0.081
0.500	2014 & 2219A1	0.458	0.237	(c)	(c)	---	---	---	---
0.500	2014A1	---	---	---	---	(d)	(d)	(d)	(d)
0.500	2219A1	---	---	---	---	0.278	0.246	0.114	0.319
0.500	6-4 & 5-2.5Ti	(c)	(c)	0.025	0.021	(c)	(c)	0.090	0.125
0.500	6Al-4V-Ti	---	---	---	---	(d)	(d)	(d)	(d)
0.500	5Al-2.5Sn-Ti	---	---	---	---	0.153	0.073	0.158	0.125
1.000	2014 & 2219A1	0.210	0.164	(c)	(c)	(c)	(c)	(c)	(c)

- (a) All dimensions in inches.  
 (b) Maximum crack length at zero indicated length.  
 (c) No correlation.  
 (d) Insufficient sample.

TABLE 5.4.9. Summary of Maximum Crack Depths Possible for Zero Indicated Crack Depths and Test Accuracies for the Ultrasonic-Shear and Delta-Testing Techniques on Four Alloys and Three Section Thicknesses

Thickness	Alloy	Maximum Crack Depth for Zero Indicated Depth and $\pm 3 \sigma$ Limit <sup>(a)</sup>					
		Ultrasonic Shear (increment)		Ultrasonic Shear (area)		Ultrasonic Delta	
		MCD <sup>(b)</sup>	$\pm 3 \sigma$	MCD <sup>(b)</sup>	$\pm 3 \sigma$	MCD <sup>(b)</sup>	$\pm 3 \sigma$
0.125	2014 & 2219 Al	(c)	(c)	(c)	(c)	(c)	(c)
0.125	6Al-4V-Ti	(c)	(c)	(c)	(c)	0.024	0.020
0.125	5Al-2.5Sn-Ti	0.034	0.015	0.033	0.024	(c)	(c)
0.500	2014 Al	(d)	(d)	(d)	(d)	(d)	(d)
0.500	2219 Al	(c)	(c)	(c)	(c)	(c)	(c)
0.500	6-4 & 2.5 Ti	(c)	(c)	(c)	(c)	(c)	(c)
0.500	6Al-4V-Ti	(d)	(d)	(d)	(d)	(d)	(d)
0.500	5Al-2.5Sn-Ti	0.069	0.042	0.083	0.058	0.099	0.090
1.000	2014 & 2219 Al	(c)	(c)	(c)	(c)	(c)	(c)

(a) All dimensions in inches.

(b) Maximum crack depth at zero indicated length.

(c) No correlation.

(d) Insufficient sample.

to crack depth. Artificial flaw correlations led to large underestimates of fatigue crack depth with the accuracy increasing with increasing stress on the flaw. The preceding deviations probably are due to a combination of factors such as crack shape, crack surface roughness, and mode conversion upon reflection. It will depend to a greater or lesser degree on equipment and probe characteristics such as frequency, mode, bandwidth, etc. An added factor is the surrounding stress field. The UT beam may be transmitted across an unloaded surface crack without much loss of intensity (transparency effect) so that the return pulse will depend on the state of stress in the region surrounding the crack.

In a complex structure, this state of stress will be a function of material properties, crack growth history, degree of stress relaxation and level

of induced stresses. A further error is an outgrowth of the simple theory which predicts a monotonic increase in reflected beam intensity with increasing crack depth. This approach ignores the very real interference effects which, depending on crack size, location and orientation, can cause minor to severe underestimations of crack depth.

#### 5.4.2.3 Real and Artificial Flaws

The data of Corbly et al.<sup>(5.4.2)</sup> for the influence of stress on real and artificial flaws can be seen in Figure 5.4.4. Figures 5.4.5a and 5.4.5b contain schematic depictions of stress effects on real and artificial flaws in terms of UT reflected peak and in terms of the Gaussian probability density function. The decreased accuracy of flaw measurement and enhanced precision with increasing stress can be seen. In the case of the artificial flaw, the large displacement between the faces results in nearly total reflection of the ultrasonic energy giving a large reflected peak at low sensitivity.

If such an artificial flaw is used to correlate actual crack depth of a real flaw through measurement of peak height, it will grossly underestimate the actual depth because the geometry of the artificial flaw does not accurately represent flaw contour.

The fatigue crack correlation also is in error because it does not consider the effects of applied stress on crack opening displacement; hence, it overestimates the size if tensile stresses are applied. Compressive stresses reverse the effect leading to an underestimation of size (Figure 5.4.4). Failure to recognize this behavior during field measurements could lead to substantial errors in sizing of flaws.

#### 5.4.3 Sizing Cladding Cracks

Saitoh and Takahashi<sup>(5.4.13)</sup> developed a twin crystal longitudinal wave optimized for the near field; 45° at 4 MHz was selected. The problem is exemplified in Figure 5.4.6 where a through-clad flaw is hidden by the "grass" echo. The authors<sup>(5.4.13)</sup> indicate that this characteristic grass echo in a 24-mm clad will disguise cracks up to 18-mm deep.

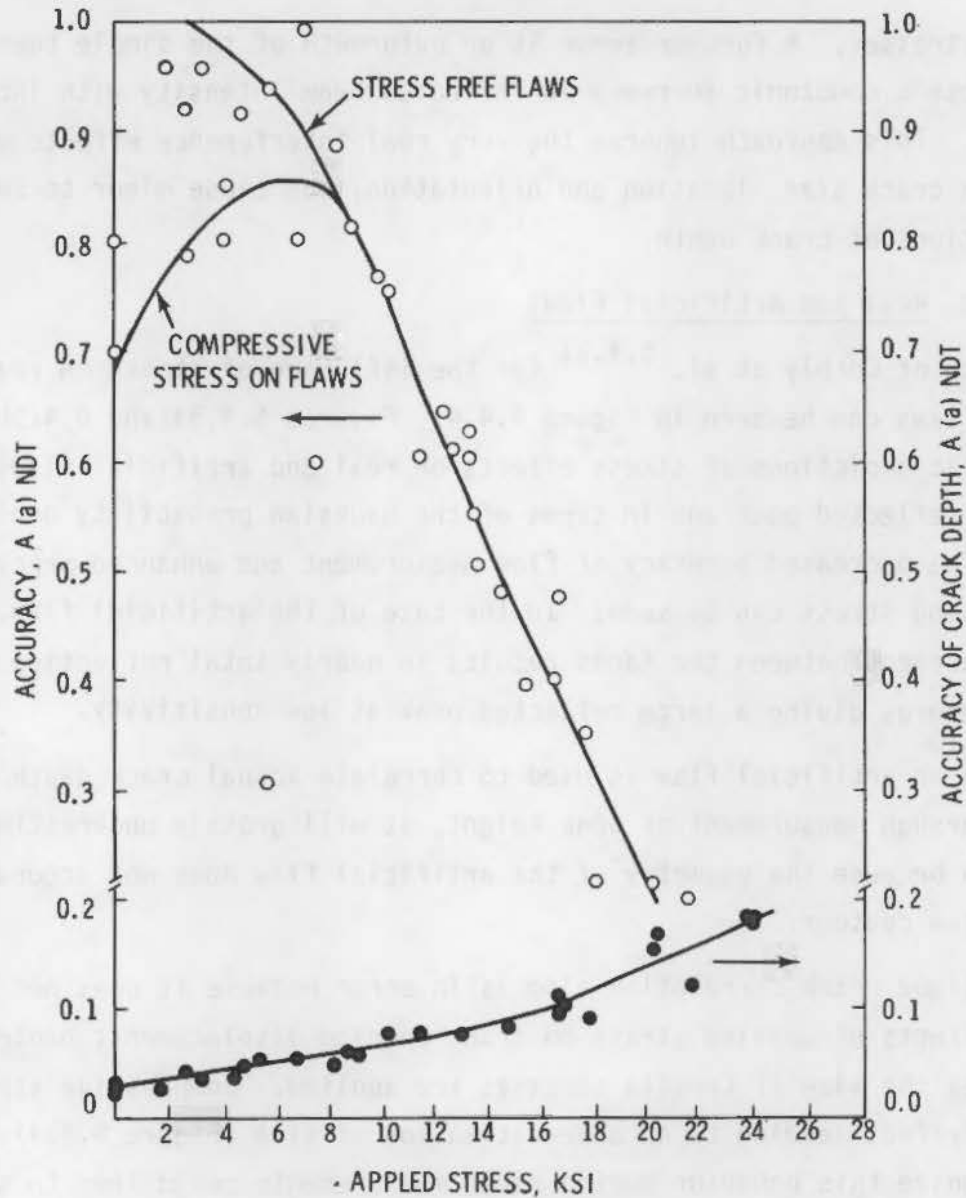


FIGURE 5.4.4. Accuracy of Crack Indication versus Applied Stress, ksi

The dead zone resulting from a combination of transmission pulse, spurious echo and grass echo was minimized or eliminated by a combination of actions. A longitudinal wave with its longer wave length will decrease the grass echo, and the twin probe erases the transmission pulse and spurious echo. Figure 5.4.7 illustrates the twin probe. The basis for selection of 45° is apparent from Figure 5.4.8 where a narrower more sharply directed beam occurs for 45° compared to 70°.

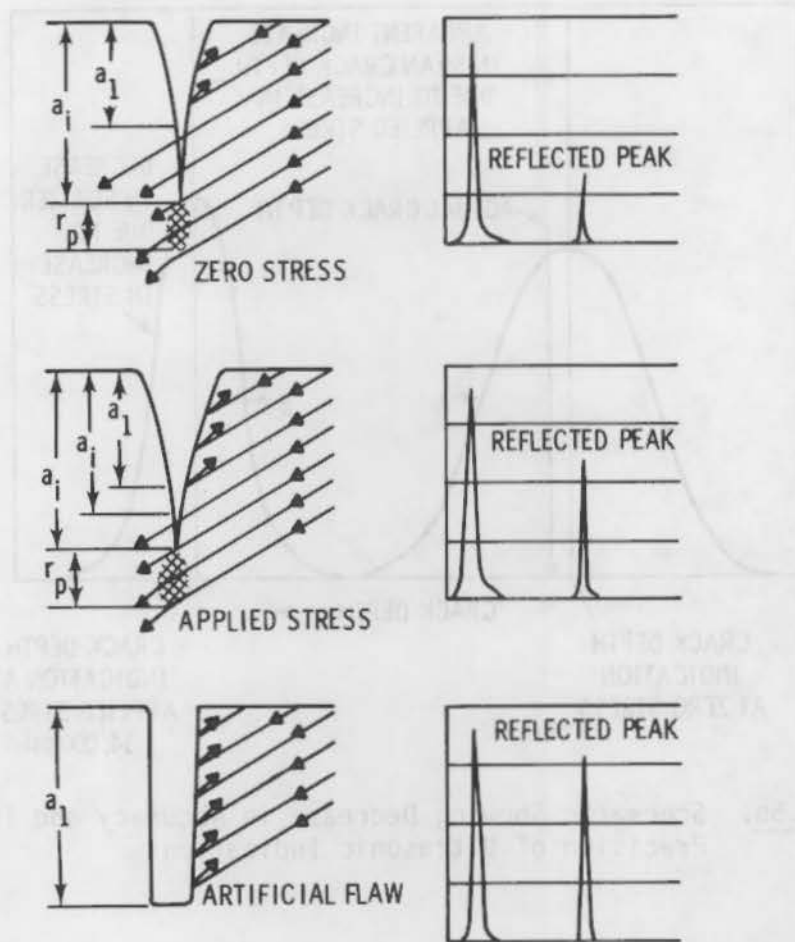


FIGURE 5.4.5a. Schematic of Effect of Stress on Reflected Peak

Table 5.4.10 is a synthesis of all data using the 45° L-wave probes. As can be seen, the cracks could be detected and sized. Usually sizes were overpredicted.

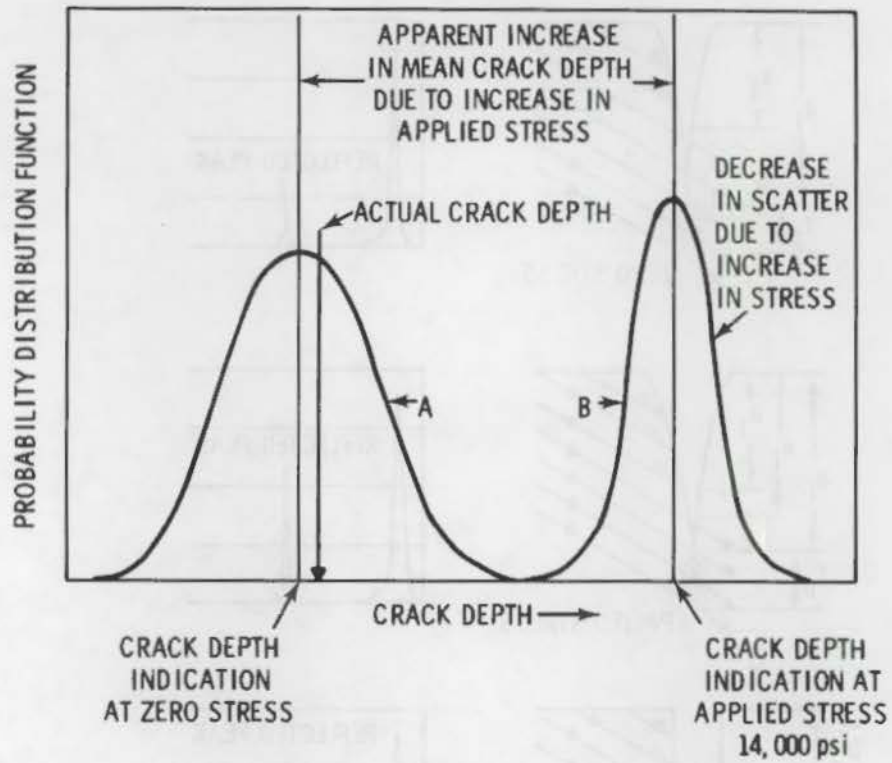
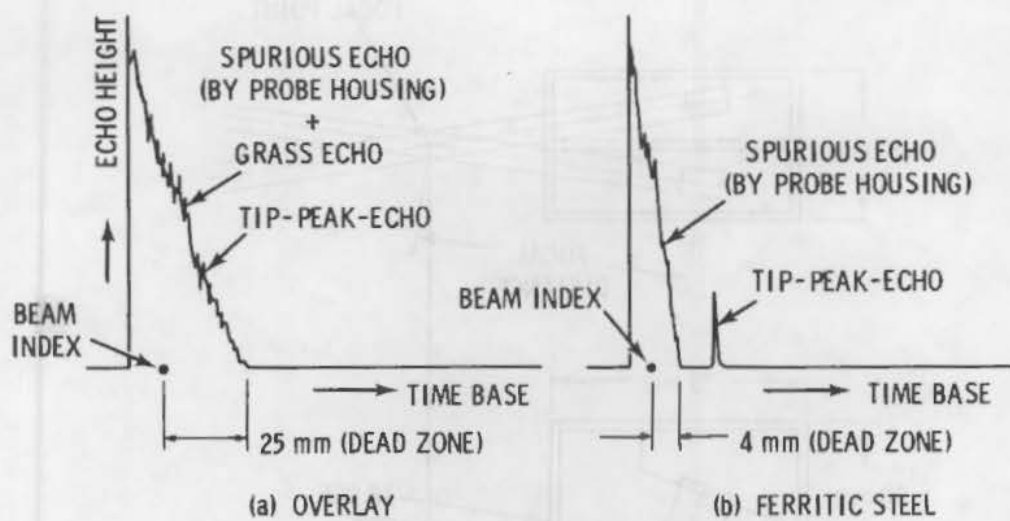


FIGURE 5.4.5b. Schematic Showing Decrease in Accuracy and Increase in Precision of Ultrasonic Indications



SENSITIVITY: REFLECTION FROM DRILLED HOLE - 80% OF CRT HEIGHT

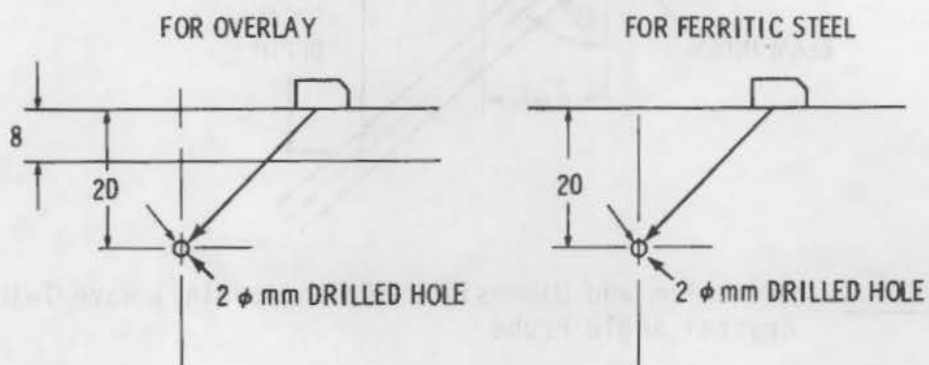


FIGURE 5.4.6. CRT Pattern from Shear-Wave Angle Probe

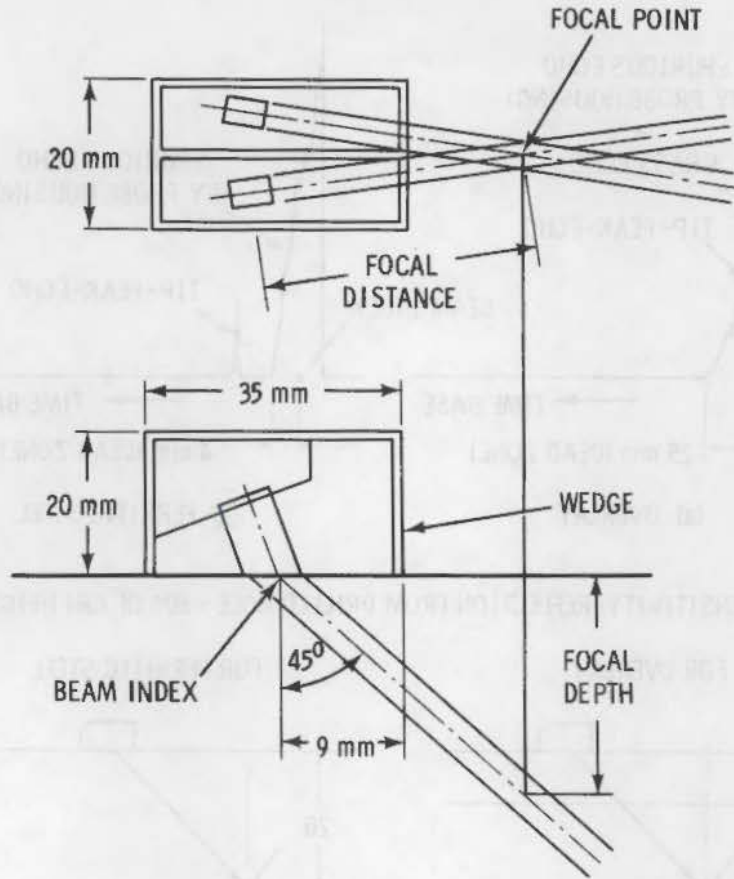


FIGURE 5.4.7. Mechanism and Dimensions of Longitudinal Wave Twin-Crystal Angle Probe

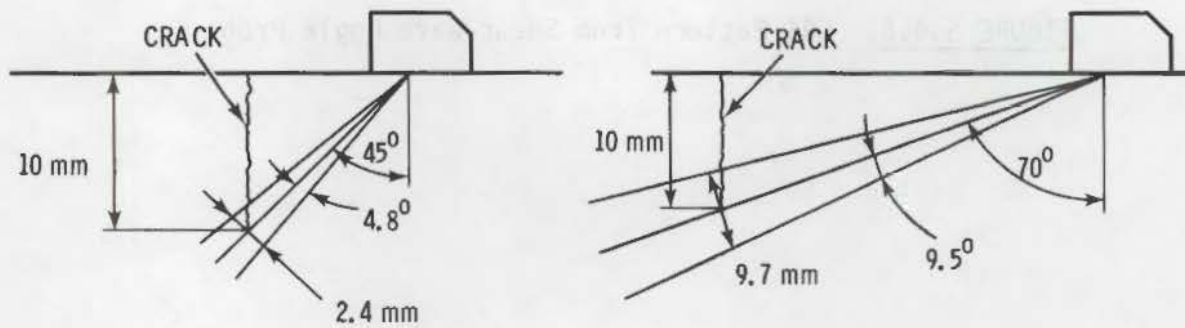


FIGURE 5.4.8. Variation in Directional Characteristics from Difference in Refraction Angle of Angle-Beam Probe



TABLE 5.4.10. Correlation Between Actual Crack Depth and Depth by Ultrasonics (L-wave)

<u>Test No.</u>	<u>Actual Depth of Crack (mm)</u>	<u>Depth of UT</u>		<u>Percent Error</u>
		<u>FD: 10mm</u>	<u>FD: 20 mm</u>	
<u>Natural Cracks - No Overlay Cladding</u>				
1	5	6.3	--	+26
2	10	10.9	--	+9
3	15	14.7	16.5	-2 (+10)
4	20		23.5	(+17.5)
5	30		30	(0)
<u>1-mm Saw Cuts into 8-mm Overlay of 309 SS and 347 SS</u>				
6a	2	2.1		+5
6b	4.5	4.6		+2.2
6c	8	8.8		+10
6d	10	10.6		+6
6e	12	12.7		+5.8
6f	14	14.8		+5.7
<u>Natural Cracks into 8-mm Overlay</u>				
7	14	16		+14.2
8	22		23.3	+5.9

TABLE 1.4.10. Correlation between total catch weight and weight of individual fish (gms)

Total Catch - no. of fish (gms)	Weight of fish		Actual Group
	100-150	150-200	
1	0.5	—	1
2	10.0	—	2
3	10.0	10.0	3
4	—	10.0	4
5	—	10.0	5

1. m. 200 fish into 5-m. weight of 100-150 and 150-200

10	2.1	—	10
20	4.0	4.0	20
30	8.0	8.0	30
40	10.0	10.0	40
50	15.0	15.0	50
60	15.0	15.0	60

Actual Catch into 5-m. weight

10	10	—	10
20	20	20	20

Ho et al.<sup>(5.5.1)</sup> used a surface-wave technique to detect and size fatigue cracks. The data differed somewhat from those of Corbly<sup>(5.4.2)</sup> in that the real and apparent crack depths were essentially the same and applied loads as high as 15 kilopounds had little effect on the apparent crack depth. There was definite evidence of crack closure on release of load which increased with increasing flaw depth.

#### 5.5.1 Delta Scan and Shear Wave

Chang et al.<sup>(5.5.2)</sup> used Delta-Scan and shear-wave UT to examine fatigue cracks in annealed Ti-6Al-4V. No significant correlation was found between signal intensity and crack length. There was a limited trend in specimens cycled to higher peak stresses; however, this could be due to differences in flaw surface roughness. Since crack width was suspected to be the important parameter, attempts were made to increase the width and reduce loss of sound through transparency. A first attempt consisted of subjecting the specimen to 35,000 compression cycles at 44 ksi which caused the crack to open up without growth. It was found that the detectability increased by an average factor of 2.8. A second experiment consisted of statically loading the cracked section which resulted in a definite increase in signal amplitude with increased stress. A reproducible hysteretic effect was observed as the static load was increased, then decreased. A third experiment consisted of removal of residual stresses by thermal annealing. This enhanced flaw detectability and gave a limited correlation.

##### 5.5.1.1 Theoretical Study

The authors<sup>(5.5.2)</sup> carried out a theoretical study to aid in interpreting their experimental results. The model consisted of longitudinal and shear waves at oblique incidence on thin cracks. They assumed an acoustic displacement field could be derived from the gradient of scalar potential for longitudinal waves and the curl of a vector potential representing polarizable shear waves. Superposition permitted the interaction of reflected and refracted waves as interfaces. An interesting conclusion of the theoretical study was that crack opening does not necessarily increase UT response. The UT response

was found to be an oscillatory function of crack openings with the period of oscillation equal to half the wavelength of sound in the crack. Theoretical calculations for the idealized case of a plane wave incident on a flat-parallel crack separation were in good agreement with their experimental results with regard to the period of oscillation; however, the derived change in amplitude is greater than the observed value. The amplitude increased with crack separation from zero to a distance of half a wavelength, then decreased during the next half wavelength opening (to  $\lambda$ ). Therefore, the prevailing assumption that UT response increases with crack opening is sound only if the crack opening is less than  $\lambda/2$  (or larger than  $\lambda$ ).

Calculations of the effects of increasing the angle of incidence indicated such increases shifted the resonance to larger values of  $\omega t$  (frequency times thickness) producing standing waves of longer wavelength in the crack. The fact that such phenomena are not commonly seen experimentally is attributed to divergence of sound beams with commercial transducers which is believed to account for the absence of sharp resonance dips.

#### 5.5.1.2 Frequency Modulation

The authors<sup>(5.5.2)</sup> suggest the introduction of a suitable frequency modulation into the UT equipment so the detected signal would not depend upon crack width. This approach could lead to the sought-after correlation between detectability and crack length, provided other variables such as crack surface texture do not present a problem. Whether such a frequency modulation scheme is feasible is not known.

#### 5.5.2 Surface (Rayleigh) Waves

Lidington and Silk<sup>(5.4.7)</sup> used single-probe surface-wave techniques to measure real flaws in addition to the artificial flaws discussed previously. A T-butt weld in a 50-mm thick plate contained a fatigue crack which ranged from 8- to 14-mm deep. The test was complicated by the changes in direction of the crack and by the high inclusion population in the steel. The results were surprisingly good considering these factors. The accuracy was about  $\pm 0.5$  microsecond corresponding to an error of  $\pm 0.8$  mm. Figure 5.5.1 presents the estimated crack depth profile and the actual profile determined by breaking

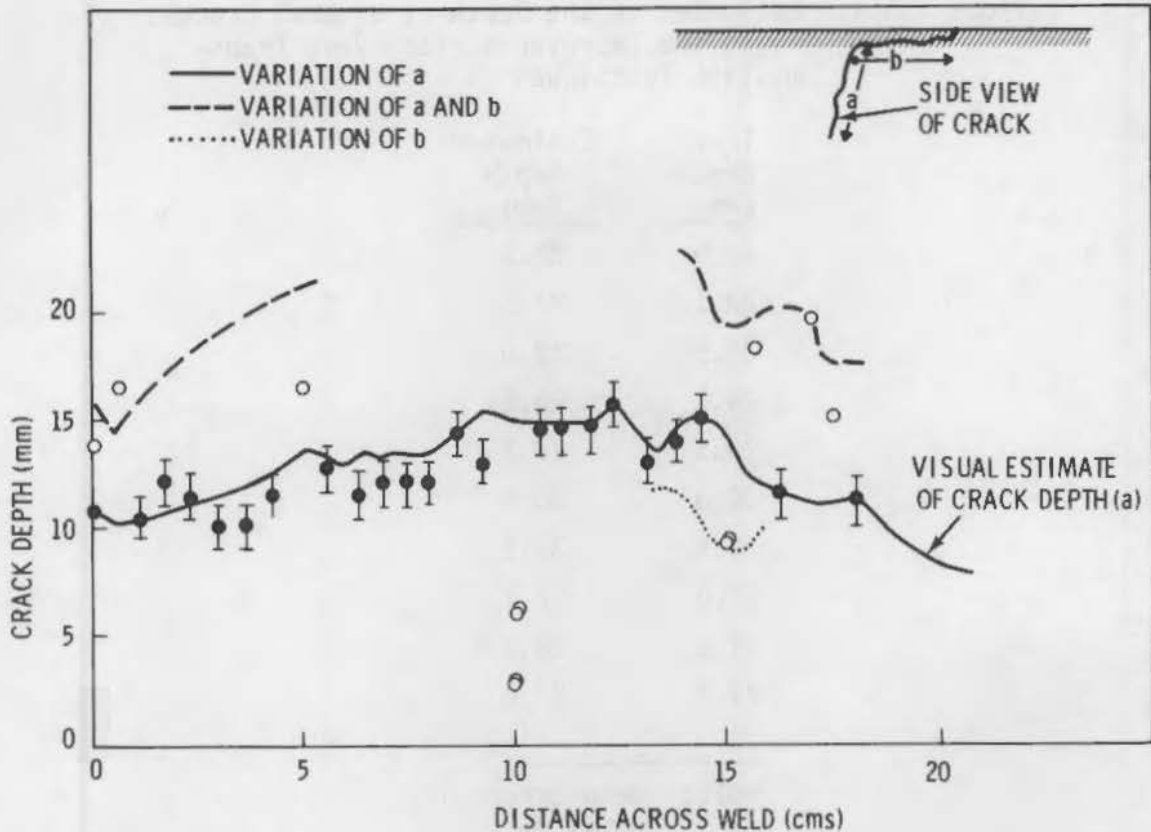


FIGURE 5.5.1. Estimates of Crack Depth in a T-Butt Weld Using a Surface-Wave Pulse Echo Technique

open the specimen. Generally, the agreement is quite good. The anomalous points are believed to occur in regions of large-scale changes in crack direction.

Silk<sup>(5.4.8)</sup> used two approaches to estimate the depth of natural cracks in parallel with similar tests on artificial flaws. The first consisted of an improved surface-wave transmission technique, relying on the timing of sample pulses between two probes. Table 5.5.1 presents data on cracks ranging from 22- to 27-mm deep. The mean error is  $\pm 0.49$ , comparing favorably to the  $\pm 0.35$  mm for the same technique with artificial slits. The second approach made use of the maximum echo position for a mode converted shear wave. Limited tests with artificial slits indicated this amplitude approach should yield an accuracy of better than  $\pm 1$  mm. As noted in Table 5.5.2, the mean error was 1.4 mm or an accuracy of about 13% for the range of crack sizes examined;

TABLE 5.5.1. Estimates of the Depth of Natural Cracks, Using the Improved Surface-Wave Transmission Techniques

<u>True Depth (mm)</u>	<u>Estimated Depth (mm)</u>
22.5	22.5
23.1	22.5
28.5	29.0
29.1	28.8
29.5	29.1
30.0	30.4
29.5	30.3
27.0	27.1
27.5	28.2
27.2	27.0

NOTE: Mean error  
±0.49 mm.

however, one would anticipate that the percentage error would decrease with an increase in crack depth and the cited level of accuracy might be acceptable for many purposes.

#### 5.5.2.1 Time Delay

Lidington et al.<sup>(5.4.3)</sup> continued their work on flaw sizing using time delay. Angled longitudinal waves were used to measure surface fatigue cracks in several steel plates. The actual flaw dimensions were determined by cooling in liquid nitrogen, then breaking open and measuring the crack profile optically. As noted in Figures 5.5.2a and 5.5.2b, there is an excellent correlation of actual and estimated crack profiles. Figure 5.5.2a presents data using transit time. Figure 5.5.2b also presents data using transit time to determine distance; however, the latter data were obtained with an electronic system rather than the visual used previously. The new system automatically measures the transit time of the signal associated with the crack tip or the back-wall echo. In essence the system is a digital crack depth meter.

TABLE 5.5.2. Estimates of the Depth of Natural Cracks, Using the Maximum Echo Position for the Mode-Converted Shear Wave

<u>True Depth (mm)</u>	<u>Estimated Depth (mm)</u>
10.0	8.0
10.8	8.5
11.5	10.5
12.5	13.0
14.0	14.5
14.2	15.0
14.5	15.5
14.2	16.0
13.9	14.1
12.5	14.0
11.0	9.0
8.5	8.0

NOTE: Mean error  $\pm 1.4$  mm.

### 5.5.3 Eddy Current

Parks<sup>(5.5.4)</sup> used eddy current techniques to measure the size of surface cracks in aluminum and titanium. The technique was able to detect cracks over the range of 0.005 in. to 0.070 in. Additionally, for specific conditions, predicted crack depths and actual crack depths agree quite well. Figure 5.5.3 is a least squares fit of the data over the range of 5 to 30 mils. The caveat above concerning specific conditions can be understood through examination of Figure 5.5.4 where two discrete families are seen to exist. The lower curve, consisting of "shaker table" cracks, can be explained on the basis that accelerated cracking leads to nearly straight crack fronts or ones with high  $c/a$  ratios so the crack area is much greater than is the case for a half-penny

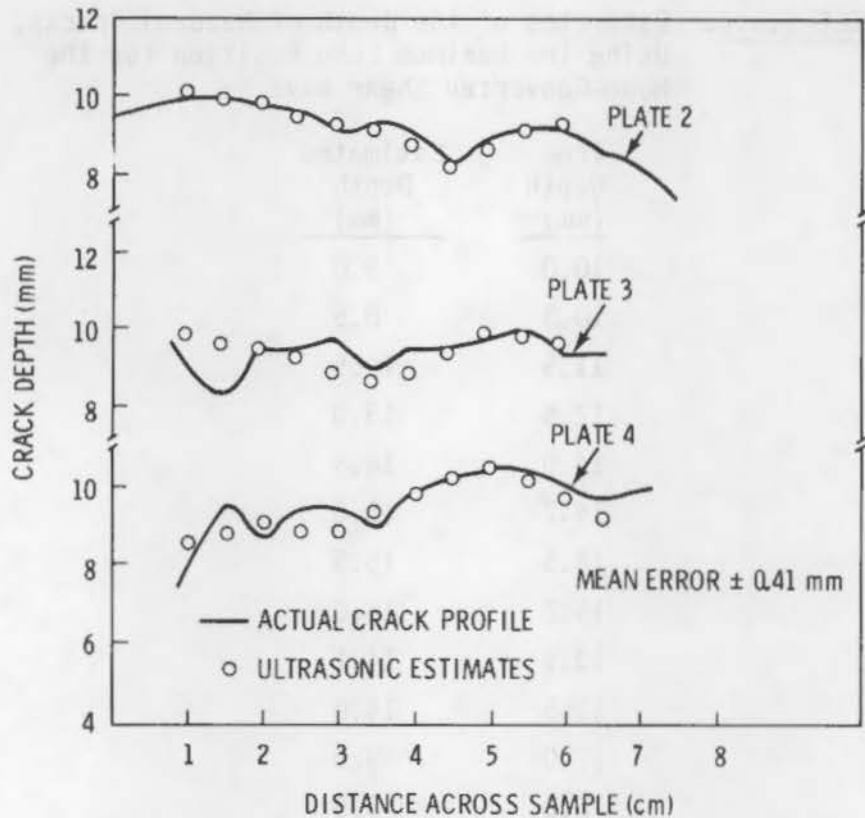


FIGURE 5.5.2a. Actual Profile Compared with Ultrasonic; Old Timing

type crack. The "natural" cracks curve is made up of the half-penny type crack with much lower crack areas for a given crack depth. The correlation in Figure 5.5.4 should be closer if the plot had been in terms of crack area.

A third item of considerable interest is the correlation of the shape of the ET signal with the type of defect. In essence, the author<sup>(5.5.4)</sup> has a simple signature analysis approach that appears to group fatigue and stress corrosion cracks into one family denoted by a smooth ET spike. These can be differentiated from corrosion, which has a broad ragged peak, and scratch or gouge, which has a sharp downward and upward deflection of the peak. These are shown in Figure 5.5.5.



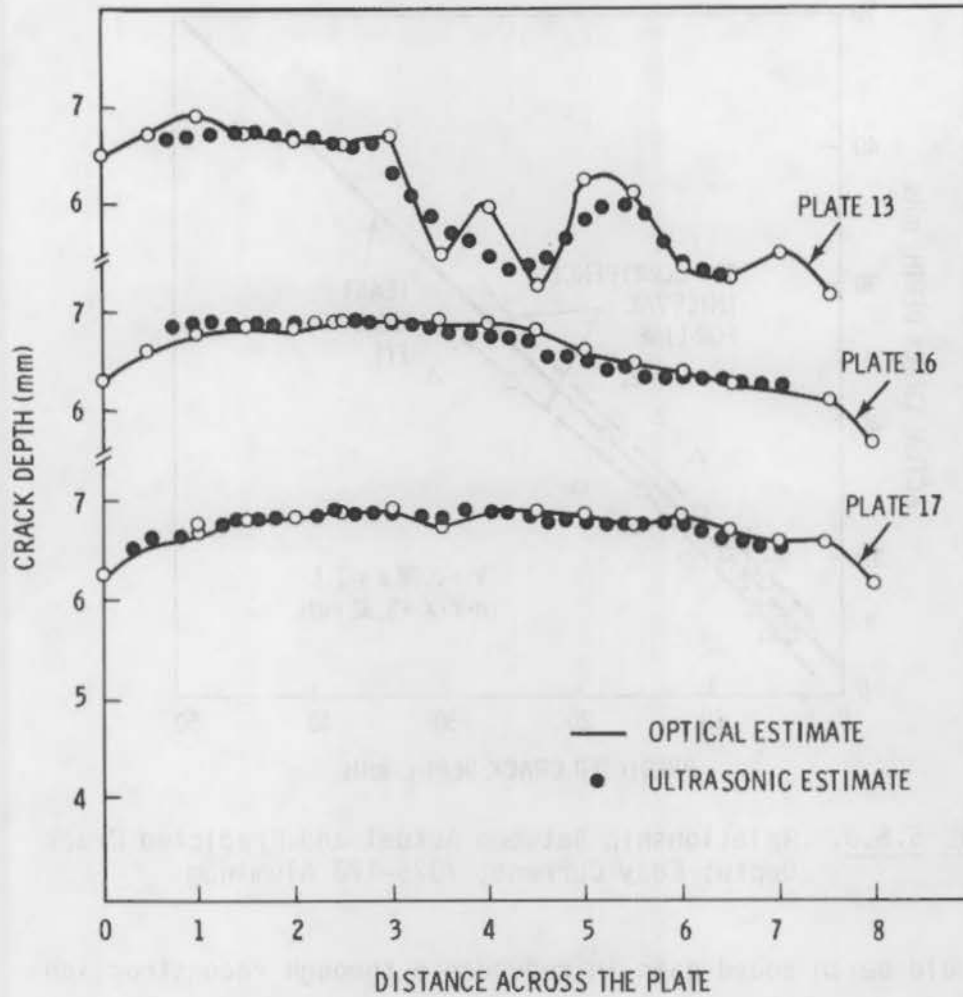


FIGURE 5.5.2b. Actual Crack Profile Compared with Ultrasonic; New Timing

#### 5.5.4 Image Reconstruction

Höller<sup>(5.3.5)</sup> discusses advanced techniques for image reconstruction directed toward meeting the following criteria:

- Any reconstruction should approach the true image of the defect as closely as possible.
- Both time or phase delay data in addition to amplitude data are necessary in reconstruction.
- Sampling procedures may be necessary unless large apertures are used.

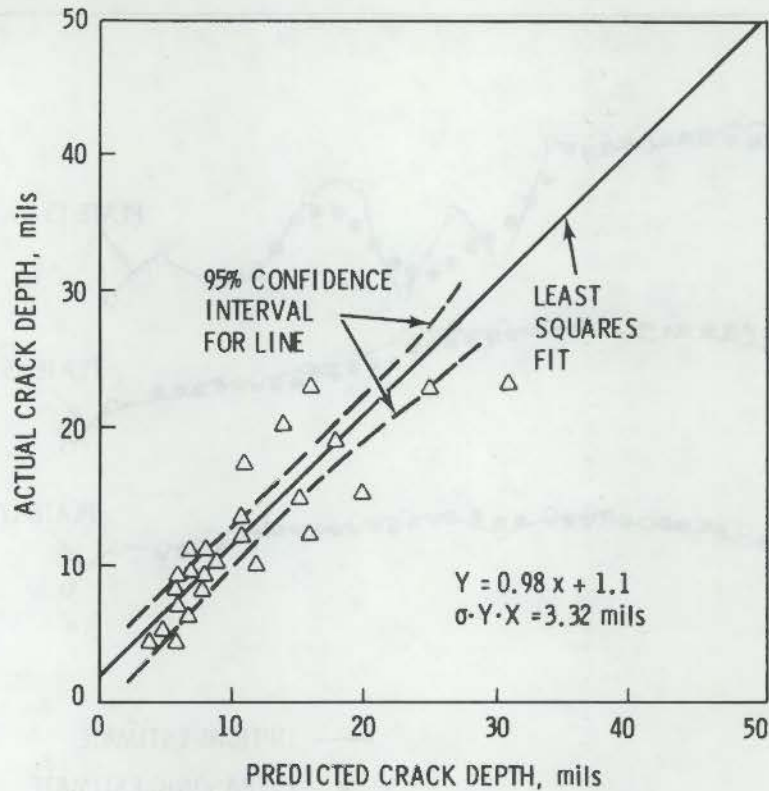
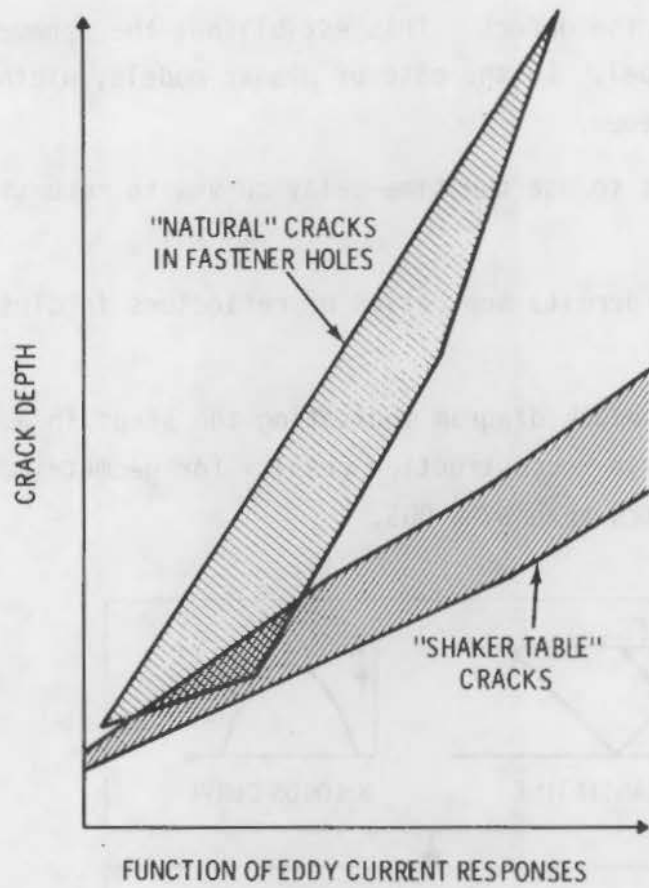


FIGURE 5.5.3. Relationship Between Actual and Predicted Crack Depth; Eddy Current, 7075-T73 Aluminum

- There should be an added gain in redundancy through reconstruction since measures are taken to focus the echo in the reconstruction.

The measurement of time-delay and amplitude during scanning will provide locus curves for time-delay and amplitude. If two incident directions are used with a given beam angle, four locus curves will be obtained. The defect may be viewed either by direct or back reflection and information is available from both the main lobe and the side lobes. With two perpendicular planes of incidence, the defect is viewed from eight directions—even more if additional beam angles are used. These data are used in the reconstruction in a two step process. The first step is to compare the locus curves to those obtained by diffraction theory for typical geometric reflectors such as spheres, discs, cylinders and strips. Pattern recognition will permit decision as to which



**FIGURE 5.5.4.** Correlations of Eddy Current Responses with Crack Depths in Titanium

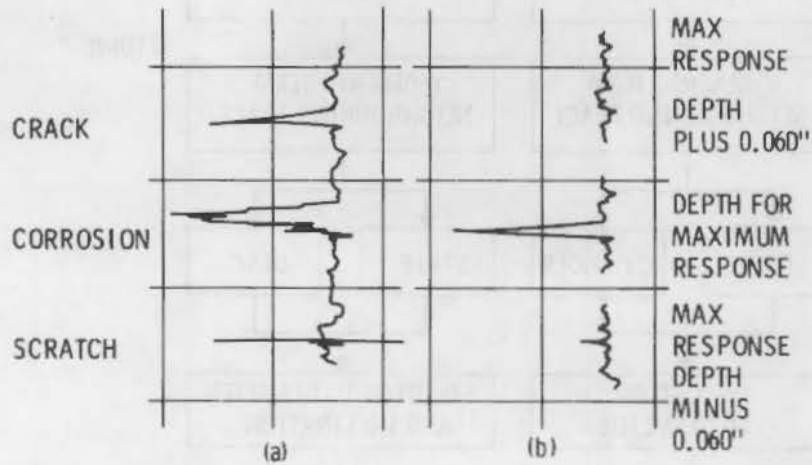


**FIGURE 5.5.5.** a) Comparison of Responses from Three Kinds of Defects; b) Responses from Crack Perpendicular to Hole Axis (i.e., delamination, exfoliation)

reflector best matches the defect. This establishes the parameters used to fit the appropriate model. In the case of planar models, width or diameter and orientation are needed.

The second step is to use the time-delay curves to reconstruct the edges of the reflector.

Use of time-delay permits separation of reflectors in close juxtaposition to one another.

Figure 5.5.6 is a block diagram indicating the steps in a reconstruction and Figure 5.5.7 displays reconstruction results for geometrical reflectors indicating a closer match than with DGS.

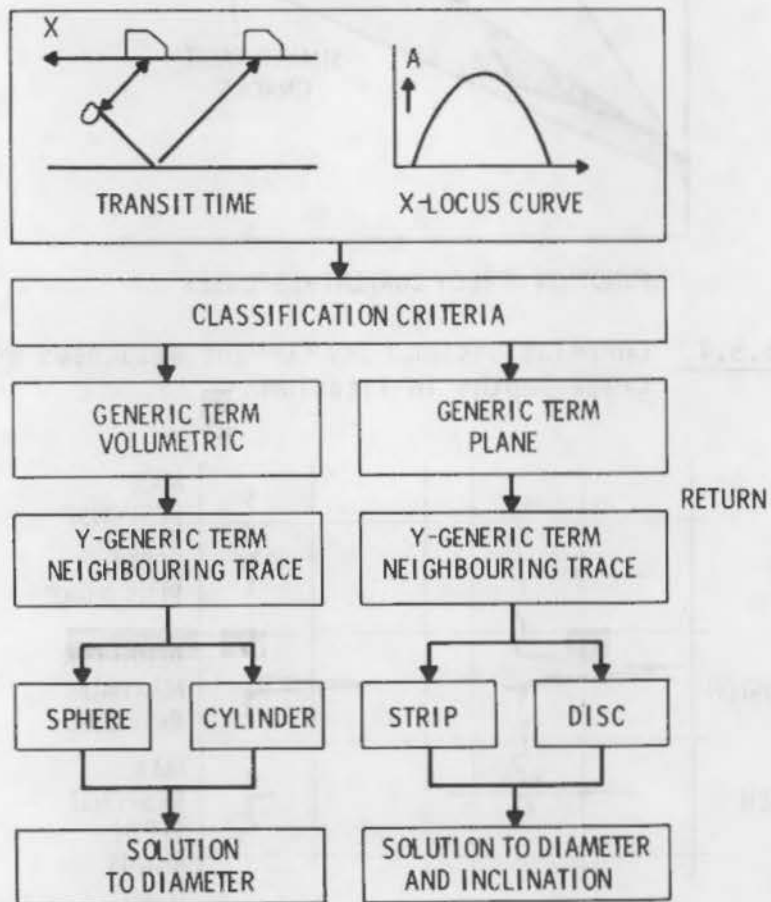


FIGURE 5.5.6. Reconstruction



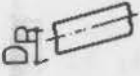

MODEL	MEASUREMENT		RECONSTRUCTION		DGS (AVG)-METHOD	
	$D_R$ (mm)	$\delta(^{\circ})$	$D_R$ (mm)	$\delta(^{\circ})$	$D_R$ (mm)	$\delta(^{\circ})$
SPHERE 	3 $\phi$	-	3.25 $\phi$	-	1.2 $\phi$	-
CYLINDER 	4 $\phi$	-	3.9 $\phi$	-	4.5 $\phi$	-
STRIP 	6	35	6.3	39	3.8	-
DISC 	6 $\phi$	40	5.1 $\phi$	43	1.8	-

FIGURE 5.5.7. Reconstruction: Results

#### 5.5.5 Possible Limitations

Hudgell et al. (5.5.5) in an excellent article spelled out the pluses and minuses of three Rayleigh wave techniques: 1) transmission around the defect, 2) mode conversion at the defect, and 3) acoustic spectroscopy. Their results can be summarized in one short statement: if they could detect the defect, they were quite successful in sizing it. Testing was on surface breaking fatigue cracks in a steel line pipe. Specific problems related to the detection were as follows:

- The transmission Rayleigh waves propagated straight across the fatigue cracks rather than around them (transparency); therefore, it was necessary to bend the specimens to open the cracks.
- The Rayleigh waves were severely attenuated by rough surfaces indicating the need to do an acceptable preparation.
- Of seven cracks investigated by transmission waves from 20 locations, five locations yielded no energy indications and, in four other locations, it was difficult to identify the signal corresponding to the energy transmitted around the crack; four of the five locations

yielding no energy indications were found to be due to the cracks being very small (<2 mm deep) so that transmission time essentially was the same as ring-down time.

One real problem and another potential problem were cited with regard to sizing:

- With mode conversion on fatigue cracks, the crack depths tend to be underestimated, possibly due to premature conversion of the Rayleigh wave from irregularities down the crack face.
- The authors did not know how well the techniques would apply to close clusters of cracks, bifurcated or multibranching cracks, or cracks with orientations other than normal to the surface. [Lidington and Silk<sup>(5.4.7)</sup> evaluated the last.]

Some idea of the accuracy of estimation of crack depth can be determined from Figure 5.5.8. While there is definite scatter the fit is quite good. Figures 5.5.9a and 5.5.9b illustrate the accuracy of the mode conversion technique in estimating the fatigue crack profile.

Lumb<sup>(5.5.6)</sup> in a recent paper reviewed the state of the art of defect sizing with emphasis on those breaking either the accessible or the inaccessible surface. The report is recommended reading since it presents an excellent review of the pros and cons of the various techniques. The author concludes the following:

- Sizing reliability probably has been oversold for state-of-the-art systems.
- It is prudent to iterate between two or more independent systems.
- It may not be possible to detect or size tight defects unless they are examined while under some tensile stress.

The author cites the excellent results obtained with Rayleigh waves on notches, but cautions regarding reliability with fatigue cracks. The need for short-pulse probes in thinner sections and errors in angled cracks have been cited previously.

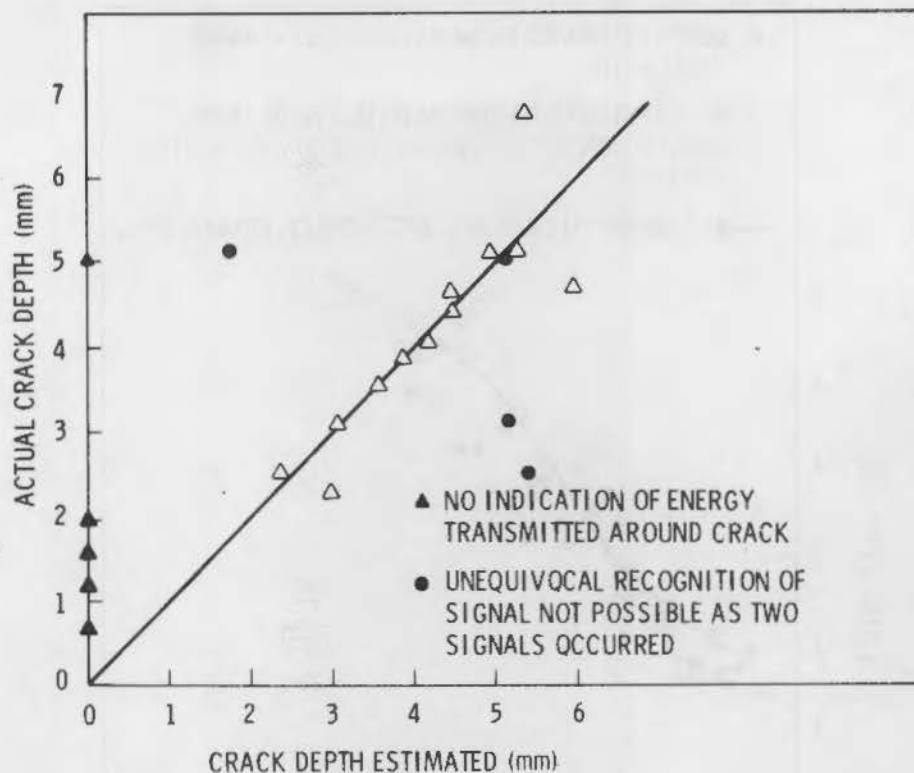


FIGURE 5.5.8. Estimation of Depth of Fatigue Cracks by Rayleigh Wave Transmission

The technical feasibility of analyzing the wave pulse (ultrasonic spectroscopy) is recognized; however, the requirements for computing hardware and software may make the technique prohibitively expensive.

The author<sup>(5.5.6)</sup> argues that it is a big step from measuring notch depths in flat plates to crack depths in situ. He cites gas-filled gaps of  $10^{-8}$  cm in steel as reflecting ~10% of the UT energy, while a gap of  $10^{-7}$  cm reflects ~90%. With water filled gaps, a gap of  $10^{-3}$  cm reflects ~90%. With fatigue cracks, which may be in compression, significant transmission (transparency) may occur, adversely affecting detection and sizing. Generally, he feels that the high sensitivity systems have been oversold since they will not deliver the needed reliability.

#### 5.5.6 Opposite Surface

A potential approach to the detection and sizing of stress corrosion cracks originating at the inner bore of piping is discussed by the

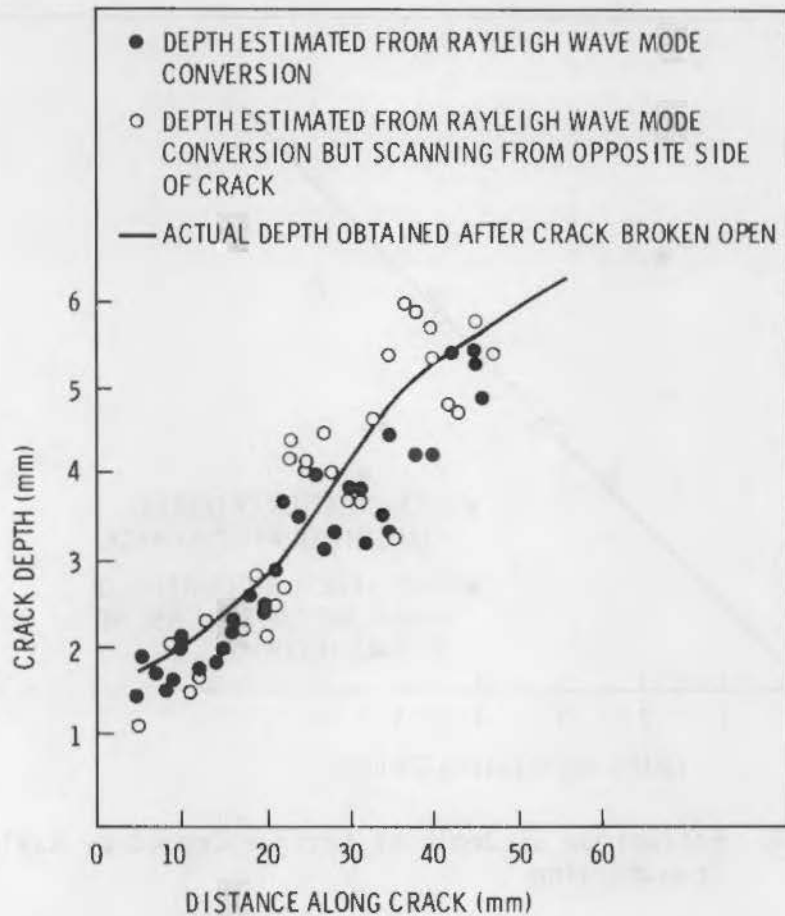


FIGURE 5.5.9a. Estimation of Depth Profile of Fatigue Cracks by Rayleigh Mode Conversion

authors.<sup>(5.5.3)</sup> Both high-angle ( $70^\circ$  to  $80^\circ$ ) shear-wave probes and angled longitudinal-wave probes were used to determine flaw profiles. Shear waves have the apparent advantage of a potential improvement in sizing accuracy because of the lower velocity of shear waves compared to longitudinal waves ( $c_s/c_l = 55\%$  for steel). This apparent advantage due to increased transit time is erased because the time domain in which the diffracted wave is expected often is dominated by stray signals from other modes and sources which make it difficult to identify the diffracted wave. Crack depth tests using high angle probes had mean accuracies of about  $0.35 \lambda$  which is worse than the longitudinal waves, probably due to interference from other signals. The authors<sup>(5.5.3)</sup> conclude there is little justification in using shear waves, and prefer to use longitudinal waves at increased frequencies.



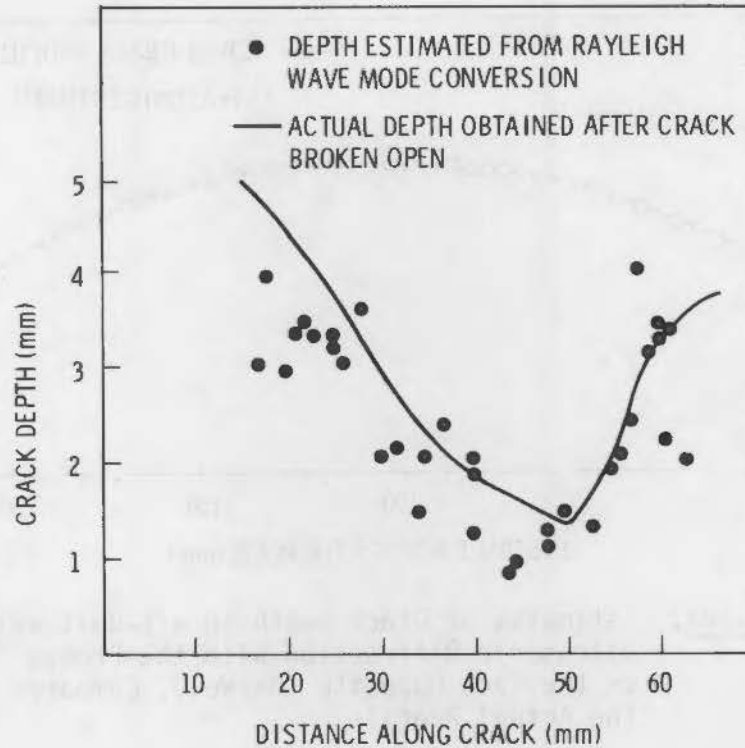
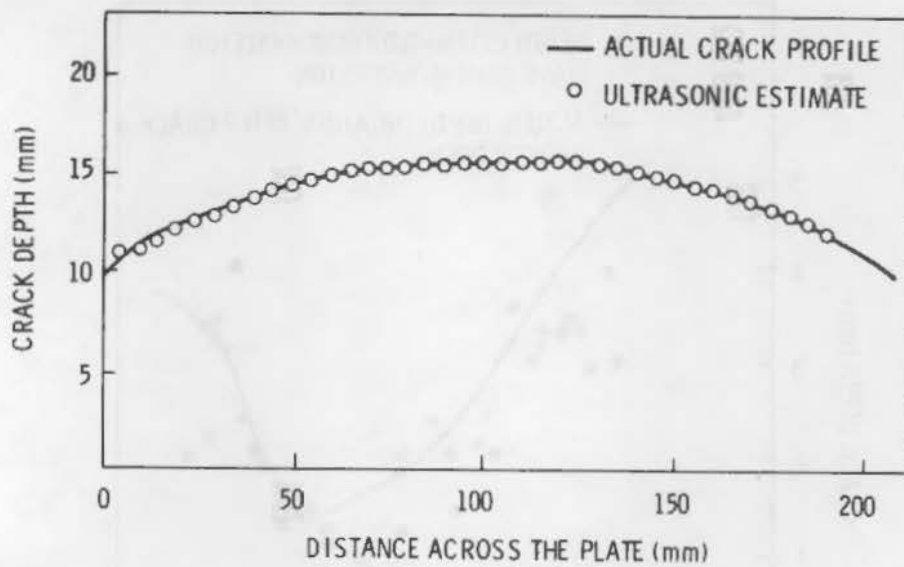


FIGURE 5.5.9b. Estimation of Depth Profile of Fatigue Cracks by Rayleigh Mode Conversion

#### 5.5.6.1 Diffraction

The diffraction technique can be used to detect and measure cracks growing from the surface opposite to that on which the probes are located. Excellent accuracies have been attained with this technique as can be seen in Figure 5.5.10a.<sup>(5.5.7)</sup> The mean accuracy was in the range 0.1 to 0.2 mm which is better than obtained in the more conventional case of the crack on the same surface as the probe. This improvement is attributed to more favorable geometric conditions; namely, the crack tip is about 35 mm from the far surface compared to 15 mm from the near surface (longer path—more discrimination). A potential source of difficulty may occur in steels with a high inclusion content which could be sources of intense reflections. The attenuation and channeling of the beam in a dendritic austenitic weld could be a problem also. Figure 5.5.10b permits a direct comparison of measurements from the same side as the flaw.



**FIGURE 5.5.10a.** Estimates of Crack Depth in a T-Butt Weld Using Ultrasonic Diffraction with the Probes Placed on the Face Opposite the Weld, Compared with the Actual Profile

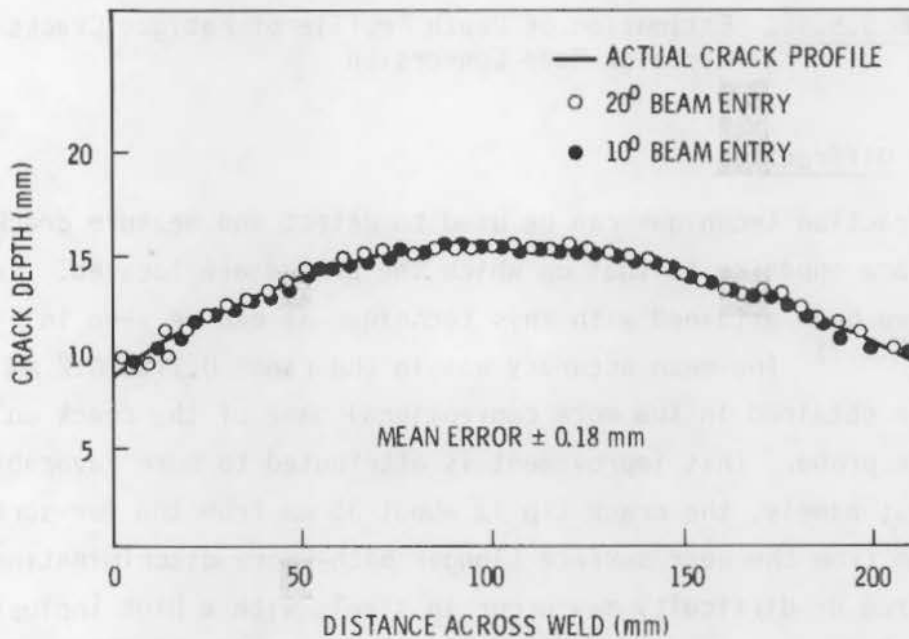


**FIGURE 5.5.10b.** Estimates of Crack Depth in a T-Butt Weld Using Diffracted Ultrasound, Compared with the Actual Crack Profile. Data points are corrected for lateral changes in the position of the crack.

The two examination options discussed above are illustrated schematically as Figure 5.5.11a and b.

Silk and Lidington<sup>(5.5.7)</sup> used a single-probe technique at normal incidence to detect and measure 10- to 30-mm deep fatigue cracks. The probe was located on the surface opposite the cracks. Four different plates containing fatigue cracks were examined. The data are presented in Table 5.5.3.

In Plate A, the data followed the general contour of the crack; however, the scatter was large, almost an order of magnitude greater than that reported

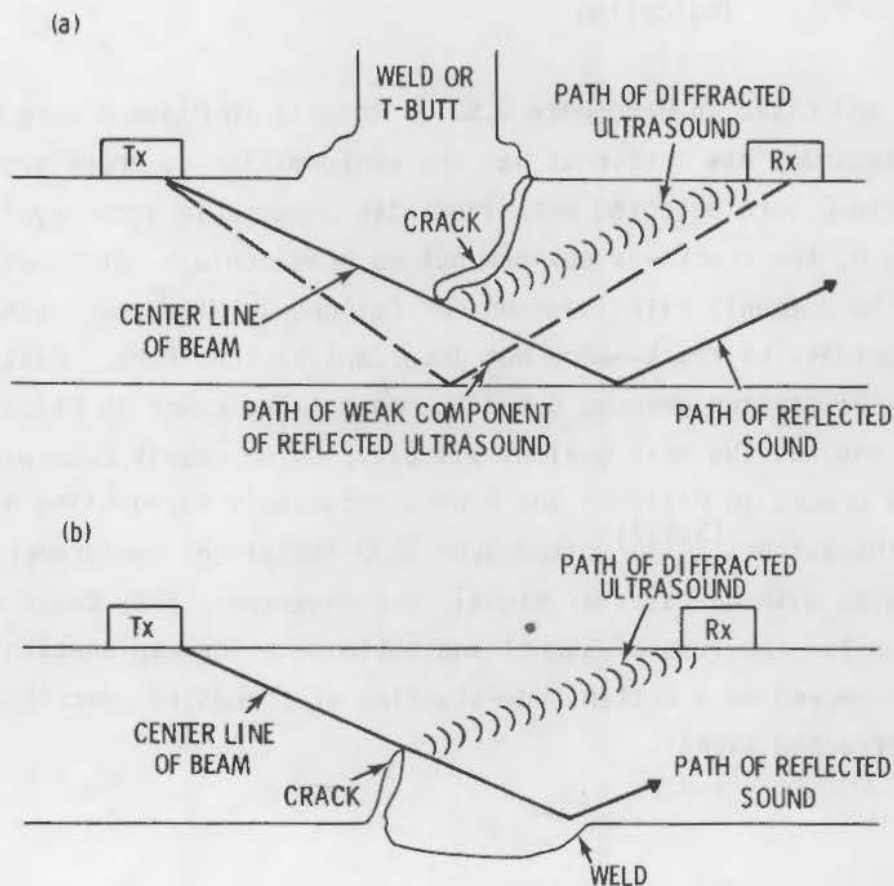


**FIGURE 5.5.11.** a) Diffracted Ultrasound used for Crack Depth Measurement with Cracks on the Same Surface as the Probe; b) Ultrasonic Diffraction Techniques also used when Cracks are Present on the Surface Opposite to the Probe

TABLE 5.5.3. Degree of Agreement Between Crack Size Measurements Using a Cathetometer and the Single-Probe Technique at Normal Incidence

Plate	Agreement	Error	
		Absolute (mm)	Percentage
A	Moderate	±2.0	13
B	Good	±0.3	3
C <sub>A</sub>	Good	±0.5	1.7
C <sub>B</sub>	Good	±0.2	2
D	No visible ultrasonic indication		

by Underwood and cited in Reference 5.5.7. Results on Plate B were much better; the accuracy was better as was the conformation to crack profile. Both cracks in Plate C were detected and sized with acceptable accuracy. In the case of Plate D, the crack was obvious but no echo could be attributed to the crack tip. The commonly cited reasons for failure in UT--poor cleanliness of steel and tightness of crack--were not important factors here. Plates C and D had the least UT scatter whereas B had the most. The crack in Plate D had been overstrained and was the most obvious visually, being nearly 2-mm wide at the surface. The cracks in Plates A and D were accurately sized using a two-probe technique. The authors<sup>(5.5.7)</sup> cited over 2000 individual measurements on some 30 crack samples with no cases of signal loss observed. They could advance no obvious reason for the loss of signal and anticipate the explanation of its behavior will depend on a better understanding of processes contributing to the scattered diffracted signal.

The embedded flaw represents the condition most often met within large thick-walled components in nuclear light water reactors such as reactor pressure vessels, pump casings, and valve bodies or steam generator shells. The operational defect due to fatigue or to stress corrosion has occurred most often in piping and safe ends; such defects have been quite rare in the thick-walled components. The problems of flaw detection are somewhat different with the embedded flaw compared to a surface fatigue crack.

#### 5.6.1 Artificial Flaws

Relatively limited work has been done with artificial flaws in the sense of quantitatively defining measurement errors from drilled holes or similar reflectors. The preceding statement is applied to conventional UT equipment. Sizing by acoustic holography, with focused probes, or using techniques such as adaptive learning will be presented in a separate chapter.

Work in France<sup>(5.6.1)</sup> on artificial defects is of interest. A 6-dB drop was used to measure the size of 60-mm long notches at depths of 50, 100, 180 mm or 4-mm flat-bottomed holes at depths of 70 and 135 mm. Beam spread as a function of depth was determined. There is a definite increase in beam diameter above 100 mm; in fact, the beam diameter doubled from 10 to 20 mm in going from 100 to 200 mm. No obvious pattern appeared to exist.

#### 5.6.2 Real Flaws

##### 5.6.2.1 Effect of Cladding

Yamaguchi et al.<sup>(5.6.2)</sup> examined the effect of cladding on flaw detection and sizing using normal beam, angle beam and pitch-catch techniques. Two methods were used to normalize the data. The first (F-method) paralleled ASME's 50% DAC; the second (FB-method) was developed to eliminate the effect of cladding on flaw detection. The method consisted of using the F/B ratio to remove such factors as surface roughness of clad. F/B consists of the reflected echo from a flaw (F) divided by the reflected echo from the opposite surface (B). Figure 5.6.1 presents the data for the F and F/B methods on a partially clad test block so that the effect of cladding can be seen. The F/B

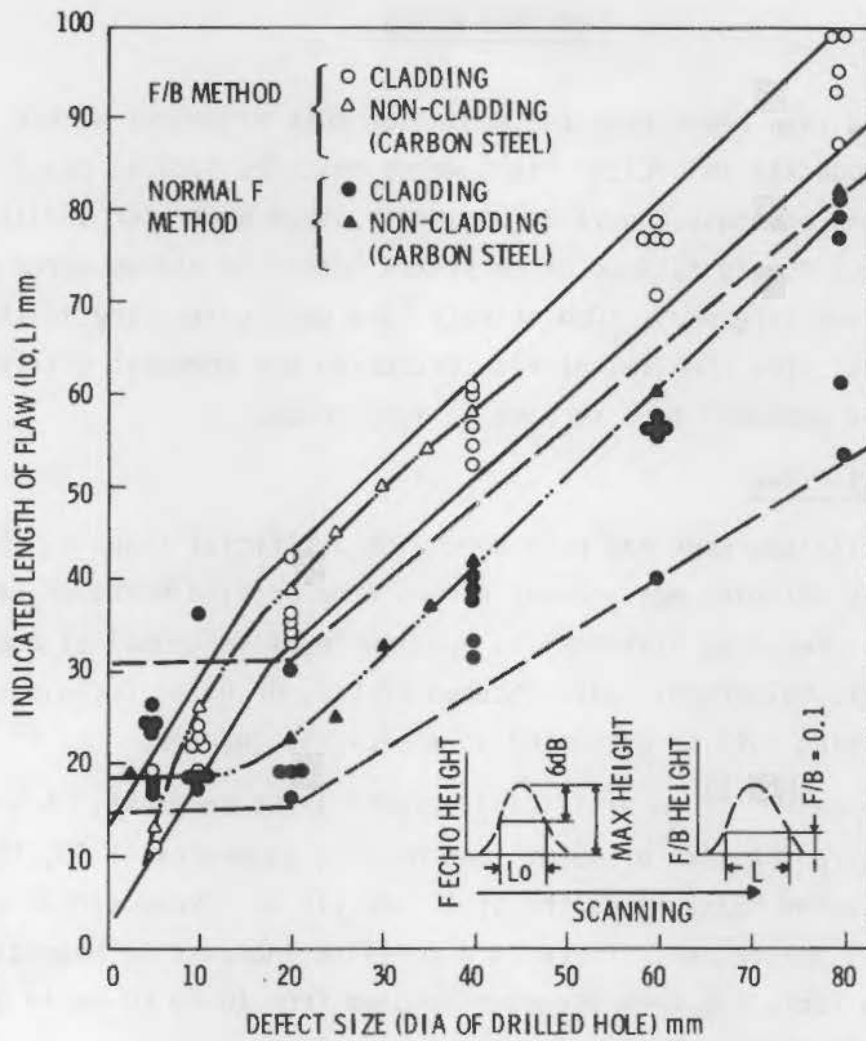


FIGURE 5.6.1. Relation Between Actual Defect Size and Indicated Length of Flaw (normal F method and F/B method)

method generally overpredicts the size while the F method underpredicts when examined through cladding. In the absence of cladding, the F method yields accurate results while F/B substantially overpredicts size.

The authors<sup>(5.6.2)</sup> reported the sizing of actual flaws in what is presumed to be nuclear structures. Both UT and RT were used with the ratio UT/RT (U/X) of measured flaw sizes given. The UT consistently gives higher estimated values than does RT. Unfortunately, the actual values were not given so the absolute accuracies cannot be cited. The values are given in Table 5.6.1.

TABLE 5.6.1. Comparison of Flaw Sizes Estimated from Ultrasonic Test and Radiography

Defect Type		Estimated Flaw Size		(U/X)
		by Mock-up Test, mm	by 12 MeV LINAC (X), mm	
Crack	a	94	17	5.7
Crack	b	65	58	12.0
Crack	c	94	62	1.5
Crack	d	100	66	1.5
Crack	e	153	107	1.4
Crack	f	81	50	1.6
Slag Inclusions	g	69	41	1.7
Slag Inclusions	h	81	54	1.5
Incomplete Penetration	i	118	125	0.9
Incomplete Penetration	j	88	Undetected	--
Incomplete Penetration	k	65	50	1.3

#### 5.6.2.2 Probe-to-Specimen Contact

Buken and Krächter<sup>(5.6.3)</sup> conducted studies of the influence of probe-to-specimen contact, properties of probes, and selection of optimum angle of incidence. Both artificial (bore-holes and grooves) and natural defects were used for the evaluations. Defects were sized by the half-width or half-depth technique which had an accuracy of  $\pm 50\%$ .

One study paralleled that of Yamaguchi et al.<sup>(5.6.2)</sup> in comparing UT and RT sizing of natural defects (porosity, slag inclusions, and a combination of both). Contrary to the Yamaguchi results, where UT consistently estimated the defect to be larger than RT, Buken and Krächter's<sup>(5.6.3)</sup> UT data consistently predicted lower values than RT. Since the defect sizes, UT flaw sizing technique and component thickness differed in the two studies, it is difficult to draw definite conclusions. Figure 5.6.2 contains the data.<sup>(5.6.3)</sup>

Root defects were sized by the UT half-height technique and the estimated values compared with the actual sizes determined metallographically. The trend was similar to that of Figure 5.6.2; the UT consistently underpredicted size.

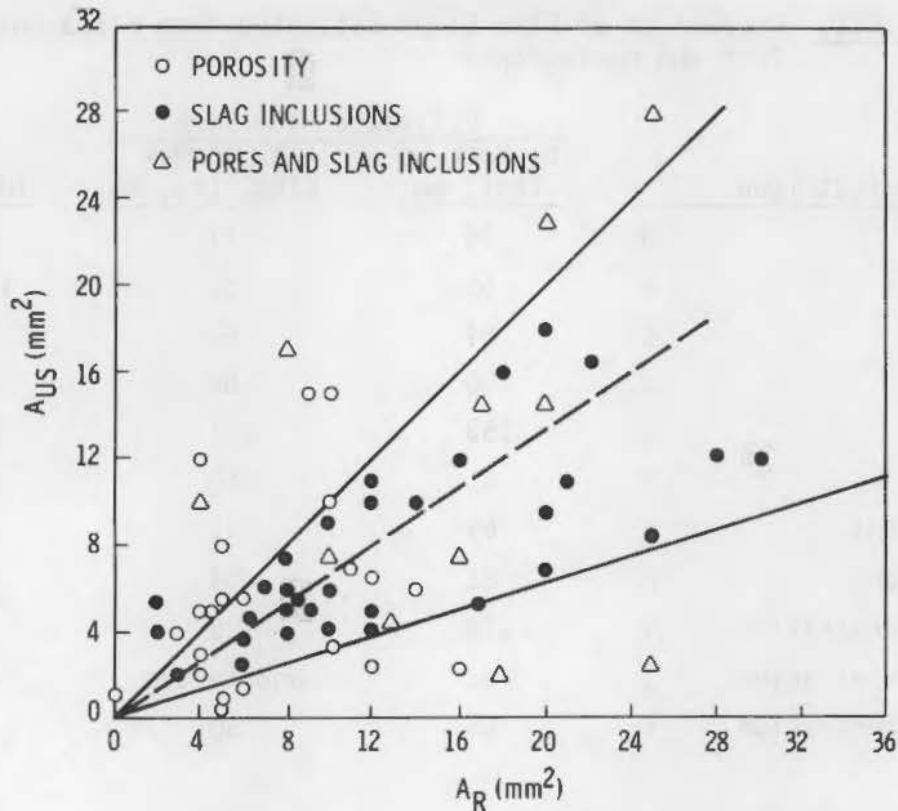


FIGURE 5.6.2. Comparison Between the Sizes of Defects Measured by Ultrasonic ( $A_{US}$ ) and Radiographic ( $A_R$ ) Testing

One further item of interest concerned the changes in signal amplitude with defect orientation (see reference 5.6.3). A flaw normal to the surface ( $\beta = 0$ ) had the maximum amplitude, about 16 dB. A minimum occurred at  $\beta = 20^\circ$  where the amplitude was -14 dB, rising to 4 dB at  $\beta = 30^\circ$ .

#### 5.6.2.3 ASME XI NDE-UT

Work in Japan<sup>(5.6.4)</sup> using ASME XI NDE-UT procedures, but sizing at 20% DAC, measured embedded flaws in pressure vessel welds. In addition, RT data were correlated with UT. A majority of the defects were slag inclusions. It was found that the UT technique consistently overestimated the flaw size both in length and depth. Only four of 19 defects were detected by RT.

Monnier et al.<sup>(5.6.5)</sup> compared several UT methods for measuring embedded defects in a thick weldment. Plane transducers in contact and immersion as well as focused transducers and acoustic holography were used. The latter will



be discussed later in the chapter covering advanced UT techniques. Contact UT with plane transducers was used with 45° probes scanning in both directions parallel to the weld and perpendicular to the weld. Table 5.6.2 summarizes the data relevant to contact and immersion plane transducers.

#### 5.6.2.4 Undercladding Cracks

A special case of flaws requiring detection and sizing are undercladding cracks immediately below an austenite stainless steel weld overlay. With UT, there are the combined problems of attenuation through stainless steel, defects in the near field and relatively small flaws. A technique was developed by deRaad and deSterke<sup>(5.6.6)</sup> using a pitch-catch compression wave. A 70° angle was used to minimize one flaw shadowing another. A 4-dB suppression was used to remove amplitude variations due to cladding irregularities. The undercladding cracks fell into two patterns; those separated by 10 mm or more, and those separated by no more than 5 mm. The pattern can be seen in Figure 5.6.3 showing the effect of clustered defects and depth of defects.

Huebner<sup>(5.6.7)</sup> used a UT pitch-catch technique to size slag inclusions located at the clad-base metal interface. In addition, artificial defects both flat-bottomed and side-drilled were evaluated.

Three evaluation techniques were used:

1. the half-value
2. 6 dB below the maximum
3. at the background noise level corrected for beam divergence.

Table 5.6.3 contains the actual flaw sizes and the UT measurements for length and width, and the length and width converted to a circular disc diameter.

The results were surprisingly good considering various sources of measurement error, such as 1) UT response  $\pm 2$  dB; 2) UT length and width measurements  $\pm 1$  mm; and 3)  $\pm 30\%$  for area measurements.

Onodera et al.<sup>(5.6.8)</sup> examined 141 large forgings for embedded flaws with UT using the German DGS method. Both longitudinal and angled beam were used. The defects were relatively small, as can be seen from the dimensions

TABLE 5.6.2. Sizing of Defects with UT Plane Transducers, Both Contact and Immersion

Actual Length (mm)	Measured Lengths (mm)					Cutoff Below Maximum Amplitude Cutoff Max Amp, dB
	Contact Long-2 MHz	Long-4 MHz	45° 2 MHz (a)	Immersion Long-4 MHz	45° 4 MHz (a)	
25.7	27	23	18 to 21	27	17 to 22	6
				35	21 to 26.5	12
				38	27 to 30	18
26.8	--	--	20 to 34	41	30 to 35	24
				18	23 to 31	6
				36	30 to 35	12
				41	34 to 38	18
				45	39 to 42	24
24.7	19	17	20 to 30	24	14 to 17.5	6
				27	21 to 23	12
				31	27	18
				37	35 to 43	24

(a) Range traverse both directions.

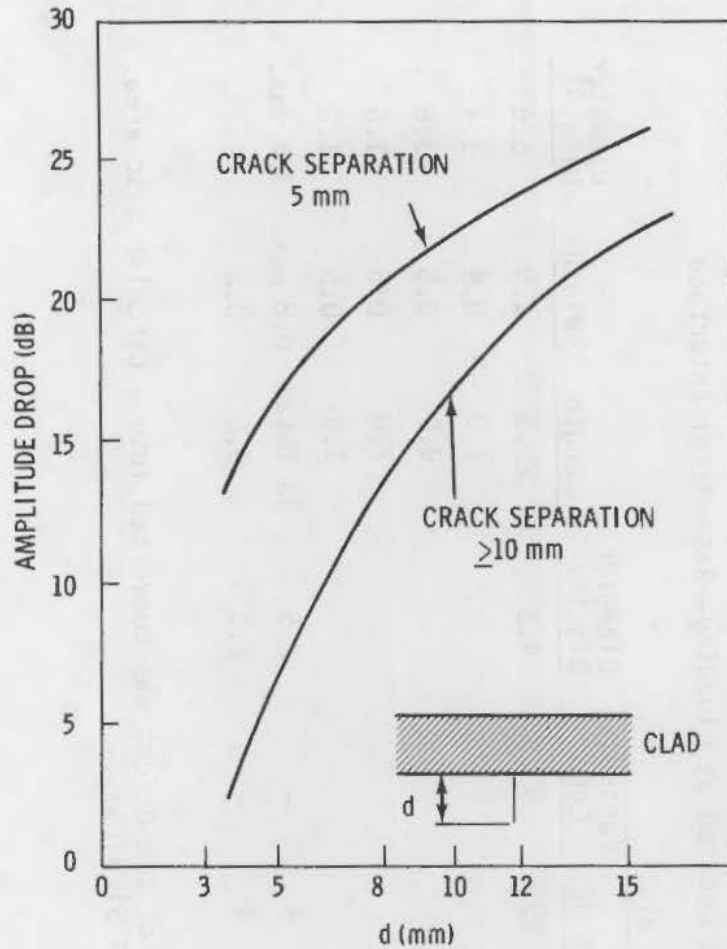


FIGURE 5.6.3. Depth-Amplitude-Drop Relation (scatter technique)

in Table 5.6.4. As noted, the UT consistently underestimated both length and areal (surface) values, which is somewhat surprising with small flaws since the tendency is to overestimate due to the focal spot size.

The possible sources of error in flaw measurement by a dB-drop technique such as 20 dB was reported in a 1971 seminar on the significance of weld defects. (5.6.9) The cumulative errors include the following:

- Error in marking position  $X_1 \pm 0.5$  mm;
- Error in marking position  $X_2 \pm 0.5$  mm;
- Error in measuring distance  $X_1 - X_2 \pm 0.5$  mm;
- Error in establishing edge of beam  $\pm 1.0$  mm in forward position;
- Error in establishing edge of beam  $\pm 1.0$  mm in backward position.

TABLE 5.6.3. Sizing of Defects Located at Cladding--Base-Metal Interface

Sample Number	Length			Width			Diameter Disc(a)	Length	Width	Diameter Disc(a)
	Half Height	6 dB	Vanishing Echo	Half Height	6 dB	Vanishing Echo				
1	12	23	22	8	10	5	4.8	20.5	1.9	5.8
2a								7.0	0.4	1.4
2b								9.0	0.8	3.6
2c								7.0	0.5	1.6
2d								3.5	0.5	1.2
2	12	7	43	-	4	-	2.5	36 Total	0.8 max.	3.6 max.
3	12	6	7	-	4	-	2.0	9.0	0.8	2.2

(a) The area obtained from the width plot of the defect was converted into a circular disc area.  
 NOTE: Ultrasonic Measurement (mm); Actual Size (mm).

TABLE 5.6.4. Comparison of Actual Flaw Sizes and UT Estimate in Large Forgings

Defect Number	Area (A) mm <sup>2</sup>	Actual Size			UT Estimate		Ratio A/A'
		Parallel to UT Beam, mm (T)	Normal to UT Beam, mm (W) (L)		(A <sup>2</sup> ) mm <sup>2</sup>	D, mm	
1	5.9	1.7	2.4	7.9	3.1	2.0	2.7
2	4.4	1.4	2.1	6.2	1.5	1.4	2.4
3	2.2	0.8	2.3	6.0	0.8	1.0	1.7
4	2.7	0.7	3.0	4.6	0.8	1.0	1.8
5	2.2	1.0	2.5	3.5	0.8	1.0	1.7
6	6.0	-	2.5	4.0	7.0	3.0	2.8
7	15.0	-	6.0	4.0	7.0	3.0	4.4

Total cumulative error possible  $\pm 3.5$  mm; error  $1^\circ$  in positioner probe translated to linear error of 0.85 mm for defect 50 mm distant (can occur at both ends)

or

- $\pm 3.5$  mm
- $\pm 1.7$  mm
- $\pm 5.2$  mm

A later paper<sup>(5.6.10)</sup> updated the information in Reference 5.6.8.

Basically, the information in Table 5.6.4 is unchanged. In excess of 150 large SA 508 Class 2 and Class 3 forgings have been examined. Otherwise the data reported in 5.6.8 are the same.

#### 5.6.2.5 Other Detection Techniques

Lumb<sup>(5.5.6)</sup> briefly reviewed embedded defects in a larger survey of surface defects. The following are two detection techniques which are discussed extensively elsewhere in this chapter:

1. Use of signal amplitude, with or without the DGS correction
2. Echo dynamic, which examines the way in which amplitude alters as the probe is scanned across a defect—

- a. Generally such methods as 6-dB, 10-dB, and 20-dB drop are not reliable.
- b. The alternate is flaw tip reflection (FTR), which is similar to the dB-drop methods, except that maximum amplitude is not measured so the invalid assumption that the center of the crack gives the maximum signal is avoided. The technique used is to estimate the defect size from the distance the probe can be scanned without reducing the amplitude below that from a fixed reference such as a 3-mm diameter cylindrical hole.

The justification for the statement concerning poor results with the various dB-drop techniques is apparent upon examination of Figure 5.6.4.

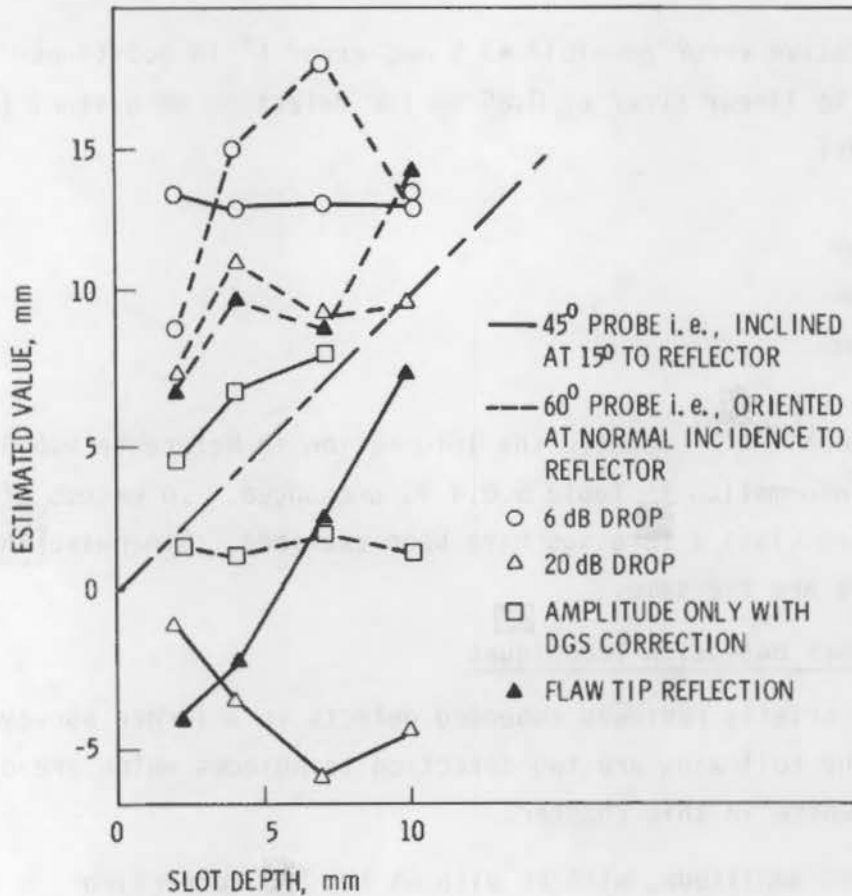


FIGURE 5.6.4. Comparison of Estimates of Size of Reflectors Inclined at 60°

#### 5.6.2.6 Defect Sizing

One of the most comprehensive studies of defect sizing and certainly the best defined statistical design of experiment is that of Kato et al.<sup>(5.6.11)</sup> The investigators examined various types of weld defects such as root cracks, internal cracks, lack of penetration at the root, internal lack of penetration, slag inclusions at the root, and internal slag inclusions. Several thicknesses of steel were examined; namely, 16, 25, 32, 40, 50 and 60 mm. The material was Japanese SM 50-steel comparable to an A242. Various welding techniques were used in the butt-welds such as manual arc, semi-automatic arc, and semi-automatic CO<sub>2</sub> arc.

In some instances, flaws were introduced by bending the specimen after laying down the initial weld beads, then completing the weld. In other cases, small saw cuts were used which may not duplicate weld cracking.

Sizing of both length and height of flaw was accomplished in UT with several techniques:

- 6-dB drop
- 10-dB drop
- vanishing echo corrected for beam width.

Radiography also was used in some instances with regard to the test data. There was a comprehensive statistical analysis. Values determined were 1) mean value of error; 2) variance; and 3) two-sided tolerance at 95% confidence and 99% population.

A total of 389 specimens were examined over the spectrum of thickness, 16 to 60 mm; with the three welding techniques; for six different defect types; and under a variety of UT (and RT) test conditions. The test matrix is given in Table 5.6.5.

The test program, both UT and RT, is presented in Table 5.6.6. The statistical data, mean value of error, variance, tolerance, and F-Test, are given in Table 5.6.7.

The F-Test results are of interest when combined with the two-sided tolerance; the vanishing echo was the most precise with the 10-dB drop next. As

TABLE 5.6.5. Test Series Data

Test Series	Plate Thickness, mm	Width of Specimen, mm	Welding Procedure(a)	Types of Artificial Weld Defects Inserted(b)	Number of Specimen	Used Probe (Ref. 5.6.10)
1	16	125	S	Cr, Cl, Pr, Pi, Sl	44	5Z9.10A70 5Z10.9A70
2	25	100	M,S,C	Cr, Cl, Pr, Pi, Si,	68	4B8.9A70
3	25	100	M,S,C	Pr, Pi	31	4B8.9A70
4	25	100	M	Cr, Cl, Pr, Pi, Sr, Si	12 + 24(c)	5Z10.10A70
5	25	100	M	Cr, Pr, Sr	30	5Z10.10A70
6	25	300	C	Cr, Cl, Pr, Pi	0.4	5Z10.10A70
7	32	250	M	Cr, Cl, Pr, Pi	14	5Z10.9A70
8	32	250	S	Cr, Cl	23	4B8.9A70
9	40	180	M,S,C	Cr, Cl, Pr, Pi, Si	112	4B8.9A45
10	50	300	C	Cr, Cl, Pr	3	5Z10.10A70
11	60	240	C	Cr, Pr	20	5Z10.10A70

(a) M--manual arc welding, S--non-gas semi-automatic arc welding; C--CO<sub>2</sub> semi-automatic arc welding.

(b) Cr--root crack; Cl--internal crack; Pr--lack of penetration at root; Pi--internal lack of penetration; Sr--slag inclusion at root; Si--internal slag inclusion.

(c) Two defects are inserted in weldments.



TABLE 5.6.6. Test Program—Outline and Terminology

	Ultrasonic Angle Beam (U)						Radiography Defect Length (L) -X <sup>L</sup>	
	Defect Length (L)			Defect Height (H)				
	A-Scope (U <sup>L</sup> A) Method	B-Scope (U <sup>L</sup> B) Method	VE(c)	A-Scope (U <sup>H</sup> A) Method	B-Scope (U <sup>H</sup> B) Method			
Test Series(d)	6 dB(a) 10 dB(b)	1,2,3,4,5, 7,8,9,11	4,8	4,5,11	6 dB(a)	1,2,7,8	4,11	2,4,5,9
Test Results Figure	5.6.5a	5.6.5b	5.6.5c	5.6.6	5.6.8	5.6.9	5.6.9	5.6.7

(a) 6-dB-dropping method.

(b) 10-dB-dropping method.

(c) Vanishing echo method.

(d) Given in Table 5.6.5.

TERMINOLOGY: Measured (S); e.g., S<sup>L</sup>, S<sup>H</sup>Measured—Arc Gouge (a); e.g., a<sup>L</sup>, a<sup>H</sup>Construction (field tests) UT—Length (G<sup>L</sup>)

TABLE 5.6.7. Statistical Data for Population Tested by Specified Method

	Ultrasonic						
	Length				Height		
	A-Scope Method		VE	B-Scope Method	RT	A-Scope Method	B-Scope Method
6 dB	10 dB	6 dB					
Sample Numbers	168	389	83	110	208	133	38
Mean Value of Error, mm	-8.01	0.15	-0.68	1.32	0.84	0.49	-0.68
Variance, mm <sup>2</sup>	119.87	47.97	9.96	12.86	12.12	9.91	6.32
Two-Sided Tolerance, mm	-39.77	-19.00	-10.20	-9.20	-8.97	--	--
	mm +23.75	+19.30	+8.82	+11.84	+10.65	--	--
F-Test Results							
6 dB	--	S	S	S	S	--	--
10 dB	--	--	S	S	S	--	--
VE	--	--	--	N	N	--	--
B-Scope	--	--	--	--	N	--	--
RT	--	--	--	--	--	--	--

NOTE: S = Significant  
N = Nonsignificant

noted, there was no statistically significant difference in reliability among the vanishing echo method, B-Scope method and radiography. The 6- and 10-dB methods differences could be due to a lack of correction for UT beam width and orientation. They feel the UK 20-dB method, which was not used, would be superior to the 6- and 10-dB methods.

The plotted data from the report<sup>(5.6.11)</sup> are reproduced in Figures 5.6.5 to 5.6.9 covering actual versus measured flaw lengths for 6 dB, 10 dB, V.E. (Figure 5.6.5a, b, c), B-Scope on length, radiography, height by 6 dB and by B-Scope. Construction UT (10 dB) results of length measurements were compared to laboratory measurements with the greater accuracy achieved by laboratory techniques.

A study by Schlengermann and Frielinghaus<sup>(5.6.12)</sup> is quite pertinent to the problem of error size in measurement and location of real defects vis-a-vis ideal defects. The specimens consisted of replicas of both fatigue and brittle fractures plus ideal specimens consisting of flat surfaces of the same size and geometry; permitting a comparison on the basis of the same areas and shapes but different reflector surfaces. Both plane and focused transducers were used. The data are presented in Chapter 6, Section 6.2. Tables 6.2.2 and 6.2.3 are particularly interesting.

Lumb et al.<sup>(5.6.13)</sup> discuss a specialized technique for monitoring the growth of fatigue cracks in situ. While the technique wouldn't be optimum for routine detection and sizing, it was both sensitive and accurate with fixed mount transducers. Growth in the range of about 0.005 mm (0.0002-in.) with accuracies of  $\pm 0.1$  mm ( $\pm 0.004$ -in.) were obtained.

Work at the Welding Institute<sup>(5.6.14,5.6.15)</sup> relates to the measurement and characterization of fabrication defects. A spectrum of defects were examined using a variety of UT techniques. The first study<sup>(5.6.14)</sup> was limited to non-planar while the second<sup>(5.6.15)</sup> concentrated on planar defects. Table 5.6.8 presents an excellent description of the UT techniques, specimen characteristics, and types of defects. Table 5.6.9 summarizes the positional and size data as well as the mean error and standard deviations.

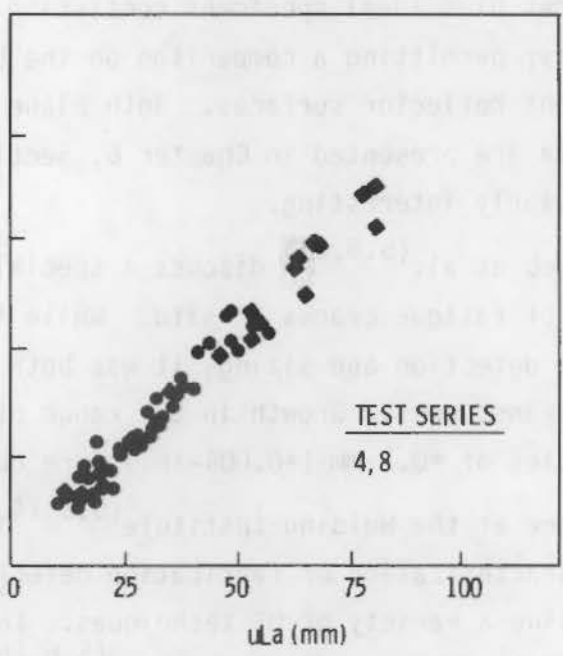
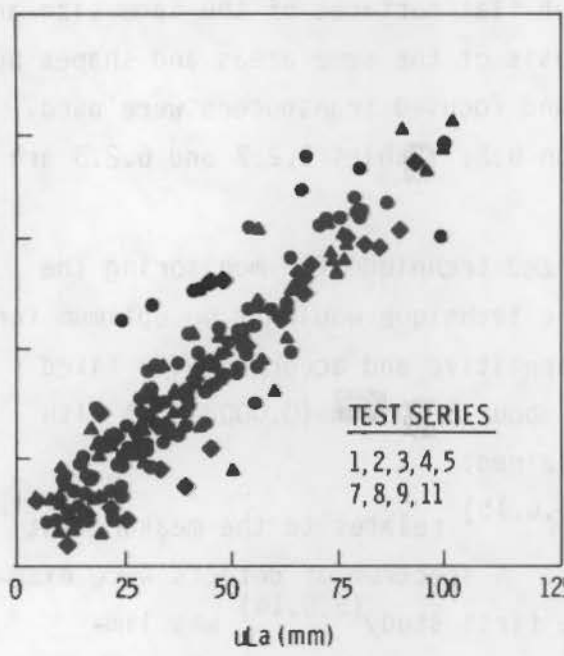
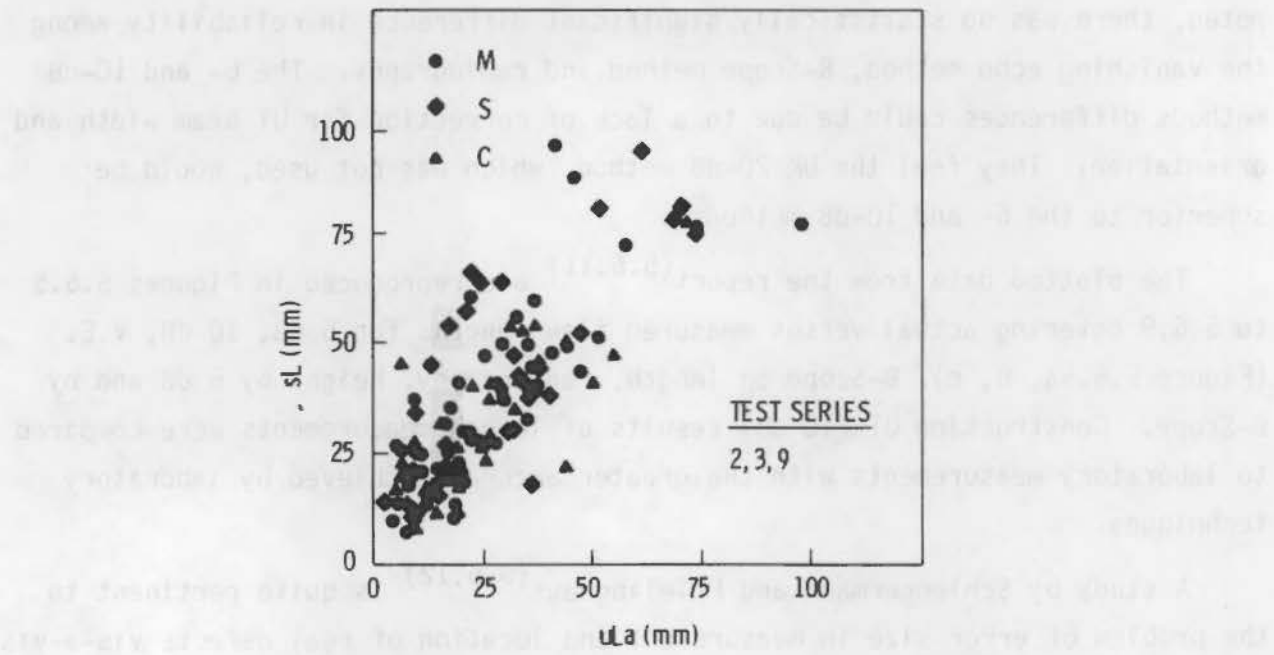


**FIGURE 5.6.5.** Comparison of Defect Lengths ( $uL_A$ ) Estimated by Various Inspection Methods to Actual Defect Lengths ( $sL$ ). a) 6-dB-dropping method; b) 10-dB-dropping method; c) vanishing echo method

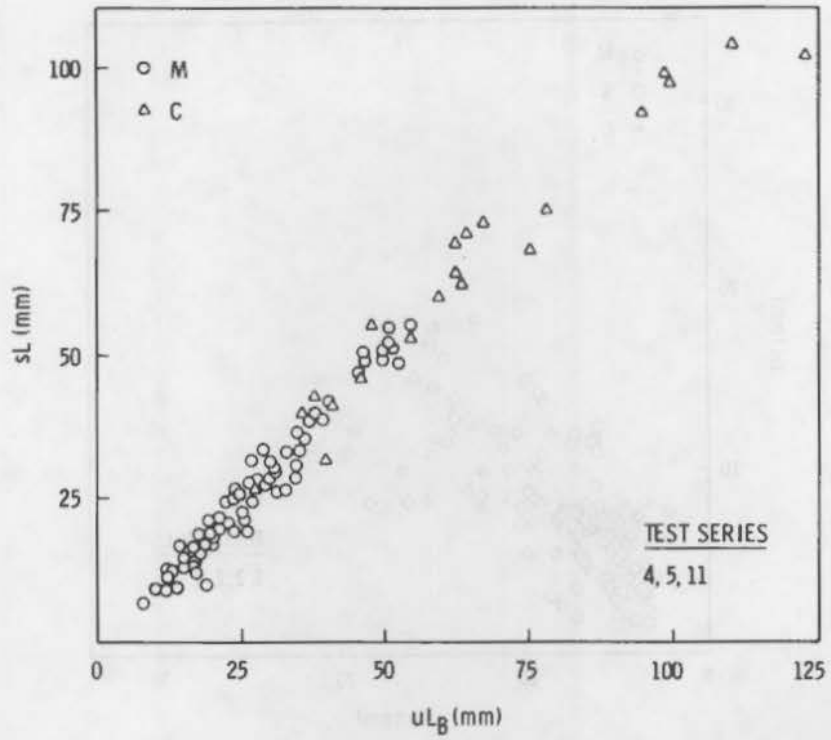


FIGURE 5.6.6. Relation Between  $uL_b$  and  $sL$

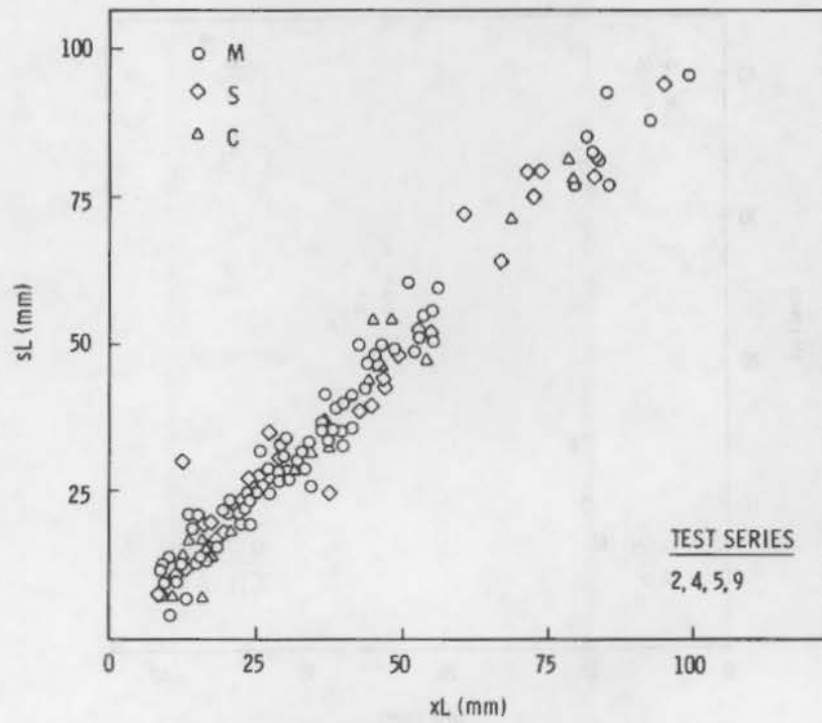


FIGURE 5.6.7. Relation Between  $xL$  and  $sL$

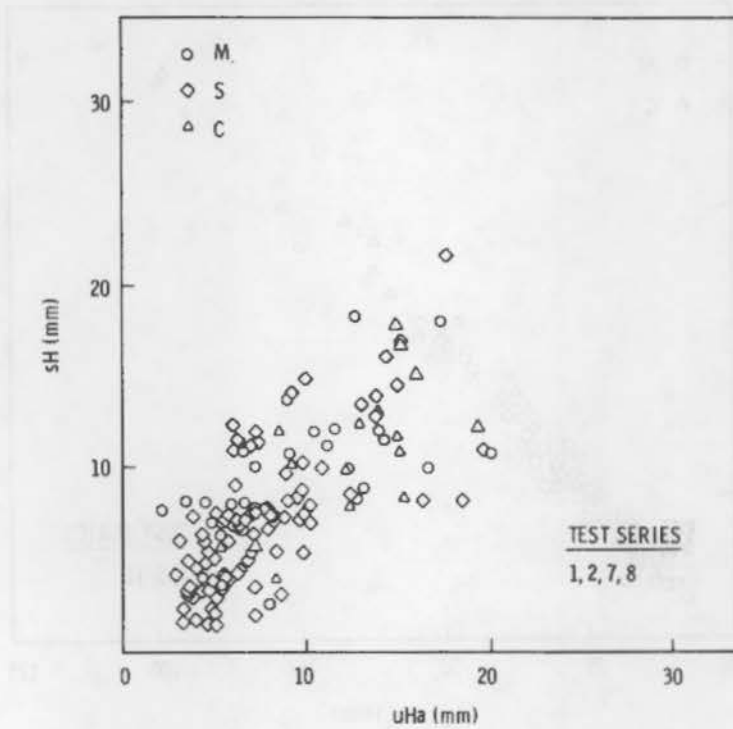


FIGURE 5.6.8. Relation Between  $uHa$  and  $sH$

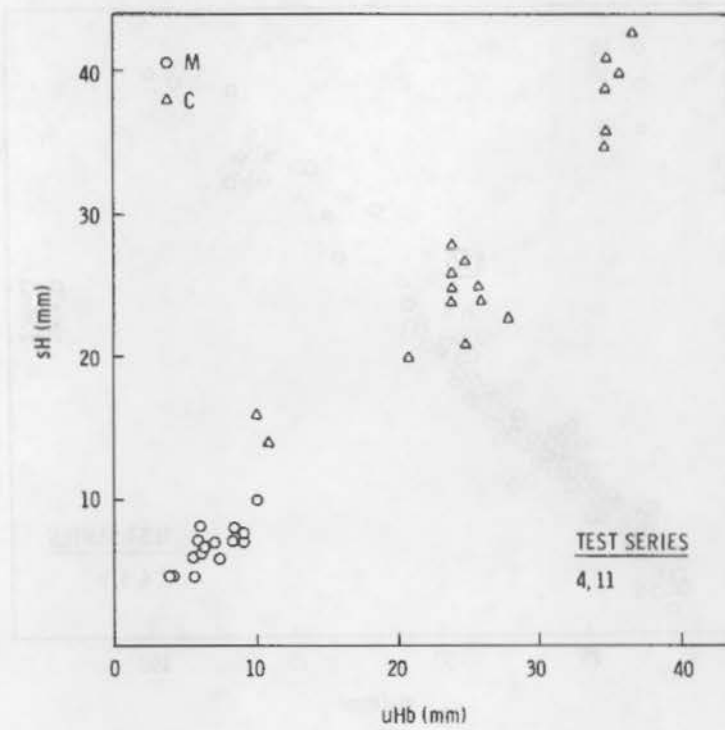


FIGURE 5.6.9. Relation Between  $uHb$  and  $sH$

**TABLE 5.6.8. Specimen Details and Testing Conducted - Welding Institute Non-Planar Defects Program(5.6.14)**

	Specimen Number									
	MMA			SA				SA		
	J3	J8	J12	J15	J18	J19	J20	J21	J22	J27
Thickness, mm	42	40	65	95	95	38	37	37	39	95
Defects Included	2 small slag lines*(1) numerous small unintended defects*	3 porosity lines*(1) 1 lack of root penetration*	3 porosity lines*(1) 1 lack of root penetration*	6 slag inclusions*(1) 6 porosity clusters**(1)	3 porosity lines*(1) 1 lack of root penetration	6 slag lines*(4)	6 slag inclusions**(3) 6 slag/porosity clusters**(3)	3 porosity lines*(3) 1 lack of root penetration	1 lack of root penetration*	6 slag lines*(4)
Defect Number	27	17 18	14 16	26 25	13	9, 10, 11, 12	19, 20, 21 22, 23, 24	6, 7, 8	5	1, 2, 3, 4
Surface Preparation	Machined both sides	Hand ground both sides	Machined both sides	Machined both sides	Machined top side only	Machined both sides	Machined both sides	Machined both sides	Machined top side only	Machined both sides
Conventional UT Tests										
Laboratory	X	X	X	X	X	X	X	X	X	X
Shop-Floor	X	X	X	X	X	X	X	X	X	X
B-Scan	X	X	X	X	X	X	X	X	X	X
C-Scan	X		X		X			X	X	X
Ultrasonic Holography				X						X
Time Domain Analysis	X	X	X	X	X	X	X	X	X	X
Destructive Test:	* Freeze Break									
	** Isolation and Radiography									
	( ) Number of defects analyzed.									

5.6.19

TABLE 5.6.9. Positional and Size Data: Various Ultrasonic Techniques(5.6.14)

Type of Test; Frequency	Type of Error	Type of Defect	Range of Measured Values	Mean Error ( $\bar{x}$ )	Standard Deviation from Mean ( $\sigma$ )	Sample Details
Conventional-Laboratory, 4 MHz	Transverse plan position error (mm)		-4.0 to +2.0	-0.6	1.5	Population 34
Conventional-Laboratory, 2 MHz			-4.5 to 3.0	0.0	1.9	Population 25
Conventional-Shop Floor			-4.0 to +3.0	-0.36	1.9	Population 25
B-Scan			-5.0 to +4.0	-0.57	1.9	Population 28
C-Scan			-4.0 to +1.0	-0.89	1.5	Population 9
Ultrasonic Holography			0.0, 0.0, +2.0, -1.0, +9.0 <sup>(a)</sup>	-	-	-
Time Domain Analysis			-	-	-	-
Conventional-Laboratory, 4 MHz	Vertical cross-section position error (mm)		-3.0 to +4.0	+0.1	1.2	Population 34
Conventional-Laboratory, 2 MHz			-5.0 to 2.5	-5.0	1.7	Population 25
Conventional-Shop Floor			-2.0 to +3.5	+0.48	1.5	Population 25
B-Scan			-5.0 to +4.0	+0.17	2.0	Population 30
C-Scan			-2.0 to +2.0	+0.50	1.4	Population 8
Ultrasonic Holography			0.0, 0.0, 0.0, -2.0, -10.0 <sup>(a)</sup>	-	-	-
Time Domain Analysis				-1.5 to +4.0	+0.35	1.3
Conventional-Laboratory, 4 MHz	Length extremities (% error) (by 6-dB-drop method)	Linear defects	-33 to +26%	0%	9.0%	Population 92 40- to 121-mm long
		Cluster and inclusion defects	-50 to +50%	+8.0%	25%	Population 30 5- to 15-mm long

(a) This defect (specimen J15, defect 25) produced an image consisting of a cluster of points. These values refer to a single bright point within that cluster.



TABLE 5.6.9. (Contd)

Type of Test; Frequency	Type of Error	Type of Defect	Range of Measured Values	Mean Error ( $\bar{x}$ )	Standard Deviation from Mean ( $\sigma$ )	Sample Details
Conventional-Laboratory, 2 MHz	Length extremities (% error) (by 6-dB-drop method)	Linear defects	-30 to 24%	-2.3%	9.7%	Population 62 40- to 121-mm long
		Cluster and inclusion defects	-100 to 100%	+19%	60%	Population 12 5- to 9-mm long
Conventional-Shop Floor		Linear defects	-14 to +27%	0.91%	8.7%	Population 34 40- to 121-mm long
		Cluster and inclusion defects	-40 to +60%	6.9%	28%	Population 16 5- to 15-mm long
B-Scan		Linear defects	-27 to +32%	-1.9%	9.2%	Population 60 40- to 121-mm long
		Cluster and inclusion defects	-30 to +100%	+27%	32%	Population 22 5- to 15-mm long
C-Scan		Linear defects only	-6 to +12%	+2.2%	6.8%	Population 18 50- to 121-mm long
Ultrasonic Holography		Linear defects only	-11 to +8%	-2.9%	6.7%	Population 8 70- to 80-mm long
Time Domain Analysis		Linear defects	-14 to +23%	+3%	7.7%	Population 34 40- to 121-mm long
		Cluster and inclusion defects	-50 to +80%	+7.1%	40%	Population 14 5- to 15-mm long
Conventional-Laboratory, 4 MHz	Cross-section size (mm) (20-dB-drop method)	Linear defects	-4.0 to +5.0	-2.0	2.1	Population 46 1.0- to 7.0-mm size
		Cluster and inclusion defects	-4.0 to +4.5	-3.3	3.2	Population 13 2.0- to 8.0-mm size

5.6.21

TABLE 5.6.9. (Contd)

Type of Test; Frequency	Type of Error	Type of Defect	Range of Measured Values	Mean Error ( $\bar{x}$ )	Standard Deviation from Mean ( $\sigma$ )	Sample Details
Conventional-Laboratory, 4 MHz	Cross-section size (mm) (max. amp. method)	Linear defects only	0.0 to +7.0	-2.1	2.0	Population 30 2.0- to 7.0-mm size
Conventional-Laboratory, 2 MHz	↓	Linear defects	1.5 to 6.0	-0.88	2.3	Population 13 1.5- to 6-mm size
		Cluster and inclusion defects	Insufficient sample - zero for all four measured			
Conventional-Shop Floor	Cross-section size (mm) (20-dB-drop method)		0.0 to 8.0	-0.8	1.4	Population 25 2.0- to 8.0-mm size
B-Scan	↓		-2.0 to +8.0	-1.3	2.2	Population 30 1.5- to 7.0-mm size
C-Scan			None			
Ultrasonic Holography			None			
Time Domain Analysis				1.6 to 7.0	-0.32	1.0
Ultrasonic Holography	Depth extension (mm)		7.5 12.5 15.0 10.0 35.0			3.5-mm actual 4.5-mm actual 2.5-mm actual 5.0-mm actual 7.0-mm actual
Distance Gain Size Data	Equivalent reflector size (mm)	Linear defects	0.8 to 5.5	-1.7	1.6	Population 100 1.5- to 7.0-mm size
	Equivalent reflector size (mm)	Cluster and inclusion defects	1.2 to 4.6	-2.7	1.8	Population 13 1.5- to 7.0-mm size

5.6.22

The program emphasizing linear defects<sup>(5.6.15)</sup> is illustrated in Table 5.6.10. Again, there is a spectrum of defects and UT techniques. Various sizing methods and their relative accuracy in sizing for both non-planar and planar defects were investigated including both positional error and dimensional error. Mean errors were relatively consistent for various sizing techniques in terms of both defect size and location.

In anticipation of future work, Table 5.6.11 covers details of complex geometry and defects as well as the proposed UT techniques.

#### 5.6.2.7 Geometric Effects

A complex geometry may complicate examination by UT. A specific example is in pressure vessel nozzles where both geometry and cladding militate against both detection and the sizing and location of defects. Data cited in Chapter 3 with regard to the PVRC nozzle blocks illustrate the problems. Such UT examinations may be done from either the outer or the inner surfaces of the nozzle or vessel wall.

Baker and Greer<sup>(5.6.16)</sup> touch on some of the difficulties of nozzle UT examinations. The authors cite the problems of geometry and cladding. For example, cladding echoes, reflection, refraction, and mode conversion may occur due to the cladding. Generally, cladding interference militates against detection of smaller cracks. The authors cite success in detecting cracks 10- to 16-mm deep and one instance of detection at 8 mm total depth.

The present apparatus (Figure 1) is illustrated in Table 1. It is a system of objects and is designed to measure the relative accuracy of using the two-dimensional and three-dimensional displays. The objects are arranged in a regular grid. The objects are arranged in a regular grid. The objects are arranged in a regular grid.

In addition to the data in Table 1, the accuracy of geometry and distance is also presented in Table 2.

### 3.1.2. Geometry Effects

A complex geometry was employed (Figure 1). It is a system of objects and is designed to measure the relative accuracy of using the two-dimensional and three-dimensional displays. The objects are arranged in a regular grid. The objects are arranged in a regular grid.

Table 1. Accuracy of geometry and distance. The accuracy of geometry and distance is also presented in Table 2. The accuracy of geometry and distance is also presented in Table 2.

TABLE 5.6.10. Specimen Details and Testing for Planar Defects - Welding Institute(5.6.15)

	Specimen Number							Specimen Number						
	J50	J52	J53	J55	J56	J57	J58	J60	J61	J62	J63	J65	J66	J67
Thickness, mm	38	38	67	94	93	67	38	94	94	38	39	47	44	34
Welding Process	SA	MMA	SA	SA	MMA	SA	MMA	MMA	SA	SA	MMA	MMA	MMA	MMA
Joint Preparation	Single V	2/3-1/3 double V	Single V	Double V	Single U	Single U	2/3-1/3 double V	Double V	2/3-1/3 double V	Single V	Double V	Single V	Single V	Single V
Defects Included	Solidification cracking	Solidification cracking	Solidification cracking	Solidification cracking	Solidification cracking	Large crack incomplete fusion	Incomplete fusion	Incomplete fusion	Large crack	Weld metal hydrogen cracking	Large crack	Incomplete side-wall fusion	Cluster of small slag inclusions on sidewall	HAZ crack
Destructively Tested Defect Number	1,2	13, 14	3, 4, 5	23, 24, 25	11a, 11b	12, 21, 22	15, 16, 17, 18	7, 8, 9, 10	20	19	6	26	27	28
Surface Preparation	As-welded	Machined both sides	Machined both sides	Machined both sides	Machined top side only	Machined top side only	Machined both sides	Machined both sides	Machined both sides	Machined both sides	Machined both sides	Machined both sides	Machined both sides	Machined both sides
Radiography	+	+	+	+	+	+	+	+	+	+	+	+	+	+
Immersion C-scan	+	+	+	+	x	+	+	+	+	+	+	+	+	+
Conventional UT Tests														
Laboratory	+	+	+	+	+	+	+	+	+	+	+	+	+	+
Shop Floor Tvoe	+	+	+	+	+	+	+	+	+	+	+	+	+	+
Manual B-scan	+	+	+	+	+	+	+	x	+	+	+	+	+	+
Accuscan	x	x	x	x	+	x	+	+	+	x	+	+	+	+
Ultrasonic Holography														
Laboratory	x	x	x	x	+	x	x	+	+	x	x	x	x	x
Commercial	x	x	x	x	x	x	x	x	+	x	x	x	x	x
Time Domain Analysis	+	+	+	+	+	+	+	+	+	+	+	+	+	+
Type of Defect Identified by Destructive Testing	Solidification cracks	Solidification cracks	Incomplete fusion	Solidification cracks	Solidification cracks (also 12)	Incomplete fusion	Incomplete fusion	Incomplete fusion	Large crack	Weld metal hydrogen cracks	Large crack	Incomplete sidewall fusion	Slag inclusions	HAZ crack
Destructive Test Method	FB(a)	FB	FB	PS(b)	FB	PS	FB	PS(b)	FB(a)	PS	FB	FB	PS	PS

(a) FB = Freeze Break  
 (b) PS = Progressive Sectioning



**TABLE 5.6.11. Details and Testing of Laboratory Specimens Having Complex Geometries -  
Welding Institute Planar Defects Program**

Configuration	Specimen Number							
	J151	J152	J153	J154	J155	J156	J157	J158
Configuration	Tee	Tee	Tee	Tee	Tee	Set-through nozzle into curved section	Tee with curved flange	Corner
Nominal Plate Thickness	38 mm both plates	38 mm both plates	38 mm both plates	38 mm both plates	38 mm both plates	30 mm	40 mm	One 60-mm plate One 80-mm plate
Joint Preparation	Unpenetrated fillet	Partially penetrated	Fully penetrated	Fully penetrated	Fully penetrated	Fully penetrated	Partially penetrated	Single J preparation
Defects Included	Cracks and linear slag	Lack of fusion and porosity	Lack of fusion and porosity	Cracks and porosity	Lack of penetration & slag	Root cracks	Lamellar tearing	Lamellar tearing
Surface Preparation	Machined on top side	Machined on top side	Machined on top side	Machined on top side	Machined on top side	As rolled	As-received	As-received
Radiography	+	+	+	+	+	X	X	X
Immersion C-Scan	+	+	+	+	+	X	+	+
Conventional UT Tests								
Laboratory	+	+	+	+	+	X	X	+
Shop-Floor	+	+	+	+	+	+	+	+
Manual B-Scan	+	+	+	+	+	+	+	+
Advanced Tests								
Accuscan	X	+	X	X	+	X	X	+
Commercial holography	X	+	X	X	X	X	X	X
Time Domain Analysis	X	X	+	+	X	X	X	X
Destructive	X	+	+	+	+	X	X	+

5.6.27





- All factors influencing the detection of defects by NDE are applicable to the sizing of defects.
- Both instrument and operator error are significant factors in sizing and location of flaws even more than they are in detecting them.
- The sizing technique used—half height 6-dB drop, 10-dB drop, 20-dB drop, vanishing echo, etc.—yield different results which in turn are dependent on the corrections or lack of corrections made with regard to beam spread.
- In flaws smaller than the focal spot, there will be a tendency to over-estimate the size because the focal spot will control. This effect will be magnified for more deeply embedded flaws; however, this source of error can be corrected partially.
- UT techniques for sizing surface flaws are more diverse and appear to yield better results than is true for embedded flaws. Part of this is due to flaw component geometry; part is due to the techniques.
- There is a need for carefully planned and statistically designed experiments to establish sources of error and means of correction for near-field flaws. The effort should include sizing and location by conventional or advanced UT techniques and confirmation by destructive testing. The tests should cover fairly thick sections on both ferritic (clad or unclad) steel and austenitic steel containing weldments.

- All factors influencing the detection of defects by the applicants to the state of defects.
- Both instrument and operator error are significant factors in sizing and location of flaws even more than they are in detecting them.
- The sizing technique used—half height 6-dB crest, 10-20 dB, 50-20 dB, various edge, etc.—gives different results when in turn the dependence on the connectors or lack of connectors made with regard to their spread.
- A flaw smaller than the focal spot, there will be a tendency to over-estimate the size because the focal spot will control. This effect will be amplified for more heavily eroded flaws; however, this source of error can be corrected partially.
- It is important for these surface flaws and some internal flaws to be graded better results than is true for internal flaws. Part of this is due to the opposite geometry; part is due to the resolution.
- There is a need for carefully planned and statistically designed experiments to establish sources of error and means of correction for the test flaw. The effort should include sizing and location by conventional techniques of techniques and comparison by destructive testing. The tests should cover fairly thick sections of both ferritic steel or austenitic steel and austenitic steel containing weldments.

- 5.1.1 Thompson, R. B. and Evans, A. G., "Goals and Objectives of Quantitative Ultrasonics." IEEE Trans. Sonics Ultrason. SU-23(5):292-299, September 1976.
- 5.2.1 "Non-Destructive Examination," ASME Section V, Article 4, "Ultrasonic Examination for Dimensioning of Indications," 1977.
- 5.2.2 Krautkrämer, J., "Determination of the Size of Defects by the Ultrasonic Impulse Echo Method." Br. J. Appl. Phys. 10(6):240-245, June 1959.
- 5.2.3 Bastien, P., "Difficulties in the Ultrasonic Evaluation of Defect Size." Nondestructive Testing 1(2):147-151, February 1969.
- 5.2.4 Bradfield, G., "Correlating Echo and Flaw Magnitudes." Nondestructive Testing 1(5):317-318, 1968.
- 5.2.5 Hislop, J. D., "Flaw Size Evaluation in Immersed Ultrasonic Testing." Nondestructive Testing 2(3):182-192, August 1969.
- 5.2.6 Krautkrämer, J., "Thirteen Years of DGS Diagrams in Ultrasonics NDT." Proceedings of Ultrasonics International 1971 Conference, London, England, pp. 39-41, 1971.
- 5.2.7 Chapman, H., "Defect Size Estimation with Ultrasonic Angle Beam Probes and the DGS (AVG) Diagram." Report B11, 6th International Conference on NDT, Hanover, Germany, pp. 121-133, 1970.
- 5.2.8 Mundry, E., "Defect Evaluation of Ultrasonics." Nondestructive Testing 5(5):290-291, October 1972.
- 5.2.9 Minton, W. C., "Flaw Sizing in Piping Welds with Ultrasonics." Nuclear Power Education Seminar, Southwest Research Institute, San Antonio, Texas, 1978.
- 5.3.1 Silk, M. G., "Estimates of the Magnitudes of Some of the Basic Sources of Error in Ultrasonic Defects Sizing." AERE-R9023, United Kingdom Atomic Energy Authority, Harwell, England, February 1978.
- 5.3.2 Coffey, J. M., "Quantitative Assessment of the Reliability of Ultrasonics for Detecting and Measuring Defects in Thick-Section Welds." Paper C85/78, Institute of Mechanical Engineers, London, England, pp. 63-70, 1978.
- 5.3.3 Haines, N. F., "The Reliability of Ultrasonic Inspection." IAEA-SM-218/41, International Symposium on Application of Reliability Technology to Nuclear Power Plants, Vienna, Austria, October 10-13, 1977.

- 5.3.4 Haines, N. F. and Langston, D. B., "The Reflection of Ultrasonic Pulses from Surfaces." RD/B/N4115, Central Electricity Generating Board, September 1977.
- 5.3.5 Höller, P., "Vortrag Anlässlich der Sitzung", Prepared for Electric Power Research Institute Pressure Vessel Study Group by Institut für Zerstörungsfreie Prüfverfahren, February 1978.
- 5.4.1 Gurvich, A. V. and Kuzmina, L. I., "Investigation of Methods of Measuring the Apparent Height of Defects in the Case of Scanning with an Inclined Probe." Sov. J. Nondestr. Test., pp. 678-684, 1971.
- 5.4.2 Corbly, D. M., Packman, P. F. and Pearson, H. S., "The Accuracy and Precision of Ultrasonic Shear Wave Flaw Measurements as a Function of Stress on the Flaw." Mater. Eval. 28:103-110, 1970.
- 5.4.3 Silk, M. G. and Lidington, B. H., "A Preliminary Study of the Effects of Defect Shape and Roughness on Ultrasonic Size Estimation." Nondestructive Testing, pp. 27-32, February 1975.
- 5.4.4 Silk, M. G. and Lidington, B. H., "Defect Sizing Using an Ultrasonic Time Delay Approach." Br. J. Nondestr. Test., pp. 33-36, March 1975.
- 5.4.5 Silk, M. G. and Lidington, B. H., "The Potential of Scattered or Diffracted Ultrasound in the Determination of Crack Depth." Nondestructive Testing, pp. 146-151, June 1975.
- 5.4.6 Lidington, B. H., Saunderson, D. H. and Silk, M. G., "Interference Effects in the Reflection of Ultrasound from Shallow Slits." Nondestructive Testing, pp. 185-190, August 1975.
- 5.4.7 Lidington, B. H. and Silk, M. G., "Crack Depth Measurements Using a Single Surface Wave Probe." Br. J. Nondestr. Test., pp. 165-167, November 1975.
- 5.4.8 Silk, M. G., "The Determination of Crack Penetration Using Ultrasonic Surface Waves." NDT Int., pp. 290-297, December 1976.
- 5.4.9 Packman, P. F., et al., "Definition of Fatigue Cracks Through Nondestructive Testing." J. Mater. 4:666-700, 1969.
- 5.4.10 Rummel, W. P. and Rathke, R. A., "Detection and Measurement of Fatigue Cracks in Aluminum Alloy Sheet by Non-Destructive Evaluation Techniques." Prevention of Structural Failure: The Role of Quantitative Non-Destructive Evaluation, T. D. Cooper and P. F. Packman, eds., American Society for Metals, pp. 146-160, 1973.
- 5.4.11 Kupcis, O. A., "Nondestructive Inspection of Pressure Tubes at the Pickering Nuclear Generating Station." 3rd Conference on Periodic Inspection, Institute of Mechanical Engineers, London, England, pp. 19-25, 1976.

- 5.4.12 Sattler, F. J., "Nondestructive Flaw Definition Techniques for Critical Defect Determination." NASA-CR-72602, TRW/ER-7419, Prepared for the National Aeronautics and Space Administration by TRW Equipment Group, Cleveland, Ohio, January 1970.
- 5.4.13 Saitoh, T. and Takahashi, S., "Measuring the Depth of Cracks in Austenitic Stainless Steel Overlays by Ultrasonic Testing." NDE in the Nuclear Industry, pp. 611-625, 1980.
- 5.5.1 Ho, C. L., Marcus, H. L. and Buck, O., "Ultrasonic Surface Wave Detection Techniques in Fracture Mechanics." Exp. Mech. 14:42-48, 1974.
- 5.5.2 Chang, F. H. S., Couchman, J. C. and Yee, B. G. W., "The Effects of Stress on the Detection of Fatigue Cracks by Ultrasonic Techniques." Proceedings of 9th Symposium on NDE, San Antonio, Texas, pp. 424-433, April 25-27, 1973.
- 5.5.3 Lidington, B. H., et al., "Ultrasonic Measurements of the Depth of Fatigue Cracks." Br. J. Nondestr. Test., pp. 165-170, November 1976.
- 5.5.4 Parks, J. W., "Detection and Definition of Environmental Damage (Fatigue, Stress, Corrosion, etc.) Using Eddy Current Techniques." Proceedings of 9th Symposium on NDE, San Antonio, Texas, pp. 291-297, April 25-27, 1973.
- 5.5.5 Hudgell, R. J., Morgan, L. L. and Lumb, R. F., "Non-Destructive Measurement of the Depth of Surface Breaking Cracks Using Ultrasonic Rayleigh Waves." Br. J. Nondestr. Test., pp. 144-149, September 1974.
- 5.5.6 Lumb, R. F., "Defect Sizing—State-of-the-Art." Paper C86/78, 4th Conference on Periodic Inspection of Pressure Vessels: Significance of Flaws, Institute of Mechanical Engineers, London, England, 1978.
- 5.5.7 Silk, M. G. and Lidington, B. H., "An Evaluation of Single Probe Bulk-Wave Time-Delay Techniques in Sizing Cracks in Steel." NDT Int., pp. 129-134, June 1977.
- 5.6.1 Dufresne, J., "Probabilistic Study of Core Pressure Vessel Rupture of Nuclear Reactors Operating on Ordinary Water." Report No. 145, September 15, 1976 to March 15, 1977, Commissariat a L'Énergie Atomique, Saclay, France, April 1977.
- 5.6.2 Yamaguchi, T., et al., "Results of Mockup Test on Ultrasonic Inservice Inspection Tool for Nuclear Reactor Pressure Vessel." 2nd International Conference on Pressure Vessels and Piping, pp. 685-699, 1973.
- 5.6.3 Buken, G. and Krachter, H., "Determination of the Size of Defects in Welds by the Ultrasonic Reflection Method." Deutscher Verband für Materialprüfung (DVM) 10(10):329-339, October 1968.

- 5.6.4 "Ultrasonic Examination Comparison of Indication and Actual Flaw in Reactor Pressure Vessel." Ishikawajima-Harima Heavy Industries Co., Ltd., Tokyo, Japan, January 1976.
- 5.6.5 Monnier, P., Touffait, A. M. and Saglio, R., "Comparison of Different Methods of Measuring Defects by Ultrasonics in a Weld of Great Thickness." Report NT 201, Commissariat a L'Énergie Atomique, Saclay, France, February 1974.
- 5.6.6 deRaad, J. A. and deSterke, A., "Ultrasonic Monitoring of Subcladding Cracks." 3rd Conference on Periodic Inspection, Institute of Mechanical Engineers, London, England, pp. 13-18, 1976.
- 5.6.7 Huebner, W., "Comparison of the Ultrasonic Test Data and the Actual Defect Dimensions of Slag Inclusions in a Submerged Arc Welded INCO Cladding." NDE Conference, Babcock and Wilcox/Technischen Überwachungs Verein e.V., Rheinland Westphalia, Washington, D.C., November 18, 1976.
- 5.6.8 Onodera, S., et al., "UT Indications in Large Forgings in NSSS." NDE Conference, Babcock and Wilcox/Technischen Überwachungs Verein e.V., Rheinland Westphalia, Washington, D.C., November 18, 1976.
- 5.6.9 "NDT Aspects of the Significance of Weld Defects." SANDT Special Seminar NDT 17, December 16, 1971.
- 5.6.10 Onodera, S., et al., "Evaluation of UT Indications in Material and Welds of LWR Components." NDE in the Nuclear Industry, American Society for Metals, pp. 34-47, 1978.
- 5.6.11 Kato, B., Morita, K. and Furuzawa, H., "Estimation of Weld Defects Through Ultrasonic Testing." Weld. J., pp. 946-953, November 1976.
- 5.6.12 Schlengermann, U. and Frielinghaus, R., "Remarks on the Practice of Determining the Size of Reflectors by Scanning." Br. J. Nondestr. Test., pp. 9-13, January 1978.
- 5.6.13 Lumb, R. F., Hudgell, R. J. and Winship, P., "Monitoring Slow Crack Growth by Ultrasonic Methods." 7th International Conference on Nondestructive Testing, Warsaw, Poland, June 4-8, 1973.
- 5.6.14 Jessop, T. J., et al., "Size Measurement and Characterization of Weld Defects by Ultrasonic Testing Part 1. Non-Planar Defects in Ferritic Steels." Welding Institute Report Series, 1979.
- 5.6.15 "Size Measurement and Characterization of Weld Defects by Ultrasonic Testing." A Seminar Coventry, Welding Institute, March 17, 1981.
- 5.6.16 Baker, R. A. and Greer, A. S., "Ultrasonic Examination of Nozzle Inner Surfaces in Heavy Wall Pressure Vessels." NDE in the Nuclear Industry, American Society for Metals, pp. 34-47, 1978.

CHAPTER 6

FLAW SIZING AND LOCATION--ADVANCED TECHNIQUES

CHAPTER II

PLANNING AND LOCATION OF FACTORIES



## CONTENTS

6.1	INTRODUCTION . . . . .	6.1.1
6.2	LIMITED VARIATIONS FROM CONVENTIONAL SIGNAL AMPLITUDE . . . . .	6.2.1
6.2.1	High-Speed Ultrasonic Imaging . . . . .	6.2.1
6.2.2	Enhanced Signal-to-Noise Ratio . . . . .	6.2.1
6.2.3	Focused Transducers . . . . .	6.2.2
6.2.4	Scattered Amplitude . . . . .	6.2.11
6.2.5	Mode-Converted Amplitude . . . . .	6.2.15
6.2.6	Pulse-Height Difference . . . . .	6.2.16
6.2.7	End-On UT to Crack . . . . .	6.2.16
6.2.8	Diffacted Amplitude . . . . .	6.2.17
6.3	ANALYSIS IN TIME DOMAIN . . . . .	6.3.1
6.4	ANALYSIS IN FREQUENCY DOMAIN . . . . .	6.4.1
6.4.1	Acoustic Spectroscopy . . . . .	6.4.1
6.4.2	Adaptive Learning . . . . .	6.4.2
6.5	ANALYSIS OF MULTI-INFORMATION DATA . . . . .	6.5.1
6.5.1	Signal-to-Interference Ratio . . . . .	6.5.8
6.6	ANALYSIS OF PHASE INFORMATION--FLAW IMAGING . . . . .	6.6.1
6.6.1	Acoustic Holography . . . . .	6.6.1
6.6.2	High-Speed Imaging . . . . .	6.6.9
6.6.3	Synthetic Aperture Focusing Techniques (SAFT-UT) . . . . .	6.6.10
6.7	ACOUSTIC EMISSION . . . . .	6.7.1
6.8	ELECTROMAGNETIC-ACOUSTIC TECHNIQUES . . . . .	6.8.1
6.9	POSITRON ANNIHILATION . . . . .	6.9.1
6.10	CAPACITANCE STRAIN GAGES . . . . .	6.10.1

6.11	INFRARED ELECTRO-THERMAL NDE	6.11.1
6.12	ELECTROMAGNETIC LEAKAGE	6.12.1
6.13	RADIOGRAPHY	6.13.1
6.13.1	Intensifying Screens	6.13.3
6.13.2	Image Processing	6.13.5
6.13.3	Neutron Radiography	6.13.7
6.13.4	Sizing	6.13.8
6.14	EDDY CURRENT	6.14.1
6.14.1	Alternative Eddy Current Systems	6.14.1
6.14.2	Eddy Current--ALN	6.14.6
6.15	LASER INTERFEROMETRIC HOLOGRAPHY	6.15.1
6.16	OTHER NON-ACOUSTIC TECHNIQUES	6.16.1
6.17	CONCLUSIONS	6.17.1
6.18	RECOMMENDATIONS	6.18.1
6.19	REFERENCES	6.19.1

## FIGURES

6.2.1	Variation of Image of the Holes as a Function of the Increase of Gain with Respect to the Level of Detection-4 MHz Transducer . . . . .	6.2.2
6.2.2	Measured Diameter as a Function of the Actual Diameter-4 MHz Transducer . . . . .	6.2.3
6.2.3	Measured Diameter as a Function of the Actual Diameter-2.25 MHz Transducer . . . . .	6.2.4
6.2.4	Measured Diameter as a Function of the Actual Diameter-1 MHz Transducer . . . . .	6.2.5
6.2.5	Scatter in the Width and Depth Dimensions of A, B, and C as Measured with Focused Probes . . . . .	6.2.12
6.2.6	Depth Measurement by Detecting S-Waves Produced by Mode Conversion of R-Waves at the Tip Using an S-Wave Detector of Known Angle $\phi$ . . . . .	6.2.13
6.2.7	Study of Scattered Energy . . . . .	6.2.14
6.2.8	Estimates of Depth of Fatigue Crack Using Maximum Echo from Mode-Converted Shear Wave . . . . .	6.2.15
6.2.9	Presumed Ray Paths Taken by the Discrete Signals Observed in the Diffraction Technique . . . . .	6.2.18
6.2.10	Typical Ultrasonic Responses: a) internal crack (hypothetical); b) crack opens to surface opposite probes; c) crack opens to same surface as probes . . . . .	6.2.19
6.2.11	Theoretical and Experimental Estimates of the Variation of the Amplitude of the Wave Scattered or Diffracted from the Crack Tip . . . . .	6.2.20
6.3.1	Determination of Fatigue Crack Profile Using Ultrasonic Surface Waves and Mode-Converted Shear Waves . . . . .	6.3.2
6.3.2	The Interaction of an Ultrasonic Shear Wave with an Inclusion-Like Defect Resulting in a Reflected Pulse and a Lagging Scattered Satellite Pulse . . . . .	6.3.5
6.3.3	Illustrating the One-to-One Correspondence Between the SPT Ultrasonically Estimated and Visually Determined Slit Depths . . . . .	6.3.5

6.4.1	Pulse Echo Dependence on Scanning Angle for Five 304 SS Reflectors . . . . .	6.4.8
6.5.1	Percentage of Downward Frequency Shift Displayed by the Various Combination of Search Unit and Instrument Types . . . . .	6.5.4
6.5.2	Crack Specimen Attenuation as Compared to the Carbon Steel IIW Block Using Various Combinations of Search Units and Instrument Types . . . . .	6.5.5
6.5.3	Signal-to-Noise Ratio Displayed by the Various Combinations of Search Unit and Instrument Types at 45° Refracted Angle . . . . .	6.5.6
6.5.4	Signal-to-Noise Ratio Displayed by the Various Combinations of Search Unit and Instrument Types at 60° Refracted Angle . . . . .	6.5.7
6.5.5	Probability Density Functions for Signal Embedded in Gaussian Reverberation . . . . .	6.5.9
6.6.1	Measurements of Surface Fatigue Crack Dimensions . . . . .	6.6.4
6.6.2	Measurements of Internal Fatigue Crack Dimensions . . . . .	6.6.5
6.6.3	Dimensional Measurements of Artificial Flaw in Safe-End Section; Longitudinal Wave 0° . . . . .	6.6.6
6.6.4	Dimensional Measurements of Artificial Flaw in Safe-End Section, 45° . . . . .	6.6.7
6.6.5	Dimensional Measurements of Artificial Flaw from Safe-End Section, 55° . . . . .	6.6.8
6.6.6	Dimensional Measurements of Artificial Flaw in Safe-End Section, 45° . . . . .	6.6.9
6.6.7	Size of Artificial Flaw Measured by Conventional Ultrasonic Flaw Detection Method . . . . .	6.6.10
6.6.8	Size of Artificial Flaw Measured by Conventional Ultrasonic Flaw Detection Method . . . . .	6.6.11
6.6.9	Measured Size of Artificial Flaw in Heavy Cast Steel Specimen versus Its Actual Size . . . . .	6.6.12
6.6.10	Isometric Images of Side-Drilled Holes . . . . .	6.6.15
6.6.11	Isometric Images of Notches and Saw Cuts . . . . .	6.6.16
6.6.12	Single Transducer Views Showing Flaw No. 1 and the Clad Overhang . . . . .	6.6.17

6.6.13	Single Transducer Views Showing Flaw No. 2 and a Number of Small Defects . . . . .	6.6.18
6.6.14	A Comparison of Array Single Block Performance versus the Array Multiple Block for Two Different Views of Weld Sections 5-1 to 5-3, at 20% DAC on the Babcock and Wilcox Test Block, Showing Flaw No. 1 . . . . .	6.6.19
6.8.1	Response of Surface Waves to Milled Slots of Various Depths, 0.9 MHz Probe . . . . .	6.8.2
6.10.1	Typical Strain Output in Power Piping Over a One-Month Period . . . . .	6.10.2
6.10.2	Gage Position Around Pipe on Power Piping . . . . .	6.10.3
6.12.1	Magnetic Flux Leakage Signal from Sawn Slots . . . . .	6.12.2
6.13.1	Radiographic Image Processing . . . . .	6.13.5
6.13.2	Measurement Method for Crack Height for an Angled Crack . . . . .	6.13.9
6.13.3	Detectability of Cracks Influenced by Geometric Unsharpness; Natural Crack; Plate Thickness 5, 10, 15, 20 mm . . . . .	6.13.9
6.13.4	Relation Between Measured Crack Height and Actual Crack Height . . . . .	6.13.10
6.14.1	Summary of Small and Large Dent, Eddy Current Flaw Assessment Data . . . . .	6.14.3
6.14.2	Eddy Current Estimated Depth versus True Depth Wastage and Axial Notches . . . . .	6.14.4
6.15.1	An Example of a Double Exposure Hologram Obtained with Laser Holographic Interferometry Illustrating Defects in a Tube Pressurized to 4.14 MN/m <sup>2</sup> . . . . .	6.15.2
6.15.2	Holographic Defect Detection Limits in Tube . . . . .	6.15.4
6.15.3	Relative Vertical and Horizontal Movement of Crack Edges Along Crack . . . . .	6.15.5
6.16.1	Crack Shape Measurements During a Random Load Fatigue Test on a Tubular Welded T-Joint . . . . .	6.16.2
6.16.2	One- and Two-Dimensional Interpretations of the Voltage Ratio for a Circular Arc Notch in a Steel Plate . . . . .	6.16.2
6.16.3	AC-Potential Drop Measurements of Fatigue Cracks in T-Joints, Cracks Located at the Weld Toe . . . . .	6.16.3

## TABLES

6.2.1a	NDE Test Conditions . . . . .	6.2.6
6.2.1b	Range of Measurements for Above Techniques . . . . .	6.2.6
6.2.2	Determination of Size Deviation in Percentage from True Value . . . . .	6.2.8
6.2.3	Determination of Position Deviation in Millimeters from True Value . . . . .	6.2.9
6.3.1	Pros and Cons of Various Defect Sizing Techniques . . . . .	6.3.4
6.4.1	Classification of Natural Defects . . . . .	6.4.2
6.4.2	Flaw Size Measurement Using UT Frequency Analysis . . . . .	6.4.5
6.4.3a	Index of Performance--Classification Results . . . . .	6.4.6
6.4.3b	Capability of Detecting a Specified Class . . . . .	6.4.6
6.5.1a	Test Specimen and Defect Summary; Flaws with Low SIR Values . . . . .	6.5.13
6.5.1b	Type III Specimen and Defect Summary . . . . .	6.5.13
6.5.2	Factors Influencing Type I and Type II Errors . . . . .	6.5.14
6.5.3	Classification of the Six Selected Ultrasonic Techniques According to the Types of the Special Probes and Operations and Type and Domain of Special Operations . . . . .	6.5.15
6.5.4	Modes of Operation and Salient Features of the Multiple-Beam-Angle Crack Detector . . . . .	6.5.16
6.5.5	Advantages and Disadvantages Cited for Six Techniques . . . . .	6.5.17
6.5.6	Automatic and/or Manual Tests Performed on the Three Specimen Types . . . . .	6.5.18
6.5.7a	Overall Performance of the Six Techniques Applied to the Three Type I and Two Type II Test Specimens . . . . .	6.5.19
6.5.7b	Overall Performance of the Six Techniques Applied to the Ten Type III Test Specimens . . . . .	6.5.19
6.6.1	Accuracy of Flaw Measurement by Acoustic Holography . . . . .	6.6.2
6.6.2	Acoustic Holography--Carbon Steel--Inconel Weld-- Stainless Steel, 80-mm Thick . . . . .	6.6.3

6.6.3	Examples of Accuracy of Flaw Sizing, Primarily with Acoustic Holography . . . . .	6.6.13
6.6.4	Composite Summary of Various NDE Techniques . . . . .	6.6.14
6.7.1	Major Parameters Included in Three-Year Weld Monitoring Effort . . . . .	6.7.2
6.7.2	Listing of Defects Detected During the Twelve Series of Tests Shown in Preceding Table . . . . .	6.7.3
6.11.1	Infrared Electro-Thermal NDE . . . . .	6.11.2
6.12.1	Comparison of Experimental and Theoretical Values for Leakage Field at 1.5 mm Lift-Off Over Sawn Slots . . . . .	6.12.2
6.13.1	Comparative Data for Fluorometallic and Lead Screen Exposures for a Range of Specimen Thicknesses and Radiographic Techniques . . . . .	6.13.4
6.14.1	Summary of Tube Support Defect Detectability, and Measurement Data for Eddy Current Using Various Types of Equipment . . . . .	6.14.5
6.15.1	Comparison of Lateral Displacement Determined by Dial Gage, by Theory, and by Laser Speckle Photography . . . . .	6.15.4

8.1.1	Examination of accuracy of the design, particularly with respect to the
8.1.2	Examination of the design of the structure, particularly with respect to the
8.1.3	Examination of the design of the structure, particularly with respect to the
8.1.4	Examination of the design of the structure, particularly with respect to the
8.1.5	Examination of the design of the structure, particularly with respect to the
8.1.6	Examination of the design of the structure, particularly with respect to the
8.1.7	Examination of the design of the structure, particularly with respect to the
8.1.8	Examination of the design of the structure, particularly with respect to the
8.1.9	Examination of the design of the structure, particularly with respect to the
8.1.10	Examination of the design of the structure, particularly with respect to the
8.1.11	Examination of the design of the structure, particularly with respect to the
8.1.12	Examination of the design of the structure, particularly with respect to the
8.1.13	Examination of the design of the structure, particularly with respect to the
8.1.14	Examination of the design of the structure, particularly with respect to the
8.1.15	Examination of the design of the structure, particularly with respect to the
8.1.16	Examination of the design of the structure, particularly with respect to the
8.1.17	Examination of the design of the structure, particularly with respect to the
8.1.18	Examination of the design of the structure, particularly with respect to the
8.1.19	Examination of the design of the structure, particularly with respect to the
8.1.20	Examination of the design of the structure, particularly with respect to the



FLAW SIZING AND LOCATION--ADVANCED TECHNIQUES

6.1

INTRODUCTION

Two classes of NDE systems will be reviewed in Chapter 6; namely,

1. modifications or improvements in ultrasonics such as SAFT-UT, Adaptive Learning Network, Acoustic Holography, etc.
2. all other systems that include thermal imaging, magnetic flux leakage, real-time radiography, etc.

Item 1 above, related to ultrasonics, is divided further into the following categories:

- limited variations from conventional signal amplitude. Focused transducers and high-speed imaging will be considered to be in this category.
- techniques for analysis of data in the time domain. The work of Silk et al. in the United Kingdom discussed in Chapter 5 as well as in this chapter fits into this category.
- techniques for analysis of data in the frequency domain and the majority of work including spectroscopy and adaptive learning network (ALN). In essence, such data are handled with a Fourier transform.
- techniques for analysis of data from more than one category of information such as frequency polarization, amplitude plus angle, etc. Most such techniques are still in the early stages of development.
- information handled by phase analysis. This includes conventional holography as well as special aspects of holography such as SAFT-UT and the holographic mode of high-speed imaging.

The following criteria will be applied in assessing the potential of each system:

- Is it primarily or exclusively a detection system?
- Is its principal use the sizing of defects?
- Is the system equally applicable to detection and sizing?

With regard to sizing, the system's ability must be in the context of generating quantitative information for input into fracture mechanics analyses; therefore, the following questions need to be addressed:

1. Will the system quantitatively locate a defect three-dimensionally with regard to the volume of the test object?
2. Can the orientation of planar defects be established with respect to critical surfaces of the test object?
3. Can the planar or three-dimensional defect be sized accurately at appropriately high sensitivity limits?
4. Have the above criteria been confirmed by appropriate tests on both artificial and real defects?
5. Does the available information indicate with a fairly high probability that item 4 will be achieved?

The following represent necessary caveats requiring definition:

- Does the NDE system being reviewed have inherent limitations in one or more of the following:
  - Are there thickness limitations; e.g., no application to thick sections, but good for thin?
  - Are there materials limitations such as only ferromagnetic materials for magnetic flux systems?
  - Is flaw location a critical parameter; e.g., applicable only to defects at or very near the outer surface?
  - Is the NDE system severely limited by a combination of factors such as inapplicable to thick sections of austenitic dendritic welds or castings because of excessive beam attenuation?

- Can geometric considerations so severely limit a system's use that it should not be pursued because of the high probability of fallacious results?
- Finally, a caveat may be required where the system is so new and the data so limited that one cannot determine what, if any, limitations apply, but a system to which one cannot be sure that such limitations do not apply.

The present consideration is given to the fact that it should not be possible to have a system of value for itself.

It is, in fact, a system of value which is not a value in itself, but a system in which the value is not a value in itself.

There is an element of arbitrariness in deciding whether a given UT system is conventional and is covered in Chapters 4 and 5, or whether it is nonconventional and discussed in Chapter 6. Three examples of systems considered to deviate to a limited degree from the "conventional" are high-speed ultrasonic imaging, enhanced signal-to-noise ratio, and focused transducers. These are described in the following paragraphs.

### 6.2.1 High-Speed Ultrasonic Imaging

The high-speed ultrasonic imaging system being developed for EPRI by BNW<sup>(6.2.1,6.2.2)</sup> has two operating modes; namely, pulse-echo and holography. The latter will be discussed in the section dealing with holography.

The computer-based inspection system utilizes multi-element linear arrays capable of developing either pulse-echo or phase (holographic) images of flaws. The long linear arrays can be electronically or phase-stressed to transmit or receive in the zero- or angle-beam mode and present the data in A-scan, or B-scan (isometric). An obvious advantage of this system is the possibility of examination with multiple angles, permitting better detection and location of defects.

### 6.2.2 Enhanced Signal-to-Noise Ratio

Work at the National Bureau of Standards (NBS)<sup>(6.2.3)</sup> has concentrated on improvement of signal-to-random-noise ratio with the purpose of locating minute flaws undetectable with conventional UT equipment. The system consists of an ultrasensitive, ultrasound inspection system with order of magnitude improvement in signal-to-random-noise ratio over conventional devices. The system incorporates real-time signal averaging, pulse compression, dynamic focusing, and transducer matching, permitting penetration of highly attenuating materials such as austenitic stainless steel weldments while detecting reflections in the presence of strong background signals due to grain scattering. The system appears to have considerable potential; however, quantitative data are not available on its ability to locate natural flaws. Until such data are presented, its potential strengths and weaknesses cannot be assessed.

### 6.2.3 Focused Transducers

Principal proponents of the use of focused transducers have been personnel of the Center for Nuclear Studies of the French Atomic Energy Commission. (6.2.4,6.2.5,6.2.6) Early work concentrated on artificial flaws; namely, a series of flat-bottomed holes, 2, 3, 4, 5, 10 and 15 mm in diameter, at a depth of 105 mm. Three longitudinal focused transducers were used:

1. 4 MHz-I-60-157; 2.7-mm dia focal spot
2. 2.25 MHz-I-60-151; 6.5-mm dia focal spot
3. 1 MHz-I-60-161; 9-mm dia focal spot.

Measurements were taken at several values of dB gain using all three transducers at appropriate frequencies. Apparent diameters of each flat-bottomed hole were measured in 2-dB steps yielding typical curves such as Figure 6.2.1.

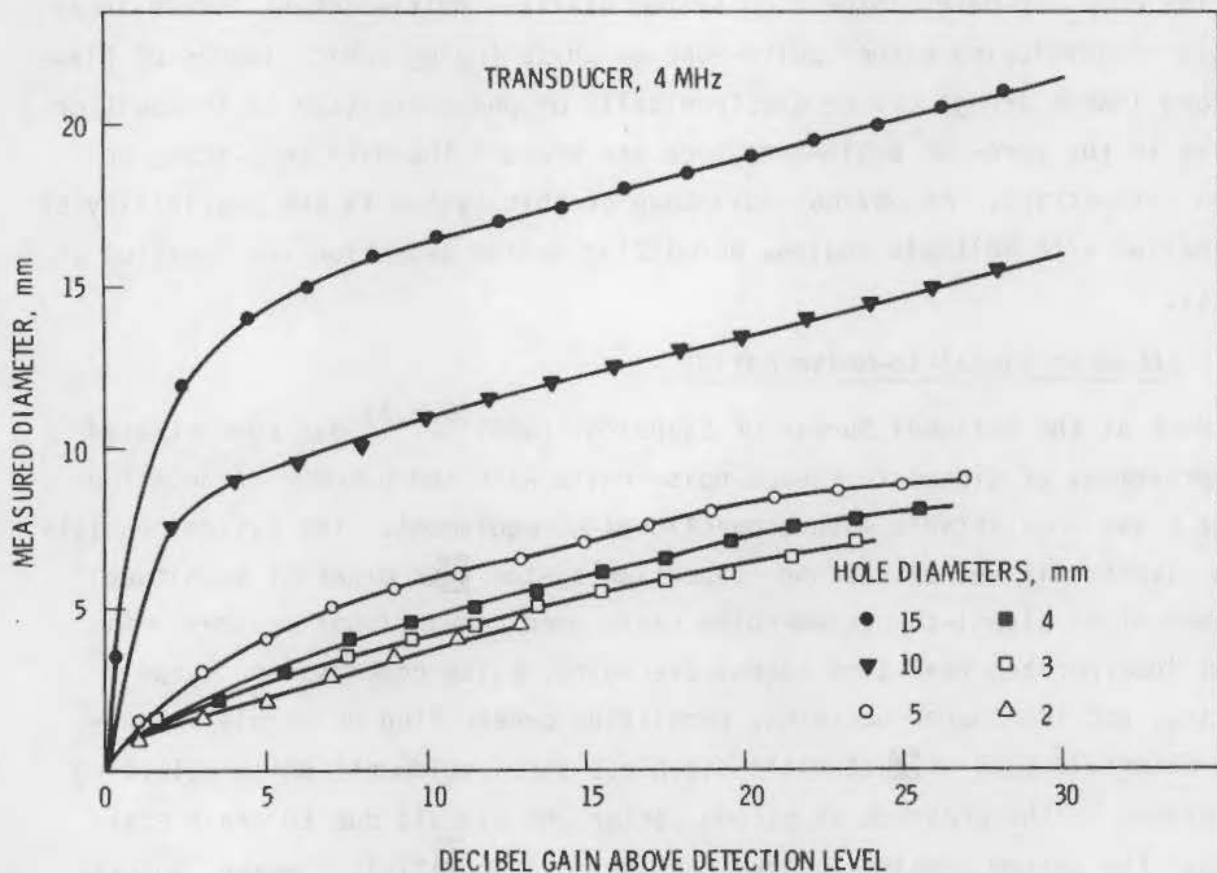


FIGURE 6.2.1. Variation of Image of the Holes as a Function of the Increase of Gain with Respect to the Level of Detection 4-MHz Transducer

The significant plots are Figures 6.2.2, 6.2.3 and 6.2.4 where measured versus actual diameters are plotted at levels of 6, 12, 18 and 24 dB. It is apparent that actual versus measured values are quite similar at 6 dB. The deviations from linearity occur at the diameter of the focal spot. As noted, measured and actual values are quite close at 6 dB whereas the measured sizes are overestimated substantially at 12, 18 and 24 dB. However, these are ratioed. For example, if the hole diameter exceeds the focal spot diameter, the 12-dB line in Figure 6.2.2 should be offset by one-half the focal spot diameter.

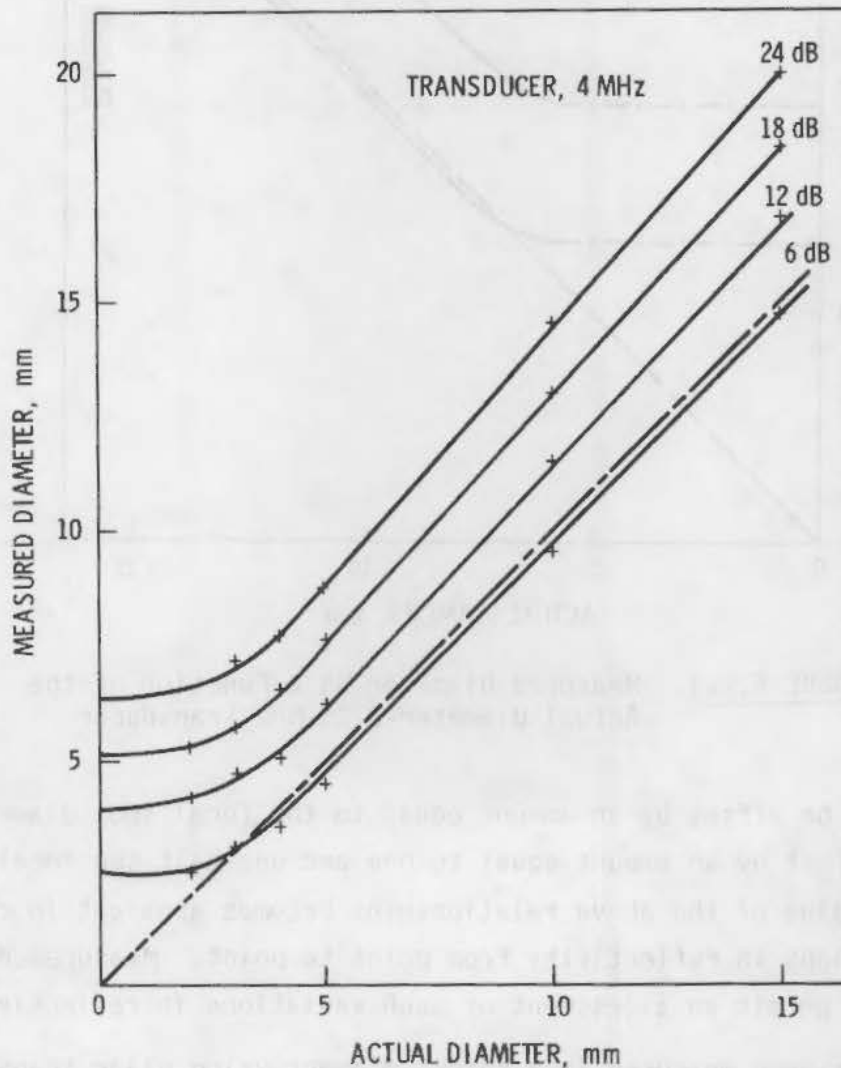


FIGURE 6.2.2. Measured Diameter as a Function of the Actual Diameter—4 MHz Transducer

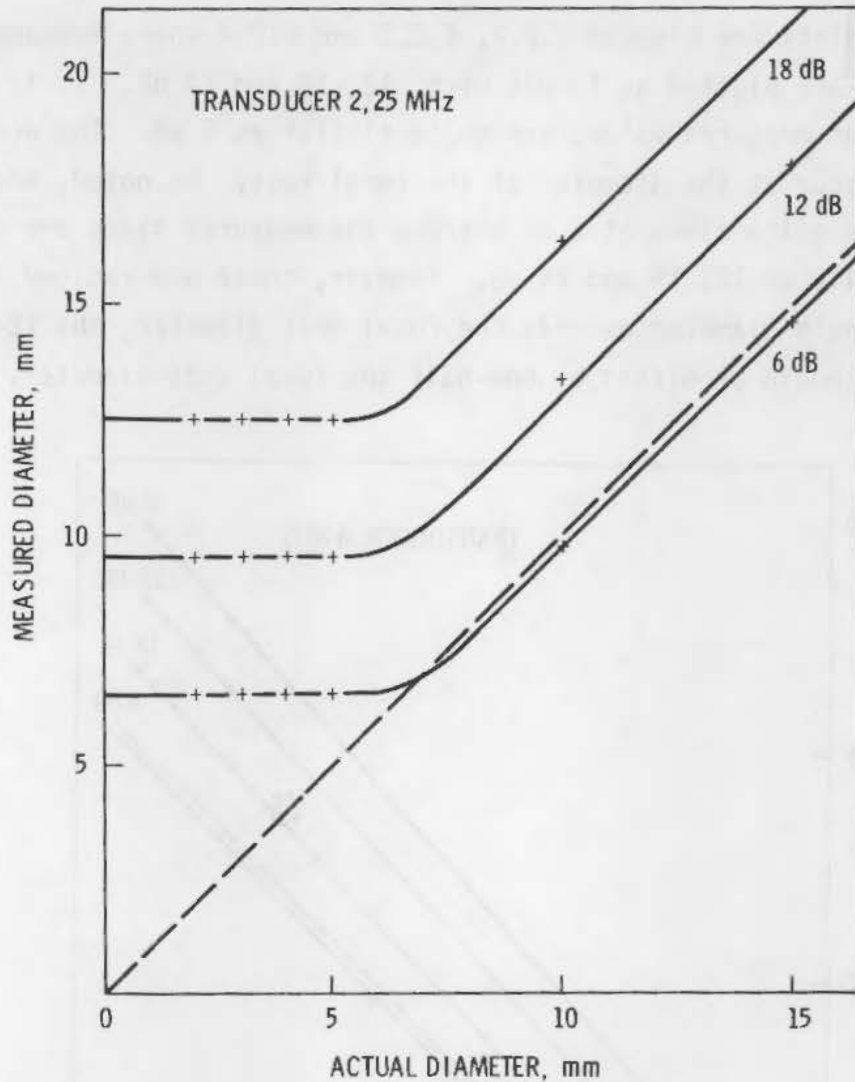


FIGURE 6.2.3. Measured Diameter as a Function of the Actual Diameter—2.25 MHz Transducer

Eighteen dB will be offset by an amount equal to the focal spot diameter and 24 dB will be offset by an amount equal to one and one-half the focal spot diameter. The value of the above relationships becomes apparent in cases where there are variations in reflectivity from point to point. Measurements at 12, 18 or 24 dB will permit an assessment of such variations in reflectivity.

Real defects were measured in a thick weldment using plane transducers in contact and immersion as well as focused transducers and acoustic holography. The weldment consisted of 710- x 390- x 122-mm (28- x 15.5- x 5-in.) block.



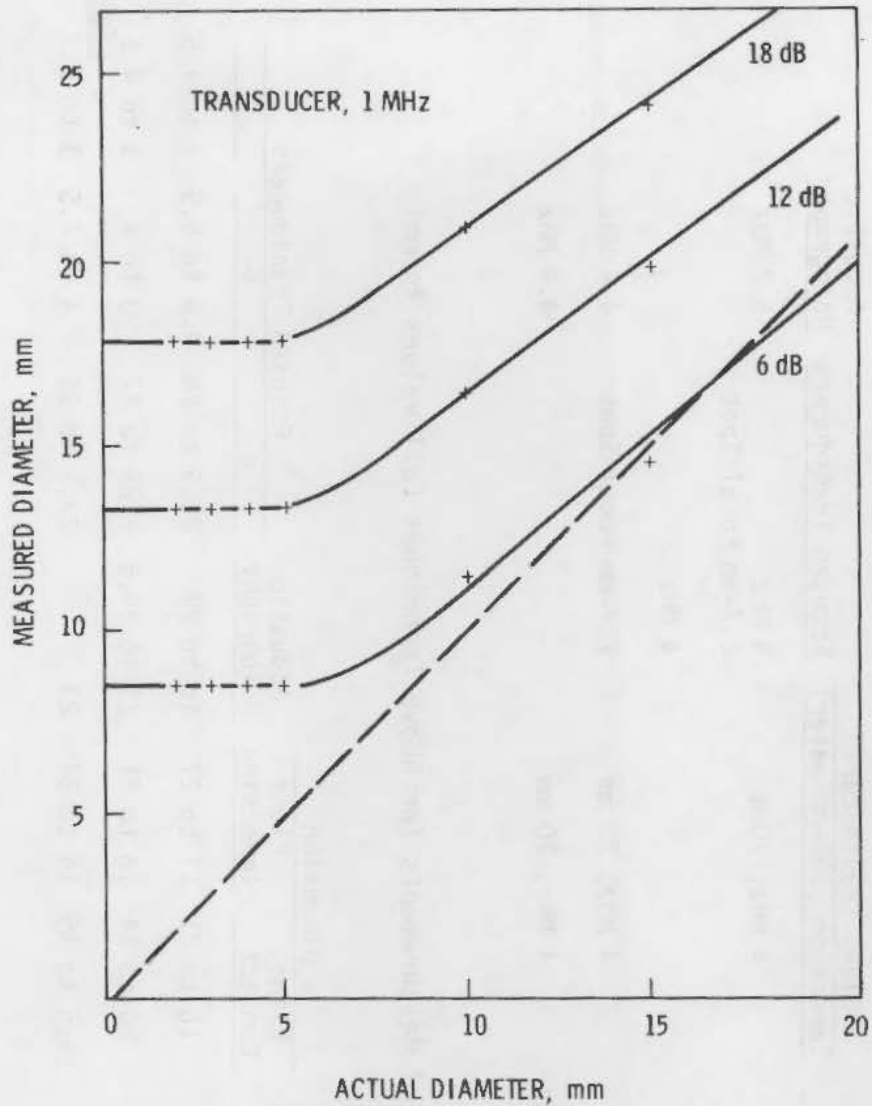


FIGURE 6.2.4. Measured Diameter as a Function of the Actual Diameter-1 MHz Transducer

Defects consisted of holes drilled into the partially completed weld, filled with ground fused flux, and covered by a manual weld; then the weld was completed. Three such flaws were inserted, all angling diagonally through the weld.

Some idea of the test conditions and the relative accuracy of measurement using the various techniques is apparent from the values in Table 6.2.1 based on examination of the values in the a dimension (parallel to weld). Error bands are quite broad for plane transducers. The values with acoustic

TABLE 6.2.1a. NDE Test Conditions

Contact	Plane Transducers	Focused Transducers	Acoustic Holography
	Immersion (100-mm water)		
Longitudinal 4 MHz 2 MHz	4 MHz, 20mm	4 MHz 2.7-mm Focal Spot	5.2 MHz
Shear 45°		4 MHz	
Parallel to Weld 2 MHz	4 MHz, 20 mm	2.7-mm Focal Spot	4.4 MHz
Perpendicular to Weld 2 MHz	4 MHz, 20 mm		4.4 MHz

TABLE 6.2.1b. Range of Measurements for Above Techniques (all values in mm)

Defect	Actual Dimensions			a Dimension		Acoustic Holography	Focused Transducers		
	a	b	c	Plane Contact	Plane Immersion		a	b	c
	Parallel to Weld	Through Thickness	Across Weld						
A	25.7	4.5	4.0	16 to 21	17 to 27	16 to 27	25.5 to 28	4.5 to 5.5	3 to 4.5
B	26.8	3.3	3.7	20 to 34	18 to 31	29 to 29.6	25 to 27	3 to 4	3 to 4.5
C	24.7	4.0	4.7	16.5 to 35	14 to 24	23	23.5 to 26	4 to 4.5	3 to 5

holography and focused transducers are better with regard to error band. Generally, the focused transducers appear to yield more accurate results.

Schlengermann and Frielinghaus<sup>(6.2.7)</sup> studied the parameters influencing the accurate sizing of defects. In some respects, this paper is comparable to the French work with focused transducers reported in this section. The authors<sup>(6.2.7)</sup> make the point that an exact determination of flaw size is possible only if the following pre-conditions are fulfilled:

- The reflector surface is smooth and even.
- The acoustical axis of the sound beam is vertical to the surface of the reflector.
- When evaluating the scanning curves, the effect of the (ideal) reflector on the (ideal) sound field is considered correctly.

Both natural and ideal reflectors were used in the study. The natural reflectors consisted of replicas of fatigue and brittle fractures of either rectangular or circular geometry. The ideal reflectors were of the same size but with accurately rectangular or circular edges and smooth surfaces. These are characterized in Tables 6.2.2 and 6.2.3.

Examination conditions consisted of two frequencies (1, 5 MHz), the same transducer diameter (~20 mm), near-field lengths of 0.25, 1 and 4 for flat transducers and the same focusing factor at the focal distance for focused transducers at both frequencies.

Evaluations were made at thresholds of 6 dB, 12 dB and 20 dB. Pronounced differences in the echo-amplitude curves were observed for natural defects when scanned in the long-axis and short-axis directions. Table 6.2.2 presents data for sizing of ideal and natural defects using plane and focused transducers. Table 6.2.3 presents data for locating the same defects. While errors are relatively limited for ideal defects, they are quite large for natural defects.

Some conclusions derived from this study are as follows:

TABLE 6.2.2. Determination of Size Deviation in Percent from True Value

Frequency	Distance	6-dB Drop				12-dB Drop				20-dB Drop				
		Ideal		Natural		Ideal		Natural		Ideal		Natural		
		X	Y	X	Y	X	Y	X	Y	X	Y	X	Y	
Fatigue Surface Rectangular (70 x 7 x 31 mm)	1 MHz	Focus	-0.8	1.2	-66.4	-21.2	0.5	4.5	-2.2	4.5	--	--	--	--
		1 N	0.9	4.4	-69.3	25.4	0.6	9.8	-44.9	24.1	0.9	6.6	-11.8	21.2
	5 MHz	Focus	-0.1	-0.3	-92.1	-64.6	1.2	2.8	-86.4	-58.1	2.7	6.1	-62.1	-24.4
		1 N	1.2	2.8	--	-93.5	2.4	5.7	-87.4	-36.6	2.4	2.5	-28.8	-16.7
Fatigue Surface Circular (43.5 mm)	1 MHz	Focus	0.0	0.0	-12.6	0.0	1.1	1.1	3.4	3.4	5.7	5.7	--	--
		1 N	0.5	0.5	-31.0	16.0	0.4	0.4	0.0	15.4	4.3	4.3	6.4	19.4
	5 MHz	Focus	-1.1	-1.1	-83.9	--	0.9	9.9	-81.6	-75.8	1.1	1.1	-56.3	-40.2
		1 N	2.2	2.2	-88.9	-59.5	1.1	1.1	-65.0	-47.3	0.9	0.9	-49.6	-35.8
Brittle Fracture Surface Rectangular (30 x 25 mm)	1 MHz	Focus	1.6	0.8	-21.6	-57.6	5.0	4.8	-16.6	-27.4	--	--	--	--
		1 N	5.6	5.1	--	-43.9	3.3	2.9	-26.0	-26.6	2.3	4.3	12.6	1.2
	5 MHz	Focus	3.3	2.8	-78.3	--	6.6	8.8	-75.0	-61.6	10.0	10.8	-70.0	0.8
		1 N	8.3	8.8	-4.6	-69.3	9.6	8.4	-10.3	-7.6	6.3	12.5	3.0	-3.6

TABLE 6.2.3. Determination of Position Deviation in Millimeters from True Value

	Frequency	Distance	6-dB Drop				12-dB Drop				20-dB Drop			
			Ideal		Natural		Ideal		Natural		Ideal		Natural	
			X	Y	X	Y	X	Y	X	Y	X	Y	X	Y
Fatigue Surface Rectangular (70 x 31 mm)	1 MHz	Focus	--	--	0.5	3.2	--	--	0.0	0.0	--	--	--	--
		1 N	--	--	-4.7	2.7	--	--	4.7	2.2	--	--	--	--
	5 MHz	Focus	--	--	-3.2	9.2	--	--	6.7	8.7	--	--	0.7	4.5
		1 N	--	--	-4.0	12.5	--	--	-1.0	7.7	--	--	-2.0	5.2
Fatigue Surface Circular (43.5 mm)	1 MHz	Focus	--	--	-2.0	1.7	--	--	0.5	2.0	--	--	--	--
		1 N	--	--	-9.2	0.7	--	--	-1.5	1.0	--	--	-3.0	0.7
	5 MHz	Focus	--	--	-12.0	--	--	--	-12.7	-3.2	--	--	-8.5	-6.0
		1 N	--	--	0.0	-10.7	--	--	-6.0	-9.5	--	--	-2.0	-8.2
Brittle Fracture Surface Rectangular (30 x 25 mm)	1 MHz	Focus	--	--	2.7	1.2	--	--	2.5	0.0	--	--	--	--
		1 N	--	--	8.0	3.7	--	--	8.7	0.0	--	--	3.7	-0.5
	5 MHz	Focus	--	--	11.2	--	--	--	11.2	2.5	--	--	11.0	0.0
		1 N	--	--	8.5	-0.2	--	--	3.0	-1.7	--	--	2.0	-2.7

- For ideal reflectors, reflector size can be determined quite accurately and almost independently of threshold and frequency; lower frequencies yield sharper images of the reflector edge and narrower sound beams lead to greater accuracy.
- The natural reflectors structure is a decisive factor when compared to wavelength. Steps taken to improve measurement of dimensions include the use of wavelengths large in comparison to defect structure, and the use of a relatively wide sound beam, provided that it is smaller than the reflector; focused beams are quite sensitive to flaw structure so that single reflectors are recorded by several indications.
- Variations in echo amplitude of natural reflectors require low relative thresholds for accuracy; a 6-dB threshold is not suitable; 20 dB or more is required.
- The effect of defect structure is reduced the less the impinging wave-front is in phase; this reduction is independent of wavelength.
- Echo deviations increase due to interference the farther one goes into the far field; i.e., approaches a flat wave-front.
- Reliable results cannot be obtained for natural reflectors by using the methods providing optimum results for ideal reflectors; geometrical concepts are of little help because the wave characteristics are so significant.
- A wide sound beam yields better results than does a narrow (focused) sound beam.
- A wave-front with phase variations (near-field/transition-field) gives better results than a flat wave-front (far-field focus);
- It is doubtful whether the optimized techniques used for ideal reflectors lead to satisfactory results for natural reflectors, regardless of phase relationships.

Saglio et al.,<sup>(6.2.8)</sup> in a continuation of their focused probe studies, examine a test block containing three flaws at different depths. They compare

the absolute size to the range of sizes obtained using focused probes, acoustic holography, contact flat probes, and immersion flat probes. Figure 6.2.5 presents their data for length as well as focused probe data for width and depth. The data confirm the author's opinion concerning the superior accuracy of focused probes.

#### 6.2.4 Scattered Amplitude

Silk<sup>(6.2.9)</sup> discusses the use of amplitude in the context of reflected amplitude from a defect. Amplitude per se is affected by variations in bulk material and coupling efficiency, both being sensitive to a variety of conditions. In recognition of these limitations, the signal arising from other sources becomes of interest. Three possibilities are

1. scattered amplitude
2. diffracted amplitude
3. mode-converted amplitude.

One approach to scattered amplitude cited in a review by Doyle and Scala<sup>(6.2.10)</sup> used two angle probes on opposite sides of a defect. A signal which is dependent on defect depth, reaches the receiver due to scattering by grain boundaries beyond the leading edge of the defect. Possible limitations to this technique include diffraction by the edge contributing to the signal, random errors caused by scattering from inclusions, and variations in transducer coupling. Another significant limitation is that cracks must be at least 3- to 4-mm deep because of physical size of transducers and beam width, together with the need to eliminate interfering surface waves.

The variation of transmission and reflection coefficients with crack depth might provide a basis for the measurement of small cracks less than half a wavelength deep. The transmission of surface waves past a crack in a fatigue test specimen has been used to monitor crack growth from an initial precrack 1.2-mm deep. The reflection coefficient for surface waves, which varies more markedly than the transmission coefficient for cracks much smaller than the wavelength, may prove more useful for the measurement of very small cracks; this possibility does not yet seem to have been thoroughly investigated.<sup>(6.2.10)</sup>

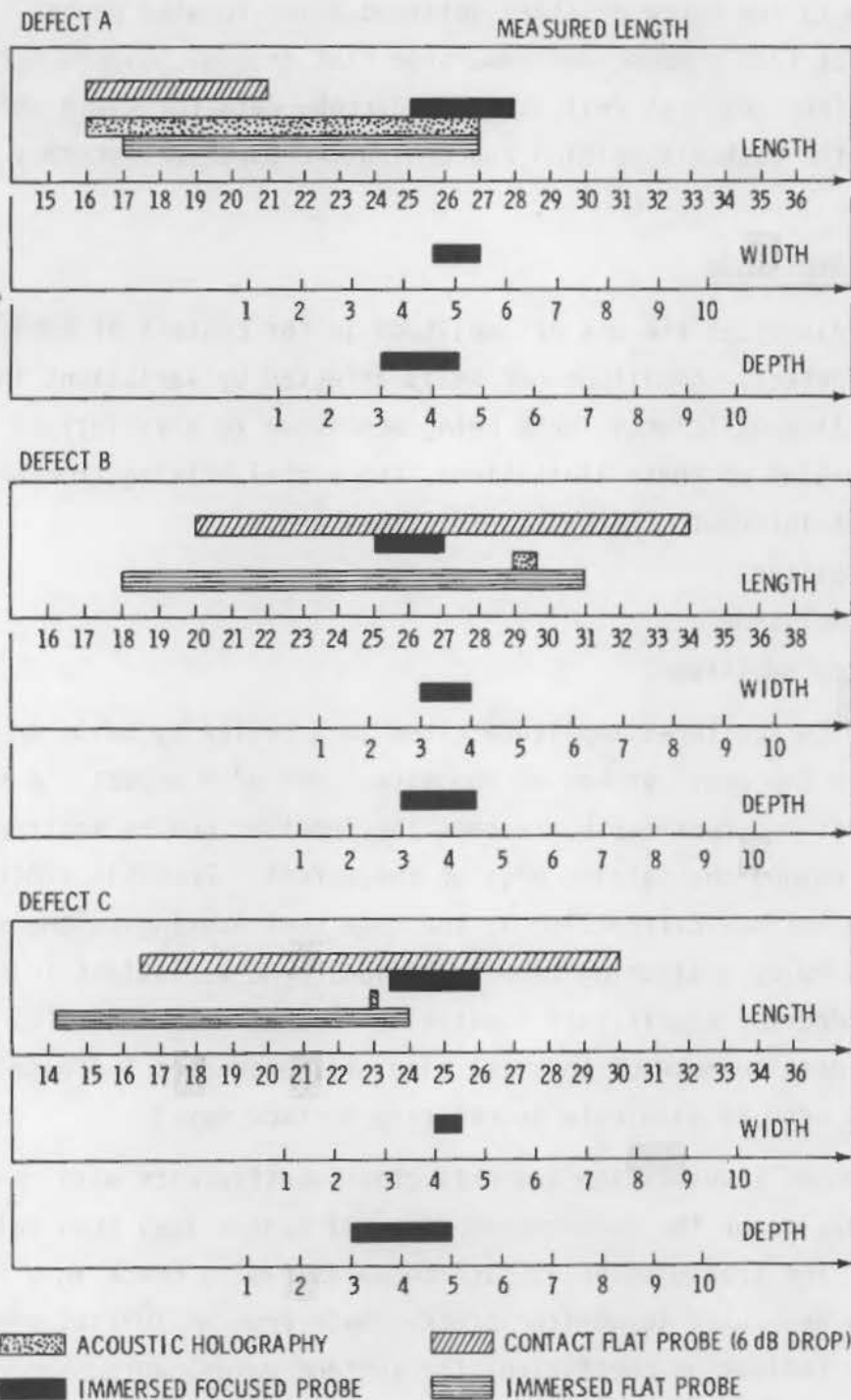


**FIGURE 6.2.5.** Scatter in the Width and Depth Dimensions of A, B, and C as Measured with Focused Probes. Ranges (max to min) in dimensions of slag inclusions A, B, C, where length was measured by four ultrasonic techniques and width and depth by focused probes alone. Values are compared to those determined by sectioning.



A different technique has been proposed recently. When a surface wave is directed towards a crack, part of the energy travels down the crack face and is radiated over a wide range of angles as S-waves from the tip (Figure 6.2.6). An S-wave detector of known angle  $\phi$  should give maximum response at two positions, one at each side of the crack tip. Once these two positions are located (for one surface of the specimen), the crack depth can be readily found geometrically. This technique has the advantage of requiring neither a reference standard nor a detailed study of the scattering process. Fatigue crack depth greater than 8 mm was measured to an accuracy of 13% with the method though it is unsuitable for application to small cracks. (6.2.10)

Another approach<sup>(6.2.9)</sup> uses two angled longitudinal-wave probes placed as shown in Figure 6.2.7a on the material surface. At low gain no signal will be observed, but with increasing gain the scattered ultrasound from the region where the beams cross will become apparent. By choosing frequency, pulse length, and electronic characteristics so that these grain boundary echoes are largely in phase, the observed signal can be made a measure of the presence of cracks. Thus, as a crack grows from the surface, it will successively block the scattered energy, causing the signal to fall.

This fall in signal amplitude is, in general, slow at first, but becomes more rapid as the crack tip enters the region close to the center line of both

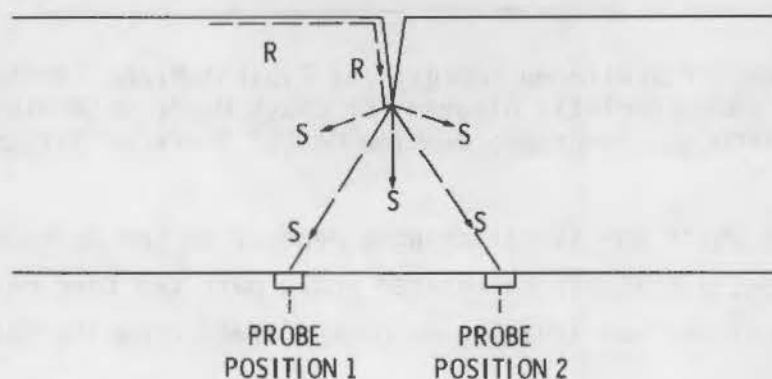


**FIGURE 6.2.6.** Depth Measurement by Detecting S-Waves Produced by Mode Conversion of R-Waves at the Tip Using an S-Wave Detector of Known Angle  $\phi$

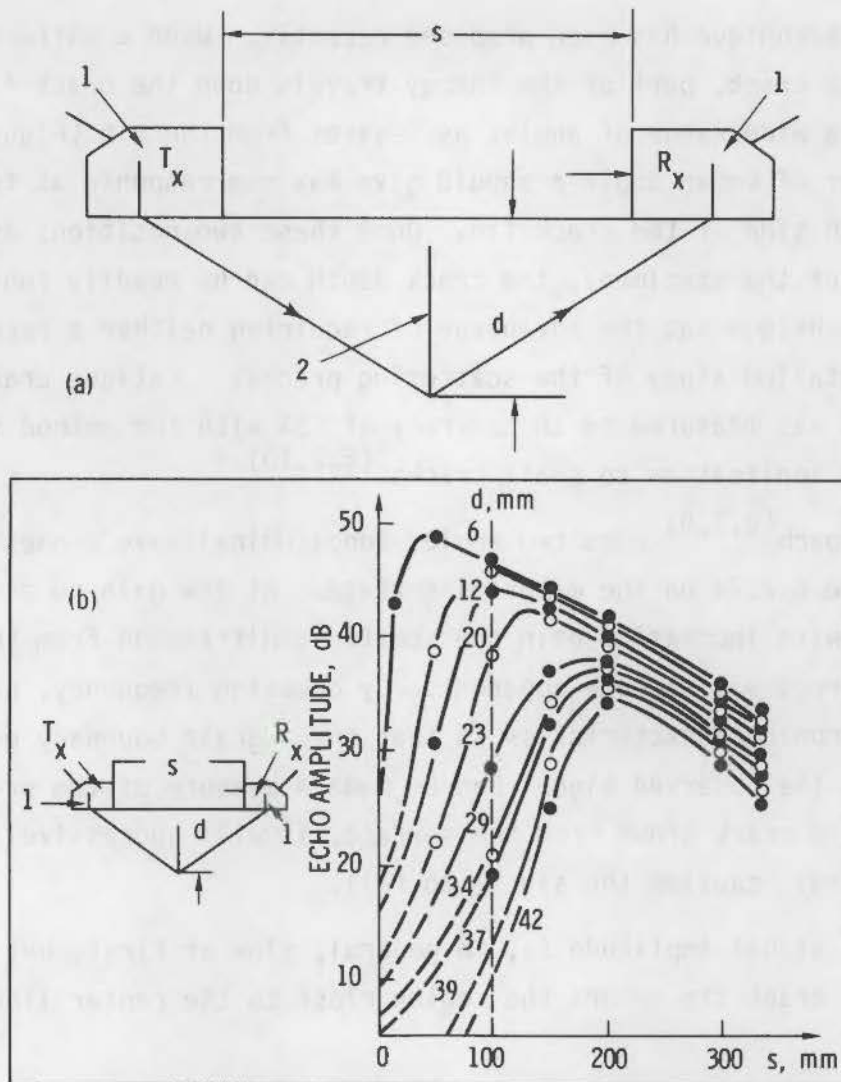


FIGURE 6.2.7. Study of Scattered Energy: a) Typical Probe Configuration, b) Characteristic Diagram for Crack Depth Determination. 1--Probes; 2--Crack; d--Flaw Depth; S--Probe Distance

beams. The point at which the signal changes depends on the probe angles and separation and, hence, a suitably calibrated probe pair can then be used to determine the depth of surface-breaking or near-surface-breaking cracks (Figure 6.2.7b).

The fundamental work on this approach has been carried out by Wüstenberg and his co-workers at Bundesanstalt für Materialprüfung (German Federal

Institute) (BAM), Berlin. It has been used in practice on cracks but the data do not yet seem to be published. The accuracy appears to be in the region of  $\pm 1$  mm.

### 6.2.5 Mode-Converted Amplitude

If a Rayleigh wave is allowed to pass along the material surface and encounters a crack, it will run down the crack face. At the crack tip, mode conversion of some of the energy into shear waves occurs giving a wave-front that is, again, moderately uniform in intensity. The remaining energy is either reflected at the crack tip or passes on up the other crack face to the surface; this phenomenon will be discussed later.

The shear-wave energy can then be used with probes of known angle to locate the crack tip exactly as described in the previous section. Some data are shown in Figure 6.2.8 for a fatigue crack sample and the error here seems to be some  $\pm 2$  to 3 mm.

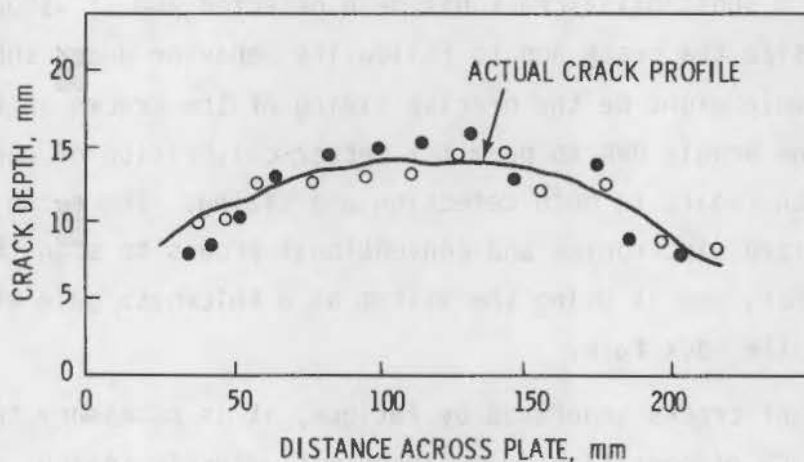


**FIGURE 6.2.8.** Estimates of Depth of Fatigue Crack Using Maximum Echo from Mode-Converted Shear Wave. Probes on same side of plate as (o) and opposite side of plate to (●) surface wave probe

### 6.2.6 Pulse-Height Difference

Cracks that grow as a function of time such as thermal or vibrational fatigue or stress corrosion have been monitored continuously. If this is done, it is necessary to consider long-term equipment drift which can be affected by temperature, variations in the voltage supply and creep in couplant, etc.

Various approaches have been used to achieve a reasonably stable signal such as measuring the UT output voltage difference  $\Delta V$  between back-wall reflection and crack reflection, recognizing that crack morphology is a significant input.

Crack growth can be monitored continuously during initiation of load quasi-stable loads and unloading to establish the significance of holding time, cycles, etc. on crack growth.

### 6.2.7 End-On UT to Crack

A specialized technique is end-on UT.<sup>(6.2.11)</sup> It might be used in special cases where a substantial crack has been detected and it is desirable to both accurately size the crack and to follow its behavior under subsequent loading. An example might be the precise sizing of the cracks in the safe ends removed from Duane Arnold BWR to permit a better calibration of conventional UT techniques with regard to both detection and sizing. The technique uses somewhat specialized electronics and conventional probes to scan the crack end-on. In essence, one is using the system as a thickness gage where the crack represents the back face.

In the case of cracks generated by fatigue, it is necessary to load the system to about 50% of operating loads to permit accurate sizing. Generally, the technique somewhat underpredicts the crack size. In the case of a crack driven under monotonic loads, it can be detected under zero stress. An estimate of the error in sizing appears to be less than 1 mm.

Sizing also is sensitive to the remaining ligament. As this dimension decreases, higher UT frequencies are required; however, with higher frequencies cracks to within 4 mm of the surface have been measured. A potential application would be on larger piping where the tradeoff of continuous

monitoring versus repair may make such an installation attractive, providing that the regulatory authorities' approval could be obtained.

#### 6.2.8 Diffacted Amplitude

A diffracted wave arises from the ends of the defect and appears not to be subject to rapid changes in intensity. If a probe of known angular characteristics,  $\theta$ , is used as a receiver, the diffracted signal will be at a maximum when the crack tip lies at the angle  $\theta$  with respect to the probe. This provides a means of delineating the defect, since the echo time delay gives the range of the crack tip and the probe angle its angle with respect to the beam entry point. Thus, the coordinates,  $R$ ,  $\theta$ , can be defined for each tip. This technique is similar in operation but possibly more accurate than the decibel-drop approach. It was one of several techniques considered by de Sterke and has also been studied at the NDT Centre Harwell.

Golan<sup>(6.2.12)</sup> Examined crack-tip ultrasonic diffraction as a technique for crack sizing. The author<sup>(6.2.12)</sup> develops the geometric-formulation for various crack locations. The following four parameters influence the efficacy of this technique:

- strength of the UT beam diffracted from the crack tip
- accuracy of sizing of the crack
- range (this parameter relates to the area covered by the UT field)
- surface resolution (the factor determining the limits of crack size that is measurable).

The low intensity of the scattered field from the crack tip is a significant limitation; however, optimization of testing conditions partially alleviates this effect.

Silk<sup>(6.2.13)</sup> discusses the crack-tip diffraction technique developed at Harwell, and indicates its application on real flaws such as fatigue cracks. Figure 6.2.9 is a schematic of the UT wave paths. The two signals from the crack tips are the bases for sizing. In addition to these signals, there will be specular reflection from the back surface plus a near-surface wave which

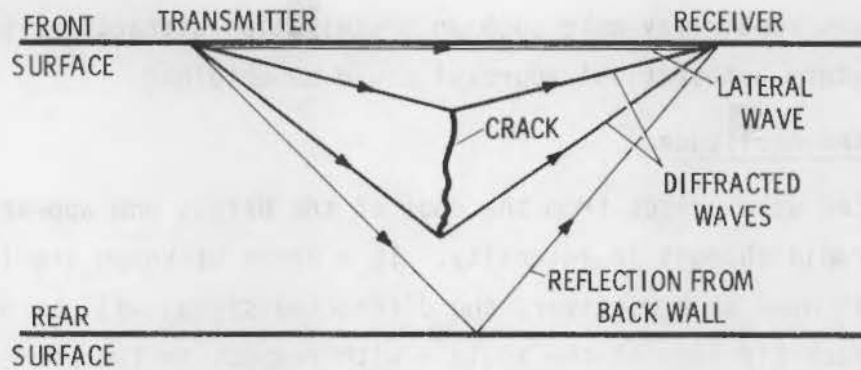


FIGURE 6.2.9. Presumed Ray Paths Taken by the Discrete Signals Observed in the Diffraction Technique

appears to take the shortest path between the probes. The author<sup>(6.2.13)</sup> defines this as the near-surface wave. With mode conversions and other signals there may be 14 to 20 discrete signals. Usually, these will appear later than the back-wall echo. Figure 6.2.10 permits a comparison of UT waves from cracks at various locations such as embedded, far surface and near surface.

The various mechanisms contributing to the UT under diffraction conditions include the near-surface wave and a composite pulse arising from grain-boundary scatter. This means that there may be marked variations from component to component being examined. A better understanding of the UT behavior will require a detailed theoretical analyses. Some theoretical work permits a comparison of response as noted in Figure 6.2.11.

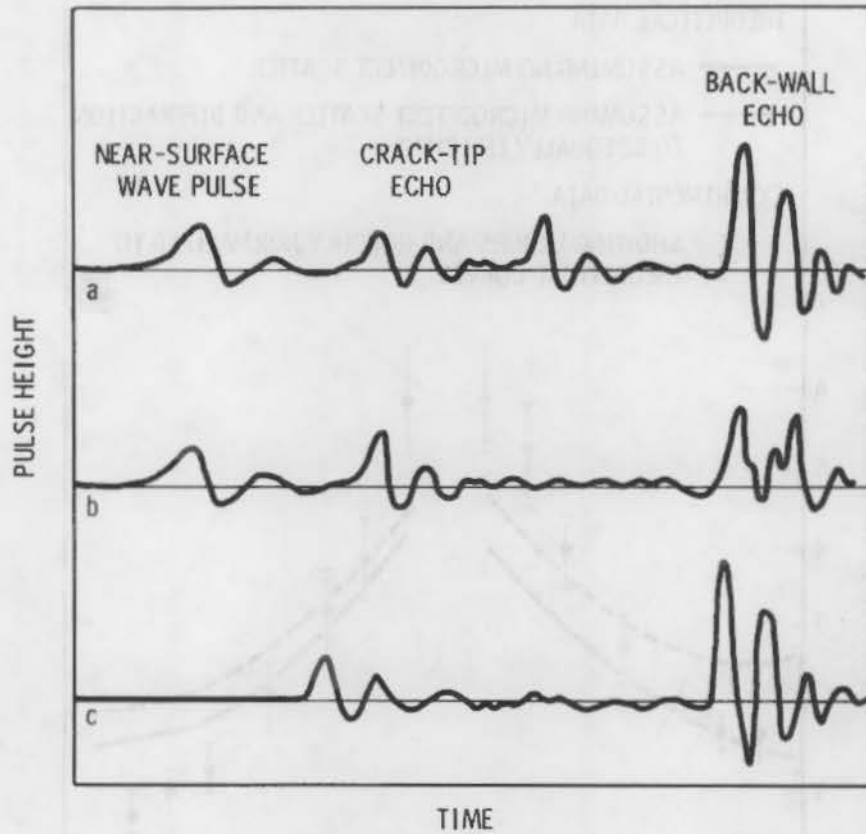


FIGURE 6.2.10. Typical Ultrasonic Responses: a) internal crack (hypothetical); b) crack opens to surface opposite probes; c) crack opens to same surface as probes

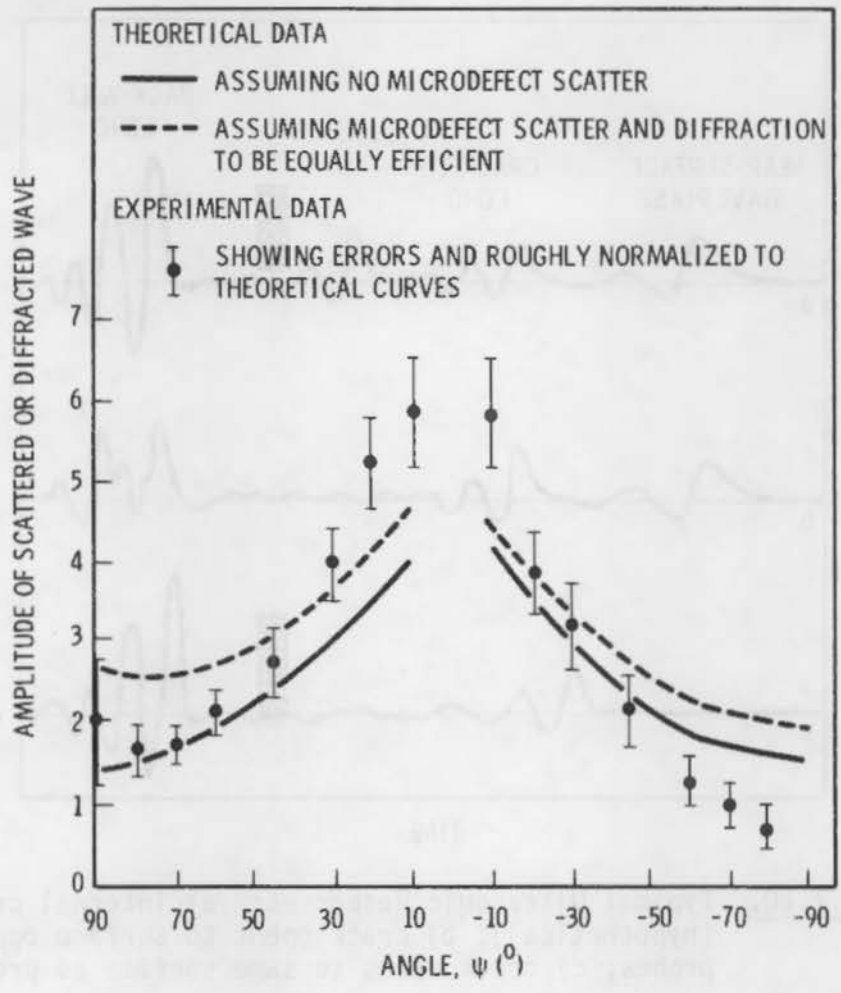


FIGURE 6.2.11. Theoretical and Experimental Estimates of the Variation of the Amplitude of the Wave Scattered or Diffracted from the Crack Tip



The time domain technique exploited by Silk et al. has been discussed in Chapters 4 and 5. (4.5.10,5.4.4,5.4.5,5.4.8,5.5.3) Both artificial slits and natural flaws have been examined. With stepped slits, accuracies of  $\pm 0.2$  to  $0.3$  mm were obtained. Some idea of the relative accuracies of time delay versus signal amplitude is given in Table 5.4.2 for a dual probe technique. The error with time delay ranged from  $0.0$  to  $1.8$  mm with maximum mean error of  $4\%$  whereas amplitude errors ranged from  $0.5$  to  $29.5$  mm with mean error of  $66\%$ . A single-probe, surface-wave technique used to measure real flaws yielded surprisingly good results, considering that the crack changed direction and that there was a high inclusion population in the steel. The accuracy was about  $\pm 0.5$  microsecond, corresponding to an error of  $\pm 0.8$  mm (see Figure 5.5.1).

Parallel studies on artificial flaws and natural cracks yielded mean errors of  $\pm 0.49$  mm for cracks versus  $\pm 0.35$  mm for artificial slits.

Both shear and angled longitudinal waves were examined by the time delay technique to determine whether there was an advantage to longer transit time due to the lower velocity of shear waves; however, stray signals due to mode conversion etc., made it difficult to identify the diffracted wave. Figures 5.5.2a and 5.5.2b indicate the relative accuracies of the time delay technique over a total crack profile.

Crack depth measurements with time delay of surface waves yields accuracies of  $\pm 0.2$  mm. (5.4.8) However, several problems require resolution insofar as practical applications are concerned such as the following:

- Length along the crack face rather than depth of penetration is measured.
- Rayleigh wave travel times are affected by surface irregularities.
- Shear-wave signals of comparable height may arrive earlier than the surface wave.

Another approach to crack sizing utilizes the additional factor of arrival time of the mode-converted shear wave described in Section 6.2.6.<sup>(6.2.8)</sup> This arrival time is taken together with the surface-wave transit time. The experiment is then repeated reversing the transmitter and receiver which permits a mathematical elimination of surface travel time and provides an estimate of depth of penetration. This now becomes the mathematical analogy to the diffraction technique described in 6.2.5 above. Results in Figure 6.3.1 have an accuracy of better than  $\pm 1$  mm.

A more general and potentially more powerful technique of sizing defects in the time domain is the satellite-pulse technique (SPT) developed at Southwest Research Institute.<sup>(6.3.1)</sup> This technique is based on an interpretation in terms of defect dimensions of the separation in time-of-arrival (TOA) between the specularly reflected pulse and its tip-diffracted or circumferentially scattered satellite. The SPT is said to improve both defect discrimination and sizing capability. It is considered to be both reliable and

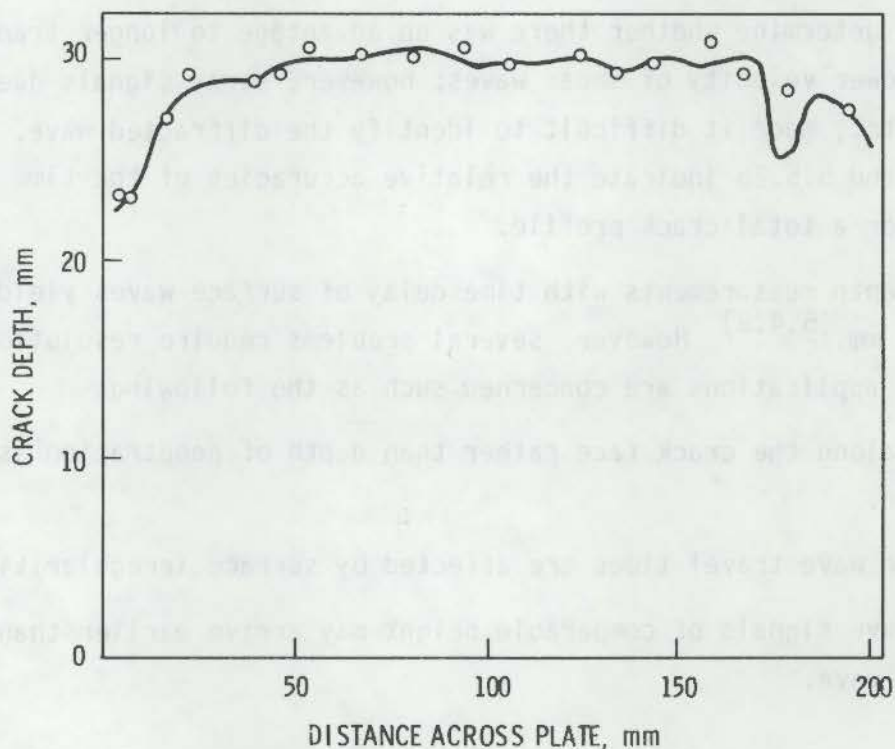


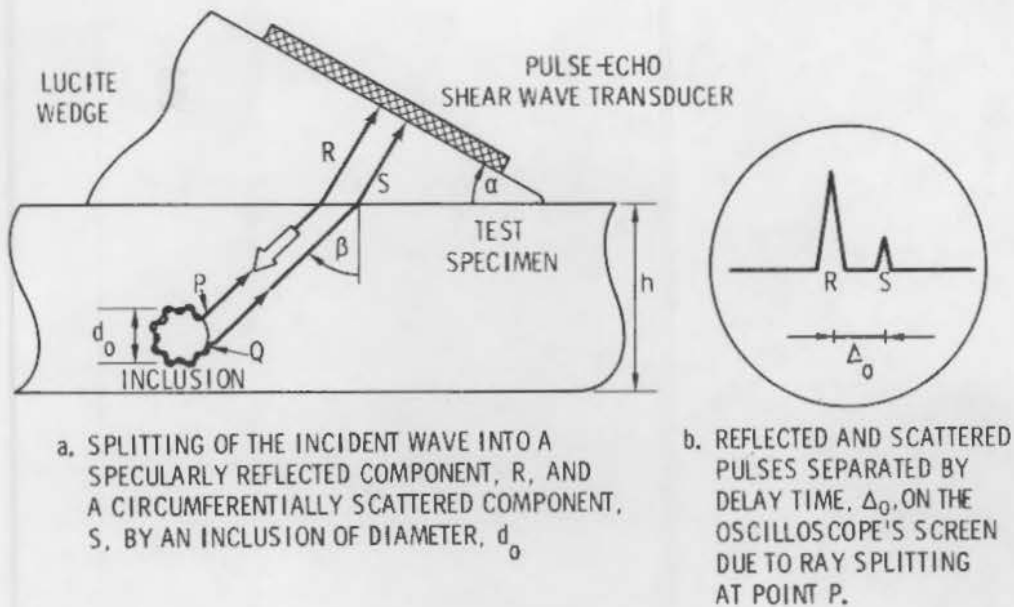
**FIGURE 6.3.1.** Determination of Fatigue Crack Profile (—) Using Ultrasonic Surface Waves and Mode-Converted Shear Waves. O—ultrasonic estimates of depth

simple because it is independent of 1) signal parameter from peak amplitude, 2) defect location, and 3) operating frequency. Furthermore, there is a linear relationship of signal parameter to defect size together with self-calibration, direct reading of defect size, and use of standard equipment.

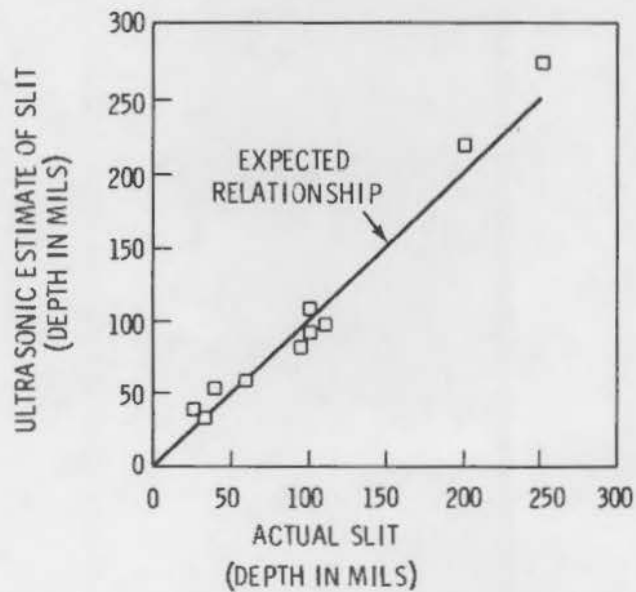
Table 6.3.1 permits a comparison of various peak amplitude, frequency content, and arrival techniques. Figure 6.3.2 illustrates the operations of SPT. Figure 6.3.3 illustrates the linear relationship between estimated and actual slit depths using SPT.

TABLE 6.3.1. Pros and Cons of Various Defect Sizing Techniques

<u>Technique</u>	<u>Manner of Analysis</u>	<u>Pros</u>	<u>Cons</u>
Artificial Defect	Peak Amplitude		Neither side-drilled holes nor notches correlate well with defects (even simple artificial). There can be a gross over- or under-estimation of flaw size.
Backwall Echo Comparison	Distance	Distance-Gain-Size permits a "universal" test block.	Size estimates unreliable for defects in near (dead) zone. Defect surface roughness adversely affects sizing. Correction factors needed for differences in coupling efficiency, frequency, attenuation, etc.
Decibel Drop			If planar defect is not normal to UT beam, then sizing will vary.
Deconvolution	Frequency Content		Deconvolution which compensates for contamination by transducer and material properties may or may not isolate effects of defect characteristics from defect signal. Therefore, may be pro or con.
Frequency Response			Conceptually, frequency response permits obtaining defect geometry information directly from the defect spectrum. While such techniques as ultrasonic spectroscopy have potential, they have not been accepted for industrial use.
Impulse Response	Arrival Time	Arrival time basically is simpler than frequency analyses.	Phase information normally is not available. To obtain requires deconvolution and inverse Fourier transformation which needs sophisticated minicomputers not generally available.
Tip-Diffraction	Delay Time	A fairly unambiguous measurement. Tip-diffraction can be used with a single probe.	Errors in probe separation measurements will result in inaccuracies in crack size estimation.
Satellite-Pulse Technique (SPT)		An extension of time-delay applicable to all types of defects. This incorporates features of the preceding four techniques. SPT presumably is immune to variations in reflected, diffracted, and scattered pulse amplitudes.	



**FIGURE 6.3.2.** The Interaction of an Ultrasonic Shear Wave with an Inclusion-Like Defect Resulting in a Reflected Pulse and a Lagging Scattered Satellite Pulse



**FIGURE 6.3.3.** Illustrating the One-to-One Correspondence Between the SPT Ultrasonically Estimated and Visually Determined Slit Depths



Figure 2. Schematic diagram of the experimental setup. The circular inset shows the waveform of the shear wave at point A.

The interaction of an ultrasonic shear wave with an inclusion is the subject of this paper. In a bilinear system, the shear wave is scattered into a reflected wave and a transmitted wave.

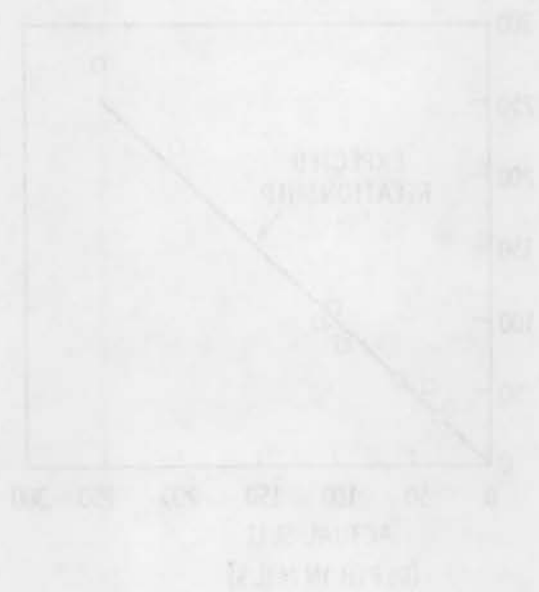


Figure 3. Relationship between the incident wave and the reflected wave.

A first step and a limited one toward frequency domain analysis was reported by Gurvich and Kuzmina<sup>(6.4.1)</sup> in 1970. A "scattering indicatrix" approach was used to enhance the volume of information relevant to a detected defect to permit a better estimate of its configuration and orientation. The "scattering indicatrix" is defined as the normal function describing the field of an ultrasonic wave reflected toward the probe.

#### 6.4.1 Acoustic Spectroscopy

Vopilkin et al.<sup>(6.4.2)</sup> used an ultrasonic spectroscope covering a bandwidth of 1 to 10 MHz to detect and classify various defects. Pictorial spectrograms were used to classify into various planar or volume defects.

Volume defects were distinguished by the following:

- the monotonic nature of spectrum from both probes for a single volume defect
- the nonmonotonic nature of the spectrum for a single or for both probes with the depth of the minima not exceeding 3 to 4 dB for a single volume defect of small dimensions
- the oscillating nature of the spectrum for one or both probes with the depth of the minima as much as 15 to 20 dB; however, the attenuation of maxima and minima is nonperiodic; these factors apply to a group of closely adjacent volume defects.

A planar defect can be distinguished by the following:

- the oscillating nature of the spectrum for both probes with depth of minima as much as 15 to 20 dB and alternation of maxima and minima periodic; the deviation in frequency interval between neighboring maxima does not exceed 0.3 of the average frequency interval; these apply to a single crack or non-fusion.
- the monotonic spectrum of the first probe and oscillating spectrum of the second probe for a single crack or planar non-fusion when oriented perpendicular to the first probe.

The preceding criteria were applied to 77 natural defects to classify them as noted in Table 6.4.1.

TABLE 6.4.1. Classification of Natural Defects

<u>Class of Defect</u>	<u>Type of Defect (Basis--Metallography)</u>	<u>Total Number of Defects</u>	<u>Number of Correctly Classified Defects</u>	<u>Probability of Correct Defect Classification</u>
Volume	Single slag or pores	16	14	0.875
	Slag clusters	13	9	0.692
	Circular non-fusion	9	8	0.888
Planar	Cracks	13	13	1.0
	Planar non-fusion	<u>26</u>	<u>23</u>	0.884
		77	67	Pa = 0.82

NOTE: Pa = mean probability.

#### 6.4.2 Adaptive Learning

Workers at Hanford Engineering Development Lab (HEDL) (6.4.3,6.4.4) investigated the implications of several parameters in austenitic stainless steel weldments in various sizes of piping. These weldments contained EDM notches and flat-bottomed holes as well as porosity and lack-of-fusion. In addition, the welds varied in grain size and dendritic structure. The objective of the study was to examine techniques to reduce the sensitivity to microstructural variations. A reduction in frequency reduced the UT noise level; however, such a reduction also reduced the sensitivity of detection. Spurious UT signals were attributed primarily to 1) the dendritic structure; 2) some noise attributed to weld metal-base metal interfaces which occurred with both homogeneous weld structures and parallel dendritic structures; and 3) some UT noise due to external geometry. For example, when the weld crown and weld root regions were machined, much of the UT noise was lost.



One other feature observed was UT beam bending with the beam following the dendritic grain interface. This phenomenon was previously cited in Japanese work.<sup>(4.5.20)</sup>

The HEDL ultrasonic automatic data processing system (UT/ADP) is a form of adaptive learning network (ALN) utilizing waveform analysis to minimize sensitivity to microstructural variations. A second-order moment algorithm was used to discriminate signals from defect notches vis-a-vis grain size. Best results were obtained with broad-band transducers because the spectral response of grains is narrow band whereas defect response is broad band. The UT/ADP technique was considered successful in discriminating between notches, porosity and grain noise.

An example of analysis of frequency domain data with computerized ALN techniques appeared in an early study by Adaptronics<sup>(6.4.5)</sup> using UT to detect and measure subsurface fatigue cracks radiating from fastener holes in aluminum plate. The ALN analysis detected and measured these subsurface cracks to about 70% of the characterized length over the size range of from 0 to 279 mils compared to approximately 50% detection for fatigue cracks larger than 30 mils and zero for cracks smaller than 30 mils using conventional UT.

An Argonne National Laboratory (ANL) study<sup>(6.4.6)</sup> examined the effects of microstructure and the use of signal enhancement in UT of austenitic stainless steel. The same trends observed in other studies occurred here; namely, beam attenuation, particularly at higher frequencies; decrease in UT velocity; and strong directionality of amplitude in dendritic structures. Signal enhancement by averaging and computer processing helped improve signal-to-noise ratios.

An ultrasonic frequency-analysis technique<sup>(6.4.7)</sup> was used to characterize flaws in an 8-in. (203-mm) thick steel weldment. A multi-transducer system was used with the spectrum of received broad-band signal frequency analyzed at two different receivers for each flaw. The two spectra permitted determination of flaw size and orientation with the aid of an analytic model.

Based on the size of weldment, location and type of flaws, it is highly probable that the specimen is PVRC Plate 201. Since the weldment is not identified specifically, the data are given here in Table 6.4.2 rather than in Chapter 3; however, the intended and actual flaw locations of PVRC 201 are included for comparison.

If, indeed, the authors<sup>(6.4.7)</sup> had access to PVRC 201, it was after cladding half the plate and prior to dividing the clad and unclad portions. While the report is not explicit, it appears that the examinations were through the cladding. If that is true, they were more successful in detecting the defects than were the five teams using conventional equipment. In fact, these results are better than were obtained with focused arc transducers. The multi-transducer technique is described elsewhere.

Rose<sup>(6.4.8)</sup> conducted a flaw sorting study using ultrasonics and pattern recognition. Twenty-three flaw geometries consisting of side-drilled holes and electro-discharge machined notches were examined. The flaws consisted of smooth cylindrical, elliptical, and sharp rectangular and triangular, in both singular and cluster arrangements. The objective of the study was to separate the 23 tests flaws into as many groups as possible on the basis of UT data acquisition and pattern recognition, while serving as a feasibility study for extension into real flaw inspection and classification.

Ultrasonic data were obtained in a scattering mode with a fixed position angle-beam transducer. Three algorithms in pattern recognition were used: 1) a minimum distance classification scheme; 2) a Fisher linear discriminant function routine; and 3) a two-layered adaptive training network.

A two-mode classification scheme, either sharp or smooth surface defects for pattern recognition algorithms, produced a 92% reliability of predicting the sharp or smooth classification. The classifications consisted of sharp singular, sharp multiple, smooth singular, and smooth multiple, using probability density functions.

The results of the various classification approaches can be seen in Table 6.4.3.a and 6.4.3b.

TABLE 6.4.2. Flaw Size Measurement Using UT Frequency Analysis(6.4.7)

PVRC 201 Plate Data		Flaw Location (in.)						Frequency Analysis Measurement (Length, in.)			Actual Length
Flaw	Type	Intended			Actual			X	Y	Z	
		X	Y	Z	X	Y	Z				
A	Crack	14.75	19.75	4.1	15.0	19.31 to 21.12	4.19	~14.5	~19.5 (~0.7)	4.0	1.8
B	Slag	15.0	3.0	2.0	15.3	2.2 to 3.6	2.0	~15.0	~3.5 (~1.0)	2.3	1.4
C	Crack	14.0	5.75	1.0	14.3	5.4 to 7.2	1.0	~15.0	~5.0 (?)	1.3	1.8
D	Crack	16.0	17.0	0.5	16.0	16.81 to 17.81	0.5		--	--	1.0
E	L-0-F	14.0	21.0	0.5	13.93	21.12 to 22.12	1.5			--	1.0
F	L-0-F	15.0	16.0	5.5	15.19	15.88 to 16.88	5.4	~15.0	~15.5 (~1.0)	5.8	1.0
G	L-0-F	14.0	0.83	7.0	14.7	0.8 to 1.2	7.6	~14.5	~1.0 (1.5)	7.3	2.0
H	Slag	16.0	5.0	7.5	15.7	4.3 to 6.0	7.4	~16.0	~5.0 (0.75)	7.5	1.3
I	Slag	15.75	1.0	7.0	15.8	0.3 to 1.6	7.9	~16.0	~1.0 (2.0)	7.1	1.3
1	Lamination				14.2	0.1 to 2.1	4.6				2.0
2	Lamination				14.2	9.1 to 9.9	4.5				0.8
12	Sponge				14.75	~2.1	2.5				--

6.4.5

TABLE 6.4.3a. Index of Performance--Classification Results

<u>Class Description</u>	<u>Minimum Distance Classifier Approach (%)</u>	<u>Fisher Linear Discriminant Function Approach (%)</u>	<u>Adaptive Training Network (%)</u>
2-Class Problem of Sharp or Smooth	92	88	92
4-Class Problem of Sharp Singular, Sharp Cluster, Smooth Singular, Smooth Cluster	82	82	Not done
23-Class Problem of Specific Class Numbers	48	Not done	Not done

TABLE 6.4.3b. Capability of Detecting a Specified Class

<u>Specified Class</u>	<u>Minimum Distance Classifier Approach (%)</u>	<u>Fisher Linear Discriminant Function Approach (%)</u>	<u>Adaptive Training Network (%)</u>
Sharp versus Smooth	92	88	92
Singular versus Multiple	88	88	Not done
Inclined Sharp Edge	94	Not done	Not done
Smooth Singular	90	93	Not done
Smooth Cluster	52	76	Not done
Sharp Edge Singular	93	77	Not done
Normal Sharp Edge Cluster	85	80	Not done

An extension of the Adaptonics work in ALN examined various defects in austenitic stainless steel with the UT techniques simulating inservice examination.<sup>(6.4.9)</sup> A two-step ALN decision process was used to 1) identify suspicious regions via a rapid nonangulating scan; and 2) examine the suspicious regions in great detail by an angulating scan pattern.

This approach enabled all cracks to be successfully sorted from weld geometrical reflectors. The ALN classified false-dismissal rate (the fraction of cracks falsely dismissed as geometrical reflectors) was zero, and the false-alarm rate (the fraction of non-defects falsely assessed as cracks) was 33%. In the second more detailed examination of suspicious regions, an ALN crack classifier was synthesized from parameters related to spectral shifts in

waveform ensemble; this approach reduced the false-alarm rate to zero; e.g., it was possible to discriminate unambiguously between cracks and benign reflectors. The ALN's utilized parameters that were independent of signal amplitude. This generally normalizes out variability due to transducer, couplant, operator technique and electronics. Differences were emphasized in a series of frequency ranges; e.g., 0 to 1 MHz, 1 to 2 MHz and 2 MHz.

While the procedure was quite successful in detecting side-drilled holes, fatigue cracks, weld crown, counterbore, etc., the study was not completely definitive since full penetration welds with pronounced dendritic formation were not examined. The study represents a good first step, but confirmation is required by destructive testing with the specimens containing both benign and hazardous defects.

Some idea of the response to various defects can be seen in Figure 6.4.1.<sup>(6.4.9)</sup>

Another ALN type study<sup>(6.4.10)</sup> concentrated on intergranular stress corrosion cracks (IGSCC) in austenitic stainless steel piping. Seven different welds in four different 4-in. pipe specimens were examined. Specific features considered in the data analysis were 1) the number of spectral peaks above 20 dB; 2) the fractional power ratio in the 2- to 2.5-MHz range; 3) total power in the 0- to 3-MHz range; 4) the 10-dB down bandwidth; and 5) 10-dB down mid-frequency.

The interim results clearly distinguished between the weld crown geometric reflector vis-a-vis IGSCC; however, further studies on additional geometric reflectors are required utilizing more advanced techniques in pattern recognition.

An early version of determining flaw size and orientation by ultrasonic spectral analysis, possibly the first, was reported in 1971.<sup>(6.4.11)</sup> The authors present both a physical and an analytical model based on an interference mechanism which compared favorably to the experimental results.

A UT technique tied to Reference 6.4.9 used a form of computer learning known as "Simu-Learning" where the computer is used to obtain specific defect information; e.g., crack-no-crack type of flaw, etc.<sup>(6.4.12)</sup> The study used

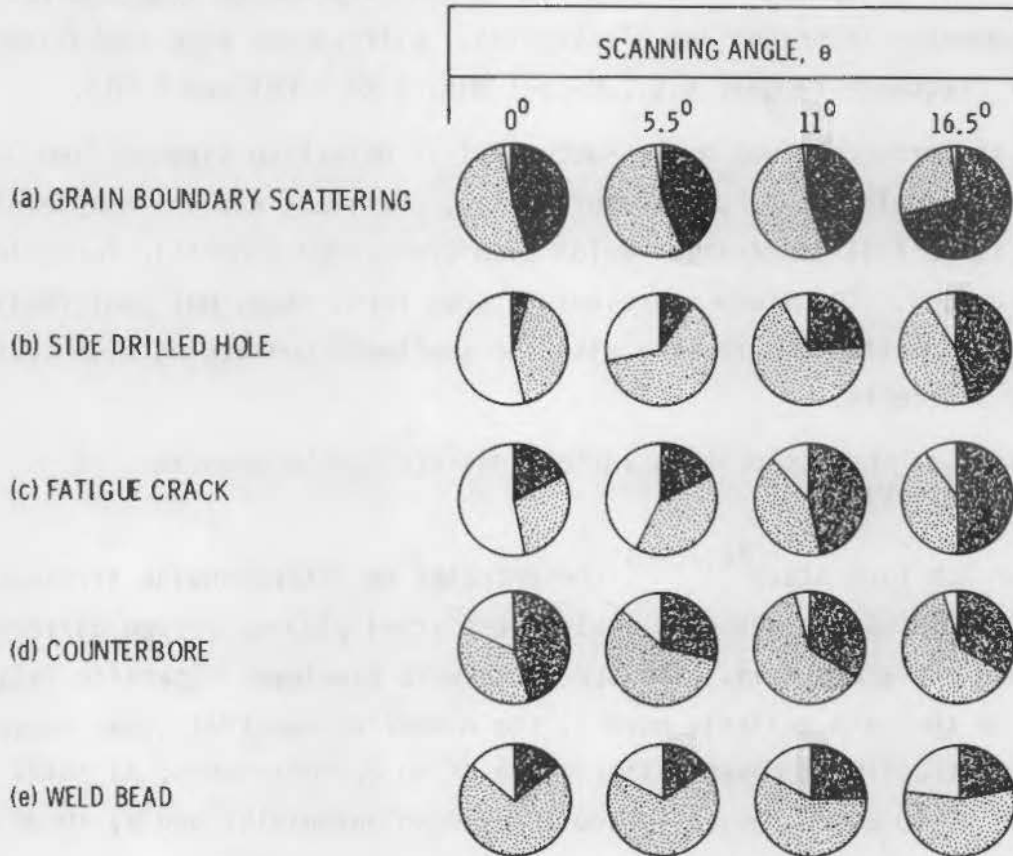
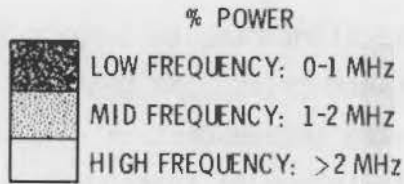


**FIGURE 6.4.1.** Pulse Echo Dependence on Scanning Angle for Five 304 SS Reflectors

real flaws and piping geometries. While no information was presented that quantitatively relates to IGSCC size, there is considerable information pertaining to difference in signals such as RF display, Fourier phase angle versus frequency, Fourier amplitude versus frequency, production of Fourier amplitude, and phase angle versus frequency.

A Russian study<sup>(6.4.13)</sup> classified defects by spectral analysis; however, fewer parameters were used than was the case with Rose.<sup>(6.4.8)</sup>

Only five defect geometries (disc, strip, sphere, cylinder, concave cylinder) and the following six size spectral criteria are used:

1. average arithmetic spectrum
2. average quadratic spectrum
3. area occupied by the spectrum
4. sum of the slope angles of the secants to the adjacent points of the spectrum
5. length of spectrum envelope
6. length of spectrum envelope of single density.

A combination of criteria 1 and 4 led to correct classification of 88 to 90% of planar defects and 88 to 95% of three-dimensional defects. A combination of five criteria (1, 4, 5, 2 and 3) improves classification somewhat, 87 to 92% versus 88 to 90%, 94 to 97% versus 88 to 95%.

While this procedure illustrates the power of spectral analysis, no apparent advantages appear to exist when compared to ALN, etc.

only two defect categories (large, small, column, column) and the following: (1) the total of the 12 sets.

1. average defect frequency
2. average defect frequency
3. area occupied by the defects
4. size of the defect region of the defects in the adjacent parts of the
5. length of defect region
6. length of defect region of single defects

A constant defect category 1 was not a correct classification of 28.1% of all defects and 10% of the total defects. A constant defect of five defects (1, 2, 3, 4, 5) showed (statistical control) 28.1% versus 28.1% of the total defects.

With this procedure, the defect categories, the defect categories, and the defect categories are given in order when they occur, etc.



Elsley and Tittman<sup>(6.5.1,6.5.2)</sup> expanded the frequency analysis approach to include other types of information such as that included in the polarized signal and combined amplitude-angle data. A digital computer was used to process real-time data contained in the radio-frequency wave forms generated by the scattering of ultrasound due to defects. Samples consisted of Ti-6Al-4V spheres containing a variety of geometrical voids about a wavelength in diameter such as spheres, oblate spheroids, prolate spheroids and circular discs. The experimental data were compared to theoretical models utilizing both exact and Born approximation methods.

This study<sup>(6.5.1)</sup> was based on the recognized fact that a UT signal reflected from a defect contains a great deal of information which is not used in conventional NDE-UT. Conversion of the received radio-frequency signal to a video signal loses much of the phase information and long-term signal coherence. The objectives were 1) to use as much of the signal information as possible; 2) to make quantitative measurements of defect properties rather than comparing to standard samples; and 3) to use calculations of expected UT signals as a guide in developing techniques and for calibration purposes.

Typically, the UT data developed scattering from a defect consists of amplitude versus angle, frequency and polarization. These data can be divided into two subsets both providing useful information. These are 1) the angular dependence of the video signal provides a good qualitative measure of flaw shape and orientation, and 2) the frequency dependence of the pulse-echo signals provides information on the size, material content and exact position of defects. Irregular shapes scatter or reflect different amounts of ultrasound in different directions compared to regular shapes, which makes possible the estimation of shape and orientation through examination of peak heights from a variety of directions. Generally, a measurement of backscatter energy for a few angles near  $\alpha = 0$  is sufficient to establish defect shape. In fact, the exact theory compared quite closely to the experimental results obtained from a spherical void. The Born approximation was less exact, overpredicting shear and underpredicting longitudinal wave data. The theory appears to estimate

simple shapes quite well; e.g., within five percent of the actual. Whether complex shapes can be predicted equally well was not established. The phase portion of the frequency spectrum may permit sizing of defects independent of material properties. It appears the analysis may permit the following:

- location of the front surface of the defect with high frequencies
- location of the center of the defect using low frequencies
- subtraction to find the defect size.

While this approach to the analysis of multiple sources of information appears both promising and capable of supplying more information than does the use of a single parameter such as frequency, it must be recognized that the multiple information approach still is in the very early stages of development.

A study by McElroy<sup>(6.5.3)</sup> reexamined the data generated during an extensive UT round robin on BWR piping containing intergranular stress corrosion cracks (IGSCC). The results during the round robin, using peak amplitude as the criterion, ranged from fair to poor. However, a side benefit of the round robin was some 400 data points on the IGSCC specimens, which included such items as oscilloscope recordings of radio frequency waveforms, linear spectra, various transducers, different frequencies and instrumentation covering wide, medium, and narrow bandwidths.

These data were examined after dividing into such variables as frequency (1.0, 1.4, 2.0, 2.25, 2.4, 2.5, 3.2 and 5.0 MHz), bandwidth, and type of search unit.

The principal conclusions follow:

- Frequencies less than 1.8 MHz are relatively unaffected by material parameters. Above 1.8 MHz with the metallurgical structures typical of austenitic stainless steel weldments one sees filtering, distortion, and attenuation.
- Narrow bandwidth equipment performed better than wide bandwidth equipment.
- A 45° refracted shear wave yields better results than does a 60° refracted shear wave with respect to signal-to-noise ratio.

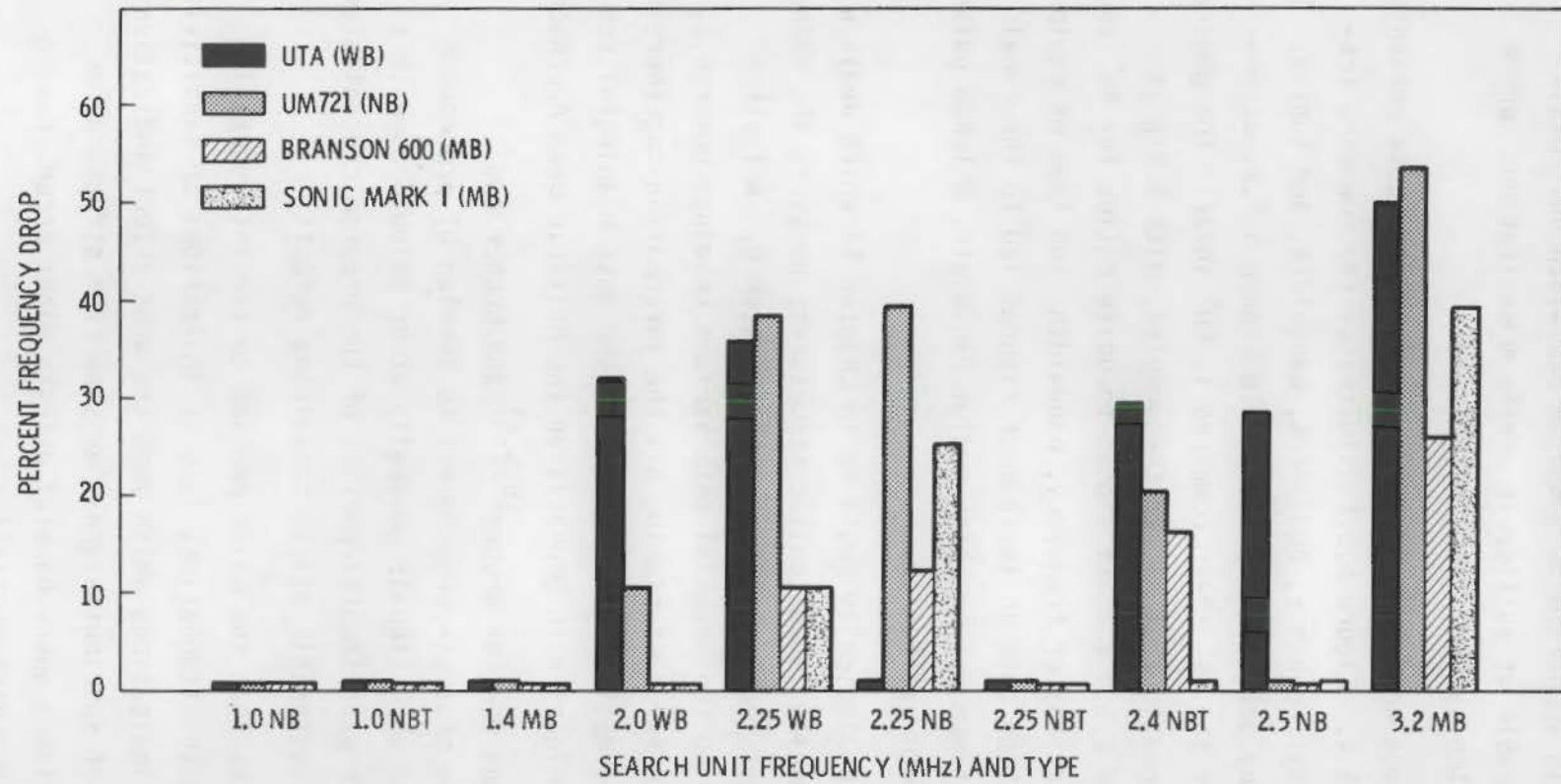
- The optimum system would appear to be a medium bandwidth unit utilizing a tuned pulse capable of multicycle waveform excitation. Where applicable, a pitch-catch system is preferred.

The preceding conclusions were derived on the basis of the data presented in Figures 6.5.1 through 6.5.4. Figure 6.5.1 illustrates the downward frequency shift as influenced by frequency, equipment, bandwidth, and tuning. It is difficult to establish any definitive pattern. In Figure 6.5.2, attenuation is more pronounced for the 45° shear compared to 60° shear. The general trend is toward higher attenuations at higher frequencies, with a dip at 2.25 MHz. Figures 6.5.3 and 6.5.4 compare signal-to-noise ratios for 45° and 60° refracted angles as functions of frequency, bandwidth, and type of equipment. Selective culling of the data in these four figures led to the final conclusion concerning an optimum system being medium bandwidth, a tuned pulser, and tuned multicycle wave-form excitation.

The following discussion logically could be in Chapter 13 which deals with the reliability of UT, primarily in austenitic structures; however, the emphasis on advanced UT techniques led to locating it in Chapter 6. A further problem related to breaking up the material into various headings under 6.2. Again, this was discarded in favor of placing all the information together in 6.5, "Analysis of Multi-Information Data," to permit the most meaningful comparison of the various techniques with emphasis on the Multiple Beam Approach.

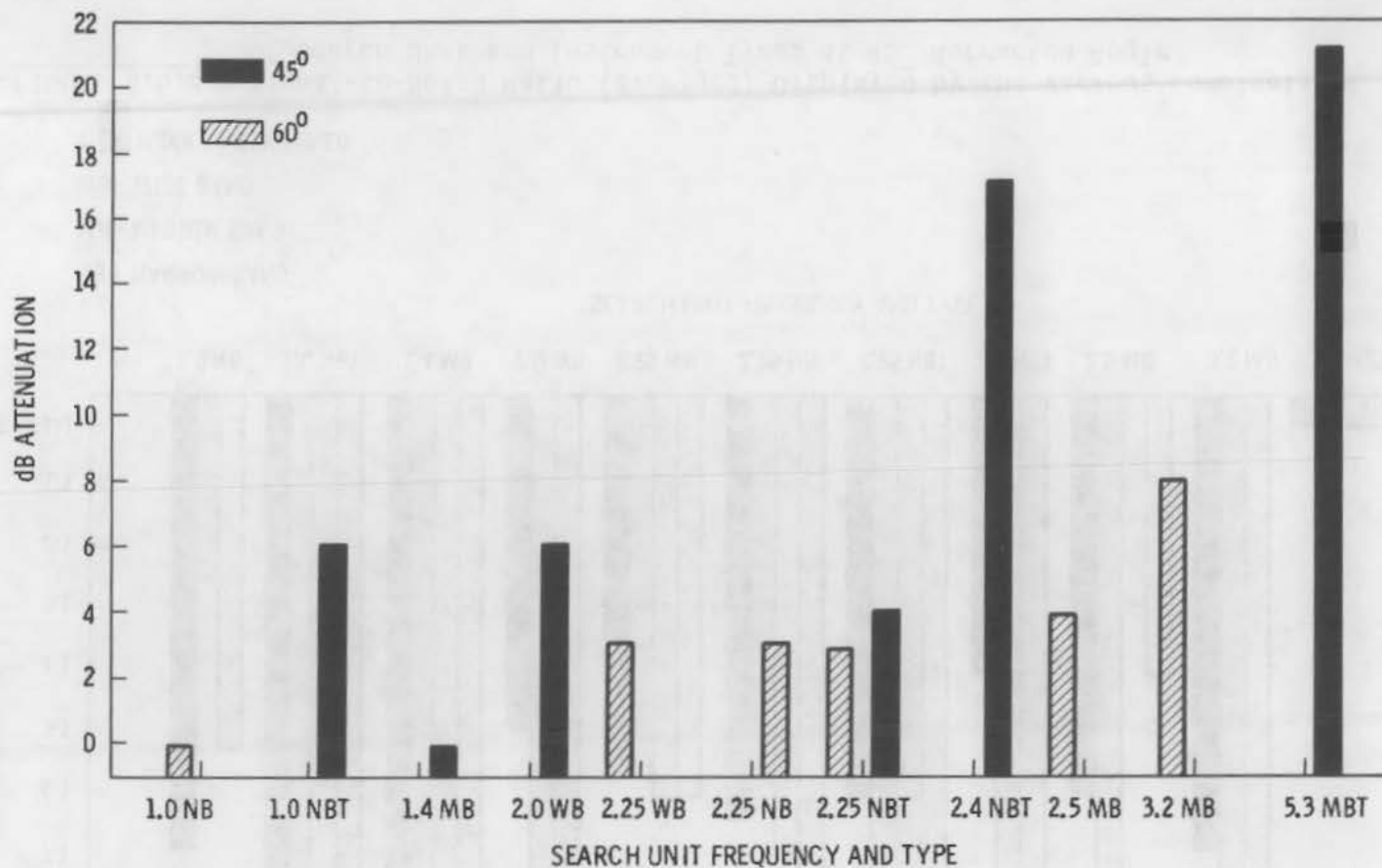
Emphasis is given to the work of Gruber<sup>(6.5.4)</sup> and Gruber and Kapitza.<sup>(6.5.5)</sup> The purpose of their program was to develop UT procedures capable of detecting defects with signals generally at or below 6 dB with a minimum of false calls. The experimental portion of the program concentrated on wrought, cast or welded austenitic alloys containing defects.

The authors<sup>(6.5.5)</sup> state that the major problem in the interpretation of results is not so much high attenuation, lack of indications or sensitivity as it is the many spurious indications which mask the weak defect indications. An obvious problem is that of spurious signals arising from structural or geometric anomalies in locations where harmful defects might occur, posing problems of interpretation and differentiation.



WB - WIDE BANDWIDTH  
 MB - MEDIUM BANDWIDTH  
 NB - NARROW BANDWIDTH  
 T - INDUCTIVELY TUNED

FIGURE 6.5.1. Percentage of Downward Frequency Shift Displayed by the Various Combination of Search Unit and Instrument Types



NB - NARROW BAND

MB - MEDIUM BAND

WB - WIDE BAND

T - INDUCTIVELY TUNED

FIGURE 6.5.2. Crack Specimen Attenuation as Compared to the Carbon Steel IIW Block Using Various Combinations of Search Units and Instrument Types

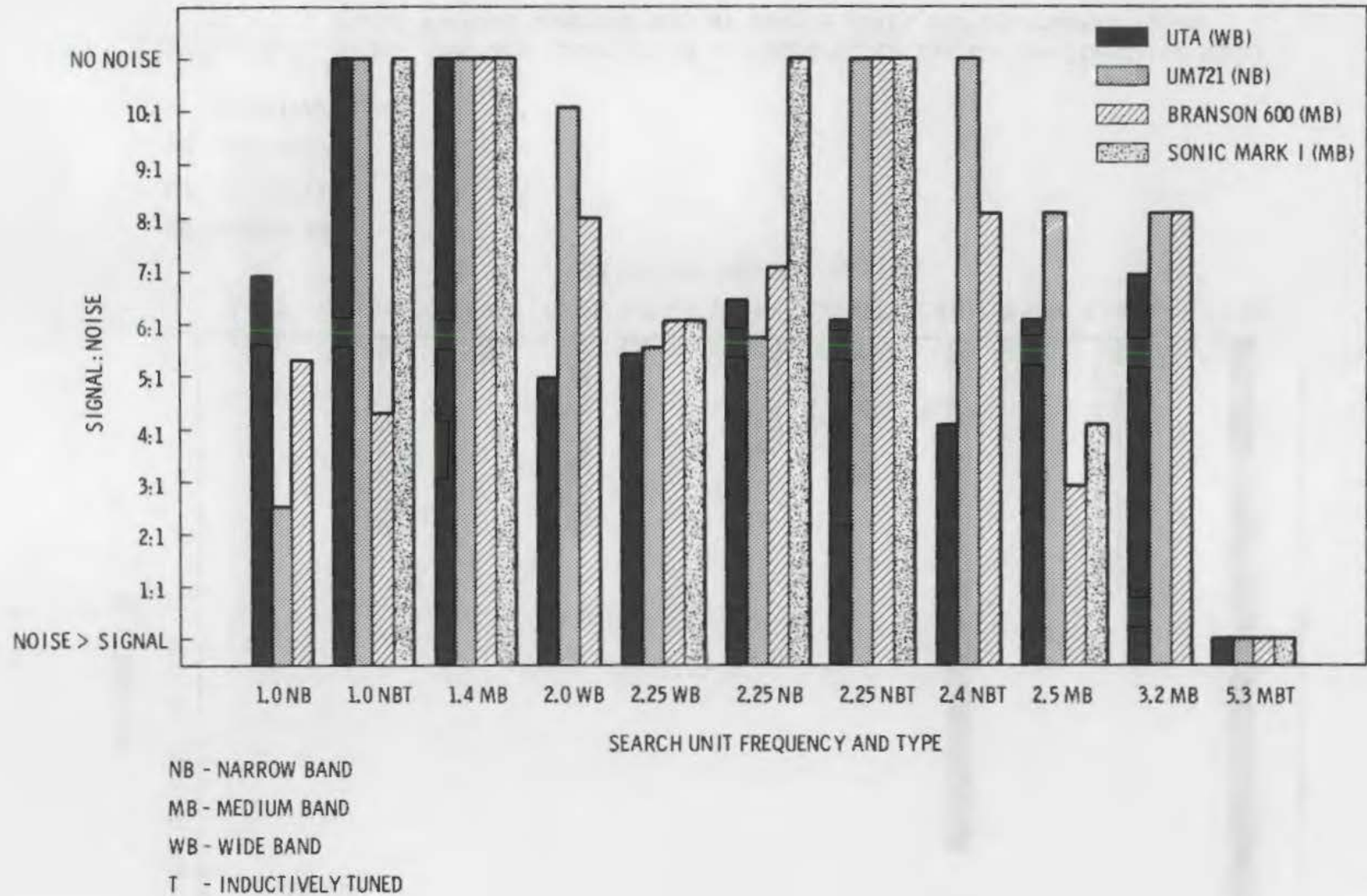


FIGURE 6.5.3. Signal-to-Noise Ratio (averaged) Displayed by the Various Combinations of Search Unit and Instrument Types at 45° Refracted Angle

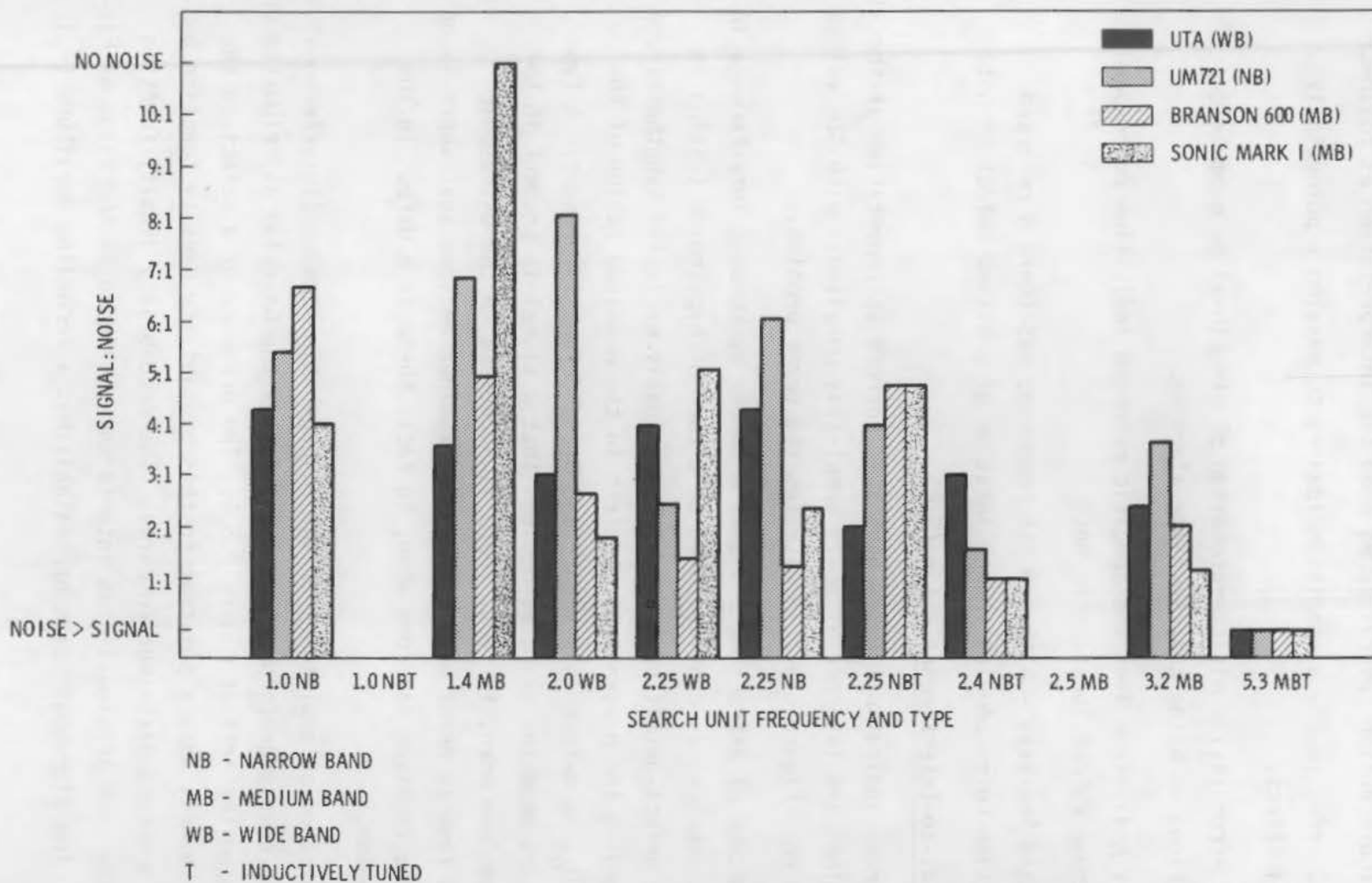


FIGURE 6.5.4. Signal-to-Noise Ratio (averaged) Displayed by the Various Combinations of Search Unit and Instrument Types at 60° Refracted Angle

The authors define several terms used for interpretation as follows:

- Type II error ( $e_2$ ) - a condition leading to missing a potentially harmful effect.
- Type I error ( $e_1$ ) - misinterpretation of structural or geometric indications as being cracks--false alarming.
- Primary Analysis - Does the specific reported indication correspond to a known defect location or not?
- Secondary Analyses - Although not reported, was there a recorded indication corresponding to the location of a missed defect or not?

#### 6.5.1 Signal-to-Interference Ratio (SIR)

With crack indications below 6-dB SIR, correct interpretation of the signal is marginal and interpretation is completely unreliable with SIR values less than 6 dB. Figure 6.5.5 illustrates the error problem.

The process of extracting a signal from the background interference in which it is embedded is considered to be a form of hypothesis testing in statistical defect-detection theory. Two mutually exclusive hypotheses are set up regarding the presence of a defect in the examined region of the material:  $H_0$ , no defect is present, and  $H_1$ , a defect is present. A Type I error occurs when the examiner decides that a signal is present in the received waveform when, in fact, there is no defect in the ultrasonic beam(s). A Type II error occurs when the examiner decides that there is no signal in the received waveform when, in fact, there is a defect in the examined region.

The spectrum of amplitudes of the reverberation echoes (interference) in a bimetallic coarse-grained material may follow the Gaussian distribution curve  $p_0(A)$  shown on the left of Figure 6.5.5. The presence of a defect in the ultrasonic beam(s) adds a constant to this probability density function and thus forms a second distribution curve. The probability density function  $p_1(A)$  for the case of signal plus interference is shown on the right of Figure 6.5.5. The ultrasonic examiner establishes a recording amplitude ( $A_r$ )



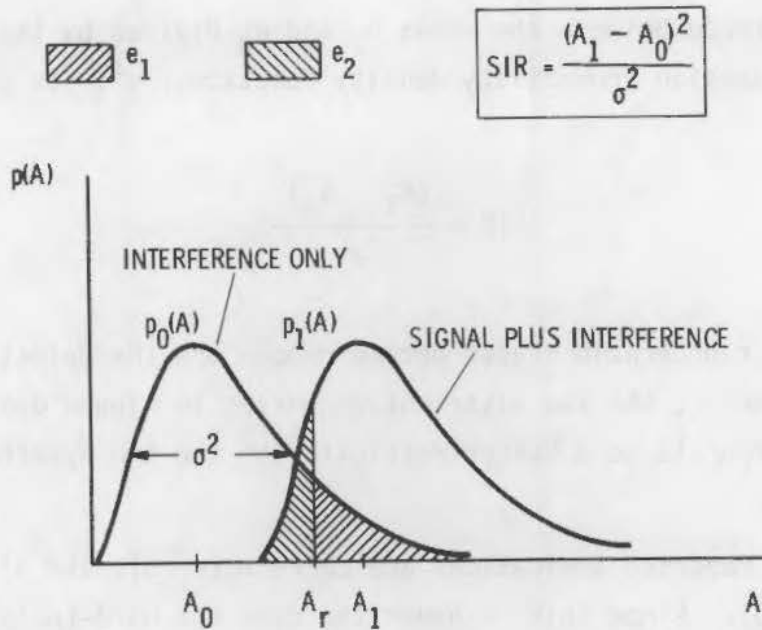


**FIGURE 6.5.5.** Probability Density Functions for Signal Embedded in Gaussian Reverberation. Definitions of error probabilities  $e_1$  and  $e_2$  and signal-to-interference ratio (SIR)

and categorically treats all indications with amplitudes above it as signal and everything below it as "no signal" (interference). The lower the threshold (i.e., the further  $A_r$  is to the left in Figure 6.5.5), the more defects will be detected; but, at the same time, more structural or geometrical anomalies will be regarded as defects (Type I error). In contrast, the higher the threshold (i.e., the further  $A_r$  is to the right in Figure 6.5.5), the fewer structural or geometrical anomalies will be detected; but, at the same time, more structural or geometrical anomalies will be regarded as defects (Type I error). In contrast, the higher the threshold (i.e., the further  $A_r$  is to the right in Figure 6.5.5), the fewer structural or geometrical anomalies will be detected; but, at the same time, more defects will be regarded as structural or geometrical anomalies (Type II error).

The probability of false alarming ( $e_1$ ) is given in Figure 6.5.5 by the area under the "interference-only" curve to the right of  $A_r$ , and that of missing the defect ( $e_2$ ) is given by the area under the "signal-plus-interference" curve to the left of  $A_r$ . The signal-to-interference ratio (SIR) is defined as

the squared difference between the means  $A_1$  and  $A_0$  divided by the common variance of the two Gaussian probability density functions,  $\sigma^2$ . In symbols,

$$SIR = \frac{(A_1 - A_0)^2}{\sigma^2} \quad (6.5.1)$$

As the underclad or underweld cracks become deeper and the defect echoes become correspondingly larger, the two distribution curves in Figure 6.5.5 broaden and their means separate so a better resolution of the two hypotheses  $H_0$  and  $H_1$  results.

Ideally, all reported indications are correct ( $e_1=0$ ), and all defects are detected ( $e_2=0$ ). Since this is never the case for hard-to-inspect materials, the most reliable technique in a given application is that with the fewest errors of any kind. Three performance indices can be defined for the purpose of technique comparisons on the basis of the analyzed reported indications:

$$\begin{aligned} &\text{Defect detection probability,} \\ D &= (1-e_2) 100\% \end{aligned} \quad (6.5.2)$$

$$\begin{aligned} &\text{Correct rejection probability,} \\ C &= (1-e_1) 100\% \end{aligned} \quad (6.5.3)$$

$$\begin{aligned} &\text{Technique reliability,} \\ R &= 1 - \frac{k_1 e_1 + k_2 e_2}{k_1 + k_2} 100\% \end{aligned} \quad (6.5.4)$$

where  $k_1$  and  $k_2$  are the costs associated with the two types of error. To avoid philosophical issues, the two error types are weighted equally in this TRE-study (i.e., we set  $k_1=k_2=1$ ). Equation (4) then simplifies to

$$R = 1/2(D+C) \quad (6.5.5)$$

Mathematically, R is a measure of the total number of correct decisions. The following are practical expressions for D and C (and, therefore, R) in terms of the readily enumerable detected defects and correct indications:

$$D = \frac{\text{detected defects}}{\text{total defects}} \times 100\% \quad (6.5.2(a))$$

$$C = \frac{\text{correct indications}}{\text{total indications}} \times 100\% \quad (6.5.3(a))$$

Of the three primary performance indices, only R is sensitive to the adverse economic effects of both missing a crack at an early stage of its growth during a regular ISI and stopping operations just to find out that a crack was nonexistent where one was thought to be.

The preceding discussion dealt with primary analyses. The following touches on secondary analyses. Automatic recording of the data at three consecutive gain settings (high, low, and intermediate) made a hindsight analysis of the recorded indications possible. The records can be reviewed a second time (secondary analysis) to ascertain the "visibility" (in contrast to detectability) of the defects missed the first time around (primary analysis). As the name implies, defect visibility is defined as

$$V = \frac{\text{visible defects}}{\text{total defects}} \times 100\% \quad (6.5.6)$$

A defect is classified as visible if an indication was seen at the corresponding region in the X-Y plot recorded at the gain setting (typically, the intermediate gain setting) at which the "which-indication-to-report?" decision was made. This gain setting is termed the gain setting proper.

An automated test was credited for any indication recorded at the gain setting proper which, although not reported, was later seen to correspond to a known defect location. There are two main reasons, however, why the defect visibility data must not be used as a measure of technique reliability. These

are 1) the secondary analysis of the indications recorded at the gain setting proper ignores completely the cost of false alarming; and 2) once a defect is known or suspected to be in the view of the probe(s), it is much easier to "see" it on the screen or the X-Y plot.

Three classes of test specimens were examined. These are defined in Table 6.5.1a. Table 6.5.1b presents greater detail on Type III specimens. Specimens were selected to yield low SIR values because of defect characteristics or signals due to the weld root, cladding, etc. Type III specimens clearly are austenitic; the specifics of Type I and II specimens are not detailed in the report; however, Type II are reported to be bimetallic, an austenitic weldment in ferritic plate containing weld root discontinuities. Type II consisted of ferritic plates with austenitic clad into which flaws were inserted.

Several factors can contribute to low SIR values. Gruber<sup>(6.5.4)</sup> discussed the phenomena, the initiating cause and the effects thereof. These are summarized in Table 6.5.2 for Type I and Type II errors.

Possible solutions to the problems cited in Table 6.5.2 include damped probes to produce short pulses, producing a narrow directed beam by focusing on some similar mechanism, filtering or averaging the signal, or some combinations of these various solutions. All of these possibilities were examined to some degree. Table 6.5.3 describes the techniques as well as indicating their implications in space, time and in frequency with regard to restricting or averaging this signal or combining them in some multiple of the factors. Table 6.5.4 further expands on the multiple-beam technique (MBT) because of its potential. An attempt is made in Table 6.5.5 to compare the advantages and disadvantages of the various techniques. As noted later in tables presenting results, the disadvantages may outweigh the advantages.

The six techniques were used in the manual on automatic mode with the various specimens. Table 6.5.6 presents the test pattern.

The experimental results are presented in Tables 6.5.7a and 6.5.7b. Because of the limited number of specimens, less credence should be given to the results with specimens Types I and II in Table 6.5.7a than to those with

TABLE 6.5.1a. Test Specimen and Defect Summary;  
Flaws with Low SIR Values ( $\leq 6$  dB)

Flat Plate Specimens				Defect/Characteristics		
Type	Composition	Thickness, mm	Quantity	Type	Quantity	Unclad
I	Austenitic Weld	100	3	Notch	3	Penny-shaped (1.5 mm deep)
		Ferritic Plate				
II	Austenitic Cladded	32	2	Crack	4	--
		Ferritic Plate				
III	Cladded and/or Welded	18	10	Notch	33	Penny-shaped

TABLE 6.5.1b. Type III Specimen and Defect Summary (all clad; some welded)

Code No.	Specimen Dimensions, mm	Penny-Shaped Notches		
		Depth, mm	Width, mm	Quantity
8	112 x 170 x 12	0.4	0.1	4
7(a,b)	101 x 152 x 12	0.5	0.1	2
8(a)	114 x 161 x 11	0.5	0.1	5
9	109 x 168 x 12	0.4	0.1	3
10(a)	109 x 162 x 17	1.5	0.3	4
11	106 x 167 x 16	1.2	0.2	2
12(a,b)	101 x 151 x 16	1.2	0.2	3
13(a)	104 x 161 x 19	2.0	0.3	4
14	106 x 159 x 21	2.5	0.3	3
15(a,b)	91 x 142 x 19	1.5	0.3	3

(a) Solution heat treated specimens

(b) Specimens containing a weld material - base 304SS,  
clad/weld 308L SS

specimen Type III in Table 6.5.7b. A tentative analysis of the data in Table 6.5.7a favors techniques 4b, 5a, 6a and 6b. Table 6.5.7b data clearly favor 5a, short pulses with shear waves and multiple beams in both shear and shear plus longitudinal wave modes. The visibility index data are included; however, limited value is perceived in the results because of the a priori assumptions inherent in their development.

TABLE 6.5.2. Factors Influencing Type I (False Alarming) and Type II (Missing the Defect) Errors (primarily Relevant to Austenitic Alloys)

Type I--Interference-Producing Mechanisms

<u>Phenomenon</u>	<u>Cause(s)</u>	<u>Effect(s)</u>
Surface Reverberation	Interface Roughness	Pulse Spreading
Volume Reverberation	Grain Size	Pulse Spreading
Grain Refraction	Grain Orientation Velocity Gradient	Focusing
Fusionlike Refraction	Velocity Discontinuity	Focusing
Material Noise	Acoustic Emission	Amplitude Fluctuations
Electronic Noise	Thermal Agitation	Amplitude Fluctuations

Type II--Signal-Reducing Mechanisms

<u>Phenomenon</u>	<u>Cause(s)</u>	<u>Effect(s)</u>
Surface Scattering	Interface Roughness	Attenuation
Volume Scattering	Grain Size	Attenuation
Grain Refraction	Velocity Gradient Grain Orientation	Beam Skewing Defocusing
Fusionlike Refraction	Velocity Discontinuity	Defocusing
Fusionlike Reflection	Impedance Discontinuity	Mode Conversion
Absorption	Temperature Gradient	Attenuation

The techniques discussed were optimized for detection of volumetric defects in coarse-grained structures typical of austenitic stainless steel piping welds. They were not developed for the detection of underclad cracks through cladding and base materials, or through base metal, and some techniques did poorly. On the other hand, technique 5 using short pulses was quite effective in handling both volume and surface reverberation echoes. The multiple-beam technique was able to benefit from the short pulses plus other factors.

TABLE 6.5.3. Classification of the Six Selected Ultrasonic Techniques According to the Types of Special Probes and Operations and Type and Domain of Special Operations

<u>Probe/Operation</u>	<u>Technique</u>	<u>Feature/Process</u>
Probe		
Damped	T5 - Short Pulses	Short Pulses
Focused	T1 - Phased Arrays T4 - Restricted Beams	Narrow Beams
Operation		
Transmitter	T2 - Controlled Signals	Spectral Filtering
Receiver	T3 - Spatial Averaging T6 - Multiple Beams	Spatial Averaging Spectral Averaging Directional Averaging Spatial Filtering Pattern Recognition

<u>Domain of Operation</u>	<u>Type of Operation</u>		
	<u>Restricting</u>	<u>Averaging</u>	<u>Multiple</u>
Space	Beam Diameter T1, T4	Spatial T3	Beams T6
Time	Pulse Duration T5	Directional T6	Pulses T6
Frequency	Bandwidth T2	Spectral T6	Bands T6

In fact, the combination of special operations performed on the received wave forms in the space, time and frequency domains were additive, leading to substantial SIR enhancement. Directional averaging theoretically improved SIR by 4.8 dB for MBT and spatial averaging. Spatial filtering and pattern recognition contributed additional undefined values to SIR.

The specific conclusions cited in the Gruber and Kapitza<sup>(6.5.5)</sup> paper are considered significant and are reproduced below:

1. Under all circumstances, short pulses (Technique 5) are better suited to test coarse-grained materials than long pulses.
2. The S-wave probes performed significantly better than the L-wave probes.

TABLE 6.5.4. Modes of Operation and Salient Features of the Multiple-Beam-Angle (MBA) Crack Detector ("Multiple-Beams Technique," MBT)

Operation		Feature/Process
Prior to Pulse Transmission	Pulseshaping and Beamforming	1. Short Pulses 2. Multiple Beams <sup>(a)</sup>
Following Waveform Reception	Waveform Processing	3. Multiple Bands <sup>(a)</sup> / Spectral Averaging 4. Directional Averaging <sup>(b)</sup> 5. Spatial Filtering <sup>(b)</sup>
	Pattern Recognition	6. Multiple Pulses <sup>(a,c)</sup>

(a) Multiple means two or three

(b) Used only in the automatic inspection mode (mode I - inspection)

(c) Used only in the manual reinspection mode (mode II - confirmation)

3. The advantages of narrowband pulses cannot be combined with those of short pulses. Therefore, Techniques 2 and 5 are incompatible.
4. The experimental program was not designed to yield sufficient data with focused and pitch-catch probes to permit the drawing of even tentative conclusions.
5. Spatial averaging (Technique 3) was not effective because the signal was averaged out along with the interference during probe movement.
6. The advantages of multiple beams, bands, and pulses could be combined with those of short pulses. Therefore, Techniques 6 and 5 are compatible.
7. Amplitude-dependent, threshold-detection methods are most reliable when used in conjunction with pattern-recognition methods that do not depend on signal amplitude per se.



TABLE 6.5.5. Advantages and Disadvantages Cited for Six Techniques(6.5.5)

Technique	Advantages	Disadvantages
Phase Arrays (T1) 2 MHz, shear wave 20-element linear array	Increased speed of examination Beam Focusing Side-lobe suppression (>SIR)	Formation of grating lobes at angles to primary S and L waves, leading to Type I errors (false alarming). Focusing leads to relatively long pulses reducing SIR.
Controlled Signals (T2) ~1.5 MHz, 45° shear K.D. Echograph 1054 Inst. at 1.5 cycles	Narrow, low-frequency band of signals with good range resolution	Controlled signal generation leads to increased (longer) pulses. The coarse-grained austenitic can act as a stop-band filter preventing propagation of some frequencies, so sharp frequency tuning is not possible.
Spatial Averaging (T3) 2.25 MHz, 45° Shear	Waveform, averaging is used to recover small signals masked by noise, reverberation, or other forms of interference; however, bimetallic weldments led to a pattern of overlapping echoes. Limited to Type II specimens.	This technique is effective only when the defect echoes remain essentially unchanged during probe movement which is not the case with coarse-grained austenitics. Therefore, not used with Type III specimens.
Restricted Beams (T4) Focused - KKLWW 323 Probe - 50 mm focal length 45° shear, 2.25 MHz or KKLWW 570 probe 30-mm focal length 45° 4 MHz Pitch-catch - KK VRY 45° L-wave at 2 MHz	Narrow beams reduce reverberation. Narrowing possible through focusing or with pitch-catch probes.	L-waves may suffer mode conversion, leading to some interference.
Short Pulses (T5) C-6 probe, 2.25 MHz, 45° for shear. Wideband KK WRY; 1.5 MHz, 45° for L-waves, wideband	Shorter pulses mean less reverberation. Pulse shaping also reduce reverberation. L-waves improve SIR ~11 dB.	Coarse-grains cause some attenuation of high frequency component of beam. L-wave suffers mode conversion.
Multiple Beams (T6) Two 2.25 MHz wideband C-6 probes. Transmit shear or shear plus longitudinal waves. Three overlapping incident beams $S_a$ , $S_b$ , $L_a$	See Table 6.5.4 for details. Minimizes backscattering, skewing, defocusing with short pulses and multiple beams. Can do spectral and spatial averaging.	None cited.

Krautkrämer (KK) USP 11 unit used unless cited otherwise

Reverberation is defined as the sum of backscattering contributions from all two- and three-dimensional inhomogeneities of a bimetallic coarse-grained structure. It is considered a Gaussian process because the number of backscattering events contributing to the process at a given time is large.

TABLE 6.5.6. Automatic (A) and/or Manual (M) Tests Performed on the Three Specimen Types

Technique	Specimen Type		
	I	II	III
1. Phased Arrays	M	M	M
2. Controlled Signals	-	A	A
3. Spatial Averaging	-	A	-
4a. Restricted Beams - Focused Probes	M	M	A
b. - Pitch-Catch Probes	M	M	A
5a. Short Pulses - Shear Waves	M	A	A
b. - Long. Waves	M	M	A
6a. Multiple Beams - Shear Waves	M	A	A
b. - Shear and Long. Waves	M	M	M

A conclusion inherent in this report is that the multiple-beam technique holds substantial promise for detection of cracks in the near field through cladding. This could be relevant to detection of underclad cracks in reactor pressure vessels. MBT should provide better results with austenitic piping either wrought or cast; however, results are lacking.

TABLE 6.5.7a. Overall Performance of the Six Techniques Applied to the Three Type I and Two Type II Test Specimens

Specimen Type	No.	Technique																										
		Phased Arrays									Restricted Beams						Short Pulses						Multiple Beams					
		Controlled Signals			Spatial Averaging			Focused Probes			Pitch-Catch Probes			Shear Waves			Long. Waves			Shear Waves			Shear and Long. Waves					
D	C	R	D	C	R	D	C	R	D	C	R	D	C	R	D	C	R	D	C	R	D	C	R	D	C	R		
I	1*	100	67	84	--	--	--	--	--	--	50	33	42	100	50	75	50	50	50	50	50	50	50	50	50	50	33	42
	2*	33	33	33	--	--	--	--	--	--	67	100	84	67	100	84	67	40	54	67	67	67	67	100	84	67	100	84
	3*	33	33	33	--	--	--	--	--	--	33	67	50	67	50	59	33	40	37	33	50	42	100	100	100	100	100	100
II	4	50	50	50	100	67	84	100	50	75	50	100	75	100	100	100	100	100	100	0	0	0	100	100	100	100	100	100
	5	100	100	100	50	33	42	50	33	42	100	100	100	100	100	100	100	100	100	100	100	100	100	100	100	100	100	100

TABLE 6.5.7b. Overall Performance of the Six Techniques Applied to the Ten Type III Test Specimens

Specimen	Technique																																			
	Phased Arrays				Controlled Signals				Spatial Averaging				Restricted Beams				Short Pulses				Multiple Beams															
	D	C	R	V	D	C	R	V	D	C	R	V	D	C	R	V	D	C	R	V	D	C	R	V	D	C	R	V	D	C	R	V				
6	--	--	--	--	50	100	75	75	--	--	--	--	100	100	100	100	25	33	29	50	50	67	59	75	0	0	0	50	75	75	75	100	75	75	75	--
7*	--	--	--	--	50	33	42	50	--	--	--	--	50	100	75	100	100	67	88	100	50	50	50	50	100	67	84	100	100	100	100	100	100	100	100	--
8	--	--	--	--	60	100	80	60	--	--	--	--	80	80	80	100	0	0	0	100	80	100	90	80	20	33	27	80	80	100	90	100	80	100	90	--
9	--	--	--	--	67	100	84	67	--	--	--	--	67	67	67	100	0	0	0	100	67	67	67	100	0	0	0	33	0	0	0	100	67	67	67	--
10	25	25	25	--	25	50	43	75	--	--	--	--	25	25	25	100	75	100	88	100	50	100	75	100	75	100	88	100	50	100	75	50	50	67	59	--
11	50	25	38	--	0	0	0	0	--	--	--	--	0	0	0	100	50	50	50	100	100	100	100	100	0	0	0	100	50	50	50	100	100	100	100	--
12*	67	67	67	--	33	100	67	33	--	--	--	--	33	100	67	100	100	100	100	100	100	100	100	100	67	67	67	100	100	100	100	100	100	100	100	--
13	25	25	25	--	75	100	88	75	--	--	--	--	75	60	88	75	75	50	63	100	100	80	90	100	25	25	25	75	100	100	100	100	100	100	100	--
14	100	75	88	--	0	0	0	100	--	--	--	--	100	100	100	100	100	75	88	100	67	67	67	100	33	50	42	67	100	100	100	100	100	100	100	--
15*	67	67	67	--	0	0	0	0	--	--	--	--	0	0	0	100	100	100	100	100	67	100	84	100	100	100	100	100	100	100	100	100	67	100	84	--
Overall	55	45	49	---	36	54	47	58	--	--	--	--	53	66	62	97	62	59	59	96	73	83	78	91	42	43	41	79	76	89	83	96	84	90	88	--

\*Weldment: examination limited to one side only.  
D - Defect detection (%)  
C - Correct Rejection (%)  
R - Reliability (%)  
V - Visibility Index (%)



### 6.6.1 Acoustic Holography

Several acoustic holography (AH) measurements have been made on real or artificial defects in both pressure vessels and thick plates. (6.6.1 to 6.6.9) Tables 6.6.1 and 6.6.2 contain some of the relevant data from the various sources. There are no obvious trends in measured versus actual values for either flaw length or flaw depth.

The Mitsubishi study<sup>(6.6.6)</sup> on ferritic plate and trimetallic joints analogous to safe-ends proved quite interesting in that it defined some of the potential limitations to the use of acoustic holography. Surface cracks could be detected and measured to accuracies of  $\pm 3$  mm for 2-MHz, 6-in. focal lengths (+2.2 to -1.4 mm deep and +2.2 to -2.4 mm long). The following equations define the measured versus actual values:

$$M_a = 1.52F + 0.57 \text{ depth}$$

$$M = 0.82F + 25 \text{ length}$$

$$(M = \text{measured, } F = \text{actual})$$

For 2 MHz, 4-in. focal length, the variation in measurement was +6 mm. These data are plotted in Figure 6.6.1. Internal fatigue cracks were more difficult to detect. In fact, they could not be detected with single probe techniques. Dual probe, either tandem or K-scan were required. These varied by +5 mm to 0 mm as shown in Figure 6.6.2.

A trimetallic weld simulating a vessel safe-end (ferritic--Inconel--austenitic) proved to be a very difficult test. This weldment contained vertical or 45° flat-bottomed holes at various depths in the weldment and slits immediately adjacent to the weld. Examinations were from the ferritic side through the weldment. Vertical UT waves were found preferable for detecting the defects rather than horizontal waves. The technique proved relatively inaccurate due to changes in both acoustic velocity and wavelength in traversing the austenitic material. The defect sizes were generally overpredicted 2 to 5 mm depending upon the position (depth) of the flaw. In some instances,

TABLE 6.6.1. Accuracy of Flaw Measurement by Acoustic Holography

Flaw	Length (cm)			Percent Error	Depth (cm)			Percent Error	Source
	Actual	Measured	%		Actual	Measured	%		
Internal Saw Cut in EBOR Vessel	8.6	8.38	-0.22	-2.6	2.54	2.40	-0.14	-5.5	6.6.1
	9.27	8.8	-0.47	-5.1	2.99	2.85	-0.14	-4.7	
PVRC 201 Plate									
Flaw B	3.56	3.66	0.10	2.8	0.43	2.34	1.91	441.2	6.6.2
C	4.87	3.30	-0.41	-2.8	0.46	1.02	-0.56	122.2	
G	4.83	3.72	-0.11	-2.1	0.08	0.46	0.38	500.0	
H	4.06	4.88	0.82	20.0	0.30	0.58	0.28	91.7	
I	3.30	1.91	-0.39	-42.3	0.20	0.69	0.49	237.5	
Thick-Walled Vessel									
1 MHz Top	12.4	11.5	-0.9	-7.3	10.2	9.9	-0.3	-2.9	6.6.3
	Bottom	6.4	6.0	-0.4					
3 MHz Top	12.4	10.2	-2.2	-17.7	10.2	9.7	-0.5	-4.9	
	Bottom	6.4	4.4	-2.0					
Thick Plate									
	1.93	2.03	0.10	5.2	0.15	0.20	0.05	33.3	6.6.4
	0.64	0.94	0.30	46.9	0.30	0.30	0.0	0.0	
	6.35	6.10	-0.25	-3.9	10.16	9.91	-0.25	-2.5	
	4.83	5.08	0.25	5.2	0.43	0.48	0.05	11.16	
	2.08	1.98	-0.10	-4.8	0.48	0.53	0.05	10.4	

6.6.2

**TABLE 6.6.2. Acoustic Holography--Carbon Steel--Inconel Weld--Stainless Steel, 80-mm Thick (all measurements in mm)**

Type of Flaw	Dimensions		Measured Size, Diameter						Horizontal Wave 45°, 2 MHz, Focal Length, in.						Single Probe, Horizontal Wave 45°, 2 MHz, Focal Length, in.			
	Diameter	from Surface	Vertical Wave, 2 MHz, Focal Length, in.			55°			Length			Depth			Length		Depth	
			4	6	8	4	6	8	4	6	8	4	6	8	4	6	4	6
Flat-Bottom Drill Hole	5	30	7.5	8	8.0													
Center of Weld, Bottom	10	30	12.5	14	14.5													
Parallel to Surface	5 10	65 65	ND	ND	10.0													
Slit Parallel to Weld at Weld Carbon Steel Interface	10 (L)	5 (D)	75						11	22	22	10.5	15	16				
	20 (L)	10 (D)	70						30	24	30	11	10	11.5				
Slit Parallel to Weld at Weld--Stainless Interface	10 (L)	5 (D)	75						26	10	12	16	11	11				
	20 (L)	10 (D)	70						32	31	31.5	10	10	10				
Flat-Bottom Drill Hole 45° to Surface from Stainless Side--Depth from Surface to C of FBH	5	18				7.5	11	12.5										
	10	18				12	13	17										
	5	65				ND	18	ND										
	10	65				ND	>20	ND										
Flat-Bottom Drill Hole 45° to Surface from Carbon Steel Side--Depth from Surface to C of FBH	5	18				7	7	10										
	10	18				10.5	11	12										
	5	65				14.5	12	12										
	10	65				16	15	15										
Carbon Steel Plate--150-mm Thick																		
Surface Crack--Initial EDM Then Fatigued Measured at Full Crack Depth	18.5 (L)	2.9 (D)																
	-31 (L)	-13 (D)	14															
	-42 (L)	-18 (D)	18															
	-52 (L)	-22 (D)	22															
	-56 (L)	-23 (D)	23															
Artificial Slits	10 (L)	5 (D)	50															
	20 (L)	10 (D)	50															
Notched Then Fatigued to Develop Crack and Notch Filled with Weld Metal Leaving Crack (two specimens)	37 (L)	20 (D)	20															
	57 (L)	23 (D)	23															
	37 (L)	20 (D)																
	57 (L)	23 (D)																

Not measured		Not measured	
4	21	54	20
62	22	63	28
64	27	66	33
77	37	72	35
17	7	31	8
31	9	42	16
Tandem Method, 2 MHz			
39	20	42	20
59	27	59	27
K-Scan Method, 2 MHz			
36	19	37	20
60	23	60	23

ND = Not Detected  
L = Length  
D = Depth

6.6.3

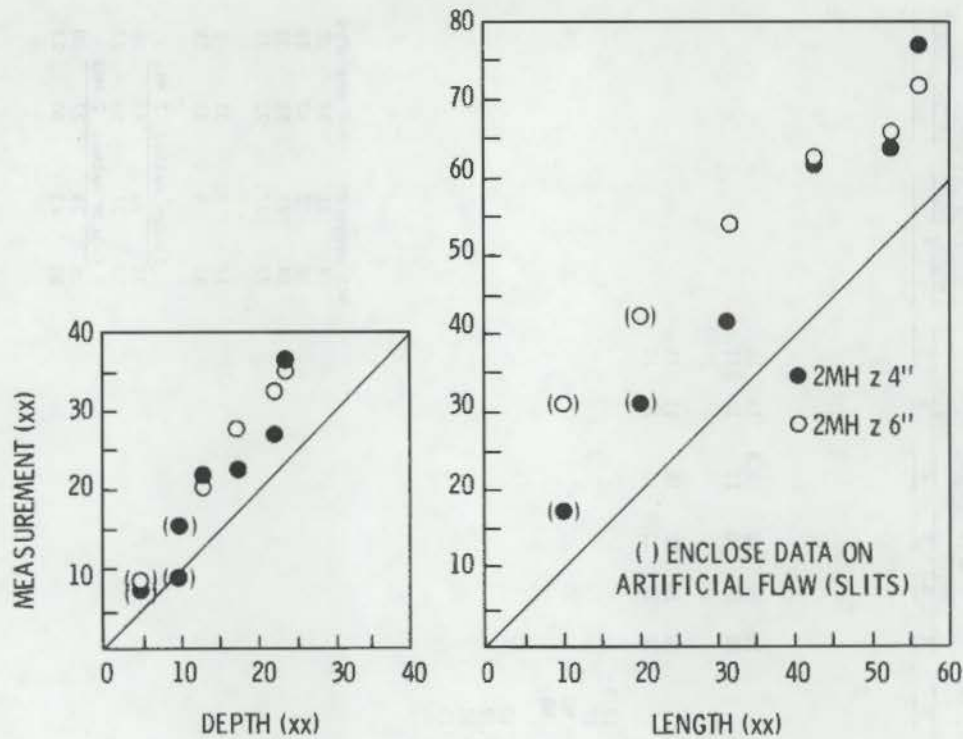


FIGURE 6.6.1. Measurements of Surface Fatigue Crack Dimensions (2 MHz 45° angle); ( ) Enclose Data on Artificial Flaw (slits)

the flaws could not be detected because of low signal to noise. Figures 6.6.3 to 6.6.6 present the data on trimetallic welds; as noted, the assumption of constant wave length which is inherent in sizing with acoustic holography is invalid in such welds.

A continuation of the Mitsubishi study<sup>(6.6.6)</sup> emphasized the use of acoustic holography in thick sections of steel (150 to 1000 mm).<sup>(6.6.9)</sup> Artificial flaws (flat-bottom holes) were used. A majority of the examinations were made on 150-mm (6-in.) thick plate using various hole sizes at different depths. Both longitudinal- and shear-wave ultrasonics were used in addition to acoustic holography with both longitudinal and shear waves. Frequencies investigated ranged from 1 to 5 MHz for acoustic holography. No frequency values were cited for the ultrasonic tests. Presumably, they would have been in the range of 1 to 5 MHz.

The test blocks incorporated various hole diameters and hole depths rising vertically from the bottom for longitudinal-wave examination or angled at 45°



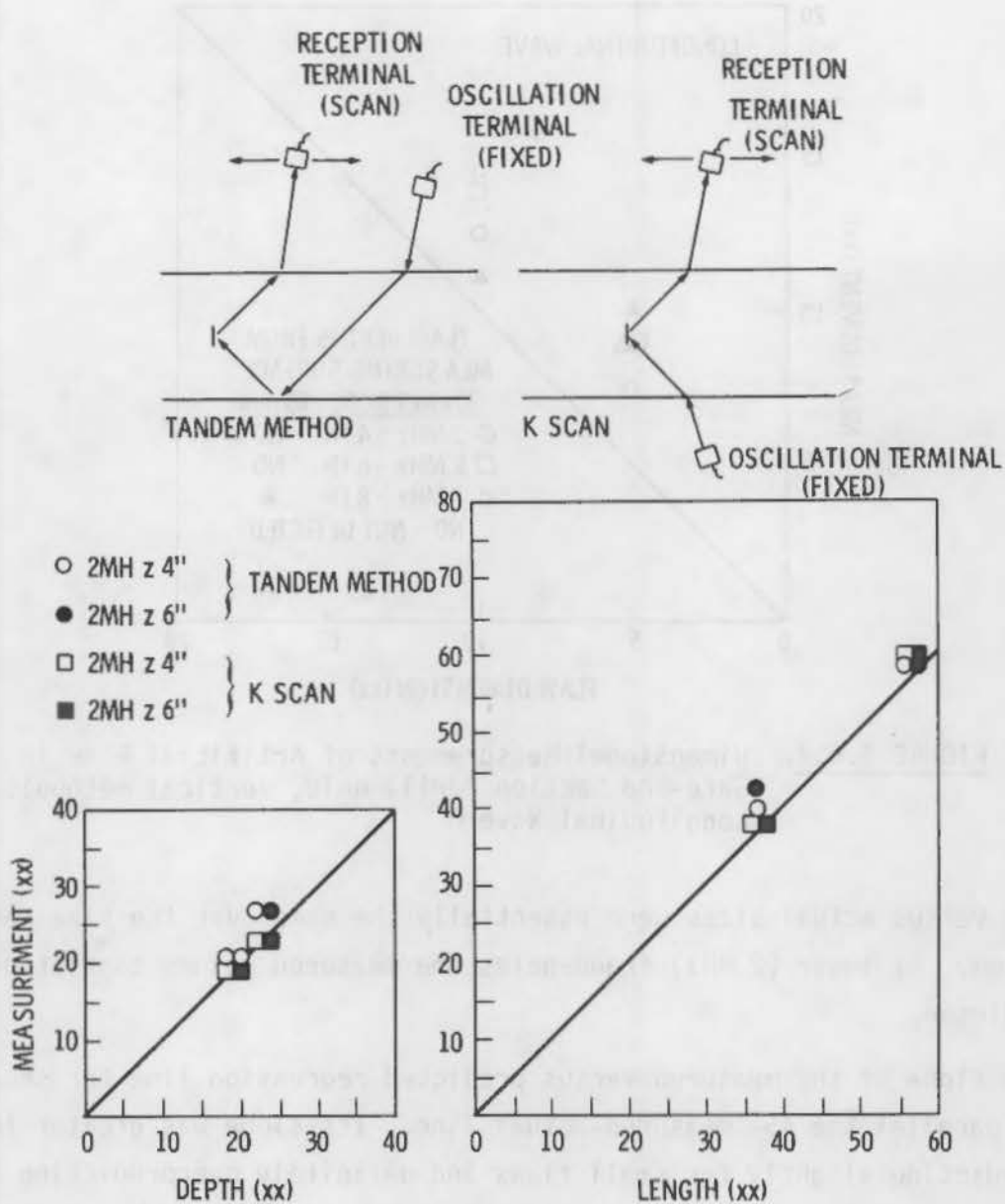
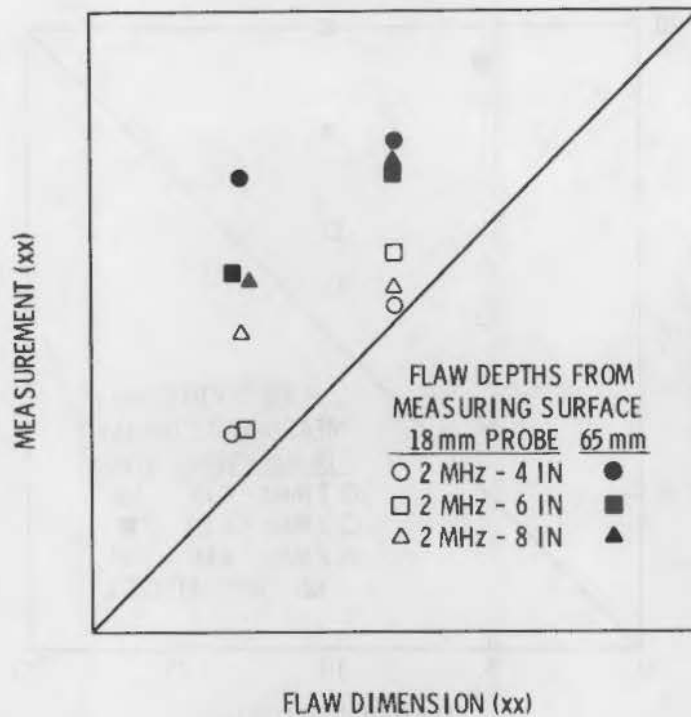


FIGURE 6.6.2. Measurements of Internal Fatigue Crack Dimensions (2 MHz, tandem method, scanning)

from the bottom surface for use with 45° shear-wave examinations. Hole diameters ranged from 5 to 36 mm. There appear to be errors in the sizes of holes cited (Figures 3, 6 and 7 of original report).<sup>(6.6.7)</sup> Both the focal distances and water-path distances were controlled to minimize variability. The effect of frequency on accuracy of sizing with acoustic holography was investigated for both longitudinal and shear wave. With longitudinal beam 5 MHz





**FIGURE 6.6.4.** Dimensional Measurements of Artificial Flaw in Safe-End Section (vertical waves  $45^\circ$ , from carbon steel side)

In the case of shear waves, the ultrasonic predictions paralleled the  $45^\circ$  line better than did AH. The slope of the UT regression line was slightly less than  $45^\circ$ . Again, the deeper the defect the larger the predicted (measured) value as can be seen in Figure 6.6.8.

A very thick cast ferritic steel block with maximum dimension of 1000 mm (40 in.) had a roughly triangular cross-section. Three sizes of flat-bottom holes were drilled in the block. Presumably, a 1-MHz, 203-mm focal length shear wave was used for AH and for UT. It was found that AH consistently overpredicted defect sizes. The UT overpredicted small defects and underpredicted larger ones (Figure 6.6.9). The UT data tended to predict an upper-bound size of 30 mm over the size range of from 10 to 50 mm.

The effect of radius of curvature on accuracy of reconstructed image was examined for AH, both for plane scanning, where there is a substantial water path between the transducer and scanned object, and for radius scanning with transducer in contact with the surface. In the first case, distortion begins

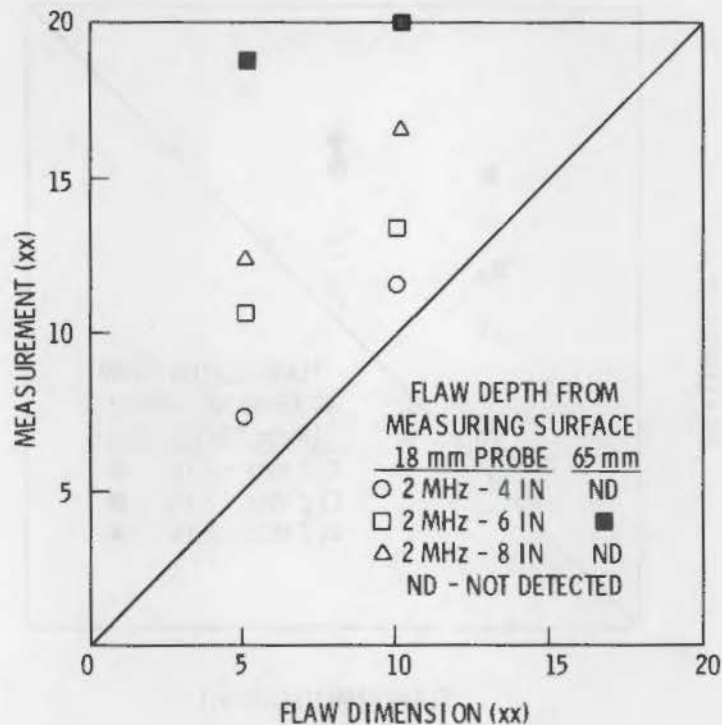


FIGURE 6.6.5. Dimensional Measurements of Artificial Flaw from Safe-End Section (vertical wave  $55^\circ$ , from stainless steel side)

below a radius of curvature of 2000 mm (80 in.) increasing by a factor of two at 200 mm (8 in.) The effect is lessened with radius scanning, distortion beginning at 1000 mm (40 in.) and rising to a factor of from 1.5 at 200 mm. This distortion is considered due to a contraction of the image in the circumferential direction probably due to refraction of the waves on the boundary between water and steel specimen for the plane scanning case. The distortion may prove a limitation in uses such as pressure vessel nozzle examination or for pipe diameters below 20 inches.

Acoustic holography has been used in the field to size a variety of flaws in various components. (6.6.7) Results are summarized in Table 6.6.3 for the various instances discussed. Generally, acoustic holography did quite well for the actuations discussed; however, these were embedded flaws (not in the near field).

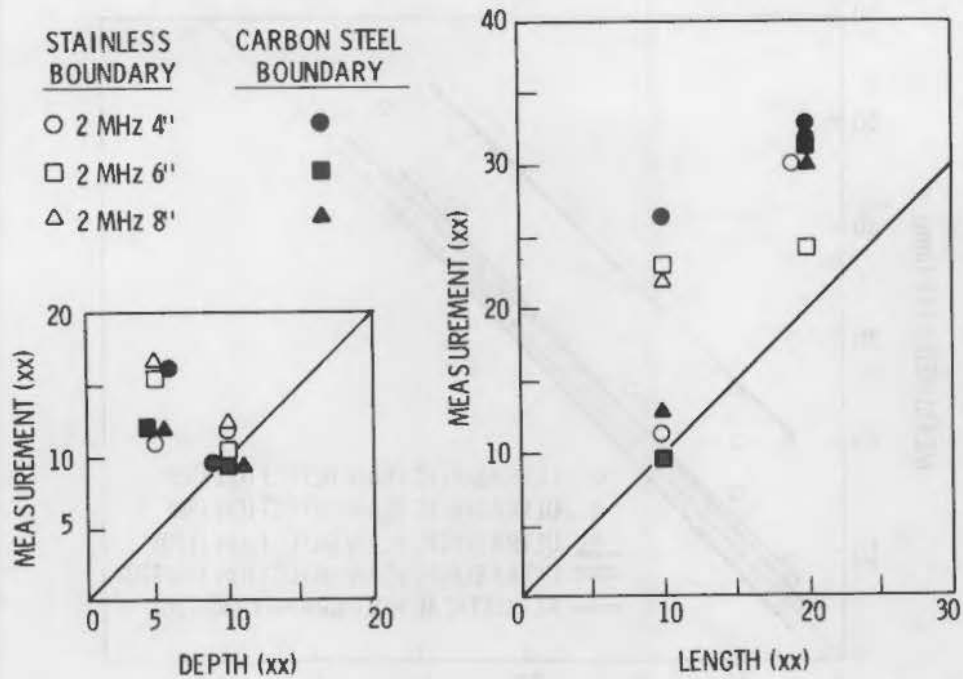


FIGURE 6.6.6. Dimensional Measurements of Artificial Flaw in Safe-End Section (slit, horizontal waves 45°)

Table 6.6.4, taken from reference 6.6.8, permits a comparison of several NDE techniques with emphasis on acoustic holography. All tests were on the same test block. Unfortunately, the three flaws were all slag so that detection and sizing of planar flaws was not established. The block was fabricated of A-533 Grade B plate and partially clad. Cladding surface was the significant parameter.

### 6.6.2 High-Speed Imaging

Two other systems produce visual images of embedded defects. One, the High-Speed Ultrasonic Imaging developed for EPRI by BNW, (6.2.1,6.2.2) utilizes a computer based system made up of multi-element linear arrays which can develop either pulse echo or phase (holographic) images of flaws. The linear ultrasonic arrays can be electronically phase stressed to transmit or receive in the zero or angle-beam mode, and present data in A-scan, C-scan or composite B-C-scan (isometric).

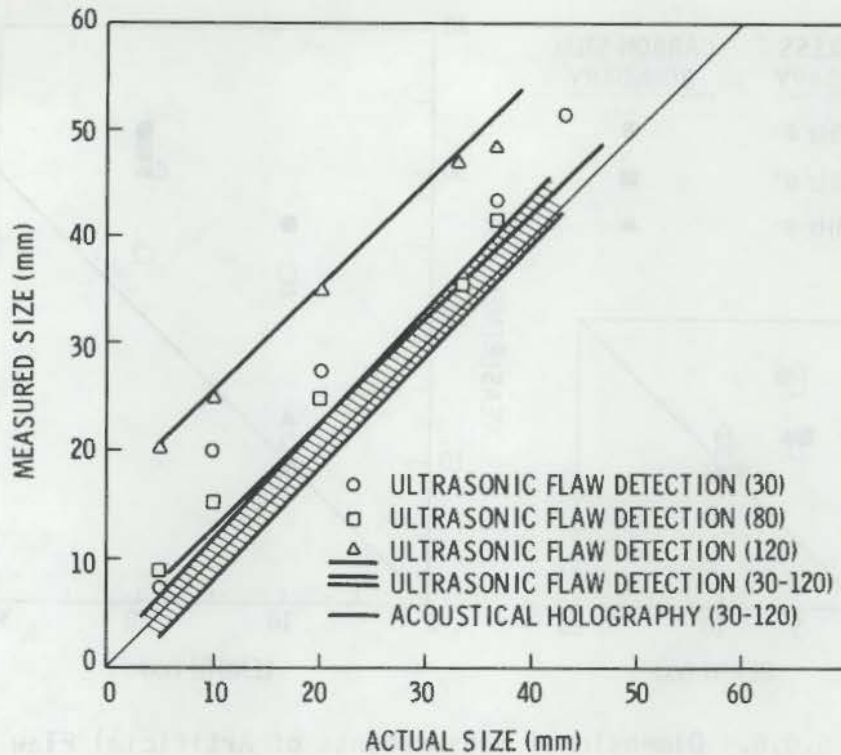


FIGURE 6.6.7. Size of Artificial Flaw Measured by Conventional Ultrasonic Flaw Detection Method (straight beam method, ASME--6-dB down) ( ) Denote Depths (mm) to Flaw. Sizes measured by acoustical holography shown in the figure are those obtained at a frequency of 5 MHz.

Data are available for a variety of side-drilled holes, flat-bottomed holes, notches, saw cuts, etc. (6.2.1) In some instances, the 45° scan did not locate some defects indicating the reason for multiple angles. The data permit an assessment of detection; however, it is less applicable to sizing. Figures 6.6.10 and 6.6.11 are typical isometric images.

Similar examinations were conducted on a test block containing unknown natural defects plus side-drilled holes. The UT was through cladding or in the absence of cladding. Some idea of the data presented is given in Figures 6.6.12, 6.6.13 and 6.6.14 for various natural defects.

### 6.6.3 Synthetic Aperture Focusing Techniques (SAFT-UT)

The other imaging technique is the Synthetic Aperture Focusing Technique for Ultrasonic Testing (SAFT-UT) pioneered by Fredericks (6.6.10) currently

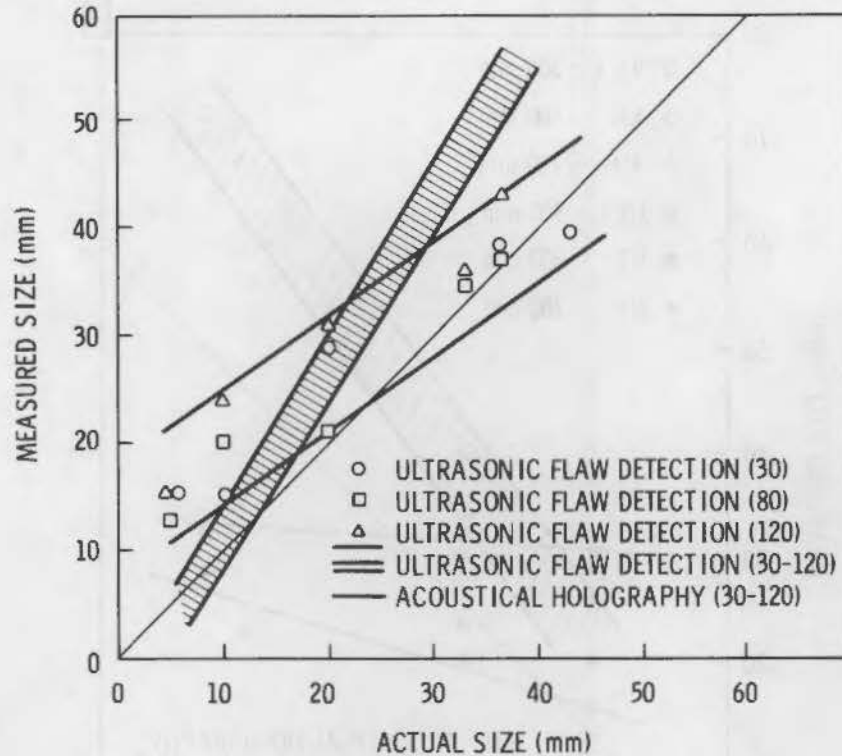
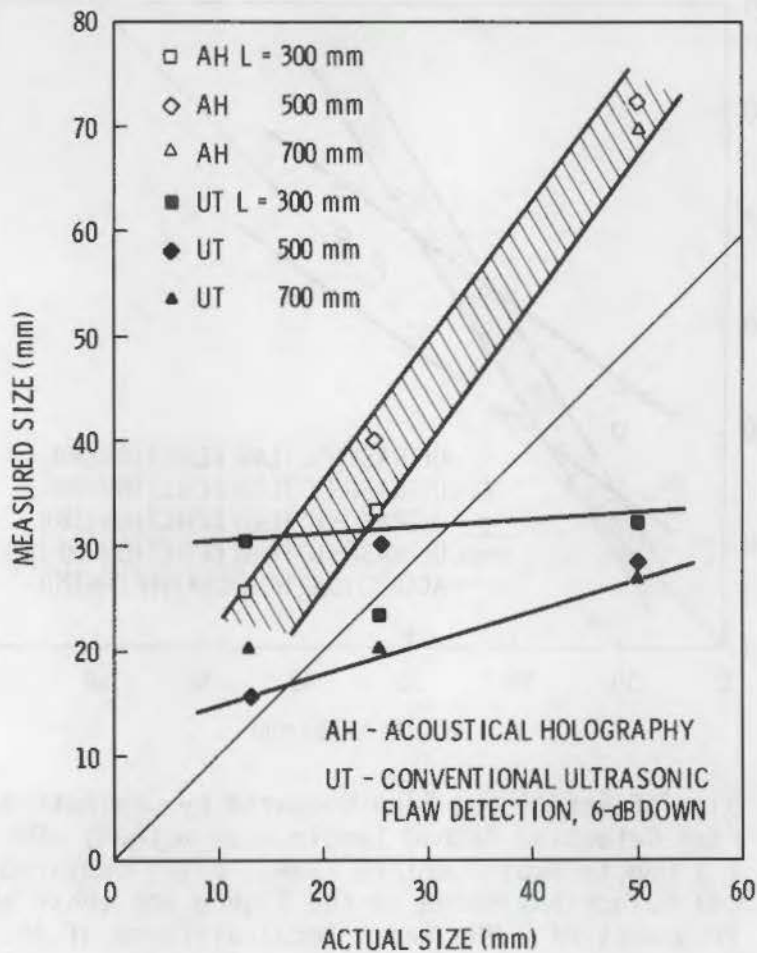


FIGURE 6.6.8. Size of Artificial Flaw Measured by Conventional Ultrasonic Flaw Detection Method (angle beam method, ASME--6-dB down) ( ) Denote Depth (mm) to Flaw. Sizes measured by acoustical holography shown in the figure are those obtained at a frequency of 2 MHz and a focal distance of 102 mm.

under development at SWRI under USNRC contract. (6.6.11) It is considered to have the following attributes:

- simultaneous high lateral and longitudinal resolution ( $\sim 1 \lambda$ )
- high signal-to-noise ratio
- wide beam width insonification (multi-angle)
- wide bandwidth insonification (multi-frequency)
- inherently quantitative and volumetric.

Fredericks (6.6.10) has examined the ability of SAFT-UT to detect flaws near the front surface and has detected 1.5-mm side-drilled holes in the range of from 2.0 to 12.0 mm from that surface. Future work will explore the effects of rough surfaces on detection.



**FIGURE 6.6.9.** Measured Size of Artificial Flaw in Heavy Cast Steel Specimen Versus Its Actual Size

Special specimens containing natural defects have been examined; e.g., PVRC block 202, the GE brittle fracture block ACB-3, ORNL ITV V-7B, and GARD weld specimens. A problem with the data, which is all visual, is one of quantification. With some effort, it would be possible to correlate presumed flaws with observed flaws from the point-of-view of detection; however, sizing would be much more difficult. Extensive pictorial data are available on the PVRC-202. Nothing was detected on the GE ACB-3 block. Extensive data exist for ORNL ITV-V-TB; however, destructive examination will be necessary to establish correlation. The GARD weld specimens did not appear to yield quantitative data.



TABLE 6.6.3. Examples of Accuracy of Flaw Sizing, Primarily with Acoustic Holography\*

Type of Flaw	Length (in.)			Depth (in.)			Comments
	Actual	NDE		Actual	NDE		
Crack in thick curved plate	2.5	3.0	(AH)	1.5	1.5	(AH)	Not detectable by other NDE.
Defects in RPV Nozzle	#1 2.0	0.75	(RT)	0.56	--		
Both 5.5 in. below surface	2.0	1.8	(AH)	0.56	0.6	(AH)	
	#2 2.2	1.0	(RT)	0.8	--		
	2.2	2.2	(AH)	0.8	0.8	(AH)	
Flaws in circular seam weldment	#21 0.4	0.438	(UT)	0.1*	--		2.875 in. below surface
	0.4	0.625	(RT)	0.1	--		
	0.4	0.45	(AH)	0.1	0.20	(AH)	
	#22 0.76	0.188	(UT)	0.088*	--		3.625 below
	0.76	0.563	(RT)	0.088	--		
	0.76	0.8	(AH)	0.088	0.08	(AH)	
	#25 0.055	0.156	(RT)	0.03*	--		2.875 below
	#26 0.50**	0.44**	(AH)	0.073	0.089	(AH)	3.625 below
	#27 0.25	0.19	(UT)	0.179	--		2.875 below
	0.25	0.31	(RT)	0.179	--		
	0.25	0.24	(AH)	0.179	0.144	(AH)	
HSST #1	0.5	0.5	(AH)				EB weld zone
	1.0	0.9	(AH)				Trepan dia.
	1.7	1.55	(AH)				Max. crack
HSST #2	0.5	0.5	(AH)				EB weld zone
	0.5	0.5	(AH)				Avg. crack extent
Acoustic Emission	#2 --	11	(UT)	--	2.21	(UT)	0.21 wide (UT)
Pressure Vessel	--	10.5	(RT)	--			0.20 wide (RT)
	#4 --	11.5	(UT)	--	0.75	(UT)	0.17 wide (UT)
		11.0	(RT)				0.24 wide (RT)
Clad Test Block (all AH)	#1 --	4.25		--	0.5		
	3 --	4.1		--	0.45		
	4 --	4.29		--	0.6		
	5 --	0.84		--	0.34		
	6,7 --	1.2		--	0.34		6,7 connecting; seen from only one direction.
	8 --	1.4		--	0.4		May be another. Discontinuity somewhat lower.
	9 --	2.3		--	0.46		
	10 --	2.6		--	0.5		

\* Said to be width.

\*\* Actual flaw consists of two: one 0.14, other 0.19, separated by 0.25. AH flaw consists of two: one 0.13, other 0.3, separated by 0.075.

TABLE 6.6.4. Composite Summary of Various NDE Techniques

Method/ Criteria	System		Normalized Result											
			Under Clad Surface				No Cladding							
			Flaw No. 1				Flaw No. 2				Flaw No. 3			
Group	Description	Length %DT	Width %DT	TWD %DT	Depth %DT	Length %DT	Width %DT	TWD %DT	Depth mm	Length %DT	Width %DT	TWD %DT	Depth %DT	
DT														
ASME III	B&W	STD	99	68	NE	NE	101	168	NE	NE	53	575	NE	NE
EXP	Risley	EXP	108	84	31	112	104	168	62	25	16	300	50	119
<u>Single-Point Non-Imaging</u>														
ASME XI-UT	SWRI	STD	153	263	500	119	105	375	266	13.5	NR	NR	NR	NR
ASME XI-UT	B&W	STD	90	128	200	106	112	475	216	12.5	NR	NR	NR	NR
RHP 5/3	KWU	STD	166	136	125	99	156	512	NR	Surface	168	850	NR	91
TIM	KWU	Autoscan	126	NR	NR	97	100	NR	NR	20	126	1500	NR	110
<u>Multiple-Point Imaging</u>														
Fcsd. Prb-UT	CEN/CEA	- - -	103	105	NE	106	90	125	NE	15-22	122	500	NE	105
Fcsd. Prb-UT	BAM	- - -	97	NR	175	90	100	NR	116	5-30	106	NR	300	108
AH-UT	B&W	- - -	101	136	62	108	103	231	108	17-34	108	250	166	106
AH-UT	Harwell	- - -	96	NR	NR	132	102	125	41	15-20	NE	NE	NE	NE
AH-UT	IZFP	- - -	77	94	75	93	NR	NR	NR	NR	98	350	333	92
AH-UT	BAM	- - -	97	NR	162	90	102	NR	116	5-30	106	NR	300	108
<u>Multiple-Point Non-Imaging</u>														
ASME XI-UT	BNW	Mul. El.	106	136	87	108	101	156	104	12-21	NR	NR	NR	NR
ASME XI-UT	Risley	B-scan	77	136	87	97	100	425	375	10	24	500	NR	110
Diffra-UT	Harwell	Dual Trans	151	NE	125	104	118	NE	41	15-20	142	NE	333	108
Ampl. & TD-UT	IZFP	ALOK	132	189	137	84	122	215	133	8	92	1050	700	89
Cmbd. Rslt-UT	BAM	Mixture	103	52	157	90	119	237	208	29	20	NR	NR	110

Flaw Description

Thin, convex top, continuous piece.

Two flaws/Angled sawcut plus series of inter-connected slag deposits.

Series of spherical slag inclusions on weld fusion line.

NOTE: NR - Not Reported RT - Radiographic Technique  
 NE - Not Examined UT - Ultrasonic Technique  
 STD - Standard AH - Acoustic Holography  
 - Less accurate than \*25% of DT result.  
 - Less accurate than \*10% of DT result.

6.6.15

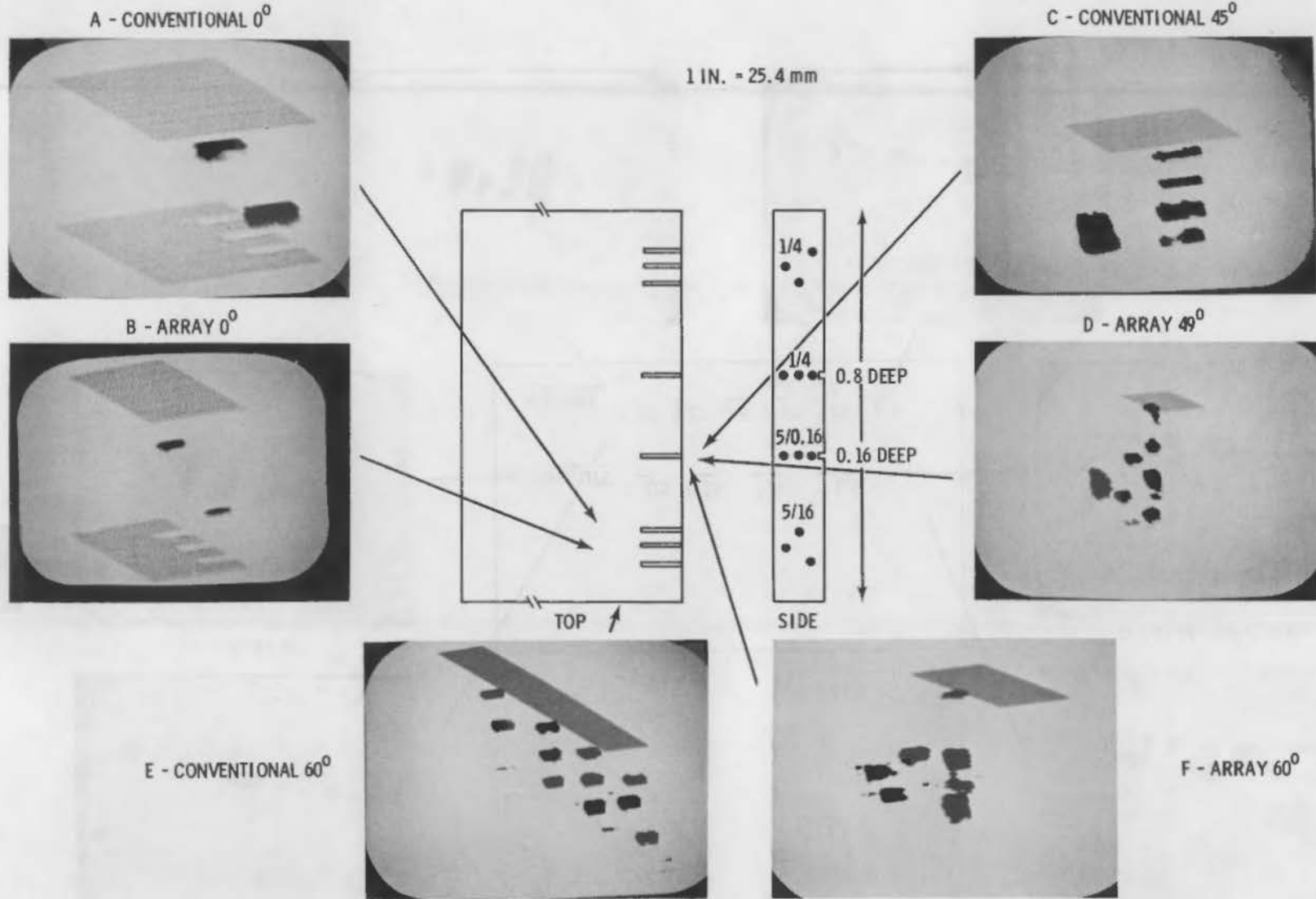


FIGURE 6.6.10. Isometric Images of Side-Drilled Holes

6.6.16

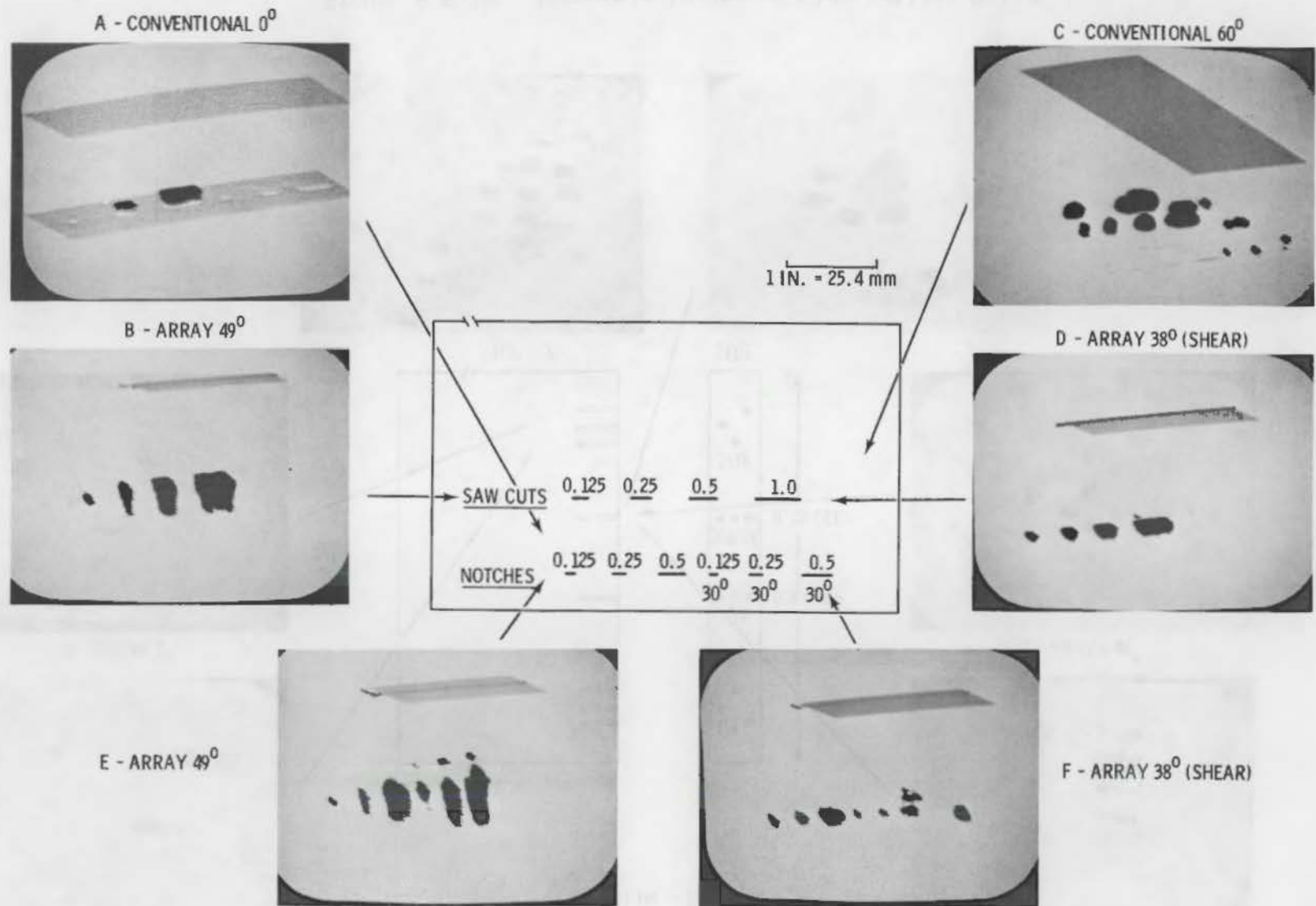
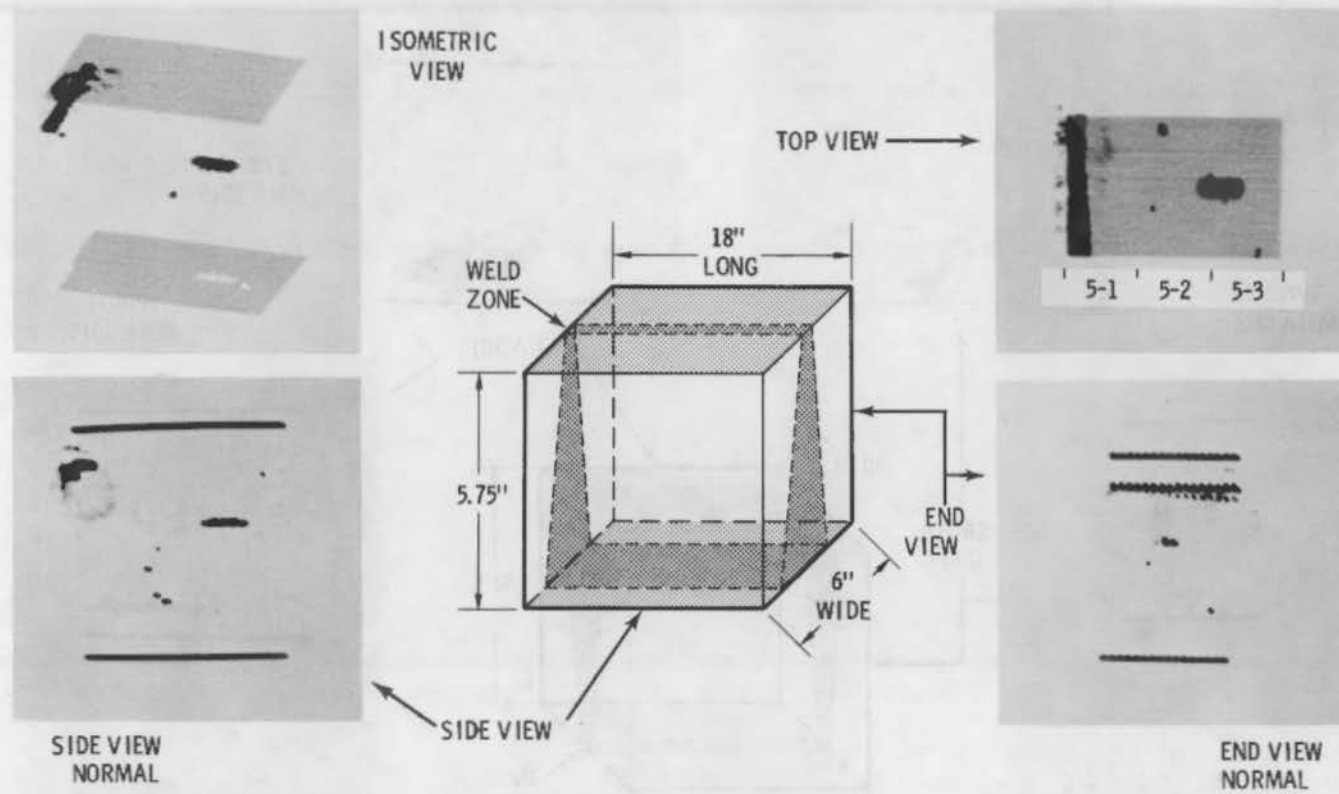


FIGURE 6.6.11. Isometric Images of Notches and Saw Cuts

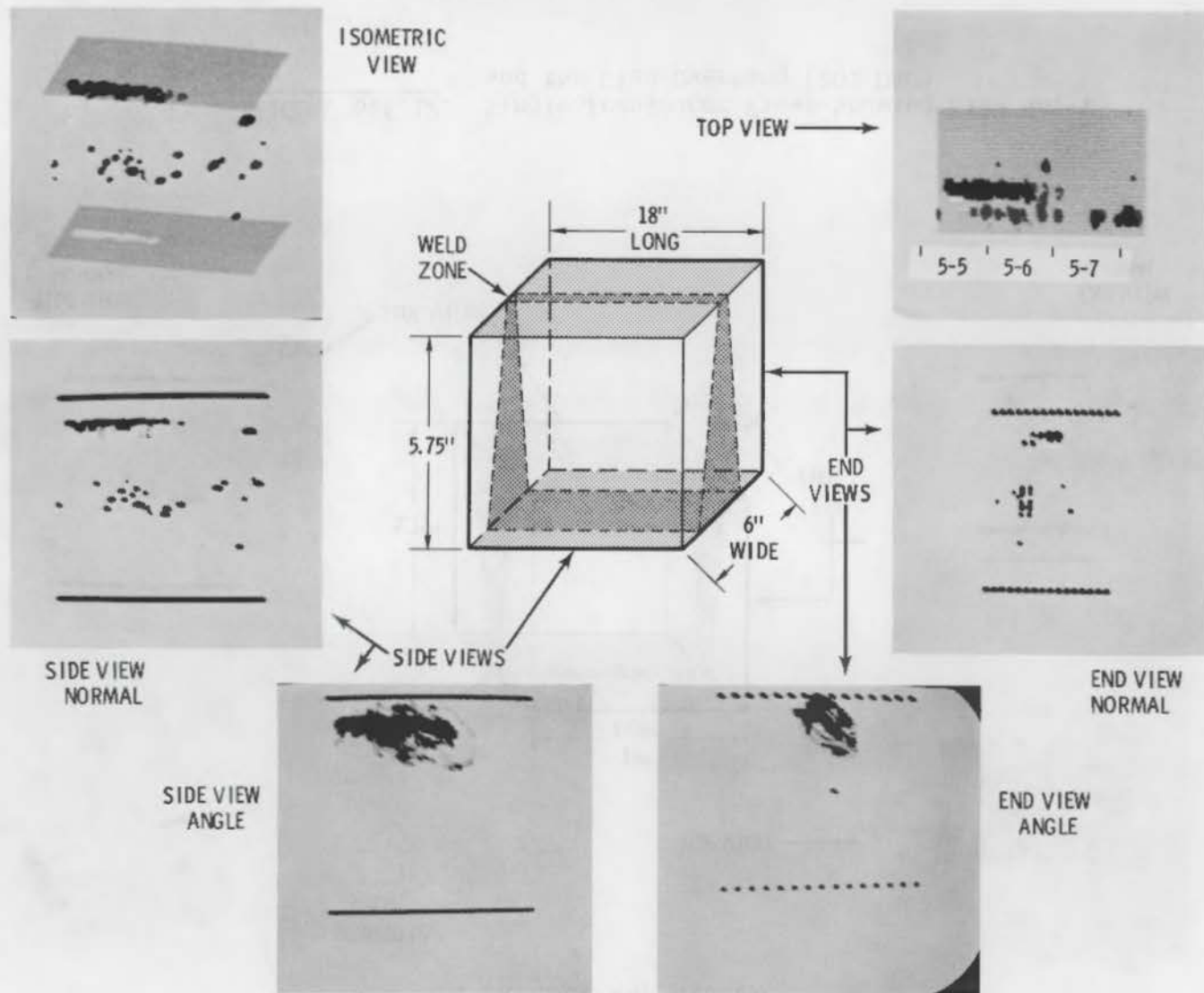
TEST BLOCK PROVIDED  
BY BABCOCK AND WILCOX



6.6.17

FIGURE 6.6.12. Single Transducer Views Showing Flaw No. 1 and the Clad Overhang (20% DAC)

TEST BLOCK PROVIDED  
BY BABCOCK AND WILCOX

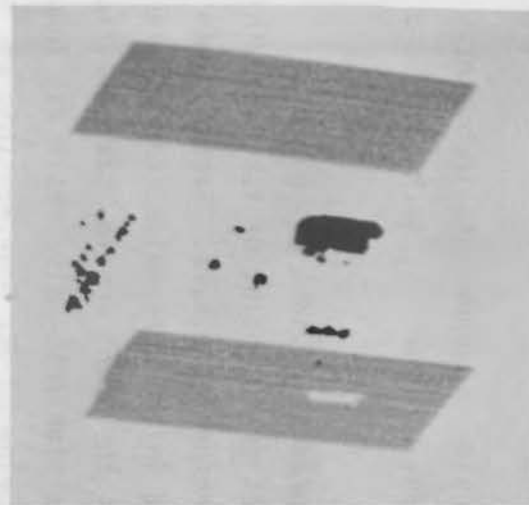


6.6.18

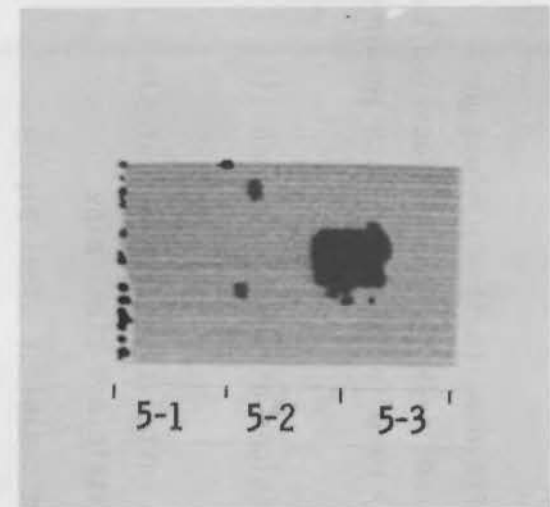
FIGURE 6.6.13. Single Transducer Views Showing Flaw No. 2 and a Number of Small Defects (20% DAC)

ARRAY:  
SINGLE BLOCK

ISOMETRIC



C-SCAN



ARRAY:  
MULTIPLE BLOCK

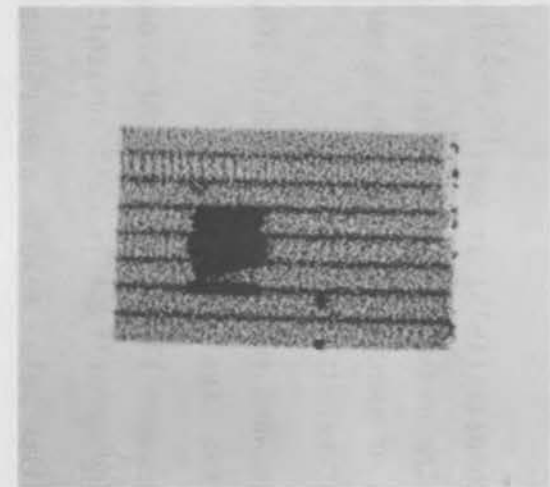


FIGURE 6.6.14. A Comparison of Array Single Block Performance Versus the Array Multiple Block for Two Different Views of Weld Sections 5-1 to 5-3, at 20% DAC on the Babcock and Wilcox Test Block, Showing Flaw No. 1

Work to date (1978) at SWRI (6.6.11) on field validation has not progressed to the measurement of defects. Substantial work has been devoted to fabrication of specimens containing a variety of defects. Four such specimens have been prepared; namely,

1. weld between two 12-in. schedule 100 sections of wrought austenitic stainless steel pipe
2. weld between 12-in. sections of wrought austenitic stainless steel pipe and centrifugally cast austenitic stainless steel pipe
3. dissimilar metal weld between carbon and stainless steel piping
4. butt-weld in carbon steel plate.

The following flaws were inserted: porosity, ID undercut, incomplete fusion, tungsten inclusion, drop through, slag, OD undercut, suck back, and incomplete penetration.

An update of the status of the SAFT-UT program at SWRI was given in 1981. (6.6.12) Equipment development continued to the point of testing both calibration blocks and test pieces cited in reference 6.6.11. Porosity and heat-affected-zone cracking could be detected in the butt-welded carbon steel plate. An examination of interest was one of the Duane Arnold nozzle sections containing IGSCC occurring in the field. The signal-to-noise ratio was lower than either aluminum or carbon steel, being below 10 dB; however, this was sufficient to identify the crack and chart its path.



The literature relevant to acoustic emission is extensive and somewhat confusing. While several references could be cited, preference is given to an excellent review by Spanner.<sup>(6.7.1)</sup> Two significant aspects covered in the review were the application of acoustic emission (AE) to monitoring the welding process and the use of AE to monitor crack growth during hydro tests or online. Tables 6.7.1 and 6.7.2 present data on an extensive three-year effort on monitoring welds. The success or lack of success in both laboratory and production tests are given in the second table. As noted, AE is relatively unsuccessful or variable in detecting porosity, tungsten inclusions, and slag inclusions, and quite successful for cracks, lack of penetration and lack of fusion. This is in the positive direction since the former have little or no safety significance whereas the latter have substantial safety significance. The preceding work was abstracted from NUREG-0035-4 by GARD.

Acoustic emission tests have been conducted on about 20 experimental vessels. Most of these vessels included machined flaws in the base metal. Only four tests had flaws located in the weldment so data are relatively limited concerning AE response during impending vessel failures due to weld associated defects. Tests to failure include PM-2A, EBOR, KEMA, AMMO, UK vessels (5), HSST (11). Generally, prediction ranges from fair to good. In a few instances noisy welds led to some difficulties.

Spanner<sup>(6.7.1)</sup> suggested that AE had considerable promise as a complementary NDE method. In conjunction with a method such as UT it can be very valuable. Sole dependence on AE is risky--I agree.

TABLE 6.7.1. Major Parameters Included in Three-Year Weld Monitoring Effort

Series	Test Article	Number of Welds	Pipe Size or Weld Thickness, cm (in.)	Total Length of Weld Bead, m (ft)	Number of Weld Beads	Material(s)	Weld Process
1	Piping Weld (Laboratory)	20	15 & 36 (6 & 14) Dia	75 (250)	5 & 7	A106, A312	GTAW, GMAW, SMAW, SAW
2	Piping Weld (Production)	18	6-30 (2-1/4-12) Dia	102 (400)	Varied	A106, A312	GTAW, GMAW, SMAW, SAW
3	Piping Weld (Production)	10	15-61 (6-24) Dia	210 (340)	Varied	A106	GTAW, SMAW, SAW
4	Vessel Weld (Laboratory)	1	16 (6-5/8)	150 (500)	95	A508	SAW
5	Vessel Weld (Laboratory)	1	17 (6-3/4)	78 (260)	65	A533	SAW
6	Piping Weld (Laboratory)	30	10 (4) Dia	87 (290)	6	A106	GTAW, GMAW, SMAW
7	Piping Weld (Production)	80	48-107 (19-42) Dia	1,740 (5,800)	3-15	A106	SAW
8	Vessel Weld (Production)	1	30.5 (12)	204 (680)	266	A508	SAW
9	Vessel Weld (Production)	1	15 (6)	540 (1,800)	850	A533	SMAW
10	Vessel Weld (Production)	3	8 & 10 (3 & 4)	600 (2,000)	42-65	A533	SAW
11	Piping Weld (Laboratory)	19	10 (4) Dia	75 (250)	5-6	A106, A312	GTAW, GMAW
12	Vessel Weld (Laboratory)	15	1.3-5 (1/2-2)	270 (900)	20-30	A533	SAW

6.7.2

TABLE 6.7.2. Listing of Defects Detected During the Twelve Series of Tests Shown in Preceding Table

Tests	No. of Welds	Number Detected by AE	Number Detected by Confirming Method(s)	Confirming Method(s)	Number of Defects Missed	Apparent % AE Accuracy
<b>Laboratory</b>						
Vessel Materials	17					
Cracks		29	27	RT, UT, VT(a)	4 (RT)(b)	93
Lack-of-Penetration(c)		21	21	RT, UT	0	100
Lack-of-Fusion		0	0	--	--	--
Porosity(a)		10	14	RT	4	71
Tungsten Inclusions		--	--	--	--	--
Slag Inclusions		43	43	RT	0	100
<b>Piping Materials</b>						
Piping Materials	64(d)					
Cracks		25	25	RT, VT	2 (RT)(b)	100
Lack-of-Penetration		6	8	RT	2	75
Lack-of-Fusion		0	23	RT	23	0
Porosity		1	24	RT	20	5
Tungsten Inclusions		0	4	RT	4	0
Slag Inclusions		0	0	--	--	--
<b>Production</b>						
Vessels(e)	5					
Cracks		1	1	VT	0	100
Porosity		2	2	VT	0	100
Slag Inclusions		6	6	VT	0	100
<b>Piping</b>						
Piping	100					
Cracks		16	16	RT, PT	0	100
Porosity		88	151	RT	63	58
Slag Inclusions		44	67	RT	23	66

- (a) VT - includes visual observations during and after welding, plus metallographic sectioning.  
 (b) Metallography confirmed 6 cracks that were detected by AE but not detected by RT.  
 (c) Detectability enhanced by associated slag inclusions for SAW welds.  
 (d) High amplitude noise signals from slag cracking precluded AE monitoring of 5 A312 pipes during Test #1, and these welds are not included in this table.  
 (e) Includes 3 welds on 1 vessel, and 1 weld on 2 other vessels.



Electromagnetic-acoustic (EMA) techniques produce ultrasonic vibrations directly in the surface of a conducting medium without the need for an external vibrating transducer with a fluid couplant. Since the EMA transducer need not touch the surface of the specimen, the term "noncontact ultrasonics" is sometimes used interchangeably with EMA. The EMA technique permits both generation and detection of ultrasound permitting a complete noncontact transmit-receive system. An obvious advantage of such a technique is its use on objects at relatively high temperatures.

A report of the EMA technique for surface and Lamb-wave testing covers both theory and experimental information.<sup>(6.8.1)</sup>

A critical parameter in EMA is gap between specimen surface and excitation transducer. At 1.5 MHz, the gap should be from 1 to 2 mm with signal strength decreasing from 6 to 8 dB/mm of added clearance. Typically, the signal strength of EMA systems is about 40 dB less than with conventional Piezo electric zirconate titanate (PZT) transducers. However, much of the loss can be recovered by increasing the excitation.

Another important parameter is signal-to-noise ratio rather than signal strength. Since EMA yields signals as clear as or clearer than conventional systems, the signal strength is less critical. Factors influencing signal strength include magnetic and electrical behavior of the material beam tested. If the material is ferromagnetic (e.g., a low-alloy steel below the Curie point) a shear wave yields the higher signal strength, whereas a longitudinal wave is highest in the vicinity of 800°C.

Surface waves can be generated with a zig-zag RF grid. However, such systems are even more dependent on liftoff because, when liftoff becomes comparable with the spacing between the grid wires, the RF fields begin to cancel. Such surface waves can be used in two ways to detect defects:

1. through use of a reflection technique
2. by measuring the increase in attenuation of a transmitted signal when defects exist.

The relative response of the two techniques can be seen in Figure 6.8.1. With surface waves, penetration is limited to a few wavelengths with saturation occurring for defects at greater than a certain depth where all energy is reflected and none transmitted.

At the other extreme, very small surface or near-surface defects whose depths are a small fraction of a wavelength will give very small signals. These extremes, in essence, predetermine the optimum wavelengths. However, in the defect size (0.3 to 3.0 mm) the most suitable frequencies are 250 to 500 MHz, permitting reasonable grid spacings and clearances.

The Lamb waves represent a natural extension of surface waves with primary applications to thin-walled products such as plates and tubes which are irrelevant to this white paper.

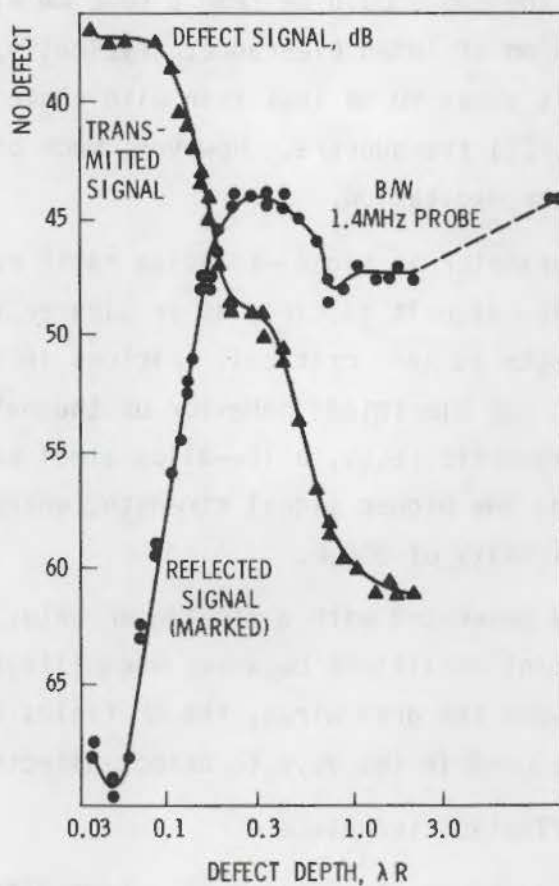


FIGURE 6.8.1. Response of Surface Waves to Milled Slots of Various Depths, 0.9 MHz Probe

Positron annihilation is a rather specialized technique using a small positron source such as  $^{22}\text{Na}$  to map cracks such as those caused by fatigue. If it is used commercially, the use will be highly specialized and will require a great deal of development. Obvious problems include but are not limited to the following:

- positron range in materials--strictly a surface phenomenon
- time--with the current system, about 20 hours per measurement is required
- sensitivity to positioning with respect to cracks--there is a very rapid drop-off to background.

Presumably, the time aspect can be solved by measurement of gamma ray line shape and Doppler broadening. There appears no obvious application in nuclear, at least at this time. (6.9.1)

Position administration is a rather special technique using a self-position source such as  $\text{C}^{14}$  or  $\text{C}^{13}$  as tracers as these cannot be taken up by the body. It is usually administered by the use of highly specialized and well-regulated a great deal of development. The main problem involved but not limited to the following:

- a position range in waterfalls—strictly structural dimensions
  - a time with the control system, about 20 hours per measurement is required
  - a sensitivity to positioning with respect to error—there is a very small error in the background.
- Therefore, the few aspects can be solved by measurement of time by the above and logical reasoning. There appears no further application in nature, at least at this time. (R. S. 1)



The CEGB has used capacitance strain gages to monitor crack growth in piping and other components of steam plants operating at elevated temperatures ( $\sim 600^{\circ}\text{C}$ ). The strain gage consists of two capacitor plates mounted between two compliant arches. A circumferential crack causes translation of one plate with respect to other. (6.10.1)

Gages are mounted over the heat-affected zones adjacent to welds since cracks commonly form there. Their use on piping in operating power plants confirmed the existence of bending moments during startup and shutdown as well as moderate steady bending under normal loads. Examples of strain, power, pressure, temperature outputs are given in Figure 6.10.1. Figure 6.10.2 illustrates changes during cooling transients over a 18-month period.

While the use of such gages would be limited to specific locations, it is possible that they could be valuable under certain circumstances.

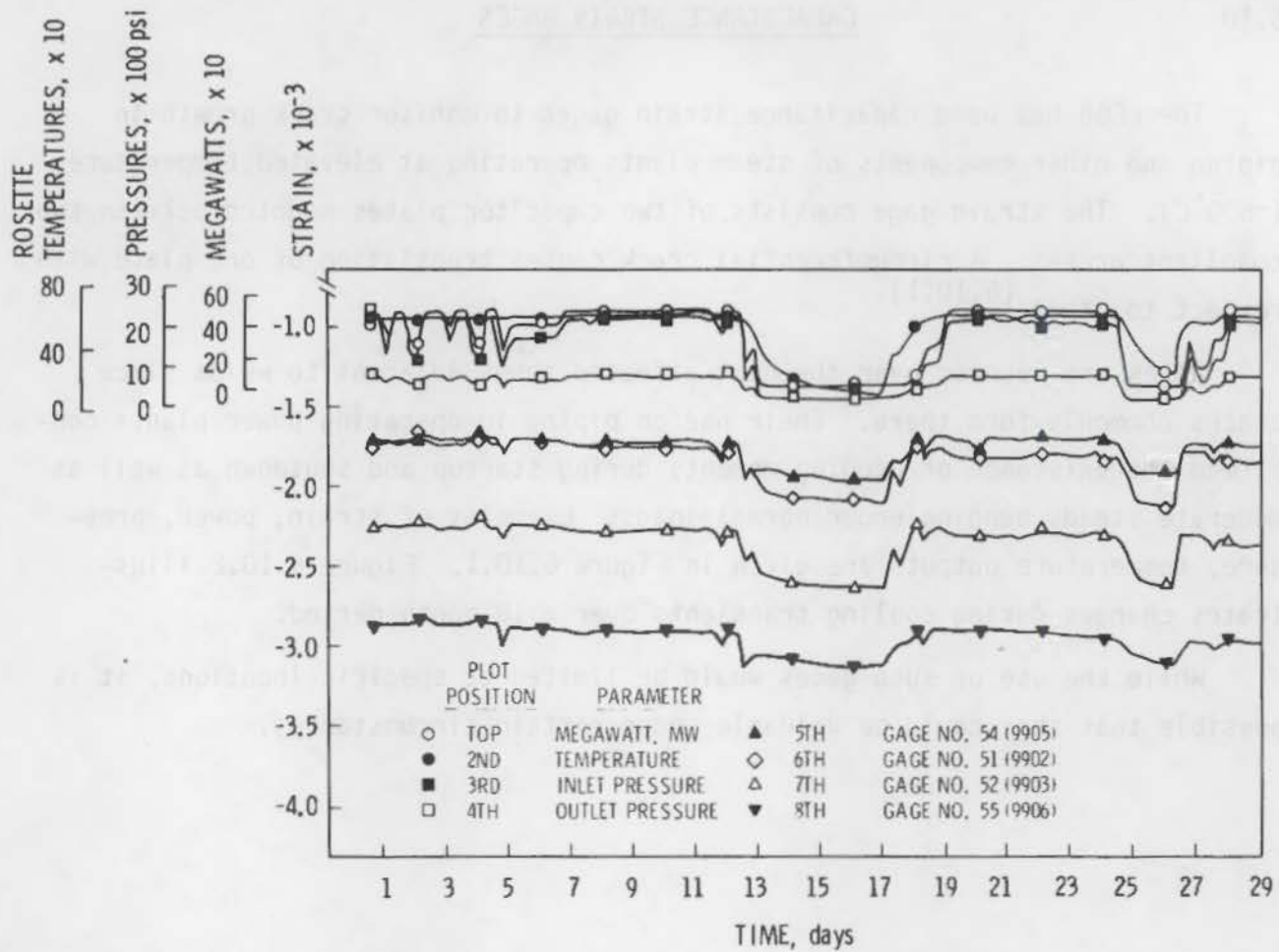


FIGURE 6.10.1. Typical Strain Output in Power Piping Over a One-Month Period

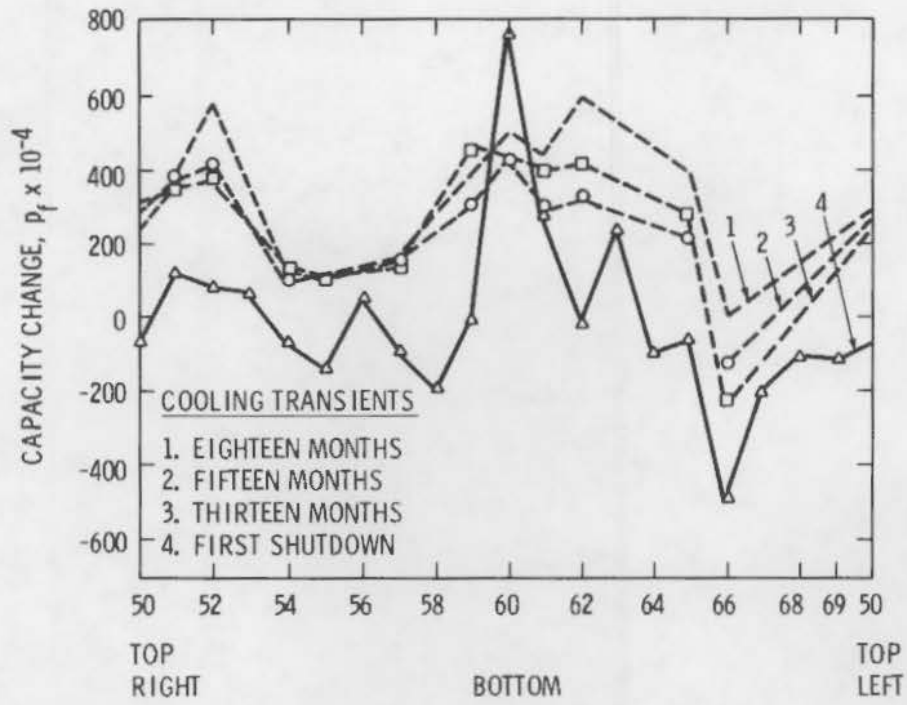


FIGURE 6.10.2. Gage Position Around Pipe on Power Piping

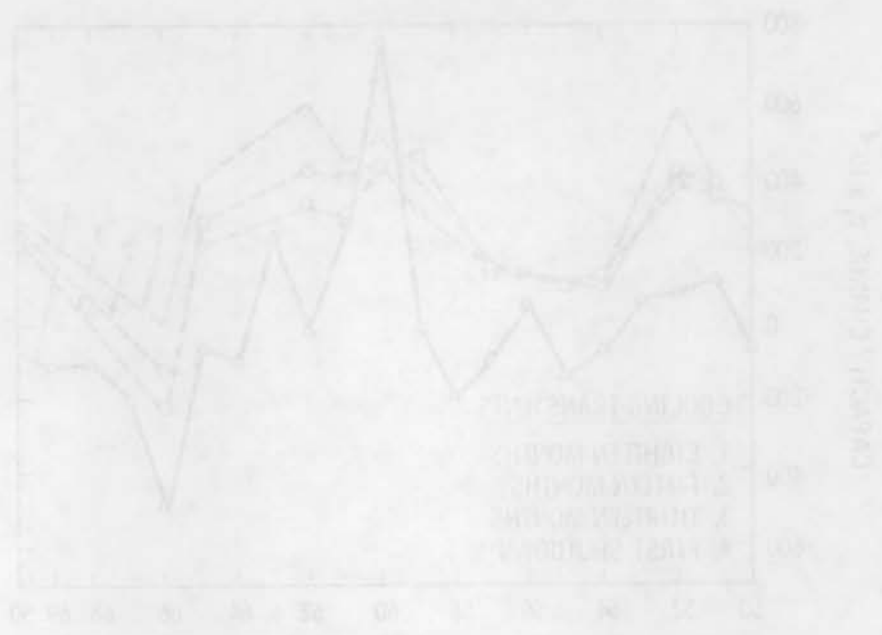


FIGURE 8.10.A. Edge position relative to the Power Rigging

A technique probably limited to thinner sections of austenitic stainless steel is infrared electro-thermal NDE. (6.11.1,6.11.2) This technique is an analog of MT tests in ferritic steels; however, it will detect embedded as well as near- and far-surface flaws. A very short (0.1 sec) high energy ac pulse is introduced through contacts either symmetrically through the cross-section by applying contacts on the near and far surfaces on both sides of the defect, or limited to the near side across the defect region. The process generally is one of detection rather than sizing. Table 6.11.1 presents the available data.

The most meaningful values in terms of tests on piping are those with near-side current applied. Detection was limited to the deeper (0.32-cm) or the longer (1.28-cm) flaws. The data are limited to artificial flaws and it is difficult to assess the detectability of tight fatigue cracks.

This technique would appear to have limited applications; however, it could be of value under some circumstances, particularly in coarse-grained austenitic stainless steels. A description of equipment and testing is given in reference 6.11.2.

TABLE 6.11.1. Infrared Electro-Thermal NDE

Application	Notch Depth cm (in.)	Notch Length--cm (in.)				
		0.08 (0.03)	0.16 (0.06)	0.32 (0.12)	0.64 (0.25)	1.28 (0.50)
Symmetric Current Near-Side Surface Defects	0.08 (0.03)	C	C	D		D
	0.16 (0.06)	C	D	D	D	D
	0.32 (0.12)		D	D	D	D
Far-Side Surface Defects	0.08 (0.03)					Q
	0.16 (0.06)			N	D	D
	0.32 (0.12)		D	D	D	D
Near-Side Surface Defects	0.08 (0.03)		D			
	0.16 (0.06)		D			
	0.32 (0.12)					
Near-Side Current Far-Side Surface Defects	0.08 (0.03)			N		D
	0.16 (0.06)			N	Q	D
	0.32 (0.12)		N	D	D	D

NOTES: 100 KVA at 6 VAC for 0.1 second-to-heat.  
 Specimens 5 x 10 x 0.5 cm (2 x 4 x 0.2 in.)  
 D - Detectable from surface temperature pattern.  
 C - Detectable only through cavity effect.  
 Q - Detection from surface pattern questionable.  
 N - Not detected.  
 Blank - Not run.  
 Width of all EDM notches 0.013 (0.005).

Electromagnetic leakage, in essence, is an instrumented electronic version of magnetic particle testing (MT) useful for surface or near-surface flaws in ferrite steel pipe or ferrite steel solid sections. The leakage of magnetic flux is measured and can be correlated with flaws. The theory substantially agrees with experimental results from slots; however, agreement is rather poor with fatigue cracks.

Work by Owston<sup>(6.12.1)</sup> represents the most meaningful experimental study known to me. Two types of specimens were investigated:

1. Mild steel plates 300 x 80 x 10 mm (12 x 3 x 0.375 in.) with slots machined across the face perpendicular to the long axis; the slot sizes were:

Width (mils)	6	10	27	63
Depth (mils)	10	--	--	--
	25	--	--	--
	100	100	100	100
	--	--	--	200

The same specimen size was used with a fatigue crack about 200 mils deep and perpendicular to the long axis.

2. Two-in. dia mild steel bars containing longitudinal machined slots.

The plate specimens had a magnetic field applied parallel to the length and a travelling search coil was used to detect flaws. The tests on machined slots indicated that the magnetic field varied with slot depth but was independent of slot width as can be seen in Figure 6.12.1.

Theoretical values of leakage flux compared relatively well with experimental values for machined slots as can be seen in Table 6.12.1.

An application of theory to the fatigue crack led to a prediction of a signal of ~500 Gauss based on depth of flaw. The experimental value was about 30 Gauss, representing a major discrepancy. Followup experiments, where the crack was opened by external loads, increased the magnetic flux. A tight flaw behaves about the same as a machined slot about half the depth. The results

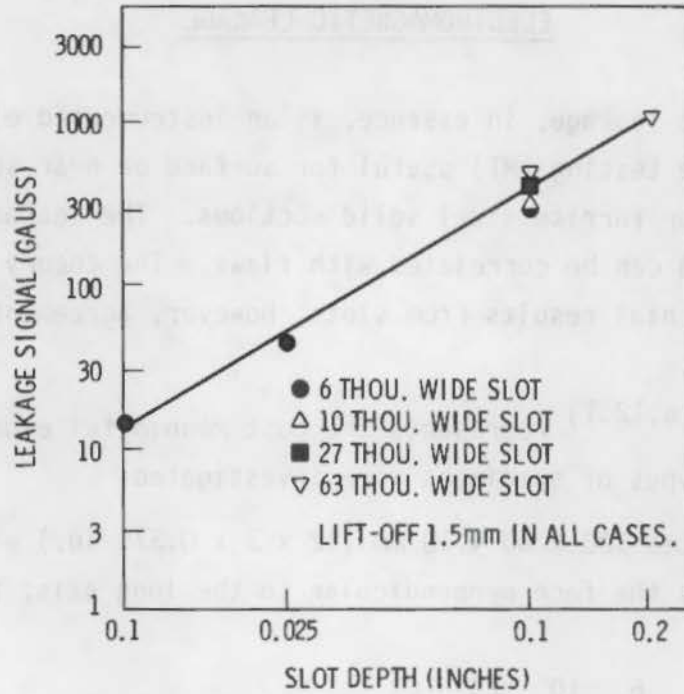


FIGURE 6.12.1. Magnetic Flux Leakage Signal from Sawn Slots

TABLE 6.12.1. Comparison of Experimental and Theoretical Values for Leakage Field at 1.5-mm Lift-Off Over Sawn Slots

Slot		Leakage Flux	
Width (mils)	Depth (mils)	Calculated Gauss	Measured Gauss
6	10	31	15
6	25	62	45
6	100	125	310
10	100	208	340
27	100	560	430
63	200	1,480	1,150



are sufficiently undefinitive to conclude that substantial experimental work needs to be done on real flaws before using such a technique.

Limited experiments were conducted on the cylindrical bar containing slots; however, the specimen conditions were poorly defined so the data are not presented here.

An earlier study<sup>(6.12.2)</sup> developed the theory for a finite defect in a magnetic field. The surface charge distribution pattern and surface charge density of the magnetizing field were calculated as functions of the defect length. These values were compared to experimental results. The correlation was relatively poor. For example, defect geometry is a critical factor. A 0.5-mm dia by 2.5-mm deep hole develops a magnetic field ~2% of the field for a long hairline crack of the same depth. While this approach may have specific applications, its use in quantifying flaw geometry is doubtful.

are sufficiently sensitive to compute that statistical significance was  
needed to be done on post-flight data using such a technique.

Adjusted values were computed for the significant parameters  
and, however, the observed correlation coefficients were not adjusted to the 0.05  
probability level.

An earlier study (1975) determined the effect of a 10% deficit in a  
certain state. The various data distributions were not adjusted  
because of the magnitude of the deficit. The results of the deficit  
study, those values were compared to experimental results. The correlation  
was relatively poor. For example, deficit severity is a critical factor. A  
50-50 mix of 2.5-sec and 10-sec a duration time 50% of the field for  
a long duration time of the field. While this approach may have resulted  
in a deficit, it is in principle the severity is constant.

The new high intensity, high-energy accelerators have resulted in expanded usage of X-ray radiography, particularly for thick sections of steel such as reactor pressure vessels; however, higher beam intensities represent only one part of the problem. Detection and quantification of small defects requires optimization of system sensitivity. An EPRI report<sup>(6.13.1)</sup> assesses the potential of thick section radiography with an analytic model. The analytic approach was selected in preference to the experimental because a comprehensive experimental investigation of high-energy X-ray radiography is practically infeasible because of the following:

- The physical processes are complex and interrelated.
- The detailed determination of system sensitivity to component changes would be very expensive and time consuming.

The analytic approach is possible because of the sophisticated radiation transport computer codes available permitting accurate simulation of scattering and beam interaction as well as assessment of such factors as incident beam contribution to image, influence of filters, buildup, collimation, backscatter and sensitivity to thickness.

The preceding approach permits a rating of the various factors from a high of those having the most potential for improvement to a low covering those where minimal gain is anticipated with the new high-energy sources. The imaging system appears to have the greatest potential for improvement or optimization. For example, substitution of metallic screens of metals such as tantalum should result in significant improvements compared to the present lead screens.

The following summary list reproduced from the EPRI report<sup>(6.13.1)</sup> cites both the positive and negative conclusions derived from the study:

- Imaging systems show the most potential for improvement because changes, such as substituting tantalum for lead intensifying screens, are relatively easy to implement. An example of the magnitude of the image system effects can be derived from the preliminary set of metal screen-film calculations that are discussed in Section 5.3. A more

comprehensive set of calculations would quantify the optimum image system for a given radiographic situation; however, the more extensive calculations would probably not alter the general conclusions.

Example of Image System Variations. Considering a 4 MeV photon only, there is roughly a factor of 7 increase in image line spread (i.e., decrease in resolution) between a front- and back-metal intensifying screen-film image system versus that of a bare double-emulsion film. Much of this increase in line spread is contributed by the back-metal screen. At the same time, there is roughly a factor of 10 increase in film density caused by this 4 MeV photon for the metal-screen image system versus the bare film. Although the radiographic image is a complex multiparameter function of several variables, it appears that for many high-energy radiography situations the best resolution is obtained with a single front emulsion film; a double emulsion only spreads this image slightly. A single intensifying screen in front significantly increases the film density for a given irradiation with a lower spread in resolution than does for a single back screen, and a front- and back-metal intensifying screen increases the film density by more than just the simple sum due to each individual intensification screen. The range of the validity of the above general comments over variations in the radiographic system parameters (source energy, object thickness, etc.) would have to be quantified by more comprehensive calculations.

- Collimators do not show much promise of improving radiographic quality.
- Optimum  $E_e$  Energy is in the 8- to 15-MeV region since higher energies will not significantly improve the buildup factors. In addition, there are indications that metal screen-film imaging systems show a decreased response at higher energies.

- Backscatter may be significant in some applications. Initial calculations indicate a 10 to 20% effect; for other more complex geometries the effect could be higher.
- Xeroradiography does not appear to be a promising approach for high-energy radiography.

While the present study has reviewed the state-of-the-art thick section radiography, and has provided new tools for understanding and optimizing thick section radiography systems, there are still a number of unresolved areas that warrant future study efforts. We list below some of these areas with brief explanatory discussions:

- Systematic Computational and Experimental Investigation of Metal Intensifying Screens. The optimum thickness and material for metal intensifying screens as a function of average photon energy should be investigated in a systematic calculational/experimental study.
- Analytical and Experimental Investigation of Backscatter. Backscatter in many practical situations can be a significant effect. A calculational effort verified with experimental results should provide some general rules of thumb. This would be incorporated in a more comprehensive set of multidimensional calculations.
- Image Enhancement Review and Test Program. The present program did not address image enhancement and its application to thick section radiography in detail. There is a great need to review the various image enhancement concepts and experimentally evaluate their application to high-energy radiographs.

#### 6.13.1 Intensifying Screens

The potential gain from improved intensifying screens is well illustrated in a study comparing fluorometallic screens to conventional lead screens. (6.13.2) The results are given in Table 6.13.1.

Initially, it was felt that the fluorometallic screen, which consists of a layer of polycrystalline calcium tungstate coated onto a thin lead foil, functions by the lead layer absorbing X-rays and emitting electrons into the

**TABLE 6.13.1.** Comparative Data for Fluorometallic and Lead-Screen Exposures for a Range of Specimen Thicknesses and Radiographic Techniques

Specimen (steel) mm	Screens	Radiation	mA	ffd, mm	Film	Density	Time	IQI, % Wire	Step/Hole
6	SMP 308	80 kV	8	500	NDT 75	2.0	0.5 min	1.6	4
	Lead	80 kV	8	500	NDT 75	2.0	5 min	1.6	4
12.5	SMP 308	120 kV		600	NDT 75	2.2	1 min	1.3	2.5
	Lead	120 kV		600	NDT 75	1.9	10 min	1.3	2.5
25	SMP 308	250 kV	6	900	NDT 75	1.8	1 min	1.1	2.5
	Lead	250 kV	6	900	NDT 75	1.8	10 min	1.1	2.5
	SMP 308	190 kV	6	900	NDT 75	1.9	1 min	1.0	2.5
50	Lead	400 kV	8	1,000	D7FM	1.9	1.5 min	1.0	2.0
	SMP 301	400 kV	8	1,000	D7FM	1.7	20 sec	1.0	2.0
	SMP 301	320 kV	8	1,000	D7FM	2.1	1.5 min	1.0	2.0
25	Lead	$^{192}\text{Ir } \gamma$		500	D7FM	1.9	80 Ci min	1.6	3.2
	SMP 303	$^{192}\text{Ir } \gamma$		500	D7FM	2.1	40 Ci min	1.6	3.2
75	Lead	$^{60}\text{Co } \gamma$		1,000	D7FM	2.5	300 Ci min	1.1	1.7
		$^{60}\text{Co } \gamma$		1,000	D7FM	2.5	150 Ci min	1.1	1.7

Purpose	Code Numbers and Letters	
	High Definition Type	High Speed Type
80 to 200 kV X-rays	SMP 108	SMP 308
200 to 400 kV X-rays $^{192}\text{Ir}$ , $^{137}\text{Cs}$ , $\gamma$ -rays	SMP 103	SMP 303
High-energy X-rays $^{60}\text{Co } \gamma$ -rays	SMP 101	SMP 301

tungstate layer which enhances the emission of ultraviolet light. The current opinion is that the calcium tungstate layer consists of very small particles of much more uniform size than is true of typical tungstate screens and the uniformity of particle size is responsible for the improved image. Limited data with so-called "tungstate screens" confirms that these "improved" screens do yield comparable image quality although the exposure times are longer than the fluorometallic.

### 6.13.2 Image Processing

A more general approach to improvement of radiographs is image processing which covers the gamut of techniques currently available for improving data retrieval from the radiographic image. (6.13.3) Figure 6.13.1 lists these

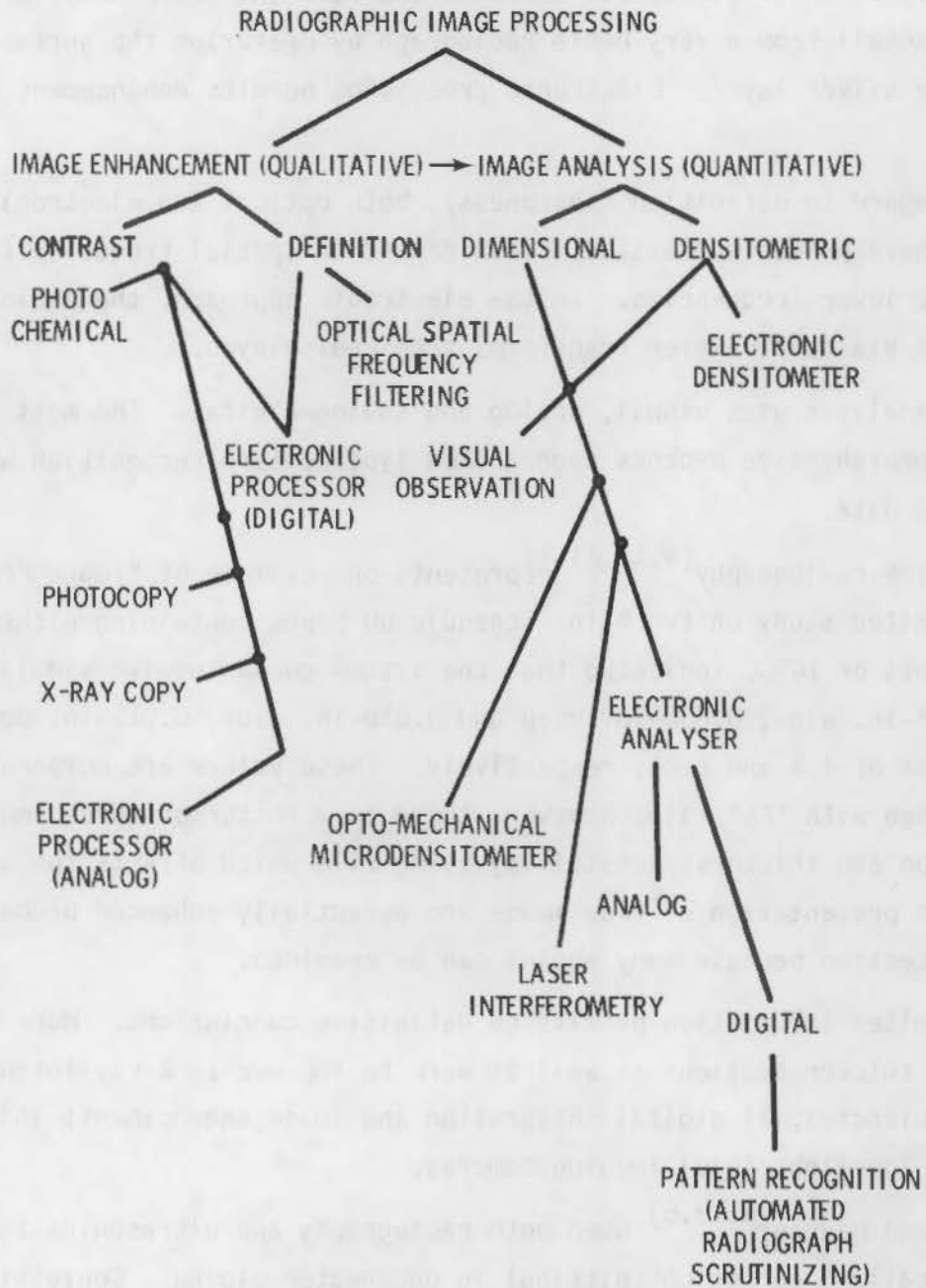


**FIGURE 6.13.1.** Radiographic Image Processing

techniques as well as illustrating the interaction among the techniques. This figure provides an excellent overview of the content of the report.<sup>(6.13.3)</sup>

For example, in the contrast area chemical reprocessing uses reducers to get rid of fog on the image and intensifiers are used to enhance low film densities. Similarly, photocopying may either reduce or intensify. X-ray copying permits delineation of burned out areas on the film and laser interferometry can obtain detail from a very dense radiograph by measuring the surface contours of the silver layer. Electronic processing permits enhancement of contrast.

With regard to definition (sharpness), both optical and electronic approaches have proven successful. Both depend on spatial frequency filtering to attenuate lower frequencies. In the electronic approach, the analog signal is digitized via fast Fourier transform, then redisplayed.

Image analysis uses visual, analog and analog-digital. The most sophisticated and comprehensive depends upon an ALN type pattern recognition with computer stored data.

Real-time radiography<sup>(6.13.4)</sup> represents one example of "Image Processing." A limited study on two 4-in. Schedule 80 pipes containing either machined slots or IGSCC indicated that the system could resolve simulated cracks 0.008-in. wide, 0.030-in. deep and 0.010-in. wide, 0.015-in. deep, or sensitivities of 4.4 and 2.2%, respectively. These values are comparable to those obtained with "AA" film; however, there is a factor of three improvement in resolution and thickness sensitivity using film which offsets the advantages of immediate presentation of flaw image and potentially enhanced probability of crack detection because many angles can be examined.

The limited information permits no definitive conclusions. More work is required on thicker sections as well as work to improve 1) X-ray intensifying screen efficiencies; 2) digital integration and image enhancement; and 3) improved low-light level imaging cameras.

Forli and Haugen<sup>(6.13.5)</sup> used both radiography and ultrasonics to detect and size localized corrosion (pitting) in underwater piping. Conventional RT and UT were used; however, the pits were accentuated by making differential



density measurements on the RT film, digitizing the data then projecting it as a pseudo-three dimensional picture. A similar approach was used for UT, where the signals were deconvoluted to differentiate the front from the rear-face signals by phase difference. This approach permits isolation of the corrosion surface signals. If 45° shear is used, pit sizes less than the UT beam diameter can be detected.

### 6.13.3 Neutron Radiography

Neutron radiography should have limited, but specific, applications to reactor systems. A report<sup>(6.13.6)</sup> summarized applications below where the large difference in attenuation coefficients between neutrons and photons can be exploited:

1. radiography of highly radioactive objects such as nuclear fuel and other reactor components
2. imaging of hydrogenous materials such as seals, gaskets, explosive charges, aluminum corrosion, plastic components, oil, and grease
3. imaging of materials in which one constituent such as boron, cadmium, or gadolinium shows particularly high neutron absorption. (This marker or contrast agent may be added deliberately, as in radiography of aeroturbine blades, for any residue of gadolinium oxide doped casting cores.)
4. imaging of materials such as those in 2 and 3, embedded in or hidden by appreciable thicknesses of heavy metals, such as copper, brass, lead, and, to some extent, steel, with notably low neutron attenuation
5. testing of materials such as nuclear fuel and reactor control elements in which the correct balance of an element's isotopes is important.

Of these five the first represents the one directly applicable to this "white paper." Either vessel or piping system that have become highly radioactive may utilize neutron radiography.

#### 6.13.4 Sizing

Sizing of defects with radiography have been reported in other chapters, notably in Chapter 5. The intent here is to examine results exclusively covering radiography in contrast to comparisons of UT versus RT. Halmshaw<sup>(6.13.7)</sup> describes two techniques for determining the height of a defect. One represents work of the author<sup>(6.13.7)</sup>; the other described by him is the work of Yokota and Ishii<sup>(6.13.8)</sup> discussed further. A densitometric method proposed by Halmshaw<sup>(6.13.7)</sup> is limited in practice to the measurement of the through-thickness dimensions of defects which are substantially wider than the unsharpness. Correction of unsharpness is too complicated to be reliable; however, it can be used for defects such as gas cavities, corrosion pits and very wide cracks. This procedure would have little application for tighter cracks.

The Japanese technique<sup>(6.13.8)</sup> is applicable to tighter cracks. A spectrum of artificial cracks was examined ranging in depth from 0.5 to 5 mm and in width from 0.01 to 0.08 mm and lengths of 10 mm plus one natural crack. The data are plotted extensively. Figure 6.13.2 illustrates the technique used in sizing. The two angles used with the RT beam permit accurate sizing.

Crack detectability depends on the geometric unsharpness ( $U_g$ ) which in turn is related to the focal spot ( $f$ ) size, distance from source to flaw ( $L_1$ ) and from flaw to film ( $L_2$ ) or

$$U_g = f (L_2/L_1)$$

An example of detectability of a natural crack is given in Figure 6.13.3. Finally, one of several relations of measured versus actual crack height is given in Figure 6.13.4. With tight cracks there is a tendency to underestimate flaw depths substantially.

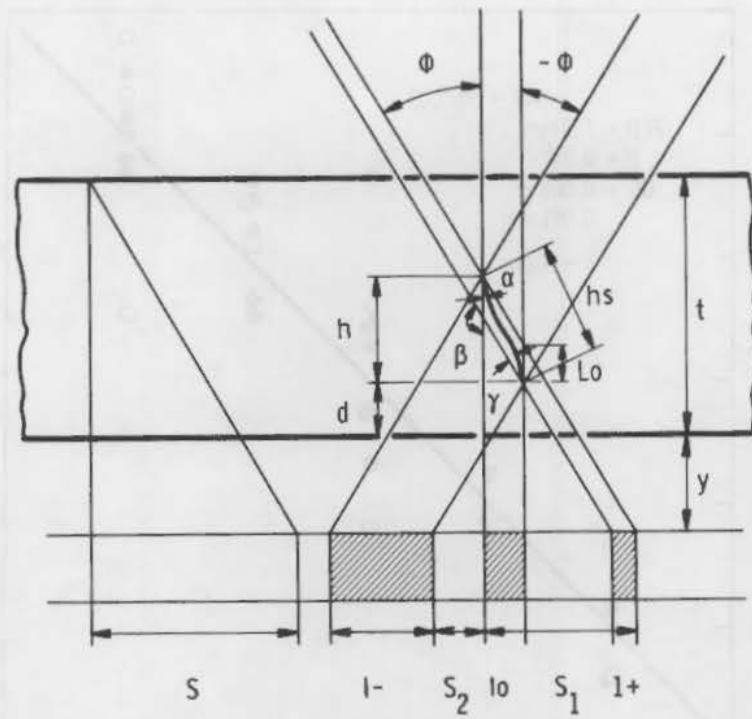


FIGURE 6.13.2. Measurement Method for Crack Height for an Angled Crack

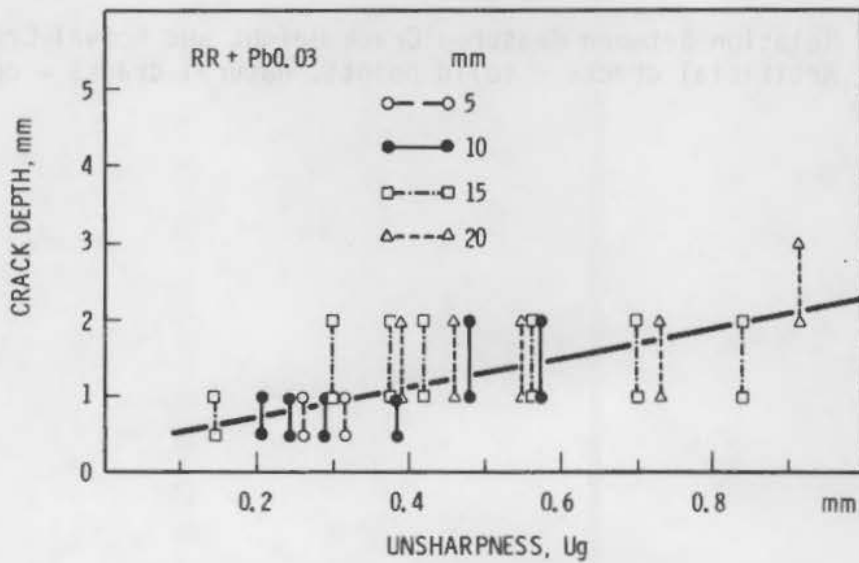
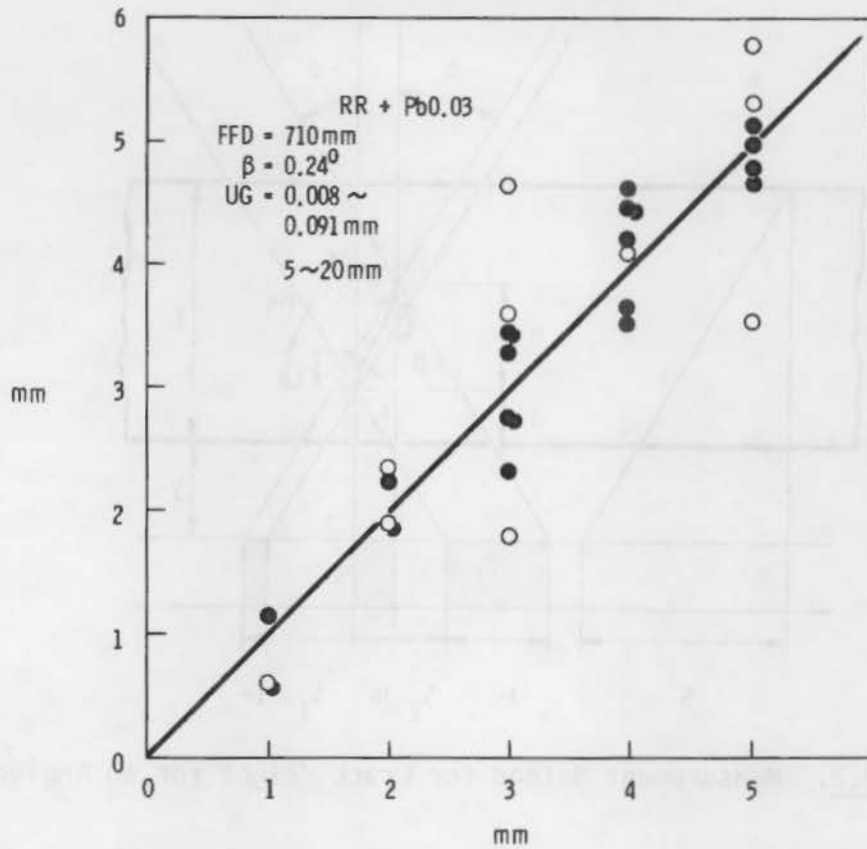


FIGURE 6.13.3. Detectability of Cracks Influenced by Geometric Unsharpness; Natural Crack; Plate Thickness 5, 10, 15, 20 mm



**FIGURE 6.13.4.** Relation Between Measured Crack Height and Actual Crack Height. Artificial cracks - solid points; natural cracks = open points.

The principal use of eddy current has been in the examination of steam generator tubing. While there may be other applications in nuclear systems, this is the most obvious. Several variations exist in such equipment. For example, there are single frequency systems and multi-frequency systems, and single or multi-parametric systems usually combined with one or more of the frequency combinations. Other variables relate to coil design, including rotating pancake coils. Another modification pertains to the manipulation of the data. Utilization of the ALN for this purpose has been investigated to a limited degree and is cited briefly in 6.14.1.

#### 6.14.1 Alternative Eddy Current Systems

A significant paper comparing four competitive systems was presented in 1978. (6.14.1) The same information has appeared in EPRI NP-636. A panel of NDE experts reviewed the testing of four different ET systems:

1. Zetec--a single frequency (state-of-the-art) unit operable at 100, 225, 400 KHz. (A rotating coil was examined also.)
2. Holosonics/Intercontrole--a French state-of-the-art three-frequency unit; manual data analysis used. (Design presumably minimized effects of variations due to tube supports and internal tubing diameters.)
3. Battelle-Northwest--a multi-frequency, multi-parametric unit now under development; using a modified Zetec probe. [Four frequencies (100, 200, 300, 400 KHz) are used; both manual and automated analysis are possible; again the unit was presumed to minimize the interference effects of tube supports and probe wobble.]
4. Failure Analysis Associates/Reluxtrol--a new approach using controlled reluctance probes to achieve high axial resolution for analysis of flaws near tube supports or in dented regions. (This is a single frequency unit.)

These four systems were examined with respect to their ability to do the following:

- How successfully they can detect large and small defects in straight sections of tubing.
- How well they can detect and characterize defects near tube supports.
- How well they can estimate the depth of defects as a percentage of tube wall.
- How well they can detect and characterize defects located in small dents.

A steam generator mockup was used for the testing. The tubes contained a variety of axial and circumferential EDM notches varying in length and depth as well as natural defects such as wastage.

Straight Sections. Wastage was relatively easy to detect even when relatively limited in depth. While some systems performed somewhat better, the differences were trivial.

Axial notches on the O.D., when relatively long (0.125 to 0.5 in.), were found with high reliability at 20 to 30% wall depth. The Holosonics/Intercontrole and Battelle-Northwest systems were essentially similar and better than Zetec for similar probe fill factors. The Zetec unit improved markedly when the fill factors were increased from 86 to 94%. Shorter notches were detected with lower reliability by the Zetec unit even with 94% fill factor.

Tube Support Effects. Figure 6.14.1 from Reference 6.14.1 permits a comparison of reliability of sizing of various defects by the different types of equipment. As noted previously, wastage can be detected with a high reliability; however, as noted in Figure 6.14.1, the accuracy of sizing is quite variable. There were both underpredictions and overpredictions of size with no obvious pattern. No system yielded consistent results.

With regard to an axial O.D. notch, only Reluxtrol detected and sized the notch; however, the size was substantially underpredicted.

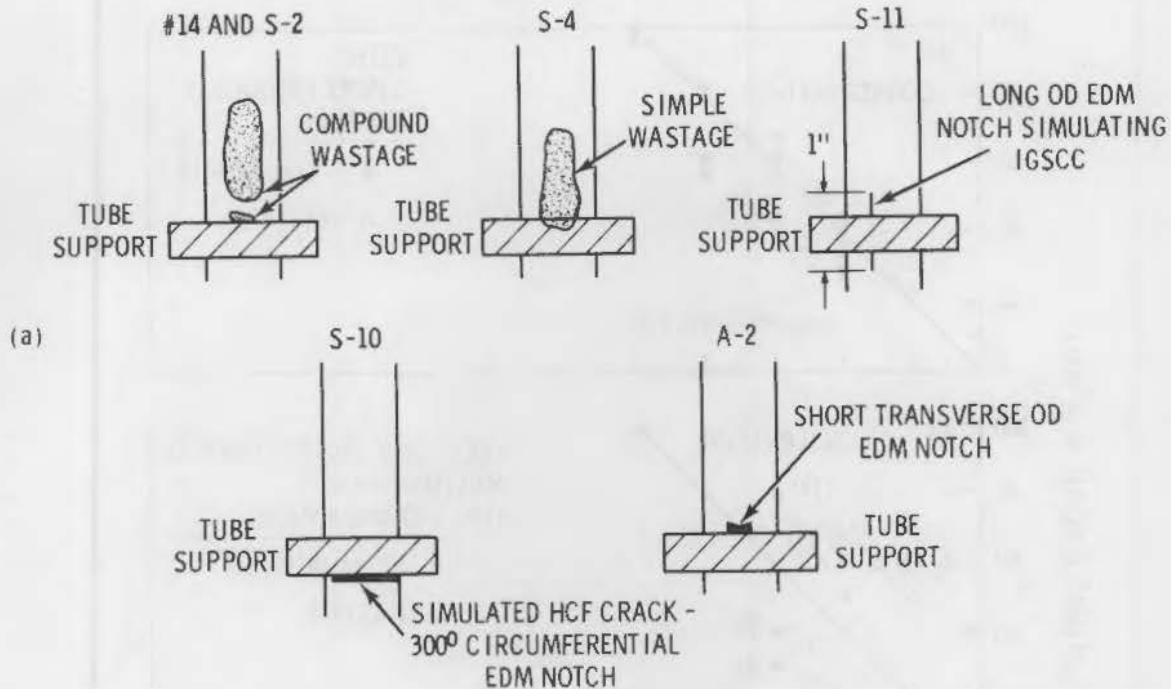


FIGURE 6.14.1. Summary of a) Small and b) Large Dent, Eddy Current Flow Assessment Data

Circumferential O.D. notches, either long transverse or short transverse, were very difficult to detect. Only the Holosonics/Intercontrolle unit detected the long transverse notch; only Reluxtrol detected the short transverse notch. Both approximated the size quite well, which could be happenstance.

Sizing. An underestimation of defect depths may represent a safety problem. An overestimation could result in the premature or unnecessary plugging of tubes. Figure 6.14.2 (Reference 6.14.1) permits a comparison of the Zetec, Holosonics/Intercontrolle and BNW systems. The Zetec system tended to be quite consistent possibly due to operator experience. The Holosonics/Intercontrolle tended to be a shotgun pattern while the BNW system tended to underpredict sizes.

Denting. The ability to detect cracks within regions of denting is a complex problem. Probably Zetec is the only company with substantial experience in examining such defects in the field. Table 6.14.1 permits an intercomparison with respect to both small and large dents. The rotating probe did yield fair to good results.

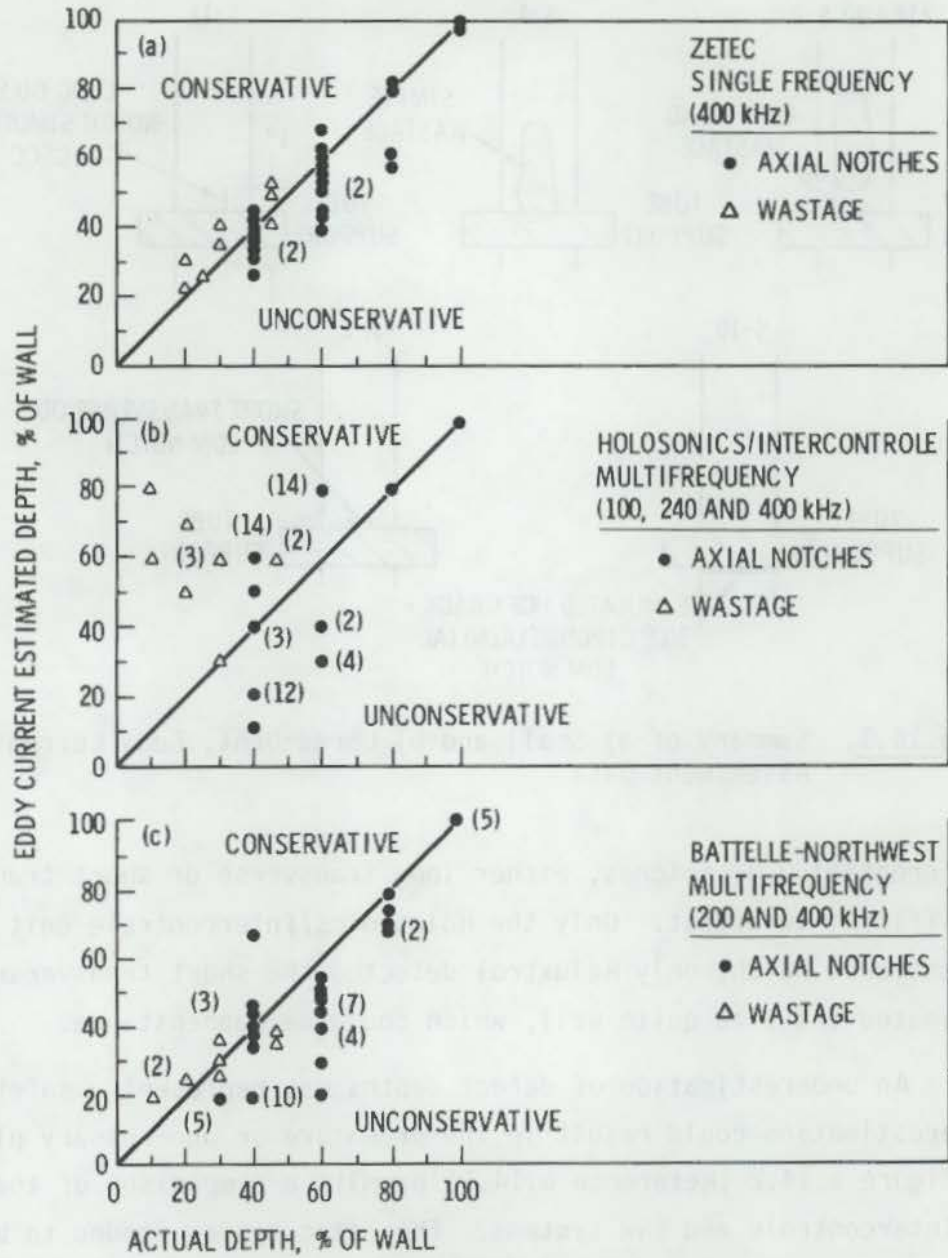


FIGURE 6.14.2. Eddy Current Estimated Depth Versus True Depth Wastage and Axial Notches

Conclusions. Since this study made so extensive a comparison of the various units, the conclusions are quite pertinent and are given verbatim:

In isolated sections of steam generator tubing free of extraneous test variables the detection capability of both single and multi-frequency methods can be equivalent. The use of low inspection frequencies, i.e., 200 to 225 KHz for 0.050-in. wall tube, is the significant factor.



TABLE 6.14.1. Summary of Tube Support Defect Detectability, and Measurement Data for Eddy Current Using Various Types of Equipment

Test Specimen	Defect Depth, % of Tube Wall	Eddy Current Estimated Depth, % of Tube Wall			
		Zetec (1f)	Holosonics Intercontrol (3f)	Battelle-Northwest (2f)	Reluxtrol (1f)
#14	20	34	60	20	No Data
S-2	60	42	65	56	53
S-4	60	82	70	20	45
S-11	60	ND	D	ND	30
S-10	60	ND	50	ND	ND
A-2	60	ND	ND	ND	50

NOTES: D - Detected, no depth reported.  
 ND - Not detected.

Multi-frequency methods have not demonstrated an advantage in defect depth measurement accuracy or precision. Measurement precision in the more important methods and the lack of precision in multi-frequency methods may result from a compression of the phase angle versus depth calibration curve. The conventional single frequency 400 KHz curve has a phase spread of approximately 140° between a 100% and 20% through wall O.D. discontinuity. For the multi-frequency systems considered in this evaluation, the phase spread varied between 55° to 90° for comparable ranges in defect depth. Thus, small variations in assigning the appropriate phase angle to the eddy current Lissajous pattern can give rise to large variations in estimated defect depth.

Single frequency eddy current inspection methods provide conservative estimates of larger volume wastage defects and unconservative estimates of small volume crack-like defects when an ASME Section XI standard is used for the establishment of phase angle versus depth calibration curve. This would suggest the existence of two different plugging criteria and also imply that the eddy current data analyst can discriminate between wastage and crack-like defects.

Multi-frequency methods demonstrate a better ability to detect defects in the tube support region than conventional single frequency inservice inspection techniques. However, on an overall percentage basis, the single frequency high resolution coil demonstrates equivalent results.

For small dents, existing single frequency bobbin-coil inspection methods are inadequate for small volume defect detection. The single frequency high axial resolution coil, the rotating coil, and multi-frequency methods offer significant advantages. For large or ovalized dents, the rotating probe is the only demonstrated inspection method.

Multi-Frequency Unit. A somewhat later study<sup>(6.14.2)</sup> of the BNW multi-frequency unit incorporating both differential and absolute examination modes indicated an improved capability with respect to both earlier multi-frequency units and single frequency units. Some specific advantages cited were as follows:

- a three- to five-fold reduction of error in assessing depth of flaws
- a 90 to 95% reduction of indications from tube supports
- an 85 to 90% reduction of probe wobble effects
- a flaw depth sensitivity equivalent to that of the conventional single frequency test
- continuous profiling of flaws and tubing wall thickness
- characterization of support corrosion and cracking, even in dented tubes
- detection and sizing of medium and large wastage flaws in dented regions.

Results with both elliptical wastage and uniform thinning indicate a reduction in scatter with the multi-frequency unit compared to a single frequency unit; however, the single frequency scatter appeared to be within reasonable limits.

#### 6.14.2 Eddy Current--ALN

A somewhat preliminary study used ALN to discriminate flaws from artifacts.<sup>(6.14.3)</sup> In addition, an attempt was made to accurately measure the depths of simulated pits and cracks using EDM notches and flat-bottomed holes, all in the outer surface for these simulated defects. The ALN system could discriminate between simulated pits and cracks regardless of tube support

plates using both single frequency (400 KHz) and multi-frequency (200 and 400 KHz). Simulated pit sizes were estimated with average absolute errors of 12% with the single frequency unit and  $\pm 2.4\%$  with the multi-frequency unit. In the case of simulated cracks, the average absolute error was 3.6% for the single frequency units and 2.6% for the multi-frequency unit.

While these results are quite impressive, we must recall that the study was limited to simulated defects. The real test will be using the system on actual not simulated defects.

11110  
11111  
11112  
11113  
11114  
11115  
11116  
11117  
11118  
11119  
11120  
11121  
11122  
11123  
11124  
11125  
11126  
11127  
11128  
11129  
11130  
11131  
11132  
11133  
11134  
11135  
11136  
11137  
11138  
11139  
11140  
11141  
11142  
11143  
11144  
11145  
11146  
11147  
11148  
11149  
11150  
11151  
11152  
11153  
11154  
11155  
11156  
11157  
11158  
11159  
11160  
11161  
11162  
11163  
11164  
11165  
11166  
11167  
11168  
11169  
11170  
11171  
11172  
11173  
11174  
11175  
11176  
11177  
11178  
11179  
11180  
11181  
11182  
11183  
11184  
11185  
11186  
11187  
11188  
11189  
11190  
11191  
11192  
11193  
11194  
11195  
11196  
11197  
11198  
11199  
11200

Holographic interferometry combined with laser speckle photographs provide a method to record and evaluate embedded defects as well as surface defects. (6.15.1,6.15.2,6.15.3) Essentially, the procedure consists of a double exposure on film. The first exposure records the initial positions of "speckles," which are minor geometric surface variations highlighted by laser illumination. (6.15.1) These "speckles" may be further highlighted, if necessary, by thin coatings. A second exposure is made after loading the system. This loading results in Young's fringes, providing the movement of the system exceeds the speckle size; hence, the term interferometric holography.

This technique can be used on internally pressurized systems, (6.15.1) vibrating components, (6.15.2) and statically and dynamically loaded beams, (6.15.3) etc. Applications directly relevant to nuclear systems are covered in References 6.15.1 and 6.15.3.

An example of a typical interferometric pattern on pressure piping is given in Figure 6.15.1.

Some real or potential advantages of this technique are listed:

- A permanent record can be made of the system status at beginning of life.
- A dynamic record can be made by recording on movie film to reproduce movement of fringes.
- Complex shapes, such as pump and valve bodies, can be examined without disassembly.
- In situ remote testing is possible without operator exposure; the producer is noncontacting.
- The holographic system generally reduces chances of missing defects.
- No special cleaning or treatment of the surface contamination such as dust or rust is necessary; in fact, surface finish has little or no effect. At most, the surface may be whitened somewhat to enhance fringe contrast.

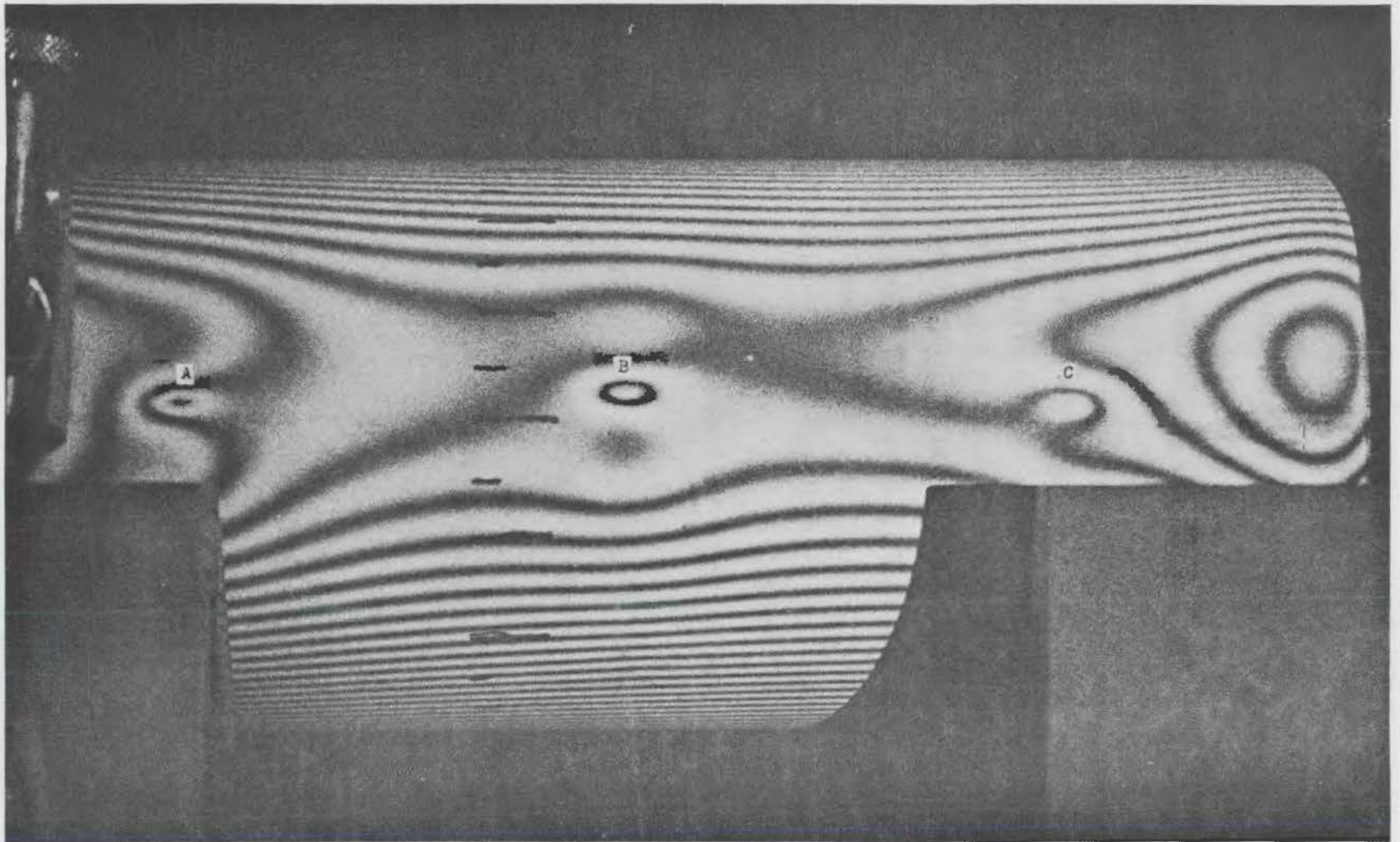


FIGURE 6.15.1. An Example of a Double Exposure Hologram Obtained with Laser Holographic Interferometry Illustrating Defects in a Tube Pressurized to  $4.14 \text{ MN/m}^2$

- Pulsed lasers permit measurement of very rapid changes in load, etc.
- Many measurements can be obtained within the field of view of the film.
- It is possible to determine both the direction of movement and the components of this motion.
- Strain gages which are susceptible to damage and failure are not used.

The preceding list is quite impressive; however, there are some limitations which must be considered:

- Differential movement, if excessive, may interfere with stability, causing difficulties in fringe interpretation; therefore, local vibrations must be minimized.
- Since detection relies on a change in movement of a surface due to some form of loading, it is necessary to apply some load vibration, mechanical pressure, vacuum, temperature, etc., which can be used and the load may be relatively small; since we are concerned with systems underload, this is not a very severe limitation.
- Immediate results such as are obtained with strain gages cannot be achieved at this time.
- Fringe recording and analyses can be a tedious and time consuming operation, particularly if many measurements are required.

One study used 100-mm O.D. mild steel tubes.<sup>(6.15.1)</sup> Some of the tubes contained spark eroded notches on the inner surface. This technique permitted a calibration of the fringes. Some idea of lower limits of detection of flaws in such tubes is given in Figure 6.15.2. Another series of experiments measured the accuracy and sensitivity of detection of small lateral deflections. These are given in Table 6.15.1.

Reference 6.15.1 develops the calculational procedure for determining the movement of a surface, a crack, etc. The formula used is

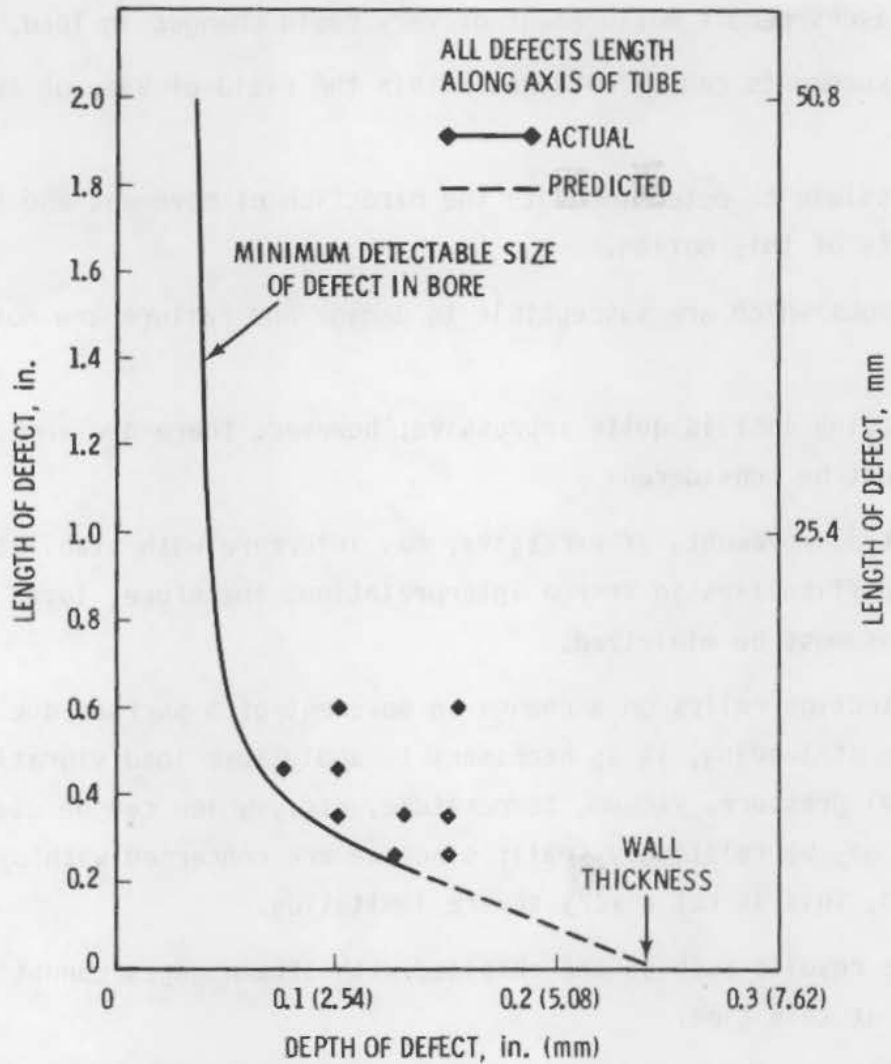


FIGURE 6.15.2. Holographic Defect Detection Limits in Tube (101-mm O.D. x 6.35-mm wall)

TABLE 6.15.1. Comparison of Lateral Displacement Determined by Dial Gage, by Theory, and by Laser Speckle Photography

Dial Gage	Theoretical	Photography
0.006934	0.0067168	0.00787



$$\text{Movement } D = \frac{nm\lambda}{\sin \alpha} \quad (6.15.1)$$

where  $n$  = fringe order number

$m$  = demagnification factor

$\lambda$  = wave length of light used

$\alpha$  = angle subtended by fringes to point on photographic plate.

A specific application of laser interferometric holography is cited by Archbold and Ennis.<sup>(6.15.3)</sup> In this instance, an actual flaw was found in a load-bearing structural component (a box-section found by the welding of four thick steel plates) in a large mechanical testing machine. Since the machine was in daily use, the preferred procedure was to monitor the flaw, a crack in one of the fillet welds. Laser interferometric photography was selected to record the growth of the crack on a semi-continuous basis. The accuracy in this specific application was  $\pm 2 \mu\text{m}$ . Figure 6.15.3 illustrates the relative vertical and horizontal movement of crack edges under load. As noted, movement could not be seen for loads less than 500 KN.

This procedure appears to have a definite potential in regions of difficult accessibility where repair would be quite difficult and where it can be rationalized that continuous monitoring of a defect will give adequate early warning if the defect begins to grow.

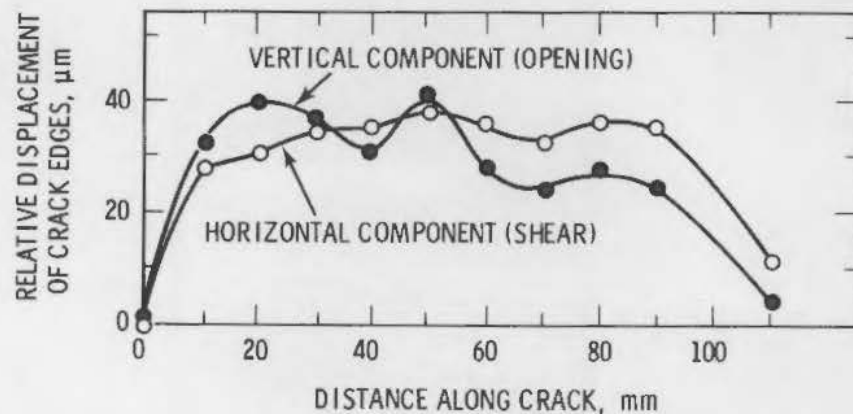


FIGURE 6.15.3. Relative Vertical and Horizontal Movement of Crack Edges Along Crack

$$f(x) = \frac{1}{2} \left( \frac{x}{a} + \frac{x}{b} \right)$$

where  $f$  = total order number  
 $n$  = domain (total order factor)  
 $x$  = value length of first row  
 $a$  = value length of first row  
 $b$  = value length of first row

A specific application of laser interferometric holography is called by  
architectural holo. In this instance, an optical film was used to  
copy the surface of a component (a 100-ohm resistor) by the reflection of  
light from a plane (in a 100-ohm resistor) in the distance. Since the surface  
was not flat, the pattern produced was in reality the film, a trace in  
one of the film's edges. Laser light interferometry was used to  
copy the pattern of the glass on a flat surface. The accuracy in  
this specific application was 70 microns (0.0027 inches) for relative  
vertical and horizontal movement of crack edges after load. At initial, movement  
could not be seen for loads less than 500 lb.

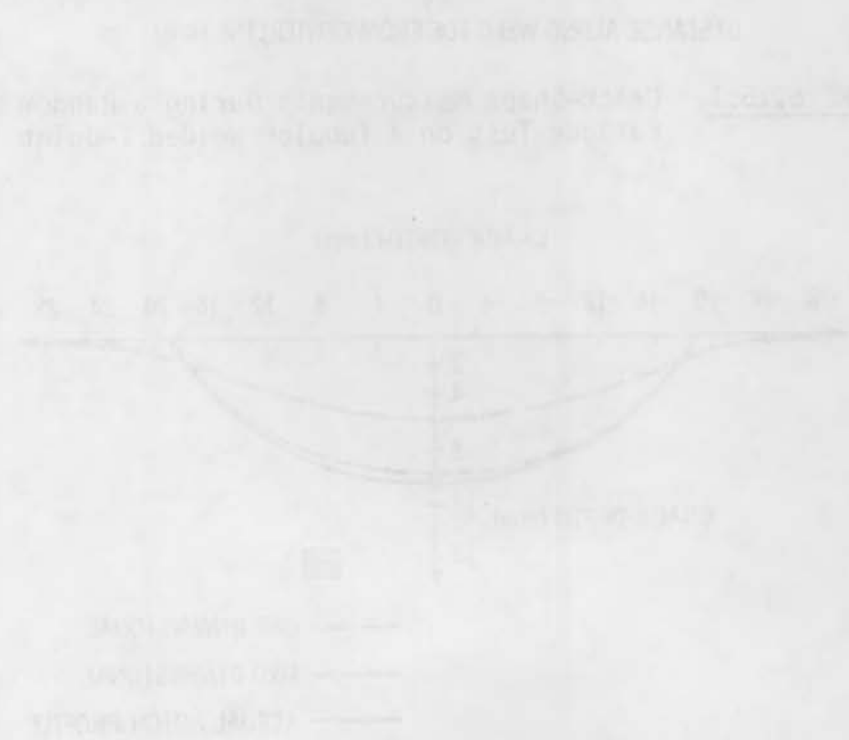
This experiment appears to have a lot more potential in regions of stress  
and discontinuity where there would be large distortions and where it had no  
potential that the continuous monitoring of a defect with the advanced early  
warning in the early stages is given.



Figure 11.11.1. Vertical and horizontal movement of crack edges after load. At initial, movement could not be seen for loads less than 500 lb.

An extension of infrared electrothermal NDE is the use of alternating currents to develop AC electric fields that predict surface flaw geometry and size quite well. Work of Dover and Collins<sup>(6.16.1)</sup> appears pertinent to complex geometrics. Figure 6.16.1, from their paper, illustrates crack shapes in tubular welded T-joints. An example of signals interpreted either one-dimensionally or two-dimensionally and compared to an actual notch profile is given in Figure 6.16.2. The paper presents details of the electrical fields schematically for those interested as well as citing further references.

An extension of the preceding work is given in a paper by Haugen and Moe<sup>(6.16.2)</sup> who use AC potential drop to monitor fatigue crack growth. The authors believe the techniques yield more reliable results than actual measurements of crack depth. Confirmation of signal was done by breaking specimens. Figure 6.16.3 presents fatigue crack measurements.



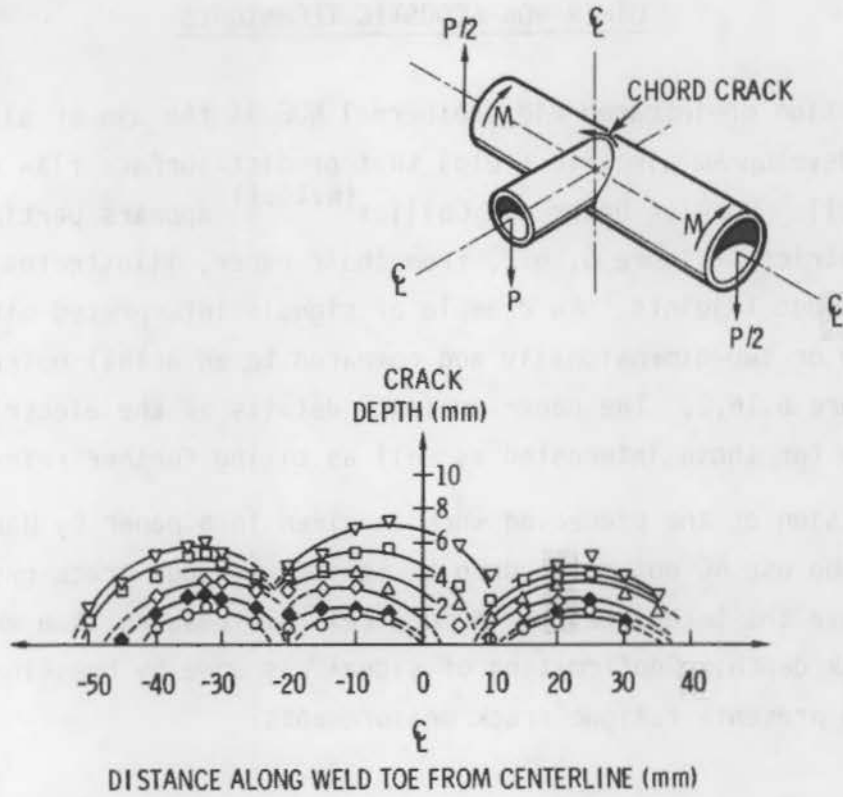


FIGURE 6.16.1. Crack-Shape Measurements During a Random Load Fatigue Test on a Tubular Welded T-Joint

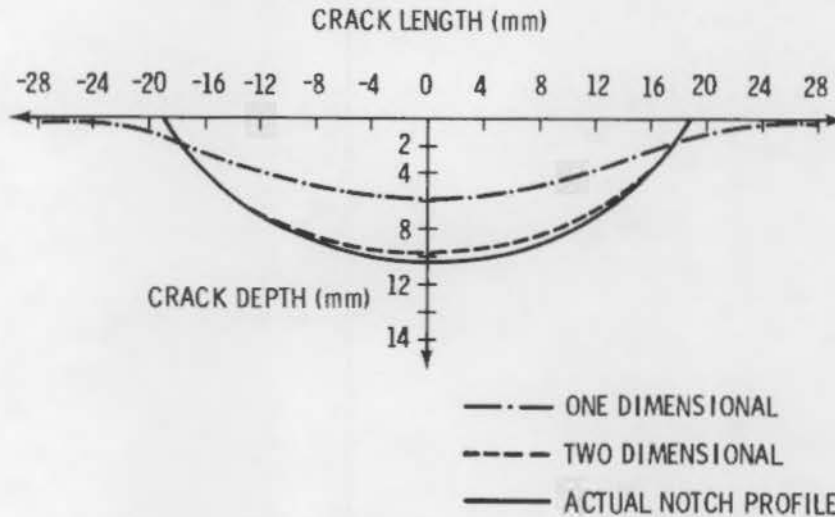


FIGURE 6.16.2. One- and Two-Dimensional Interpretations of the Voltage Ratio for a Circular Arc Notch in a Steel Plate

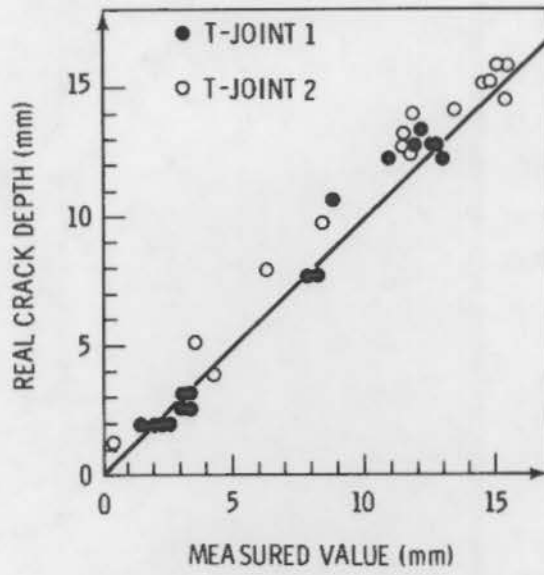


FIGURE 6.16.3. AC-Potential Drop Measurements of Fatigue Cracks in T-Joints; Cracks Located at the Weld Toe

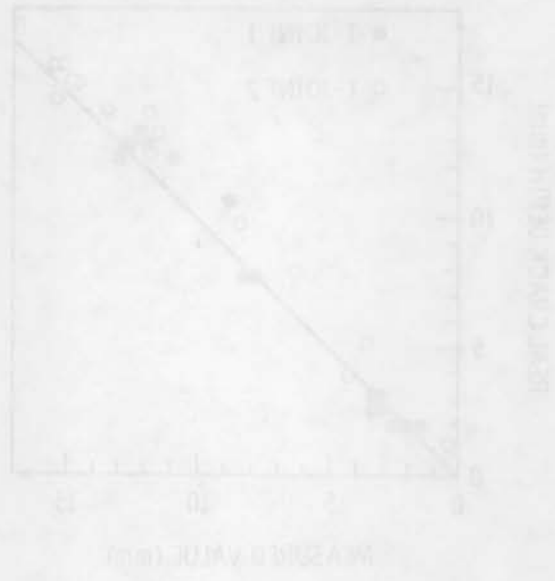


FIGURE 6.18.3. All-terrain-type Measurements of Fatigue Cracks  
 1-7 meters; Cracks located at the joints

- Focused transducers appear to have considerable promise in the sizing of embedded flaws; however, their accuracy in bimetallic and trimetallic welds, or in coarse-grained dendritic austenitic structures has not been established.
- New techniques such as scattered, diffracted and mode-converted amplitude, either in conventional signal or in the time domain, have not been proven experimentally so that their potential is not known.
- The various time domain techniques appear to yield very high accuracies insofar as flaw sizing is concerned. However, work is inadequate to permit a definitive evaluation. Limitations in surface waves exist because the flaw length rather than depth is measured; surface irregularities may prove to be a major limitation and a multiplicity of waves, both shear and surface, can be generated leading to confusion in the time measurements.
- Results in the frequency domain using ALN have been very successful under certain circumstances; however, insufficient work has been done on coarse-grained dendritic austenitic weldments to permit a quantification of ANL's success ratio. The adverse effects of dendrites, weld-base metal interface, and external geometry need quantification.
- Results with ALN on austenitic weldments containing intergranular stress corrosion cracking (IGSCC) have been excellent on limited specimens. Again the caveats cited in the preceding conclusion above need to be examined.
- While excellent results have been obtained with acoustic holography and SAFT-UT in sizing defects, such success has been under specific conditions. In bimetallic and trimetallic weldments, changes in wavelength, velocity, and beam angle should adversely influence sizing accuracy. In some instances, known defects have not been detected. The reason for this lack of detection should be quantified.

- Acoustic emission is a potentially powerful tool for the continuous monitoring of crack growth; however, AE is not completely dependable so its probable role appears to be as a complementary tool to other NDE techniques.
- Infrared electro-thermal NDE appears to have limited application to pressure systems. One possibility would be in coarse-grained dendritic structures where UT attenuation is too great to permit flaw detection.
- Electro-magnetic leakage techniques would appear to have limited application to pressure boundaries. While they probably could detect flaws, the interpretation of sizing is dubious. Considerable work would be necessary to correlate signals with a spectrum of flaw sizes and geometries; however, there does not appear to be sufficient incentive insofar as major benefits in detection and sizing to lead to promotion of the technique.
- Radiographic techniques appear to be undergoing a renaissance primarily because of the new high intensity accelerators. Areas with major potential include intensifier screens and some of the digital image enhancement techniques.



The same problem seems to relate to many of the advanced NDE techniques such as time domain, focused transducers, adaptive learning, acoustic holography, SAFT-UT, etc.; namely, their applicability to bimetallic or trimetallic weldments and to coarse-grained dendritic austenitic weldments has not been established. Problems such as change in wavelength, change in velocity, probe angle shift, beam attenuation, etc., need to be examined and their adverse effects quantified. Since such weldments are relatively common in many nuclear reactors, they represent a potential limitation. A controlled program utilizing existing data and developing samples for examination appears essential.



- 6.2.1 Becker, F. L., et al., "Development of an Ultrasonic Imaging System for the Inspection of Nuclear Reactor Pressure Vessels." Third Progress Report prepared for Electric Power Research Institute by Battelle, Pacific Northwest Laboratories, Richland, Washington, July 1, 1977 to September 15, 1977.
- 6.2.2 Becker, F. L., et al., "Development of an Ultrasonic Imaging System for the Inspection of Nuclear Reactor Pressure Vessels." Fourth Progress Report prepared for Electric Power Research Institute by Battelle, Pacific Northwest Laboratories, Richland, Washington, September 15, 1977 to September 15, 1978.
- 6.2.3 Linzer, M., Dietz, D. and Parks, S. I., "Development of High Sensitivity Ultrasonic Techniques for In-Service Inspection of Nuclear Reactors." NUREG/CR-0560, U.S. Nuclear Regulatory Commission, Washington, D.C., October 1978.
- 6.2.4 Huard, J., et al., "Utilization of Focused Ultrasonic Transducers for Measurement of Defects." DMECN-DT-ECS-STA NT 112, February 1973.
- 6.2.5 Monnier, P., et al., "Comparison of Different Methods of Measuring Defects by Ultrasonics in a Weld of Great Thickness." DMECN-DT-ECS-STA NT-201, February 1976.
- 6.2.6 Saglio, R., "Better Detection of Large Poorly Oriented Plane Defects by Ultrasonics." NDT Int., pp. 193-196, August 1976.
- 6.2.7 Schlengerman, U. and Frielinghaus, R., "Remarks on the Practice of Determining the Size of Reflectors by Scanning." Br. J. Nondestr. Test., pp. 9-13, January 1978.
- 6.2.8 Saglio, R., Prot, A. C. and Touffait, A. M., "Determination of Defect Characteristics Using Focused Probes." Mater. Eval., pp. 62-66, January 1978.
- 6.2.9 Silk, M. G., "New Approaches to Crack Sizing by Ultrasonics." Recent Developments in Non-Destructive Testing, Welding Journal, American Welding Society, pp. 40-45, 1978.
- 6.2.10 Doyle, P. A. and Scala, C. M., "Crack Depth Measurement by Ultrasonics: A Review." Ultrasonics, pp. 164-170, July 1978.
- 6.2.11 Underwood, J. H., Winters, D. C. and Kendall, D. P., "End-On Ultrasonic Crack Measurements in Steel Fracture Toughness Specimens and Thick-Wall Cylinders." The Detection and Measurement of Cracks, Welding Journal, American Welding Society, pp. 31-39, 1976.

- 6.2.12 Golan, S., "Optimization of the Crack Tip Ultrasonic Diffraction Technique for Sizing of Cracks." Mater. Eval., pp. 166-169, February 1981.
- 6.2.13 Silk, M. G., "The Transfer of Ultrasonic Energy in the Diffraction Technique for Crack Sizing." Ultrasonics, pp. 113-121, May 1979.
- 6.3.1 Gruber, G. J., "Defect Identification and Sizing by the Ultrasonic Satellite-Pulse Technique." J. Non-Destr. Eval. 1(4):263-276, 1980.
- 6.4.1 Gurvich, A. K. and Kuzmina, L. I., "Scattering Indicatrix as a Source of Additional Information on Detected Defects." Sov. J. Nondestr. Test., pp. 670-672, November-December 1970.
- 6.4.2 Vopilkin, A. K., Ermolov, I. N. and Staseev, V. G., "Experimental Investigation of an Ultrasonic Spectral Method of Determining the Nature of Defects." Sov. J. Nondestr. Test. 14, pp. 34-43, 1978.
- 6.4.3 Peterson, R. O., Spanner, J. C. and Mech, S. J., "Developments of Ultrasonic Methods for Examining Stainless Steel Welds--Interim Progress Report." HEDL-TME-75-134, Hanford Engineering Development Laboratory, Richland, Washington, November 1975.
- 6.4.4 Mech, S. J., et al., "Development of Ultrasonic Examination Methods for Austenitic Stainless Steel Weld Inspection." HEDL-SA-1348, Hanford Engineering Development Laboratory, Richland, Washington, August 1977.
- 6.4.5 Shankar, R., et al., "Adaptive Nonlinear Signal Processing for Characterization of Ultrasonic NDE Waveform Task 2: Measurement of Subsurface Fatigue Crack Size." AFML-TR-76-44, USAF Technical Report, June 1976.
- 6.4.6 Kupperman, D. S. and Reimann, K. J., "Microstructural Effects and Signal Enhancement Techniques in Ultrasonic Examination of Stainless Steel." ANL-76-115, Argonne National Laboratory, September 1976.
- 6.4.7 Adler, L., et al., "Flaw Size Measurement in a Weld Sample by Ultrasonics Frequency Analysis." Mater. Eval., pp. 44-50, March 1977.
- 6.4.8 Rose, J. L., "A 23 Flaw Sorting Study in Ultrasonics and Pattern Recognition." Mater. Eval., pp. 87-96, July 1977.
- 6.4.9 Shankar, R., et al., "Development of Adaptive Learning Networks for Pipe Inspection." NP-688, Electric Power Research Institute, Palo Alto, California, March 1978.
- 6.4.10 Rose, J. L. and Singh, G. P., "Ultrasonic Pattern Recognition Study of Intergranular Stress Corrosion Cracks versus Weld Crown Reflectors in Stainless Steel Piping." NP-891, Electric Power Research Institute, Palo Alto, California, September 1978.

- 6.4.11 Whaley, J. L. and Adler, L., "Flaw Characterization by Ultrasonic Frequency Analysis." Mater. Eval., pp. 182-192, August 1971.
- 6.4.12 "A Feasibility Study of Advanced Signal Processing and Pattern Recognition for Analyzing Flaws in Stainless Steel Piping." Study to Define NDE Research for Inspection of Stainless Steels by Ultrasonics International, Inc., NP-797-SR, Electric Power Research Institute, Palo Alto, California, August 1978.
- 6.4.13 Staseev, V. G. and Ermolov, I. N., "Development of the Principles of Automatic Classification of Defects by an Ultrasonic Spectral Method." Sov. J. Nondestr. Test. 14(7):624-634, July 1978.
- 6.5.1 Elsley, R. K. and Tittmann, B. R., "Quantitative Estimation of Defect Properties by Computerized Ultrasonic Methods." 11th Symposium on Non-Destructive Evaluation, Southwest Research Institute, San Antonio, Texas, pp. 55-61, 1977.
- 6.5.2 Elsley, R. K. and Tittman, B. R., "Defect Characterization by Ultrasonic Signal Process Techniques." Proceedings of Ultrasonics Symposium, Cat. No. 77CH1264-ISU, The Institute of Electrical and Electronics Engineers, pp. 48-52, 1977.
- 6.5.3 McElroy, J. T., "Detailed Analysis of the Fundamental Ultrasonic Response Data from Stainless Steel Stress Corrosion Crack Specimens." NP-676-SR, Electric Power Research Institute, Palo Alto, California, February 1978.
- 6.5.4 Gruber, G. J., "Detection of Cracks in Bimetallic Structures by the Ultrasonic Multiple-Beams Technique." Southwest Research Institute Seminar, San Antonio, Texas, 1981.
- 6.5.5 Gruber, G. J. and Kapitza, H., "Reliability Evaluation of Six Ultrasonic Techniques for Cladded Pipe Examination." Southwest Research Institute Seminar, San Antonio, Texas, 1981.
- 6.6.1 Reinhart, E. R., "In-Service Inspection Program for Nuclear Reactor Vessels—Final Technical Report and Addendum (V-II)." Southwest Research Institute, San Antonio, Texas for Edison Electric Institute/Tennessee Valley Authority, May 21, 1973.
- 6.6.2 Collins, H. D. and Gribble, R. P., "PVRC Plate-Weld Specimen 201 Inspection by Acoustic Holography." Holosonics, Inc. Report, September 1972.
- 6.6.3 Holt, A. E., "Characterization of Defects in Thick-Walled Pressure Vessels Using Acoustic Holography." 3rd Conference on Periodic Inspection, London, England, pp. 165-171, 1976.

- 6.6.4 Holt, A. E., "The Role of Acoustical Holography in the Characterization of Defects in Thick-Section Components." NDE Conference, Babcock and Wilcox/Technischen Überwachungs Verein e.V., Rheinland Westphalia, November 18, 1976.
- 6.6.5 Sharon, G. M. and Witek, R. R., "Acoustic Holography Examination of PVRC Plate-Weld Specimen 251J." NEDO-20735, General Electric, Nuclear Energy Division, December 1974.
- 6.6.6 Ando, Y., et al., "Study of Flaw Size Measurement by Acoustical Holography." NUREG/TR-0034, U.S. Nuclear Regulatory Commission, Washington, D.C., August 1978.
- 6.6.7 Holt, A. and Brophy, J. "Defect Characterization by Acoustic Holography." Volume 1: Imaging in Field Environments, NP-1534, Research Project 605-1, Electric Power Research Institute, Palo Alto, California, September 1980.
- 6.6.8 Holt, A. and Brophy, J. "Defect Characterization by Acoustic Holography." Volume 2: Effects of Cladding on AH Imaging and Test-Block Results, NP-1534, Research Project 605-1, Electric Power Research Institute, Palo Alto, California, May 1981.
- 6.6.9 Yamamoto, M., et al., "A Study on the Dimensioning of Flaws by Acoustical Holography." Welding Research Abroad 25(3):2-9, March 1979. Originally Mitsubishi Heavy Industries Technical Review 15(2):42, June 1978.
- 6.6.10 Fredericks, J. R., et al., "Improved Ultrasonic Non-Destructive Testing of Pressure Vessels." NUREG/CR-0135, U.S. Nuclear Regulatory Commission, Washington, D.C., May 1978.
- 6.6.11 Jackson, J. L., "Program for Field Validation of the Synthetic Aperture Focusing Technique for Ultrasonic Testing (SAFT-UT) Midyear Progress Report." NUREG/CR-0290, U.S. Nuclear Regulatory Commission, Washington, D.C., 1978.
- 6.6.12 Hamlin, D. R. and Jackson, J. L., "Evaluation of the Synthetic Aperture Focusing Technique for Ultrasonic Testing." Southwest Research Institute Seminar, San Antonio, Texas, 1981.
- 6.7.1 Spanner, J. C., "Acoustic Emission—Some Examples of Industrial Maturity." HEDL-SA-1541 at American Society for Testing and Materials Symposium on Acoustic Emission Monitoring of Pressurized System, January 25-26, 1979.
- 6.8.1 Whittington, K. R., "Inspection with Surface and Lamb Wave EMA Techniques." Recent Developments in Non-Destructive Testing, Welding Journal, American Welding Society, 1978.

- 6.9.1 Tao, S. J., The Use of Positron Annihilation for Mapping Defects in Surface Zone. The New England Institute, Ridgefield, Connecticut, pp. 207-213, 1977.
- 6.10.1 Owen, C. K. W., Capacitance Strain Gages for Monitoring Cracks. Welding Journal, American Welding Society, pp. 2-6, 1976.
- 6.11.1 Green, D. R. and Hassberger, J. A., "Feasibility Study on Infrared Electro-Thermal NDE of Stainless Steel." HEDL-TME-75-133, Hanford Engineering Development Laboratory, Richland, Washington, November 1975.
- 6.11.2 Green, D. R., "Experimental Electro-Thermal Method for Nondestructively Testing Welds in Stainless Steel Pipes." Mater. Eval., pp. 54-60, October 1979.
- 6.12.1 Owston, C. N., "The Magnetic Flux Leakage Technique of Non-Destructive Testing." Br. J. Nondestr. Test., pp. 162-168, November 1974.
- 6.12.2 Shcherbinin, V. E. and Pashagin, A. I., "Influence of the Extension of a Defect on the Magnitude of Its Magnetic Field." Sov. J. Nondestr. Test., pp. 441-447, 1972.
- 6.13.1 Rundquist, D. E., et al., "Assessment of Thick-Section Radiography." NP-461, Electric Power Research Institute, Palo Alto, California, June 1977.
- 6.13.2 Halmsaw, R., "Fluorometallic Radiographic Intensifying Screens." Recent Developments in Non-Destructive Testing, Welding Journal, American Welding Society, pp. 2-4, 1978.
- 6.13.3 Pullen, D. A. W., "Radiographic Image Processing." Recent Developments in Non-Destructive Testing, Welding Journal, American Welding Society, pp. 5-12, 1978.
- 6.13.4 Patricelli, F., et al., "Utilization of Real-Time X-Radiography for In-Service Inspection of Nuclear Reactor Piping: Feasibility Investigation." NP-950, Electric Power Research Institute, Palo Alto, California, December 1978.
- 6.13.5 Forli, O. and Haugen, R., "Corrosion Detection by Ultrasonics and Radiography." 9th World Conference on Nondestructive Testing, 1979.
- 6.13.6 Hawkesworth, M. R., "Neutron Radiography in Industry." Recent Developments in Non-Destructive Testing, Welding Journal, American Welding Society, pp. 13-27, 1978.
- 6.13.7 Halmsaw, R., "Defect Size Measurement by Radiography." Br. J. Nondestr. Test., pp. 245-298, September 1979.

- 6.13.8 Yokota, O. and Ishii, Y. "Crack Detectability by Radiography." Br. J. Nondestr. Test., pp. 239-244, September 1979, (Originally J. NDI 27 ID, 1978).
- 6.14.1 Brown, S. D. and Reinhart, E. R., "Steam Generator Tubing Degradation." Proceedings of International Conference on Nondestructive Evaluation in the Nuclear Industry, sponsored by ASM, ASTM, ASNT, and ANS, Salt Lake City, Utah, pp. 169-190, February 13-15, 1978.
- 6.14.2 Davis, T. J., "Advances in Multi-frequency Eddy Current Instrumentation." Battelle, Pacific Northwest Laboratories, BN-SA-946, Periodic Inspection of Pressurized Components, Institute of Mechanical Engineers, London, England, pp. 1-9, May 8-10, 1979.
- 6.14.3 Shankar, R., et al., "Feasibility of Using Adaptive Learning Networks for Eddy Current Signal Analysis." NP-723 TPS 77-723, Electric Power Research Institute, Palo Alto, California, March 1978.
- 6.15.1 Martin, D. J. V., "Laser Holographic and Speckle Photography Methods for Defect Detection and Strain Evaluation in Pressure Vessels." SRD-R-60, United Kingdom Atomic Energy Authority, Harwell, England, pp. 1-30, September 1976.
- 6.15.2 Querido, R. J., "Interference Holography: A Means of Non-Destructive Testing." Recent Developments in Non-Destructive Testing, Welding Journal, American Welding Society, pp. 64-69, 1978.
- 6.15.3 Archbold, E. and Ennos, A. E., "Laser Photography to Measure the Deformation of Weld Cracks Under Load." The Detection and Measurement of Cracks, Welding Journal, American Welding Society, pp. 12-15, 1976.
- 6.16.1 Dover, W. D. and Collins, R., "Recent Advances in the Detection and Sizing of Cracks Using Alternating Current Field Measurements (A.C.F.M.)." Br. J. Nondestr. Test., pp. 291-295, November 1980.
- 6.16.2 Haugen, R. and Moe, E. T., "AC - Potential Drop Method for Fatigue Crack Monitoring in Tubular Joints." Interim paper, Det Norske Veritas, Oslo, Norway, May 9, 1980.



DISTRIBUTION

No. of  
Copies

No. of  
Copies

OFFSITE

Division of Technical Information  
and Document Control  
U.S. Nuclear Regulatory  
Commission  
7920 Norfolk Avenue  
Bethesda, MD 20014

Division of Engineering  
Technology  
Office of Nuclear Regulatory  
Research  
U.S. Nuclear Regulatory  
Commission  
Washington, DC 20555

W. F. Anderson  
U.S. Nuclear Regulatory  
Commission  
Mail Stop NL-5650  
Washington, DC 20555

C. Y. Cheng  
U. S. Nuclear Regulatory  
Commission  
Office of Nuclear Reactor  
Regulation  
Engineering Branch  
Mail Stop P-1030  
Washington, DC 20555

Mr. Robert Hermann  
U.S. Nuclear Regulatory  
Commission  
Mail Stop 516  
Washington, DC 20555

Martin Hum  
U.S. Nuclear Regulatory  
Commission  
Mail Stop P-1000  
Washington, DC 20555

E. L. Jordan  
U.S. Nuclear Regulatory  
Commission  
Inspection and Enforcement  
Main Stop EW-359  
Washington, DC 20555

Dr. Thomas G. McCreless  
Asst. Exec. Director of  
Technical Activity  
1717-H USNRC-ACRS  
Washington, DC 20555

12 Joseph Muscara  
U.S. Nuclear Regulatory  
Commission  
Division of Reactor Safety  
Research  
Mail Stop SS-1130  
Washington, DC 20555

S. S. Pawlicki  
U.S. Nuclear Regulatory  
Commission  
Mail Stop TS-1000  
Washington, DC 20555

G. A. Walton  
U.S. Nuclear Regulatory  
Commission  
Office Inspection & Licensing  
631 Park Avenue  
King of Prussia, PA 19406

C. W. Allison  
Dept. of Labor  
Boiler Inspection & Codes  
Division  
501 Union Bldg./Suite 200B  
Nashville, TN 37219

No. of  
Copies

No. of  
Copies

W. H. Bamford  
Westinghouse Electric Corp.  
Nuclear Energy Systems  
P.O. Box 355  
Pittsburgh, PA 15230

F. L. Becker  
EPRI NDE Center  
J. A. Jones Applied Research  
1300 Harrison  
Charlotte, NC 28221

Carl Bennett  
Battelle-Human Affairs Research  
Center  
4000 N.E. 41st Street  
Seattle, WA 98105

F. C. Berry  
Chicago Bridge & Iron Co.  
P.O. Box 277  
Birmingham, AL 35201

M. Buckley  
Science Center  
Rockwell International  
1049 Camina Des Rios  
P.O. Box 1085  
Thousand Oaks, CA 91360

H. Burger  
National Bureau of Standards  
Materials Building  
Washington, DC 20234

Hans Burte, Chief  
Metals and Ceramics Division  
Airforce Materials Laboratory  
(APSC)  
Wright Patterson  
Air Force Base, OH 45433

L. J. Chockie  
General Electric Company  
Nuclear Energy Division  
175 Curtner Avenue M/C 827  
San Jose, CA 95125

R. C. Cipolla  
Aptech Eng. Services  
795 San Antonio Road  
Los Altos, CA 94303

W. E. Cooper  
Teledyne Engineering Services  
303 Bear Hill Road  
Waltham, MA 02154

A. E. Curtis  
Rochester Gas & Electric Co.  
89 E. Avenue  
Rochester, NY 14649

J. Danko  
Electric Power Research Institute  
3412 Hillview Avenue  
P.O. Box 10412  
Palo Alto, CA 94303

G. J. Dau/K. Stahlkopf  
Electric Power Research Institute  
3412 Hillview Avenue  
P.O. Box 10412  
Palo Alto, CA 94303

F. J. Dodd/W. C. Ham  
Pacific Gas & Electric Co.  
3400 Crow Canyon Road  
San Ramon, CA 94583

F. T. Duba  
Hartford Steam Boiler  
Inspection & Insurance Co.  
56 Prospect Street  
Hartford, CT 06102

J. H. Gieske/D. Ballard  
Sandia Laboratories  
P.O. Box 5800  
Albuquerque, NM 87115

K. Hannah  
Washington Public Power Supply  
System  
3000 George Washington Way  
Richland, WA 99352

No. of  
Copies

O. F. Hedden/D. J. Ayres  
Combustion Engineering, Inc.  
1000 Prospect Hill Road  
Dept. 9004-2226  
Windsor, CT 06095

A. E. Holt  
Babcock and Wilcox Co.  
P.O. Box 1260  
Lynchburg, VA 24505

L. R. Katz/J. S. Caplan  
Westinghouse Electric Corp.  
PWR Systems/Forest Hill Site  
P.O. Box 355  
Pittsburg, PA 15230

J. R. Knoke  
Power Production Engineering  
P.O. Box 1325  
San Clemente, CA 92672

Dave Kupperman  
Argonne National Laboratories  
9700 South Cass Avenue  
Argonne, IL 60439

J. J. Lance  
Yankee Atomic Electric Co.  
20 Turnpike Road  
Westboro, MA 01581

W. Lawrie  
Babcock and Wilcox Co.  
Alliance Research Center  
1562 Beeson Street  
Alliance, OH 44601

N. R. MacDearman  
Combustion Engineering, Inc.  
911 W. Main Street  
Chattanooga, TN 37401

R. W. McClung  
Oak Ridge National Laboratory  
Post Office Box X  
Oak Ridge, TN 37830

No. of  
Copies

J. G. Merkle  
Oak Ridge National Laboratory  
P.O. Box X  
Oak Ridge, TN 37830

Thomas A. Nemzek, Vice President  
Special Projects Services  
Division  
J. A. Jones Construction Co.  
One South Executive Park  
Charlotte, NC 28231

P. F. Packman  
Southern Methodist University  
Department of Mechanical  
Engineering  
Dallas, TX 75275

Prof. Steven Serabian  
University of Lowell  
Mechanical Engineering Dept.  
North Campus  
Lowell, MA 01854

Jack C. Spanner, P.E.  
Spanner Engineering, Inc.  
2042 George Washington Way  
Richland, WA 99352

R. M. Stone  
J. A. Jones Construction Co.  
One South Executive Park  
Charlotte, NC 28231

D. O. Thompson  
Ames Lab., U.S. DOE  
Iowa State University  
Ames, IA 50011

W. A. Van Der Sluys  
Babcock and Wilcox Company  
Alliance Research Center  
1562 Beeson Street  
Alliance, OH 44601

No. of  
Copies

A. R. Whiting/A. Greer  
Southwest Research Institute  
6220 Culebra Road  
Post Office Drawer 28510  
San Antonio, TX 78284

Howard Woo  
Lawrence Livermore Laboratories  
P.O. Box 808  
Mail Stop L-90  
Livermore, CA 94550

Edward Wright  
Department of Energy  
Clinch River Project  
P.O. Box U  
Oak Ridge, TN 37830

Sumio Yukawa  
General Electric Company  
Large Steam Generator Division  
Building 55/Rm 111  
One River Road  
Schenectady, NY 12345

R. Zong  
Philadelphia Electric Company  
2301 Market Street  
Philadelphia, PA 19101

I. P. Bell  
Risley Nuclear Power Development  
Laboratories  
United Kingdom Atomic Energy  
Authority  
Risley, Warrington WA3 6AT  
England

John Darlaston/R. P. Harrison  
Central Electricity Generating  
Board  
Research Department  
Berkeley Nuclear Laboratories  
Berkeley Gloucestershire GL13 9PB  
England

No. of  
Copies

N. F. Haines  
Central Electricity Generating  
Board  
Research Department  
Berkeley Nuclear Laboratories  
Berkeley Gloucestershire GL13 9PB  
England

J. D. Harrison/T. J. Jessop  
The Welding Institute  
Research Laboratory  
Abington Hall  
Abington Cambridge CBI 6 AL  
England

R. W. Nichols  
Risley Nuclear Power Development  
Laboratories  
United Kingdom Atomic Energy  
Authority  
(Northern Division)  
Risley Warrington WA3 6AT  
England

Mr. R. O'Neil  
Safety and Reliability Directorate  
United Kingdom Atomic Energy  
Authority  
Wigshaw Lane  
Culcheth, Warrington WA3 4NE  
England

R. Sharpe/G. Silk  
Nondestructive Testing Centre  
Atomic Energy Research  
Establishment  
Harwell Oxfordshire OX11 0RG  
England

B. Watkins  
Risley Nuclear Power Development  
Laboratories  
United Kingdom Atomic Energy  
Authority  
(Northern Division)  
Wigshaw Lane  
Culcheth, Warrington WA3 6AT  
England

No. of  
Copies

Jacques Pierre Dufresne  
Commissariat a l'Energie Atomique  
CEN SAR BN06  
92260 Fontenay-aux-Roses  
France

P. Oliver  
Nuclear Safety Division  
OECD Nuclear Energy Agency  
38 bld Suchet  
75016 Paris  
France

Andre C. Prot/Robert Saglio  
Centre D'Etudes Superieure de  
Mecanique et D'Aerotechnique  
B.P. N 91190 Gif-sur-Yvette  
France

J. Eisenblatter  
Battelle Institut e.V.  
Am Romerhof 35  
6000 Frankfurt am Main 90  
West Germany

Guenter Engl  
K.W.U.  
Hammerbackerstr  
P.O. Box 3220  
D-852 Erlangen  
Dept. R214  
Germany

P. Höller  
Institut für Zerstörungsfreie  
Prüfverfahren  
Saarbrücken  
West Germany

Otto Kellerman, Dipl-Ing.  
Direktor des Institut für  
Reaktorsicherheit  
5 Köln 1  
Glockengasse 2  
West Germany

No. of  
Copies

H. J. Meyer  
Machinenfabrik Augsburg-Nürnberg AG  
Katzwangstr. 101  
85 Nürnberg 2  
West Germany

E. Mundry/Ing. H. Wüstenberg  
Bundesanstalt für  
Materialprüfung  
Unter den Eichen 87  
D-1000 Berlin 45  
West Germany

Professor D. Munz  
Universität Karlsruhe (TH)  
7500 Karlsruhe 1, den  
Postfach 3640  
West Germany

A. J. Tietze  
Technischen Überwachungs-Verein  
Rheinland e.V.  
5000 Köln 1  
Postfach 101750  
West Germany

R. Trumpfheller  
Deputy Director  
Rheinisch-Westfälischer  
Technischen Überwachungs-Verein  
E. V. 43 Essen 1  
Steubenstr. 53  
West Germany

Serge Crutzen  
Commission of the European  
Communities  
Joint Research Centre  
Ispra Establishment  
21020 Ispra (VA)  
Italy

A. deSterke  
Röntgen Technische Dienst, B.V.  
Delftweg 144  
NL 3046 Rotterdam  
The Netherlands

No. of  
Copies

No. of  
Copies

Prof. Ir. D.G.H. Latzko  
Dept. of Mechanical Engineering  
University of Technology  
Delft  
The Netherlands

A. Nielsen/P. Becher  
RISO Research Establishment  
DK-4000 Roskilde  
Denmark

Lars-Ake Kornvik  
Section Manager  
Nuclear Department  
Kemistvagen 21  
Box 51  
S-183 21 TABY  
Sweden

Dr. Gustaf Ostberg  
Engineering Materials  
Lund Institute of Technology  
Box 725  
S-220 07 - Lund 7  
Sweden

Xaver Edelmann  
Sulzer Brothers Limited  
GH-8401  
Winterthur, Switzerland

Dr. Yoshio Ando  
Professor, Nuclear Engineering  
Dept. of Nuclear Engineering  
Faculty of Engineering  
University of Tokyo  
7-3-1 Hongo  
Bunkyo-Ku  
Japan

K. Iida  
Professor, Naval Architecture  
Faculty of Engineering  
University of Tokyo  
7-3-1 Hongo  
Bunkyo-Ku  
Japan

T. Matsubara  
Mitsubishi Heavy Industries, LTD  
Takasago Technical Institute  
2-1-1 Shinhama, Arai-Cho  
Takasago 676  
Japan

Dr. Shinsaku Onodera  
Associate Director Engineering  
The Japan Steel Works, Ltd  
Hibiya-Mitsui Bldg  
1-1-2 Yurakucho, Chiyoda-Ku  
Tokyo, Japan

Y. Saiga  
Ishikawajima-Harima Heavy  
Industries Co., Ltd  
1-15, Toyosu 3  
Koto-Ku  
Tokyo, 135-91  
Japan

S. Sasaki  
Hitachi Research Lab  
4026 Kuji-Machi  
Hitachi-Shi  
Baraki-Ken  
Japan

J. Watanabe  
Japan Steel Works, Ltd  
4 Chatsu-Machi  
Muroran, Hokkaido  
Japan

T. Yamaguchi  
Mitsubishi Heavy Industries, Ltd  
Takasago Technical Institute  
2-1-1 Shinhama, Arai-Cho  
Takasago 676  
Japan

No. of  
Copies

ONSITE

50 Pacific Northwest Laboratory

S. H. Bush (39)  
S. R. Doctor  
P. G. Heasler  
G. J. Posakony  
F. C. Simonen  
Publishing Coordination (2)  
Technical Information (5)

HEDL - Westinghouse

T. E. Michaels

100-44  
100-44  
100-44

Department of Health Laboratory

- 1. Mr. John (28)
- 2. Mr. Jackson
- 3. Mr. Hill
- 4. Mr. Taylor
- 5. Mr. Green
- 6. Mr. White
- 7. Mr. Brown
- 8. Mr. Black
- 9. Mr. Gray
- 10. Mr. Blue

100-44-100

J. L. Nichols



<b>NRC FORM 335</b> <small>(11 81)</small>		<b>U.S. NUCLEAR REGULATORY COMMISSION</b> <b>BIBLIOGRAPHIC DATA SHEET</b>		<b>1. REPORT NUMBER (Assigned by DDC)</b> NUREG/CR-3110, Vol. 1 PNL-4584	
<b>4. TITLE AND SUBTITLE (Add Volume No., if appropriate)</b> Reliability of Nondestructive Examination Chapters 1 - 6				<b>2. (Leave blank)</b>	
<b>7. AUTHOR(S)</b> Spencer H. Bush, Senior Staff Consultant				<b>3. RECIPIENT'S ACCESSION NO.</b>	
<b>9. PERFORMING ORGANIZATION NAME AND MAILING ADDRESS (Include Zip Code)</b> Pacific Northwest Laboratory Operated by Battelle Memorial Institute P.O. Box 999 Richland, WA 99352				<b>5. DATE REPORT COMPLETED</b> MONTH August   YEAR 1983	
<b>12. SPONSORING ORGANIZATION NAME AND MAILING ADDRESS (Include Zip Code)</b> Division of Engineering Technology Office of Nuclear Regulatory Research U.S. Nuclear Regulatory Commission Washington, D.C. 20555				<b>6. (Leave blank)</b>	
<b>13. TYPE OF REPORT</b> Technical				<b>PERIOD COVERED (Inclusive dates)</b> October 1979 to August 1983	
<b>15. SUPPLEMENTARY NOTES</b>				<b>8. (Leave blank)</b>	
<b>16. ABSTRACT (200 words or less)</b> This eighteen-chapter, three-volume study evaluates the various nondestructive examination (NDE) techniques now used to detect flaws in components of nuclear systems so that the reliability of the techniques may be increased. The significance of flaws at various locations in pressure boundary components are assessed along with ways to optimize the NDE procedures needed to detect, locate and size them. Emphasis is placed on an integrated program which also considers design, fabrication procedures, and materials. The data available on the reliability of detecting, locating and sizing flaws by NDE are used to construct a probabilistic fracture mechanics model. The model highlights the significance of the failure to detect flaws, and to accurately locate or size them in the context of component failure probability. This study was conducted under the U.S. Nuclear Regulatory Commission program on the "Integration of NDE Reliability and Fracture Mechanics." Its objectives include 1) improving examination procedures for incorporation into the American Society for Mechanical Engineers (ASME), Boiler and Pressure Vessel Codes, Section III, V, XI; and 2) gaining a better insight into the influence of improved reliability of NDE in detecting, locating and sizing flaws on component failure probabilities.				<b>10. PROJECT/TASK/WORK UNIT NO.</b>	
<b>17. KEY WORDS AND DOCUMENT ANALYSIS</b> Ultrasonics Reliability Nondestructive Examination Austenitic Metals Flaws Flaw Detection Flaw Sizing				<b>11. FIN NO.</b> B-2289	
<b>17b. IDENTIFIERS, OPEN-ENDED TERMS</b>				<b>14. (Leave blank)</b>	
<b>18. AVAILABILITY STATEMENT</b> Unlimited				<b>19. SECURITY CLASS (This report)</b> Unclassified	
<b>20. SECURITY CLASS (This page)</b> Unclassified				<b>21. NO. OF PAGES</b>	
<b>22. PRICE</b> S					

1. TITLE OF PROJECT 2. AUTHOR(S) 3. INSTITUTION(S) 4. DATE OF REPORT 5. PERIOD COVERED 6. TYPE OF REPORT 7. AVAILABILITY STATEMENTS 8. PRICE(S) 9. AVAILABILITY STATEMENTS 10. AVAILABILITY STATEMENTS	11. AUTHOR(S) 12. INSTITUTION(S) 13. DATE OF REPORT 14. PERIOD COVERED 15. TYPE OF REPORT 16. AVAILABILITY STATEMENTS 17. PRICE(S) 18. AVAILABILITY STATEMENTS 19. AVAILABILITY STATEMENTS
20. TITLE OF PROJECT 21. AUTHOR(S) 22. INSTITUTION(S) 23. DATE OF REPORT 24. PERIOD COVERED 25. TYPE OF REPORT 26. AVAILABILITY STATEMENTS 27. PRICE(S) 28. AVAILABILITY STATEMENTS 29. AVAILABILITY STATEMENTS	30. AUTHOR(S) 31. INSTITUTION(S) 32. DATE OF REPORT 33. PERIOD COVERED 34. TYPE OF REPORT 35. AVAILABILITY STATEMENTS 36. PRICE(S) 37. AVAILABILITY STATEMENTS 38. AVAILABILITY STATEMENTS
39. TITLE OF PROJECT 40. AUTHOR(S) 41. INSTITUTION(S) 42. DATE OF REPORT 43. PERIOD COVERED 44. TYPE OF REPORT 45. AVAILABILITY STATEMENTS 46. PRICE(S) 47. AVAILABILITY STATEMENTS 48. AVAILABILITY STATEMENTS	49. AUTHOR(S) 50. INSTITUTION(S) 51. DATE OF REPORT 52. PERIOD COVERED 53. TYPE OF REPORT 54. AVAILABILITY STATEMENTS 55. PRICE(S) 56. AVAILABILITY STATEMENTS 57. AVAILABILITY STATEMENTS
58. TITLE OF PROJECT 59. AUTHOR(S) 60. INSTITUTION(S) 61. DATE OF REPORT 62. PERIOD COVERED 63. TYPE OF REPORT 64. AVAILABILITY STATEMENTS 65. PRICE(S) 66. AVAILABILITY STATEMENTS 67. AVAILABILITY STATEMENTS	68. AUTHOR(S) 69. INSTITUTION(S) 70. DATE OF REPORT 71. PERIOD COVERED 72. TYPE OF REPORT 73. AVAILABILITY STATEMENTS 74. PRICE(S) 75. AVAILABILITY STATEMENTS 76. AVAILABILITY STATEMENTS
77. TITLE OF PROJECT 78. AUTHOR(S) 79. INSTITUTION(S) 80. DATE OF REPORT 81. PERIOD COVERED 82. TYPE OF REPORT 83. AVAILABILITY STATEMENTS 84. PRICE(S) 85. AVAILABILITY STATEMENTS 86. AVAILABILITY STATEMENTS	87. AUTHOR(S) 88. INSTITUTION(S) 89. DATE OF REPORT 90. PERIOD COVERED 91. TYPE OF REPORT 92. AVAILABILITY STATEMENTS 93. PRICE(S) 94. AVAILABILITY STATEMENTS 95. AVAILABILITY STATEMENTS
96. TITLE OF PROJECT 97. AUTHOR(S) 98. INSTITUTION(S) 99. DATE OF REPORT 100. PERIOD COVERED 101. TYPE OF REPORT 102. AVAILABILITY STATEMENTS 103. PRICE(S) 104. AVAILABILITY STATEMENTS 105. AVAILABILITY STATEMENTS	106. AUTHOR(S) 107. INSTITUTION(S) 108. DATE OF REPORT 109. PERIOD COVERED 110. TYPE OF REPORT 111. AVAILABILITY STATEMENTS 112. PRICE(S) 113. AVAILABILITY STATEMENTS 114. AVAILABILITY STATEMENTS
115. TITLE OF PROJECT 116. AUTHOR(S) 117. INSTITUTION(S) 118. DATE OF REPORT 119. PERIOD COVERED 120. TYPE OF REPORT 121. AVAILABILITY STATEMENTS 122. PRICE(S) 123. AVAILABILITY STATEMENTS 124. AVAILABILITY STATEMENTS	125. AUTHOR(S) 126. INSTITUTION(S) 127. DATE OF REPORT 128. PERIOD COVERED 129. TYPE OF REPORT 130. AVAILABILITY STATEMENTS 131. PRICE(S) 132. AVAILABILITY STATEMENTS 133. AVAILABILITY STATEMENTS
134. TITLE OF PROJECT 135. AUTHOR(S) 136. INSTITUTION(S) 137. DATE OF REPORT 138. PERIOD COVERED 139. TYPE OF REPORT 140. AVAILABILITY STATEMENTS 141. PRICE(S) 142. AVAILABILITY STATEMENTS 143. AVAILABILITY STATEMENTS	144. AUTHOR(S) 145. INSTITUTION(S) 146. DATE OF REPORT 147. PERIOD COVERED 148. TYPE OF REPORT 149. AVAILABILITY STATEMENTS 150. PRICE(S) 151. AVAILABILITY STATEMENTS 152. AVAILABILITY STATEMENTS
153. TITLE OF PROJECT 154. AUTHOR(S) 155. INSTITUTION(S) 156. DATE OF REPORT 157. PERIOD COVERED 158. TYPE OF REPORT 159. AVAILABILITY STATEMENTS 160. PRICE(S) 161. AVAILABILITY STATEMENTS 162. AVAILABILITY STATEMENTS	163. AUTHOR(S) 164. INSTITUTION(S) 165. DATE OF REPORT 166. PERIOD COVERED 167. TYPE OF REPORT 168. AVAILABILITY STATEMENTS 169. PRICE(S) 170. AVAILABILITY STATEMENTS 171. AVAILABILITY STATEMENTS
172. TITLE OF PROJECT 173. AUTHOR(S) 174. INSTITUTION(S) 175. DATE OF REPORT 176. PERIOD COVERED 177. TYPE OF REPORT 178. AVAILABILITY STATEMENTS 179. PRICE(S) 180. AVAILABILITY STATEMENTS 181. AVAILABILITY STATEMENTS	182. AUTHOR(S) 183. INSTITUTION(S) 184. DATE OF REPORT 185. PERIOD COVERED 186. TYPE OF REPORT 187. AVAILABILITY STATEMENTS 188. PRICE(S) 189. AVAILABILITY STATEMENTS 190. AVAILABILITY STATEMENTS
191. TITLE OF PROJECT 192. AUTHOR(S) 193. INSTITUTION(S) 194. DATE OF REPORT 195. PERIOD COVERED 196. TYPE OF REPORT 197. AVAILABILITY STATEMENTS 198. PRICE(S) 199. AVAILABILITY STATEMENTS 200. AVAILABILITY STATEMENTS	201. AUTHOR(S) 202. INSTITUTION(S) 203. DATE OF REPORT 204. PERIOD COVERED 205. TYPE OF REPORT 206. AVAILABILITY STATEMENTS 207. PRICE(S) 208. AVAILABILITY STATEMENTS 209. AVAILABILITY STATEMENTS
210. TITLE OF PROJECT 211. AUTHOR(S) 212. INSTITUTION(S) 213. DATE OF REPORT 214. PERIOD COVERED 215. TYPE OF REPORT 216. AVAILABILITY STATEMENTS 217. PRICE(S) 218. AVAILABILITY STATEMENTS 219. AVAILABILITY STATEMENTS	220. AUTHOR(S) 221. INSTITUTION(S) 222. DATE OF REPORT 223. PERIOD COVERED 224. TYPE OF REPORT 225. AVAILABILITY STATEMENTS 226. PRICE(S) 227. AVAILABILITY STATEMENTS 228. AVAILABILITY STATEMENTS
229. TITLE OF PROJECT 230. AUTHOR(S) 231. INSTITUTION(S) 232. DATE OF REPORT 233. PERIOD COVERED 234. TYPE OF REPORT 235. AVAILABILITY STATEMENTS 236. PRICE(S) 237. AVAILABILITY STATEMENTS 238. AVAILABILITY STATEMENTS	239. AUTHOR(S) 240. INSTITUTION(S) 241. DATE OF REPORT 242. PERIOD COVERED 243. TYPE OF REPORT 244. AVAILABILITY STATEMENTS 245. PRICE(S) 246. AVAILABILITY STATEMENTS 247. AVAILABILITY STATEMENTS
248. TITLE OF PROJECT 249. AUTHOR(S) 250. INSTITUTION(S) 251. DATE OF REPORT 252. PERIOD COVERED 253. TYPE OF REPORT 254. AVAILABILITY STATEMENTS 255. PRICE(S) 256. AVAILABILITY STATEMENTS 257. AVAILABILITY STATEMENTS	258. AUTHOR(S) 259. INSTITUTION(S) 260. DATE OF REPORT 261. PERIOD COVERED 262. TYPE OF REPORT 263. AVAILABILITY STATEMENTS 264. PRICE(S) 265. AVAILABILITY STATEMENTS 266. AVAILABILITY STATEMENTS
267. TITLE OF PROJECT 268. AUTHOR(S) 269. INSTITUTION(S) 270. DATE OF REPORT 271. PERIOD COVERED 272. TYPE OF REPORT 273. AVAILABILITY STATEMENTS 274. PRICE(S) 275. AVAILABILITY STATEMENTS 276. AVAILABILITY STATEMENTS	277. AUTHOR(S) 278. INSTITUTION(S) 279. DATE OF REPORT 280. PERIOD COVERED 281. TYPE OF REPORT 282. AVAILABILITY STATEMENTS 283. PRICE(S) 284. AVAILABILITY STATEMENTS 285. AVAILABILITY STATEMENTS
286. TITLE OF PROJECT 287. AUTHOR(S) 288. INSTITUTION(S) 289. DATE OF REPORT 290. PERIOD COVERED 291. TYPE OF REPORT 292. AVAILABILITY STATEMENTS 293. PRICE(S) 294. AVAILABILITY STATEMENTS 295. AVAILABILITY STATEMENTS	296. AUTHOR(S) 297. INSTITUTION(S) 298. DATE OF REPORT 299. PERIOD COVERED 300. TYPE OF REPORT 301. AVAILABILITY STATEMENTS 302. PRICE(S) 303. AVAILABILITY STATEMENTS 304. AVAILABILITY STATEMENTS
305. TITLE OF PROJECT 306. AUTHOR(S) 307. INSTITUTION(S) 308. DATE OF REPORT 309. PERIOD COVERED 310. TYPE OF REPORT 311. AVAILABILITY STATEMENTS 312. PRICE(S) 313. AVAILABILITY STATEMENTS 314. AVAILABILITY STATEMENTS	315. AUTHOR(S) 316. INSTITUTION(S) 317. DATE OF REPORT 318. PERIOD COVERED 319. TYPE OF REPORT 320. AVAILABILITY STATEMENTS 321. PRICE(S) 322. AVAILABILITY STATEMENTS 323. AVAILABILITY STATEMENTS
324. TITLE OF PROJECT 325. AUTHOR(S) 326. INSTITUTION(S) 327. DATE OF REPORT 328. PERIOD COVERED 329. TYPE OF REPORT 330. AVAILABILITY STATEMENTS 331. PRICE(S) 332. AVAILABILITY STATEMENTS 333. AVAILABILITY STATEMENTS	334. AUTHOR(S) 335. INSTITUTION(S) 336. DATE OF REPORT 337. PERIOD COVERED 338. TYPE OF REPORT 339. AVAILABILITY STATEMENTS 340. PRICE(S) 341. AVAILABILITY STATEMENTS 342. AVAILABILITY STATEMENTS
343. TITLE OF PROJECT 344. AUTHOR(S) 345. INSTITUTION(S) 346. DATE OF REPORT 347. PERIOD COVERED 348. TYPE OF REPORT 349. AVAILABILITY STATEMENTS 350. PRICE(S) 351. AVAILABILITY STATEMENTS 352. AVAILABILITY STATEMENTS	353. AUTHOR(S) 354. INSTITUTION(S) 355. DATE OF REPORT 356. PERIOD COVERED 357. TYPE OF REPORT 358. AVAILABILITY STATEMENTS 359. PRICE(S) 360. AVAILABILITY STATEMENTS 361. AVAILABILITY STATEMENTS